Universidade do Minho
Escola de Engenharia

Catarina Vilaça Silva

Tall buildings using CLT. An integrated design considering moisture induced effects

outubro de 2020

Tall buildings using CLT. An integrated design considering moisture induced effects
Catarina Vilaça Silva
UMinho | 2020

Universidade do Minho
Escola de Engenharia

Catarina Vilaça Silva

Tall buildings using CLT. An integrated design considering moisture induced effects

Tese de Doutoramento

Trabalho efectuado sob a orientacao de
Professor Jorge Manuel Goncalves Branco
Professor Paulo Jose Barbosa Lourenco

outubro de 2020

ACKNOWLEDGES

The present Phd research was the most individual and lonely project I had to develop until now. However, I couldn't make it happen without the precious help of some important persons who allowed this research to be deleloped. This way, I must thank to some important people:

- My advisores, Professor Jorge Branco and Professor Paulo B. Loureço, for all the technical support during definition and execution of present research;
- Researcher José Xavier, for all the support related with the experiments based on DIC technique;
- Professor Gerhard Schickhofer, researcher Andreas Ringhofer and all technical staff from LAB, who welcome me at *Institut für Holzbau und Holztechnologie* - Graz Technical University (Austria) and gave me all the conditions and support to conclude the tasks developed in there;
- Professor Eduarda Luso, who made available the facilities of Instituto Politecnico de Bragança where we perform some experimental tests;
- Technical staff of structures laboratory of Civil Engineering Department at University of Minho for the for the crucial role in realizing a great part of experiments of this thesis, specially to my dear husband Marco Jorge, who had all the patience when the work didn't seem to go well;
- My closest family, parents and syster, for all the emotional support;
- my sweet daughters, Maria and Inês, who were born when this research was under development making it longer than expected.
- At last, I must thanks to Fundação para a Ciencia e Tecnologia that fund present research by means of the scholarship with the reference SFRH / BD / 79972 / 2011, funded by POPH - QREN - Tipology 4.1 - Advanced Training, co-funded by the European Social Fund and MEC national funds.

STATEMENT OF INTEGRITY

I hereby declare having conducted this academic work with integrity. I confirm that I have not used plagiarism or any form of undue use of information or falsification of results along the process leading to its elaboration.

I further declare that I have fully acknowledged the Code of Ethical Conduct of the University of Minho.

Edifícios em altura com MLCC. Um projeto integrado considerando os efeitos da humidade.

RESUMO

Conscientes das vantagens associadas ao uso da Madeira Lamelada Colada Cruzada (MLCC) nas construções localizadas nos grandes centros urbanos e considerando a falta de conhecimento relativo aos efeitos resultantes de variações de humidade nesse mesmo material, a presente tese foi dividida em duas partes complementares.

A Parte I é dedicada ao desenvolvimento de uma vasta campanha experimental focada essencialmente na quantificação dos esforços induzidos pela humidade na MLCC e na quantificação da resistência ao arrancamento de parafusos auto perfurantes inseridos em painéis de MLCC. Os esforços induzidos pela variação no teor de humidade foram quantificados considerando um intervalo de humidade relativa entre 30% e 90%, sendo utilizadas três técnicas de medição diferentes, nomeadamente: Correlação Digital de Imagem, sensores de deslocamento (LVDT) e paquímetro. No que respeita á quantificação da capacidade de arrancamento dos parafusos auto perfurantes, foi desenvolvida uma campanha experimental na qual foram efetuados 590 testes de arrancamento. De modo a compreender melhor a relação entre MLCC e os parafusos auto perfurantes, foram tidos em conta três parâmetros principais: (i) mudanças simples e cíclicas no teor de humidade, (ii) número de *gaps* e (iii) a largura dos mesmos *gaps*.

A parte II apresenta uma proposta para um sistema estrutural para a construção de edifícios de vários pisos, no qual a MLCC é o principal material de cariz estrutural. Este sistema foi apelidado de *Urban Timber (UT) system* e foi desenhado tendo sempre presente os efeitos causados pelas variações no teor de humidade quer nos elementos individuais de MLCC, nas ligações mecânicas ou nas soluções propostas para as fachadas. Paralelemente, o UT system foi submetido a uma avaliação estrutural e as suas potencialidades arquitetónicas foram exploradas.

Palavras-chave: Madeira Lamelada colada cruzada; parafusos auto perfurantes; efeitos induzidos pela humidade; construção de madeira em altura; resistência ao arrancamento.

Tall buildings using CLT. An integrated design considering moisture induced effects.

ABSTRACT

Aware about the advantages of using Cross Laminated Timber (CLT) as a construction material on the urban environments, and considering the lack of knowledge related with the behaviour of CLT regarding moisture induced effects, present thesis was developed in two parts that complement each other.

Part I is based on the development of laboratorial experiments focused on the quantification of moisture induced strains on CLT panels and on the quantification of withdrawal capacity of Self Tapping Screws (STS) inserted in CLT panels. Moisture induced strains were quantified considering a range of relative humidity that varies between 30% and 90% and three different measure techniques were used, namely: Digital Image Correlation (DIC), LVDT's acquisition and Calliper ruler measurements. Regarding quantification of withdrawal capacity of STSs, a large experimental campaign comprising 590 withdrawal tests was carried out. In order to understand deeply the composite model "CLT-STS", tests performed considered three main parameters: (i) simple and cyclic on moisture changes, (ii) number of gaps and (iii) the width of gaps.

Part II present a proposal for a new structural system for multi-story timber buildings, in which CLT is the main structural material. The proposed structural system was called Urban Timber (UT) system and it was designed always taking into account moisture induced effects either on individual structural elements, mechanical connections or on facade solutions. Independent of limitations imposed by moisture induced effects, a structural evaluation of UT system is performed and architectural potentialities are presented individually.

Keywords: Cross laminated timber; self-tapping screws; moisture induced effects; multi-storey timber buildings; withdrawal strength.

CONTENTS

FIGURE INDEX

TABLE INDEX

LIST OF ABBREVIATIONS AND ACRONYMS

CNC	Computerized Numerical Control
CLT	Cross Laminated Timber
GL	Glulam
STS	Self-tapping Srews
UT sytem	Urban Timber System
RH	Relative Humidity
DIC	Digital Image Correlation
EMC	Equilibrium Moisture Content
MC	Moisture Content
FSP	Fiber Saturation Point
MG	Moisture Gradients
MIS	Moisture induced stresses
ROI	Region of interest
2D DIC	2D Digital Image Correlation
CoV	Coefficient of variation
C1	Test configuration in which three directions allow free moisture flow
C2	Test configuration in which only tangential direction allow free moisture flow
C3	Test configuration in which only longitudinal direction allow free moisture flow
C4	Test configuration in which only radial direction allow free moisture flow
OL	Outer layers
IL	Inner layers
FL	First layer
BC	Before cut specimens
AC	After cut specimens
MOE	Modulus of elasticity, in MPa
REF	Test configuration in which STS is inserted without the presence of gaps
GAP_FL	Test configuration in which STS is inserted through one gap present in first layer of CLT panel
GAP_ML	Test configuration in which STS is inserted through one gap present in middle layer of CLT panel
GAP_OL	Test configuration in which STS is inserted through two gaps present in outer layers of CLT panel

GAP_3L	Test configuration in which STS is inserted through three gaps present in all three layers of CLT panel
GAP	Line or space between two boards glued side by side in a CLT pan
GAP0	Gap with 0mm
GAP4	Gap with 4mm
SD	Standard deviation
P5	5th percentile
T	Temperature, in °C
FFTT	Find forests through the threes
CREE	Creative Renewable Energy & Efficiency
STC	Sound transmission classes
IIC	Impact insulation class
ε_{mean}	Mean Strain
σ_{mean}	Mean stress (MPa)
$E(u)$	Modulus of Elasticity as a function of moisture content
$\mathbf{f_{ax,k}}$	characteristic withdrawal resistance
$\mathbf{l_{ef}}$	screw penetration depth
$\boldsymbol{\rho_k}$	timber characteristic density
α	angle between the screw and grain direction
$R_{ax,s,pred}$	Predicted values for withdrawal resistance of self-tapping screws in CLT, in N
ε_{rest}	Restrained strains
ε_{rel}	Released strains
σ	Stresses. In MPa
$E_{(u)}$	Modulus of elasticity as a function of moisture content present in the specimen at measuring time, in MPa
ρ	Density, in Kg/m^3
ρ_{12}	Density considering a moisture content of 12%, in Kg/m^3
Δ	Ratio between restrained strains obtained for Y and X directions
Δ_{OL}	Ratio obtained between strains measured for radial and tangential directions, in outer layers
Δ_{IL}	Ratio obtained between strains measured for radial and longitudinal, in inner layers
Δ_Y	Ration obtained between strains measured for tangential and longitudinal directions, considering relation between adjacent layers
E_{sta}	Static modulus of elasticity, in MPa

E_{dyn}	Dynamic modulus of elasticity, in MPa
V_p	velocity of sound propagation, in m/s
m	Mass of test piece, in grams
V	Volume of test piece, in cm^3
$f_{ax,test}$	Maximum withdrawal resistance obtained by mechanical test, in N/mm^2
F_{max}	Maximum withdrawal load given by test machine, in
d	Screw diameter, in mm
l_p	Length of penetration, in mm
m_1	Mass of specimen before drying, in g
m_0	Mass of specimen after drying, in g
$\rho_{12,i}$	Density with 12% of moisture content for each specimen, in kg/m^3
$\rho_{MC,i}$	Density with a different moisture content for each specimen, in kg/m^3
$f_{ax,corr,i}$	Corrected withdrawal resistance for each test specimen, in N/mm^2
$f_{ax,test,i}$	Withdrawal resistance for each specimen resulted from test machine, in N/mm
ρ_{ref}	Density of reference (mean value for ρ_{12} obtained with entire data of tests performed), in kg/m^3
$\rho_{12,i}$	Density of each specimen with a moisture content of 12%.
η_{gap}	Effect of number and width of gaps in withdrawal resistance of STSs
k_{gap}	Effect of each gap added in the withdrawal resistance
η_{MC}	Effect of simple MC changes on the withdrawal resistance of STSs
k_{MC}	Effect of each percentage unit of MC added/subtracted in the withdrawal resistance
ε	Angle between screw axis and grain direction.

INTRODUCTION

The continuous increase of the urban density all around the world forced cities to grow bigger, making tall buildings an ordinary typology in developed cities. The urban population keeps growing, foreseeing that until 2050 the world population living in cities will reach 70% (Green & Eric Karsh 2012). This reality will reinforce the demand for large building solutions and it is necessary to be aware that urban density becomes an increasingly important component when addressing climate change. So, it is necessary to reformulate the current construction practice in order to answer the higher standard of living and higher energy efficiency required today. Unfortunately, tall buildings are generally linked to large negative impacts on environment, raising the need to look for new environment friendly solutions. Tall timber buildings are a concept that emerged connected with this need, stressing the wood sustainable profile as the key factor to reduce the negative environmental impact of the construction sector. In some countries where timber has a social character, such as Sweden, German and Japan, timber is positively appreciated as a building material (Stehn & Bergström 2002). However, this subject can face serious barriers in countries where wood culture does not exist. Regardless of these difficulties, tall timber buildings are an exciting and current topic, expecting that their qualitative advantages overcome remaining socio-cultural barriers.

Sustainable profile linked to timber as a construction material can be a strong ally to recent European environmental policies, namely EU's 20-20-20 plan and 2050 Energy Roadmap, as well as the 2030 Agenda for Sustainable Development. Indeed, timber is a natural material, renewable, recyclable and able to capture carbon dioxide (CO^2). This last feature is the most important once, similarly to forests, harvested timber can be used for carbon storage. However, in order to guarantee the wanted positive environmental effects, the carbon emissions during manufacturing of wood products should be reduced and these materials should have significant long lifespans assuring a useful carbon sequestration (Esbjörnsson et al., 2014). Using timber as a structural material in construction sector is one solution that fits on long-lasting carbon storage, assuring that CO^2 stored will only be emitted into the atmosphere upon combustion or decay of timber. Wood stores more carbon than the equivalent CO^2 emitted by the harvesting, processing, transport and fabrication (Cambiaso & Pietrasanta, 2014). While each ton of solid wood panels sequester around 1.6 tons of CO^2, the production of one ton of steel and cement releases 1.5 and 1.1 tons of carbon, respectively. (Stehn & Bergström, 2002).

The economic sustainability of timber construction is closely related with savings provided by technical facilities, construction speed and long-term savings. Firstly, material production is industrialized and

controlled by a computerized numerical control (CNC) system which ensures the high quality of construction elements, reduces the amount of material waste and makes the execution of connections easier. Secondly, the simplicity of construction associated to timber (easy handling and prefabrication) allows a significant reduction of construction time, simplifies the building site yard, requires reduced teams and increases the on-site safety. Lastly, dependent on construction system chosen, significant long-term savings related with energy consumption, operation and maintenance can be more relevant than costs resulted directly from the erection of building (Lehmann, 2012).

Despite the large number of advantages associated to the use of timber as a structural material, there are some important barriers to be overcome. During the last century, wood was qualified as an inflammable material with low durability, fact that resulted on stagnation of timber as a construction material and allowed steel and reinforced concrete to completely domain construction sector. In some cultural contexts, the negative connotation imposed to timber was so ingrained that the idea of building a large-scale multi-story timber building is not well accepted, even nowadays (Langenbach, 2008). However, taking a look into the past, it is possible to find interesting examples of tall timber buildings/structures, erected with archaic technologies that are still standing.

Cross laminated timber (CLT) is an engineered timber product that has been largely associated to the concepts of tall timber buildings due to its excellent mechanical properties, relatively low mass and easy application. CLT constructions are often cited as a great sustainable solution due to their capacity for storing a large amount of carbon dioxide (Green & Eric Karsh 2012, Omland & Tonning 2009).

Analyzing the progressive increase of tall timber constructions, it can be observed that CLT is a transversal material, being the leading material in the majority of the constructed buildings as well as in the proposals for new construction systems. There are examples of monolithic construction systems that are fully based on CLT as structural material. Other buildings combine CLT with concrete cores or with linear elements made from steel and other wood-based products. In this thesis, CLT will be presented as a structural material and its advantages and disadvantages will be listed. Furthermore, demonstration buildings in which CLT is applied will be described as well as their construction systems.

The present research addresses multi-story timber buildings, but also discusses the innovative role that CLT can play in this type of construction. The initial motivation for this research was to give some contribute to the implementation of timber construction in urban context through the development of a new CLT based construction system thought to be applied in multi-story buildings, in which some important parameters would be analyzed: architectural versatility, either for the organization of interior

space, or for the shape or exterior appearance of the building; cost competitiveness; functional requirements such as structural behavior, fire protection and placement of building services. As a result, some case studies would be developed in order to demonstrate the versatility of developed system. However, as the research progressed, the author felt that proposing a system based on a material and structure rather different from traditional systems brings new challenges. In fact, it became clear why architects who are not familiar to the system do not risk to propose a solution based on a timber structural system. Here, it was decided to perform an experimental campaign that would allow the author to in-depth characterize a new exciting: Cross Laminated Timber (CLT).

Despite the advantages associated with timber construction, many architects and engineers do not feel confident suggesting timber in projects where other materials are more traditional. These professionals suffer a lack of knowledge and experience in timber construction. To empower architects, the knowledge must be expanded in material properties, production and construction as well as in building physics and economy of timber construction. This way architects would have a stronger voice in the decision making for sustainable solutions to urban building construction (Esbjörnsson et al., 2014) .

After some in-depth research on the subject of CLT characterization, a gap in the knowledge regarding the hygroscopic behavior of CLT as well as the behavior of screwed connections subjected to moisture induced effects was detected. At that moment, the research was divided into two different parts. One would be dedicated to the development of an experimental campaign focused in the evaluation of hygroscopic behavior of CLT elements and in the evaluation of moisture induced effects on withdrawal capacity of self-tapping screws inserted in CLT elements. The other part would be dedicated to the development of a structural system using CLT as main structural material and designed to shape multi-story timber buildings. Joining these two subjects in the same doctoral thesis may seems not evident, however, it must be said that without the laboratorial tests performed by the author, the structural system proposed would not be the same. That is because the system was developed taking special attention to the moisture induced effects. The position of structural elements, the building sequence, the connection between elements and façade composition were defined considering the behavior of CLT regarding changes on its moisture content.

Wood hygroscopic behavior varies according to the wood species, but it can also vary between solid wood and timber engineering materials. Cross lamination of CLT can restrict moisture induced movements, reducing swelling and shrinkage movements when comparing with solid timber or Glulam. Besides the changes on geometry, moisture variations can also lead to changes on timber mechanical properties,

such as shear strength and modulus and, consequently, changes on the load-carrying capacity of timber elements. Moisture gradients are another important moisture effect which may affect the stress of wood. This effect results of the slow moisture diffusion in wood when *humidity load* is variable or different from initial equilibrium. As previously mentioned, when wood is exposed to variable humidity conditions it absorbs and releases moisture from / to the air. However wood needs long time periods to reach equilibrium for different levels of relative humidity and, depending on timber size, this can take several weeks or even months (Time, 1998). This means that timber structures are affected by climatic variations (fast climatic changes), which do not let wood reach equilibrium. As result, moisture gradients are induced in wood sections and hence internal stresses arise. Moisture gradients induce important differences in shrinkage and swelling of wood, which will develop so-called moisture induced-stresses (MIS), due to constrained volume variations.

Regarding connections, in Europe, self-tapping screws (STS) are the solution most used, essentially because, the results are satisfactory and the system is extremely simple to apply, without the need of predrilled holes. STS are able to combine axial and lateral loads and also allow their withdrawal. STS are positively known as an easy and economical solution and recommended by manufacturers for most joint details. Therefore, the interest in obtaining further knowledge about STS's performance has been growing. The advantages associated to this kind of fasteners allowed an easy implementation in the field of timber construction, but further research is still needed. Actually it is essential to develop an adequate design formula, considering factors related with CLT specificities, such as gaps in unglued cross boards and other sawn grooves (necessary in case of vacuum press production procedure), and other parameters not considered in building codes, such as moisture induced effects or service classes with moisture contents above the fiber saturation point.

So, considering the relation between the two parts of the present thesis, the research question is: How to consider moisture induced effects when a CLT structural system for a multi-story building is being designed?

Figure 1 presents the goals considered in the present thesis and also indicates in which way the different goals are related with each other. Different goals are presented here by numbers, even if it does not mean that goals were reached in such sequence. In fact, most of tasks were being developed simultaneously. Bibliographic research was a permanent action during the development of the work, and as the results of experimental campaigns were obtained while the Urban Timber (UT) system was being developed.

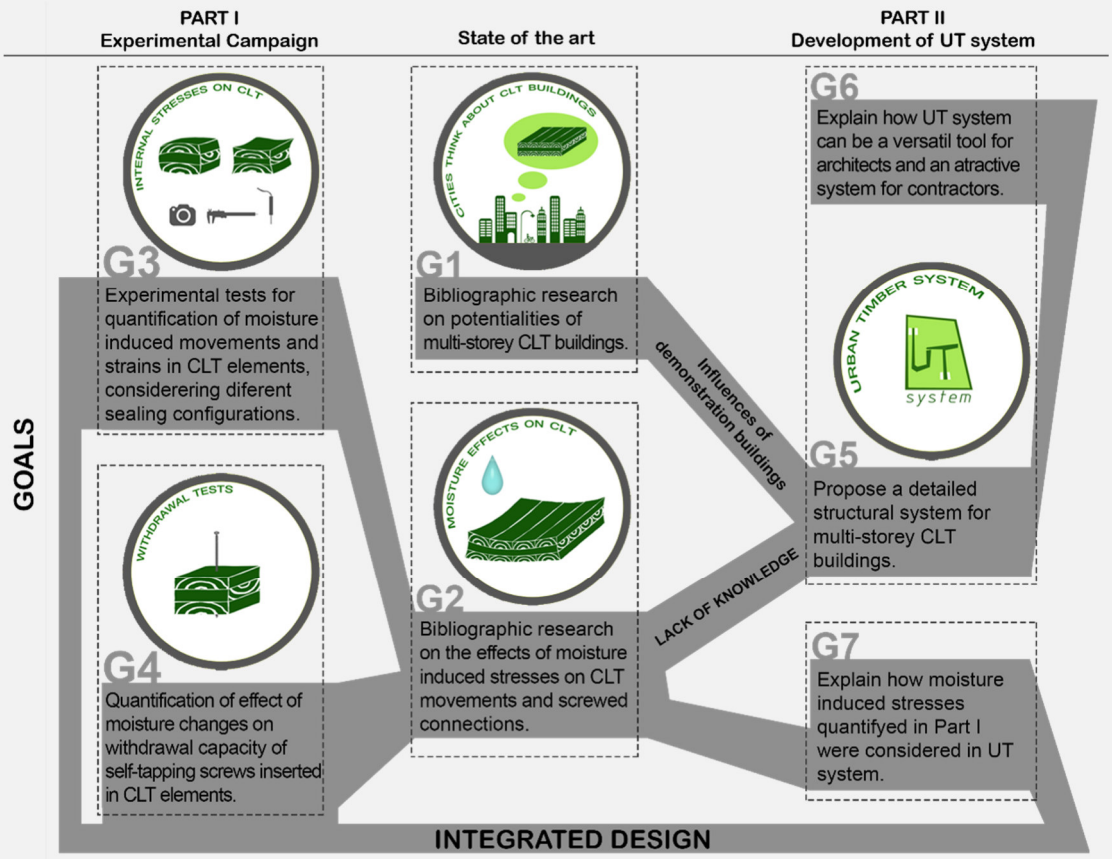

Figure 1. Scheme relating main goals involved in the present thesis.

The first goal (G1) is dedicated to bibliographic research on potentialities of multi-story CLT buildings. Analyzed the available publications, the role of timber in modern cities was presented: the main barriers to multi-story timber construction were identified, solutions were gathered and the sustainable profile of timber construction was discussed. Then, the role of CLT on multi-story timber buildings was defined and main advantages and disadvantages were pointed out. At last, most important demonstration buildings and innovative proposals were described. All these issues are presented in chapter 1 of Part II.

The second goal (G2) emerged from the need to acquire knowledge about the behavior of CLT regarding moisture induced effects and it is presented in chapter 1 of Part I. After a research about all characteristics of CLT as a structural material, it was observed that the information about the behavior of CLT and its connections to moisture change was scarce. So, an in-depth research was performed in this field: hygroscopic behavior of timber was explained in order to introduce all phenomena that occur in timber when it is submitted to moisture change; existing information about the behavior of CLT in particular, regarding moisture changes was collected; the role of connections on timber construction was explained, as well as the significance of withdrawal capacity of self-tapping screws.

The third goal (G3) is discussed in chapter 2 of part I and it is focused on the quantification of moisture induced strains in CLT elements, when it is submitted to Relative Humidity (RH) changes in the environment, considering different sealing conditions: radial, tangential and longitudinal direction. Three different measuring techniques were used, namely: Digital image correlation (DIC), LVDT's and caliper ruler. Test specimens were submitted to RH cycles in which RH varies between 30% and 90% in order to simulate aging effect.

The fourth goal (G4) is dedicated to the quantification of the effect of moisture changes on the withdrawal capacity of self-tapping screws inserted in the main face and side face of CLT elements. Performed tests considered several configurations regarding location and width of gaps. Test specimens were submitted to simple moisture changes as well to cyclic changes. Using the obtained results, the influence of gaps location and width was modelled using a predicting model develop by Uibel and Blaß (2007). Tests that considered simple moisture changes were performed at *Institut für Holzbau und Holztechnologie* - Graz Technical University (Austria) and tests in which STS was inserted in the side face of CLT panels were developed at Civil Engineering Department of University of Minho and at Instituto Politécnico de Bragança (IPB). The experimental campaigns related with the withdrawal capacity of STS's are presented in chapters 3, 4 and 5 of part I.

The fifth goal (G5) and sixth goal (G6) are treated in chapter 2 of part II. G5 is dedicated to the development of a new structural system for multi-story timber buildings, in which CLT is the main structural material. The proposed structural system was called Urban Timber (UT) system and ended up to be a hybrid structural system, once it was concluded that beams should be shaped by Glulam elements, instead of CLT. The structural design of the UT system was made in a partnership with (Dias, 2017), who developed the structural evaluation of the UT system, designing a 3D model in *RFEM-5* software*,* a finite element software by Dlubal. However, the UT system was developed considering not just structural behavior but also architectural issues and adaptive design, production of structural elements, and construction sequence (G6). In the present thesis, the architectural potentialities are presented individually and no demonstration building was developed. Silva (2014) used the potentialities to present a building solution as the main goal of her master thesis. The author resorted to the UT system to propose a solution for a multi-story timber building in which architectural possibilities and adaptive design was explored.

At last, goal 7 (G7) is dedicated to apply the knowledge obtained by the conclusion of part I of present thesis. All the decisions taken related with location of structural elements, design of connections and

development of façade configurations in which moisture induced effects were considered are explained in chapter 3 of Part II. This is where Part I and Part II intercept making this thesis make sense.

PART I : QUANTIFICATION OF MOISTURE INDUCED STRAINS IN CROSS LAMINATED TIMBER AND THEIR EFFECTS ON WITHDRAWAL CAPACITY OF SELF-TAPPING SCREWS

CHAPTER 1 (I)

1 STATE OF THE ART

1.1 Cross laminated timber and moisture changes

1.1.1 Absorption and sorption phenomenon

Softwood is composed by longitudinally oriented tapered cells composed by consecutive cavities called lumens. Tapered cells are connected by pits which allow moisture flow on tangential direction and combined with ray cells which facilitate moisture flow in radial direction (V. R. McClung, 2013). This complex structure is responsible for the characteristic hygroscopic behavior of wood.

Putting it quite simply, wood hygroscopicity means that it is permanently ready to release and absorb water (absorption and desorption phenomenon) when exposed to fluctuating atmospheric humidity. The called sorption isotherms exhibited in Figure (I) 1:1 are the simplest way to explain this phenomenon. The sorption isotherms illustrate the relation between equilibrium moisture content (EMC) and the respective relative humidity (RH) at a constant temperature. Further, they also show the phenomenon of hysteresis, which in the case of wood results in a loop between absorption and desorption isotherms. In other words, the relation between EMC and RH differs when wood is losing or gaining moisture, and as result the curves do not overlap with each other.

When wood presents high moisture content (MC), water is housed in the material in two different ways. There is free water, located in cell lumens, and bound water, located within the cell wall. In a drying situation, the first water to leaves the material is the free water, remaining the bound water. This concept is important because at the point when all free water left the material and all bound water remain, the MC level is called fiber saturation point (FSP). According to Skaar (1988) (cited by (Time, 1998)) this moisture content level is between 26 and 32% moisture content, and depends of the wood species. Referring back to Figure (I) 1:1, it is possible to check that desorption isotherm represents loss of bound water, while absorption isotherm represents gain of bound water.

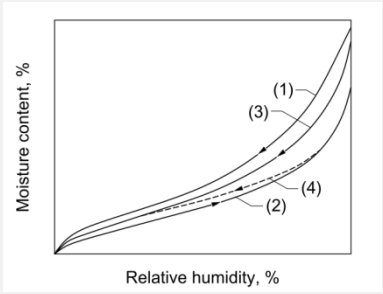

Figure (I) 1:1. Wood schematic sorption isotherms. (1) initial desorption isotherm, (2) absorption isotherm, (3) secondary desorption isotherm and (4) intermediate isotherm/a scanning curve.

1.1.2 Effects of hygroscopic behavior of wood on CLT

1.1.1.1 Swelling and shrinkage

As it is well known, wood shrinks and swells depending on the surrounding environment, which is defined by air temperature and relative humidity (RH). Wood hygroscopic behavior varies between wood species, but it can also vary between solid wood and timber engineering materials built from the same wood species. One example is cross laminated timber (CLT) which with its cross-wise lamination restrict moisture induced movements obtaining reduced rates of shrinkage/swelling in plane directions when compared with solid wood of the same species. Schwab et al. (1997) studied the in-plane dimensional variation of three-layered cross-laminated panels from Norway spruce with a thickness of 20mm and calculated its swelling coefficients[1]: α_x = 0,012...0,020%%[-1] and α_y = 0,034...0,042%%[-1] (percentage change in length per 1% change in MC). Brandner (2013) indicates that the rates for swelling and shrinkage of CLT of Norway spruce (*Picea abies*), with MC kept between 6% and 22% are: 0,02% per each percentage unit of MC added, for both directions in the plane. Bengtsson (2001) performed tests on solid timber of the same species with MC kept between 8% and 20% and obtained the following range values: 0,001...0,035%/% and 0,18...0,46%/% for longitudinal and tangential directions, respectively.

1.1.1.2 Changes on mechanical properties of CLT

Besides the changes on geometry, moisture variations can also lead to changes on wood mechanical properties, such as shear strength and modulus and, consequently, changes on the load-carrying capacity of timber elements. Gülzow et al. (2010) realized a study to understand the impact of changes on moisture content on stiffness parameters of CLT panels. For that, they measured MOE and shear Modulus on all directions of similar specimens with different moisture contents, namely 12 +/-2%, 18.5 +/-1.4%, and 10.6 +/-1.4%. According to Hoffmeyer (1995) (cited by Gülzow et al. (2010)) *the modulus of elasticity (MOE) in grain direction of defect free timber drops by approximately 1.5% if the wood moisture is increased by 1%*, the results obtained by Gülzow et al. (2010) showed that all investigated stiffness parameters decrease at they mean level towards an increase of MC. However, authors emphasized that swelling of the timber grain leads to an apparent increase in the modulus of elasticity for small service loads due to internal component friction. In the other hand, cracking resulted from the reduction of

[1] – α_x grain direction of outer layers; α_y – grain direction of middle layer

moisture content leads directly to a distinct decrease in the bending stiffness perpendicular to the grain direction on the face layers.

1.1.1.3 Moisture gradients

Moisture gradients are an important moisture effect which may affect the stress of wood. This effect results of the slow moisture diffusion in wood when *humidity load* is variable or different from initial equilibrium. As previously mentioned, when wood is exposed to variable humidity conditions it absorbs and desorbs moisture from the air. However, wood needs long time periods to reach equilibrium for different levels of relative humidity, depending on timber size it can take several weeks or even months (Time, 1998). This means that timber structures are affected by climatic variations (fast climatic changes), which do not let wood reach equilibrium. As result, moisture gradients are induced in wood sections and hence internal stresses arise. Moisture gradients induce important differences in shrinkage and swelling of wood, which will develop so-called moisture induced-stresses (MIS), due to constrained swelling or shrinkage strains. Often MIS lead to cracks either in timber surface or in its central part of timber sections, which can affect significantly the safety and serviceability of timber members. One solution to prevent these disadvantages is based on the drastic application of *coatings on the timber surfaces exposed to weather conditions in order to keep the moisture exchange with the environment and thus moisture induced stresses low* (Angst & Malo, 2012b). Some researchers have been proving by measurements and experimental work that MIS can exceed tensile strength of timber, in particular, in the case of glulam cross-sections, perpendicular to the grain (J. Jönsson, 2004) (Angst & Malo, 2012a).

Güzlow et al. (2011) points out the importance to study the consequences of changes in moisture content caused by changes in the environmental conditions surrounding the CLT panels. They refer the importance of all individual wood layers to contain the same moisture content within the hygroscopic range, otherwise residual stresses will develop between adjacent layers as each layer independently shrinks or expands depending on the environmental situation. This phenomenon can significantly weaken the bond strength and can lead to excessive cracking of the CLT.

Ignoring these recent evidences, actual design standards do not consider effects of MIS accurately, fact that may lead to unforeseen failures. Regarding timber construction, Eurocode 5 (EN 1995-1-1, 2004) classify the stresses and strains derived from humidity changes as material properties. However, as defended by Svensson et al. (2011), humidity influence on timber structures should be classified as an

action, similarly to the influence of temperature in steel. This topic is relatively new and few publications are available.

Fragiacomo et al. (2011) developed a diffusion analysis using FE model and a three-dimensional Fickian equation to modeling moisture transfer. The main goal was to evaluate *moisture-induced stresses perpendicular to grain in cross-sections of timber members exposed to different climates*. Authors subjected three different cross sections of three different timber materials (sawn timber, glulam and CLT) to the 10-year relative humidity histories of thirteen different climatic regions. The main parameters evaluated were the initial moisture content, type of exposure, size of the timber member and the presence of protective coating. In the case of CLT, it should be referred that the different directions of different layers were not considered. Their main findings emphasize that the climates which present larger yearly variations of RH induce higher stresses in timber cross sections; in some simulations were found induced stresses perpendicular to the grain that exceeds the tensile and compressive strength perpendicular to the grain of timber warning about the possibility of cracking and the protective coating has proven to be an effective solution on reduction of moisture variations.

This kind of work is of extreme importance regarding the development of knowledge in the field of timber construction. For that, the knowledge developed by wood science society is of great utility, but to substantiate adequately this kind of models it is of great importance develop experimental tests. There is some published work which is focused on the experimental evaluation and numerical analyses of effects of moisture induced stresses on glulam (J. Jönsson, 2004), (Angst & Malo, 2012a) and on CLT (Gereke, 2009). Some other studies have been developed as an attempt to quantify the loading action of Moisture gradients (MG) on glulam elements, either on bending (Ranta-Maunus, 2001) or on tensile strength perpendicular to the grain (J. Jönsson & Thelandersson, 2003), concluding that MG is a predictable action. Sjödin & Johansson (2003) tested the influence of initial MIS on glulam multiple steel-to-timber dowel joints. Authors verified that the highest decreases of load bearing capacity were linked to connection configurations which restrained the shrinkage deformations.

Jönsson (2004) performed an experimental research in which he determined moisture induced effects perpendicular to the grain in glulam after subject the specimens to moisture variations. The released strains were determined by measuring the distance between two points, through digital image correlation (DIC) technique, before and after cutting the specimens as shown in Figure (I) 1:2. The mean strain and mean stress were calculated as present in equation (1:1) and equation (1:2), respectively. But, as explained by authors, the moisture distribution is not uniform along the slice, so as the measurements

were only based in two points it should be included an end effect to obtain the maximum stress ($\sigma_{max} = 1.30\sigma_{mean}$).

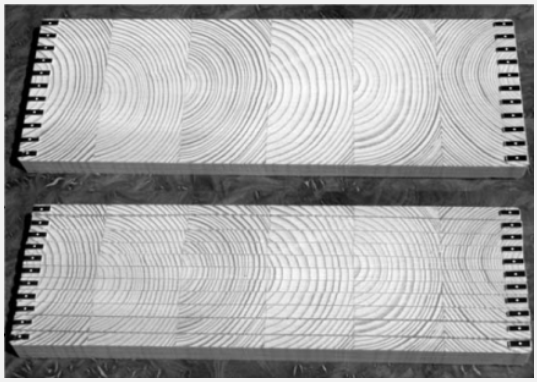

Figure (I) 1:2. Test specimen, before and after sawing into eleven slices (J. Jönsson, 2004).

$$\varepsilon_{mean} = \frac{\Delta l}{l} = \frac{L_2 - L_1}{L_1} \quad (1:1)$$

$$\sigma_{mean} = \varepsilon_{mean} \cdot E(u) \quad (1:2)$$

ε_{mean}	Mean Strain
L_1	Distance between two measure points before cutting specimen into slices
L_2	Distance between two measure points after cutting specimen into slices
σ_{mean}	Mean stress (MPa)
$E(u)$	Modulus of Elasticity as a function of moisture content

Different groups of specimens were divided and subjected to different actions: seasoned in constant humidity, subjected to a single climate change, exposed to cyclic climate change, and exposed to natural outdoors under shelter. Sub-groups of each group were tested in different times during climatic exposure (see Table (I) 1:1). The results showed that even without RH changes it was found maximum tension and compressions stresses in the order of 0,2 MPa. For the specimens with moisture induced gradient the tensile stresses were two times higher (sometimes higher than characteristic tensile strength perpendicular to the grain), and compressive were three times higher. The cycle exposure did not present any cumulative effect.

In a posterior study, Jönsson and Thelandersson (2003) realized an analysis of the *effect of moisture gradients on tensile strength perpendicular to the grain in glulam*, using the same experimental program. The study was based on the combination between initial moisture induced stresses and stresses from external loading during tension tests. Their main conclusions indicate that specimens subjected to a drying process present a marginal reduction of tension capacity, because moisture induces compression stresses, while specimens subjected to a swelling process present a significant reduction of tension

capacity since moisture gradients induce tension stresses. Similarly to previous investigation performed by J. Jönsson (2004), cyclic exposures did not present significant differences in comparison with single climate changes.

Table (I) 1:1. Relative humidity changes used on experimental program performed by Jönsson (2004).

GROUP	RH [%]	CLIMATE EXPOSURE	TOTAL NUMBER OF SPECIMENS	NUMBER OF SPECIMENS TESTED	DAYS OF TESTING
A	40% 80%	40% 80%	14 14	– –	– –
B	40% 80%	80% 40%	14 14	2 2	1,3,5,6,11,24,38 1,3,5,6,11,24,38
C	60%	Cyclic: 40% and 80% (seven days interval)	30	2	3,5,10,17,24,31,38,45,52,59,66,73,80,87,94,101
D	60%	Natural climate	52	2	0,3,11,20,33,42,62,69,76,90,104,118,132,146,161,175,188,203,221,230,244,258,272,287,304,317

Angst and Malo (2012b) also developed an experimental work with glulam which provided important data to understand the effect of climate variations on timber cross section. Their main goal was to extend the basis for a numerical model. For that, based on Jönsson (2004), they quantified moisture induced strains (restrained and released and moisture induced stresses perpendicular to the grain direction for glulam specimens subjected to an single climate changes (Table (I) 1:2).

Angst and Malo (2012a) developed another study in this field in order to understand the effect of moisture induced stresses on the behavior of self-tapping screws used as reinforcement elements in glulam structures. The climatic conditions and swelling/drying procedures used were the same described at (Angst & Malo, 2012a). *After first seasoning, a self-tapping screw was inserted in the center of each glulam specimen. The RH levels were selected to represent typical conditions for sheltered, unheated structures in Nordic countries. The application of single instead cyclic climate changes was selected, because annual changes in RH are more significant than daily changes* (Angst & Malo, 2012b). Combining experimental and numerical results they could conclude that screw reinforcement can lead to a reduction of between 30-70% of tensile stresses perpendicular to the grain located in the center of a glulam cross section.

Table (I) 1:2. Test program developed by Angst and Malo (2012b).

TEST SERIES (MEASUREMENTS)	SEASONED IN RH	EXPOSED TO RH	TOTAL NUMBER OF SPECIMENS	PARALLEL SPECIMENS	DAYS OF WETTING/DRYING UNTIL TESTING
MOISTURE INDUCED STRAINS AND MOISTURE CONTENT	50%	90%	20	5	5,12,21,38
	90%	50%	20	5	5,12,21,38
MODULUS OF ELASTICITY	50%	90%	12	3	5,12,21,38
	90%	50%	12	3	5,12,21,38
HYDRO EXPANSION COEFFICIENT	50%	90%	3	3	At increasing time intervals (hours to days)
	90%	50%	3	3	At increasing time intervals (hours to days)

Relatively to studies focused on effects of moisture induced stresses on CLT, the sources are scarce. Some work in this field was developed by Gereke (2009), who measured linear swelling in three direction of a CLT panel (Figure (I) 1:3), between relative humidifies of 35% and 85%. Considering the same RH range, Gereke (2009) also realized comparative measurements of internal stresses of CLT specimens with three layers, in which the material of middle layer varies. The measurements were made manually by means of a linear gage, which can lead with significant inaccuracy. Author concluded that the free swelling and shrinkage of adjacent layers differs by a factor of 10 (radial/longitudinal) to 20 (tangential/longitudinal) resulting in serious structural damages and shape distortions which may reduce the material serviceability. Often MIS exceeds the tensile strength of timber perpendicular to the grain, leading to cracks (either on the surface of timber or in the central part of timber sections), shape distortions and reduction of load bearing capacity (by splitting failure).

The present thesis presents an experimental work performed with three layered CLT panels with the same objectives of the described work, but presenting some new parameters, such as: the digital image correlation (DIC), which will be adequately described ahead in the text and the conditioning of moisture flow by means of insulation of different layers.

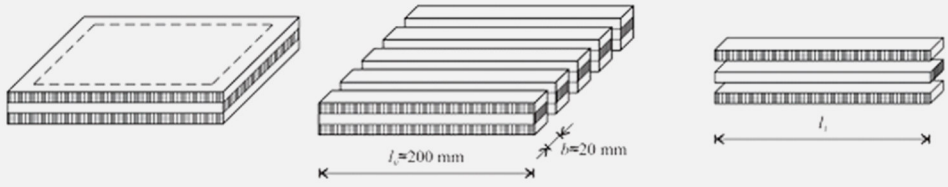

(a) (b) (c)

Figure (I) 1:3. Procedure to determine the internal stress state of laminated wood panels: (a) removal of the edges, (b) cutting into strips, (c) release of strain by sawing in the glue lines (Gereke, 2009).

1.2 CLT connections

1.2.1 The role of connections on timber construction

In a general way, connections are key points for all kinds of timber structure. This statement of timber structures stands for CLT, being the connections essential elements to guarantee the integrity of the structure and to provide strength, stiffness, stability and ductility. For example, the structural efficiency of the floor acting as a diaphragm and the walls resisting to lateral loads in a CLT structures are dependent on fastening connection details.

The efficient design and fabrication of connections often determines the level of success of timber buildings. This is an issue that has to be carefully studied in the field of multi-storey heavy timber structures, either for buildings entirely made of timber or buildings composed by hybrid structures. To get an idea, according to Wells (2011), in the case of a connection between walls and floor subjected to high loads, generally pointed out as a weak link in a CLT structure, a connection made of screws or nail arrays is crucial to ensure safety.

One important advantage of the CLT structures is the high accuracy guarantee by the computer numerical control (CNC) technology, which allows sophisticated connection systems. Moreover, the good dimensional stability recognized to CLT helps to ensure an accurate execution of connection. CLT systems accept different kinds of fasteners that are required for different functions. There are fasteners to connect different CLT elements in different contexts (roof/wall, wall/floor, and inter-storey connections – see Figure (I) 1:4) and there are fasteners suitable to connect CLT to other wood-based materials or to steel or concrete.

Self-tapping screws are the solution typically recommended by manufacturers and are essentially used to connect panels to panels in floors and floor to walls. Other efficient solutions to connect panel elements are: wood screws rivets, bolts and dowels. When high loads are involved connections resort to split rings, shear plates and tooth plates. Some innovative glued-in rods connection systems have been emerged associated to high degree of prefabrication of CLT, examples are: Geka connectors and KNAPP© (FPInnovations2, 2011).

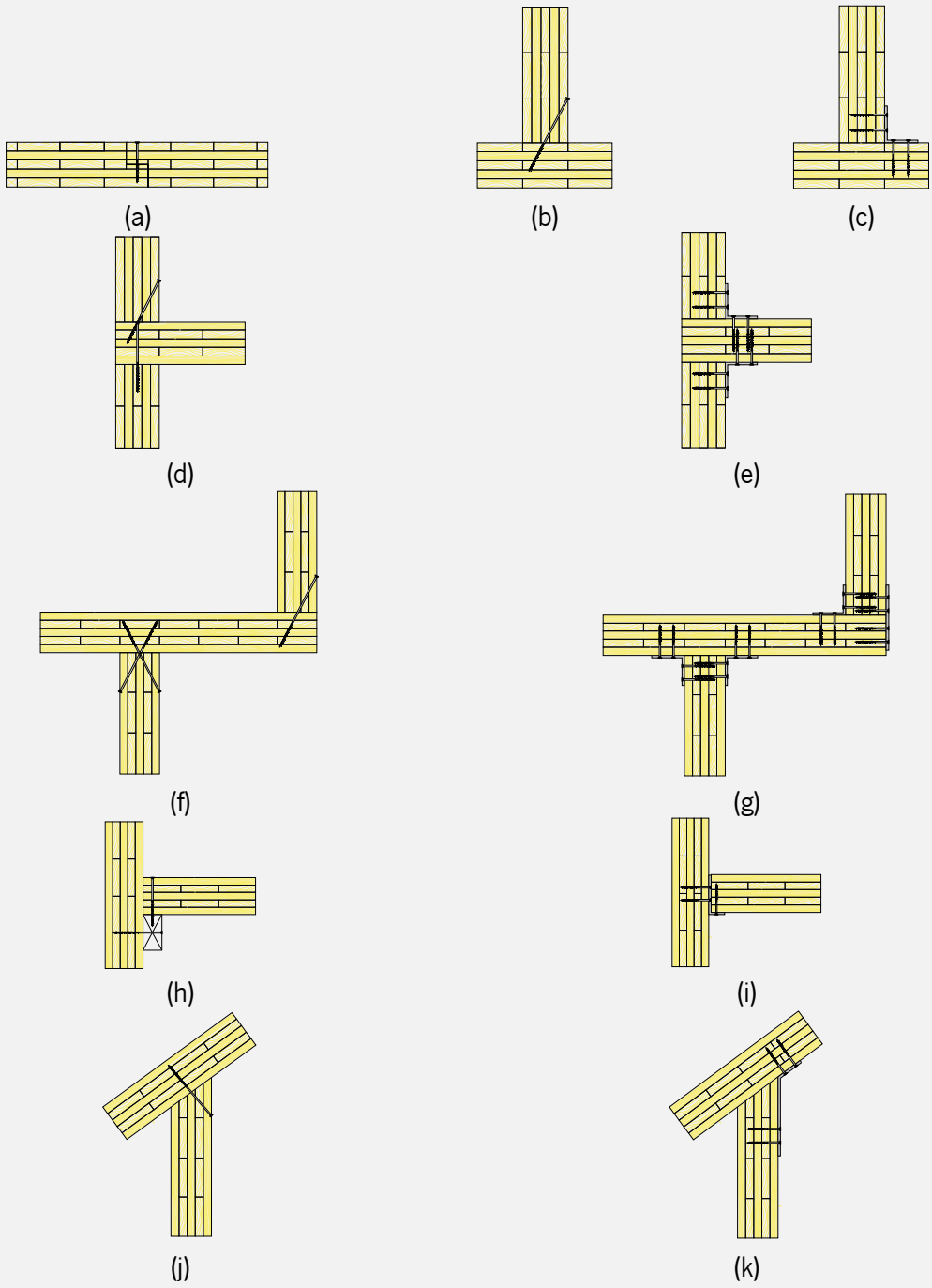

Figure (I) 1:4. Examples of connection between CLT elements. (a) connection between floor panels with self-tapping screws, (b) connection between wall panels with self-tapping screws, (c) connection between wall panels with screws and steel plates, (d) connection between floor and walls elements with self-tapping screws in a platform construction system, (e) connection between floor and walls elements with screws and steel plates in a platform construction system, (f) connection used to assemble balconies with self-tapping screws, (g) connection used to assemble balconies with screws and steel plates, (h) connection between floor and walls elements with self-tapping screws in a balloon construction system, (i) connection between floor and walls elements with screws and steel plates in a balloon construction system, (j) connection between roof and wall elements with self-tapping screws, (k) connection between roof and wall elements with screws and steel plates.

In Europe self-tapping screws (STS) are the solution most required, essentially because the results are satisfactory and the system is extremely simple dismissing predrilled holes. They are able to combine axial and lateral loads and also allow its withdrawal. In a general way, the application of inclined screws in timber-to-timber connections, arranged under an angle of 45° between screw axis and member axis, have a higher load-carrying capacity compared to common shear connections due to the high withdrawal capacity of the self-tapping screws. Further, the additional use of steel plates with special holes, incorporating the geometry of the screw head, leads to a further increase in load-carrying capacity and stiffness. The ultimate load of these joints is mainly limited by the withdrawal capacity, the tensile capacity of the screw and the friction between the steel plate and the timber member (Krenn & Schickhofer, 2009).

1.2.2 Self-tapping screws and withdrawal resistance

Despite the large variety of fasteners and types of connections compatible with CLT construction, nowadays STSs are widely used. They are positively known as an easy and economical solution and recommended by manufacturers for most joint details. Therefore, the interest in obtaining further knowledge about STSs performance has been growing.

The advantages associated to this kind of fasteners allowed an easy implementation in the field of timber construction, but further research is still needed. Actually it is essential to develop an adequate design formula, considering factors related with CLT specificities, such as gaps in unglued cross boards and other sawn grooves (necessary in case of vacuum press procedure), and some other parameters not considered in building codes procedures, such as moisture induced effects or service classes with moisture contents above the fiber saturation point. Further, there is the question related to the angle between the screw and the grain direction.

When compared with standard screws, STS present some important advantages, such as: (i) the special shape of the thread region allows a high load transmission into the surrounding wood; (ii) generally, they are hardened after rolling the thread, increasing the yield moment, the torsional strength and the steel tensile capacity; (iii) the stiffness of the connection increases while the danger of "slipping" decreases (Frese & Blaß, 2009). Furthermore, STS are characterized by a high load-carrying capacity when axially stressed, essentially due to the combination of two characteristics: (i) the long thread lengths and (ii) the hardened steel with tensile strengths up to 1200N/mm^2 (A Ringhofer et al., 2015).

The characteristic withdrawal resistance of a fastened timber connection is an essential parameter to be considered, especially if the screws are inserted at an angle (α) to the timber grain. In this case, the

load-carrying capacity of screws loaded in withdrawal becomes more important than the load-carrying capacity of screws loaded perpendicular to their axis. Eurocode 5 (EN 1995-1-1, 2004) specifies the methodology to determine characteristic withdrawal resistance ($f_{ax,k}$) for the composite model "timber-screw", which is based on a relation between screw penetration depth (l_{ef}), screw nominal diameter (d), timber characteristic density (ρ_k) and the angle between the screw and grain direction (α) (see equation (1:3).

In recent years, several studies have been performed aiming to improve this standardized proposal, considering advances on screws technology and timber products as well as introducing new parameters to the equation. Recent publications are focused on the study of the slenderness of screws (Ellingsbø & Malo, 2012), the angle between screws and grain direction (Bejtka & Blaß, 2002) (Krenn & Schickhofer, 2009) (Grabner, 2013), the moisture content (Andreas Ringhofer et al., 2014) (Abukari et al., 2012) (A Ringhofer et al., 2015) and temperature (Pirnbacher et al., 2009).

Considering the specific case of CLT, some important researches were developed looking for a withdrawal equation that considers CLT specificities. Uibel & Blaß (2007) performed an extensive test program to analyze withdrawal resistance of self-tapping screws inserted, either in plane side or in narrow side, in CLT plates. As a result, they suggest a withdrawal equation which combines the following parameters: nominal or outer diameter (d) of the screw, effective pointside penetration length (l_{ef}), angle (α) between screw axis and grain direction and CLT density (ρ) (see equation (1:4)). In the present study, this prediction equation is adjusted in order to include new variables related with the changes in MC and the existence of gaps.

Muñoz et al. (2010) developed an experimental study in which the withdrawal resistance of a CLT wall-to-floor connection using self-tapping screws, was tested. Test results were compared using various withdrawal equations concluding that most equations tend to over-estimate the withdrawal resistance, which leads to the need of revising the proposed equations, especially those proposed by design standards. The comparison used the equations proposed by Canadian and European standards (CSA O86-09 (Canadian Standard Association) (equation (1:5) and equation(1:6)), Eurocode 5 (equation (1:3)), the model proposed by Uibel & Blaß (2007) (equation (1:4)) and the equation proposed by the screws manufacturer *Würth* (equation (1:7)).

Ringhofer et al. (2014) collected, from different sources, data related with the effect of changes in MC on withdrawal resistance of STS inserted either in solid timber, CLT and Glulam (GL). Authors used data

collected to develop a simple bilinear model approach for a MC range between 8% and 20% (equation (1:8)). The same bi-linear model is applied in the present paper adding new variables: the number and width of gaps. Aware about the differences between solid timber and laminated timber products, Ringhofer et al. (2015) developed a stochastic model, verified by laboratorial test results, in which they treat withdrawal resistance as dependent on the density and on the number of layers penetrated by the screw.

$$f_{ax,k} = 0.52 \cdot d^{-0.5} \cdot l_{ef}^{-0.1} \cdot \rho_k^{0.8} \quad (1:3)$$

$f_{ax,k}$ Withdrawal resistance of self-tapping screws in CLT, in N;
d Thread diameter in mm;
l_{ef} Effective penetration length of the threaded part (mm);
ρ_k Characteristic density, in kg/m³.

$$R_{ax,s,pred} = \frac{0.44 \cdot d^{0.8} \cdot l_{ef}^{0.9} \cdot \rho^{0.75}}{1.25 \cdot cos^2\varepsilon + sin^2\varepsilon} \quad (1:4)$$

$R_{ax,s,pred}$ Predicted values for withdrawal resistance of self-tapping screws in CLT, in N;
d Nominal or outer diameter of the screw, in mm;
l_{ef} Effective pointside penetration length, in mm;
ρ For joints in the plane side of CLT: density of CLT (whole cross section), in kg/m³;
For edge joints in CLT: density of the relevant layer(s), in kg/m³;
ε Angle between screw axis and grain direction.

CSA O86-09 – Withdrawal resistance for wood screws (clause 10.11.5.2)

$$Y_w = 68 \cdot d^{0.82} \cdot G^{1.77} \cdot L_{pt} \cdot 1.25, \text{ in N} \quad (1:5)$$

d Screw diameter, in mm;
G Mean relative density of main member;
L_{pt} Threaded length penetration in the main member, in mm.

CSA O86-09 – Withdrawal resistance for lag screws (clause10.6.5 – table 10.6.5.1)

$$Y_w = a \cdot L_{pt} \cdot 1.25, \text{ in N} \quad (1:6)$$

d Screw diameter, in mm;
a Tabulated value for the withdrawal resistance of lag screws, in kN/mm;
L_{pt} Threaded length penetration in the main member, in mm.

Würth – Stress in the screw shaft direction (clause 3.3.2)

$$R_{ax,k} = 10 \cdot l_{ef} \cdot d, \; in \; N \quad (1:7)$$

d Screw diameter, in mm;
l_{ef} Point-side penetration length of the threaded part minus one screw diameter, in mm.

$$\eta_u = \begin{cases} 1.00 \\ 1.00 - k_{mc} \cdot (u[\%] - 12) \end{cases} for \begin{cases} 8\% \leq mc \leq 12\% \\ 12\% \leq mc \leq 20\% \end{cases} \quad (1:8)$$

For solid timber, k_{mc} is 0.031 or 0.036, when α is 90° and 0°, respectively.

1.3 Digital image correlation - DIC

1.3.1 Fundamentals

During last decade, contact free measurement techniques, such as two-dimensional digital image correlation (2D DIC), are raising fans in the field of experimental solid mechanics. Its success is essentially related with few attractive advantages: first, the simplicity of test setup that requires just a fixed camera, a white light or natural light source and a computer program to process the images; second, test specimens just need to receive a black and white surface painting with a random gray intensity distribution, which is typically obtained by aerosol spray or airbrush painting; third, 2D DIC method is compatible with most of digital image acquisition devices; and fourth, this technique provides full-field measurements for displacements and strains. However, such a simple method also entails some disadvantages: first, the 2D DIC method are totally dependent on the quality of imaging system; and second, the accuracy of strain measurements is lower than the interferometric techniques (Pan et al., 2009). The great argument to fight this fact is that DIC has the ability to perform measurements over an entire region of interest (ROI). It provides full-field displacements and strains by comparing a set, with a minimum of two images, acquired in different test stages.

The first step for images computation is defining ROI at initial (reference) image, which is divided into evenly spaced virtual grids (facets). Motion registered between images acquired before and after deformation is measured by tracking the same points (or pixels) between images. However, to compute properly the displacements, each point of interest is centered at a square reference facet, which will be used to track the location of same point. The unique pattern of each facet will ensure that each point is accurately located once its neighborhood is also verified. The facet should be large enough to distinguish itself from the other facets and allow enough strain precision, however if it is too big, the spatial resolution of the data field is reduced (Crammond et al., 2013). According to (Pan et al., 2008b) and (Lecompte et al., 2006), there is a trade-off between using large and small facet sizes: facet size must be properly selected according to random intensity distributions of speckled patterns.

To identify reference and deformed facets as being the same a displacement mapping function has to be chosen. The most commonly used are first and second-order shape functions once both consider the expected shape change of reference facet instead of simple rigid body translations. Then, a correlation criterion must be chosen and solved with regard to the desired deformation vector (p) using a proper algorithm to optimize correlation coefficient (e.g. Newton- Raphson or Levenberg-Marquardt methods).

According to literature (Pan et al., 2009) (Pan & Li, 2011), the zero normalized sum of squared differences (ZNSSD) is the correlation criterion that offers the most robust noise-proof performance and is insensitive to the offset and linear scale in illumination lighting (Equation ((1:9)).

In summary, the accuracy of displacement measurements performed by DIC can be influenced by several variables: sub-pixel optimization algorithm, subset shape function, subset interpolation scheme, image noise as well as camera lens distortion (Pan et al., 2008a).

$$C_{ZNSSD}(p) = \sum_{\Omega}[\frac{f(x_i, y_i) - f_m}{\sqrt{\sum_{\Omega}[f(x_i\ , y_i\ ) - f_m]^2}} - \frac{g(x'_i, y'_i) - g_m}{\sqrt{\sum_{\Omega}[g(x'_i, y'_i) - g_m]^2}} \quad (1:9)$$

where, Ω is the facet domain, $f(x_i, y_i)$ is the pixel gray level at location (x_i, y_i) in the reference image, $g(x'_i, y'_i)$ is the pixel gray level at location (x'_i, y'_i) in the deformed image, and f_m is the mean gray level value over the subset in the reference image, and g_m is the mean gray level value over the facet in the deformed image.

In the case of timber research, this technique has been used to perform measurements on material exposed to humidity changes in order to quantify shrinkage or swelling coefficients (Angst & Malo, 2012b) (Girma Kifetew et al., 1997) (Grima Kifetew, 1996) and moisture induced stresses (Angst & Malo, 2012a) (Gereke, 2009) (J. Jönsson, 2004) (Johan Jönsson & Svensson, 2004). Other studies focus on the behavior of timber connections or on the development of timber cracking for elements submitted to mechanical actions.

CHAPTER 2 (I)

2 QUANTIFICATION OF MOISTURE INDUCED STRAINS IN CROSS LAMINATED TIMBER

2.1 Variables and techniques involved

The main goal of the present experimental campaign was the measurement of strains and calculation of consequent stresses induced in CLT panels by cyclic moisture changes. Strains were measured both in the surface of the main face of CLT panels and in the lateral face of panels. The measurements performed in the main face of panels registered the timber movements for longitudinal (X) and tangential (Y) directions separately, while the measurements performed in the lateral face of panels registered the timber movements on radial direction (Z) (see Figure (I) 2:1). Additionally, measurements made in lateral face of panels registered the movements of timber on radial (Z) and tangential (Y) directions, considering the behavior of different layers separately.

Measurements of timber movements were performed by means of three different techniques (see Figure (I) 2:2): Digital Image Correlation (DIC); LVDTs; and caliper ruler. DIC technique is an optical, contact free and full-field measurement technique which can be valuable to better understand the effects of cyclic humidity changes on amplitude and distribution of strains on CLT surfaces. Acquisition of images was performed at different moments in order to register the movements on material surface during the defined periods. LVDTs were selected in order to register continuously the timber movements during the relative humidity (RH) cycles. At last, the caliper ruler was used to get measurements that could not be taken by the other two techniques used.

This experimental campaign was performed considering two distinct parameters: the RH cycle (test I) and the direction of free moisture flow (test II). Regarding test I, the effect of extreme environmental conditions was evaluated, concerning relative humidity (RH) changes, by means of compressive and tensile strains observed at CLT specimens. Besides, the effects from repeated RH cyclic changes on measured strains was also verified. So, damages caused in CLT and possible modifications on timber fibers in the course of the conditioning period were analyzed. For that purpose, CLT specimens were conditioned in climatic chambers (Fitoclima 1000EC45 and Fitoclima 28000 (see Figure (I) 2:3)) for a period of 324 days and submitted to an humidity cycle that varied between 30% and 90%, for periods of around 21 days, while temperature remained constant (20°C) (see Figure (I) 2:4). The RH cycle ends with a period in which the RH remains constant at 65% for a period 142 days to ensure standard conditioning conditions and stabilization. Dots shown in Figure (I) 2:4 mark the moments of testing, which were selected in order to understand the differences between compressive and tensile stresses obtained at the beginning and at the end of RH cycle. Each testing moment considers either DIC and caliper ruler measurements.

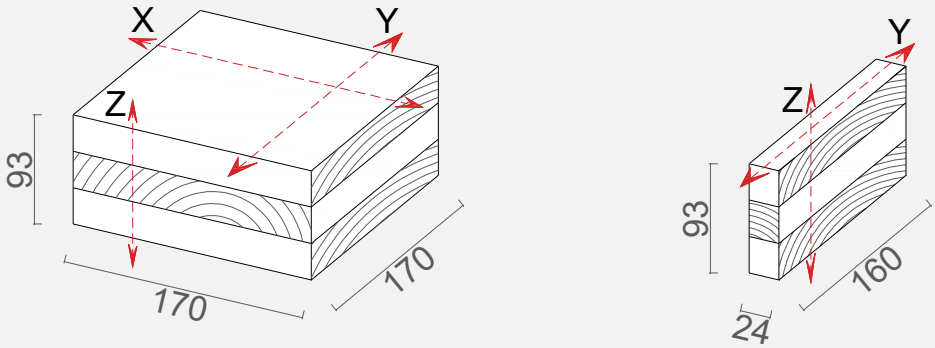

Figure (I) 2:1. Different directions used to perform measurements on CLT specimens and adopted dimensions (in mm).

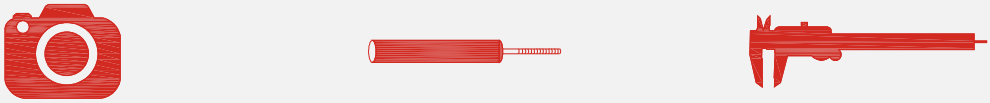

DIC LVDTs Caliper ruler

Figure (I) 2:2. Different measurement techniques used to obtain strains on CLT specimens.

Figure (I) 2:3. Fitoclima 1000EC45.

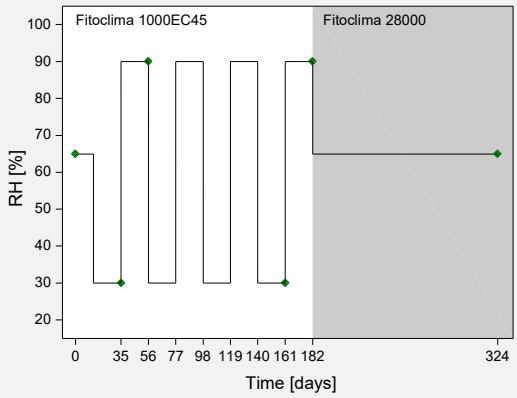

Figure (I) 2:4. Humidity cycle performed by two climatic chambers.

Concerning test II, the goal was to understand the relation between the direction of moisture flow and the strains and stresses obtained. This relation was important to study because, considering cross wise lamination of CLT, the restriction of moisture flow in specific directions could result on a different behavior towards its hygroscopic behavior when compare with CLT panels with free moisture flow.

Test configurations were designed considering both parameters described below. This way, two groups of specimens, A and B, were defined considering different geometries: group A is composed by small CLT panels with dimensions of 170x170x93 mm and group B is composed by CLT slices with dimensions of 160x93x24 mm (Figure (I) 2:1). These last has a shorter length because extremities of specimens had to be regularized in order to obtain a straight surface to perform measurements. Specimens of group A

were used to obtain restrained strains (ε_{rest}) on three different directions X, Y (F1) and Z (F2 and F3) and released strains (ε_{rel}) on Y direction of panel surface (F1). The faces are clearly shown below. Specimens of group B were used to get released and restrained strains for different CLT layers (Y direction). Each group of specimens is composed by 4 different configurations which are similar for group A and B: configuration 1 (C1) allows a free moisture flow through all three timber directions; configuration 2 (C2) allows moisture flow only in tangential direction; configuration 3 (C3) allows moisture flow only in longitudinal direction; and configuration 4 (C4) allows moisture flow only in radial direction.

2.2 Production and preparation of tests specimens and sampling

Preparation of test specimens in which the DIC technique was applied followed six main steps: firstly, CLT was produced; secondly, specimens were cut with defined dimensions; thirdly, timber directions were sealed; fourthly, specimens were painted with a random pattern; fifthly, specimens were photographed; and sixthly, specimens were conditioned in climatic chamber.

The production of CLT was carried out at *Rusticasa®* and adapted to the facilities of the factory. So, it was impossible to completely avoid knots and to control the density distribution. CLT was produced in the shape of three layered big beams (4200x170x102 mm), laminated with adhesive 1247 from *AkzoNobel* and pressed by a hydraulic pressing device with a pressure of 1 N/mm^2 for a period of 2,5 hours. The timber used for CLT production was Spruce C24, with a density range between 410kg/m^3 and 513kg/m^3 (CoV=0,05 and mean=460kg/m^3) and a moisture range between 16,5% and 20,2% (CoV=0,08 and mean=18,4%). Despite the high moisture content at production time, specimens were subsequently conditioned until a moisture content of around 14% be reached.

Once stabilized, specimens with configurations C2, C3 and C4 were carefully sealed by means of an elastic membrane *Dakorub* by Soudal®, in such a way that only one direction allows the free flow of moisture (Figure (I) 2:5). The next step was to prepare the surfaces of specimens in which the DIC technique would be applied. So, these surfaces were painted with a speckled pattern by means of black and white aerosol painting. This painting was carefully made in order to obtain a random pattern of black dots on a white background. This way, the camera obtains high quality image information.

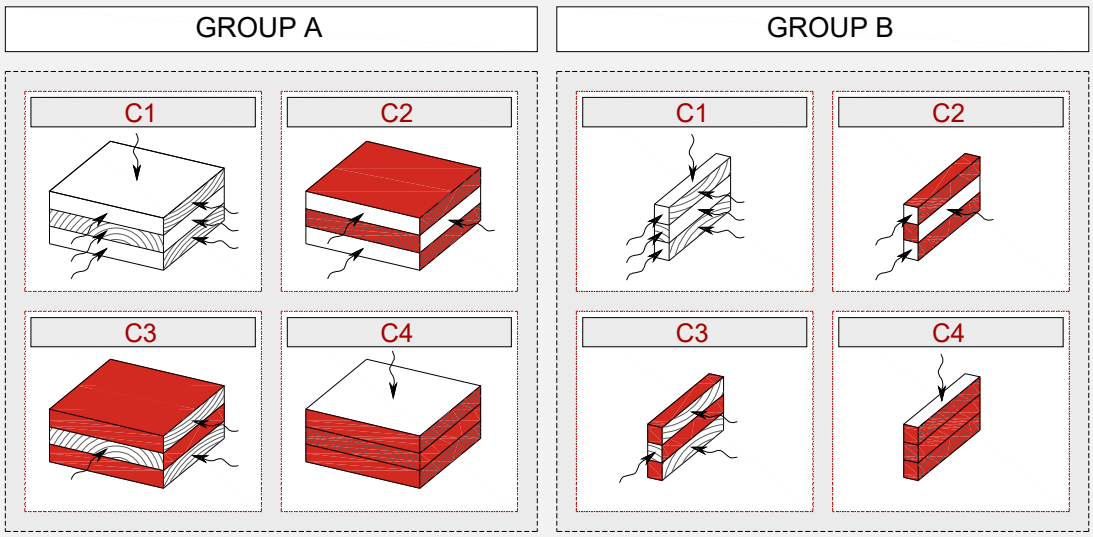

Figure (I) 2:5. Different specimen configurations for both groups of specimens A and B and respective dimensions and directions for measurements. **C1 -** Three directions allow free moisture flow; **C2 -** Only tangential direction allow free moisture flow; **C3 -** Only longitudinal direction allow free moisture flow; **C4 -** Only radial direction allow free moisture flow.

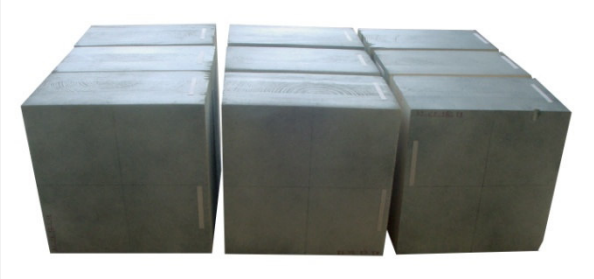

Figure (I) 2:6. Painted specimen of group A.

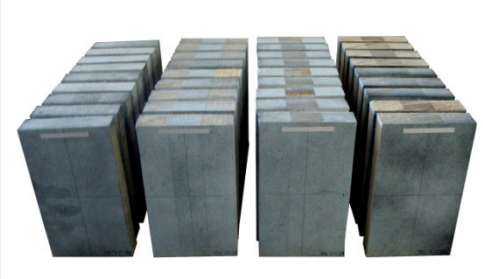

Figure (I) 2:7. Painted specimen of group B.

Specimens of group A, depicted in Figure (I) 2:6, were painted in three faces, in order to obtain general information about the shrinkage/swelling of CLT panels. On these faces two axes were drawn, dividing the faces in 4 similar parts. These axes will be of great help at the time of positioning specimens for the camera. Specimens of group B, shown in Figure (I) 2:7, were painted only in its main face in which the same two axes were also drawn.

Per each configuration, either for group A or B, 10 specimens were prepared. Configuration 1 was an exception, being prepared 14 specimens. Two of these extra specimens were used to perform the tests with LVDTs, while the other two were used to measure released strains at day 0 in order to quantify the effect of high moisture content at production time. Figure (I) 2:8 summarizes the entire experimental campaign and shows that, at each test moment, two similar specimens were tested.

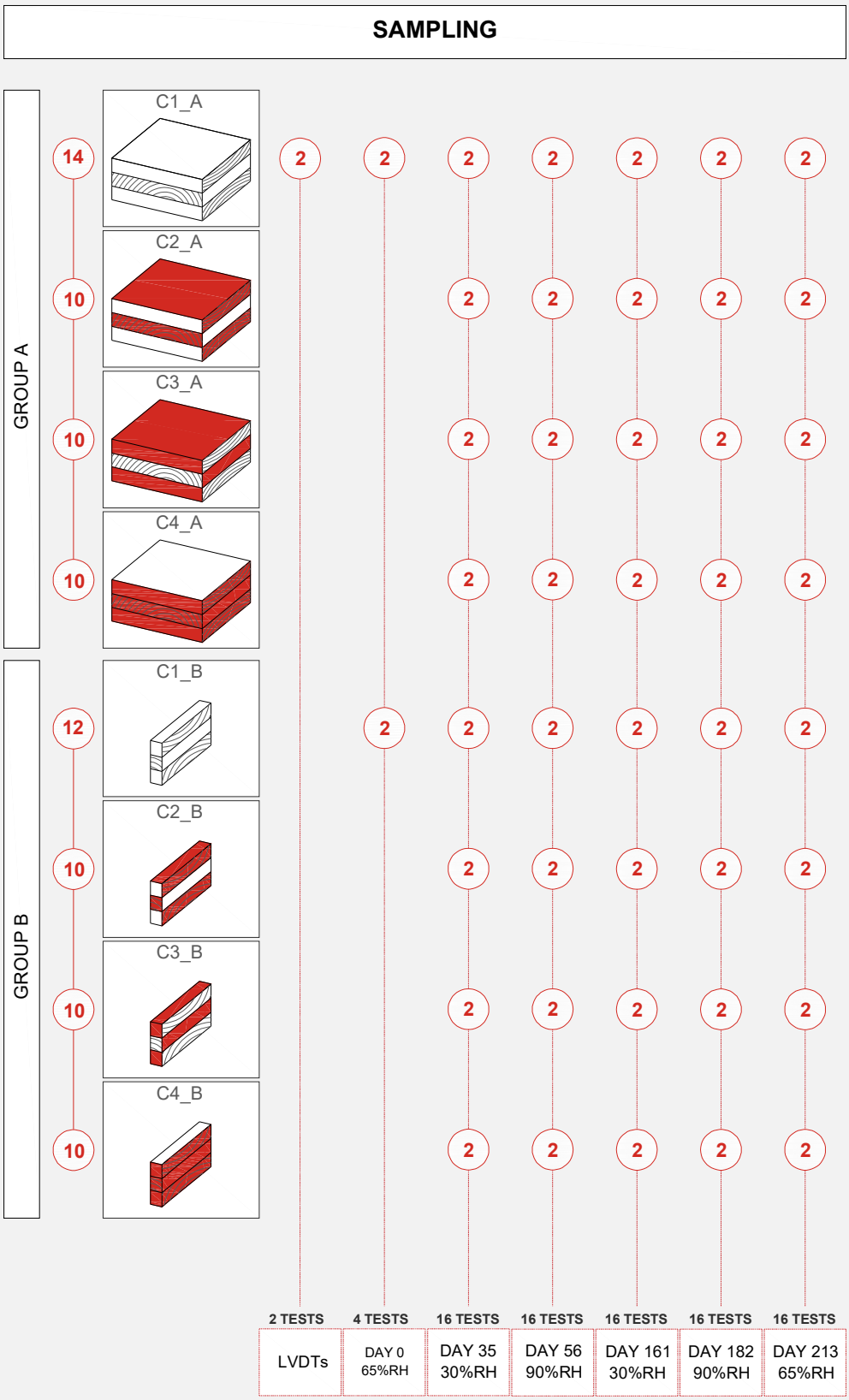

Figure (I) 2:8. Test campaign for group A and group B.

2.3 Test setup and test procedure

2.3.1 DIC technique

The test setup used for measurements performed with DIC technique was one of the main concerns of this experimental campaign. As required by the technique, it was mandatory to ensure that the object is planar, parallel to the camera and keeps a constant distance from the camera for all test moments. However, as the camera and specimen had to be placed at test setup every time image capture was required, it was not simple to guarantee that the relation between both was always the same. Figure (I) 2:9 depicts the steel structure that was designed for this propose. It is composed by a steel base and two perforated L-section steel columns in which a horizontal *Rexroth* aluminum profile can be fixed at the most favorable height. It is in the *Rexroth* profile that camera and lights are fixed, every test day, in the most similar position possible.

Despite the care to keep the camera always at the same position, the zoom position was recorded in order to reconstruct the test setup with the same reference. Once these two positions (camera and zoom) were fixed, replacing specimens was guaranteed by the axis drawn in the specimen surface, which should overlap the camera axis (see section 2.2). Furthermore, the conversion factor between pixels and millimeters was done for each tested specimen individually using a graph paper (5 x 50 mm) glued at surface of specimens.

Image acquisition was performed by a 8-bit Charged-Coupled Device (CCD) Baumer Optronic FWX20 digital camera equipped with a Nikon AF Micro-Nikkor 200 mm f/4D lens (Table (I) 2:1) using the GOM ARAMIS® DIC-2D v6.02 software. Camera and specimen were positioned in the test setup with a distance between them that varies dependent on geometry of specimens, leading to different conversion factors (Table (I) 2:1). Lens aperture was fixed to *f*/11 improving the depth of field and shutter time was set to 5 ms. Two lighting sources (LEDMHL10) were used to guarantee the adequate lighting of the specimen surface.

Once acquisition of each reference image was done, the region of interest (ROI) was defined and subdivided by means of a virtual grid (facets). To define the facet size (3375 x 3375 pixels), three main parameters were considered, namely: the size of ROI, the optical system and the quality of speckled pattern (average of speckle size). The facet step was set to 2197 x 2197 pixels. Then, the in-plan displacements were computed and the full-field strain distribution determined. In terms of evaluation of

displacements, typical resolution is in the range of 0,01-0,02 pixel. Evaluation of strains was done considering a typical resolution that varies between 0,01-0,03%.

DIC was used to compare the behavior of different configurations designed to understand the effect of moisture flow on CLT hygroscopic behavior. This choice was essentially based on two points: first, DIC offers full field measurements and second, the technique requires a simple testing apparatus making possible to test a large quantity of specimens.

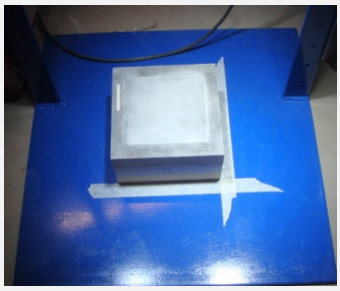

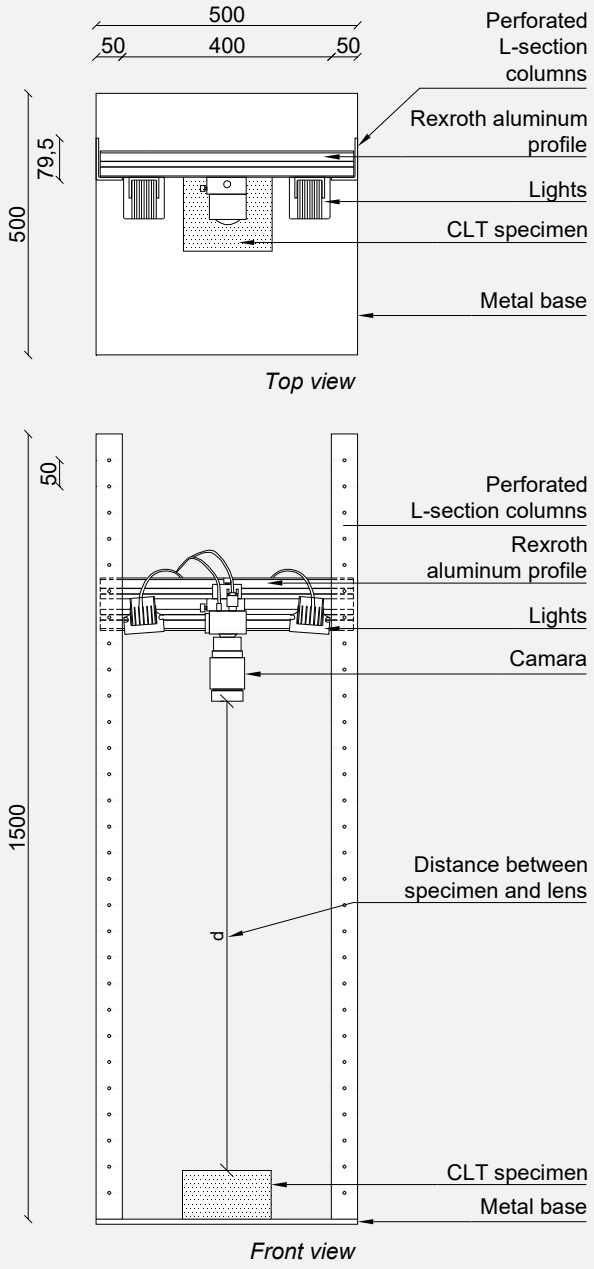

Figure (I) 2:9. Test layout: at left side pictures of steel structure during the test and at right side drawing of the same steel structure (dimensions in mm).

Table (I) 2:1. Components of the optical system and measurement parameters.

CCD camera		
Model		*Baumer Optronic FWX20 (8 bits, 1624 x 1236 pixels, 4.4 µm/pixel)*
Shutter time		*5 ms*
Acquisition frequency		*1 Hz*
Lens		
Model		*Nikon AF Micro-Nikkor 200 mm f/4D*
Aperture		*f/11*
Lighting		LEDMHL10 (color temperature: 6000 K)
Working distance		
Group A	*F1*	*966 mm*
	F2 and F3	*884 mm*
Group B		*1024 mm*
Conversion factor		
Group A	*F1*	*0,127 mm/pixel*
	F2 and F3	*0,096 mm/pixel*
Group B		*0,097 mm/pixel*
Project parameter – facet		
Facet size		*3375 x 3375 pixel*
Step size		*2197 x 2197 pixel*
Project parameter – Strain		
Computation size		*5 x 5 facets*
Validity code		*55%*
Strain compotation method		*Total*
Image recording		
Acquisition frequency		*1 Hz*

As mentioned before, all test specimens were pictured before being submitted to the RH cycles (day 0) and then pictured again for the remaining test days (day 35, day 56, day 161, day 182 and day 324). Similarly to some published work (Angst & Malo (2012), Gereke (2009) and Jönsson (2004)) two different DIC maps were done at each test day: first DIC map was done considering the effect of humidity loads on the unchanged specimens, measuring restrained strains (ε_{rest}), while second DIC map were done

considering the effect of humidity loads on the sliced specimens, measuring released strains (ε_{rel}) caused by cross lamination either through the panel surface (Figure (I) 2:10) or between CLT layers (Figure (I) 2:11). Restrained and released strains were calculated as given in following equations:

$$\varepsilon_{rest} = \frac{L_1 - L_0}{L_0} \quad (2:1)$$

L_0 Initial length taken at Day 0, in mm;
L_1 Length taken at remaining test days to the unchanged specimen, in mm.

$$\varepsilon_{rel} = \frac{L_2 - L_1}{L_1} \quad (2:2)$$

L_2 Length taken at remaining test days after cutting specimens into slices (group A) or after separation of CLT layers (Group B), in mm.

Regarding group A, the first DIC map measured compressive/tensile restrained strains developed over the specimen surfaces at all three directions (X – longitudinal in outer layers (OL) and tangential in inner layers (IL), Y - tangential in outer layers and longitudinal in inner layers and Z - radial) of CLT panels. Immediately afterwards, specimens were sliced into 7 pieces (of which just 5 were inside the defined ROI) and pictured again just in their main face (F1) in order to measure compressive/tensile released strains (Figure (I) 2:10). This procedure allowed to evaluate the role of crosswise lamination over the cross section of CLT panels. The specimens were sliced through Y direction, in which higher deformations were expected.

As depicted in Figure (I) 2:11, two different DIC maps were also performed for specimens of group B. The first DIC map was made to analyze compressive/tensile restrained strains distribution on lateral face of CLT slices (Y and Z directions), while the second DIC map analyses the compressive/tensile released strains distribution on separated layers of CLT slices. Here, the effect of crosswise lamination on hygroscopic behavior of different CLT layers was evaluated.

Values obtained for ε_{rel} were used to quantify stresses through the surface CLT panels (σ_{FL}) as well as to quantify stresses for outer and inner layers (σ_{OL} and σ_{IL}). Stresses were calculated as follows according to equation (2:3).

Once image acquisition was finished, all timber pieces were measured and weighted, before and after oven dried, in order to obtain density and moisture content levels for all tested specimens. This way, it was possible to evaluate density distribution and the moisture content variation as the RH varies.

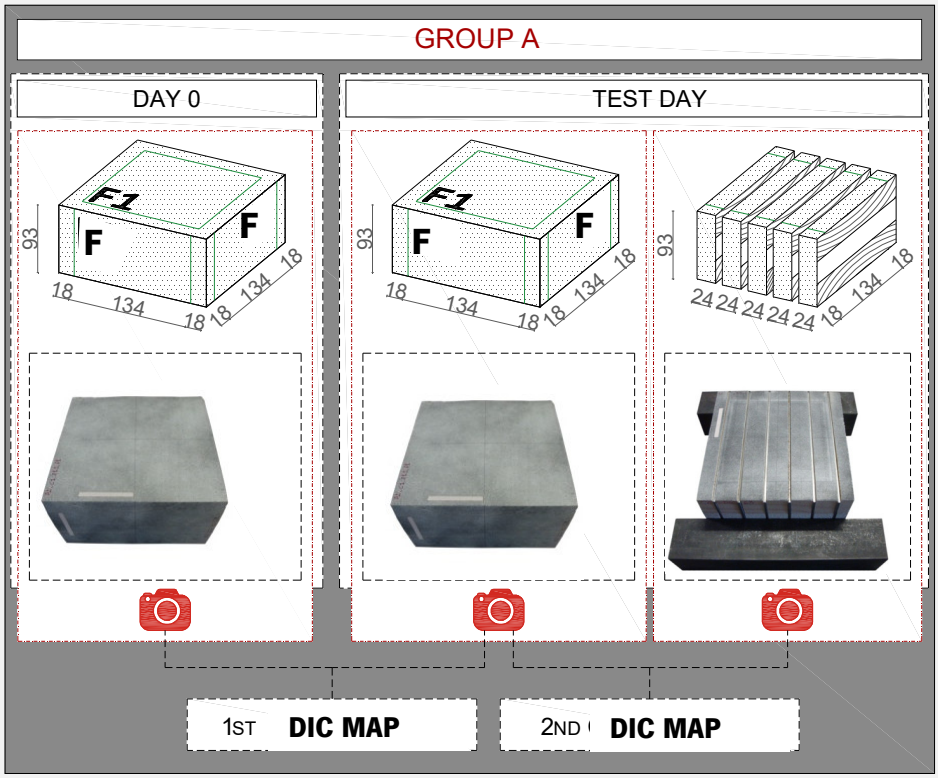

Figure (I) 2:10. Measurements made on different test days for specimens from group A (dimensions in mm).

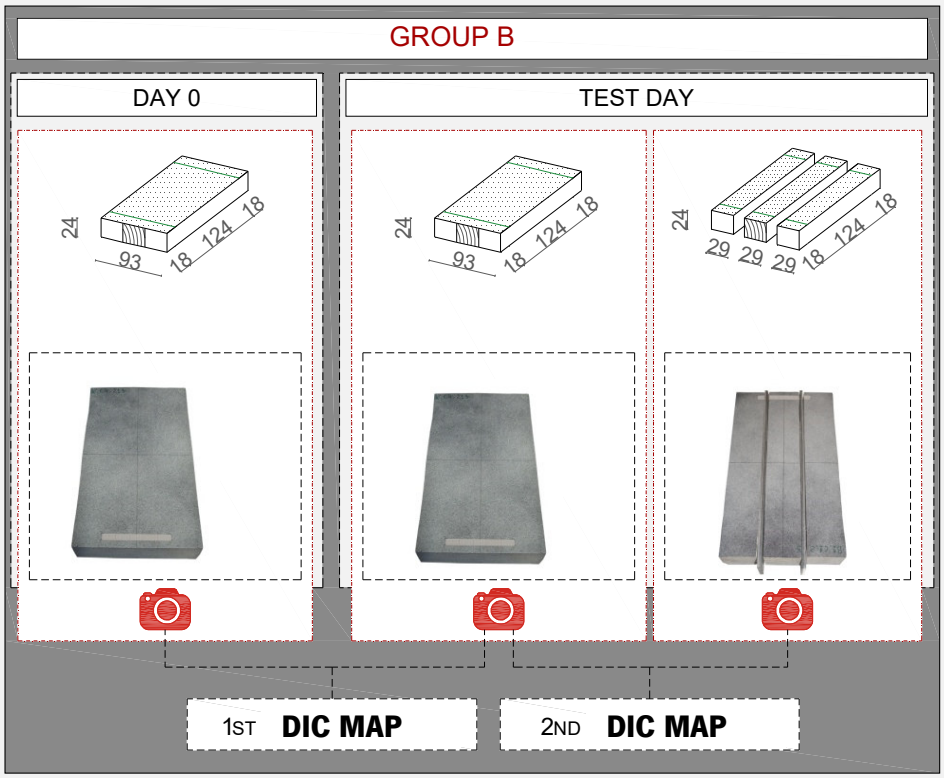

Figure (I) 2:11. Measurements made on different test days for specimens from group B (dimensions in mm).

$$\sigma_{mean} = \varepsilon_{rel,mean} \cdot E_{(u)} \quad (2:3)$$

σ_{mean}	Mean value of stress, in MPa;
$\varepsilon_{rel,mean}$	Mean value of released strain;
$E_{(u)}$	Modulus of elasticity as a function of moisture content present in the specimen at measuring time, in MPa.

2.3.2 LVDTs acquisition

To complement the measurements performed by means of DIC technique, during the same RH cycles, another technique was used to quantify moisture induced movements. In order to obtain a continuous measurement of timber shrinkage/swelling, two CLT specimens from group A and C1 were instrumented with LVDTs in order to register timber movements on all studied directions (X, Y and Z).

Taking the work performed by Gereke (2009) as reference, a stainless steel structure to fix LVDTs and CLT specimens was developed (Figure (I) 2:12) in such a way that only movements on measurement directions were allowed. Each CLT specimen was perforated with four hex head lag screws until the depth of first layer. This way, it was expected to obtain measurements close to those obtained with surface measurements made by DIC technique. These screws had a M3 threaded hole in their heads in which LVDTs and fixing elements were curled up.

Unguided D5W submersible LVDT displacement transducers from RDP group were used. D5/100WRA LVDTs with a range of +/- 2,5 mm and a linearity error of <ą 0,5/ą 0,25 (% F.S.) were used to perform measurements in X and Y directions, while D5/200WRA LVDTs with a range of ą 5 mm and a linearity error of < ą 0,5/ą 0,25/ą 0,1 (% F.S.) were used to perform measurements in Z direction. Here, F.S if full scale or the full measurement range.

Timber movements were registered by a data acquisition hardware from *National Instruments* while instruments were controlled by LabVIEW. Measurements were registered every hour during the period of RH cycles (182 days). During the final period of stabilization (until day 324) specimens were moved to another climatic chamber preventing the continuation of measurements with LVDTs acquisition system.

Obtained data was used to calculate compressive/tensile strains, taking the initial dimension of the specimen as reference. This initial dimension was considered as the dimension at day 0, in order to evaluate compressive strains during all RH cycles. However, the initial dimension was also considered as the dimension at the beginning of each different humidity period in order to compared different

drying/wetting periods. Compressive/tensile strains were calculated as indicated in previous section by equation (2:1).

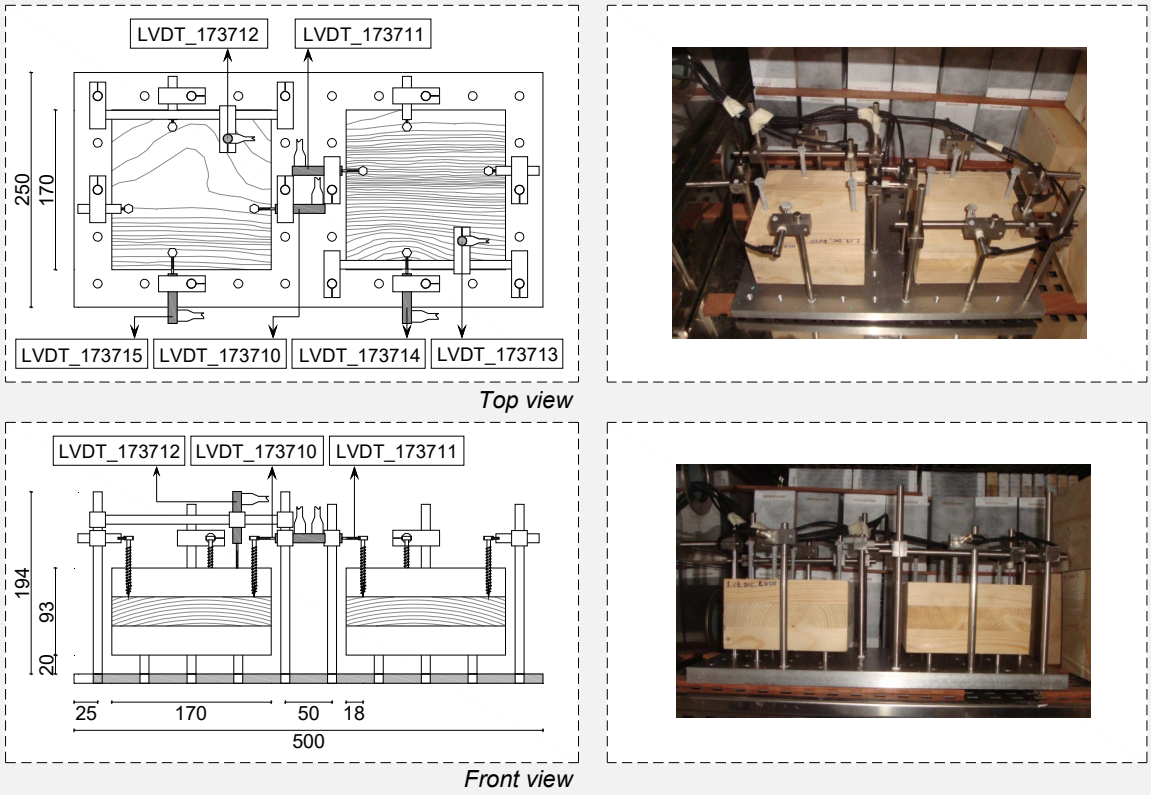

Figure (I) 2:12. Test setup for measuring shrinkage and swelling by means of LVDTs. At left side drawing of test setup (dimensions in mm), and at right side photos of test setup inside the climatic chamber.

2.3.3 Caliper ruler

Manual measurements were performed by means of a digital caliper ruler and used to perform a third analysis for specimens from group A. This technique was used just to take measurements that could not be taken by the other techniques used (DIC or LVDTs). Once specimens of group A were sliced, the caliper ruler was used to measure the total length of different layers on each slice. Then, the same measurements were done after the separation of different layers (Figure (I) 2:13). Registered values were used to calculate released strains for inner and outer layers individually and to evaluate the differences between outer and inner slices.

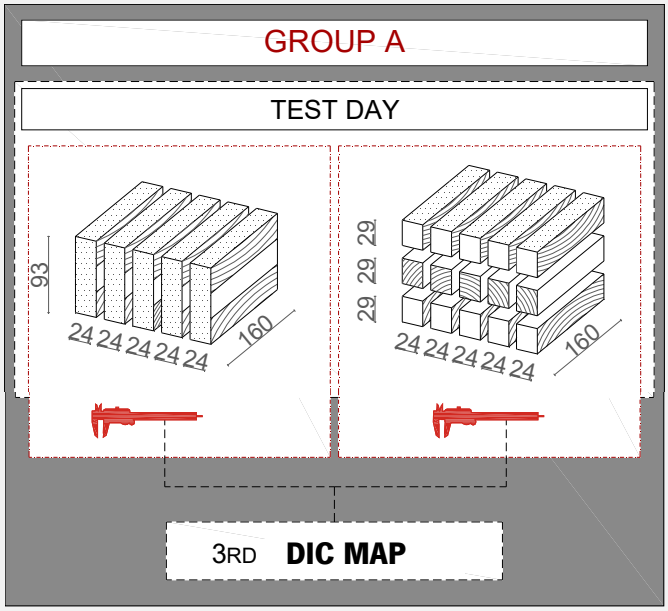

Figure (I) 2:13. Manual measurements performed by caliper ruler on specimens from group A (dimensions in mm).

2.3.4 Controlling the environment of climatic chamber and timber moisture content during RH cycles

During all RH cycles the environment in climatic chamber and moisture content of timber elements were monitored. Figure (I) 2:14 depicts relative humidity and temperature registered during RH cycles and shows that for periods with RH=90% defined environment was easy/fast to reach. This means that during wetting periods the RH remains constant. Differently, drying periods present difficulties to reach the defined environment (RH=30%), which keeps constant for less than half of the entire drying period. This is related with the slow release of moisture from timber to the environment.

A set of ten samples with the same dimensions of the test specimens were placed in the climatic chamber during the entire conditioning period in order to control moisture content changes on CLT elements. The results obtained are depicted in Figure (I) 2:15 and Table (I) 2:2, showing that the percentage of moisture content responds to the drying and wetting cycles, however it does not reach the equilibrium for any of the cycles. For drying cycles, moisture content present values between 9,0% and 10,5% while for wetting cycles, moisture content is between 20,1% and 22,3%.

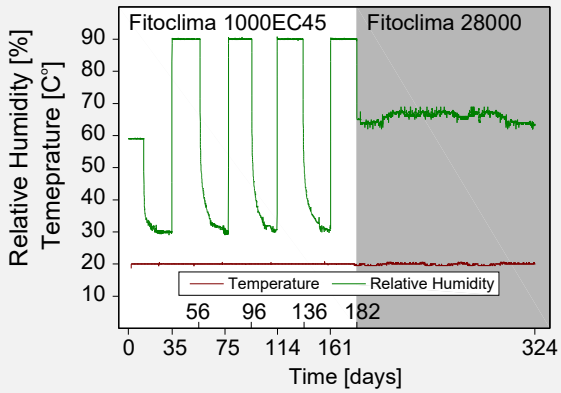

Figure (I) 2:14. Relative humidity and temperature registered by Fitoclima 1000EC45 and Fitoclima 28000 during 324 days.

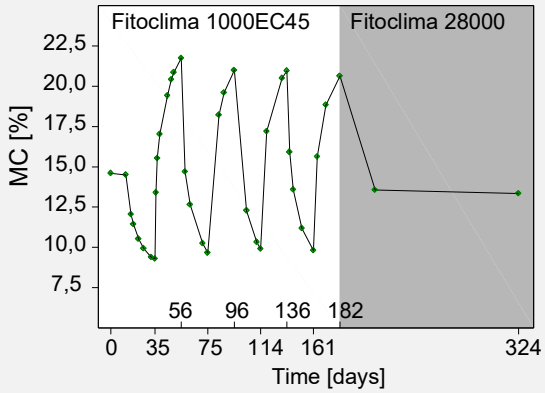

Figure (I) 2:15. Moisture content registered by control specimens during 324 days.

Table (I) 2:2. Descriptive statistics of results obtained by control specimens for moisture content during the RH cycles.

DAY		0	35	56	77	98	119	140	161	182	324
MC [%]	MAX.	14,8	9,5	22,3	9,8	21,5	10,1	21,5	10,5	21,2	13,7
	MEAN	14,5	9,3	21,7	9,7	21,0	9,9	20,9	9,8	20,6	13,5
	MIN,	13,9	9,0	20,8	9,5	20,2	9,6	20,2	9,4	20,1	13,2
	COV	0,018	0,015	0,019	0,011	0,018	0,017	0,017	0,030	0,016	0,015

2.4 Test Results

As mentioned before, displacements, strain distribution, moisture content and density were measured at six different moments: before initiating RH cycles (day 0); at the end of first and last drying and wetting cycles (days 35, 56, 161 and 182); and at the end of final stabilization period (day 324).

In a preliminary observation of results, an important phenomenon was noticed regarding different moisture flow conditions. Analyzing the variation of moisture content levels for different test moments, it is possible to understand that, for configurations in which longitudinal direction is sealed (C2 and C4), the range of MC variation is shorter. This behavior is a consequence of slower water absorption and desorption. Table (I) 2:3, Figure (I) 2:16 and Figure (I) 2:17 present mean values and CoV of moisture content registered for outer and inner layers for all four test configurations and for all test days. Slower water absorption/desorption was registered for middle layers of C2 and C4, in which MC increases/decreases in a range of 3,4 – 4,5% and 2,8 – 3,1%, respectively. In contrast, C1 and C3 present higher moisture content variations, presenting increases/decreases in a range of 6,3 – 8,9% and

7,4 – 8,3%, respectively. Considering outer layers, differences registered were not so substantial, however water absorption/desorption remains slower for C2 and C4 in which moisture content increases/decreases in a range of 4,3 – 7,1% and 3,8 – 6,4%, respectively. Remaining configurations present increases/decreases of moisture content in a range of 7,5 – 8,6% and 9,7 – 8,8%, respectively. Obtained CoV values are low for all test configurations (0,01 – 0,07).

Density distribution was analyzed comparing values of corrected density considering a moisture content of reference of 12% (ρ_{12}).

Table (I) 2:4 presents descriptive statistics of obtained values showing that ρ_{12} varies in a range of 350 - 636 kg/m^3 and 327 – 757kg/m^3 for outer and inner layers, respectively (Figure (I) 2:18 and Figure (I) 2:19). Despite the wide ranges, considering the variability of natural wood and that density was not controlled at production time, the obtained CoV values are considered low (0,08 – 0,15). Mean values obtained for outer and inner layers vary in a tighter range of 438 – 465 kg/m^3.

2.4.1 DIC technique

2.4.1.1 Group A_F1 (CLT panels with dimensions of 170x170x93 mm)

The DIC maps performed for specimens from group A resulted on full-field restrained strains measured on F1, for Y and X directions (see Figure (I) 2:10 for indication of face F1). Table (I) 2:5 and Figure (I) 2:20 present descriptive statistics and graphs of obtained results. Mean values were obtained considering the data of the entire ROI (around 75 x 75 subsets).

Regarding the first RH cycle, it is evident that tangential direction (Y) presents restrained strains that are significantly higher than those observed for longitudinal direction (X), from -0,012 to 0,012 and from -0,006 to 0,006, respectively. However, observing the differences between first and last RH cycles, Y and X directions present different trends. While for Y direction, it is possible to relate easily compressive and tensile strains associated with drying and wetting cycles, X direction does not verify the same trend. Contrary to what was expected, restrained strains measured for last drying and wetting periods present opposite trends: tensile strains for drying period and compressive strains for wetting periods.

Table (I) 2:3. Moisture content registered for outer and inner layers for all test configurations at each test day.

MOISTURE CONTENT [%]								
	MEAN COV							
TEST DAY	OUTER LAYERS				INNER LAYERS			
	C1	C2	C3	C4	C1	C2	C3	C4
35	10,7	12,5	10,3	11,7	11,1	13,2	10,2	13,5
	0,04	*0,02*	*0,04*	*0,02*	*0,04*	*0,03*	*0,02*	*0,01*
56	19,3	17,4	18,8	18,8	18,8	17,7	19,1	17,8
	0,02	*0,05*	*0,04*	*0,04*	*0,04*	*0,02*	*0,03*	*0,02*
161	10,5	13,6	10,0	12,5	11,5	14,6	10,8	15,0
	0,07	*0,02*	*0,05*	*0,02*	*0,05*	*0,02*	*0,04*	*0,01*
182	19,0	17,9	17,5	19,5	17,7	18,0	18,0	18,4
	0,02	*0,04*	*0,02*	*0,02*	*0,03*	*0,03*	*0,02*	*0,03*
324	12,8	13,3	12,9	13,3	13,4	13,9	13,2	13,9
	0,01	*0,02*	*0,02*	*0,01*	*0,02*	*0,01*	*0,01*	*0,01*

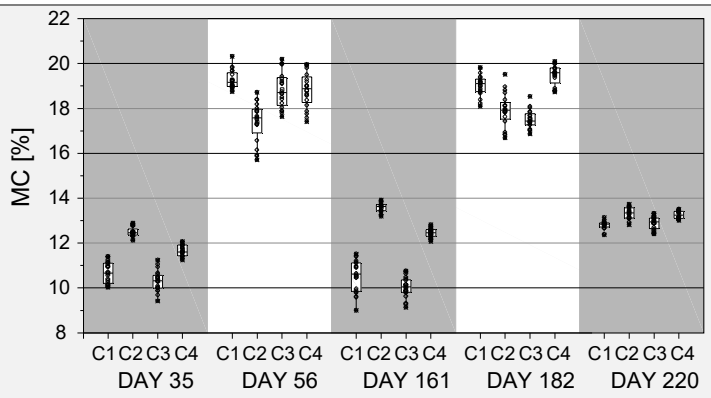

Figure (I) 2:16. Boxplots of moisture content obtained for outer layers of all specimens tested considering different test configurations and all test days.

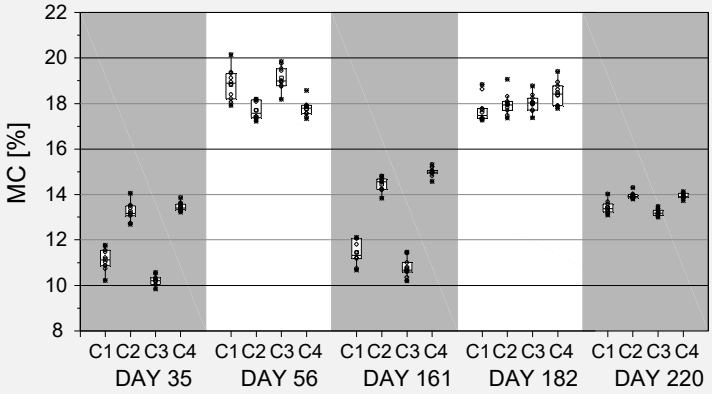

Figure (I) 2:17. Boxplots of moisture content obtained for inner layers of all specimens tested considering different test configurations and all test days.

Table (I) 2:4. Descriptive statistics of corrected density (ρ_{12}) registered for outer and inner layers for all test configurations.

CORRECTED DENSITY ρ_{12} [kg/m³]								
	OUTER LAYERS				INNER LAYERS			
	C1	C2	C3	C4	C1	C2	C3	C4
SAMPLING	120	100	100	100	60	50	50	50
MAXIMUM	580	623	636	582	531	757	513	536
MEAN	**452**	**465**	**464**	**458**	**438**	**447**	**444**	**459**
MINIMUM	350	372	369	364	352	346	353	327
COV	*0,11*	*0,11*	*0,12*	*0,08*	*0,11*	*0,15*	*0,10*	*0,10*
P5	358	388	375	391	360	355	361	383

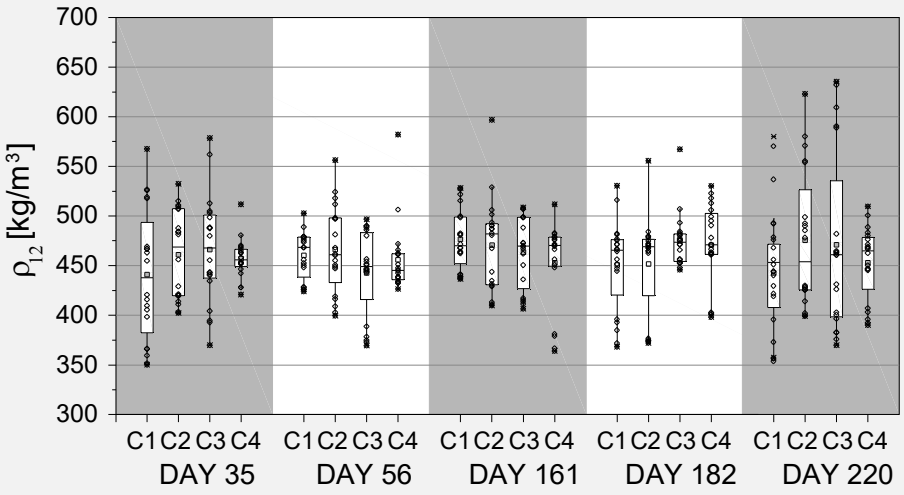

Figure (I) 2:18. Boxplots of corrected density (ρ_{12}) obtained for outer layers of all specimens tested considering different test configurations and all test days.

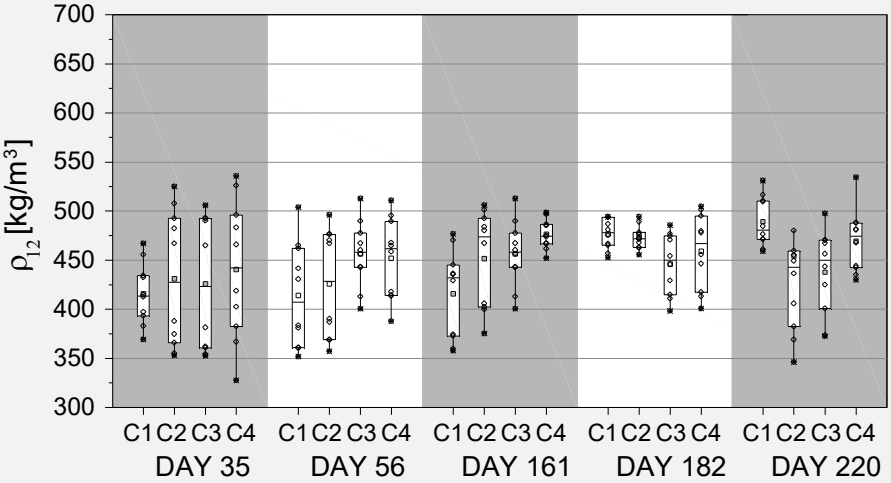

Figure (I) 2:19. Boxplots of corrected density (ρ_{12}) obtained for inner layers of all specimens tested considering different test configurations and all test days.

Analyzing the results obtained for Y direction, it was observed that the influence of different moisture flow conditions on restrained strains is similar (though not so obvious) to that observed for moisture content variations. Again, C1 allows a free moisture flow through all three timber directions, C2 only in tangential direction, C3 only in longitudinal direction and C4 only in radial direction. Taking C1 as reference, C2 and C4 present a tendency for lower restrained strains: restrained compressive strains are 75% and 50% lower for the first drying period and 167% and 84% lower for the last drying period, respectively. Because of that, a lower range of strain variation between absorption and desorption periods is also registered. However, differently from what was observed for moisture content variation, restrained strains tend to reduce significantly from first to last drying cycles (Table (I) 2:5 and Figure (I) 2:20). It was observed that configurations that block moisture flow on longitudinal direction present higher restrained strains decreases between the first and last drying periods. Taking day 35 as reference, from the first to the last drying period, restrained compressive strains reduce 50% and 0% for configurations C1 and C3, and -234% and 84% for configurations C2 and C4, respectively. Differently, taking day 56 as reference, losses observed between the first and the last wetting periods present a more homogeneous behavior: tensile restrained strains reduce 100% for configurations C1, C2 and C3 and 84% for configuration C4. These values agree with the fact that absorption/desorption process is significantly slower when longitudinal direction is sealed, especially if combined with sealing of radial direction (C2). In fact, due to its moisture flow conditions, C2 present a behavior that is more in line with what was observed for X direction, inverting the expected strain tendency at the last wetting/drying periods. Finally, in order to quantify the total effect of RH cycles on CLT specimens, and assuming that restrained strains at day 0 are absent, measurements taken at the end of stabilization process (day 324) indicate a slightly tendency for compressive strains on tangential direction (0,00 to -0,002).

Regarding X direction, different moisture flow conditions present some effects during the first drying and wetting periods but on a different way. Taking C1 as reference, registered compressive strains for first drying period are 80%, 60% and 80% lower for remaining configurations (C2, C3 and C4, respectively). At the end of first wetting period C1 does not reach tensile strains, presenting compressive strains of around 0,001, while the remaining configurations present tensile strains around 0,004. During the last drying and wetting periods the differences registered between test configurations are not so substantial. However, it is important to mention that restrained strains do not tend to decrease substantially as the number of cycles increase, as verified for Y direction. Finally, observing mean values obtained for day 324, the causing effects of successive RH cycles provide restrained strains close to zero with a slightly tendency for tensile strains, with the exception of C1 that present compressive strains of -0,001. This can

mean that restraining moisture flow on CLT panel causes observed tensile strains, however the obtained values are too small to allow a firm conclusion.

Table (I) 2:5. Descriptive statistics of full-field restrained strains measured on F1 of specimens from group A, for Y and X directions, during first DIC mapping, before cut (BC) the specimens.

RESTRAINED STRAINS (ε_{rest})										
MAXIMUM **MEAN** MINIMUM *COV*										
	Y DIRECTION (ε_{rest_Y})					**X DIRECTION (ε_{rest_X})**				
	DAY					**DAY**				
	35	**56**	**161**	**182**	**324**	**35**	**56**	**161**	**182**	**324**
C1	0,006 **-0,012** -0,024 ***-0,28***	0,025 **0,008** -0,041 ***0,77***	0,177 **-0,006** -0,028 ***-3,81***	0,023 **0,000** -0,013 ***-0,27***	-0,055 **-0,002** 0,016 ***-1,40***	0,003 **-0,005** -0,013 ***-0,37***	0,007 **-0,001** -0,007 ***-1,00***	0,026 **0,002** -0,049 ***1,46***	0,003 **-0,006** -0,013 ***-0,30***	0,087 **-0,002** -0,020 ***1,69***
C2	0,028 **-0,003** -0,026 ***-1,06***	0,026 **0,007** -0,005 ***0,48***	0,034 **0,004** -0,010 ***1,17***	0,043 **0,000** -0,020 ***28,67***	0,013 **0,000** -0,012 ***13,36***	0,014 **-0,001** -0,023 ***-2,90***	0,021 **0,004** -0,009 ***0,56***	0,030 **0,005** -0,066 ***1,15***	0,011 **-0,003** -0,024 ***-1,25***	0,020 **0,001** -0,018 ***3,64***
C3	0,008 **-0,009** -0,034 ***-0,36***	0,079 **0,011** -0,125 ***0,60***	0,047 **-0,009** -0,028 ***-0,53***	0,040 **0,000** -0,042 ***-0,22***	0,049 **-0,001** -0,020 ***-13,79***	0,019 **-0,002** -0,079 ***-1,29***	0,022 **0,005** -0,024 ***0,47***	0,015 **0,000** -0,014 ***-26,18***	0,018 **-0,004** -0,025 ***-0,82***	0,025 **0,001** -0,029 ***10,41***
C4	0,022 **-0,006** -0,021 ***-0,64***	0,026 **0,012** -0,013 ***0,45***	0,010 **-0,001** -0,015 ***-3,30***	0,014 **0,002** -0,016 ***3,44***	0,068 **-0,002** -0,023 ***-6,52***	0,005 **-0,001** -0,016 ***-0,95***	0,011 **0,004** -0,003 ***0,20***	0,016 **0,001** -0,012 ***1,31***	0,004 **-0,004** -0,009 ***-0,48***	0,011 **0,000** -0,011 ***10,07***

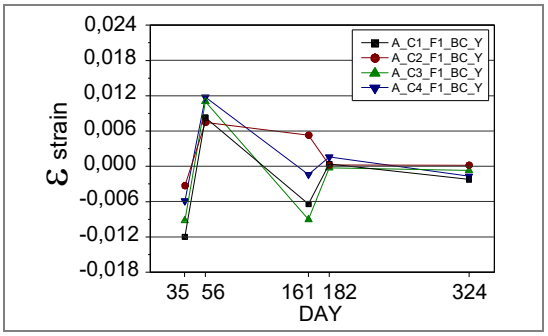

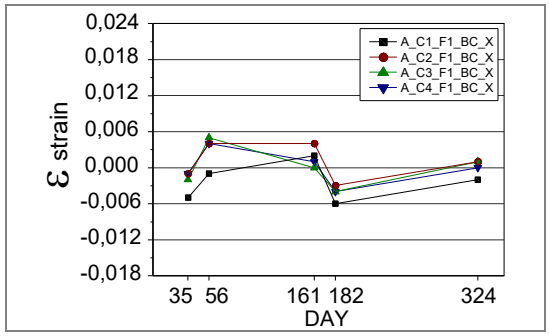

Figure (I) 2:20. Mean values of full-field restrained strains distribution measured on F1 of specimens from group A for all four configurations in Y and X directions.

In order to analyze the relations between tangential (Y) and longitudinal (X) directions on the main face of CLT panels, the ratio between restrained strains obtained for Y and X directions (Δ_{F1}) was analyzed (Table (I) 2:6). Observing the results, it is possible to realize that the ratio between tangential and longitudinal directions tend to be lower at the last RH cycle. As a consequence of low strains measured in Y direction at the end of the last wetting period, the lowest differences between Y and X direction are verified at the same moment, varying between -0,4 and 0,1.

Table (I) 2:6. Ratio between restrained strains obtained for Y and X directions during the first DIC mapping of group A.

RATIO	DAY	CONFIGURATIONS			
		C1	C2	C3	C4
$\Delta=\left(\frac{Y_{mean}}{X_{mean}}\right)$ $\quad \Delta_{F1}=\left(\frac{T}{L}\right)$	**35**	2,5	3,2	4,9	4,2
	56	-6,6	2,1	2,3	3,1
	161	-4,2	1,0	-59,8	-1,1
	182	-0,1	-0,1	0,1	-0,4
	324	2,0	1,2	-1,3	-8,3

Some values are negative, meaning that strains measured at different directions present opposite signs. In other words, at the same moment when Y direction present compressive strains, X direction present tensile strains. This phenomenon is observed for C1 from the first wetting period to the last wetting period, however at the end of stabilization period it turns positive again, meaning that successive RH cycles do not cause cumulative strains on CLT. Remaining configurations do not present exactly the same behavior, for which $\Delta_{F1} < 0$ on different moments just during the last RH cycle and at the end of stabilization process. Here, it is important to underline that C3 and C4 present the same inverted tendency at the end of stabilization process. So, assuming that the tendency observed for C1 presents the typical behavior for CLT $\Delta_{F1\_C1\_324}$= 2,0, successive RH cycles change the effects of crosswise lamination for configurations in which tangential direction is sealed.

Actually there is no published research studying the effect of cyclic humidity changes on dimensional variations of CLT. Jönsson (2004) performed an experimental study with glulam submitted to successive RH cycles in which RH varies between 40% and 80% for periods of 7 days during 101 days on total. However, the author did not found any effects of RH cycles on measured strains. Surprisingly, the present research suggests that restrained strains in tangential direction tend to decrease as cycles are repeated.

To explain this phenomenon more research is required, however three possible causes can be pointed out:

- Results obtained for tangential direction (outer layers) suggest that there is a tendency for restrained strains to reduce as the number of cycles increase. So, restriction of timber movements caused by crosswise lamination can be more effective after successive RH cycles, probably due to some exhaustion of timber fibers;
- The long duration (21 days) of each drying/wetting period can also be a cause for the observed behavior of CLT. Large drying/wetting periods allow a uniform distribution of moisture content through the CLT cross section and consequently less moisture gradients are generated;
- Successive RH cycles can cause warping/twisting on CLT, which can result on unrealistic strains distribution, once the DIC method takes the measurements just on the surface of CLT panels.

Regarding the observed behavior for longitudinal direction, the explanation should also be related with the same causes: crosswise lamination; possible fatigue of timber fibers caused by successive RH cycles; and with warping/twisting of CLT panels. It is possible that, due to a combination of these three factors, during the last drying and wetting periods, as the middle layers shrinks or swells on tangential direction, outer layers present the opposite tendency on longitudinal direction.

Graphs depicted in Table (I) 2:7 show the full field restrained strain distribution in F1 of some test specimens from group A regarding Y direction (tangential) for C1 and C2 (remaining graphs are depicted in Annex 1:1). Observing color fill graphs, it is possible to identify easily compressive (cold colors) and tensile (warm colors) strains associated with drying and wetting cycles, respectively. It is also possible to observe through Y direction, especially for configurations that were not sealed at the main face of panel (C1 and C4), that there are differences between strains measured for early and latewood. Table (I) 2:8 depicts some color fill graphs obtained for restrained strains measured through X direction of main face of CLT specimens with C1 and C2 (remaining graphs are depicted in Annex 1:2).

Surprisingly, for configurations in which main face is not sealed (C1 and C4), strains distribution is not symmetric, presenting in some cases opposite tendencies between right and left borders. The only explanation found for this tendency is the influence of tangential moisture movements of inner layers which restricts movements of outer layers on longitudinal direction. For configurations C2 and C3 this opposite tendency is not so clear, probably due to some influence of elastic membrane on timber movements.

As described in 2.3.1 a second DIC mapping was performed. Specimens were sliced in Y direction and pictured again in order to take released strains distribution (ε_{rel}). Table (I) 2:9 presents the mean released strain values taken from all five slices for all four configurations and for all test days, while Figure

(I) 2:21 depicts the graphs of same mean values. Mean values were taken from the central longitudinal section of each slice in order to avoid any sawing effects, considering a central area of around 4 x 74 facets. Results show that for test days 0, 35, 161and 324, released strains are close to zero and tensile strains are predominant independent of the test day/moisture content. So, contrary to what was observed for restrained strains, a clear relation between drying/wetting periods and compressive/tensile strains was not observed.

The effect of high moisture level at production of CLT panels seems not to induce significant released strains, once $\varepsilon_{rel\_mean\_0\_C1\_Y}$ = 0,000. Obtained released strains present significantly higher values for first wetting period (day 56), in which mean tensile strains are around 0,019 for all four tested configurations. This phenomenon shows that the effect of crosswise lamination is more evident during the first wetting period: despite the tensile restrained strains observed during the first DIC mapping, after sliced, timber still tends to swell substantially. Despite being low, compressive strains were registered just at the end of second wetting period (day 182), which presents the opposite tendency of that observed for day 56. So, similarly to what was observed for restrained strains, there is a clear effect of successive RH cycles on hygroscopic behavior of CLT panels. This effect is easily observed in color fill graphs depicted in Table (I) 2:10. C1 and C2 present here the typical behavior observed for all four configurations but the remaining graphs are depicted in Annex 1:3.

All four configurations present similar values meaning that there are no causing effects related with different moisture flow conditions. Differently, comparing released strains obtained in day 0 and 324, it can be concluded that successive RH cycles cause a slightly increase of tensile strains. This tendency proves the existence of a restriction of timber movements caused by crosswise lamination once compressive restrained strains observed at first DIC map became tensile released strains at second DIC map.

2.4.1.2 Group A_F2 and F3 (CLT panels with dimensions of 170x170x93 mm)

DIC map performed to specimens from group A included the three different faces of CLT panels. F1 was analyzed in the previous section and herein F2 and F3 (see Figure (I) 2:10 for indication of faces) will be also analyzed. F2 is one of the lateral faces of CLT panel in which outer layers are subjected to movements in tangential direction and inner layer in longitudinal direction. F3 present exactly the opposite arrangement.

Table (I) 2:7. Restrained strains measured by DIC technique for configurations C1 and C2, on F1 of specimens by group A in Y direction, for all five test days, before cut (BC) the specimens.

Y DIRECTION (ε_{rest})			
TEST DAY RH [%]	**C1**	**C2**	**SCALE**
DAY 35 [RH=30%]	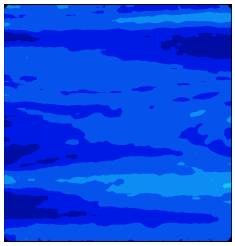 A1_C1_F1_BC_35	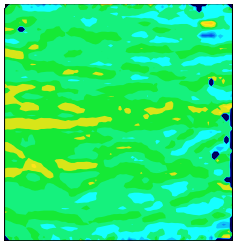 A2_C2_F1_BC_35	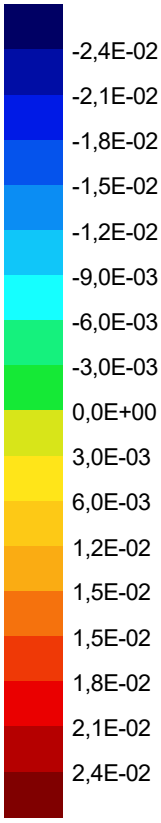 -2,4E-02 -2,1E-02 -1,8E-02 -1,5E-02 -1,2E-02 -9,0E-03 -6,0E-03 -3,0E-03 0,0E+00 3,0E-03 6,0E-03 1,2E-02 1,5E-02 1,5E-02 1,8E-02 2,1E-02 2,4E-02
DAY 56 [RH=90%]	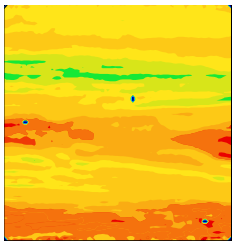 A1_C1_F1_BC_56	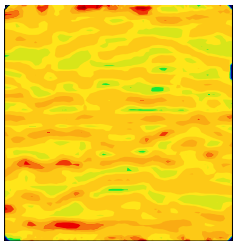 A2_C2_F1_BC_56	
DAY 161 [RH=30%]	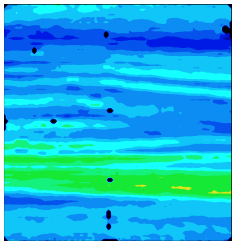 A1_C1_F1_BC_161	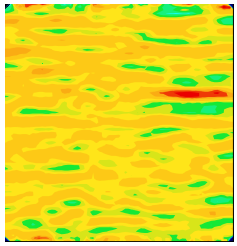 A2_C2_F1_BC_161	
DAY 182 [RH=90%]	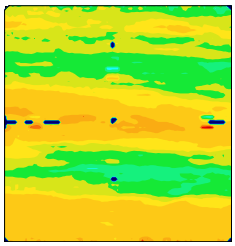 A1_C1_F1_BC_182	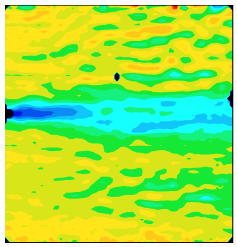 A2_C2_F1_BC_182	
DAY 324 [RH=65%]	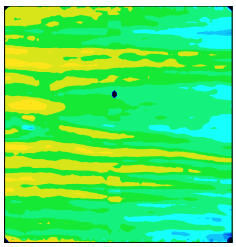 A2_C1_F1_BC_324	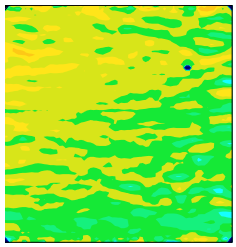 A1_C2_F1_BC_324	

Table (I) 2:8. Restrained strains measured by DIC technique for configurations C1 and C2, on F1 of specimens by group A in X direction, for all five test day, before cut (BC) the specimens.

X DIRECTION (ε_{rest})			
TEST DAY RH [%]	**C1**	**C2**	**SCALE**
DAY 35 [RH=30%]	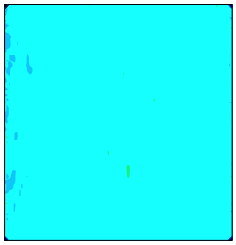 **A1_C1_F1_BC_35**	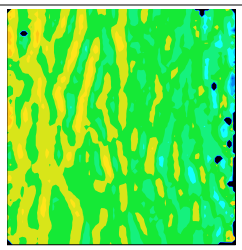 **A2_C2_F1_BC_35**	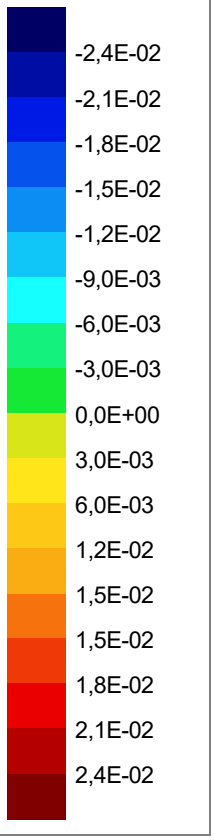 -2,4E-02 -2,1E-02 -1,8E-02 -1,5E-02 -1,2E-02 -9,0E-03 -6,0E-03 -3,0E-03 0,0E+00 3,0E-03 6,0E-03 1,2E-02 1,5E-02 1,5E-02 1,8E-02 2,1E-02 2,4E-02
DAY 56 [RH=90%]	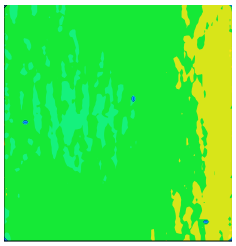 **A1_C1_F1_BC_56**	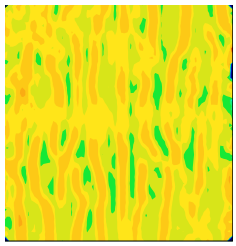 **A2_C2_F1_BC_56**	
DAY 161 [RH=30%]	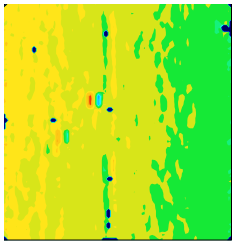 **A1_C1_F1_BC_161**	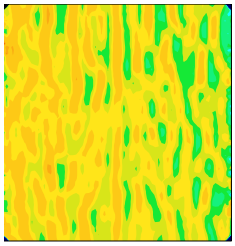 **A2_C2_F1_BC_161**	
DAY 182 [RH=90%]	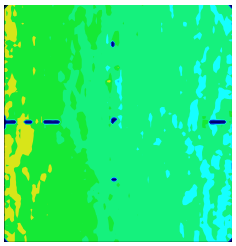 **A1_C1_F1_BC_182**	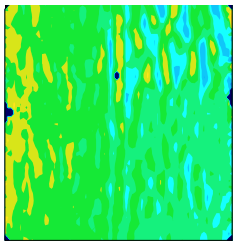 **A2_C2_F1_BC_182**	
DAY 324 [RH=65%]	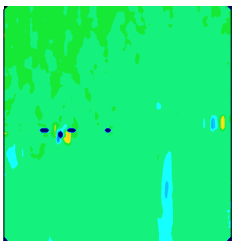 **A2_C1_F1_BC_324**	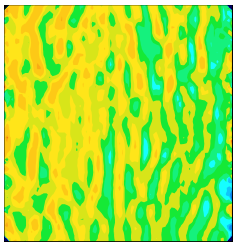 **A1_C2_F1_BC_324**	

Table (I) 2:9. Descriptive statistics of full-field released strains measured on F1 of specimens from group A during second DIC mapping, after cut (AC) the specimens.

RELEASED STRAINS (ε_{rel})

MAXIMUM
MEAN
MINIMUM
COV

	DAY 0	35	56	161	182	324
C1	0,006	0,003	0,024	0,010	0,003	0,003
	0,000	**0,000**	**0,020**	**0,000**	**0,000**	**0,001**
	-0,004	-0,002	0,016	-0,004	-0,004	-0,001
	1,82	*-0,90*	*0,04*	*-4,23*	*0,59*	*0,26*
C2		0,027	0,022	0,004	0,003	0,003
		0,001	**0,019**	**0,000**	**0,000**	**0,002**
		-0,028	0,017	-0,003	-0,006	-0,003
		1,28	*0,03*	*0,16*	*-0,08*	*0,25*
C3		0,008	0,025	0,040	0,004	0,020
		0,000	**0,019**	**0,001**	**0,000**	**0,002**
		-0,005	0,014	-0,005	-0,003	0,000
		-6,28	*0,04*	*1,22*	*-0,91*	*0,54*
C4		0,003	0,024	0,003	0,002	0,003
					-	
		0,000	**0,019**	**0,000**	**0,001**	**0,002**
		-0,002	0,015	-0,002	-0,004	0,000
		-3,88	*0,06*	*0,87*	*-0,22*	*0,26*

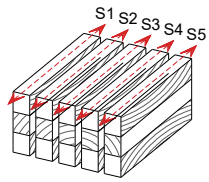

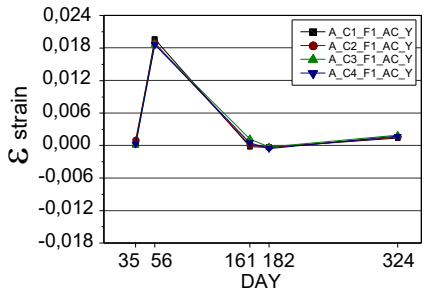

Figure (I) 2:21. Mean values of released strains measured on central longitudinal section of all slices (S1-S5) of specimens from group A for all four test configurations.

Regarding F2, Table (I) 2:11 and Figure (I) 2:22 summarize the behavior of all four configurations for inner and outer layers separately. Inner layers present predominant compressive strains during the first RH cycle while during the last RH cycle they present tensile strains for drying periods and compressive strains for wetting periods. It is important to mention here that for the last RH cycle, the results obtained for F1 presented the same tendency in X direction, which also quantify the movements in longitudinal direction. Surprisingly, during the last RH cycle, the outer layers present the opposite tendency of that observed for F1 in Y direction (tangential). This may be related with restrictions of timber movements caused by crosswise lamination. In fact, observing full field strains distribution presented in Table (I) 2:12 it is possible to notice that outer layers suffer tensile and compressive strains through Y direction which are also dependent on growth ring orientation. That is why shear strains present the diagonal symmetry depicted by color fill graphs. On contrast, inner layers present a more homogeneous strains distribution.

Table (I) 2:12 presents C1 as example however, remaining graphs obtained for F2 in Y direction are depicted in Annex 1:4.

Table (I) 2:10. Typical behavior of released strain distribution observed after CLT specimens being cut (AC) into slices for all six test moments.

Y DIRECTION			
TEST DAY RH [%]	**C1**	**C3**	**SCALE**
DAY 0 [RH=65%]	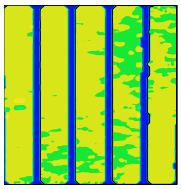 A2_C1_F1_AC_0		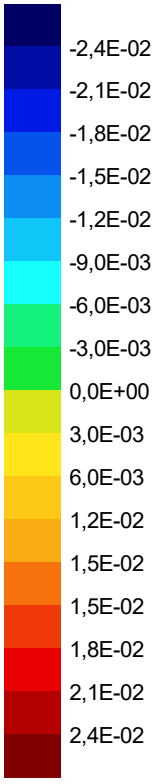 -2,4E-02 -2,1E-02 -1,8E-02 -1,5E-02 -1,2E-02 -9,0E-03 -6,0E-03 -3,0E-03 0,0E+00 3,0E-03 6,0E-03 1,2E-02 1,5E-02 1,5E-02 1,8E-02 2,1E-02 2,4E-02
DAY 35 [RH=30%]	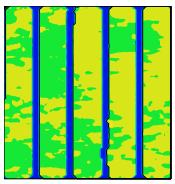 A1_C1_F1_AC_35	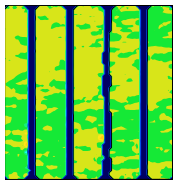 A1_C3_F1_AC_35	
DAY 56 [RH=90%]	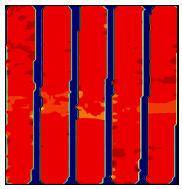 A1_C1_F1_AC_56	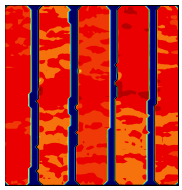 A1_C3_F1_AC_56	
DAY 161 [RH=30%]	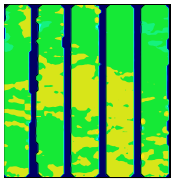 A1_C1_F1_AC_161	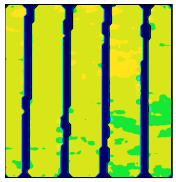 A1_C3_F1_AC_161	
DAY 182 [RH=90%]	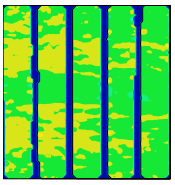 A1_C1_F1_AC_182	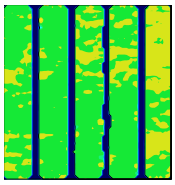 A1_C3_F1_AC_182	
DAY 324 [RH=65%]	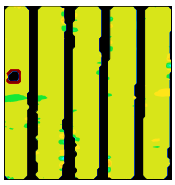 A1_C1_F1_AC_324	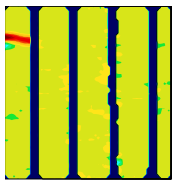 A2_C3_F1_AC_324	

Table (I) 2:11. Descriptive statistics of full-field restrained strains measured on specimens from group A_F2 in Y direction, for inner and outer layers, during first DIC mapping, after cut (AC) the specimens.

MEAN RESTRAINED STRAINS (ε_{rest_mean})										
MAXIMUM **MEAN** MINIMUM *COV*										
F2_Y DIRECTION										
	INNER LAYERS (IL)					**OUTER LAYERS (OL)**				
	DAY					**DAY**				
	35	**56**	**161**	**182**	**324**	**35**	**56**	**161**	**182**	**324**
C1	0,000 **-0,002** -0,004 ***-0,21***	0,001 **-0,001** -0,004 ***-0,74***	0,017 **0,009** 0,006 ***0,04***	0,001 **-0,004** -0,005 ***-0,11***	0,057 **0,001** -0,011 ***1,07***	0,011 **-0,004** -0,015 ***-0,85***	0,022 **0,003** -0,039 ***3,80***	0,065 **0,002** -0,015 ***6,95***	0,050 **-0,003** -0,023 ***-0,79***	0,009 **-0,002** -0,009 ***1,03***
C2	0,003 **-0,002** -0,010 ***-0,28***	0,005 **-0,002** -0,008 ***-0,44***	0,011 **0,009** 0,006 ***0,04***	0,007 **-0,004** -0,025 ***-0,25***	0,015 **0,000** -0,019 ***10,66***	0,018 **-0,003** -0,014 ***-1,12***	0,030 **0,000** -0,013 ***-3,81***	0,026 **0,009** -0,003 ***0,69***	0,029 **-0,002** -0,020 ***-4,54***	0,012 **0,000** -0,010 ***0,87***
C3	0,012 **-0,002** -0,017 ***-0,59***	0,017 **-0,003** -0,033 ***-1,58***	0,026 **0,009** -0,038 ***0,45***	0,077 **-0,004** -0,104 ***-1,71***	0,032 **0,001** -0,012 ***4,44***	0,016 **-0,005** -0,016 ***-0,90***	0,012 **0,001** -0,010 ***1,23***	0,098 **0,004** -0,018 ***2,95***	0,010 **-0,002** -0,017 ***-2,75***	0,095 **-0,002** -0,017 ***3,68***
C4	0,007 **-0,002** -0,010 ***-0,91***	0,006 **-0,003** -0,015 ***-0,46***	0,025 **0,009** -0,003 ***0,21***	0,003 **-0,004** -0,013 ***-0,21***	0,013 **0,001** -0,009 ***2,42***	0,005 **-0,004** -0,014 ***-0,70***	0,013 **0,001** -0,016 ***1,85***	0,026 **0,008** 0,000 ***0,38***	0,014 **-0,001** -0,012 ***8,06***	0,021 **0,000** -0,010 ***-14,82***

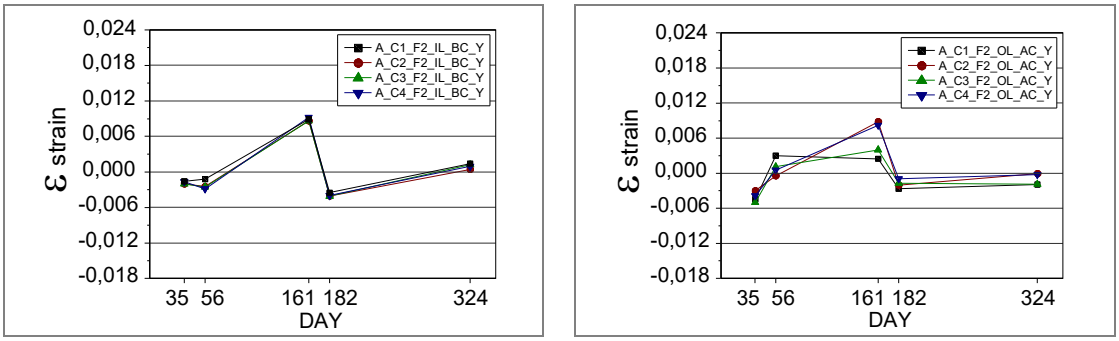

Figure (I) 2:22. Mean values of full-field restrained strains distribution measured on specimens from group A_F2 in Y direction, for inner and outer layers, during first DIC mapping.

Table (I) 2:12. Typical behavior (C1) of full field restrained strain distribution in Y and Z directions and in shear observed before CLT specimens from group A_F2 for all test moments.

RESTRAINED STRAINS FOR A_F2_C1 (ε_{rest})					
TEST DAY RH [%]	Y	Z	SHEAR	PICTURES	SCALE
DAY 35 [RH=30%]	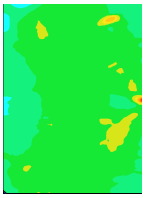	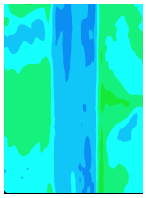	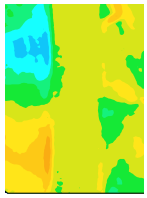	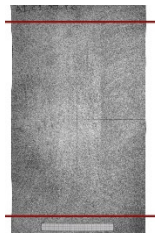	
DAY 56 [RH=90%]	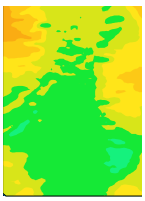		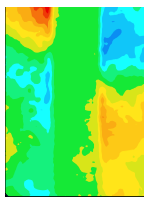		
DAY 161 [RH=30%]	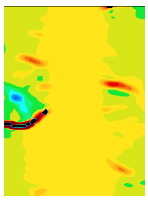	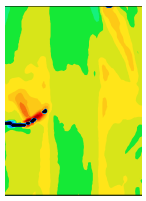	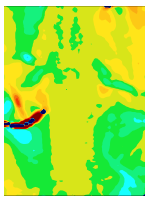	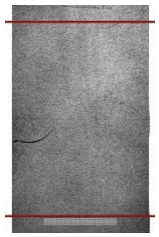	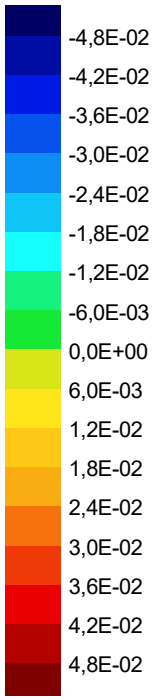 -4,8E-02 -4,2E-02 -3,6E-02 -3,0E-02 -2,4E-02 -1,8E-02 -1,2E-02 -6,0E-03 0,0E+00 6,0E-03 1,2E-02 1,8E-02 2,4E-02 3,0E-02 3,6E-02 4,2E-02 4,8E-02
DAY 182 [RH=90%]			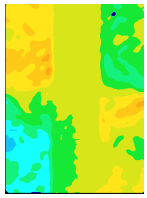	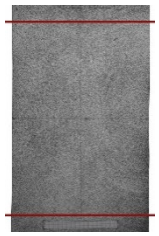	
DAY 324 [RH=65%]	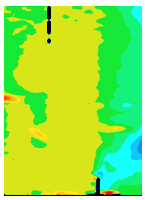	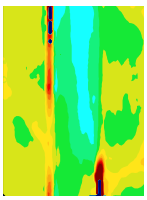	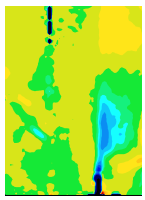	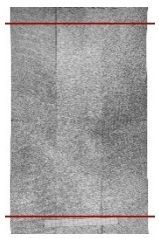	

Note: Red lines at pictures represent the end of ROI considered by DIC measurements.

Regarding inner layers, different moisture flow conditions do not affect the results and no differences between test configurations were observed. On contrary, outer layers present some differences at last drying period (day 161). Last drying period presents the highest tensile strains observed either for inner layers or outer layers. However, while inner layers present the same mean value for all four configurations $\varepsilon_{rest\_mean\_161\_C1\ /C4\_IL\_Y}$ = 0,009, outer layers present different ranges: for C1 and C3 0,002 ≤ $\varepsilon_{rest\_mean\_161\_C1/C3\_OL\_Y}$ ≤ 0,004 and for C2 and C4 0,008 ≤ $\varepsilon_{rest\_mean\_161\_C2/C4\_OL\_Y}$ ≤ 0,009. This difference should be directly related with sealing of longitudinal direction which delays the desorption process during drying period resulting in a lower ratio between tangential and longitudinal directions (1,0 ≤ $\frac{\varepsilon_{rest\_161\_C2/C4\_Ol\_Y}}{\varepsilon_{rest\_161\_C2/C4\_Il\_Y}}$ ≤ 1,1).

At the end of stabilization period, the same tendency observed for F1 is also verified for measures taken in F2: outer layers (tangential direction) present predominant compressive strains while inner layers (longitudinal direction) present predominant tensile strains. Despite this tendency, obtained mean strains are very close to zero meaning that successive RH cycles do not causes cumulative strains.

Regarding Z direction, inner layers of F2 answer to RH cycles as expected, presenting shrinking/swelling movements for drying/wetting periods, respectively (Table (I) 2:13). The influence of moisture flow conditions is verified again at day 161, in which slow desorption process do not let C2 and C4 to reach compressive strains. Independent of moisture flow conditions, radial direction of inner layers seems to be affected by successive RH cycles specially regarding drying periods. It can be observed in Figure (I) 2:23 that last drying period present lower compressive strains for C1 and C3 while C2 and C4 present tensile strains. Decreases presented by C1 and C3 are of 66,6% and 30,7%, respectively. At the end of stabilization period inner layers tend to be under compressive strains for all test configurations (-0,013 ≤ $\varepsilon_{rest\_mean\_324\_C1-C4\_IL\_Z}$ ≤ -0,004).

Surprisingly, and similarly to what was observed for Y direction, outer layers tend to present predominant tensile strains at last RH cycle. Observing full field strains distribution for Z direction depicted in Table (I) 2:12, outer layers also present tensile and compressive strains depending on growth rings orientation. However, with the exception of C3, even during drying periods tensile strains tend to be predominant (0,006 ≤ $\varepsilon_{rest\_mean\_161\_C1/C2/C4\_OL\_Z}$ ≤ 0,011). Table (I) 2:12 presents C1 as example but, remaining graphs obtained for F2 in Z direction are depicted in Annex 1:5. Configurations that restricts moisture flow in tangential direction (inner layers) are the only configurations that present shrinking movements

between first wetting and last drying periods for outer layers. This may mean that sealing tangential direction changes the effect of crosswise lamination as the number of cycles increase.

Regarding wetting periods, the differences obtained between days 56 and 182 are not so substantial. Higher differences were registered for C3 which presents strains 29,4% lower at day 182. Successive RH cycles seems to reduce the range between drying and wetting periods and at the end of stabilization period strains tend to zero for all test configurations.

Strains measured in F3 are summarized in Table (I) 2:14 and Figure (I) 2:24 for all four configurations considering inner and outer layers separately. As expected, the differences observed between inner and outer layers are not so relevant in this CLT lateral face once the layer that present tangential movements (inner layer) is restricted by layers that shrinks/swells in longitudinal direction (outer layers). Observing full field strains distribution, regarding X direction, presented in Table (I) 2:15 this restriction is very obvious once the obtained patterns are much more homogeneous than those obtained for F2_Y (remaining graphs obtained for F3 in X direction are depicted in Annex 1:4). This way, graphs depicted in Figure (I) 2:24 are more in line with what was observed for inner layers from F2, presenting high tensile strains during last drying period, shrinking tendency during last wetting period and swelling tendency during stabilization period.

Despite the small differences observed for outer layers of F2, mean restrained strains measured in F2 and F3, for Y and X directions, either for inner or outer layers varies within the same range (-0,005 ≤ $\varepsilon_{rest\_mean\_Y/X}$ ≤ 0,009).

Evaluating results obtained for F3 in Z direction the tendency is inverted when comparing with results obtained for F2. Movements in radial direction are not restrained by crosswise lamination so, the range of compressive/tensile strains are just dependent on grain orientation. This way, ranges obtained for F2 (outer layers) and F3 (inner layers) are very close to each other: -0,016 ≤ $\varepsilon_{rest\_mean\_F2\_OL\_Z}$ ≤ 0,017 and -0,009 ≤ $\varepsilon_{rest\_mean\_F3\_IL\_Z}$ ≤ 0,015. Ranges obtained for F2 (inner layers) and F3 (outer layers) are slightly higher for F2: -0,026 ≤ $\varepsilon_{rest\_mean\_F2\_IL\_Z}$ ≤ 0,023 and -0,016 ≤ $\varepsilon_{rest\_mean\_F3\_OL\_Z}$ ≤ 0,018. However the behavior through the RH cycles is similar (Figure (I) 2:23 and Figure (I) 2:25).

Table (I) 2:13. Descriptive statistics of full-field restrained strains measured on specimens from group A_F2 in Z direction, for inner and outer layers, during first DIC mapping, before cut (BC) the specimens.

MEAN RESTRAINED STRAINS (ε_{rest_mean})										
MAXIMUM **MEAN** MINIMUM *COV*										
F2_Z DIRECTION										
	INNER LAYERS (IL)					**OUTER LAYERS (OL)**				
	DAY					**DAY**				
	35	**56**	**161**	**182**	**324**	**35**	**56**	**161**	**182**	**324**
C1	-0,016 **-0,024** -0,033 ***-0,15***	0,023 **0,014** 0,006 ***0,24***	-0,003 **-0,008** -0,015 ***-2,15***	0,020 **0,009** 0,002 ***0,43***	0,006 **-0,006** -0,014 ***-1,01***	-0,004 **-0,012** -0,023 ***-0,31***	0,018 **0,006** -0,007 ***-0,52***	0,031 **0,008** -0,009 ***0,84***	0,019 **0,007** -0,002 ***1,28***	0,008 **-0,001** -0,007 ***-0,14***
C2	-0,006 **-0,016** -0,023 ***-0,14***	0,035 **0,019** 0,001 ***0,35***	0,008 **0,001** -0,004 ***2,17***	0,030 **0,017** -0,010 ***0,29***	0,003 **-0,006** -0,014 ***-0,57***	0,005 **-0,007** -0,015 ***-0,48***	0,034 **0,008** -0,010 ***1,13***	0,035 **0,011** -0,007 ***0,62***	0,036 **0,008** -0,012 ***1,28***	0,010 **0,001** -0,007 ***-4,38***
C3	-0,016 **-0,026** -0,038 ***-0,14***	0,087 **0,023** -0,112 ***0,75***	-0,003 **-0,018** -0,038 ***-0,30***	0,077 **0,011** -0,105 ***1,42***	0,003 **-0,013** -0,026 ***-0,39***	-0,002 **-0,016** -0,027 ***-0,33***	0,031 **0,017** 0,004 ***0,38***	0,035 **-0,005** -0,020 ***-1,69***	0,027 **0,012** 0,001 ***0,48***	0,033 **0,000** -0,017 ***0,84***
C4	-0,004 **-0,010** -0,015 ***-0,18***	0,026 **0,016** 0,004 ***0,24***	0,019 **0,012** 0,003 ***0,17***	0,031 **0,020** 0,007 ***0,22***	0,003 **-0,004** -0,009 ***-0,45***	-0,002 **-0,010** -0,023 ***-0,38***	0,027 **0,012** 0,000 ***0,44***	0,016 **0,006** -0,007 ***0,82***	0,035 **0,016** 0,000 ***0,49***	0,023 **0,000** -0,007 ***0,02***

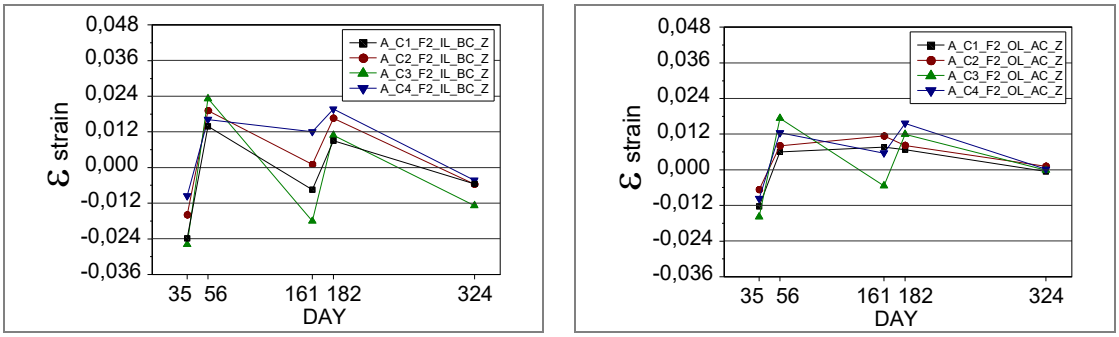

Figure (I) 2:23. Mean values of full-field restrained strains distribution measured on specimens from group A_F2 in Z direction, for inner and outer layers, during first DIC mapping.

Table (I) 2:14. Descriptive statistics of full-field restrained strains measured on specimens from group A_F3 in X direction, for inner and outer layers, during first DIC mapping.

MEAN RESTRAINED STRAINS (ε_{rest_mean})										
MAXIMUM **MEAN** MINIMUM *COV*										
F3_X DIRECTION										
	INNER LAYERS (IL)					**OUTER LAYERS (OL)**				
	DAY					**DAY**				
	35	**56**	**161**	**182**	**324**	**35**	**56**	**161**	**182**	**324**
C1	0,026	0,016	0,167	0,056	0,179	0,002	0,005	0,011	-0,001	0,015
	-0,002	**0,001**	**0,006**	**-0,002**	**-0,002**	**-0,002**	**-0,001**	**0,009**	**-0,003**	**0,001**
	-0,011	-0,084	-0,018	-0,009	-0,032	-0,006	-0,006	0,005	-0,007	-0,002
	-0,81	*9,74*	*2,31*	*-2,49*	*-9,33*	*-0,31*	*-1,59*	*0,05*	*-0,12*	*-3,39*
C2	0,015	0,059	0,025	0,018	0,015	0,002	0,002	0,010	0,003	0,006
	-0,002	**-0,001**	**0,009**	**-0,003**	**0,000**	**-0,002**	**-0,002**	**0,009**	**-0,004**	**0,001**
	-0,009	-0,082	-0,001	-0,044	-0,011	-0,006	-0,008	0,004	-0,011	-0,003
	-0,91	*-3,62*	*0,31*	*-2,06*	*56,92*	*-0,21*	*-0,47*	*0,06*	*-0,20*	*-1,95*
C3	0,212	0,012	0,307	0,027	0,207	0,005	0,015	0,025	0,012	0,019
	-0,004	**-0,001**	**0,002**	**-0,003**	**-0,003**	**-0,002**	**-0,002**	**0,008**	**-0,004**	**0,001**
	-0,028	-0,016	-0,033	-0,014	-0,028	-0,011	-0,014	-0,002	-0,014	-0,011
	-7,83	*-2,96*	*-10,83*	*-1,95*	*-12,43*	*-0,78*	*-1,55*	*0,47*	*-0,91*	*12,29*
C4	0,043	0,012	0,042	0,018	0,079	0,004	0,003	0,014	0,005	0,005
	-0,002	**-0,002**	**0,009**	**-0,003**	**0,000**	**-0,002**	**-0,002**	**0,009**	**-0,004**	**0,001**
	-0,014	-0,015	0,002	-0,016	-0,081	-0,007	-0,010	0,003	-0,013	-0,004
	-1,88	*-1,53*	*0,13*	*-1,21*	*12,51*	*-0,44*	*-0,61*	*0,07*	*-0,47*	*-3,07*

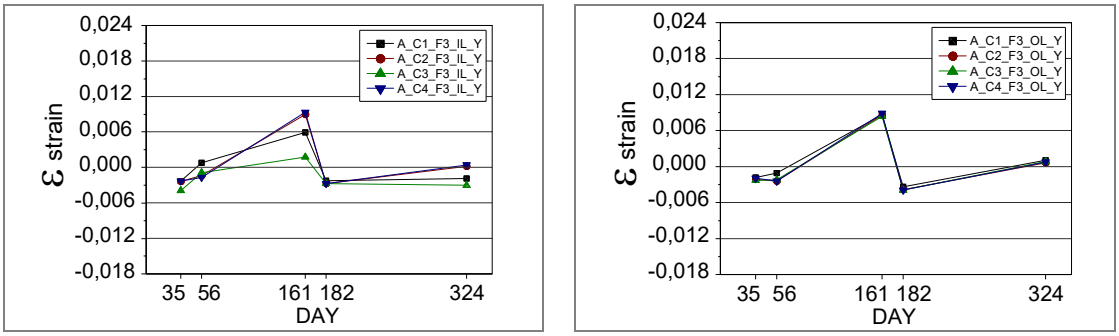

Figure (I) 2:24. Mean values of full-field restrained strains distribution measured on specimens from group A_F3 in X direction, for inner and outer layers, during first DIC mapping.

Table (I) 2:15. Typical behavior (C1) of full field restrained strain distribution in X and Z directions and in shear observed for group A_F3, before cut (BC) the specimens.

RESTRAINED STRAINS FOR A_F3_C1 (ε_{rest})					
TEST DAY RH [%]	**X**	**Z**	**SHEAR**	**PICTURES**	**SCALE**
DAY 35 [RH=30%]	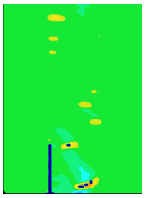	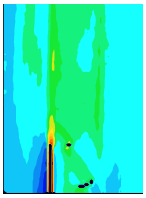	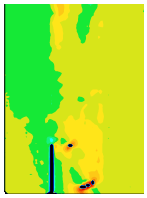	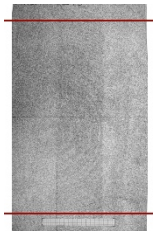	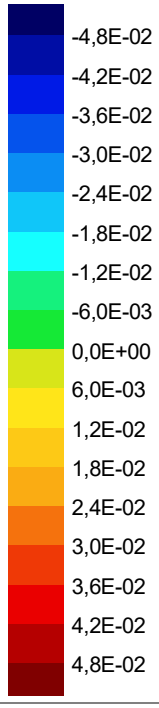
DAY 56 [RH=90%]	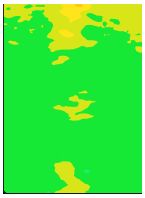		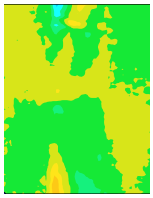		
DAY 161 [RH=30%]	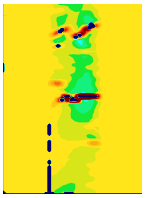	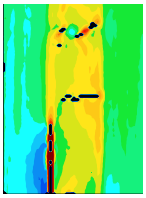	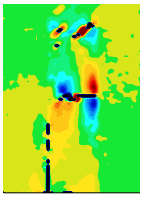	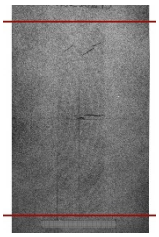	
DAY 182 [RH=90%]	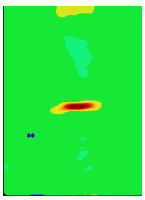		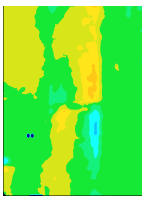	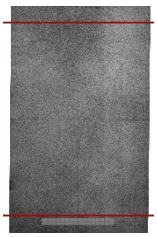	
DAY 324 [RH=65%]	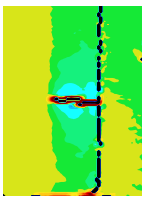	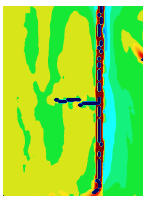	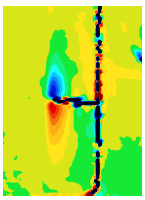		

Note: Red lines at pictures represent the end of ROI considered by DIC measurements.

Table (I) 2:16. Descriptive statistics of full-field restrained strains measured on specimens from group A_F3 in Z direction, for inner and outer layers, during first DIC mapping.

MEAN RESTRAINED STRAINS (ε_{rest_mean})										
MAXIMUM **MEAN** MINIMUM *COV*										
F3_Z DIRECTION										
	INNER LAYERS (IL)					**OUTER LAYERS (OL)**				
	DAY					**DAY**				
	35	**56**	**161**	**182**	**324**	**35**	**56**	**161**	**182**	**324**
C1	0,002 **-0,003** -0,007 ***-0,31***	0,017 **0,006** -0,041 ***4,11***	0,029 **0,005** -0,011 ***0,76***	0,012 **0,006** 0,000 ***0,43***	0,029 **0,001** -0,016 ***3,68***	-0,005 **-0,009** -0,015 ***-0,23***	0,012 **0,007** 0,001 ***-1,06***	0,000 **-0,006** -0,018 ***-0,87***	0,022 **0,012** 0,004 ***0,32***	0,008 **-0,002** -0,011 ***1,59***
C2	0,002 **-0,005** -0,012 ***-0,38***	0,029 **0,004** -0,030 ***4,22***	0,029 **0,010** -0,003 ***0,28***	0,024 **0,007** -0,013 ***0,98***	0,016 **0,001** -0,009 ***2,25***	-0,012 **-0,016** -0,020 ***-0,10***	0,028 **0,019** 0,009 ***0,20***	0,003 **-0,004** -0,010 ***-0,53***	0,028 **0,016** 0,009 ***0,18***	0,000 **-0,004** -0,009 ***-0,44***
C3	0,058 **-0,009** -0,019 ***-0,81***	0,025 **0,015** 0,002 ***0,24***	0,026 **0,000** -0,020 ***-0,32***	0,023 **0,010** -0,005 ***0,36***	0,029 **0,000** -0,062 ***1,93***	-0,012 **-0,016** -0,021 ***-0,11***	0,043 **0,014** -0,008 ***0,71***	0,000 **-0,010** -0,018 ***-0,25***	0,034 **0,010** -0,015 ***1,08***	0,009 **-0,004** -0,015 ***0,21***
C4	0,002 **-0,003** -0,007 ***-0,41***	0,014 **0,005** -0,006 ***0,74***	0,017 **0,013** 0,008 ***0,07***	0,030 **0,007** -0,009 ***0,69***	0,008 **0,002** -0,004 ***0,47***	-0,003 **-0,009** -0,015 ***-0,28***	0,023 **0,013** 0,005 ***0,25***	0,015 **0,007** -0,002 ***0,54***	0,033 **0,018** 0,001 ***0,28***	0,005 **0,000** -0,005 ***0,43***

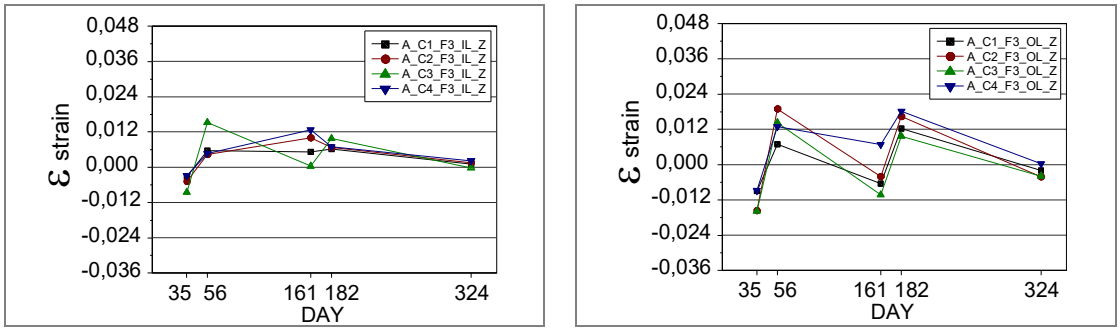

Figure (I) 2:25. Mean values of full-field restrained strains distribution measured on specimens from group A_F3 in Z direction, for inner and outer layers, during first DIC mapping.

2.4.1.3 Group B (CLT slices with dimensions of 160x93x24 mm)

Restrained strains of specimens from group B were evaluated considering measurements taken for Y (tangential) and Z (radial) directions. Table (I) 2:17 and Table (I) 2:18 present descriptive statistics for inner and outer layers for all four test configurations and all five test days, for Y and Z directions, respectively. Figure (I) 2:26 and Figure (I) 2:27 depicts mean restrained strains presented in Table (I) 2:17 and Table (I) 2:18.

Regarding mean values obtained for Y direction and taking C1 as reference, C2 and C4 present lower strains for measurements taken on outer layers. This fact may be directly related with moisture flow conditions, once both configurations block moisture flow on longitudinal direction. The C4 also restrain moisture flow on tangential direction, presenting lower restrained strains during first and last RH cycles. The C2 just registered lower values for last drying and wetting periods. The higher differences were observed for last drying period, in which C2 and C4 present mean restrained strains that are 46% and 54% lower than value registered for C1 ($\varepsilon_{rest\_OL\_161\_Y\_C1\_mean}$ = -0,013), respectively. Differently, restrained strains registered for inner layers show that moisture flow conditions do not affect substantially timber movements in Y direction. It was observed that only one value is offbeat: the C4, which is the configuration with the larger sealed area, presents a mean restrained tensile strain that is 25% lower than value obtained for C1 at first wetting period ($\varepsilon_{rest\_IL\_56\_Y\_C1\_mean}$ = -0,012).

Taking days 35 and 56 as reference, higher decreases are again linked to C2 and C4. Inner layers present decreases of 67% and 50% for drying periods and 100% for wetting periods, while outer layers presented decreases of 12,5% and 0% for drying periods and 70% and 71% for wetting periods, respectively.

Evaluating the effect of successive RH cycles, it was observed a different behavior between results obtained for group B and for group A_F2. Results obtained for group A_F2 at day 324, present compressive restrained strains for outer layers and tensile strains for inner layers. The results obtained for group B present predominant restrained tensile strains either for inner layers or outer layers. This difference must be directly related with the size of test specimens. The specimens from group B are considerably smaller than those from group A, resulting in more pronounced effects of successive RH cycles.

Analyzing mean values obtained for Z direction it was observed that, regarding outer layers, the tendency is similar to that observed for Y direction. Taking C1 as reference, C2 and C4, presented lower restrained strains for all test days. Higher differences were observed for first and last drying periods: in day 35

configurations C2 and C4 presented restrained strains that are 38% and 33% lower than value registered for C1 ($\varepsilon_{rest\_OL\_35\_Z\_C1\_mean}$ = -0,021), respectively, while in day 161 same configurations presented restrained strains 36% and 42% lower than value registered for C1 ($\varepsilon_{rest\_OL\_161\_Z\_C1\_mean}$ = -0,019, respectively.

Table (I) 2:17. Descriptive statistics of full-field restrained strains measured on specimens from group B in Y direction, for inner and outer layers, during first DIC mapping.

MEAN RESTRAINED STRAINS (ε_{rest_mean})										
MAXIMUM **MEAN** MINIMUM ***COV***										
Y DIRECTION										
	INNER LAYERS (IL)					**OUTER LAYERS (OL)**				
	DAY					**DAY**				
	35	**56**	**161**	**182**	**324**	**35**	**56**	**161**	**182**	**324**
C1	0,001	0,016	0,007	0,004	0,013	0,022	0,041	0,335	0,022	0,103
	-0,002	**0,012**	**-0,002**	**0,001**	**0,009**	**-0,009**	**0,021**	**-0,013**	**0,007**	**0,005**
	-0,006	0,009	-0,006	-0,002	0,000	-0,023	-0,027	-0,039	-0,012	-0,015
	-0,21	***0,09***	***-0,34***	***0,80***	***0,08***	***-0,57***	***0,40***	***-1,19***	***0,84***	***1,17***
C2	0,012	0,018	0,015	0,004	0,019	0,030	0,042	0,010	0,037	0,018
	-0,003	**0,012**	**-0,001**	**0,000**	**0,009**	**-0,008**	**0,020**	**-0,007**	**0,006**	**0,006**
	-0,012	0,005	-0,018	-0,002	0,006	-0,021	0,002	-0,023	-0,007	-0,008
	-0,36	***0,11***	***-0,49***	***4,40***	***0,07***	***-0,46***	***0,37***	***-0,57***	***0,93***	***0,38***
C3	0,002	0,018	0,005	0,008	0,023	0,057	0,041	0,060	0,031	0,050
	-0,003	**0,012**	**-0,002**	**0,000**	**0,009**	**-0,010**	**0,021**	**-0,012**	**0,008**	**0,002**
	-0,007	0,005	-0,010	-0,006	-0,002	-0,023	0,004	-0,032	-0,018	-0,014
	-0,20	***0,10***	***-0,50***	***2,11***	***0,12***	***-0,82***	***0,40***	***-0,66***	***0,91***	***0,70***
C4	0,006	0,018	0,002	0,006	0,016	0,004	0,036	0,006	0,018	0,014
	-0,002	**0,009**	**-0,001**	**0,000**	**0,009**	**-0,006**	**0,017**	**-0,006**	**0,005**	**0,006**
	-0,009	0,002	-0,005	-0,004	0,003	-0,022	-0,016	-0,025	-0,007	-0,010
	-0,34	***0,15***	***-0,34***	***1,40***	***0,12***	***-0,53***	***0,45***	***-0,61***	***0,96***	***0,52***

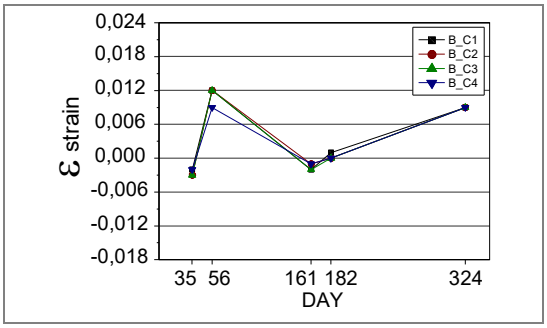

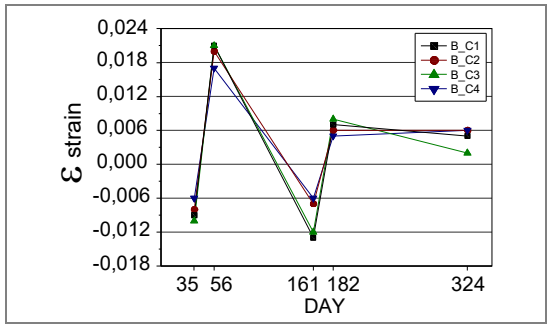

Figure (I) 2:26. Mean values of full-field restrained strains distribution measured on specimens from group B in Y direction, for inner and outer layers, during first DIC mapping.

Table (I) 2:18. Descriptive statistics of full-field restrained strains measured on specimens from group B in Z direction, for inner and outer layers, during first DIC mapping.

	RESTRAINED STRAIN (ε_{rest})									
	MAXIMUM **MEAN** MINIMUM *COV*									
	Z DIRECTION									
	INNER LAYERS					**OUTER LAYERS**				
	DAY					**DAY**				
	35	**56**	**161**	**182**	**324**	**35**	**56**	**161**	**182**	**324**
C1	-0,014 **-0,024** -0,037 ***-0,17***	0,050 **0,041** 0,027 ***0,11***	-0,012 **-0,019** -0,032 ***-0,13***	0,025 **0,014** 0,006 ***0,21***	0,013 **0,007** 0,001 ***0,23***	-0,004 **-0,021** -0,042 ***-0,33***	0,082 **0,043** 0,018 ***0,27***	0,023 **-0,019** -0,055 ***-0,42***	0,060 **0,024** 0,005 ***0,43***	0,024 **0,007** -0,006 ***0,60***
C2	-0,006 **-0,017** -0,028 ***-0,16***	0,047 **0,028** 0,014 ***0,12***	-0,006 **-0,019** -0,037 ***-0,22***	0,035 **0,023** 0,008 ***0,17***	0,026 **0,012** 0,000 ***0,35***	-0,006 **-0,013** -0,028 ***-0,30***	0,073 **0,038** 0,014 ***0,28***	0,000 **-0,012** -0,029 ***-0,38***	0,048 **0,020** 0,001 ***0,42***	0,048 **0,014** 0,001 ***0,37***
C3	-0,017 **-0,025** -0,034 ***-0,18***	0,044 **0,029** 0,000 ***0,15***	-0,007 **-0,024** -0,037 ***-0,13***	0,039 **0,023** 0,011 ***0,11***	0,609 **0,008** -0,005 ***2,35***	-0,01 **-0,02** -0,04 ***-0,30***	0,08 **0,04** 0,02 ***0,28***	0,01 **-0,02** -0,05 ***-0,44***	0,07 **0,03** 0,00 ***0,40***	0,04 **0,01** -0,01 ***0,65***
C4	-0,006 **-0,009** -0,015 ***-0,12***	0,052 **0,033** 0,014 ***0,12***	-0,002 **-0,007** -0,012 ***-0,24***	0,026 **0,017** 0,006 ***0,17***	0,012 **0,007** 0,000 ***0,25***	-0,004 **-0,014** -0,026 ***-0,27***	0,066 **0,034** 0,012 ***0,26***	-0,001 **-0,011** -0,037 ***-0,36***	0,041 **0,020** 0,003 ***0,35***	0,026 **0,007** -0,001 ***0,38***

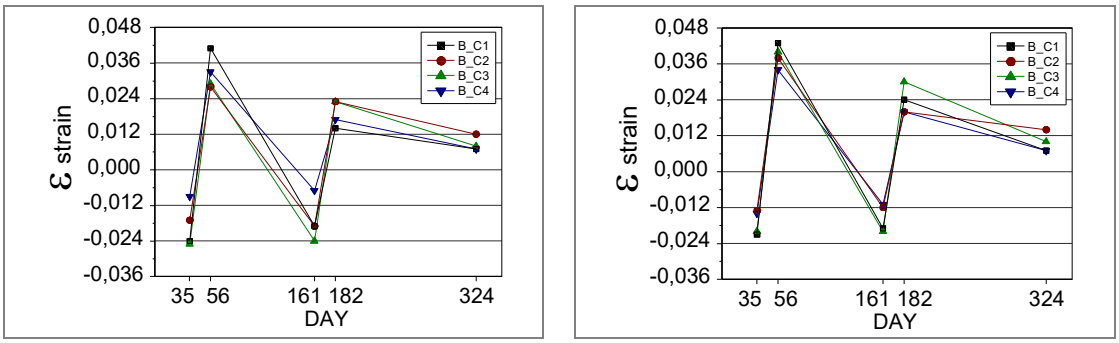

Figure (I) 2:27. Mean values of full-field restrained strains distribution measured on specimens from group B in Z direction, for inner and outer layers, during first DIC mapping.

The results obtained for inner layers presented substantial differences when comparing C1 with other configurations. In one hand, C4 presented restrained strains that are 63%, 20% and 63% lower than values registered for C1 in days 35, 56 and 161, respectively. In the other hand, results obtained for day 182 stand out, presenting higher restrained strains when comparing with value registered for C1 ($\varepsilon_{rest\_IL\_182\_Z\_mean}$ = -0,014): 64% for C2 and C3 and 21% for C4.

Taking days 35 and 56 as reference, it was observed that restrained compressive and tensile strains tend to decrease at last drying/wetting periods for all tested configurations either for outer and inner layers. However, differently to what was observed for Y direction, influence of moisture flow conditions is not so obvious, once higher decreases were registered for configurations C1 and C4, instead of C2 and C4. Differences registered between first and last wetting periods were the highest, however lower than those observed for Y direction. Regarding outer layers, C2 and C4 still suggest that sealing longitudinal direction delays the absorption/desorption process, presenting decreases of restrained tensile strains of 47% and 41%. However, inexplicably, C1 stands out presenting decreases of restrained tensile strains of 44% and 65%, for outer and inner layers, respectively. Finally, and similarly to results obtained for Y direction, at the end of stabilization period tensile strains are predominant either for inner or outer layers.

Table (I) 2:19 presents the ratio between restrained strains obtained for Y and Z directions $\left(\Delta = \frac{Z_{mean}}{Y_{mean}}\right)$ for all tested configurations at all test days, for outer and inner layers. Considering outer layers, obtained ratios represent the relation between strains measured for radial and tangential $\left(\Delta_{OL} = \frac{Z_{mean\_OL}}{Y_{mean\_OL}} = \frac{R}{T}\right)$ directions and for inner layers obtained ratios represent the relation between radial and longitudinal $\left(\Delta_{IL} = \frac{Z_{mean\_IL}}{Y_{mean\_IL}} = \frac{R}{L}\right)$ directions. Table (I) 2:19 also presents the relation between adjacent layers by the ratio between tangential and longitudinal directions $\left(\Delta_{Y} = \frac{Y_{mean\_OL}}{Y_{mean\_IL}} = \frac{T}{L}\right)$.

As expected, Δ_{OL} (R/T) presented the lowest values, once it is relating the directions with higher moisture movements. Results obtained for outer layers suggest that $\boldsymbol{\Delta_{OL}}$ is affected by successive RH cycles and not affected, at least not clearly, by moisture flow conditions. Considering all four configurations and days 35, 56 and 161, $\boldsymbol{\Delta_{OL}}$ is in a range of 1.5 - 2.3, while for day 182 a higher difference between radial and tangential directions is verified, obtaining ratios that are around 3.3. At the end of stabilization period C3 stands out with a ratio of 4.4 while the remaining configurations present a range of 1.3 - 2.4.

Similarly, the results obtained for $\boldsymbol{\Delta_{IL}}$ (R/L) also suggest that just successive RH cycles influence the relation between radial and longitudinal directions. Lower ratios were registered for days 35, 56 and 161: at days 35 and 161 $\boldsymbol{\Delta_{IL}}$ is in a range of 3,9 – 13,4, while at day 56 $\boldsymbol{\Delta_{IL}}$ is in a range of 2,4 – 3,8. Day

182 present the higher ratios in a wide range of 24,7-179,6. At the end of stabilization period, Δ_{IL} tend to decrease presenting a range of 0,7 – 1,3.

Regarding the relation between tangential and longitudinal directions (Δ_Y) the tendency is exactly the same observed for Δ_{OL} and Δ_{IL}, what means that Δ_Y (T/L) tends to increase from first to last RH cycle. Days 35 and 161 registered ranges of 2,4 – 3,9 and 4,4 – 7,3, respectively. Day 56 registered a range of 1,7 – 1,9, while day 182 stands out with a range of 12,3 – 50,5. At the end of stabilization period, Δ_Y tend to decrease presenting a range of 0,2 – 0,7.

As already mentioned, some possible influence of moisture flow conditions on analyzed ratios is not clear. It must be referred that Δ_{IL} and Δ_Y presented values at day 182 for C2 and C3 that are considerably higher than those observed for remaining configurations. However, the reason for this phenomenon is not clear, once what these two configurations have in common is sealing the radial direction.

Table (I) 2:20 exhibit the color fill graphs of typical behavior of full field restrained strains registered distribution for Y and Z direction and shear, considering C1 and all test days. C1 is presented as example and remaining full field graphs can be observed in Annex 1:6 and Annex 1:7.

Analyzing color fill graphs, it is evident that restrained strains are higher for radial direction (Z), and outer and inner layers are clearly identified. Regarding Y direction, lower compressive/tensile strains are observed for inner layers, fact that clearly restricts the movements of outer layers, especially closer to the outer borders of specimens. Due to the location and orientation of growth rings (see figure at left in Table (I) 2:20), higher strains are located at central part of outer layers. Furthermore, the effects of successive RH cycles are visible at day 182, in which restrained strains observed for middle layers suggest timber shrinkage rather than the expected swelling.

Regarding Z direction, outer and middle layers are even easily identified because cross lamination does not influence the timber movements in radial direction. Also due to the location and position of growth rings, but differently of what was observed for Y direction, higher compressive/tensile strains are located at the outer parts of outer layers. Here, the influence of successive RH cycles is also verified at day 182, in which tensile strains are lower than those observed for day 56.

Mean released strains measured during second DIC mapping are summarized at Table (I) 2:21 and depicted in Figure (I) 2:28. Obtained mean values considered a central part of each independent layer (an area of around 10 x 107 subsets) in order to avoid any possible effect of sawing action. This DIC map

just considered strains measured in Y direction once the goal was to quantify strains resulted from separation of different layers.

According to mean values presented in Table (I) 2:21, inner layers do not exhibit a relation between drying/wetting periods and compressive/tensile strains. Tensile strains are predominant, which means that independent of moisture content levels CLT inner layers tend to swell after being released. Furthermore, different moisture flow conditions do not affect the results. Obtained released strains are close to zero for majority of test days, however high tensile released strains are registered at last drying period (0,002 ≤ $\varepsilon_{rel\_IL\_161\_Y\_mean}$ ≤ 0,003). Contrary to what was observed for group A_F1, successive RH cycles lead to an increase of released strains, especially during drying periods. C4 presents high tensile strains at day 56 probably due to its small area open to moisture flow ($\varepsilon_{rel\_C4\_IL\_56\_Y\_mean}$ = 0,002). Taking day 0 as reference ($\varepsilon_{rel\_C1\_IL\_0\_Y\_mean}$ = 0,000), it can be concluded that successive RH cycles do not causes cumulative moisture induced strains, once -0,001 ≤ $\varepsilon_{rel\_IL\_324\_Y\_mean}$ ≤ 0,000.

Table (I) 2:19. Ratio between restrained strains obtained for Y and Z directions for inner and outer layers, during first DIC mapping of group B.

RATIO	DAY	CONFIGURATIONS			
		C1	C2	C3	C4
$\Delta = \left(\frac{Z_{mean}}{Y_{mean}}\right)$ $\Delta_{IL} = \left(\frac{R}{L}\right)$	35	10,6	5,5	8,6	3,9
	56	3,5	2,4	2,4	3,8
	161	10,6	13,3	13,4	5,5
	182	24,7	179,6	65,0	38,8
	324	0,7	1,3	0,9	0,8
$\Delta_{OL} = \left(\frac{R}{T}\right)$	35	2,3	1,8	2,0	2,1
	56	2,0	1,9	2,0	2,0
	161	1,5	1,8	1,7	1,8
	182	3,3	3,2	3,2	3,7
	324	1,4	2,4	4,4	1,3
$\Delta = \left(\frac{Y_{mean\_OL}}{Y_{mean\_IL}}\right)$ $\Delta_Y = \left(\frac{T}{L}\right)$	35	3,9	2,4	3,5	2,7
	56	1,8	1,7	1,8	1,9
	161	7,3	4,7	6,8	4,4
	182	12,8	50,5	22,6	12,3
	324	0,5	0,7	0,2	0,6

Table (I) 2:20. Typical behavior (C1) of full field restrained strain distribution in Y and Z directions and in shear observed group B, before cut (BC) the specimens.

RESTRAINED STRAINS FOR C1 (ε_{rest})					
TEST DAY RH [%]	**Y**	**Z**	**SHEAR**	**PICTURES**	**SCALE**
DAY 35 [RH=30%]		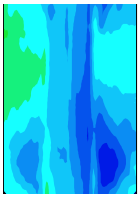	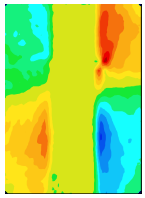	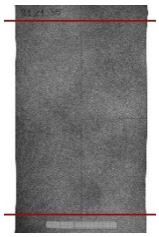	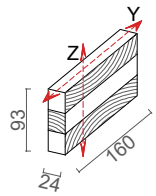
DAY 56 [RH=90%]	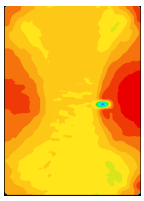	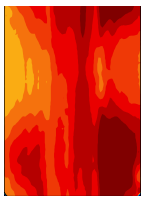	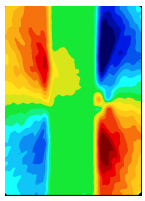	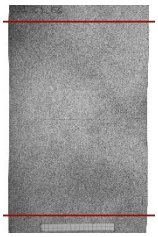	
DAY 161 [RH=30%]	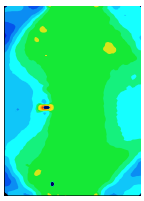	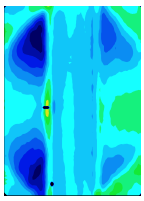	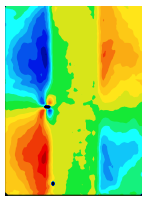		
DAY 182 [RH=90%]	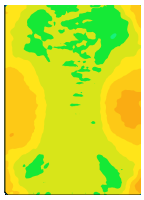	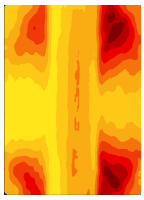	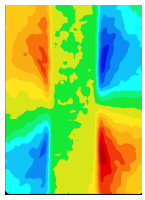	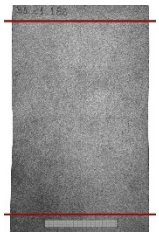	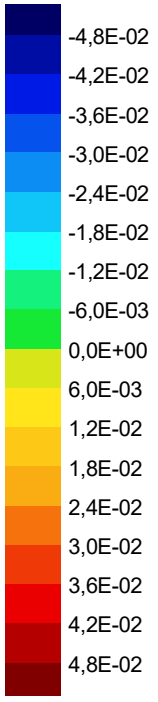
DAY 324 [RH=65%]	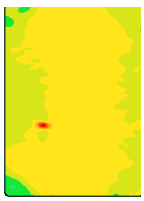		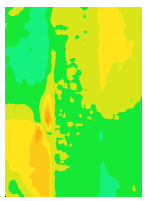	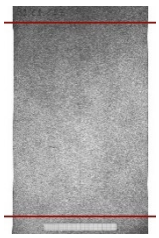	

Note: Red lines at pictures represent the end of ROI considered by DIC measurements.
(dimenstions are in mm)

Regarding outer layers, and similarly to tendency observed for inner layers, the influence of different moisture flow conditions was not observed. However, contrary to what was observed for inner layers, there is a relation between compressive/tensile strains and drying/wetting periods, especially during first RH cycle. Compressive released strains registered at day 35 stand out presenting values between -0,002 and -0,003 while last drying period present values between 0,000 and 0,001. This behavior is more in line of what was observed for group A_F1, in which successive RH cycles suggest the tendency of strain reduction as the number of cycles increase. This way, it seems that during first RH cycle inner layers restrict moisture movements of outer layers, but during last RH cycle it is not observed. Taking day 0 as reference ($\varepsilon_{rel\_C1\_OL\_0\_Y\_mean}$ = 0,001), it can be concluded that reduced tensile strains observed at day 0 become into substantial compressive strains after successive RH cycles ($\varepsilon_{rel\_OL\_324\_Y\_mean}$ = -0,002. This value was considered significant once they are very close to those observed for first drying period.

Typical behavior of full field released strain distribution in Y direction for second DIC map is depicted at Table (I) 2:22 (remaining graphs of released strains measured for specimens of group B can be seen in Annex 1:8). Analyzing color fill graphs, it is possible to observe that just at last RH cycle, the position and orientation of timber growth rings of outer layers is noticeable. At day 161 compressive strains are located at the side of inner layers while tensile strains are located on the outer part, but the opposite tendency is observed at day 182. Furthermore, regarding inner layers, tensile strains are evenly distributed at day 161 while, regarding compressive strains, the most uniform patterns are observed at days 35 and 324, either for outer or inner layers.

2.4.1.4 Correlation between dynamic and static Modulus of Elasticity

Modulus of elasticity (MoE) is a fundamental parameter to calculate internal stresses (σ) presented either in CLT slices or in CTL different layers. So, due to the huge number of test specimens, MoE was measured with a dynamic method (E_{dyn}) and then converted to a static MoE (E_{sta}). To obtain the relation between (E_{dyn}) and (E_{sta}) a group of 20 CLT slices were static and dynamically tested. First the entire CLT slice were tested and then different layers were tested separately, perpendicular and parallel to the grain for outer and inner layers, respectively. This way, two different geometries were tested, namely CLT slices (170 x 24 x 93 mm) and CLT individual layers (170 x 24 x 29 mm).

Table (I) 2:21. Descriptive statistics of full-field released strains measured on specimens from group B in Y direction, for inner and outer layers, during second DIC mapping.

	RELEASED STRAIN (ε_{rel})											
	MAXIMUM **MEAN** MINIMUM *COV*											
	Y DIRECTION											
	INNER LAYERS						**OUTER LAYERS**					
	DAY						**DAY**					
	0	**35**	**56**	**161**	**182**	**324**	**0**	**35**	**56**	**161**	**182**	**324**
C1	0,001 - **0,000** -0,003 ***-1,10***	0,002 - **0,001** -0,004 ***-0,58***	0,002 **0,000** -0,002 ***-0,29***	0,005 **0,002** 0,000 ***0,15***	0,002 **0,000** -0,002 ***-1,89***	0,002 - **0,001** -0,002 ***-0,63***	0,011 - **0,001** -0,005 ***6,61***	0,001 - **0,003** -0,008 ***-0,50***	0,004 **0,001** -0,002 ***0,76***	0,014 **0,000** -0,310 ***-2,19***	0,003 **0,000** -0,003 ***2,05***	0,002 - **0,002** -0,009 ***-0,56***
C2		0,001 **0,000** -0,011 ***-1,70***	0,003 **0,000** -0,002 ***11,79***	0,010 **0,002** -0,001 ***0,24***	0,002 **0,000** -0,002 ***-0,76***	0,004 - **0,001** -0,005 ***-0,64***		0,003 - **0,003** -0,009 ***-0,60***	0,004 **0,001** -0,002 ***0,57***	0,005 **0,000** -0,005 ***6,62***	0,004 **0,001** -0,016 ***0,79***	0,004 - **0,002** -0,009 ***-0,60***
C3		0,001 **0,000** -0,002 ***-1,67***	0,003 **0,000** -0,002 ***1,36***	0,005 **0,003** 0,000 ***0,15***	0,004 **0,000** -0,003 ***2,78***	0,002 **0,000** -0,003 ***-1,26***		0,002 - **0,002** -0,033 ***-1,13***	0,005 **0,000** -0,004 ***2,48***	0,007 **0,001** -0,029 ***1,72***	0,012 - **0,001** -0,007 ***-0,97***	0,014 - **0,002** -0,032 ***-0,78***
C4		0,003 - **0,001** -0,005 ***-0,92***	0,007 **0,002** -0,003 ***1,35***	0,005 **0,003** 0,000 ***0,14***	0,003 **0,000** -0,004 ***8,09***	0,001 **0,000** -0,003 ***-0,81***		0,002 - **0,003** -0,008 ***-0,59***	0,007 **0,003** -0,003 ***0,77***	0,008 **0,000** -0,004 ***10,53***	0,003 **0,000** -0,004 ***-7,68***	0,005 - **0,002** -0,006 ***-0,55***

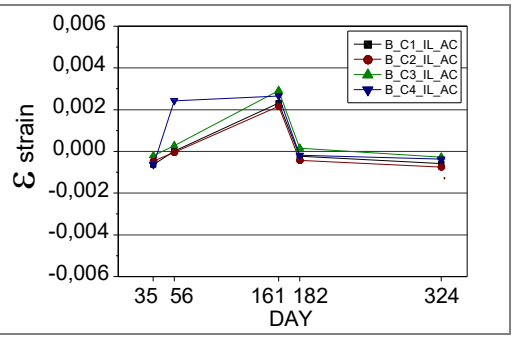

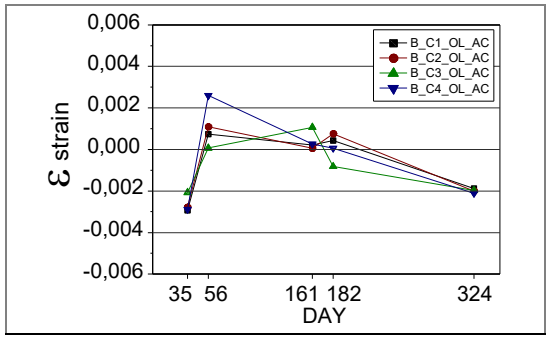

Figure (I) 2:28. Mean values of full-field released strains distribution measured on specimens from group B in Y direction, for inner and outer layers, during second DIC mapping, after cut specimens (AC).

Dynamic MoE was defined by means of ultrasound tests using a Pundit Lab equipment from Proceq with 150 kHz frequency transmission transducers. Ultrasound equipment measures the velocity of sound propagation (V_p), which can be related with E_{dyn} if the density (ρ) of timber element is known (H. S. Sousa et al., 2014). Equation (2:4) shows how E_{dyn} was obtained.

$$E_{dyn} = v_p{}^2 \cdot \rho \quad (2:4)$$

E_{dyn} Dynamic modulus of elasticity, in MPa;

$\mathrm{v_p}$ Velocity of propagation, in m/s;

ρ Wood density, in kg/m³.

As depicted in Figure (I) 2:29 and Figure (I) 2:30, ultrasound acquisitions in CLT slices considered four different measurements: crossing all three layers at the same time (cross 1 & cross 2), crossing two layers per time (cross 3 & cross 4), measuring one layer per time when they are still glued together (glued A+B+C) and measuring one layer per time after separate layers (cut A+B+C). This procedure aimed to guarantee the best correlation between dynamic and static MoE.

Due to reduced dimensions of test specimens, E_{sta} was obtained by compressive. Also due to reduced dimensions of test specimens, both test setup and procedure (Table (I) 2:23) do not follow strictly any standard. However, parameters like h_0 (96mm) and test time (180 +/- 60 s) were based on recommendations present in EN 408: 2003. Specimens were compressed by a load cell integrated on a hydraulic system, and a different test procedure was defined for each specimen configuration considering specimen dimensions as well as orientation of timber fibers (Table (I) 2:23).

Correlation between E_{dyn} and E_{sta} were made by means of linear fittings, but previously some outliers had to be excluded from the data set. The definition of outliers were made by the analysis of results obtained by the ratio $\frac{E_{sta}}{E_{dyn}}$. Results obtained for this relation are detailed in Annex 1:9. Nevertheless, sampling is still between 17 and 37 specimens per each group of tested specimens. Descriptive statistics of values obtained for E_{dyn} and E_{sta} are presented in Table (I) 2:24, while linear obtained fittings are depicted in Figure (I) 2:29 and Figure (I) 2:30.

Table (I) 2:22. Typical behavior (C1) of full field released strain distribution in Y direction observed for group B, after cut (AC) the specimens.

Y DIRECTION					
TEST DAY RH [%]	C1	PICTURES	C3	PICTURES	SCALE
DAY 0 [RH=65%]	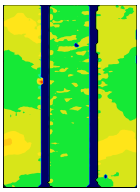	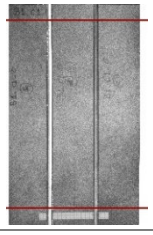			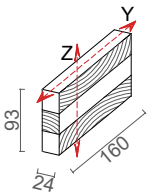
DAY 35 [RH=30%]		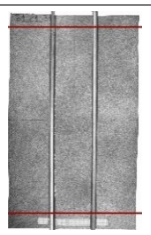	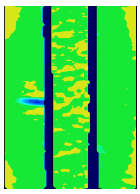	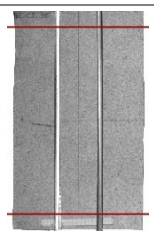	
DAY 56 [RH=90%]	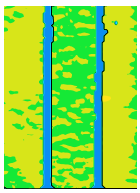	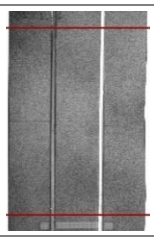	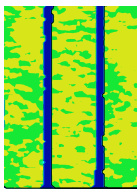	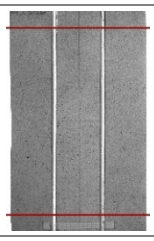	
DAY 161 [RH=30%]			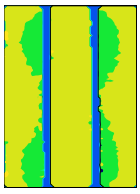		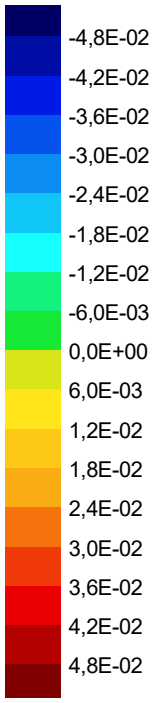
DAY 182 [RH=90%]	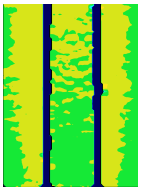	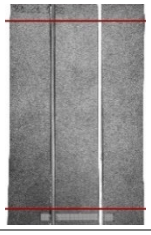	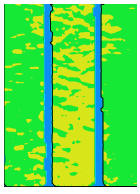		
DAY 324 [RH=65%]	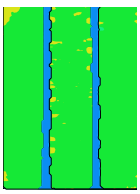		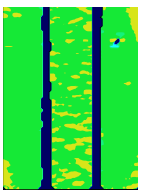	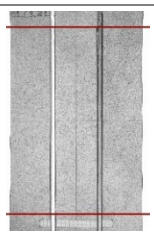	

Note: Red lines at pictures represent the end of ROI considered by DIC measurements.
(dimentions are in mm)

Table (I) 2:23. Test procedures for determination of E_{sta} for CLT slices and individual CLT layers.

SPECIMEN	MAXIMUM LOAD [KN]	VELOCITY [KN/S]	GRAPH
CLT SLICE	3,0	0,10	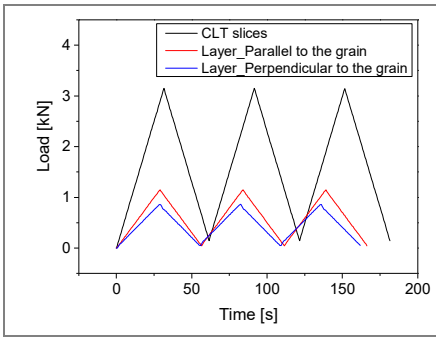
CLT LAYER – PERPENDICULAR TO THE GRAIN	0,8	0,03	
CLT LAYER – PARALLEL TO THE GRAIN	1,1	0,04	

Analyzing E_{dyn} obtained for CLT slices, it is obvious that higher dynamic modulus of elasticity are related with higher propagation velocities and consequently related with measurements that included longitudinal direction (inner layers), namely measurements taken for three layers individually either before cutting (mean = 16043 MPa; CoV=0,47) or after cutting (mean=27342 MPa; CoV=0,23). However, due to high CoV values obtained for measurements taken with the three layers still glued together ($0{,}38 \leq \text{CoV} \leq 0{,}47$), obtained linear fittings do not exhibit a good correlation with R^2 values below 0,40 (Figure (I) 2:29). So, best correlation was obtained through the mean obtained by measurements taken from separated layers individually, which presents a reduced CoV value that is closer to that obtained by static tests ($CoV_{dyn} = 0{,}23$ and $CoV_{sta} = 0{,}25$). This way, relationship between E_{dyn} and E_{sta} was determined as $E_{sta} = 0{,}15 \cdot E_{dyn} + 497$ with a $R^2 = 0{,}64$.

Regarding correlations performed with CLT individual layers, both linear fittings obtained R^2 values above 0,51 suggesting relations between E_{dyn} and E_{sta} that are acceptable: $E_{sta} = 0{,}15 \cdot E_{dyn} + 29{,}8$ with a $R^2 = 0{,}51$ and : $E_{sta} = 0{,}12 \cdot E_{dyn} + 2532$ with a $R^2 = 0{,}74$, for outer and inner layers, respectively (Figure (I) 2:30).

2.4.1.5 Calculation of internal stresses

As described in section 2.3.1 either group A or B were used to obtain a second DIC map. This was done immediately after cutting specimens into slices (for group A) or after separation of different layers (for group B). Strains obtained with these measurements quantify the restriction of moisture movements forced by cross-lamination. Similarly to work developed by Jönsson (2004), Gereke (2009) and Angst & Malo (2012b), internal stresses were calculated by the relation $\sigma_{mean} = \varepsilon_{mean} \cdot E_{(u)}$, in which $E_{(u)}$ is

the modulus of elasticity as a function of moisture content present on specimens at measuring time. It is important to mention that just E_{dyn} was taken in function of moisture content, while E_{sta} was obtained just for specimens with a mean moisture content of 14,0% (CoV=0,03).

Table (I) 2:24. Descriptive statistics of obtained E_{dyn} and E_{sta}.

TEST CONFIGURATIONS		SAMPLE	E_{dyn} (MPa)	E_{sta} (MPa)
			MAXIMUM	
			MEAN	
			MINIMUM	
			COV	
CLT SLICE	CROSS 1 & CROSS 2 (MEAN)	18	2199	6388
			1161	**4410**
			522	2639
			0,44	*0,26*
	CROSS 3 & CROSS 4 (MEAN)	17	23693	6388
			14966	**4552**
			3969	2639
			0,38	*0,25*
	GLUED A+B+C (MEAN)	20	31302	6388
			16043	**4425**
			5821	2639
			0,47	*0,25*
	CUT A+B+C (MEAN)	17	38364	6388
			27342	**4540**
			17763	2639
			0,23	*0,25*
CLT LAYERS	A & C (PERPENDICULAR TO THE GRAIN)	37	2636	423
			1179	**204**
			842	108
			0,26	*0,30*
	B (PARALLEL TO THE GRAIN)	20	112802	16442
			74562	**11545**
			37816	6789
			0,29	*0,26*

Mean stresses were calculated similarly to mean strains, considering areas of 4 x 74 subsets per slice and 10 x 107 subsets per layer, for group A and B, respectively. Internal stresses of group A were calculated considering the modulus of elasticity of the entire slice, once three layers are still glued together, in which $E_{sta} = 0{,}15 \cdot E_{dyn} + 497$. For group B, as CLT layers were detached, tangential and longitudinal directions were considered separately, in which: $E_{sta} = 0{,}15 \cdot E_{dyn} + 29{,}8$ and $E_{sta} = 0{,}12 \cdot E_{dyn} + 2532$, respectively (see section 2.4.1.4).

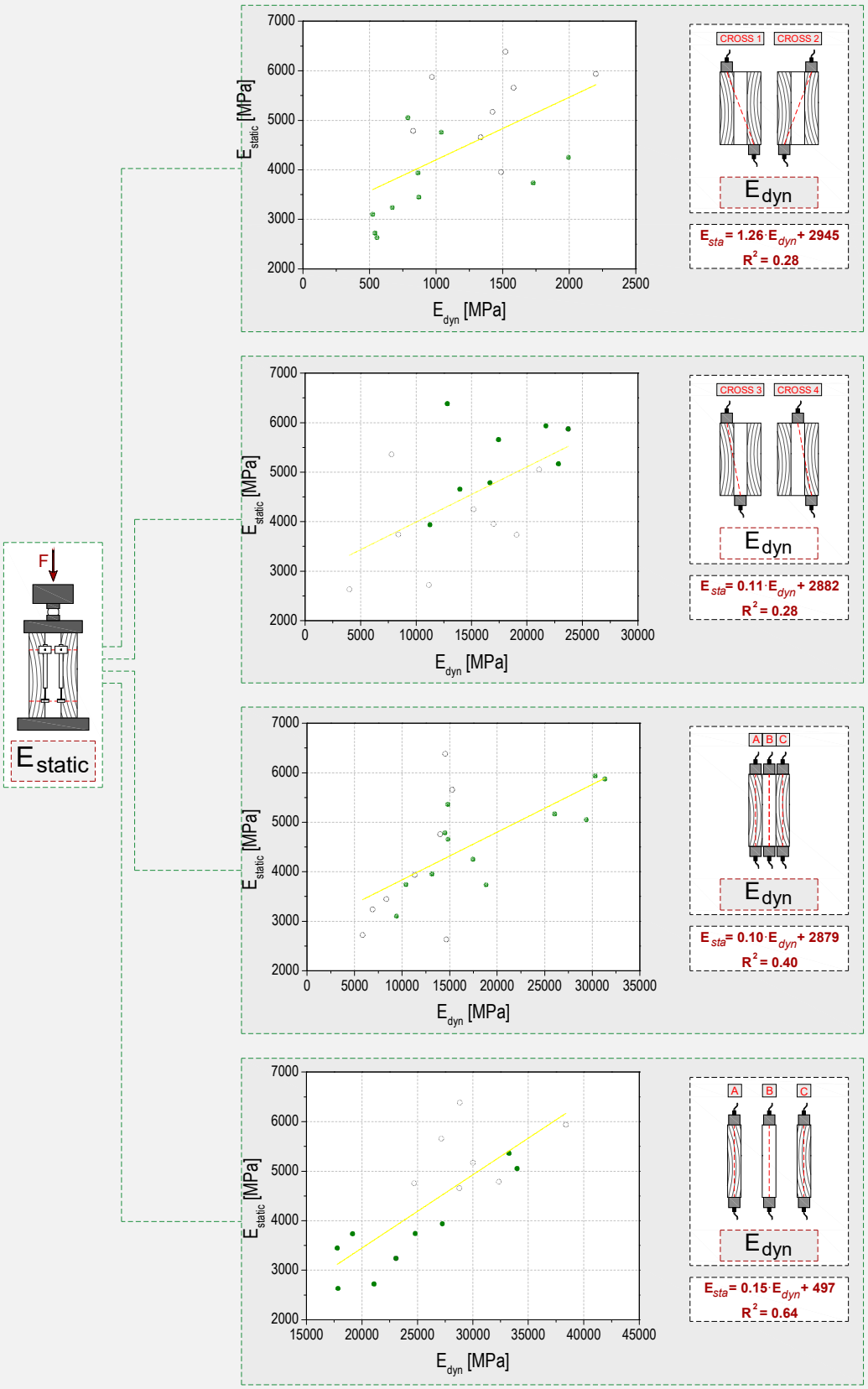

Figure (I) 2:29. Linear fittings between E_{sta} and E_{dyn} performed to obtain best correlation for entire CLT slice.

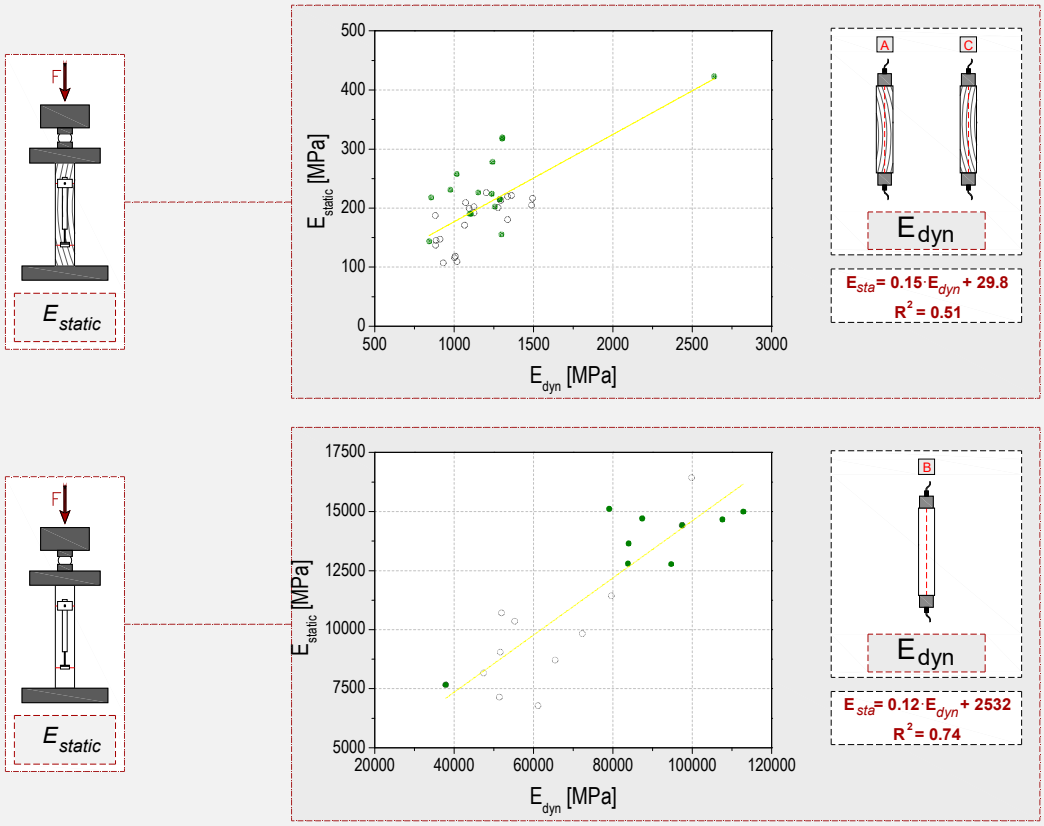

Figure (I) 2:30. Linear fittings between E_{sta} and E_{dyn} performed to obtain a correlation for different CLT layers considering their grain direction.

Regarding group A, Table (I) 2:25 presents the mean values obtained for all five slices cut from the entire specimens for all four configurations. As expected, and similarly to what was observed for released strains, highest tensile stresses were registered at the end of first wetting period (day 56). Mean released stresses at day 56 are: 75,9 MPa, 89,9 MPa, 97,3 MPa and 99,6 MPa for configurations C1, C2, C3 and C4, respectively. However, it is important to mention that higher strains registered at day 56 are reflected in dynamic modulus of elasticity which are also higher at this test day. As consequence of successive RH cycles, predominant compressive stresses are just registered at last wetting period (day 182). Furthermore, configurations C1 and C2 present the lowest effect of successive RH cycles at the end of stabilization period.

Figure (I) 2:32 depicts the mean values of released stresses measured on longitudinal section of all five slices of specimens from group A for all four test configurations and all five test days. Evaluating the behavior of different slices, compressive stresses are also present at day 0 and at both drying periods, namely day 35 for C3 and C4 and day 161 for C1 and C2 (Figure (I) 2:32 (a) and (c)). As expected, these compressive stresses are registered at outer layers which are firstly affected by drying causing effects.

Observing Figure (I) 2:32 wetting causing effects are also more evident on outer layers which present higher tensile released stresses at day 56 and lower compressive stresses at day 182 (Figure (I) 2:32 (b) and (d)). As a consequence of cross lamination and timber possible timber defects, curves depicted in Figure (I) 2:32 do not present a clear symmetry for all test configurations at all test moments.

Table (I) 2:25. Mean values of full-field released stresses measured on F1 (S1 to S5) of specimens from group A during second DIC mapping.

		MEAN RELEASED STRESSES (σ_{rel}) [MPA] (S1 TO S5)					
		DAY					
		0	35	56	161	182	324
C1	S1	4,1	0,3	84,8	-0,4	0,6	2,1
	S2	2,3	-0,2	73,6	-0,2	-0,6	2,0
	S3	2,0	0,7	69,6	-0,2	-1,4	1,8
	S4	0,7	1,0	77,5	-0,2	-1,7	2,0
	S5	1,6	1,2	73,8	-0,9	-1,7	2,2
	MEAN	**2,1**	**0,6**	**75,9**	**-0,4**	**-1,0**	**2,0**
C2	S1		2,1	89,	-0,52	-1,3	1,8
	S2		3,7	88,7	0,3	-2,2	2,0
	S3		3,6	90,6	0,7	-1,4	2,2
	S4		1,2	90,6	0,5	-0,5	2,1
	S5		0,9	90,1	-0,4	-1,5	2,5
	MEAN		**2,3**	**89,9**	**0,1**	**-1,4**	**2,1**
C3	S1		-0,7	102,6	4,3	-0,6	3,1
	S2		-0,1	95,5	6,9	-1,0	3,0
	S3		0,9	90,3	5,2	-1,2	3,1
	S4		0,6	97,7	4,3	-1,0	2,1
	S5		0,0	100,3	0,3	-0,1	2,0
	MEAN		**0,1**	**97,3**	**4,2**	**-0,8**	**2,7**
C4	S1		-0,2	95,5	1,9	-1,5	2,3
	S2		-1,3	92,0	1,8	-1,5	2,8
	S3		3,8	96,9	2,5	-1,6	2,0
	S4		-0,3	99,1	1,6	-2,0	1,9
	S5		-0,6	114,4	1,5	-2,1	2,9
	MEAN		**0,3**	**99,6**	**1,9**	**-1,8**	**2,4**

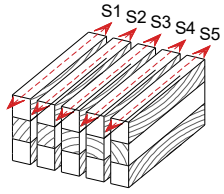

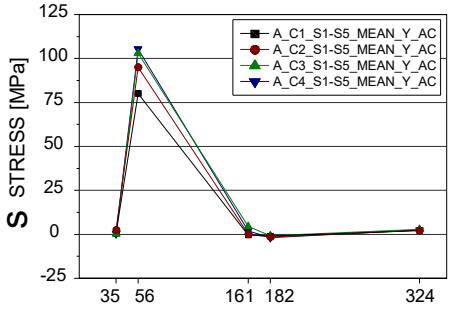

Figure (I) 2:31. Mean values of released stresses measured on longitudinal section of each slice (S1-S5) of specimens from group A for all four test configurations.

Regarding group B, Table (I) 2:26 presents the mean values of released stresses obtained for outer and inner layers of specimens from group B for all four test configurations and all five test days. Similar to

what happens with specimens from group A, highest tensile stresses were registered at first wetting period (0,1-0,4 MPa). Higher compressive stresses are observed at days 35 (-0,4 to -0,2 MPa) and 324 (-0,3 MPa). So, considering that mean initial stresses for C1 (day 0) are of 0,2 MPa (tensile stresses), it can be concluded that successive RH cycles causes internal compressive stresses in outer layers of CLT elements.

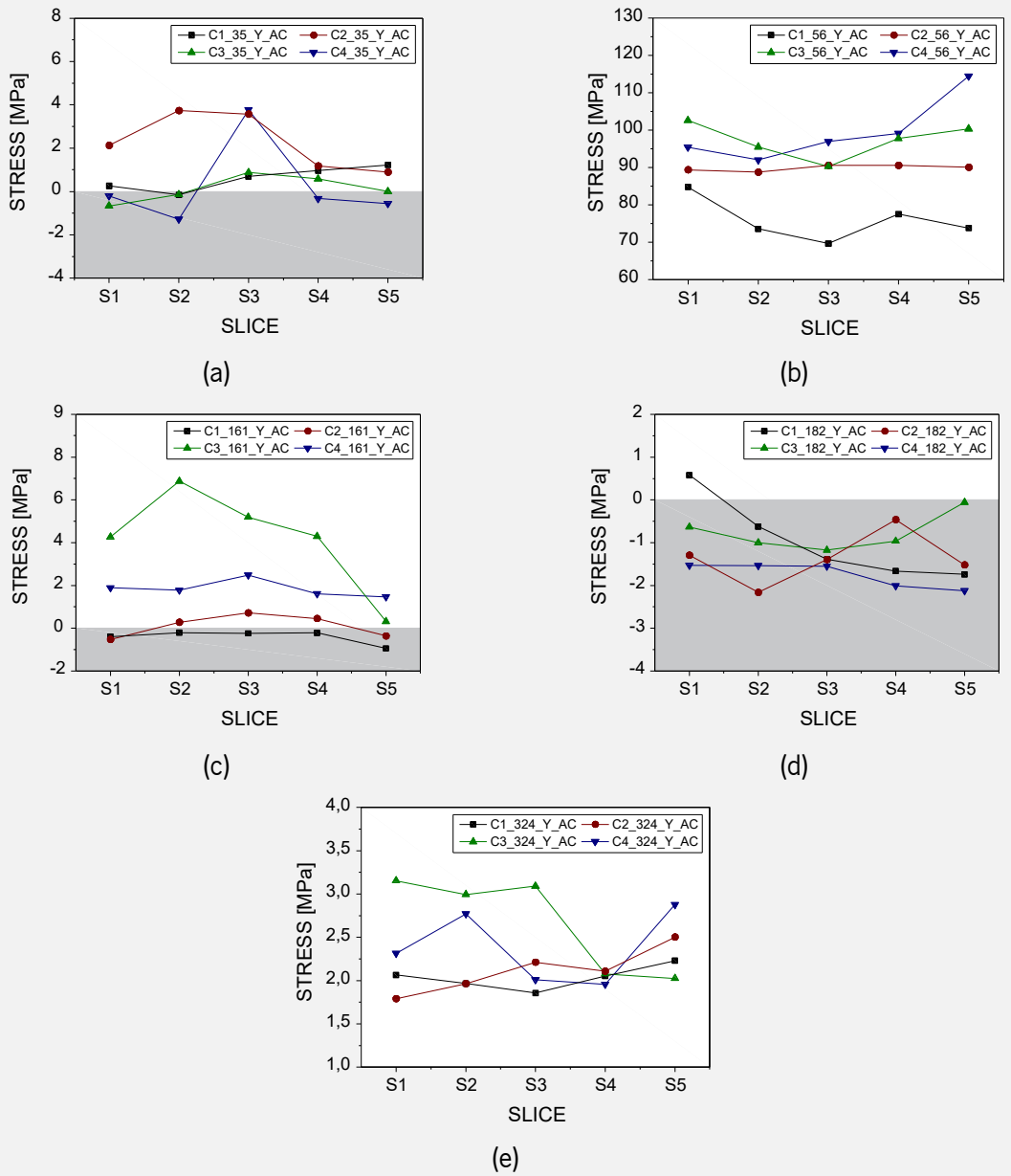

Figure (I) 2:32. Mean values of released stresses measured on longitudinal section of all five slices of specimens from group A for all four test configurations and all five test days.

In contrast, inner layers present the highest tensile stresses at last drying period (22,0 - 25,7 MPa). Despite the drying process, either inner and outer layers, present tensile stresses at this stage as consequence of successive RH cycles and crosswise lamination. Highest tensile stresses registered for

inner layers are closely related with growth rings orientation. In fact, considering growth ring orientation it was expected that outer and inner layers present opposite tendencies as observed at last cycle. Highest compressive stresses are observed at day 35 (-0,9 - 5,6 MPa) and also contrary to moisture content tendency, day 182 also present predominant compressive stresses (-3,2 to 1,2 MPa). Regarding effect of successive RH cycles, it is important to mention here that, due to the high moisture content at lamination process, days 0 and 324 present similar compressive stresses (-2,7 MPa and -3,5 to -1,3 MPa). However, it can be concluded that successive RH cycles do not cause any effects on inner layers of CLT.

Table (I) 2:26. Mean released stresses measured on specimens from group B in Y direction, for inner and outer layers, during second DIC mapping.

MEAN RELEASED STRESSES (σ_{rel}) [MPA] (OUTER AND INNER LAYERS)												
	INNER LAYERS						OUTER LAYERS					
	DAY						DAY					
	0	35	56	161	182	324	0	35	56	161	182	324
C1	-2,7	-5,1	0,2	22,0	-1,5	-2,5	0,2	-0,4	0,1	0,0	0,1	-0,3
C2		-3,4	-0,3	20,7	-3,2	-3,5		-0,4	0,1	0,0	0,1	-0,3
C3		-0,9	2,4	25,7	1,2	-1,3		-0,2	0,0	0,2	-0,1	-0,3
C4		-5,6	17,5	24,6	-1,3	-1,8		-0,4	0,4	0,0	0,0	-0,3

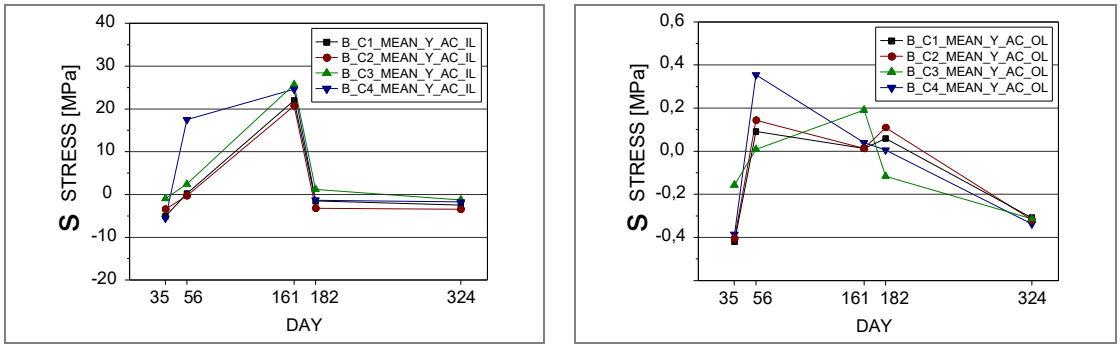

Figure (I) 2:33. Mean values of full-field released stresses distribution measured on specimens from group B in Y direction, for inner and outer layers, during second DIC mapping.

Regarding different moisture flow conditions, configurations that block tangential direction (C3 and C4) present lower compressive stresses and highest tensile stresses for inner layers as a consequence of slower absorption/desorption processes. Observing behavior of outer layers, the influence of moisture flow conditions is not so clear. Configurations that block longitudinal direction (C2 and C4) present higher tensile stresses at day 56, however the same tendency is not observed at last wetting period. Surprisingly,

the configuration that presents a behavior completely out of pattern is C3. It is possible that sealing of tangential and radial directions cause some effects on outer layers, especially at last wetting period in which outer layers present predominant compressive stresses while inner layers present predominant tensile stresses (Figure (I) 2:34 (d)). However, before take final conclusions more research is required, once this phenomenon can be just a result of reduced sampling.

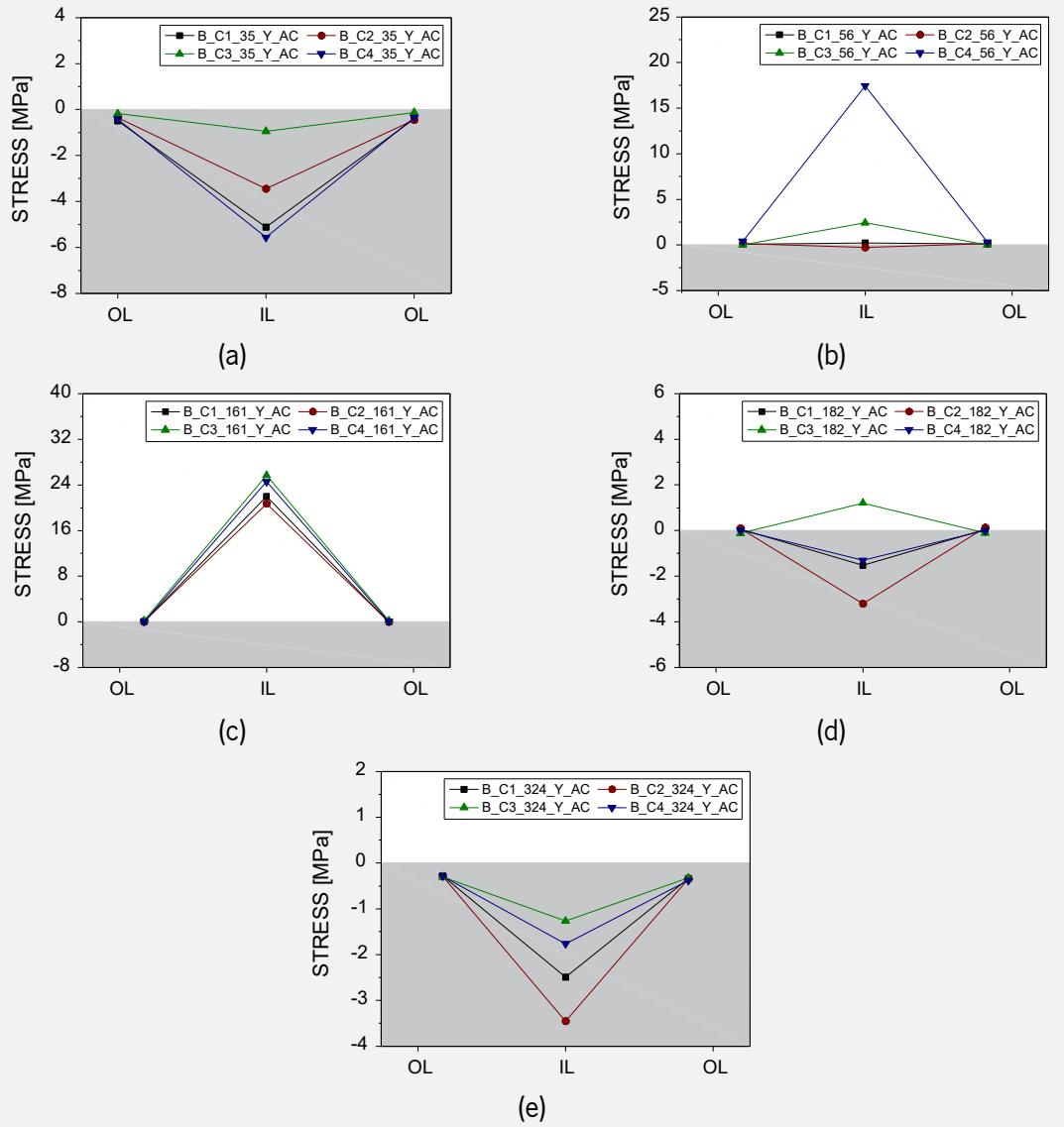

Figure (I) 2:34. Mean values of released stresses measured on outer and inner layers of specimens from group B for all four test configurations and all five test days.

2.4.2 LVDTs acquisition

As explained at point 2.3.2, constant measurements of moisture induced movements were taken until the end of last wetting period (day 182) of RH cycle using two specimens similar to C1 from group A. Taking initial dimensions of specimens (day 0) as reference, Table (I) 2:27 presents mean compressive

restrained strains registered at the end of each drying/wetting period, while Figure (I) 2:35 depicts the continuous compressive strains registered during the 182 test days. Both, Table (I) 2:27 and Figure (I) 2:35 present obtained results for all three monitored directions (X, Y and Z).

Regarding X direction (longitudinal direction of outer layers), just the measurements of one specimen was considered for this analysis, once due to technical issues the other LVDTs does not take the measurements properly. As expected, X direction was the one with lower moisture induced movements. However, it presents predominant negative compressive strains during all the RH cycles, which means that swelling movements tend to be wider than shrinking movements. This way, CLT panels never recover its initial shape keeping it always larger. Furthermore, negative compressive strains (-0,01% to -0,34%) are registered for drying periods, meaning that X direction present exactly the opposite of expected tendency. In other words, X direction present a clear tendency to swell when timber dries. This tendency tends to emphasize as the number of cycles increase and must be related with crosswise lamination.

Differently, Y direction present predominant positive compressive strains either for drying or wetting periods. Contrary to what was observed for X direction, shrinking movements tend to be wider than swelling movements. Furthermore, compressive strains tend to increase as the number of cycles also increase either for drying or wetting periods. It can be observed in Figure (I) 2:35 that for drying periods timber does not reach an equilibrium, while for wetting periods timber tends to stabilize few days after RH being changed. At the end of last drying period (day 161) CLT panel is 2,34% smaller in its Y direction and present a reduced moisture content of 9,8%. Surprisingly, at the end of last wetting period CLT panel is 1,09% smaller when comparing with its initial dimensions, despite its moisture content being around 20,6%.

Z direction is the one that present the expected relation between positive/negative compressive strains and drying/wetting periods, respectively. Contrary to what was observed for Y direction, specimens show a tendency to stabilize at the end of drying periods, while during wetting periods specimens indicate the tendency to keep swelling (Figure (I) 2:35). For all RH cycles, values registered for wetting periods are clearly more substantial than those registered for drying periods. Furthermore, either shrinkage or swelling movements tend to decrease as the number of cycles increase. Considering initial dimensions of CLT panels, at the end of last wetting period CLT panel is 1,90% larger while at the end of last drying period CLT panel is 0,38% smaller.

Table (I) 2:27. Restrained compressive strains considering initial dimension of specimens at day 0.

COMPRESSIVE STRAINS [%]									
DIRECTION	LVDT	DAY / RELATIVE HUMIDITY							
		35 30%	56 90%	75 30%	96 90%	114 30%	136 90%	161 30%	182 90%
X	173710	n.a.	n.a.	n.a.	n.a.	n.a.	n.a.	n.a.	n.a.
	173711	-0,01	0,07	-0,13	-0,00	-0,30	-0,04	-0,339	-0,073
	MEAN	**-0,01**	**0,07**	**-0,13**	**-0,00**	**-0,30**	**-0,04**	**-0,34**	**-0,07**
Y	173714	1,21	0,427	1,86	0,70	2,06	0,91	2,38	1,15
	173715	1,18	0,24	1,90	0,72	1,77	0,94	2,30	1,04
	MEAN	**1,19**	**0,33**	**1,88**	**0,71**	**1,92**	**0,92**	**2,34**	**1,09**
Z	173712	0,98	-1,97	0,66	-1,96	0,56	-1,98	0,48	-1,89
	173713	0,91	-2,35	0,28	-2,10	0,29	-2,06	0,27	-1,89
	MEAN	**0,95**	**-2,16**	**0,47**	**-2,03**	**0,42**	**-2,02**	**0,38**	**-1,90**

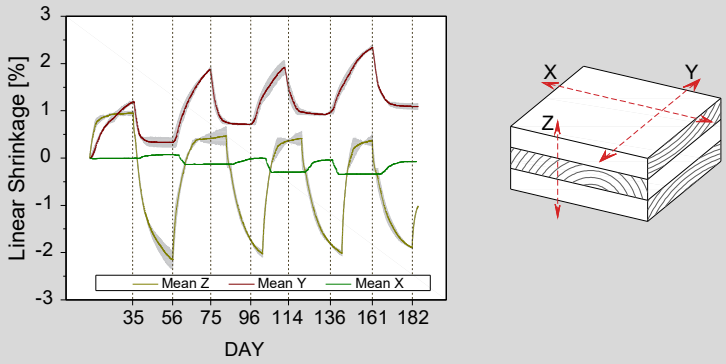

Figure (I) 2:35. Linear shrinkage considering initial dimension (day 0) of test specimens.

Observing compressive/tensile strains separately and taking the dimensions at the beginning of each drying/wetting period as reference, differences between successive RH cycles can be compared easily. Table (I) 2:28 presents percentages of compressive strains obtained at the end of all four drying periods for three analyzed directions, and Figure (I) 2:36 depicts curves of compressive strains registered continuously for the same periods and CLT directions. Analyzing the data, it can be observed that for all directions the first drying period is the less significant, especially for X and Z directions. Y direction present the greatest similarity between different drying periods (1,19% to 1,55%) and is the unique direction in which specimens do not stabilize. Differences between minimum and maximum linear shrinkage are of 0,29%, 0,36% and 1,61% for X, Y and Z directions, respectively. Exhibiting negative compressive strains (-0,01% to -0,30%), X direction tends to stabilize around 5th day of each drying period. This means that during first five days while CLT panel shrinks in Y direction it swells in X direction. As a consequence of

wider shrinking movements (0,95% to 2,56%), Z direction tends to stabilize later, around in the middle of each drying period.

Table (I) 2:29 presents tensile strains (%) obtained at the end of all four wetting periods for three analyzed directions, and Figure (I) 2:37 depicts curves of tensile strains registered continuously for the same periods and CLT directions. Similar to what was observed for drying periods, first wetting period is the less significant for X and Y direction. On contrary, Z direction present the first wetting period as the most significant and successive periods present a descendent tendency. Higher differences observed between successive drying periods for X and Z directions are less significant regarding wetting periods. Differences between minimum and maximum tensile strains are of 0,19%, 0,41% and 0,84% for X, Y and Z directions, respectively. Despite low percentages, X direction present again negative values (-0,08% to -0,27%). During swelling periods Y and Z direction switch their behaviors and Y direction stabilizes around 10th day of each period, while Z direction swells continuously until the end of wetting period. As expected, Z direction still present higher percentages for tensile strains (2,23% to 3,07%) than Y direction (0,87% to 1,28%).

The effect of successive RH cycles on compressive/tensile strains is not well studied and few studies are found regarding this subject. Sousa (2010) performed some experiments with solid maritime pine (*Pinus pinaster, ait*), submitting specimens to three successive drying/wetting cycles and evaluating the shrinkage/swelling coefficients during stabilization periods for radial and tangential directions. Results shown that moisture movements tend to increase as the number of cycles also increases concluding that timber fibers suffer some kind of laxity, changing its hygroscopic behavior. Regarding present study, this tendency was also observed, with the exception of swelling movements in radial direction.

Comparing restrained strains obtained with DIC technique and LVDTs measurements for first and last RH cycles some important differences were registered. Table (I) 2:30 presents the mean values of restrained strains obtained by means of both techniques for first and last RH cycles and for all three measured directions. Figure (I) 2:38 depicts the comparative curves. Mean values presented for DIC technique are obtained from average of full-filed measurements considering the entire ROI of F1 for X and Y directions and F2 and F3 for Z direction (Figure (I) 2:10), while mean values presented for LVDTs acquisition are obtained by the linear measurements, according to test setup (Figure (I) 2:12), taken at each test day.

Table (I) 2:28. Compressive strains considering initial dimension of specimens at the beginning of each drying period.

COMPRESSIVE STRAINS [%]					
DIRECTION	**LVDT**	**DRYING PERIODS**			
		1st	**2nd**	**3rd**	**4th**
X	**LVDT_173710**	n.a.	n.a.	n.a.	n.a.
	LVDT_173711	-0,01	-0,21	-0,29	-0,30
	MEAN	**-0,01**	**-0,21**	**-0,29**	**-0,30**
Y	**LVDT_173714**	1,21	1,44	1,37	1,49
	LVDT_173715	1,18	1,66	1,06	1,38
	MEAN	**1,19**	**1,55**	**1,22**	**1,43**
Z	**LVDT_173712**	0,98	2,56	2,43	2,36
	LVDT_173713	0,91	2,55	2,30	2,24
	MEAN	**0,95**	**2,56**	**2,37**	**2,30**

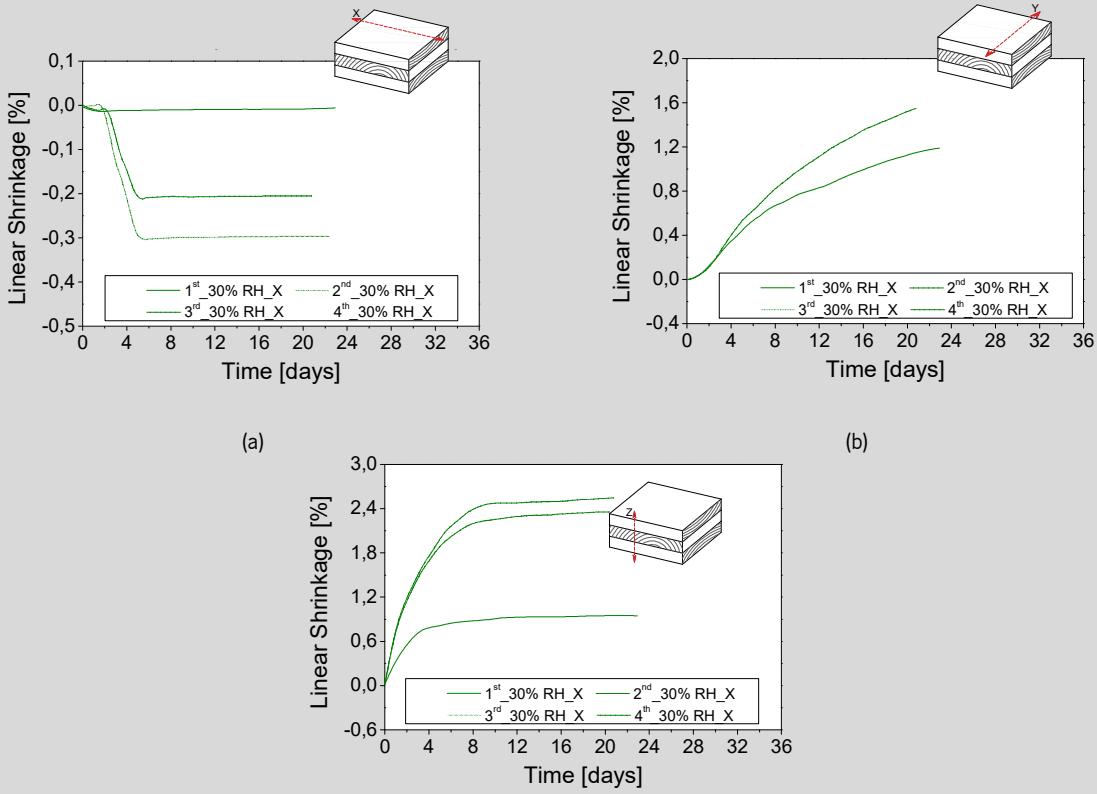

Figure (I) 2:36. Curves of compressive strains considering initial dimension of each cycle with 30% RH. (a) X direction; (b) Y direction; (c) Z direction.

Table (I) 2:29. Tensile strains considering initial dimension of specimens at the beginning of each wetting period.

TENSILE STRAINS [%]					
DIRECTION	**LVDT**	**WETTTING PERIODS**			
		1st	**2nd**	**3rd**	**4th**
X	**LVDT_173710**	n.a.	n.a.	n.a.	n.a.
	LVDT_173711	-0,08	-0,13	-0,25	-0,27
	MEAN	**-0,08**	**-0,13**	**-0,25**	**-0,27**
Y	**LVDT_173714**	0,79	1,19	1,18	1,27
	LVDT_173715	0,95	1,20	0,86	1,29
	MEAN	**0,87**	**1,19**	**1,02**	**1,28**
Z	**LVDT_173712**	2,92	2,58	2,52	2,34
	LVDT_173713	3,22	2,33	2,32	2,12
	MEAN	**3,07**	**2,46**	**2,42**	**2,23**

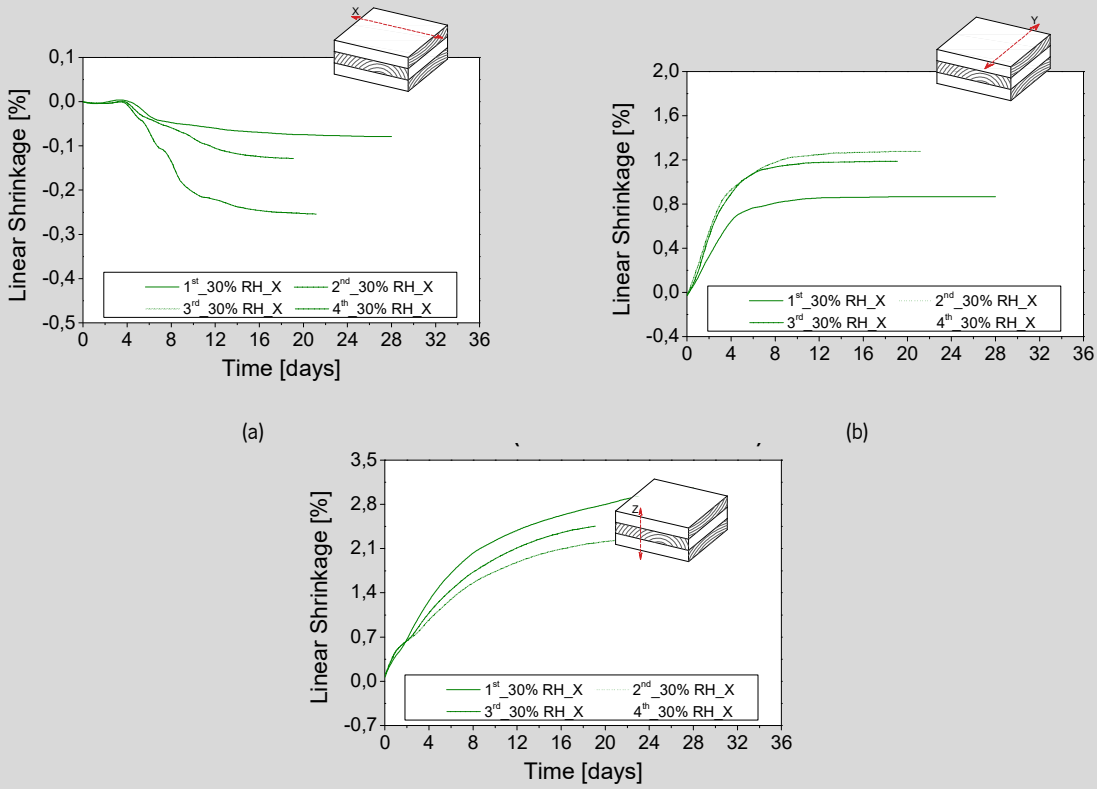

Figure (I) 2:37. Curves of tensile strains considering initial dimension of each cycle with 90% RH. (a) X direction; (b) Y direction; (c) Z direction.

Regarding X direction (Figure (I) 2:38 (a)), it is possible to conclude that both techniques suggest that, as a consequence of successive RH cycles, tensile strains tends to be predominant as the number of cycles increase, however DIC technique present wider differences between compressive and tensile strains (-0,005 to -0,001 for first RH cycle and 0,002 to -0,006 for last RH cycle).

Concerning Y direction (Figure (I) 2:38 (b)), it is during the first wetting period that the most important difference happens, once according to LVDTs acquisition outer layers of CLT panels does not reach tensile strains. As a consequence, Y direction measured by LVDTs acquisition never presents tensile strains during the entire test period. When comparing first and last wetting periods, both techniques present similar decreases for tensile/compressive restrained strains. However, when comparing first and last drying periods, DIC technique suggest a decrease of compressive strains (-0,012 to -0,006) while LVDTs acquisition suggest an increase of compressive strains (-0,012 to -0,023). So, the final effect of RH cyclic changes on Y direction is different depending on measurement technique. While DIC technique suggest that the moisture induced movements reduce as the RH cycles increases, LVDTs acquisition suggest that successive RH cycles causes cumulative compressive strains on CLT panel.

Finally, observing the behavior of Z direction (Figure (I) 2:38 (c)), higher differences between both techniques are registered for wetting periods. For first and second wetting periods DIC technique present restrained strains that are 56% and 63% lower than those registered by LVDTs acquisition, respectively. This difference is directly related with the way measurements were taken. While DIC technique used external lateral surfaces of CLT panels, LVDTs acquisitions were made perpendicular to the main face of CLT panel. This way, results suggest that timber swelling is higher in central parts of CLT panel than in its borders. Despite these differences both techniques suggest that successive RH cycles tends to nullify compressive strains and keep tensile strains predominant.

2.4.3 Caliper ruler

Digital Caliper ruler were used to perform measurements on slices obtained after slicing specimens from group A. Measurements were taken on the length of CLT slices before and after separation of CLT layers. Each specimen was sliced into seven slices and central five slices were measured using a digital caliper ruler. However, the accuracy of this method is dependent on the operator technique as well as on the device quality. This way, obtained values present some contradictory results. Table (I) 2:31 presents mean released strains obtained for outer and inner layers, considering the measurements taken on all five slices of each specimen and Figure (I) 2:39 depicts the same released strains.

Table (I) 2:30. Mean restrained values obtained for X, Y and Z directions using DIC technique and LVDTs acquisitions at first and last RH cycles.

MEAN ε_{rest}					
TEST DAY		**35**	**56**	**161**	**182**
X	**DIC**	-0,005	-0,001	0,002	-0,006
	LVDTs	0,000	-0,001	0,003	0,001
Y	**DIC**	-0,012	0,008	-0,006	0,000
	LVDTs	-0,012	-0,003	-0,023	-0,011
Z	**DIC**	-0,012	0,009	0,001	0,007
	LVDTs	-0,009	0,022	-0,004	0,019

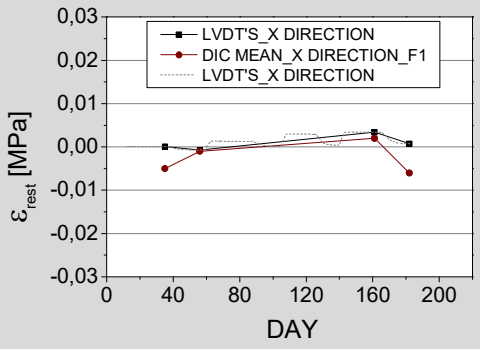

(a)

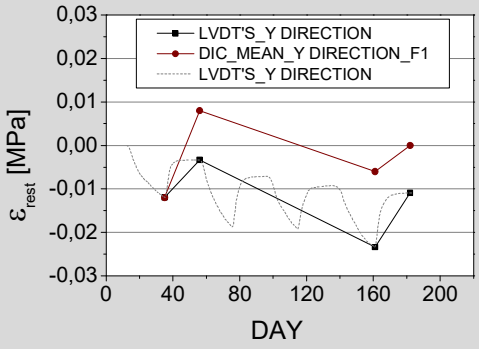

(b)

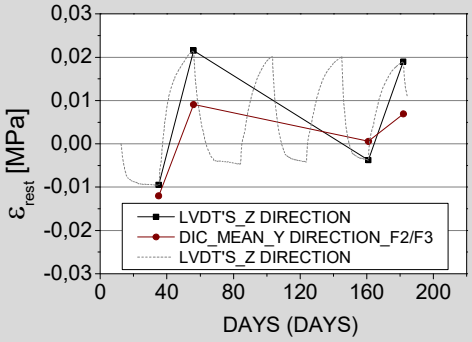

(c)

Figure (I) 2:38. Curves comparing restrained strains obtained by DIC technique and LVDTs measurements. (a) X direction; (b) Y direction; (c) Z direction.

Table (I) 2:31. Descriptive statistics of mean released strains measured on specimens from group A in Y direction, for inner and outer layers, using digital caliper ruler and considering measurements taken on all five slices.

	RELEASED STRAIN (ε_{rel})											
	MAXIMUM **MEAN** MINIMUM *COV*											
	INNER LAYERS						**OUTER LAYERS**					
	DAY						**DAY**					
	0	**35**	**56**	**161**	**182**	**324**	**0**	**35**	**56**	**161**	**182**	**324**
C1	0,001	0,001	0,000	0,001	0,002	0,004	0,000	0,000	-0,001	0,002	0,001	0,000
	0,000	**0,000**	**-0,001**	**-0,001**	**0,000**	**0,001**	**-0,001**	**-0,002**	**-0,002**	**-0,002**	**-0,002**	**-0,003**
	-0,001	-0,002	-0,003	-0,004	-0,001	-0,001	-0,002	-0,004	-0,004	-0,004	-0,004	-0,005
	-9,51	*-2,05*	*-1,05*	*-1,63*	*2,97*	*1,59*	*-0,47*	*-0,61*	*-0,38*	*-1,06*	*-0,83*	*-0,62*
C2	0,001	0,001	0,002	0,001	0,003		0,000	0,000	0,002	0,001	0,000	
	0,000	**0,000**	**0,000**	**0,000**	**0,001**		**-0,002**	**-0,001**	**-0,002**	**-0,001**	**-0,003**	
	-0,001	-0,001	-0,005	-0,001	-0,001		-0,007	-0,002	-0,005	-0,007	-0,010	
	-5,63	*1,29*	*-20,25*	*2,75*	*1,27*		*-0,67*	*-0,82*	*-1,00*	*-1,12*	*-0,77*	
C3	0,002	0,001	0,004	0,002	0,002		0,001	-0,001	0,001	0,003	0,003	
	0,000	**0,000**	**0,000**	**0,000**	**0,000**		**-0,001**	**-0,002**	**-0,003**	**-0,001**	**-0,001**	
	-0,002	-0,002	-0,002	-0,001	-0,003		-0,003	-0,004	-0,008	-0,004	-0,003	
	-84,84	*-1,77*	*-4,06*	*3,61*	*12,67*		*-1,37*	*-0,43*	*-0,66*	*-1,30*	*-1,38*	
C4	0,001	0,001	0,001	0,001	0,003		0,002	0,001	0,000	0,000	0,003	
	0,000	**0,001**	**0,000**	**0,000**	**0,000**		**-0,001**	**-0,001**	**-0,002**	**-0,001**	**-0,003**	
	-0,002	0,000	-0,001	-0,002	-0,002		-0,004	-0,003	-0,004	-0,003	-0,005	
	-7,81	*0,96*	*5,12*	*-2,31*	*3,59*		*-0,87*	*-1,05*	*-0,50*	*-0,56*	*-0,77*	

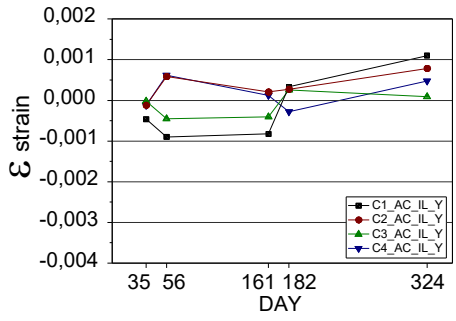

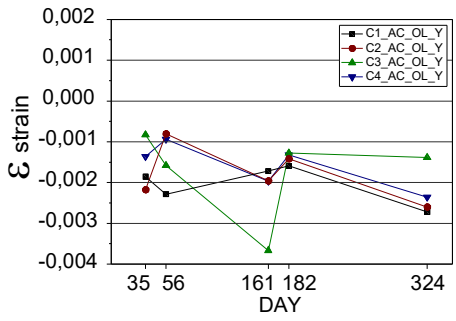

Figure (I) 2:39. Mean values of mean released strains measured on specimens from group A in Y direction, for inner and outer layers, using digital caliper ruler and considering measurements taken on all five slices.

Despite the reduced strains, it is possible to observe the effect of drying and wetting periods either for inner or outer layers. However, some important differences are observed between test configurations. C1 and C3 present behaviors completely different from those presented by C2 and C4. Fact that could be justified by the effects of different moisture flow conditions. It is important to state here that similar differences were not observed for specimens from group B (in which DIC technique was applied) however, this fact can be related with different dimensions of original specimens. Anyway, results obtained for group B were taken here as a reference to compare the tendencies of all configurations during the RH cycles however, obtained values are not comparable.

Considering inner layers, C2 and C4 present compressive/tensile strains for drying/wetting periods during first RH cycle, while C1 and C3 present predominant compressive strains. Despite the differences between configurations, at the end of stabilization period (day 324) all four configurations present predominant tensile strains (0,000 to 0,001). On contrary, results obtained for group B suggest predominant compressive strains for all four configurations at Day 324, while high tensile strains were registered at day 161.

Released strains obtained for outer layers present predominant compressive tendency for all four configurations. However, while C2 and C4 present higher compressive strains associated to drying periods and lower compressive strains associated to wetting periods (agreeing with the tendency observed for specimens from group B), C1 and C3 present the opposite tendency during first RH cycle. Finally, at the end of stabilization period, and similarly to results obtained for group B, all configurations present predominant compressive strains (-0,001 to -0,003).

As depicted in Figure (I) 2:40 and Figure (I) 2:41 released strains obtained for inner and outer layers were analyzed considering all five slices separately. Observing these figures, it is possible to verify that the expected symmetry centered at slice 3 (S3) was not always registered. However, some tendencies can be pointed out regarding released strains registered for inner layers (Figure (I) 2:40): released strains measured at S3 are closer when comparing drying and wetting periods (green and red lines, respectively); released strains measured for S3 at the end of wetting periods show the lowest tensile/compressive strains; at the end of stabilization period just C4 present compressive strains at S3, while remaining configurations present the highest tensile strains. Some other tendencies can be pointed out regarding outer layers (Figure (I) 2:41): wetting periods present closer results and a more evident symmetry while drying periods present higher differences and symmetry is not verified; at the end of stabilization period compressive strains tends to be higher, however a high variance is observed between different slices.

Regarding different moisture flow conditions, it is possible to observe that configurations that seal longitudinal direction (C2 and C4) present predominance of tensile strains for inner layers and the lowest compressive strains for outer layers.

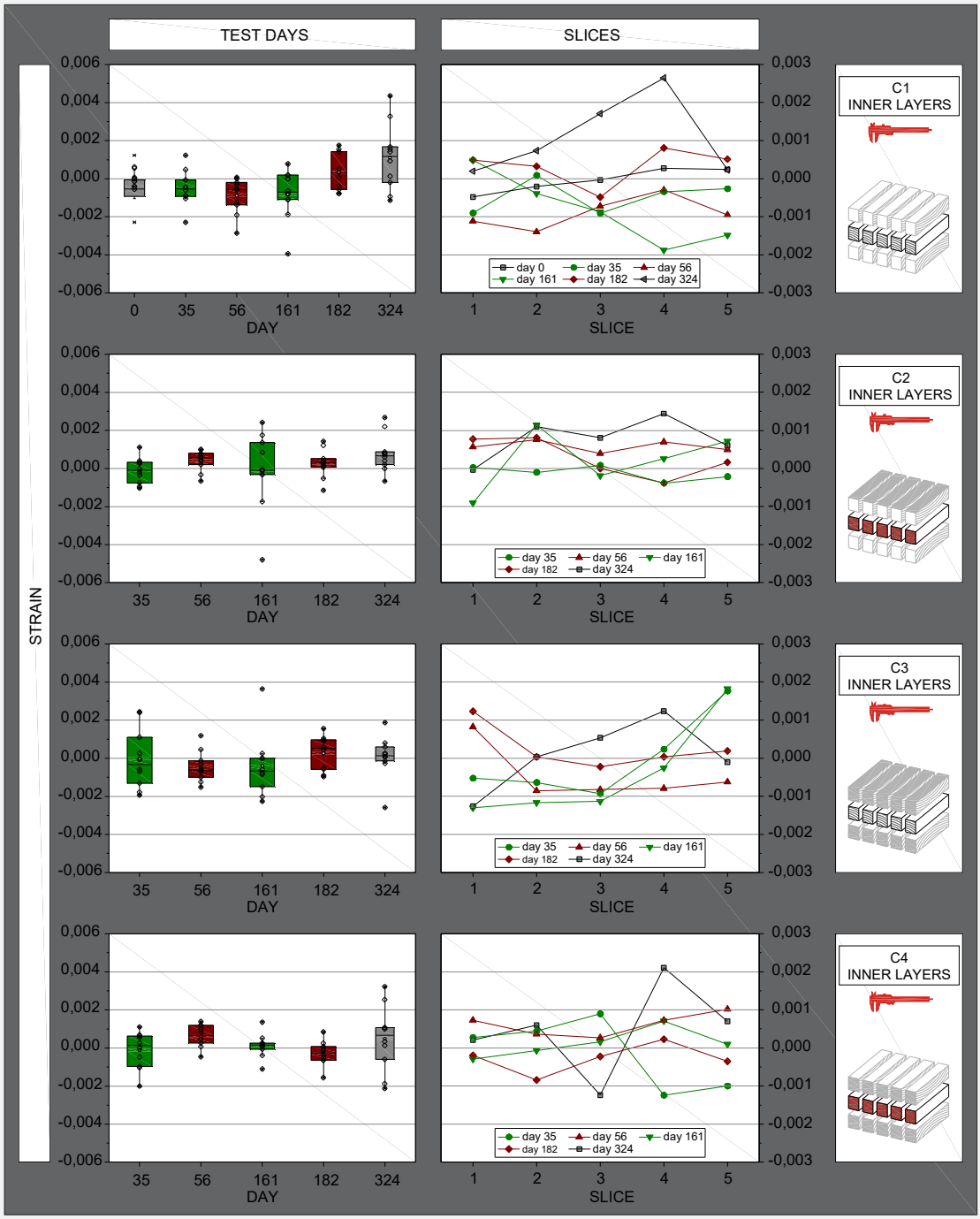

Figure (I) 2:40. Released strains obtained for inner layers for all four configurations and for all five slices.

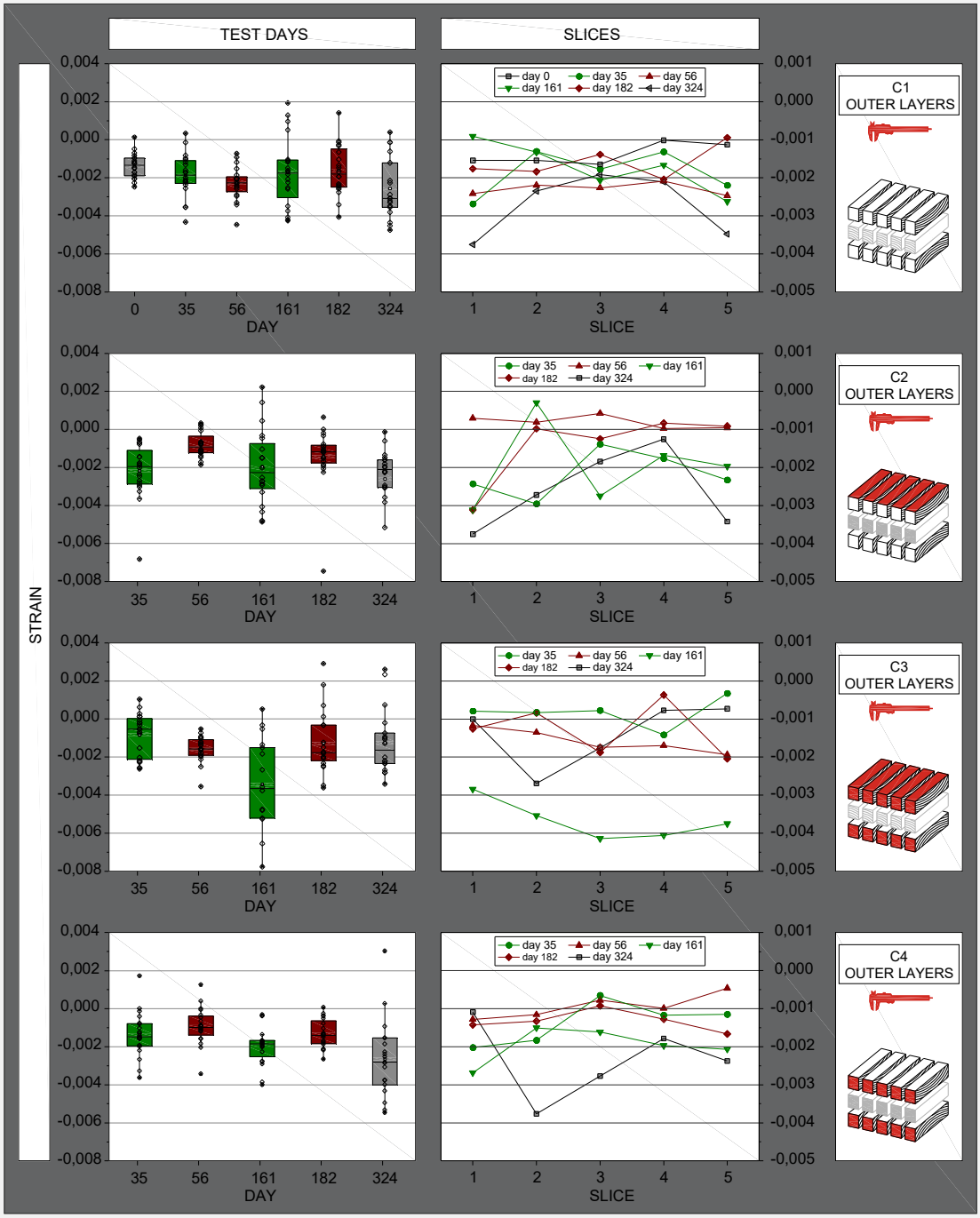

Figure (I) 2:41. Released strains obtained for outer layers for all four configurations and for all five slices.

2.5 Main conclusions

Analysis performed to restrained strains for specimens from group A suggest some important conclusions:

- When evaluating restrained strains in longitudinal direction, measurements performed in main face of CLT panels (F1 – X direction) suggest that successive RH cycles tend to invert the normal tendency of wood movements when submitted to drying/wetting environments. In other words, drying periods present tensile strains while wetting periods present compressive strains. One possible explanation for this phenomenon is the accumulation of strains during several cycles;
- Otherwise, when evaluating restrained strains in tangential direction (F1 – Y direction), measurements performed in main face of CLT panels suggest that, differently from what was observed for moisture content variation, restrained strains tend to reduce significantly from first to last drying cycles for all test configurations;
- However, when restrained strains in tangential direction are measured in lateral face of CLT panels (F2 – outer layers), drying period present tensile strains while wetting period present compressive strains. This fact may be related with restrictions caused by crosswise lamination and growth ring orientation;
- Regarding different moisture flow conditions, configurations that restricts moisture flow on longitudinal direction (C2 and C4) present slower water desorption and because of that suggest a tendency for lower restrained strains measured through Y direction of main face of CLT panels (F1), during drying periods;
- Measurements taken on F1 of specimens from group A suggest that the ratio between tangential and longitudinal directions tend to decrease with the number of RH cycles;
- Assuming that ratio between tangential and longitudinal directions (T/L) at the end of stabilization period (day 324) for configuration C1 is 2,0 ($\Delta_{F1\_C1\_324}$ =2,0), it can be concluded that successive RH cycles changes the effects of crosswise lamination for configurations in which tangential direction is sealed (C3 and C4): $\Delta_{F1\_C3\_324}$ = -1,3 and $\Delta_{F1\_C4\_324}$ = -8,3;
- At the end of stabilization period, CLT tend to present always reduced strain values, meaning that successive RH cycles do not cause cumulative strains on CLT. However, tangential direction presents a slightly tendency for compressive strains while longitudinal direction presents a slightly tendency for tensile strains;

- Regarding measurements taken in Z direction, it can be concluded that movements in radial direction are not restrained by crosswise lamination being just dependent on timber grain orientation.

Regarding released strains measured in main face (F1) of CLT panels some assumptions can be pointed out:

- Tensile strains are predominant independent of the test day/moisture content;
- No effect of different moisture flow conditions was observed;
- It is during first wetting period that effects of crosswise laminations are more evident: despite the tensile restrained strains observed during first DIC mapping, after sliced timber still tends to swell substantially;
- Released strains tend to reduce as the number of cycles increase;
- Compressive restrained strains observed at first DIC map became tensile released strains at second DIC map, proofing the existence of restriction of timber movements caused by crosswise lamination.

Concerning released strains measured in specimens from group B it can be stated that:

- Contrary to strains measured in tangential direction, strains measured in longitudinal direction (inner layers) do not exhibit a correlation between drying/wetting periods and compressive/tensile strains. Tensile strains are predominant, which means that independent of moisture content levels CLT inner layers tend to swell after being released;
- Different moisture flow conditions do not affect the results;
- Taking day 0 as reference, the effect of successive RH cycles is different for inner and outer layers: while for inner layers no substantial effects were observed, for outer layers significant compressive released strains were measured at day 324.

Measurements taken with LVDTs acquisition in comparison with DIC technique resulted in following main conclusions:

- Regarding X direction, both techniques suggest that tensile strains tends to be predominant as the number of cycles increase, however DIC technique present wider differences between compressive and tensile strains. Furthermore, both techniques suggest that in X direction the normal tendency of wood movements when submitted to drying/wetting environments is inverted;

- Due to reduced swelling movements registered by LVDTs during first wetting period, both techniques present different final effects for successive RH cycles: while DIC technique suggest that RH cycles decrease the moisture induced movements caused by cross wise lamination, LVDTs acquisition suggest that successive RH cycles causes cumulative compressive strains on CLT panel;
- Z direction present a similar behavior for both techniques, however LVDTs acquisition tend to present high tensile strains during wetting periods;
- Despite the similarities observed between two techniques, LVDTs still raise some doubts related with the efficiency of test setup, especially for points in which specimen is screwed to fix measurements in X and Y directions.

Measurements performed with caliper ruler helped to understand how released strains are distributed inside the CLT panel:

- Differences between compressive and tensile strains tend to be reduced at the center of CLT panels (S3 of inner layers), maybe because inner part of CLT panels are not significantly affected by moisture changes;
- Higher tensile strains measured at the center of specimens (S3 of inner layers) were observed at the end of stabilization period, with the exception of C4;
- Regarding different moisture flow conditions, it is possible to observe that configurations that seal longitudinal direction (C2 and C4) present predominance of tensile strains for inner layers and the lowest compressive strains for outer layers.

CHAPTER 3 (I)

3 WITHDRAWAL RESISTANCE OF SELF-TAPPING SCREWS INSERTED ON MAIN FACE OF CLT PANELS WHEN SUBMITTED TO SIMPLE CHANGES ON MOISTURE CONTENT

3.1. Experimental Campaign

The experimental campaign described in the present chapter was carried out at *Institut für Holzbau und Holztechnologie* - Graz Technical University (Austria) - with the background support of Professor Gerhard Schickhofer and PhD Andreas Ringhofer. This task was performed as a training program during a period of six months thanks to financial support of Portuguese foundation for science and technology (FCT) and Erasmus Placement program (University of Minho).

3.1.1 Main goals and parameters involved

The performed experiments pretend to understand the influence of three different parameters on the axial withdrawal resistance of self-tapping screws (STS) inserted perpendicular to the main face of three layered CLT panels. The first parameter is related with simple moisture content changes on CLT. For that, it was considered a range limited by moisture content values established by service classes of Eurocode 5. In other words, the moisture content changes respected the limits imposed by service classes 1 and 2, described in point 2.3.1.3. of Eurocode 5. This way, the tests performed considered three different moisture levels, namely: 8% and 12%, respecting the limits of service class 1, and 18%, respecting the environmental conditions considered by service class 2. The decision of respect the limits of service classes 1 and 2 is justified by the warnings of CLT producers, who say that CLT is still considered a material incompatible with service class 3 (KLH-Massivholzplatten, 2011).

Second parameter is related to the possible existence of gaps on the STS path through CLT thickness. It is called gaps to the line or space between two boards glued side by side in a CLT panel. To explore this parameter, CLT was produced considering the insertion of STSs through a different number of gaps across all CLT layers. CLT was produced with three layers, which allowed five different gap configurations, namely: reference (REF) – STS is inserted without the presence of gaps; gap in first layer (GAP_FL) – STS is inserted through one gap present in first layer of CLT panel; gap in middle layer (GAP_ML) - STS is inserted through one gap present in middle layer of CLT panel; gap in outer layers (GAP_OL) - STS is inserted through two gaps present in outer layers of CLT panel; gap in three layers (GAP_3L) - STS is inserted through three gaps present in all three layers of CLT panel. The drawings present in Figure (I) 3:1 illustrate these five configurations.

Last parameter is related with gap width, which can be 0mm or 4mm. Gaps with 0mm (GAP0) were selected as the reference for the better scenario, once the boards glued side by side are touching each

other, and gaps with 4mm (GAP4) were selected to simulate the worst scenario, once there is a void between boards. The decision of a maximum width of 4mm was based on the research of Brandner et al. (2013), who presented a summary of main geometrical characteristics of European CLT producers. They concluded that the most common gap width varies between 2mm and 6mm. However, they also refer that producers are looking for improvements for CLT pressing procedures, namely lateral pressing, in order to reduce the width of gaps. So, considering these future improvements, present research fixed a gap width of 4mm as the worst scenario.

The combination of these three parameters resulted in nine different test configurations and 270 withdrawal tests. Figure (I) 3:1 presents a summary of experimental campaign and illustrates different test configurations.

3.1.2 Production of specimens and main steps of experimental procedure

CLT used to build the test specimens was entirely produced in laboratory in order to obtain specimens free of significant knots and with similar density distribution between MC (moisture content) groups and test configurations. To avoid significant knots, CLT panels with fixed dimensions of 600x400x102mm^3 and three similar layers with a thickness of 34mm each were produced. This way, each produced panel contained six test specimens of 170x170x102mm^3. The configuration of CLT panels depended on the test configuration (Figure (I) 3:2). Density of timber boards was calculated by equation (3:1), according to ISO 3131:1975, and a random distribution was realized between different configurations. Densities varied between 345kg/m^3 and 576kg/m^3 (CoV=0,09 and mean=462kg/m^3) (Table (I) 3:1). In order to save time and avoid unexpected problems, the production of panels was planned in advance following pre-defined steps:

1. Cut (avoiding significant knots), plane and rectify four different types of boards needed to produce different layer configurations (Figure (I) 3:2 (a));
2. Weight all boards and realize a similar density distribution between all configuration groups and a good distribution, close to a normal one, was obtained (Figure (I) 3:3);
3. Glue and press CLT panels (Figure (I) 3:4 (a) and (b));
4. Saw the gaps in groups which include it (Figure (I) 3:4 (c) and (f));
5. Glue and press last layer in configurations with GAP4 in middle layers (Figure (I) 3:4 (d) and (e)).

Relatively to production of CLT, it is also important to refer that the timber used was spruce (*Picea abies*), with a nominal strength class C24 according to EN 338 (2009), and different layers were glued with

PURBOND® HB110 applied by a MINDA gluing equipment (Figure (I) 3:4 (a)). Furthermore, all CLT panels were pressed by a hydraulic pressing LANGZAUNER for 3 hours with a constant pressure of 0.4N/mm² (Figure (I) 3:4 (b) and (e)).

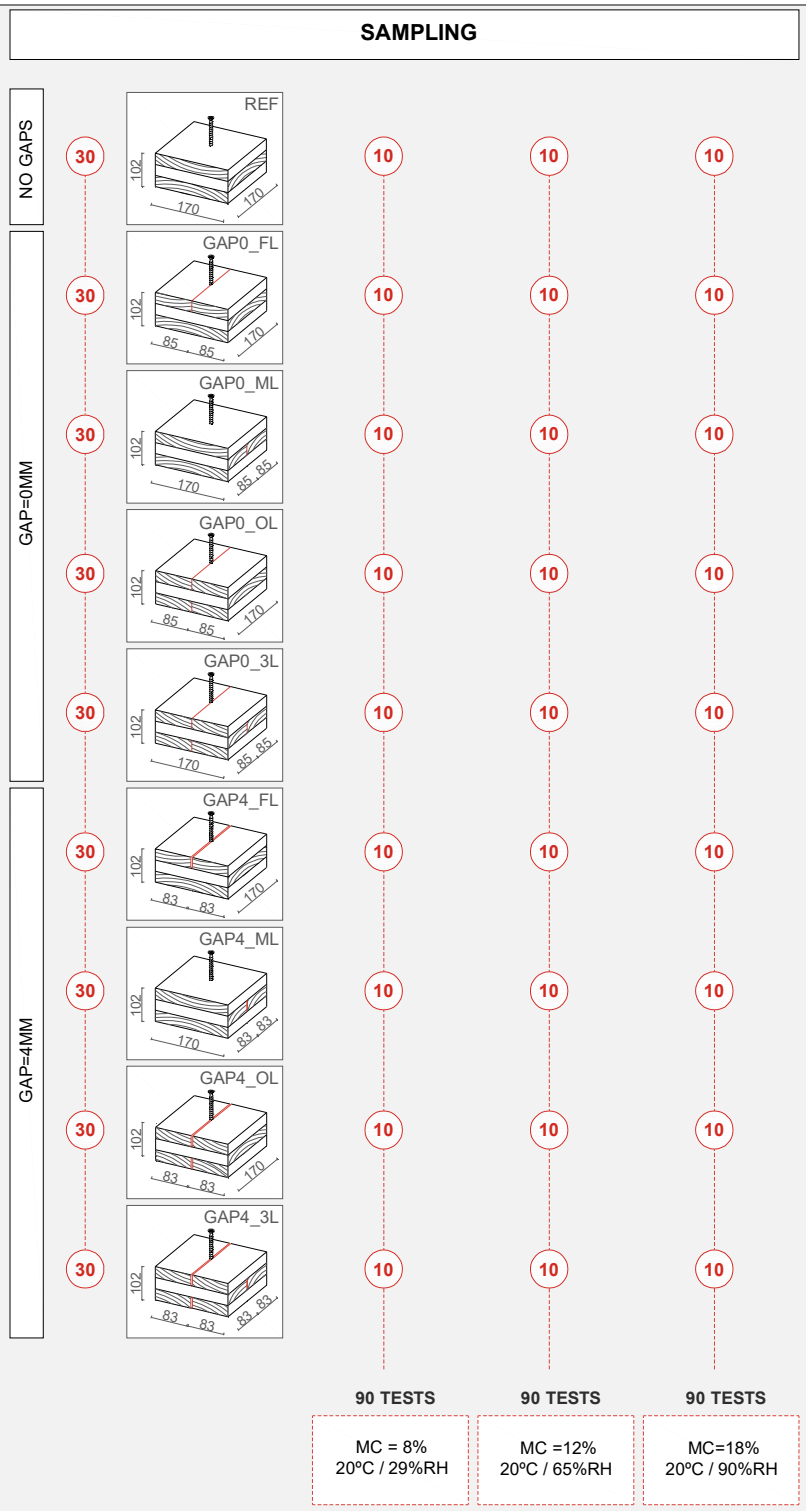

Figure (I) 3:1. Different test configurations and sampling used for different groups and test days (dimensions in mm).

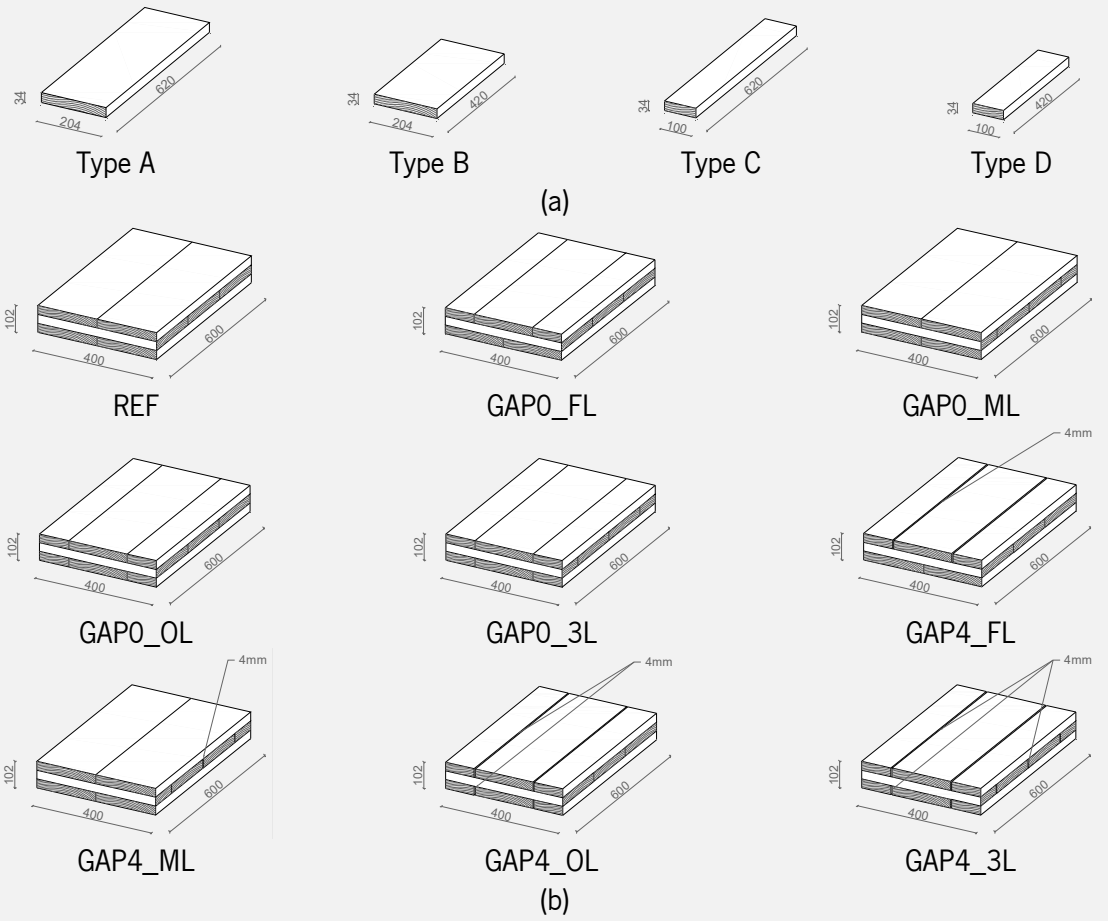

Figure (I) 3:2. CLT panels produced at Laboratory. (a) Four different types of boards needed to produce CLT panels for different test configurations; (b) different configurations of CLT panels.

$$\rho = \frac{m}{V} \tag{3:1}$$

ρ Density of each test piece, in grams per cm^3
m Mass of test piece, in grams
V Volume of test piece, in cm^3

Table (I) 3:1. Descriptive statistics of density distribution for all nine different CLT panels.

CONF.	Nº OF BOARDS	MEAN	SD	COV	MINIMUM	MEDIAN	MAXIMUM	P5
REF	42	473	51,7	0,11	345	473	576	397
GAP0_FL	40	457	41,3	0,09	354	463	532	377
GAP0_ML	40	456	34,5	0,08	378	457	520	395
GAP0_OL	45	465	43,2	0,09	367	466	559	394
GAP0_3L	50	456	44,0	0,10	351	459	558	367
GAP4_FL	40	462	37,4	0,08	390	466	542	395
GAP4_ML	40	462	36,9	0,08	390	462	576	405
GAP4_OL	45	469	41,5	0,09	397	468	560	401
GAP4_3L	50	462	41,1	0,09	369	463	560	396

SD – standard deviation; **CoV** – coefficient of variation; **P5** – 5th percentile

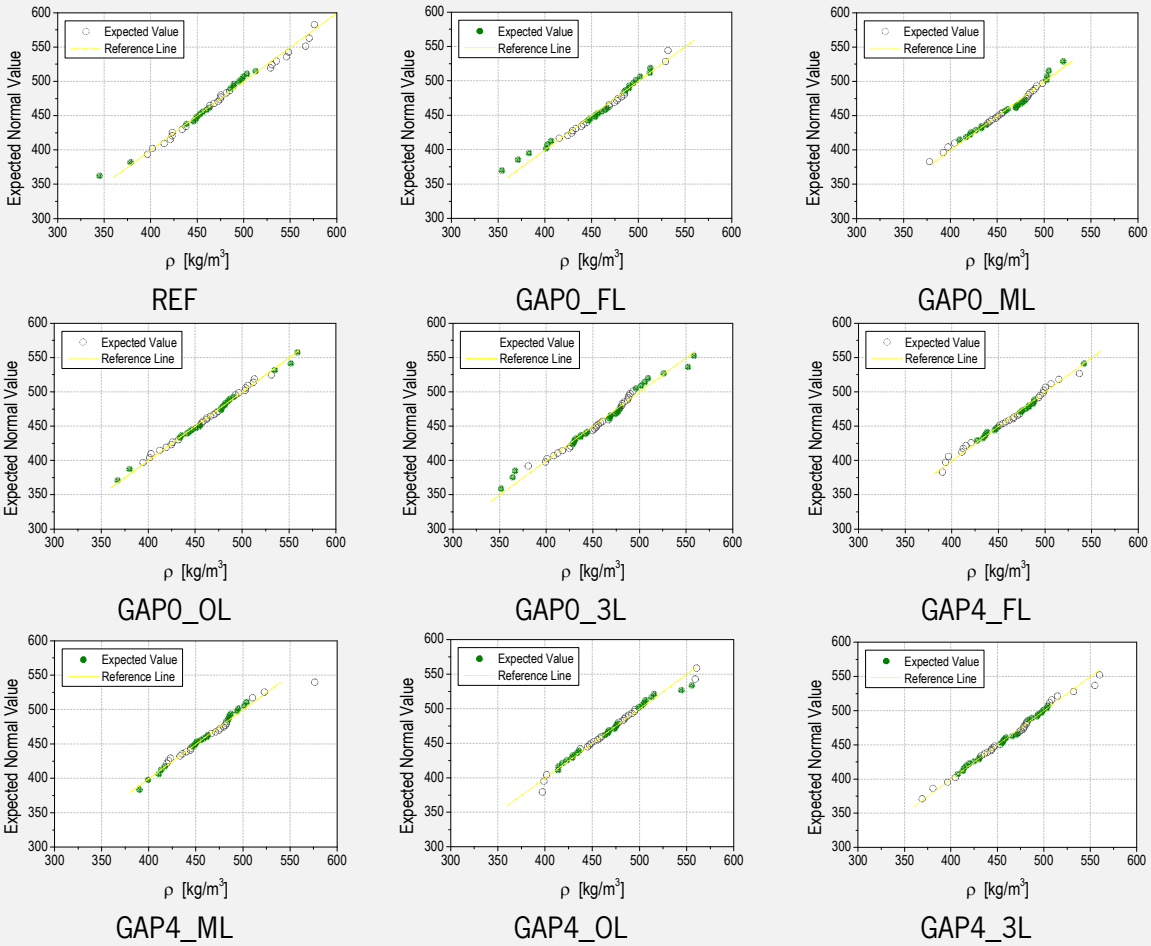

Figure (I) 3:3. Similar density distribution between different configurations. Graphs were plotted based on Normal distribution and Renard score method - (i – 0,3) / (n + 0,4).

After CLT production, 6 test specimens were cut from each CLT panel (Figure (I) 3:5 (a)). Small timber samples were saved and dried in order to quantify the timber moisture content at that time. After weighted and oven dried, those samples indicated a moisture content of approximately 10%. The goal was to produce CLT with stabilized timber with 12% of moisture content however, due to timing issues, it was not possible to conditioning timber boards for a longer period. So, in order to achieve a moisture content of approximately 12% at screwing time, specimens were conditioned again, in a climatic chamber with environmental conditions of 20°C and 65% RH, for more 10 days. After that, all specimens were pre-drilled with a hole of 5mm adequate for screws with a diameter of 8mm (EN 1995-1-1:2004) (Figure (I) 3:5 (b)). The decision of pre-drilling test specimens is justified by the difficulty to ensure the correct insertion of STS through CLT gaps.

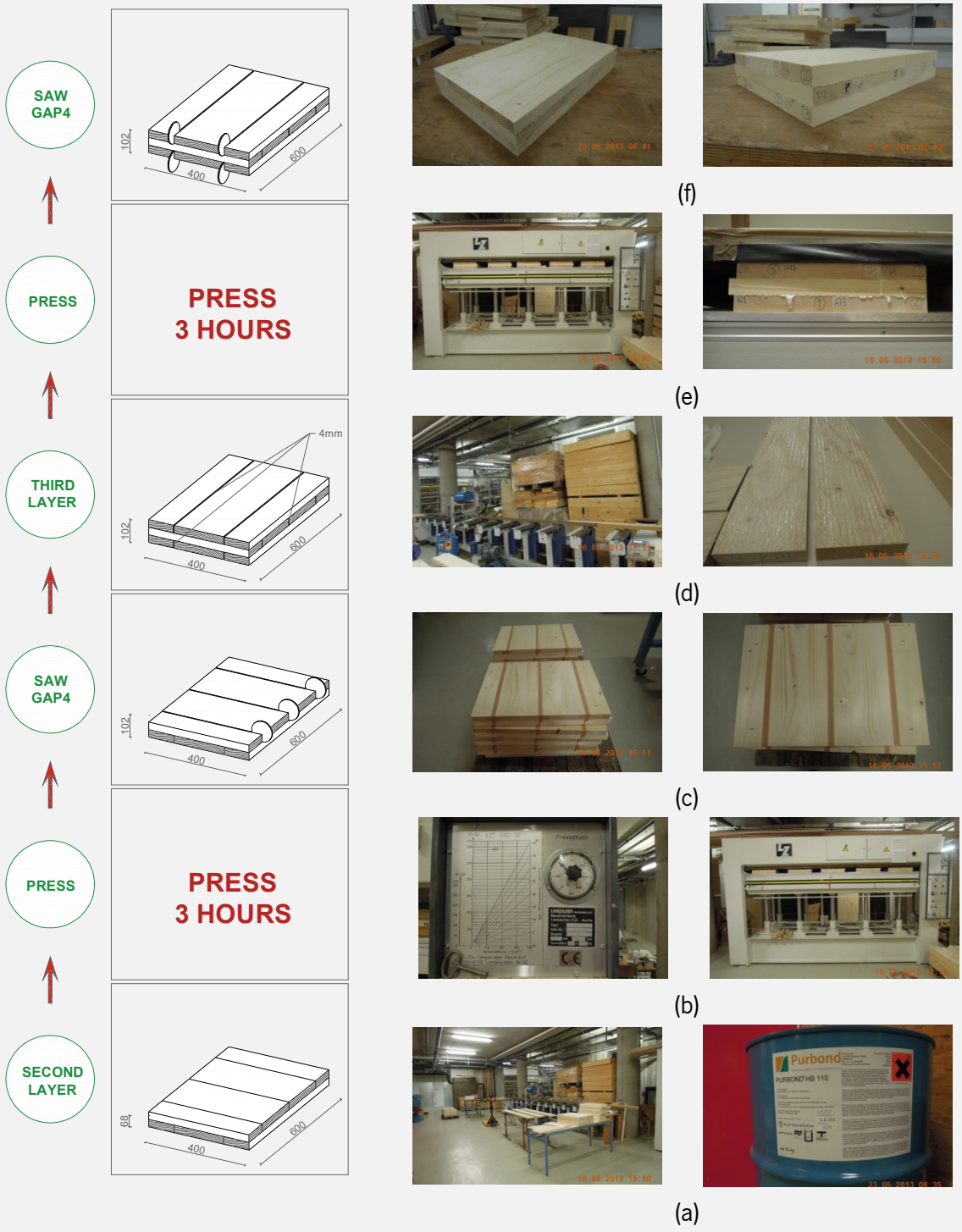

Figure (I) 3:4. Procedure to build CLT panels in laboratory. (a) assembling line and glue used to bond layers (PURBOND® HB110); (b) hydraulic pressing machine (LANGZAUNER) bonding two CLT layers; (c) gaps with four millimeters protected to the next bonding procedure; (d) glue line (MINDA equipment) with glue dispenser and timber boards with glue before assembly panel; (e) pressing the third layer; (f) final CLT panels before saw the external gaps. (Note: dimensions are in mm)

Still before these 10 days of conditioning, all specimens were again weighted and measured in order to perform another random density distribution between three defined moisture groups. Density distribution exhibited again good results with a density distribution close to a normal one, with median and mean densities close to each other, and with low CoV values between 0,07 and 0,12 (Figure (I) 3:6 and Table (I) 3:2).

After ten days of conditioning, specimens were screwed. Moisture content did not reach exactly 12%, but it was close, ≈11%. STSs used were full threaded Rapid® Vollgewinde from Schmid with a diameter of 8mm and length of 180mm (Figure (I) 3:5 (b)). It is important to refer that in order to avoid tip influence in test results, STSs were inserted through the specimen thickness until the tip of STS trespass the entire thickness of specimen (Figure (I) 3:5 (c)).

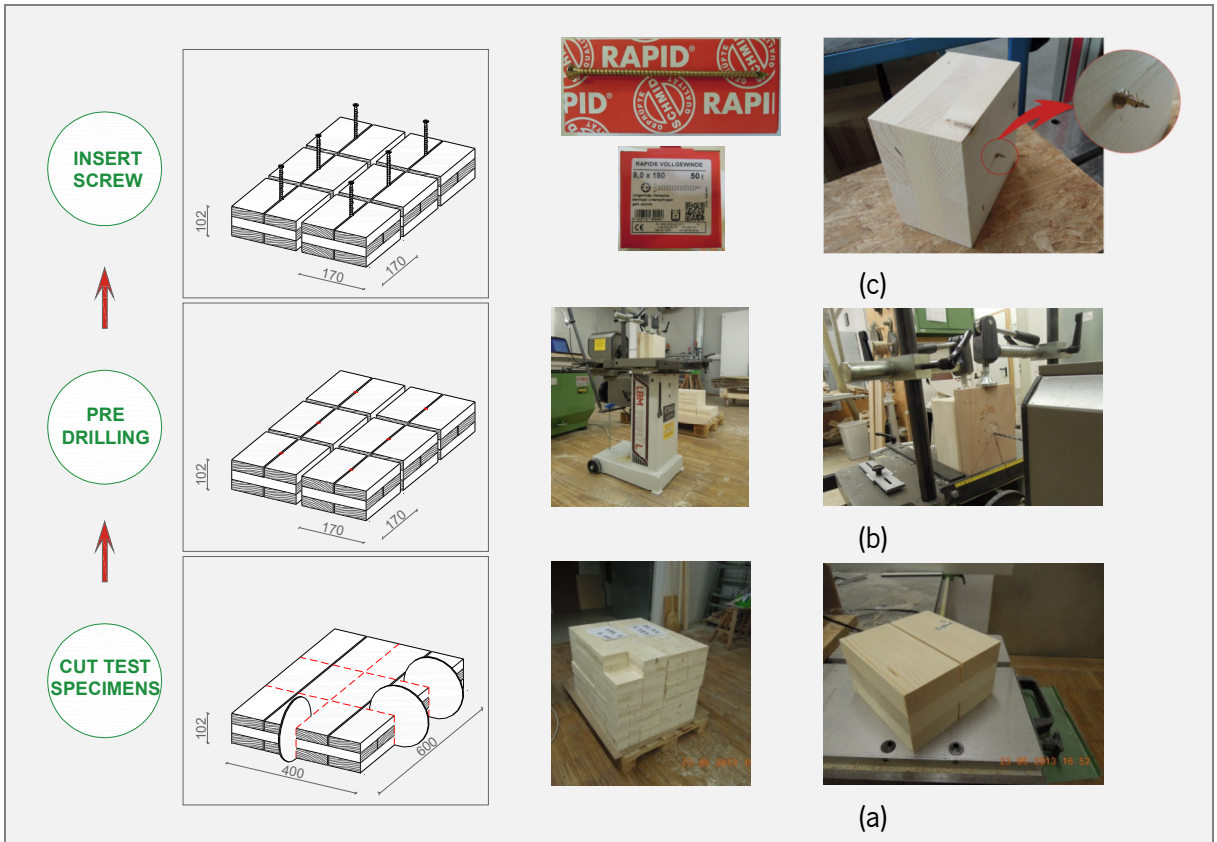

Figure (I) 3:5. Procedure to finish test specimens. (a) test specimens cut from CLT panels; (b) pre-drilling equipment; (c) STS used to perform withdrawal tests (Rapid® Vollgewinde from Schmid with diameter of 8mm and length of 180mm) and the penetration of STS through entire specimen thickness until avoids the tip effect.

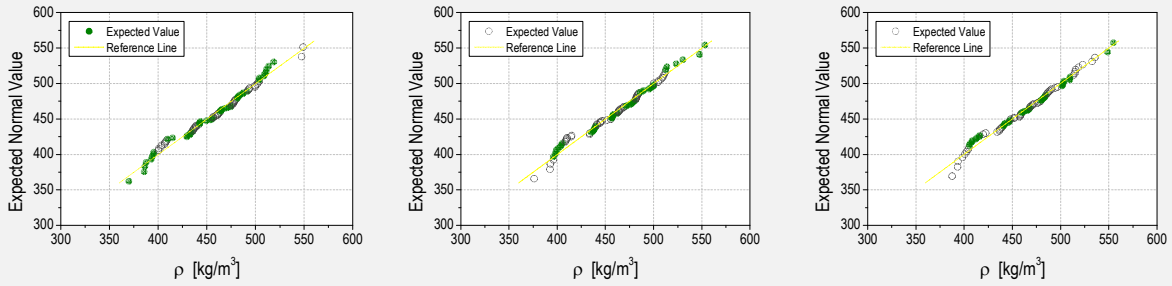

Figure (I) 3:6. Similar density distribution for different MC groups. Graphs were plotted based on Normal distribution and Renard score method - (i – 0,3) / (n + 0,4).

Table (I) 3:2. Descriptive statistics of density distribution (ρ) for all nine different configurations between three MC groups.

CONF.	MC GROUP	Nº OF SPECIMENS	MEAN	SD	COV	MIN	MEDIAN	MAX	P5
REF	8%	10	468	57,1	0,12	370	471	549	370
	12%	10	472	55,9	0,12	376	471	553	376
	18%	10	475	53,7	0,11	388	474	555	388
GAP0_FL	8%	10	453	40,1	0,09	388	459	509	388
	12%	10	455	39,2	0,09	393	460	511	393
	18%	10	460	40,0	0,09	394	463	519	394
GAP0_ML	8%	10	453	35,8	0,08	393	455	499	393
	12%	10	456	35,1	0,08	396	459	500	396
	18%	10	459	34,3	0,07	404	463	502	404
GAP0_OL	8%	10	457	41,3	0,09	386	461	514	386
	12%	10	461	41,7	0,09	396	463	523	396
	18%	10	465	42,3	0,09	401	466	535	401
GAP0_3L	8%	10	453	40,1	0,09	386	460	502	386
	12%	10	455	39,2	0,09	392	461	505	392
	18%	10	458	40,2	0,09	393	463	509	393
GAP4_FL	8%	10	453	35,8	0,08	394	457	504	394
	12%	10	457	36,4	0,08	398	461	510	398
	18%	10	461	36,0	0,08	405	465	515	405
GAP4_ML	8%	10	457	35,5	0,08	401	462	511	401
	12%	10	461	34,6	0,08	405	466	512	405
	18%	10	464	36,1	0,08	408	467	523	408
GAP4_OL	8%	10	462	37,4	0,08	407	466	519	407
	12%	10	466	39,4	0,08	409	468	530	409
	18%	10	469	38,9	0,08	412	468	533	412
GAP4_3L	8%	10	458	37,7	0,08	400	459	511	400
	12%	10	459	38,4	0,08	401	460	512	401
	18%	10	461	38,7	0,08	402	463	515	402

SD – standard deviation; **CoV** – coefficient of variation; **P5** – 5th percentile

Finished the production of specimens, it was time to conditioning three groups of specimens in different environmental conditions in order to stabilize CLT with the pre-defined MC levels, namely: 8%, 12% and 18% (Figure (I) 3:1). The first approach to choose the right environmental conditions was based on suggestions of Hartl & Ramberger (1985) (Figure (I) 3:7). However, final decision was grounded on some recent data obtained by Wallner (2012) during his deep research on the evaluation of moisture induced stresses in glulam. Considering a fixed temperature (T) of 20°C, only relative humidity (RH) levels were changed. Regarding a moisture content of 12%, both authors suggest the same level of relative humidity – 65%. But, based on his recent research, Wallner (2012) suggest different relative humidity levels to reach moisture contents of 8% and 18% (for a temperature of 20°C): respectively 29% RH and 90% RH. So, three groups of specimens with similar configurations and densities, were conditioned in three different environmental conditions, namely: 20°C and 29% RH to reach MC=8%; 20°C and 65% RH to reach MC=12%; and 20°C and 90% RH to reach MC=18% (Figure (I) 3:1).

As the moisture content at screwing time was not 12%, specimens from group that should reach MC=12% were conditioned again for more ten days before being tested. Specimens from group with MC=8% were conditioned in a climatic chamber for a period of twenty days, while specimens from group with MC=18% were conditioned in a climatic room for a period of forty-five days.

It is important to refer that, to predict the MC levels of conditioned specimens, a group of control specimens was produced. Those specimens were oven-dried, according to ISO 3130:1975, and their dried weight was used to know when specimens conditioned in different environments reach the expected MC level.

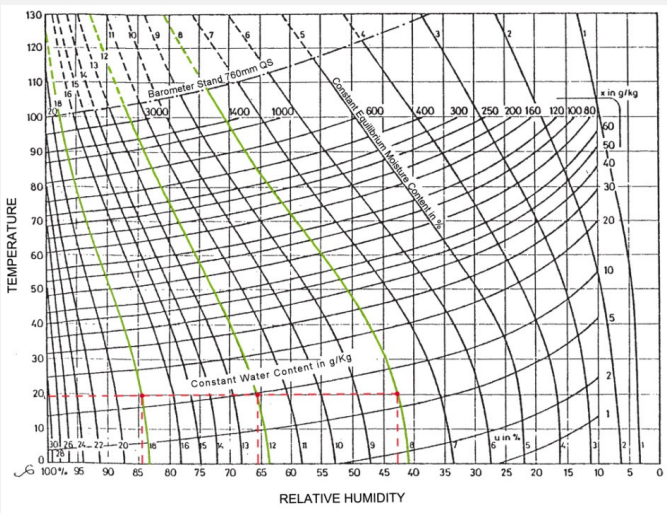

Figure (I) 3:7. Relation between temperature and relative humidity for reaching different moisture contents for spruce, suggested by Hartl & Ramberger (1985).

3.1.3 Test procedure

Axial withdrawal test procedure for screws is simple and it is clearly normalized at EN 1382:1999. Figure (I) 2:8 and Figure (I) 3:9 depict the test layout used to perform these tests and normally used to perform all withdrawal tests at *Institut für Holzbau und Holztechnologie* - Graz Technical University (Austria).

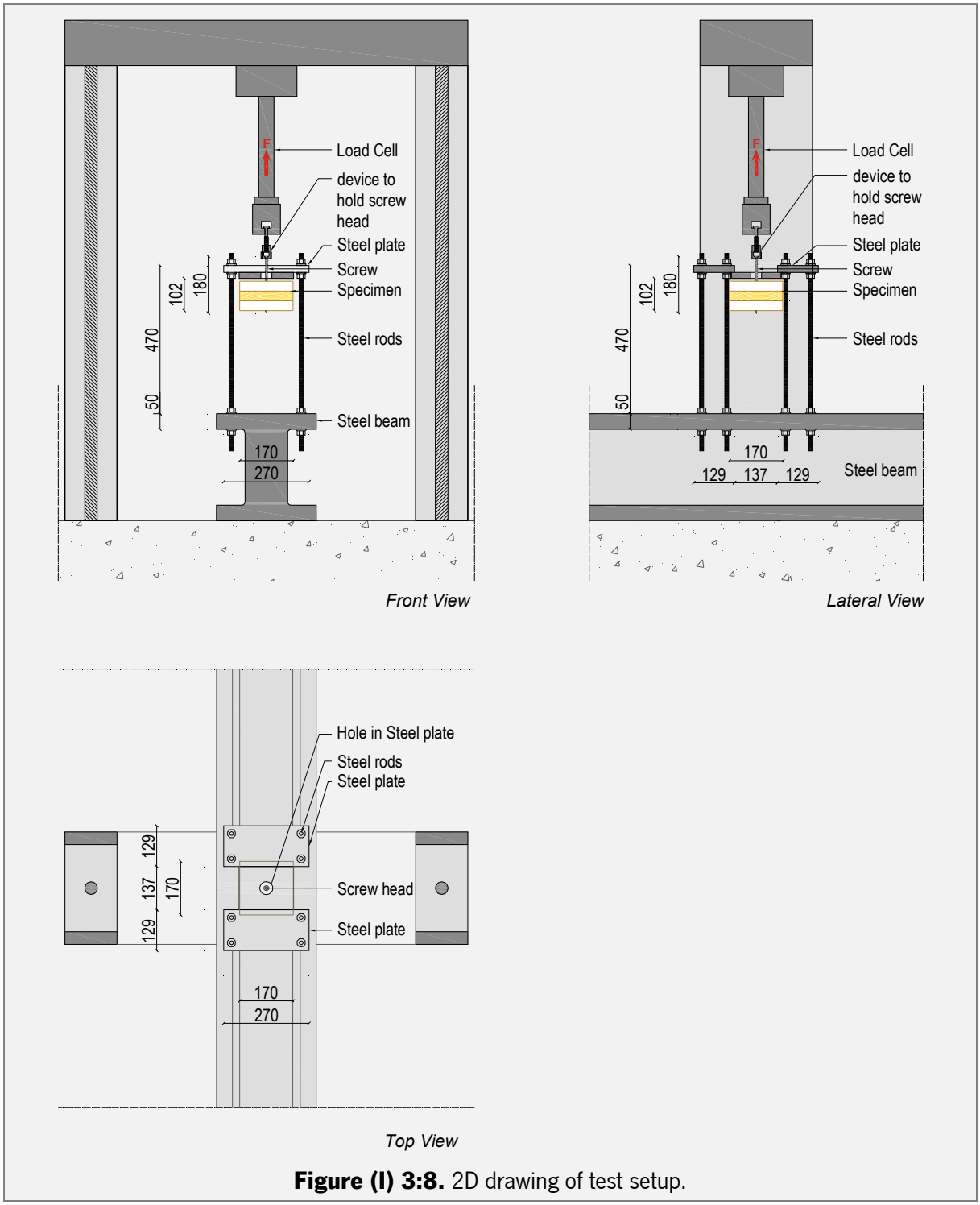

Figure (I) 3:8. 2D drawing of test setup.

Both test layout and test procedure, followed almost all recommendations of EN 1382:1999:

- Tests were performed in LIGNUM-UNI-275, a test rig manufactured by Zwick-Roell, with a maximum force of 275 kN (Figure (I) 3:10 (a));
- The device responsible to connect the screw with the load cell, ensured the application of the withdrawal force along the screw axis (Figure (I) 3:10 (b) and (c));
- Time taken to reach F_{max} was 90+/- 30 seconds with a test velocity of 2,4mm/min.

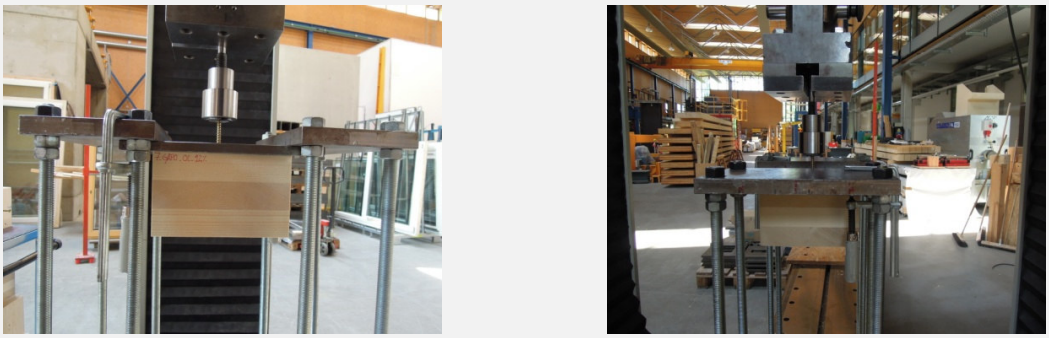

(a) (b)

Figure (I) 3:9. Photos of test setup. (a) lateral view; (b) front view.

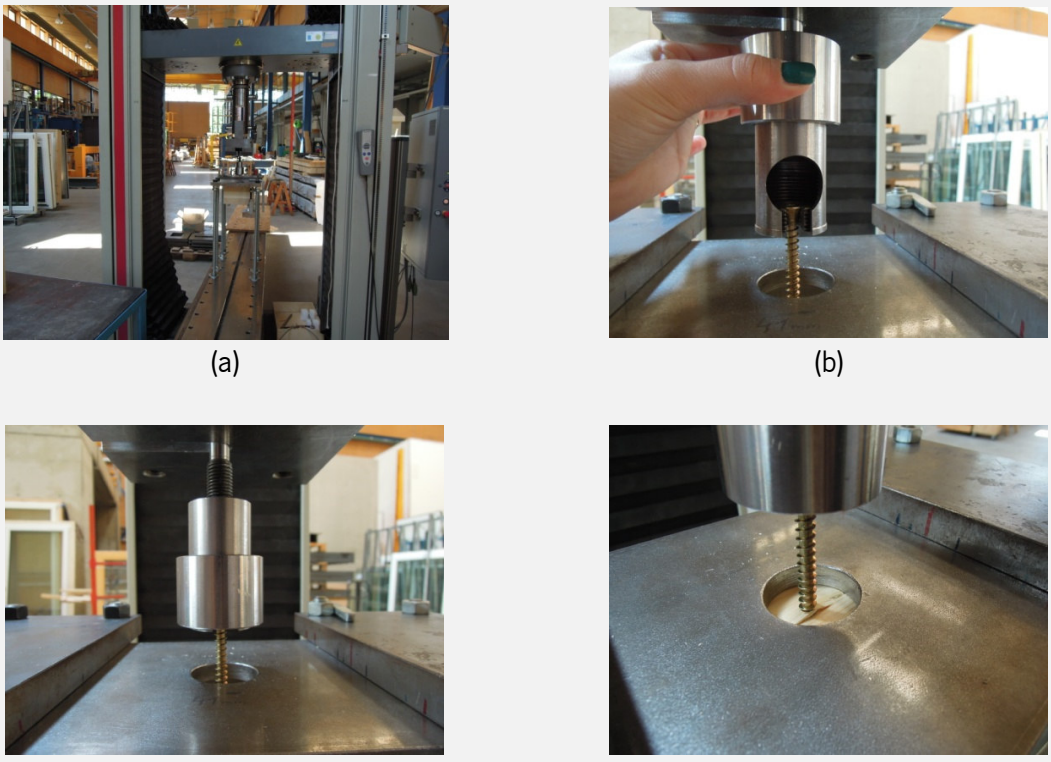

(a) (b) (c) (d)

Figure (I) 3:10. Equipment involved in test procedure. (a) test machine; (b) and (c) device to ensure the application of the withdrawal force along the screw axis and hold screw head; (d) required free area around the screw axis.

Only two parameters present in that standard were not followed. These parameters are related with the relation between screw penetration depth and the thickness of specimen, and the free area around screw axis. According to the standard, the thickness of specimen, in direction of screw insertion, should be at least $2lp + 5d$. But, as mentioned before, for present experimental campaign, screw crossed the entire thickness of specimens. This fact was not considered significant because, as already proved by Pirnbacher et al. (2009), the relation between withdrawal resistance and screw penetration is linear. Relatively to the free circular area around screw axis, standard fix a radius of 3d, but in present test setup it is a bit smaller - 2.5d (Figure (I) 3:10 (c)).

3.2 Description of test results

First step to analyze test results was to calculate the maximum withdrawal resistance ($f_{ax,test}$) that, according to EN1382:1999, should be calculated as presented in equation (3:2). However, to perform the following statistical analysis, f_{ax} was calculated according to equation (3:3), which is based on the so-called shell strength (Grabner, 2013).

Second step was to define real moisture content of all tested specimens at test time. For that, specimens were weighted at test time and posteriorly oven dried at 103°C. Once specimens reach an anhydrous state, they were weighted again. With obtained weights and following the recommendations of ISO 3130:1975, moisture content was calculated by equation (3:4). Obtained real MC levels, density of reference (ρ_{12}) was defined for all specimens, in order to compare density values considering a MC=12%. Density of reference was defined by equation (3:5), suggested at ÖNORM EN384:2010.

In an initial phase of analysis, the three moisture groups were observed individually. Obtained results for groups with 12%, 8% and 18% of moisture content will be present in the next three sub-sections, respectively.

$$f_{ax,test} = \frac{F_{max}}{d \cdot l_p} \quad (3:2)$$

$f_{ax,test}$	Maximum withdrawal resistance obtained by mechanical test, in N/mm²;
F_{max}	Maximum withdrawal load given by test machine, in N;
d	Screw diameter, in mm;
l_p	Length of penetration, in mm.

$$f_{ax,test} = \frac{F_{max}}{\pi \cdot d \cdot l_p} \quad (3:3)$$

$f_{ax,test}$ Maximum withdrawal resistance obtained by mechanical test, in N/mm²;
F_{max} Maximum withdrawal load given by test machine, in N;
d Screw diameter, in mm;
l_p Length of penetration, in mm.

$$\mathrm{MC} = \frac{\mathrm{m_1} - \mathrm{m_2}}{\mathrm{m_2}} \cdot 100 \quad (3:4)$$

MC Moisture content level, in%;
m_1 Mass of specimen before drying, in g;
m_0 Mass of specimen after drying, in g.

$$\rho_{12,i} = \rho_{MC,i} \cdot (1 - (0.5 \cdot MC - 0.12)) \quad (3:5)$$

$\rho_{12,i}$ Density with 12% of moisture content for each specimen, in kg/m³;
$\rho_{MC,i}$ Density with a different moisture content for each specimen, in kg/m³;
MC Moisture content, different of 12%, for same specimen, in %.

3.2.1 Test results for MC=12%

Regarding real MC levels obtained for the group which intended to stabilize with MC=12%, it varies in a range between 10,4% and 12,8% (11,0% ≤ Mean ≤ 11.7% and 0.02 ≤ CoV ≤ 0.06) and suggest a good distribution (Figure (I) 3:11). Large part of specimens presented MC levels lower than 12%. This fact indicates that probably specimens should be stored for a larger period under controlled environment. However, this fact is not alarming once the range of moisture content obtained is not far from the expected values and the range of values present a variation of approximately +/- 2 percentage units than the desirable MC level.

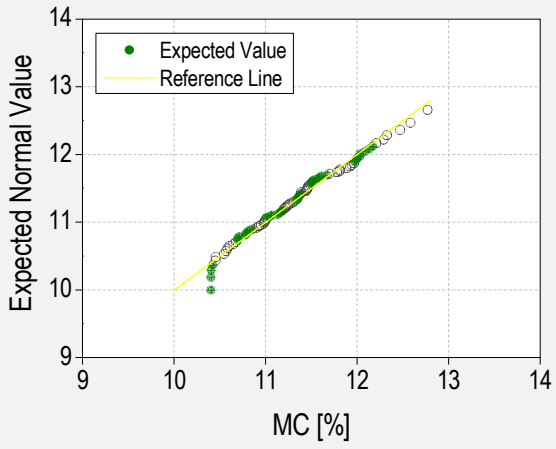

Figure (I) 3:11. Moisture distribution for group with 12% of moisture content. Graph was plotted based on Normal distribution and Renard score method - (i – 0,3) / (n + 0,4).

Table (I) 3:3 presents mean values and descriptive statistics concerning: withdrawal capacity, $f_{ax,test}$, density of reference (ρ_{12}) and moisture content (MC). For all these three variables, CoV values are positively low and median values are close to mean values, meaning a good distribution and absence of outliers.

Analyzing results obtained for $f_{ax,test}$, highest and lowest values registered are of 7,31N/mm^2 and 4,76Nmm^2, for configurations GAP0_3L_12% and GAP4_3L_12%, respectively. A slightly difference is observed between REF_12% and GAP0_12% configurations. This difference was expected to be represented by a small decrease of $f_{ax,test}$ but, contrary to expectations, values of GAP0_12% are higher than values of REF_12% (Figure (I) 3:12 (a)). Concerning configurations with GAP0, the configuration that showed the highest discrepancy comparing with REF_12% is GAP0_3L_12%, registering an increase of $f_{ax,test,mean}$ of 13,9%. Obviously, the highest losses of $f_{ax,test}$ are observed for GAP4_12% configurations. Here, the influence of the number of gaps is also evident being possible to observe a progressive decrease of $f_{ax,test}$ as the number of gaps increase (Figure (I) 3:12 (b)). So, less favorable configurations are GAP4_OL_12% and GAP4_3L_12%, with significant decreases of 16,4% and 25,9%, when compared with REF_12%, respectively.

Figure (I) 3:13 compares the results obtained by similar configurations from groups GAP0_12% and GAP4_12% with REF_12% configuration. Observing graphs, it is obvious the opposite behavior of configurations with GAP0 and GAP4 regarding the position of REF configuration. Comparing the differences between GAP0 and GAP4 configurations, the discrepancy between both tends to increase with the number of gaps: 13,8%, 11,6%, 23,2% and 34,9% for configurations GAP_FL_12%, GAP_ML_12%, GAP_OL_12% and GAP_3L_12%, respectively.

Figure (I) 3:14 depicts visual damages caused by STS failures. Screw pull-out caused minor located timber destruction in all configurations. As expected and expressed in curves depicted by Figure (I) 3:15, results presented a yielding failure mode. More detailed information about test results obtained for group with 12% of moisture content are shown in Annex 1:1.

Table (I) 3:3. Mean values and descriptive statistics of $f_{ax,test}$, ρ_{12} and MC of different test configurations with 12% of moisture content.

GROUPS	MEAN VALUES			DESCRIPTIVE STATISTICS						
	MC [%]	$f_{ax,test}$ [N/MM²]	ρ_{12} [KG/M³]	N.º OF TESTS	$f_{ax,test}$ / ρ_{12} / MC	SD	COV	MIN	MAX	MEDIAN	P5
REF_12%	**11,7**	**6,42**	**476**	**10**		**0,65**	**0,10**	**5,41**	**7,56**	**6,59**	**5,41**
						54,70	**0,12**	**382**	**559**	**474**	**382**
						0,69	**0,06**	**10,6**	**12,5**	**12,0**	**10,6**
GAP0_FL_12%	11,0	6,88	461	10		*0,93*	*0,14*	*5,45*	*8,41*	*6,66*	*5,45*
						39,00	0,08	399	518	464	399
						0,47	0,04	10,4	11,5	10,9	10,4
GAP0_ML_12%	11,2	6,66	461	10		*0,52*	*0,08*	*6,06*	*7,5*	*6,54*	*6,06*
						34,70	0,08	401	504	463	401
						0,47	0,04	10,4	12,0	11,2	10,4
GAP0_OL_12%	11,1	6,99	466	10		*0,59*	*0,08*	*5,9*	*7,73*	*7,08*	*5,9*
						40,60	0,09	403	527	467	403
						0,48	0,04	10,4	12,0	11,2	10,4
GAP0_3L_12%	11,2	7,31	460	10		*0,48*	*0,07*	*6,34*	*7,92*	*7,38*	*6,34*
						38,20	0,08	399	509	467	399
						0,49	0,04	10,5	11,8	11,3	10,5
GAP4_FL_12%	11,9	5,93	460	10		*0,68*	*0,12*	*5,12*	*7,09*	*5,98*	*5,12*
						35,60	0,08	403	512	463	403
						0,51	0,04	11,4	12,8	11,9	11,4
GAP4_ML_12%	11,2	5,89	466	10		*0,43*	*0,07*	*5,29*	*6,74*	*5,9*	*5,29*
						34,30	0,07	411	518	471	411
						0,26	0,02	10,8	11,5	11,3	10,8
GAP4_OL_12%	11,4	5,37	470	10		*0,68*	*0,13*	*4,49*	*6,53*	*5,42*	*4,49*
						38,60	0,08	414	536	471	414
						0,56	0,05	10,7	12,3	11,2	10,7
GAP4_3L_12%	11,3	4,76	464	10		*0,53*	*0,11*	*3,79*	*5,43*	*4,89*	*3,79*
						37,30	0,08	408	514	464	408
						0,46	0,04	10,7	12,0	11,3	10,7

MC – moisture content, f_{ax} - maximum withdrawal resistance, ρ_{12} – density of reference, **SD** – standard deviation, **CoV** – coefficient of variation, **P5** – 5th percentil, **REF_12%** - configuration without gaps tested with 12% of moisture content, **GAP0_FL_12%** - configuration with a gap of 0mm in first layer and tested with 12% of moisture content; **GAP0_ML_12%** - configuration with a gap of 0mm in middle layer and tested with 12% of moisture content, **GAP0_OL_12%** - configuration with a gap of 0mm in outer layers and tested with 12% of moisture content, **GAP0_3L_12%** - configuration with a gap of 0mm in three layers and tested with 12% of moisture content, **GAP4_FL_12%** - configuration with a gap of 4mm in first layer and tested with 12% of moisture content; **GAP4_ML_12%** - configuration with a gap of 4mm in middle layer and tested with 12% of moisture content, **GAP4_OL_12%** - configuration with a gap of 4mm in outer layers and tested with 12% of moisture content, **GAP4_3L_12%** - configuration with a gap of 4mm in three layers and tested with 12% of moisture content.

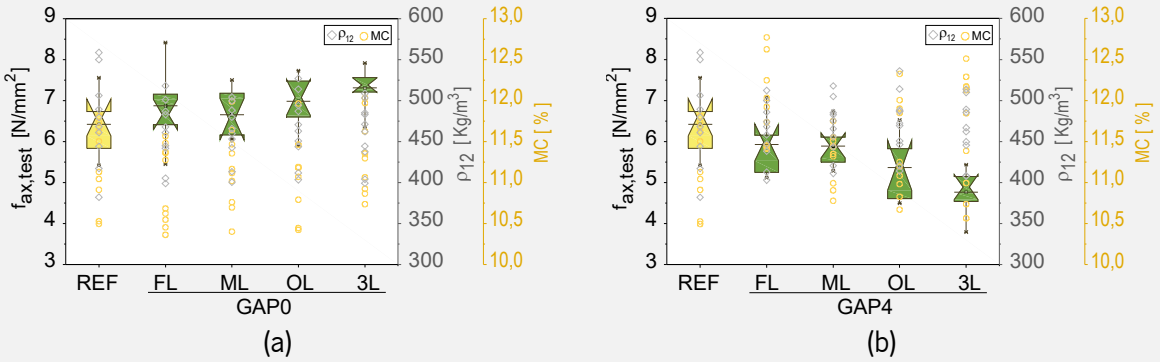

(a) (b)

Figure (I) 3:12. Box chart with notched boxes of $f_{ax,test}$ and scatter plot of density of reference and moisture content for the following groups: (a) REF_12% and GAP0_12%; (b) REF_12% and GAP4_12%.

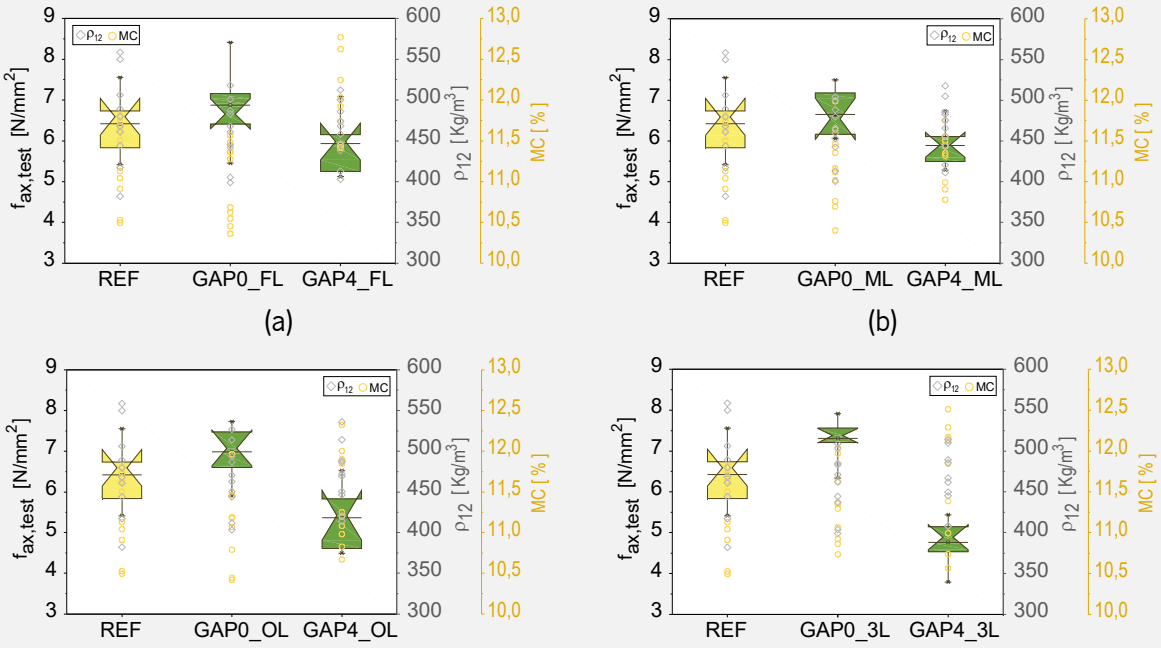

(a) (b)

(c) (d)

Figure (I) 3:13. Box chart with notched boxes of $f_{ax,test}$ and scatter plot of density of reference and moisture content for the following groups: (a) REF_12% and GAP_FL_12%; (b) REF_12% and GAP_ML_12%; (c) REF_12% and GAP_OL_12%; and (d) REF_12% and GAP_3L_12%.

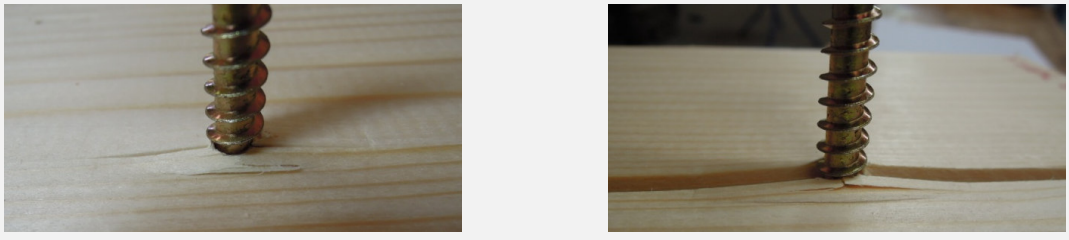

(a) (b)

Figure (I) 3:14. Visual inspection of failures for tests performed with 12% moisture content. (a) typical failure for configurations REF_12%, GAP4_ML_12% and configurations belonging to GAP0_12%; (b) typical failure for remaining configurations belonging to GAP4_12%.

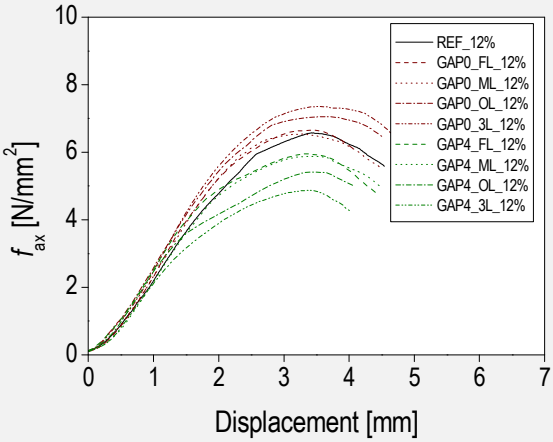

Figure (I) 3:15. Mean test curves for all configurations with 12% of moisture content, expressing the expected yielding failure mode.

3.2.2 Test results for MC=8%

Concerning results obtained for specimens tested with MC=8%, the real MC levels vary between 7,7% and 8,9% and present a good distribution (Figure (I) 3:16). However, due to low levels of MC reached, some damages in CLT specimens were observed after conditioning period in an environment of 20°C and 29% RH. Damages in specimens were detected by direct visual inspection and are listen bellow:

- Two specimens (8_GAP0_ML_8% and 9_GAP0_8%) exhibited large cracks through the STS location, in first layer, however it seems to not influence obtained $f_{ax,test}$ (Figure (I) 3:17 (a));
- Some specimens exhibited cracks through STS location in bottom layer (Figure (I) 3:17 (b));
- Specimens of groups with GAP0/GAP4 in one or both outer layers (GAP_FL, GAP_OL and GAP_3L) exhibited an enlargement of gap width of approximately 1mm (Figure (I) 3:17 (c));
- Some specimens present some cracks parallel to the grain in middle layer, for configurations that do not consider gaps in the same layer (Figure (I) 3:17 (d));
- A reduced delamination between layers was verified only in few cases (Figure (I) 3:17 (e)).

Furthermore, as a result of some test problems, sampling of group GAP4_ML_8% was reduced from ten to eight specimens.

Table (I) 3:4 presents descriptive statistics of results obtained by the group of specimens that intended to reach MC=8%, concerning: $f_{ax,test}$, ρ_{12} and MC. Similarly to group with MC=12%, obtained results suggest a good distribution and absence of outliers. The highest obtained mean value for $f_{ax,test}$ was 7,34 N/mm^2 for configuration GAP0_3L_8% and lowest was 4,10N/mm^2 for configuration GAP4_3L_8%.

Figure (I) 3:18 (a), the tendency to $f_{ax,test}$ increase with number of gaps remains. Also due to enlargement of gaps, GAP4_8% configurations present higher decreases for $f_{ax,test}$ than those observed in group with MC=12%. Again the configurations GAP4_OL_8% and GAP4_3L_8% exhibit the higher decreases (Figure (I) 3:18 (b)): 28,4% and 37,3%, respectively. Figure (I) 3:19 compares the results obtained by similar configurations with GAP0 and GAP4. Considering only gap width, the differences still increase with number of gaps: 19,3%, 14,6%, 30,4% and 44,1%, for configurations GAP_FL_8%, GAP_ML_8%, GAP_OL_8% and GAP_3L_8%, respectively. Due to lower $f_{ax,test}$ obtained for configurations with GAP4, these differences are larger than results obtained by group with MC=12%.

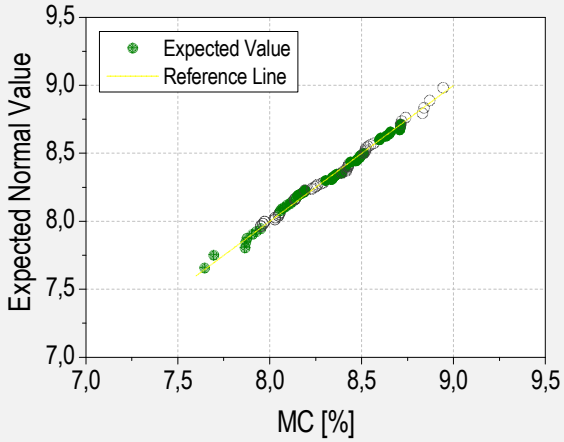

Figure (I) 3:16. Moisture distribution for group with 8% of moisture content.

(a) (b) (c)

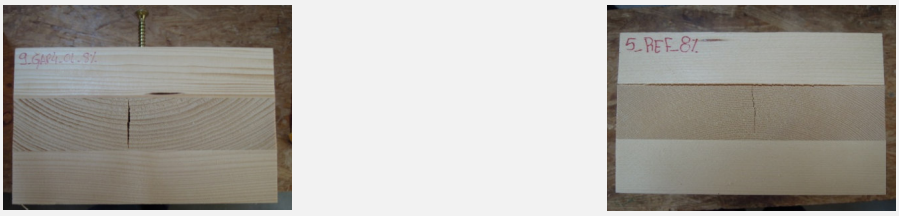

(d) (e)

Figure (I) 3:17. Cracking resulted from conditioning period. (a) crack through the STS location; (b) opening of GAP0 on an exterior layer; (c) lateral view of a crack in an outer layer; (d) and (e) lateral view of delamination and crack in middle layer.

Table (I) 3:4. Mean values and descriptive statistics of $f_{ax,test}$, ρ_{12} and MC of different test configurations with 8% of moisture content.

GROUPS	MEAN VALUES			DESCRIPTIVE STATISTICS						
	MC (%)	$f_{ax,test}$ (N/MM²)	ρ_{12} (KG/M³)	NUMBER OF TESTS	$f_{ax,test}$ / ρ_{12} / MC	SD	COV	MIN	MAX	MEDIAN	P5
REF_8%	**8,4**	**6,54**	**472**	**10**	***0,68***	***0,10***	***5,47***	***7,96***	***6,52***	***5,47***
					55,70	**0,12**	**376**	**553**	**472**	**376**
					0,35	**0,04**	**7,9**	**8,9**	**8,6**	**7,9**
GAP0_FL_8%	8,0	6,69	458	10	*0,73*	*0,11*	*5,75*	*8,12*	*6,73*	*5,75*
					39,00	0,09	395	514	463	395
					0,29	0,03	7,9	8,7	8,3	7,9
GAP0_ML_8%	8,1	6,29	457	10	*0,31*	*0,05*	*5,91*	*6,82*	*6,23*	*5,91*
					35,30	0,08	398	504	460	398
					0,28	0,03	7,9	8,6	8,4	7,9
GAP0_OL_8%	8,0	6,72	461	10	*0,43*	*0,06*	*5,92*	*7,26*	*6,76*	*5,92*
					40,40	0,09	393	517	464	393
					0,33	0,04	7,7	8,8	8,2	7,7
GAP0_3L_8%	8,1	7,34	458	10	*0,46*	*0,06*	*6,42*	*7,77*	*7,54*	*6,42*
					39,50	0,09	391	505	466	391
					0,24	0,03	8,0	8,7	8,4	8,0
GAP4_FL_8%	8,1	5,4	457	10	*0,74*	*0,14*	*3,93*	*6,62*	*5,28*	*3,93*
					34,10	0,07	401	505	461	401
					0,19	0,02	8,0	8,7	8,4	8,0
GAP4_ML_8%	7,9	5,37	455	8	*0,38*	*0,07*	*4,72*	*5,84*	*5,41*	*4,72*
					36,20	0,08	405	516	455	405
					0,33	0,04	7,7	8,7	8,4	7,7
GAP4_OL_8%	8,0	4,68	467	10	*0,34*	*0,07*	*4,25*	*5,32*	*4,64*	*4,25*
					36,50	0,08	412	522	469	412
					0,19	0,02	7,9	8,5	8,1	7,9
GAP4_3L_8%	7,8	4,10	462	10	*0,45*	*0,11*	*3,25*	*4,66*	*4,2*	*3,25*
					36,30	0,08	407	513	463	407
					0,19	0,02	8,0	8,7	8,2	8,0

MC – moisture content, f_{ax} - maximum withdrawal resistance, ρ_{12} – density, **SD** – standard of deviation, **CoV** – coefficient of variation, **P5** – 5th percentil, **REF_8%** - configuration without gaps tested with 8% of moisture content, **GAP0_FL_8%** - configuration with a gap of 0mm in first layer and tested with 8% of moisture content; **GAP0_ML_8%** - configuration with a gap of 0mm in middle layer and tested with 8% of moisture content, **GAP0_OL_8%** - configuration with a gap of 0mm in outer layers and tested with 8% of moisture content, **GAP0_3L_8%** - configuration with a gap of 0mm in three layers and tested with 8% of moisture content, **GAP4_FL_8%** - configuration with a gap of 4mm in first layer and tested with 8% of moisture content; **GAP4_ML_8%** - configuration with a gap of 4mm in middle layer and tested with 8% of moisture content, **GAP4_OL_8%** - configuration with a gap of 4mm in outer layers and tested with 8% of moisture content, **GAP4_3L_8%** - configuration with a gap of 4mm in three layers and tested with 8% of moisture content.

Figure (I) 3:20 depicts the visual failures of tested specimens with MC=8%, which are more pronounced than observed failures for specimens with MC=12%. In bottom part, tip of STS crushes timber, while on top, timber breaks and comes out inside free area around the STS provided by test setup. However, the failure mode remains the same: Figure (I) 3:21 shows the yielding failure mode, through the mean curves obtained by relation between $f_{ax,test}$ and STS displacement. More detailed information about test results of specimens with MC=8% can be seen in Annex 1:11.

Analyzing $f_{ax,test}$ values obtained in 8% of moisture content group, it was verified that due to reduced moisture content and consequent small enlargement of gaps, the discrepancy between REF_8% and GAP0_8% configurations became reduced. The higher discrepancy is of 12,23% for configuration GAP0_3L_8%. However, as expected and shown in Figure (I) 3:18, the tendency to $f_{ax,test}$ increase with number of gaps remains. Relatively to GAP4_8% configurations, the withdrawal capacity decrease more than in group with 12% of moisture content also due to gap enlargement. Again the configurations of GAP4_OL_8% and GAP4_3L_8% exhibit the higher discrepancies (Figure (I) 3:18): 28,44% and 37,31%, respectively. Figure (I) 3:19 compares the results obtained by similar configurations of GAP0 and GAP4. Considering only gap width, the differences still increase with number of gaps: 19,28%, 14,63%, 30,36% and 44,14%, for configurations GAP_FL_8%, GAP_ML_8%, GAP_OL_8% and GAP_3L_8%, respectively. These differences are larger than results obtained by group with 12% of moisture content.

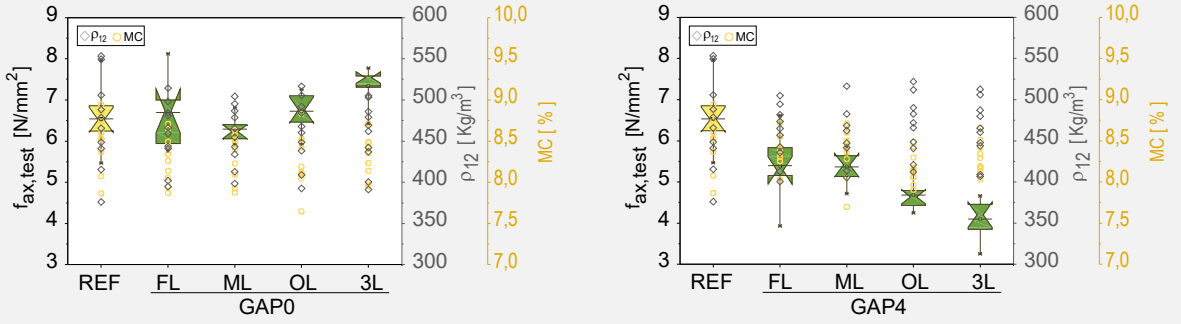

Figure (I) 3:18. Box chart with notched boxes of $f_{ax,test}$ and scatter plot of density of reference and moisture content for the following groups: (a) REF_8% and GAP0_8%; (b) REF_8% and GAP4_8%.

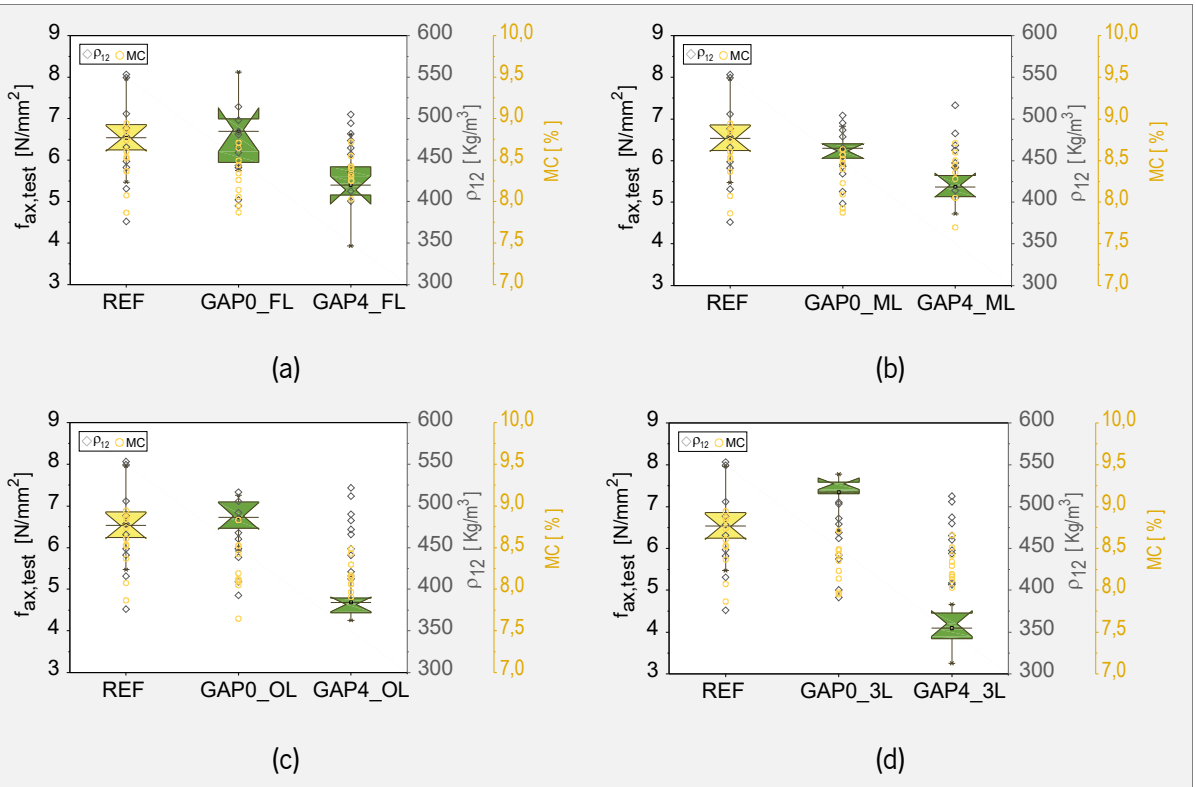

Figure (I) 3:19. Box chart with notched boxes of $f_{ax,test}$ and scatter plot of density of reference and moisture content for the following groups: (a) REF_8% and GAP_FL_8%; (b) REF_8% and GAP_ML_8%; (c) REF_8% and GAP_OL_8%; and (d) REF_8% and GAP_3L_8%.

Figure (I) 3:20. Visual failures of tests performed with 8% of moisture content. (a) Visual failure for configurations REF, GAP0 and GAP4_ML; (b) Visual failure for remaining configurations GAP4.

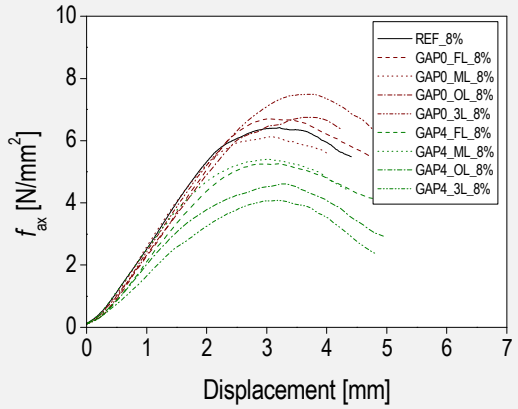

Figure (I) 3:21. Mean test curves for all configurations with 8% of moisture content, expressing the expected yielding failure mode.

3.2.3 Test results for MC=18%

Considering the group of specimens in which a MC=18% was intended, the range of moisture content values vary between 16,5% and 18,7%, and similarly to both previous groups, obtained values exhibit a good distribution (Figure (I) 3:22). Furthermore, similarly to what was observed to low levels of MC (MC=8%), high levels of MC caused some damages on CLT specimens, namely:

- Wood swelling caused the deformation of CLT specimens, which exhibit concave or convex side faces depending on dominant timber direction (Figure (I) 3:23 (a));
- GAP4 close significantly, crushing against the thread of STSs (Figure (I) 3:23 (b)).

Table (I) 3:5 presents descriptive statistics of $f_{ax,test}$, ρ_{12} and MC, for all test configurations with MC=18%. Withdrawal resistance varies in a range between 3,77 N/mm² and 7,76 N/mm² and, similarly to both moisture groups described before, configurations GAP0 present the highest values (Figure (I) 3:24 (a)) and configurations GAP4 present the lowest values (Figure (I) 3:24 (b)). Both follow the same tendency to increase/decrease $f_{ax,test}$ with the increase of number of gaps. However, differently to what was observed for remaining MC groups, the decrease of $f_{ax,test}$ registered for GAP4 configurations is not so significant. This change is the result of timber swelling and consequent closing of GAP4. The difference between mean $f_{ax,test}$ of configurations REF_18% and GAP4_3L_18% is 18,3%. It is important to remind that for the group with MC=8% the difference between these configurations was of 37,3%.

Following the same tendency, similar configurations with GAP0 and GAP4 also present lower differences between them. Figure (I) 3:25 depicts exactly this fact which can be expressed by following percentages: 15,1%, 11,1%, 15,0% and 23,5%. Relatively to visual damages after testing, they were quite similar to those observed for group tested with MC=8%. Due to higher moisture content, crushing close to the tip

of STS, caused by pulling out action, was a bit more evident, but on the top of specimen timber fractured less (Figure (I) 3:26). Figure (I) 3:27 depicts the mean curves representative of relation between $f_{ax,test}$ and displacement (mm). As expected, and similarly to the remaining MC groups, curves depict a yielding failure mode. More detailed information about test results for configurations with MC=18% can be seen in Annex 1:12.

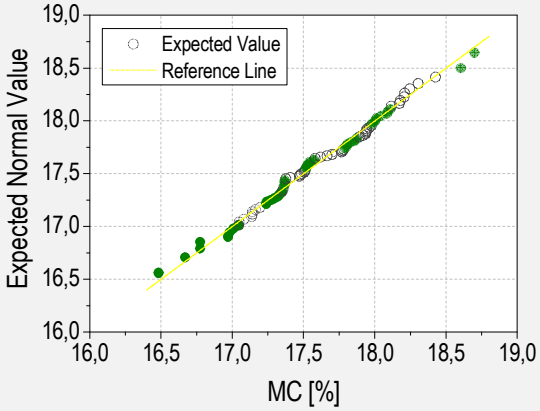

Figure (I) 3:22. Moisture distribution for group with 18% of moisture content.

(a) (b)

Figure (I) 3:23. Damages caused by high MC levels. (a) deformations on CLT shape caused by timber swelling depending on grain direction; (b) closing of GAP4 after conditioning period.

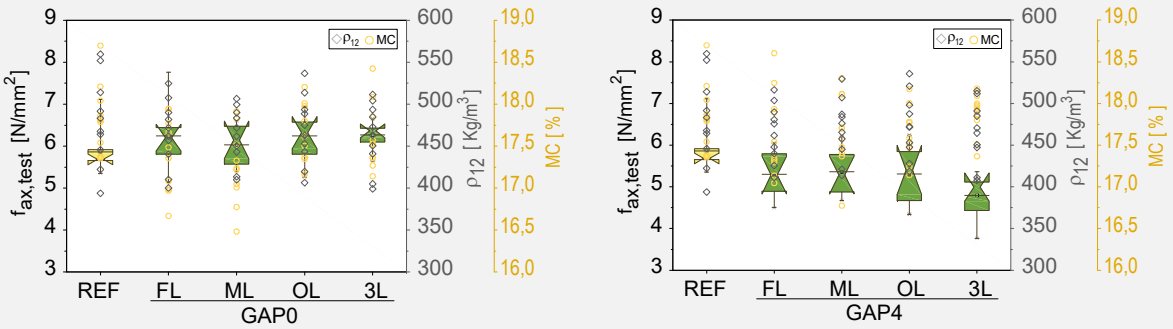

(a) (b)

Figure (I) 3:24. Box chart with notched boxes of $f_{ax,test}$ and scatter plot of density of reference and moisture content for the following groups: (a) REF_18% and GAP0_18%; (b) REF_18% and GAP4_18%.

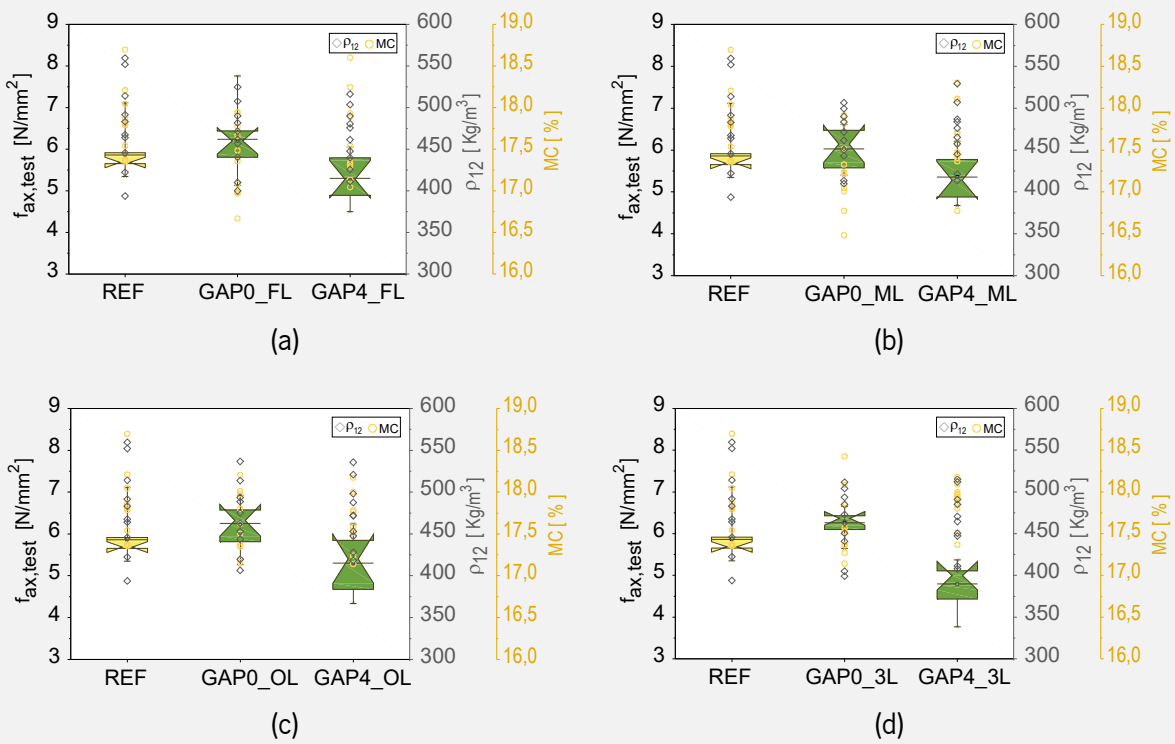

Figure (I) 3:25. Box chart with notched boxes of $f_{ax,test}$ and scatter plot of density of reference and moisture content for the following groups: (a) REF_18% and GAP_FL_18%; (b) REF_18% and GAP_ML_18%; (c) REF_18% and GAP_OL_18%; (d) REF_18% and GAP_3L_18%; and (e) REF_18% and GL_18%.

(a) (b)

Figure (I) 3:26. Visual STS failures of tests performed with 18% of moisture content. (a) Visual failure on top of specimen; (b) Visual failure on bottom of specimen.

Table (I) 3:5. Mean values and descriptive statistics of $f_{ax,test}$, ρ_{12} and MC for different test configurations with 18% of moisture content.

	MEAN VALUES			DESCRIPTIVE STATISTICS						
GROUPS	MC (%)	$f_{ax,test}$ (N/MM²)	ρ_{12} (KG/M³)	NUMBER OF TESTS	$f_{ax,test}$ / ρ_{12} / MC					
					SD	COV	MIN	MAX	MEDIAN	P5
REF_18%	**17,5**	**5,86**	**479**	**10**	***0,53***	***0,09***	***5,35***	***7,12***	***5,68***	***5,35***
					52,90	**0,11**	**394**	**560**	**475**	**394**
					0,43	**0,02**	**17,4**	**18,7**	**17,8**	**17,4**
GAP0_FL_18%	17,0	6,24	465	10	*0,70*	*0,11*	*5,13*	*7,76*	*6,2*	*5,13*
					39,80	0,09	400	525	467	400
					0,45	0,03	16,7	17,9	17,4	16,7
GAP0_ML_18%	17,0	6,03	463	10	*0,45*	*0,07*	*5,4*	*6,61*	*6,15*	*5,4*
					33,80	0,07	410	507	467	410
					0,44	0,03	16,5	17,9	17,2	16,5
GAP0_OL_18%	17,4	6,25	469	10	*0,52*	*0,08*	*5,26*	*6,93*	*6,32*	*5,26*
					40,70	0,09	406	537	469	406
					0,36	0,02	17,2	18,2	17,6	17,2
GAP0_3L_18%	17,3	6,26	463	10	*0,33*	*0,05*	*5,65*	*6,66*	*6,37*	*5,65*
					39,00	0,08	399	512	468	399
					0,40	0,02	17,1	18,4	17,5	17,1
GAP4_FL_18%	17,4	5,3	465	10	*0,55*	*0,10*	*4,5*	*6,05*	*5,28*	*4,5*
					34,20	0,07	411	516	469	411
					0,51	0,03	17,1	18,6	17,4	17,1
GAP4_ML_18%	17,3	5,36	469	10	*0,52*	*0,10*	*4,67*	*6,21*	*5,28*	*4,67*
					36,10	0,08	414	529	471	414
					0,45	0,03	16,8	18,3	17,6	16,8
GAP4_OL_18%	17,4	5,31	473	10	*0,68*	*0,13*	*4,34*	*6,24*	*5,4*	*4,34*
					38,20	0,08	418	536	472	418
					0,32	0,02	17,1	18,2	17,6	17,1
GAP4_3L_18%	17,4	4,79	466	10	*0,55*	*0,12*	*3,77*	*5,37*	*5*	*3,77*
					37,30	0,08	408	515	468	408
					0,25	0,01	17,4	18,2	18,0	17,4

MC – moisture content, $f_{ax,test}$ - maximum withdrawal resistance obtained with test, ρ_{12} – density, **SD** – standard of deviation, **CoV** – coefficient of variation, **P5** – 5th percentil, **REF_18%** - configuration without gaps and tested with 18% of moisture content, **GAP0_FL_18%** - configuration with a gap of 0mm in first layer and tested with 18% of moisture content; **GAP0_ML_18%** - configuration with a gap of 0mm in middle layer and tested with 18% of moisture content, **GAP0_OL_18%** - configuration with a gap of 0mm in outer layers and tested with 18% of moisture content, **GAP0_3L_18%** - configuration with a gap of 0mm in three layers and tested with 18% of moisture content, **GAP4_FL_18%** - configuration with a gap of 4mm in first layer and tested with 18% of moisture content; **GAP4_ML_18%** - configuration with a gap of 4mm in middle layer and tested with 18% of moisture content, **GAP4_OL_18%** - configuration with a gap of 4mm in outer layers and tested with 18% of moisture content, **GAP4_3L_18%** - configuration with a gap of 4mm in three layers and tested with 18% of moisture content.

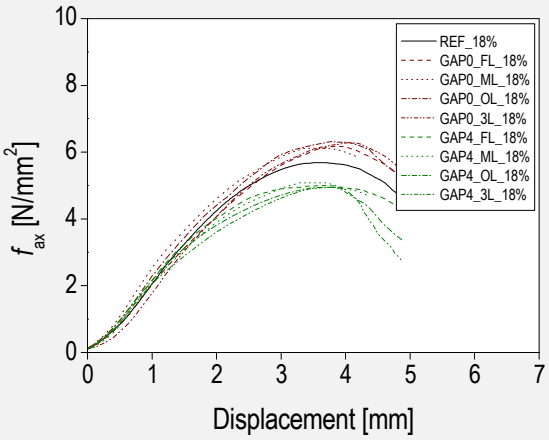

Figure (I) 3:27. Mean test curves for all configurations with 8% of moisture content, expressing a yielding failure mode.

3.3 Modeling the influence of number of gaps (η_{gap}) and MC levels (η_{MC}) on withdrawal resistance of STSs inserted in main face of CLT panels

3.3.1 Correction of density of reference ($\rho_{12,corr}$) and withdrawal resistance ($f_{ax,corr}$)

As observed in previous points, against the expectations, GAP0 configurations exhibited higher $f_{ax,test}$ than REF configurations for all moisture groups, always depending on number of gaps. Those results incited the suspicion that the density at GAP location could be higher depending on the way the boards were placed during CLT production. Annual growing rings could be closer to each other in the location where STS was inserted (Figure (I) 3:28). Considering this suspicion, density was corrected by measure and weight a smaller volume of timber around the STS (Figure (I) 3:29). However, corrected density ($\rho_{12,corr}$) present a bit lower values (Figure (I) 3:30) than ρ_{12}, a difference that was not considered significant. Table (I) 3:6 presents density values, before and after correction, respective CoV and the ratio between both for all configurations tested with different MC levels.

Considering values obtained for $\rho_{12,corr}$, f_{ax} was also corrected ($f_{ax,corr}$) according to equation (3:6), suggested by CUAP 06.03/08 (2010). Despite this formula has been conceived to be used only in case of high differences between densities of specimens, it was decided to apply it in order to perform some comparisons with results obtained for the experimental campaigns presented in next two chapters. Table (I) 3:7 shows the descriptive statistics of $f_{ax,corr}$, which are the values used to perform the analysis presented hereafter.

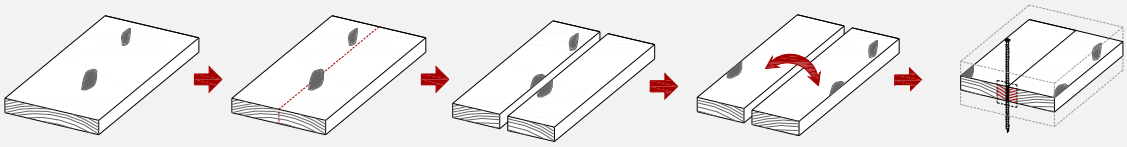

Figure (I) 3:28. Sketch explaining the reason why density is higher in gap location.

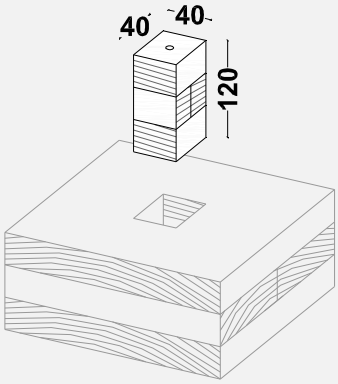

Figure (I) 3:29. GAPO_ML configurations cut to correct the density close to STS location (dimensions in mm).

$$f_{ax,corr,i.} = f_{ax,test,i} \cdot \left(\frac{\rho_{ref,i}}{\rho_{12}}\right)^{0,8} \quad (3:6)$$

$f_{ax,corr,i}$	Corrected withdrawal resistance for each test specimen, in N/mm²;
$f_{ax,test,i}$	Withdrawal resistance for each specimen resulted from test machine, in N/mm²;
ρ_{ref}	Density of reference (mean value for ρ_{12} obtained with entire data of tests performed), in kg/m³;
$\rho_{12,i}$	Density of each specimen with a moisture content of 12%.

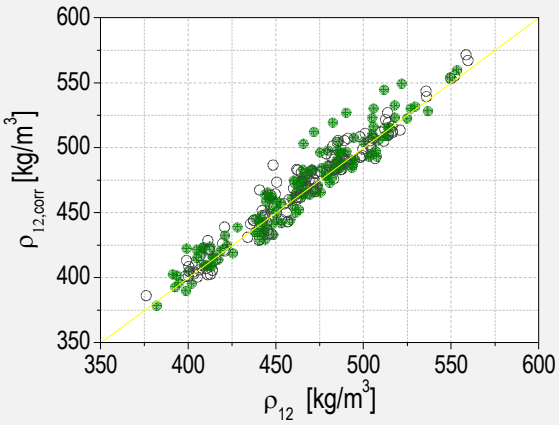

Figure (I) 3:30. Relation between density of reference concerning the entire specimen (ρ_{12}) and corrected density considering a small sample of CLT close to STS location ($\rho_{12,corr}$).

Table (I) 3:6. Median values of ρ_{12} and $\rho_{12,corr}$ for different test configurations, respective CoV values and ratio between them.

MEAN VALUES						
GROUPS		ρ_{12} (KG/M³)	COV (ρ_{12}) [%]	$\rho_{12,corr}$ (KG/M³)	COV ($\rho_{12,corr}$) [%]	$\frac{\rho_{12}}{\rho_{12,corr}}$
REF	**8%**	**472**	**11,80**	**466**	**12,11**	**1,01**
	12%	**476**	**12,05**	**463**	**13,21**	**1,02**
	18%	**472**	**11,04**	**472**	**11,33**	**1,02**
GAP0_FL	**8%**	458	8,51	446	8,69	1,03
	12%	461	8,46	452	9,39	1,02
	18%	465	8,57	452	8,69	1,03
GAP0_ML	**8%**	457	7,73	446	7,59	1,02
	12%	461	7,54	453	7,64	1,02
	18%	463	7,31	451	7,11	1,03
GAP0_OL	**8%**	461	8,75	454	8,69	1,02
	12%	466	8,72	461	8,29	1,01
	18%	469	8,67	460	8,56	1,02
GAP0_3L	**8%**	458	8,64	453	7,86	1,01
	12%	460	8,31	456	7,13	1,01
	18%	463	8,43	456	6,62	1,01
GAP4_FL	**8%**	462	6,99	458	7,94	1,01
	12%	460	7,74	454	7,87	1,01
	18%	465	7,35	453	7,98	1,03
GAP4_ML	**8%**	455	7,95	454	7,76	1,00
	12%	466	7,37	461	8,55	1,01
	18%	469	7,70	461	8,29	1,02
GAP4_OL	**8%**	467	7,82	487	8,67	0,96
	12%	470	8,21	463	7,87	1,01
	18%	473	8,07	461	8,21	1,03
GAP4_3L	**8%**	462	7,86	466	7,83	0,99
	12%	464	8,03	468	7,63	0,99
	18%	465	8,01	467	7,42	1,00

ρ_{12} – density, **CoV** – coefficient of variation, **REF** - test configuration with no gaps, **GAP0_FL** - test configuration with a gap of 0mm in first layer; **GAP0_ML** - test configuration with a gap of 0mm in middle layer, **GAP0_OL**- test configuration with a gap of 0mm in outer layers, **GAP0_3L**- test configuration with a gap of 0mm in three layers, **GAP4_FL**- test configuration with a gap of 4mm in first layer; **GAP4_ML** - test configuration with a gap of 4mm in middle layer, **GAP4_OL** - test configuration with a gap of 4mm in outer layers, **GAP4_3L** - test configuration with a gap of 4mm in three layers.

Table (I) 3:7. Descriptive statistics of $f_{ax,corr}$ for different test configurations with 8%, 12% and 18% of moisture content.

GROUPS		SAMPLE	MEAN	SD	COV [%]	MEDIAN	MIN	MAX	P5
REF	8%	10	6,48	0,42	6,41	6,54	5,87	7,07	5,87
	12%	9	6,46	0,22	0,03	6,44	6,12	6,80	6,12
	18%	10	5,75	0,24	4,14	5,69	5,44	6,11	5,44
GAP0_FL	8%	10	6,85	0,49	7,15	6,88	5,90	7,58	5,90
	12%	10	6,95	0,51	7,40	6,97	6,26	7,76	6,26
	18%	10	6,32	0,36	5,66	6,22	5,74	7,11	5,74
GAP0_ML	8%	10	6,46	0,43	6,65	6,57	5,69	6,95	5,69
	12%	10	6,74	0,33	4,84	6,81	6,15	7,17	6,15
	18%	10	6,11	0,21	3,38	6,17	5,78	6,44	5,78
GAP0_OL	8%	10	6,80	0,32	4,69	6,83	6,14	7,33	6,14
	12%	10	6,97	0,28	4,03	6,94	6,57	7,54	6,57
	18%	10	6,24	0,26	4,22	6,17	5,90	6,74	5,90
GAP0_3L	8%	10	7,42	0,17	2,31	7,39	7,25	7,81	7,25
	12%	10	7,36	0,28	3,87	7,36	6,91	7,72	6,91
	18%	10	6,31	0,25	4,04	6,33	5,74	6,62	5,74
GAP4_FL	8%	9	5,57	0,32	0,06	5,44	5,20	6,21	5,20
	12%	10	5,97	0,38	6,43	5,91	5,45	6,68	5,45
	18%	10	5,36	0,32	5,98	5,24	5,01	5,87	5,01
GAP4_ML	8%	8	5,41	0,09	1,73	5,45	5,20	5,49	5,20
	12%	10	5,87	0,11	1,92	5,89	5,70	6,08	5,70
	18%	10	5,34	0,24	4,46	5,30	4,95	5,63	4,95
GAP4_OL	8%	10	4,48	0,30	6,71	4,39	4,09	5,06	4,09
	12%	10	5,32	0,38	7,07	5,35	4,82	5,83	4,82
	18%	10	5,28	0,38	7,14	5,31	4,74	5,75	4,74
GAP4_3L	8%	10	4,04	0,27	6,63	4,04	3,58	4,42	3,58
	12%	10	4,68	0,29	6,13	4,76	4,12	5,03	4,12
	18%	10	4,72	0,34	7,11	4,74	4,20	5,17	4,20

f_{ax} - maximum withdrawal resistance, **CoV** – coefficient of variation, **REF** - test configuration with no gaps, **GAP0_FL** - test configuration with a gap of 0mm in first layer; **GAP0_ML** - test configuration with a gap of 0mm in middle layer, **GAP0_OL**- test configuration with a gap of 0mm in outer layers, **GAP0_3L**- test configuration with a gap of 0mm in three layers, **GAP4_FL**- test configuration with a gap of 4mm in first layer; **GAP4_ML** - test configuration with a gap of 4mm in middle layer, **GAP4_OL** - test configuration with a gap of 4mm in outer layers, **GAP4_3L** - test configuration with a gap of 4mm in three layers.

3.3.2 Defining η_{gap} and η_{MC}

In order to quantify properly the influence of each GAP0/GAP4 added to the STS path (k_{gap}) as well as the influence of each percentage unit of MC added/subtracted to CLT elements (k_{MC}), linear fittings based on the method of least squares were performed. These linear fittings resulted in the suggestion of

bi-linear models able to quantify the influence of number and width of gaps (η_{gap}) and MC levels (η_{MC}) in the withdrawal resistance of STSs inserted in the main face of CLT panels.

It is important to refer that, for the following analysis, two extreme outliers were excluded from data because, obtained data points lie upper or lower the outer fences defined by each individual boxplot construction (Table (I) 3:8). Relatively to the performed linear fittings, it is also important to note that R^2 tends to be lower than desirable and the reason for that should be related with reduced sampling.

Table (I) 3:8. Outliers excluded from data considered for bilinear modeling.

SPECIMEN NAME	NUMBER OF GAPS	GAP WIDTH [MM]	$f_{ax,corr}$ [N/MM²]	ρ_{12} [KG/M³]
8_REF_12%	0	n.a.	5,46	499
2_GAP4_FL_8%	1	4	4,29	411

3.3.2.1 η_{GAP}

In order to analise the effect of number and width of gaps in withdrawal resistance of STSs (η_{gap}), all three moisture groups were analysed separatly. Considering the REF configuration of each MC group as reference (equation (3:7)), linear fittings, depicted in Figure (I) 3:31, were performed and mean k_{gap} values, shown in Table (I) 2:23, were defined. The effect of each gap added in the withdrawal resistance is represented by k_{gap} values, which were defined by the average between slopes given by linear fittings performed regarding different number of GAPs (slopes obtained for different linear fittings can be seen at tables presented in Figure (I) 3:31). Here, configurations GAP_FL and GAP_ML were considered part of the same group (one gap), once location of gaps does not suggest a significant influence on obtained results.

As already verified in section 0, f_{ax} presents a slight increase as the number of GAP0 in the STS path also increase for all MC levels (Figure (I) 3:31 (a)). It was verified that this phenomenon is not related with higher density located close to the STSs. So, our suspicion is that it can be related with the crosswise lamination of CLT however, further research is required before state it as a fact. Because of that, this study consider that GAP0 has no influence on the test results. This way, bi-linear model proposed (3:8) will not consider it.

Anyway, results obtained with linear fittings show that configurations tested with MC=8% presented the lower increase of f_{ax} as the number of GAP0 increases (Figure (I) 3:31 (a)). While group with MC=8% suggest an increase for f_{ax} of 3,7% per each GAP0 added, groups with MC=12% and MC=18% suggest an increase of 4,7% and 5,0% per each GAP0 added to the STS path, respectively.

$$\frac{f_{ax,corr,gap(i)(,8/12/18\%)}}{f_{ax,corr,REF\ (mean\ 8/12/18\%)}} \quad (3:7)$$

$f_{ax,corr}$	Withdrawal resistance corrected considering density, in N/mm²;
$f_{ax,corr,gap(i)(\ 8/12/18\%)}$	$f_{ax,corr}$ obtained in experimental campaign for REF configuration with 8, 12 or 18% of moisture content, in N/mm²;
$f_{ax,corr,REF\ (mean\ 8/12/18\%)}$	Mean $f_{ax,corr}$ obtained in experimental campaign for remaining configurations with 8, 12 or 18% of moisture content, in N/mm².

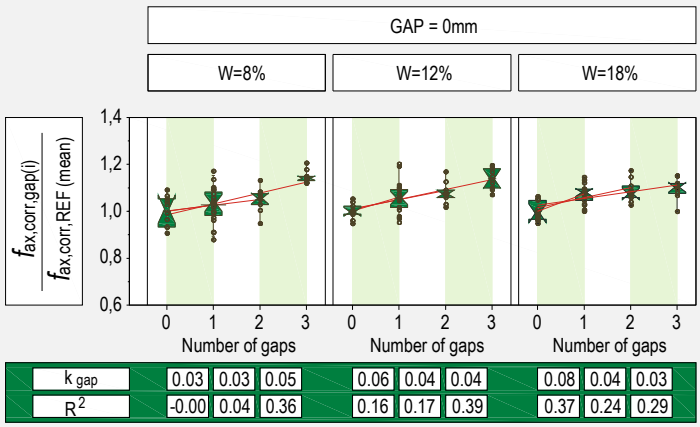

(a)

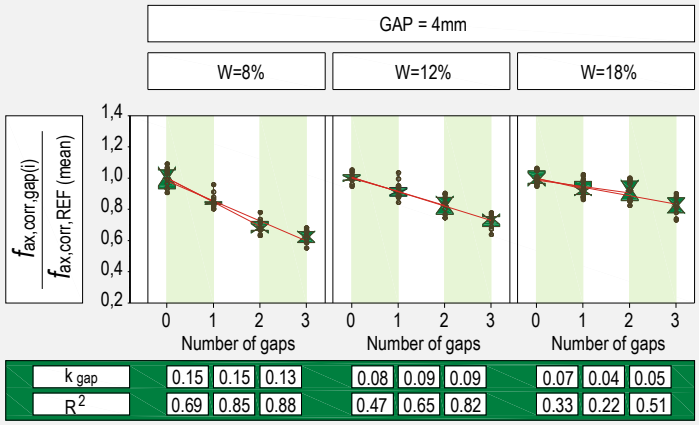

(b)

Figure (I) 3:31. Linear fittings performed between REF configuration and remaining configurations: (a) configurations with GAP0; (b) configurations with GAP4. k_{gap} and R^2values are presented in tables bellow respective graphs.

As expected, configurations with GAP4 present significant decreases for f_{ax} when comparing with REF and a downward trend as the number of gaps increase. As shown in Table (I) 2:23 and Figure (I) 3:31 (b), the test group with MC=8% registers the highest decreases (f_{ax} decreases 14,4% per each GAP4 added), while group with MC=18% registers the lowest decreases (f_{ax} decreases 5,7% per each GAP4 added).

Low f_{ax} values obtained by test group with MC=8 % resulted from the enlargement of the gap width due to wood shrinkage. Considering the reduced decrease of f_{ax} registered for the group with MC=18%, it means that the increase of MC levels can be beneficial for withdrawal resistance in some scenarios. This phenomenon is related with the consequent reduction of gap width when wood swells.

Table (I) 3:9. Obtained values for $\mathrm{k_{gap}}$, depending on moisture content and gap width.

MOISTURE CONTENT		8%	12%	18%
k_{gap}	GAP0	0,03	0,05	0,05
	GAP4	- 0,14	- 0,09	- 0,06

$$\eta_{gap} = \frac{f_{ax,gap(i)}}{f_{ax,REF,mean}} = \begin{cases} 1{,}00, when\ gap = 0\ mm \\ 1{,}00 + k_{gap} \cdot N, when\ gap = 4\ mm \end{cases} \quad (3:8)$$

Where $\mathrm{f_{ax,gap(i)}}$ is the mean withdrawal resistance of a given configuration, $\mathrm{f_{ax,REF,mean}}$ is the mean withdrawal resistance of REF configuration with the same range of moisture content, k_{gap} is the effect of each gap added in the withdrawal resistance and N is the number of gaps.

3.3.2.2 η_{MC}

In order to analise the effect of simple MC changes on the withdrawal resistance of STSs (η_{MC}), all tested configurations were analysed separatly. Considering test configurations with MC=12% as reference (equation (3:9)), the effect of each percentage unit of MC added/subtracted was quantified (k_{MC}). Similarly to k_{gap}, k_{MC} was defined by the average obtained between slopes given by individual linear fittings performed regarding different MC levels (these individual results can be seen at tables presented in Figure (I) 3:32). Linear fittings were set for all configurations considering two different ranges of moisture content: from 8% to 12% and from 12% to 18%.

Table (I) 3:10 shows $\mathrm{k_{MC}}$ values obtained by linear fittings depicted in Figure (I) 3:32. Considering the MC range between 8% and 12%, obtained values show that REF and GAP0 configurations present similar behaviour. As shown in Figure (I) 3:32 (a) and (b) and

Table (I) 3:**10**, when MC is between 8 % and 12 %, f_{ax} remains the same for both MC levels. This way, and similarly to what was suggested by Grabner (2012), proposed linear model (equation (3:10)) says that $\eta_{MC,REF\ and\ GAP0}$ = 1,00, for 8% ≤ MC ≤ 12%.

Still in the range 8%≤MC≤12%, GAP4 configurations present a high influence of MC decease due to timber shrinkage. The insertion of a STS in a GAP4 in itself implies a decrease of f_{ax}, once the thread of STS is

not totally filled with timber. But, when timber is forced to reduce its MC to 8%, GAP4 enlarges, further reducing the contact area between timber and STS. This way, the decrease of f_{ax} is directly related with the number of gaps. As shown in Figure (I) 3:32 (c), f_{ax} becomes smaller as the number of gaps increase. For configurations GAP4_FL, GAP4_ML, GAP4_OL and GAP4_3L, each percentage unit of MC subtracted to timber element implies decreases for f_{ax} of 2,1%, 2,7%, 4,8% and 4,7%, respectively. To understand the significance of these numbers it is important to remember that in similar situation, REF presents a decrease of 0.3%. As shown in

Table (I) 3:10, considering the number of gaps, it is possible to divide the results into two groups: one group for configurations with one gap (GAP4_FL and GAP4_ML), that in average suggest a decrease for f_{ax} of 2,4% per each percentage unit of MC subtracted, and another group for configurations with 2 and 3 gaps (GAP4_OL and GAP4_3L), that in average suggest a decrease for f_{ax} of 4,8% per each percentage unit of MC subtracted to timber element. However, it is important to note that, for configurations with only one GAP, there is no significant difference when GAP is located in middle layer or in an outer layer and, the presence of a gap in the middle layer of GAP4_3L is not reflected on results.

Relatively to MC range between 12% and 18%, linear fitting for REF suggests a decrease for f_{ax} of 1,8% per each percentage unit of MC added. Here it is important to mention that the obtained decrease for REF configuration is significantly lower than the decreases obtained for solid timber and GL. According to Ringhofer et al. (2014), withdrawal resistance of a STS inserted in solid timber and GL decreases 3,1 % and 2,5 %, respectively, per each percentage unit of MC added to the timber element. The difference between results obtained for CLT and solid timber are significant (1,3% per each percentage unit of MC added), and the reason for that is not clear. Similarly to the effect of GAP0 on increase of f_{ax}, cross lamination is also pointed as a possible reason. But, to fix a feasible conclusion, further research is required.

Still regarding MC range between 12% and 18%, GAP0 configurations present a behavior close to REF, presenting decreases for f_{ax} of 2,0 %, in average, per each percentage unit of MC added (Figure (I) 3:32 (a) and (b)).

At last, results related with GAP4 configurations for 12% ≤ MC ≤ 18% show that timber swelling had a significant effect on f_{ax}. The reduction of f_{ax}, caused by GAP4 and high levels of MC, tend to be avoided as the number of GAPs increase. When exposed to environments with high relative humidity (90%RH) timber swells substantially almost closing the GAP4, action that creates an important pressure against

the thread of STS. In this case, instead of STS drills the timber is the timber that goes inside the STS thread, and maybe this makes the difference. Linear regressions depicted in Figure (I) 3:32 (c), show the decreases of f_{ax} per each percentage unit of MC added for all GAP4 configurations: 1,7%, 1,4%, 0,0% and 0,2% for configurations GAP4_FL, GAP4_ML, GAP4_OL and GAP4_3L, respectively. Considering obtained values, GAP4_FL and GAP4_ML configurations were grouped with REF and GAP0 configurations which suggest, in average, a decrease for f_{ax} of 2,0% per each percentage unit of MC added. GAP4_OL and GAP4_3L were grouped together considering that increasing of MC does not affect f_{ax}. Similarly to what was verified for MC range between 8% and 12%, the influence of GAP4 in the middle layer of configuration GAP4_3L was not noticeable.

Performed linear fittings present low R^2 values which are related with lower line slopes and with reduced sample. To obtain better statistical results, experimental tests with larger samples and with intermediate MC levels should be performed. The range of R^2 values is too large from 0,01 to 0,86. When line tend to be horizontal, R^2 express no correlation between data. But, in other cases, correlation is considered reasonably good. The better correlation obtained was for configuration GAP4_ML and MC range between 8% and 12%, with a R^2 of 0,86.

$$\frac{f_{ax,corr,(MC=8/18\%)}}{f_{ax,corr,(mean,MC=12\%)}} \quad (3:9)$$

$f_{ax,corr}$	Withdrawal resistance corrected considering density, in N/mm²;
$f_{ax,corr,(MC=8/18\%)}$	$f_{ax,corr}$ obtained in experimental campaign for configurations with MC=8% or MC=18%, in N/mm²;
$f_{ax,corr,(mean,MC=12\%)}$	Mean $f_{ax,corr}$ obtained in experimental campaign for configurations with MC=12, in N/mm².

Modeling η_{gap} and η_{MC} resulted in two bi-linear models (equations (3:9) and (3:10)) designed to predict the influence of gaps and the influence of moisture content changes on the withdrawal resistance of STSs inserted in main face of CLT panels considering different configurations. The obtained values for k_{gap} and k_{MC}, presented in Table (I) 2:23 and

Table (I) 3:10, respectively, are the variables that should be applied in the suggested models. It is important to underline that, despite the increase/decrease of f_{ax} observed for GAP0 configurations, these models considered that as the number of gaps with 0mm increases, f_{ax} remains the same. The obtained models are an important step to introduce the influences of the studied variables on practical applications. However, despite being based on results obtained with rigorous experimental tests, the presented models

should still be verified and some further research is needed. The width of the gaps, for example, is a variable that should be deeply studied in order to complement the proposed models. Gaps with 1mm, 2mm and 3mm should also be tested in order to verify if the expected linearity exists.

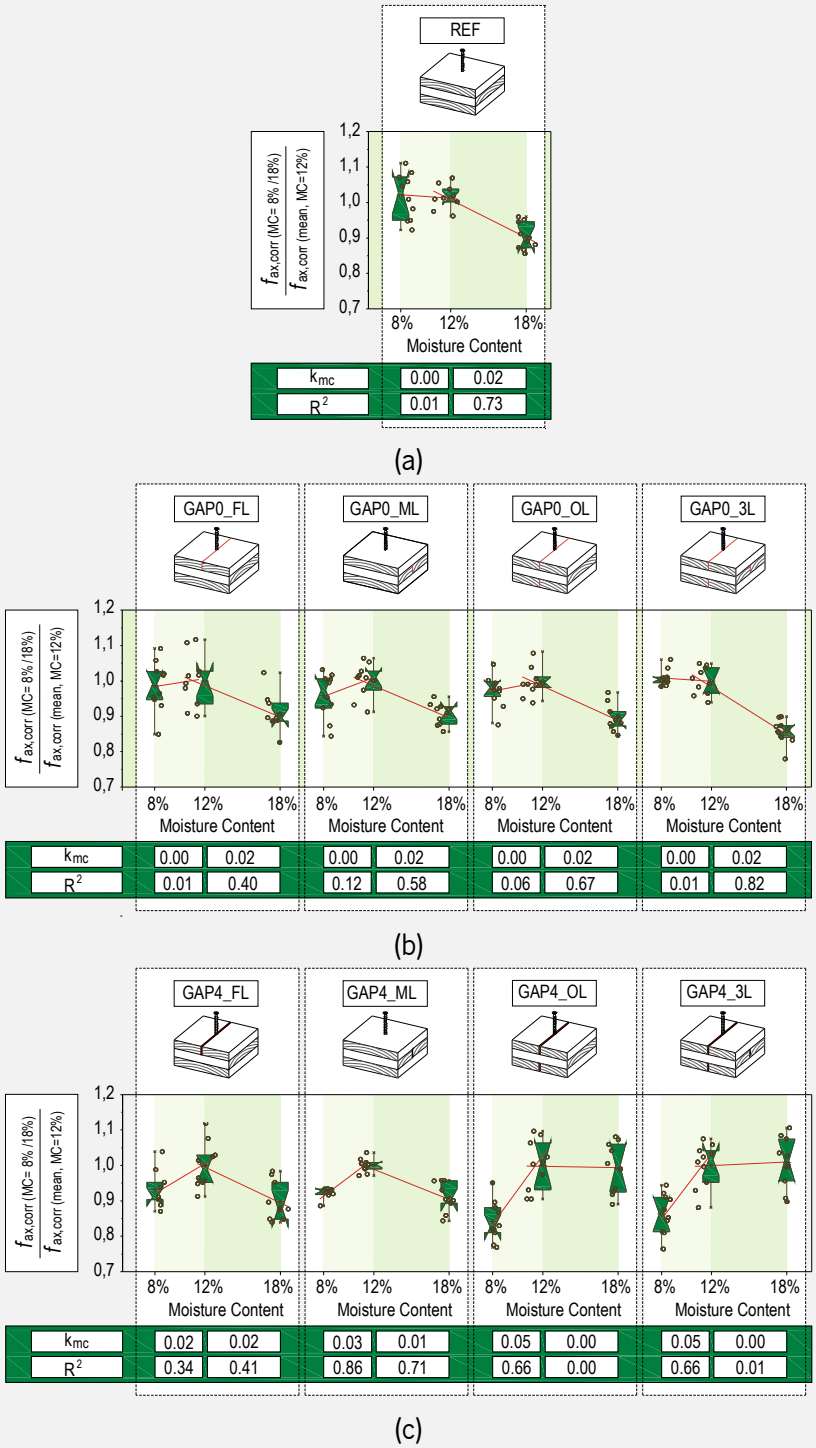

Figure (I) 3:32. Graphs of linear fittings between different moisture levels for all configurations: (a) REF configuration; (b) GAP0 configurations; and (c) GAP4 configurations. k_{MC} and R^2 values related with same linear fittings are presented bellow respective graphs.

Table (I) 3:10. Obtained values for k_{MC}, depending on moisture content, gap width and number of gaps.

	MOISTURE RANGE	REF	GAP0	GAP4_FL AND GAP4_ML	GAP4_OL AND GAP4_3L
k_{MC}	8%-12%	0,00		-0,02	-0,05
	12%-18%	-0,02			0,000

$$\eta_{MC} = \frac{f_{ax,MC(i)}}{f_{ax,MC(12)}} = \begin{cases} 1{,}00, for \begin{cases} REF \\ GAP0 \end{cases}, when\ 8\% \leq MC \leq 12\% \\ 1{,}00 + k_{MC} \cdot (MC - 12), for \begin{cases} GAP4, when\ 8\% \leq MC \leq 18\% \\ REF/\ GAP0, when\ 12\% \leq MC \leq 18\% \end{cases} \end{cases} \quad (3:10)$$

3.3.3 Applying η_{gap} and η_{MC} to Uibel & Blaß Model

In order to evaluate the defined η_{gap} and η_{MC} models, the model proposed by Uibel & Blaß (2007), was applied as it is shown in equation (3:11). This way, predicted withdrawal resistance of STSs in CLT ($f_{ax,pred}$) could be compared with the test results ($f_{ax,test}$) analyzed in previous sections. Uibel & Blaß (2007) Model, presented in chapter 1 (Part I), is the most known model to predict withdrawal resistance of STSs in CLT depending on the angle between screw axis and grain direction.

$$F_{ax,s,pred} = \frac{0.44 \cdot d^{0.8} \cdot l_{ef}^{0.9} \cdot \rho^{0.75}}{1.25 \cdot cos^2\varepsilon + sin^2\varepsilon} \quad (3:11)$$

$F_{ax,s,pred}$	Predicted values for withdrawal resistance of STS inserted in the plane side of CLT, considering moisture content level, number and width of gaps present in screw path, in N;
d	Nominal or outer diameter of the screw, in mm;
l_{ef}	Effective pointside penetration length, in mm;
ρ	For joints in the plane side of CLT: density of CLT (whole cross section), in kg/m³; For edge joints in CLT: density of the relevant layer(s), in kg/m³;
ε	Angle between screw axis and grain direction.

Table (I) 3:11 shows descriptive statistics for $f_{ax,pred}$, considering an angle of 90° between screw axis and grain direction, while Figure (I) 3:33 depicts the correlations between $f_{ax,pred}$ and $f_{ax,test}$, considering different MC levels and different width of gaps. Analyzing both, it is clear that predicted values are placed on conservative side.

Table (I) 3:11. Descriptive statistics of $f_{ax,pred}$ for different test configurations with 8%, 12% and 18% of moisture content.

GROUPS		N.TESTS	MEAN	SD	COV	MEDIAN	MIN	MAX	P5	$\frac{f_{ax,pred}}{f_{ax,test}}$
REF	8%	10	5,91	0,54	0,09	5,94	5,07	6,70	5,07	0,91
	12%	9	5,87	0,58	0,10	5,83	4,99	6,80	4,99	0,91
	18%	10	5,28	0,46	0,09	5,21	4,61	6,04	4,61	0,90
GAP0_FL	8%	10	5,73	0,37	0,07	5,82	5,16	6,25	5,16	0,86
	12%	10	5,78	0,41	0,07	5,89	5,10	6,37	5,10	0,85
	18%	10	5,16	0,36	0,07	5,22	4,65	5,77	4,65	0,83
GAP0_ML	8%	10	5,73	0,33	0,06	5,78	5,21	6,11	5,21	0,91
	12%	10	5,79	0,33	0,06	5,79	5,25	6,16	5,25	0,87
	18%	10	5,17	0,31	0,06	5,22	4,67	5,53	4,67	0,86
GAP0_OL	8%	10	5,80	0,38	0,07	5,90	5,13	6,26	5,13	0,86
	12%	10	5,87	0,37	0,06	6,00	5,23	6,43	5,23	0,84
	18%	10	5,21	0,34	0,07	5,32	4,63	5,69	4,63	0,83
GAP0_3L	8%	10	5,80	0,34	0,06	5,85	5,23	6,23	5,23	0,79
	12%	10	5,82	0,31	0,05	5,91	5,30	6,21	5,30	0,80
	18%	10	5,17	0,29	0,06	5,17	4,73	5,51	4,73	0,83
GAP4_FL	8%	9	4,66	0,29	0,06	4,68	4,18	5,11	4,18	0,84
	12%	10	5,24	0,33	0,06	5,21	4,72	5,70	4,72	0,89
	18%	10	4,83	0,27	0,05	4,79	4,45	5,23	4,45	0,92
GAP4_ML	8%	8	4,63	0,29	0,06	4,67	4,21	5,01	4,21	0,86
	12%	10	5,26	0,36	0,07	5,36	4,65	5,80	4,65	0,89
	18%	10	4,90	0,35	0,07	4,98	4,34	5,48	4,34	0,92
GAP4_OL	8%	10	3,56	0,26	0,07	3,66	3,11	3,88	3,11	0,76
	12%	10	4,69	0,35	0,08	4,73	4,13	5,14	4,13	0,88
	18%	10	5,17	0,32	0,06	5,15	4,76	5,76	4,76	0,98
GAP4_3L	8%	10	2,80	0,19	0,07	2,78	2,51	3,11	2,51	0,69
	12%	10	4,20	0,33	0,08	4,24	3,67	4,68	3,67	0,89
	18%	10	4,87	0,27	0,06	4,90	4,34	5,16	4,34	1,02

$f_{ax,pred}$ - predicted withdrawal resistance, obtained by Uibel & Blaß Model, η_{MC} - reduction factor of moisture influence on f_{ax}, η_{gap} - reduction factor of GAPs influence on f_{ax}, **SD** – Standard of Derivation, **CoV** – Coefficient of Variation, **P5** – 5th percentil. **REF** - configuration without gaps, **GAP0_FL** - configuration with a gap of 0mm in first layer; **GAP0_ML** - configuration with a gap of 0mm in middle layer; **GAP0_OL** - configuration with a gap of 0mm in outer layers; **GAP0_3L** - configuration with a gap of 0mm in three layers; **GAP4_FL** - configuration with a gap of 4mm in first layer; **GAP4_ML** - configuration with a gap of 4mm in middle layer; **GAP4_OL** - configuration with a gap of 4mm in outer layers; **GAP4_3L** - configuration with a gap of 4mm in three layers.

Figure (I) 3:34 shows the relation between mean test results and the predicted mean values. Despite the good data trend, mean values obtained by tests present higher values than the predicted withdrawal resistance, suggesting that Uibel & Blaß model is conservative. Regarding REF configuration, it is important to mention that it presents similar relation between $f_{ax,pred}$ and $f_{ax,test}$ for all MC groups ($0{,}90 \leq \frac{f_{ax,pred,REF}}{f_{ax,test,REF}} \leq 0{,}91$). As the effect of GAP0 was not considered for definition of $f_{ax,pred}$, configurations with GAP0 ($0{,}79 \leq \frac{f_{ax,pred,GAP0}}{f_{ax,test,GAP0}} \leq 0{,}91$) present a lower range for the ratio between $f_{ax,pred}$ and $f_{ax,test}$ than configurations with GAP4 ($0{,}69 \leq \frac{f_{ax,pred,GAP4}}{f_{ax,test,GAP4}} \leq 1{,}02$).

Most conservative results were obtained for some configurations tested with MC=8%, namely: GAP4_OL_8% $\left(\frac{f_{ax,pred}}{f_{ax,test}} = 0{,}76\right)$ and GAP4_3L_8% $\left(\frac{f_{ax,pred}}{f_{ax,test}} = 0{,}69\right)$. As k_{gap} and k_{MC} were suggested based on the average of slops obtained by linear fittings performed for different configurations, some test configurations did not present such conservative predicted values, namely: GAP4_OL_18% $\left(\frac{f_{ax,pred}}{f_{ax,test}} = 0{,}98\right)$ and GAP4_3L_18% $\left(\frac{f_{ax,pred}}{f_{ax,test}} = 1{,}02\right)$ (Figure (I) 3:34 (e)). Furthermore, due to closing of gaps as a consequence of high MC levels , these configurations obtained low values for k_{gap} and k_{MC}.

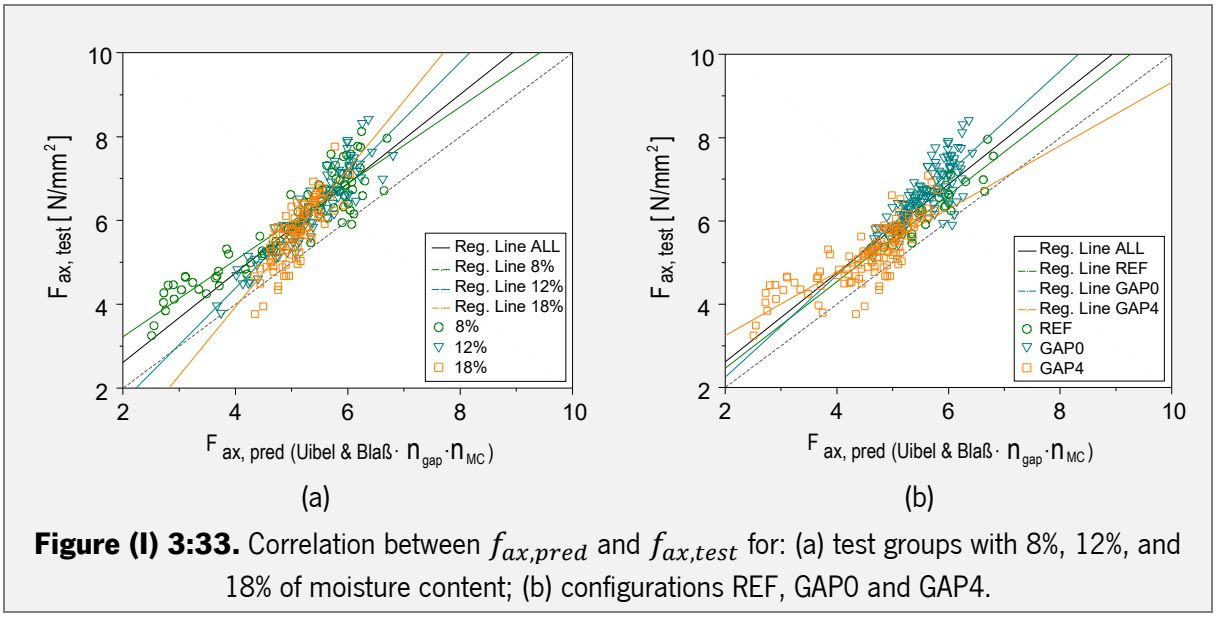

Figure (I) 3:33. Correlation between $f_{ax,pred}$ and $f_{ax,test}$ for: (a) test groups with 8%, 12%, and 18% of moisture content; (b) configurations REF, GAP0 and GAP4.

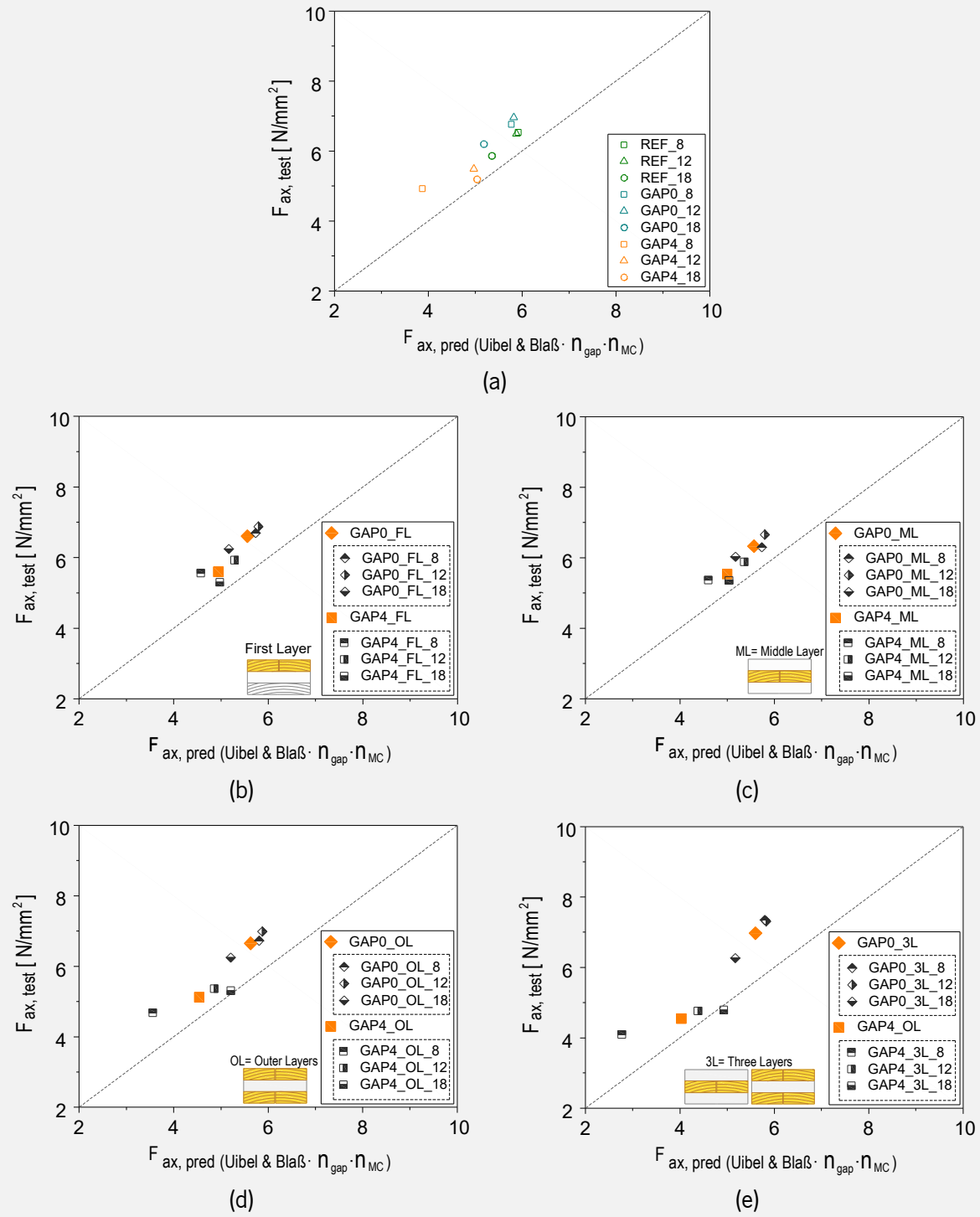

Figure (I) 3:34. Correlation between mean values obtained for $f_{ax,pred}$ and $f_{ax,test}$. a) mean values for all tested configurations considering MC level and gap width; b) mean values for GAP_FL configurations; c) mean values for GAP_ML configurations; d) mean values for GAP_OL configurations; e) mean values for GAP_3L configurations.

3.4 Main conclusions

The present research showed and discussed the results of an experimental campaign focused on the quantification of effects caused by MC variation and the existence of gaps and their width on the withdrawal behavior of axially loaded STSs inserted in the side face of CLT panels.

Moisture content covered a range between 8 % and 18 %, number of the gaps presented in the STS path varied from 0 to 3 and gap widths were of 0mm and 4mm.

After the analysis and modeling of the test results, some important conclusions can be pointed out:

- It was observed that the insertion of GAP0 in the STS path can result on an improvement of f_{ax}, while the insertion of gaps with 4mm result on a decrease of f_{ax}, which tends to reduce its significance as the moisture content increases. The surprising behavior of GAP4 configurations is related with timber swelling which causes the closing of gaps and consequently results on an improvement of the withdrawal resistance. The behavior of GAP0 configurations can be related with CLT crosswise lamination. Nevertheless, further research is needed to solidify the conclusions;
- Regarding the influence of gap width and location, configurations with GAP4 present significant decreases for f_{ax} when comparing with REF and a downward trend as the number of gaps increase. The test group with MC=8% registers the highest decreases (f_{ax} decreases 14,4% per each GAP4 added), while group with MC=18% registers the lowest decreases (f_{ax} decreases 5,7% per each GAP4 added);
- It was observed that for a MC range between 12% and 18%, REF configuration presented a decrease for f_{ax} of 1,8% per each percentage unit of moisture content added. This result proves that the reduction of withdrawal resistance caused by increase of moisture is lower for STS inserted in CLT than for solid timber and GL;
- Still regarding effects of changes on moisture content, but in a range between 8% and 12%, REF and GAP0 configurations present similar behaviour ($\Pi_{MC,REF\ and\ GAP0}$ = 1,00, for 8% ≤ MC ≤12%), while GAP4 configurations present a high influence of MC decease due to timber shrinkage (GAP4_3L present a decreases for f_{ax} 4,7%);
- The adjusted Uibel & Blaß (2007) model showed accuracy in predicting the obtained test results, presenting higher conservative results for configurations with GAP4.

Beyond the suggestions for future research already mentioned in present chapter, another theme that should be studied is the influence of moisture content variations and gaps on withdrawal resistance of STS inserted in side face of CLT panels. Some research performed about this topic is presented further on present thesis (chapter 5 – Part I).

CHAPTER 4 (I)

4 WITHDRAWAL RESISTANCE OF OF SELF-TAPPING SCREWS WHEN SUBMITTED TO CYCLIC CHANGES ON MOISTURE CONTENT

4.1 Experimental campaign

The present chapter presents an experimental campaign performed at Laboratory of structures of Civil Engineering Department of University of Minho aiming to complete the experiments performed at Institut für Holzbau und Holztechnologie (Graz University of Technology-Austria) presented in previous chapter.

4.1.1 Main goals and parameters involved

The present experimental campaign aims to understand the influence of cyclic humidity changes on the withdrawal resistance of self-tapping screws inserted in the main face of CLT panels. Here, the same parameters analyzed in the previous chapter (changes on levels of moisture content, number of gaps through the screw path and the width of gaps) were again evaluated but now using specimens which were submitted to successive cyclic changes on relative humidity, instead of simple humidity changes (Figure (I) 4:1).

During cyclic changes, relative humidity varied between 30% and 90% in order to keep moisture content levels between 8% and 18%, respectively. This way, the changes respect the limits imposed by Eurocode 5 regarding service classes 1 and 2, once according to CLT producers these are the service classes in which CLT can be applied (KLH-Massivholzplatten, 2011). The evaluation of influence of cyclic humidity changes on withdrawal resistance of self-tapping screws were performed through the comparison between specimens tested on day 0 and on day 324. Before being tested, specimens tested on day 0 were stabilized in an environment of 20°C and 65% RH and not submitted to any cyclic humidity changes. Differently, specimens tested on day 324 were conditioned for a period of 182 days in a climatic chamber in which relative humidity varied between 30% and 90%, completing 4 complete drying-wetting cycles of around 45 days. Before being tested, these specimens were conditioned again in a climatic chamber, with a constant environment of 20°C and 65% RH during a period of 142 days. This way, specimens tested on day 0 and day 324 have approximately the same levels of moisture content. Present RH cycle is the same used for tests described at chapter 2.

Again, CLT specimens were produced considering nine different configurations, which were defined cautioning the possible existence of gaps through screw path as well as the width of same gaps. All nine configurations were described in section 3.1.1. from chapter 3.

Here, a fourth parameter was introduced as an attempt to evaluate the influence of cross lamination in withdrawal resistance of STS inserted in the main face of CLT elements. For that, a tenth configuration

was tested and two groups of glulam (GL) specimens with the same dimensions and prepared and conditioned exactly in the same way of the CLT specimens were tested on day 0 and day 324.

The combination of these three parameters resulted in ten different test configurations and 200 withdrawal tests. Figure (I) 4:3 presents a summary of experimental campaign and illustrates different test configurations.

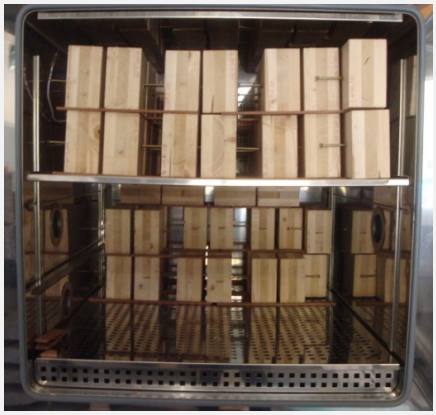

Figure (I) 4:1. Specimens conditioned inside the climatic chamber.

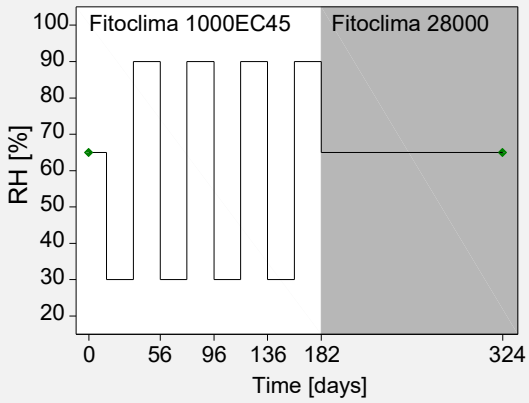

Figure (I) 4:2. Cycle performed by climatic chamber in which specimens were conditioned.

4.1.2 Production of specimens and main steps of experimental procedure

CLT and GL used to prepare the test specimens were produced in a partnership with a Portuguese timber industry, *Rusticasa*. Due to industry limitations, the production procedure was not so rigorous as the production of CLT performed at *Institute of Timber Engineering and Wood Technology* (chapter 3), at Graz University of Technology (Austria), especially regarding avoiding knots and density distribution.

CLT and GL specimens were produced using Spruce (nominal strength class C24 according to EN 338 (2009)) and with the shape of big beams (4200x170x102mm^3). The position of different layers varied depending on test configuration. CLT and GL elements were produced with three layers with a thickness of 34mm each. This way, each produced beam contained twenty-four test specimens of 170x170x102mm^3 (Figure (I) 4:4).

In order to save time and avoid unexpected problems, the production of test specimens was planned in advance following pre-defined steps:

6. Cut, plane and rectify different types of boards needed to produce different layer configurations (Figure (I) 4:5 (a));
7. Timber boards passed through the glue dispenser (Figure (I) 4:5 (b));
8. CLT and GL beams were mounted in the press structure (Figure (I) 4:5 (c));

9. Six beams were pressed per time (Figure (I) 4:5 (d));
10. Saw the gaps with 4mm in groups which include it;
11. Test specimens were cut from beams.

Relatively to production of CLT, it is also important to refer that layers were glued with adhesive 1247 from *AkzoNobel* and pressed by a hydraulic pressing device with a pressure of 1 N/mm^2 for a period of 2,5 hours.

Despite the non-controlled position and quantification of knots, test specimens were cut from the big beams and randomly distributed between groups.

Table (I) 4:1 present the descriptive statistics of density distribution for all ten different configurations and for both test days. Density values were calculated according to equation 3:1 (chapter 3) and varied between 410kg/m^3 and 513kg/m^3 (mean=460kg/m^3). Density distribution exhibited good results with a density distribution close to a normal one, with median and mean densities close to each other, and with low CoV values between 0.01 and 0.05. Figure (I) 4:6 depicts the similarity of density distribution for groups tested on day 0 and day 324.

In order to know the moisture content at production time some small samples were arbitrarily collected and weighted immediately. Obtained moisture content levels (equation 3:4) varied between 16,5% and 20,2% (CoV=0,08 and mean=18,4%). The high moisture content at production time allowed to understand if the CLT lamination with higher levels of moisture content has some effect on the withdrawal resistance when comparing the results obtained by REF configuration for both phases of the experiments.

Back to the lab, specimens were conditioned in a climatic controlled room (20 °C and 65 %RH) in order to reduce the MC. Reaching MC~14 %, specimens were pre-drilled with a hole of 5mm and screwed using full threaded Rapid® Vollgewinde from Schmid with a diameter of 8mm and length of 180mm. At this stage, one group of each configuration was tested (Day 0), following exactly the same test procedure used for tests performed at *Institute of Timber Engineering and Wood Technology* (chapter 3 – section 3.1.2), while remaining groups were conditioned in a climatic chamber and submitted to the RH cycle for a period of 324 days (Figure (I) 4:2). Finalized the cycle, specimens were tested also following exactly the same procedure.

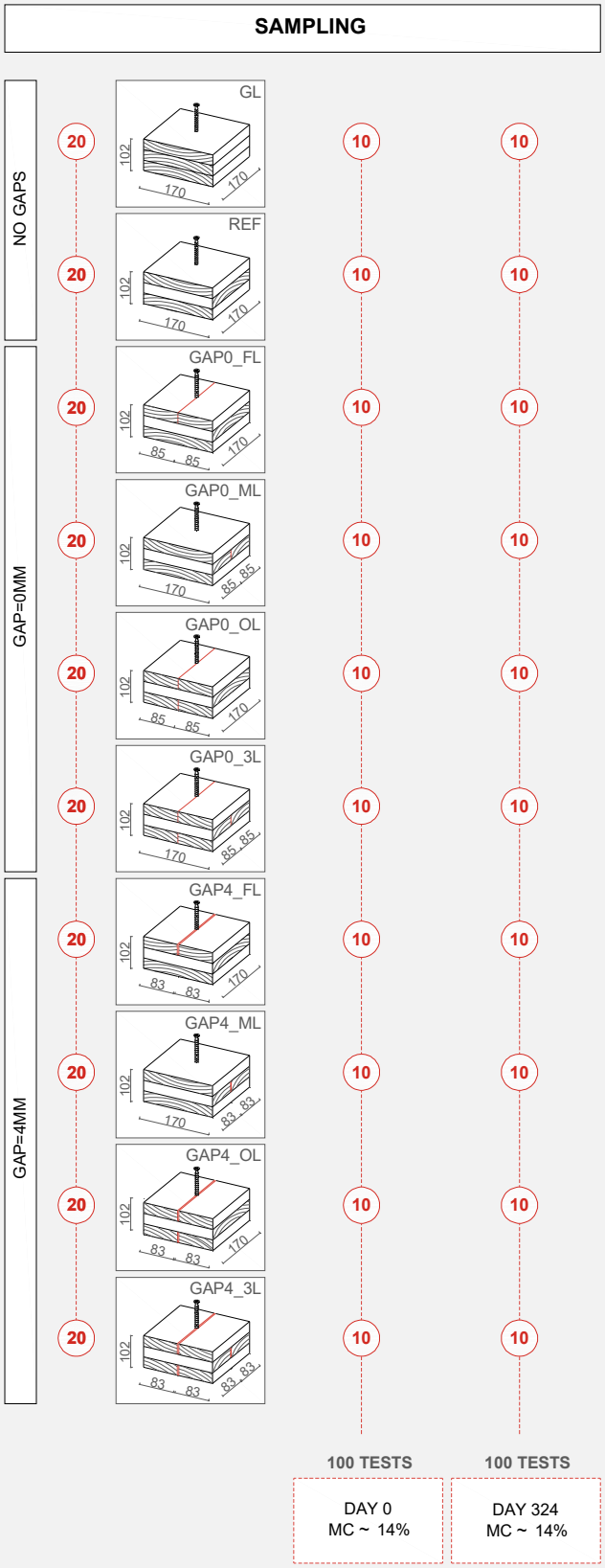

Figure (I) 4:3. Different test configurations and sampling used for different groups and test days.

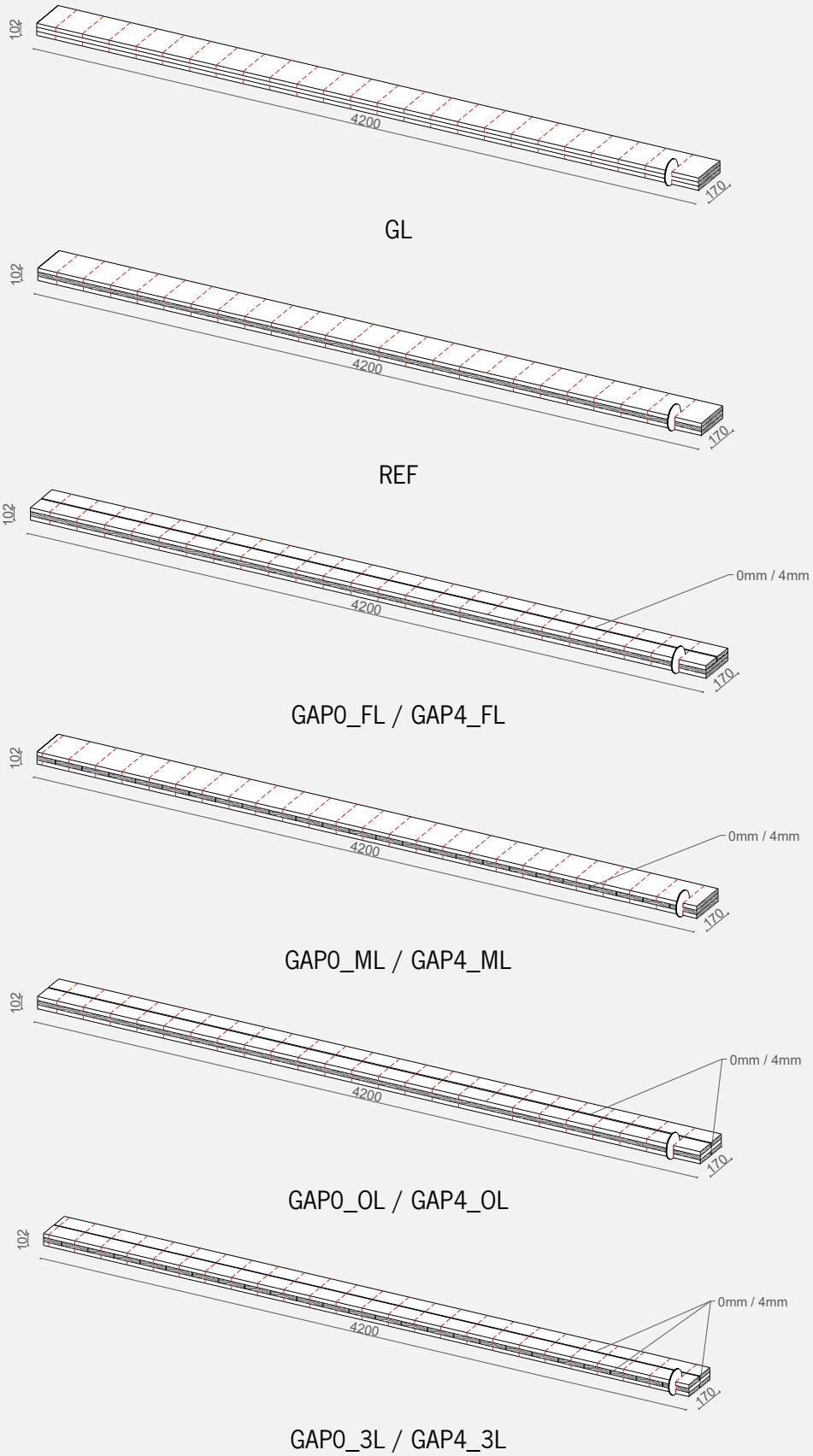

Figure (I) 4:4. CLT and GL beams produced at *Rusticasa* for different test configurations.

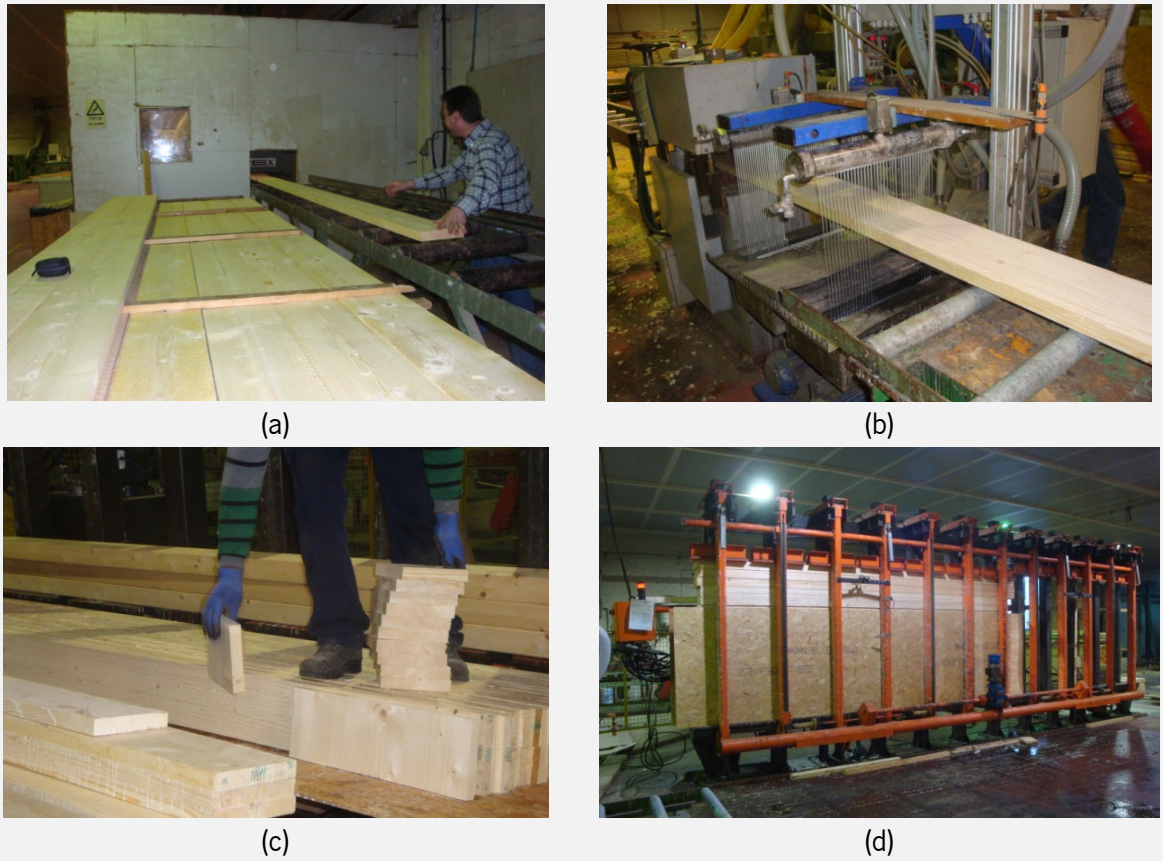

Figure (I) 4:5. Procedure to build CLT and GL beams using *Rusticasa* facilities. (a) rectifying timber boards; (b) timber boards passing through glue dispenser; (c) adhesive 1247 from *AkzoNobel*; (d) glue dispenser; (e) and (f) CLT and GL beams being mounted in the press structure; (g) and (h) pressing device.

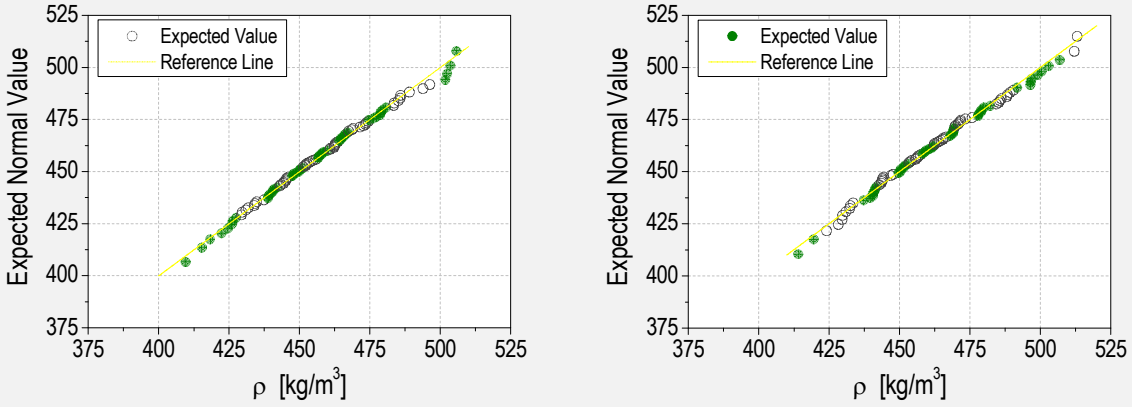

Figure (I) 4:6. Similar density distribution for different test days. Graphs were plotted based on Normal distribution and Renard score method - (i – 0,3) / (n + 0,4).

Table (I) 4:1. Descriptive statistics of density distribution (ρ) for all ten different configurations and for different test days.

CONF.	MC GROUP	Nº OF SPECIMENS	MEAN	SD	COV	MIN	MEDIAN	MAX	P5
REF	DAY 0	10	465	5,8	0,01	454	465	474	454
	DAY 324	10	470	5,0	0,01	463	469	479	463
GAP0_FL	DAY 0	10	479	17,5	0,04	448	480	506	448
	DAY 324	10	487	14,7	0,03	462	488	512	462
GAP0_ML	DAY 0	10	440	20,3	0,05	410	442	465	410
	DAY 324	10	445	21,1	0,05	414	447	470	414
GAP0_OL	DAY 0	10	471	16,0	0,03	443	477	489	443
	DAY 324	10	475	15,8	0,03	447	481	497	447
GAP0_3L	DAY 0	10	444	11,2	0,03	430	443	463	430
	DAY 324	10	449	12,6	0,03	432	447	469	432
GAP4_FL	DAY 0	10	459	18,5	0,04	422	464	479	422
	DAY 324	10	464	17,8	0,04	430	468	486	430
GAP4_ML	DAY 0	10	448	8,9	0,02	435	449	462	435
	DAY 324	10	454	12,0	0,03	437	454	479	437
GAP4_OL	DAY 0	10	452	25,0	0,06	418	449	494	418
	DAY 324	10	455	24,3	0,05	424	450	499	424
GAP4_3L	DAY 0	10	447	14,2	0,03	426	447	474	426
	DAY 324	10	452	14,0	0,03	431	452	478	431
GL	DAY 0	10	467	25,3	0,05	437	459	504	437
	DAY 324	10	476	26,8	0,06	441	467	513	441

SD – standard of deviation; **CoV** – coefficient of variation; **P5** – 5th percentile

During all RH cycles, the environment in climatic chamber and moisture content of timber elements were monitored. Registers of relative humidity and temperature suggest that for periods with RH=90% defined environment was easy/fast to reach, while for drying periods difficulties to reach the defined environment (RH=30%) were observed. Moisture content changes during conditioning period show that for drying periods moisture content present values between 9.0% and 10.5% and for wetting periods moisture content is between 20.1% and 22.3%. Detailed information is present in section 2.3.4. of chapter 2.

4.1.3 Test procedure

Axial withdrawal test procedure for screws is simple and it is clearly normalized at EN 1382:1999. Figure (I) 4:7 depicts the test layout used to perform present experimental campaign, which is normally used to perform all withdrawal tests at laboratory of structures at University of Minho. An auxiliary suspended structure was built on the base of the test machine in order to lock the specimen when the screw is pulled

out. Force was applied by a load cell, with a capacity of 100kN, integrated on a hydraulic system and fixed to a steel frame. Data acquisition was done by a Modular 600 system from MRA and *Dyna Tester* software.

Despite the differences on test setup and equipment used, the test procedure was exactly the same applied at *Institut für Holzbau und Holztechnologie* (see section 3.1.3 from chapter 3).

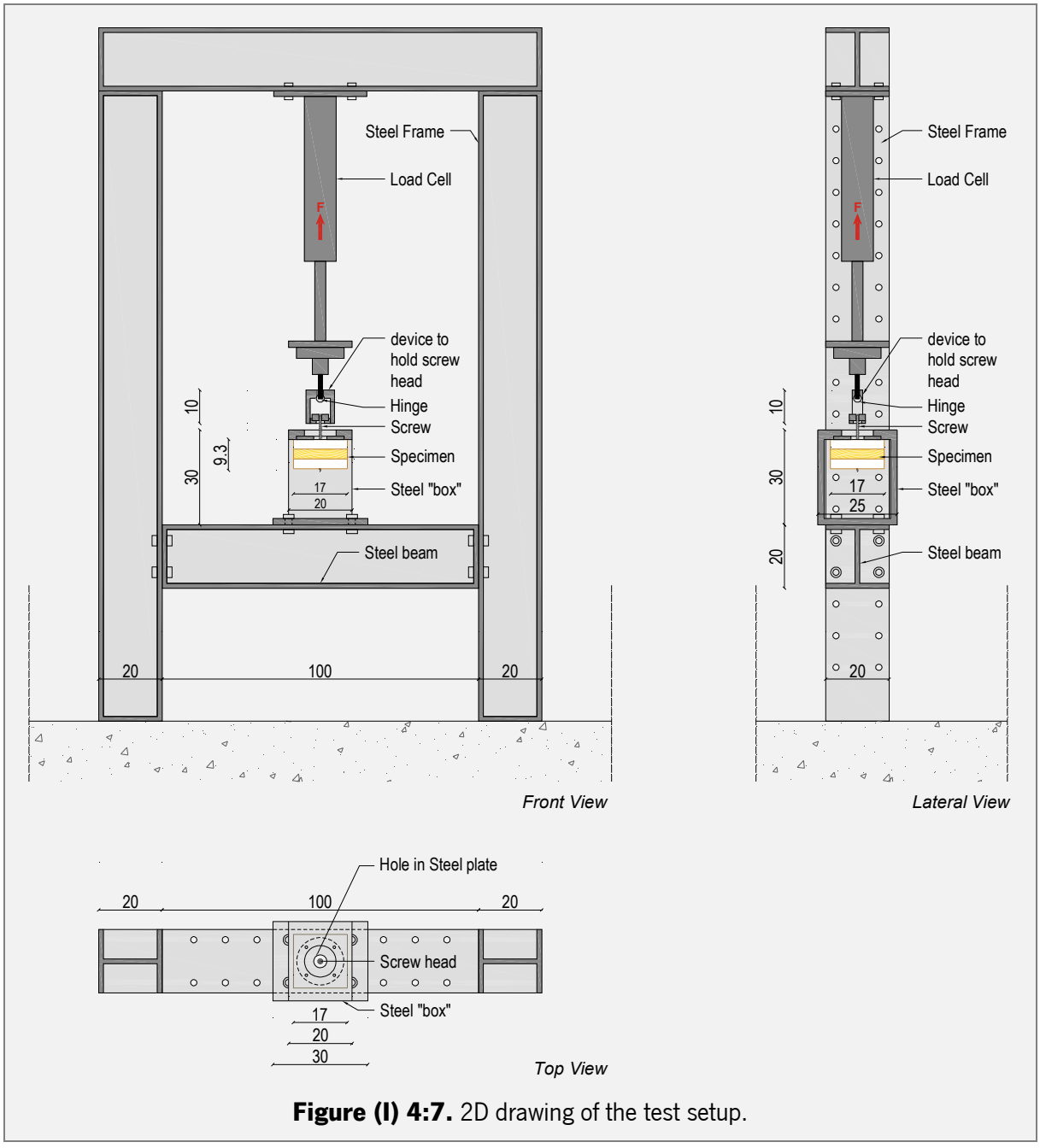

Figure (I) 4:7. 2D drawing of the test setup.

4.2 Description of test results

Similarly to what was described in previous chapter, first analysis of test results followed the three next steps: firstly, maximum withdrawal resistance ($f_{ax,test}$) was calculated according to equation (3:3); secondly, real moisture content at test time was defined for all tested specimens according to ISO 3130:1975; and thirdly, density of reference (ρ_{12}) was calculated as suggested at ÖNORM EN384:2010.

In present section, results obtained for tests performed on day 0 and day 324 are presented separately.

4.2.1 Test results for day 0

The moisture content obtained for specimens tested on day 0 varied between 13,9% and 14,9% (14,3% ≤ Mean ≤ 14,6% and CoV=0.01) and suggest a good distribution (Figure (I) 3:11). All specimens tested present a moisture content level higher than 12%, fact that indicates that specimens should be conditioned for a longer period. However, due to time issues specimens had to be tested before stabilize its moisture content levels.

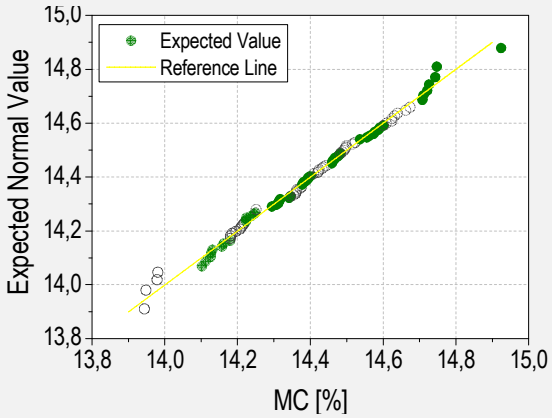

Figure (I) 4:8. Moisture distribution for group tested at day 0.

As a result of non-stabilization of moisture levels, internal gradients were present at test specimens. Regarding CLT specimens, a quantification of internal stresses was done for configuration of reference and is described in section 2.4.1.2. of chapter 2. Moisture content levels are, in average, 0.5 percentage units higher in middle layers than in outer layers (MC_{mean_Il} = 14,8% (CoV = 0,02) and MC_{mean_Ol} = 14,3% (CoV = 0,03)). Table (I) 3:3 present mean values and descriptive statistics of $f_{ax,test}$, ρ_{12} and MC of different configurations tested on day 0. Figure (I) 4:9 presents some specimens that was considered outliers, not due to test results but due to the location of significant timber knots on screw path which resulted on the highest withdrawal resistance.

Table (I) 4:2. Mean values and descriptive statistics of $f_{ax,test}$, ρ_{12} and MC of different configurations tested on day 0.

	MEAN VALUES			DESCRIPTIVE STATISTICS						
GROUPS	MC [%]	$f_{ax,test}$ [N/MM²]	ρ_{12} [KG/M³]	N.º OF TESTS	$f_{ax,test}$ / ρ_{12} / MC	SD	COV	MIN	MAX	MEDIAN	P5
REF_D0	**14,2**	**7,05**	**448**	**10**		**0,72**	**0,10**	**5,50**	**7,70**	**7,32**	**5,50**
						18,82	**0,04**	**404**	**476**	**452**	**404**
						0,21	**0,01**	**13,9**	**14,6**	**14,2**	**13,9**
GAP0_FL_D0	14,5	7,86	461	10		*0,44*	*0,06*	*7,20*	*8,75*	*7,81*	*7,20*
						22,20	0,05	431	502	455	431
						0,22	0,01	14,2	14,9	14,5	14,2
GAP0_ML_D0	14,4	7,26	431	9		*0,55*	*0,08*	*6,34*	*8,23*	*7,21*	*6,34*
						33,40	0,08	396	484	413	396
						0,14	0,01	14,1	14,6	14,5	14,1
GAP0_OL_D0	14,3	7,13	476	9		*0,60*	*0,08*	*5,82*	*7,60*	*7,48*	*5,82*
						34,13	0,07	444	547	464	444
						0,14	0,01	14,2	14,5	14,2	14,2
GAP0_3L_D0	14,6	7,64	448	10		*0,57*	*0,07*	*6,87*	*8,84*	*7,59*	*6,87*
						24,37	0,05	421	495	445	421
						0,08	0,01	14,5	14,7	14,6	14,5
GAP4_FL_D0	14,5	6,80	439	10		*0,42*	*0,06*	*6,29*	*7,37*	*6,86*	*6,29*
						23,90	0,05	410	471	431	410
						0,19	0,01	14,3	14,7	14,4	14,3
GAP4_ML_D0	14,4	5,79	444	10		*0,40*	*0,07*	*5,33*	*6,43*	*5,79*	*5,33*
						19,94	0,04	419	480	438	419
						0,17	0,01	13,9	14,6	14,4	13,9
GAP4_OL_D0	14,3	5,53	437	10		*1,27*	*0,23*	*2,72*	*7,49*	*5,61*	*2,72*
						24,71	0,06	387	462	438	387
						0,15	0,01	14,1	14,5	14,4	14,1
GAP4_3L_D0	14,3	3,84	439	10		*0,52*	*0,14*	*3,08*	*4,48*	*4,04*	*3,08*
						13,65	0,03	424	463	435	424
						0,14	0,01	14,0	14,4	14,3	14,0
GL_D0	14,4	7,67	455	9		*0,45*	*0,06*	*7,14*	*8,41*	*7,61*	*7,14*
						23,46	0,05	420	486	452	420
						0,13	0,01	14,1	14,6	14,4	14,1

MC – moisture content, f_{ax} - maximum withdrawal resistance, ρ_{12} – density of reference, **SD** – standard of derivation, **CoV** – Coefficient of Variation, **P5** – 5th Percentil. **REF_D0** - configuration tested on day 0, **GAP0_FL_D0** - configuration with a gap of 0mm in first layer tested on day 0; **GAP0_ML_D0** - configuration with a gap of 0mm in middle layer tested on day 0, **GAP0_OL_D0** - configuration with a gap of 0mm in outer layers tested on day 0, **GAP0_3L_D0** - configuration with a gap of 0mm in three layers tested on day 0, **GAP4_FL_D0** - configuration with a gap of 4mm in first layer tested on day 0; **GAP4_ML_D0** - configuration with a gap of 4mm in middle layer tested on day 0, **GAP4_OL_D0** - configuration with a gap of 4mm in outer layers tested on day 0, **GAP4_3L_D0** - configuration with a gap of 4mm in three layers tested on day 0, **GL_D0** – configuration of GL tested on day 0.

7_GAP0_OL_D0 6_GAP0_ML_D0 7_GL_D0

Figure (I) 4:9. Specimens defined as outliers due to the location of knots on screw path for tests performed on day 0.

Analyzing $f_{ax,test}$ values, highest and lowest values registered are of 8,84N/mm² and 2,72Nmm², for configurations GAP0_ML_D0 and GAP4_OL_D0, respectively. Differently to what was observed for specimens tested with 12% of moisture content at *Institut für Holzbau und Holztechnologie* (section 3.2.1 from chapter 3), the configurations with gaps of 0mm (GAP0_D0) present a constant trend as the number of gaps increase. A slightly increase of $f_{ax,test}$ is observed when comparing with REF_D0 results however, observing the overlapping of boxplots it can be concluded that this difference is not significant (Figure (I) 3:12 (a)). The configuration that exhibits the highest discrepancy comparing with REF_D0 is GAP0_FL_D0, registering an increase for $f_{ax,test,mean}$ of 10,3%. This fact must be related with high level of moisture content at time of CLT production, once it was observed that gaps with 0mm tend to open during the reduction of moisture content level, especially for outer layers. Another possible cause is related with the high level of moisture content at the test moment.

As expected, the highest losses of $f_{ax,test}$ are observed for configurations with gaps of 4mm (GAP4_D0). Here, the influence of number of gaps remains, being observed a decreasing trend for $f_{ax,test}$ as the number of gaps increase (Figure (I) 3:12 (b)). So, taking REF_D0 as reference, less favorable configurations are GAP4_OL_D0 and GAP4_3L_D0, with significant decreases of 21,6% and 45,5%, respectively. Observed decreases are higher than those observed in section 3.2.1 from chapter 3. Again, this fact must be related with the high moisture content level at time of CLT lamination and consequent enlargement of gaps and with the high level of moisture content at the test moment.

Figure (I) 3:13 ((a)-(d)) compares the results obtained by similar configurations GAP0_D0/GAP4_D0 with configuration REF_D0. Observing graphs, it is obvious the opposite behavior of configurations with GAP0 and GAP4 regarding REF configuration. Comparing the differences between GAP0 and GAP4

configurations, the discrepancy between both tends to increase with the number of gaps: 13,5%, 22,2%, 22,4% and 49,7% for configurations GAP_FL_D0, GAP_ML_D0, GAP_OL_D0 and GAP_3L_D0, respectively.

Regarding tests performed with GL, it was observed that GL presents $f_{ax,test,mean}$ 8,1% higher than that observed for REF configuration. However, considering the overlapping of boxplots this difference is not significant (Figure (I) 3:13 (e)).

Figure (I) 3:15 depicts the expected yielding failure mode observed during screw pull-out test. More detailed information about results obtained for tests performed on day 0 are shown in Annex 1:1.

4.2.2 Test results for DAY 324

The moisture content obtained for specimens tested on day 324 varied between 12,6% and 14,2% (13,2% ≤ Mean ≤ 13,7% and CoV=0,01) and suggest a good distribution (Figure (I) 3:11). All tested specimens present a moisture content level higher than 12%, fact that indicates that specimens should be conditioned for a longer period. However, due to time issues specimens had to be tested before stabilize its moisture content levels.

As a result of non-stabilization of moisture levels, moisture gradients were present in test specimens. Regarding CLT specimens, a quantification of internal stresses was done for configuration of reference and is described in section 2.4.1.2. of chapter 2. Moisture content levels are, in average, 0.6 percentage units higher in inner layers (MC_{mean_Ol} = 12,8% (CoV = 0,01) and MC_{mean_Il} = 13,4%(CoV = 0,02)).

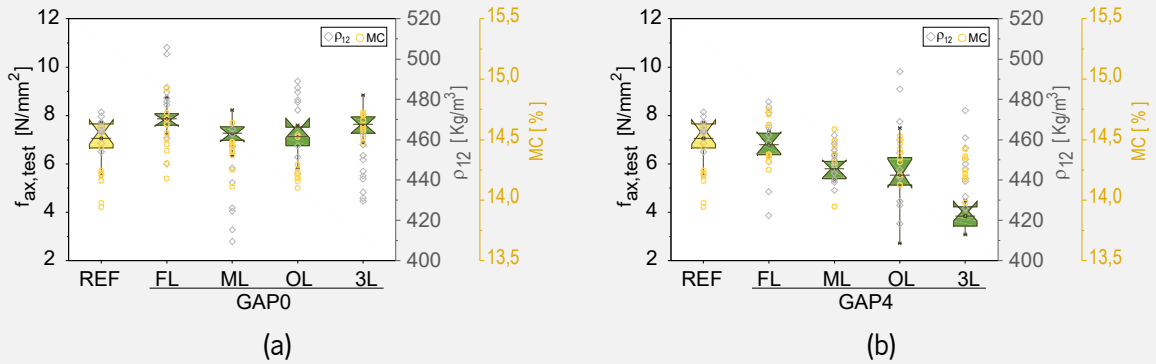

Figure (I) 4:10. Box chart with notched boxes of $f_{ax,test}$ and scatter plot of density of reference and moisture content for the following groups: (a) REF_D0 and GAP0_D0; (b) REF_D0 and GAP4_D0.

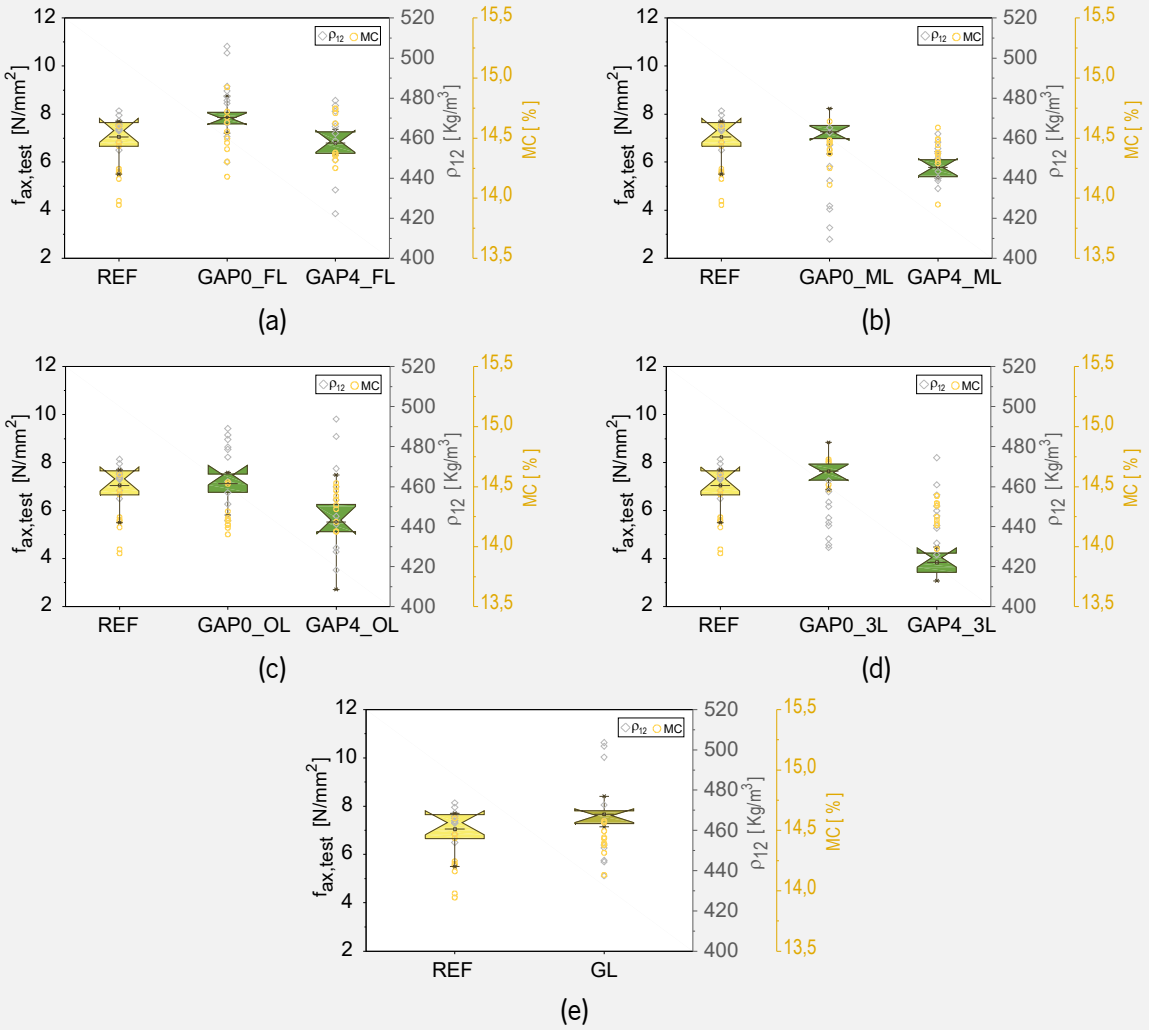

Figure (I) 4:11. Box chart with notched boxes of $f_{ax,test}$ and scatter plot of density of reference and moisture content for the following groups: (a) REF_D0 and GAP_FL_D0; (b) REF_D0 and GAP_ML_D0; (c) REF_D0 and GAP_OL_D0; (d) REF_D0 and GAP_3L_D0; and (e) REF_D0 and GL_D0.

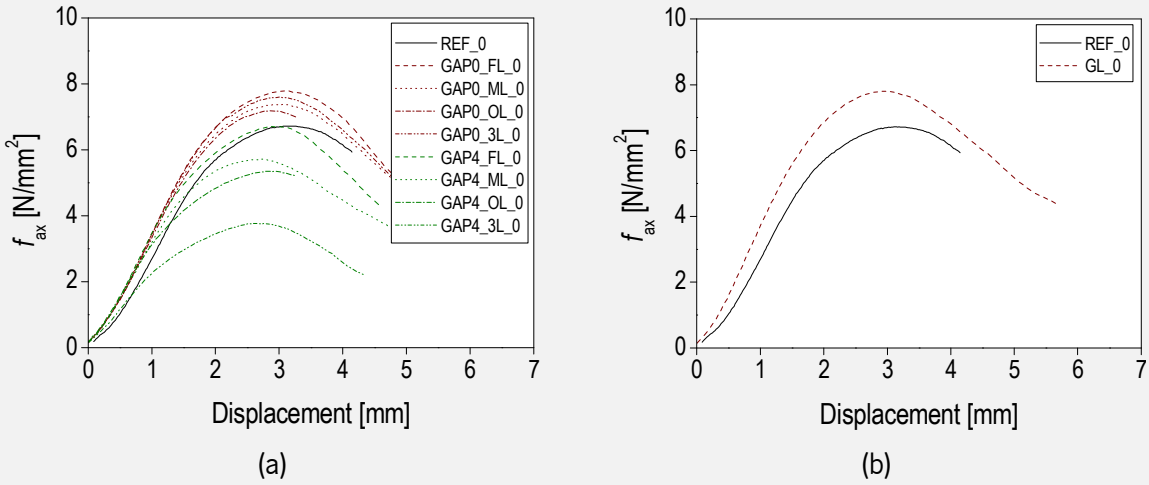

Figure (I) 4:12. Mean test curves for all configurations tested on day 0, expressing the expected yielding failure mode. (a) nine CLT configurations; (b) REF_D0 and GL_D0.

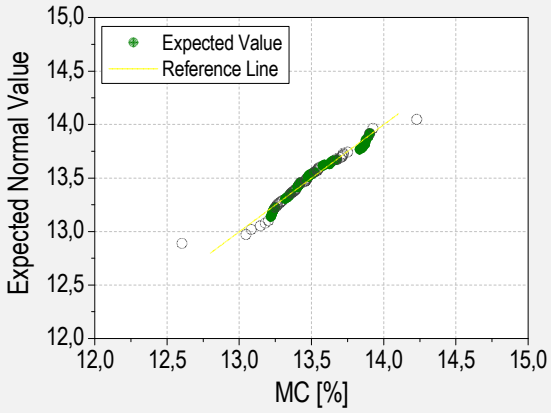

Figure (I) 4:13. Moisture distribution for group tested on day 324.

As mentioned before specimens tested on day 324 were submitted to an humidity cycle in which RH varied between 30% and 90% on a total of four complete cycles (Figure (I) 4:2). As a consequence, some damages were observed by simple visual inspection (Figure (I) 4:14). Typical observed damages are listen bellow:

- Opening of cracks, on outer layers, parallel to the timber grain and close to heartwood and screw location;
- Opening of cracks, on inner layers, also parallel to the timber grain;
- Delamination between boards;
- Enlargement of gaps.

Table (I) 4:3 presents mean values and descriptive statistics concerning $f_{ax,test}$, ρ_{12} and MC. For all these three variables, CoV values are positively low and median values are close to median values representing a good distribution and absence of outliers. Figure (I) 4:15 presents some specimens that was considered outliers, not due to test results but due to the location of significant timber knots on screw path which resulted on the highest withdrawal resistance.

Analyzing $f_{ax,test}$ values, highest and lowest values registered are of 8,08N/mm² and 2,67N/mm², for configurations GAP0_FL_D324 and GAP4_3L_D324, respectively. Differently to what was observed for specimens on day 0, the configurations with gaps of 0mm (GAP0_D324) present a decreasing trend as the number of gaps increase. A slightly decrease of $f_{ax,test}$ is observed when comparing with results obtained for REF_D324 (Figure (I) 4:16 (a)). The configuration that exhibits the highest discrepancy comparing with REF_D324 is GAP0_3L_D324, registering a decrease for $f_{ax,test,mean}$ of 15,4%. This inversion of the normal tendency must be related with damages caused by RH cycle and consequent enlargement of GAP0 (Figure (I) 4:14). The highest losses of $f_{ax,test}$ are again observed for configurations

with gaps of 4mm (GAP4_D324). Similarly to tests performed on day 0, it was observed a pronounced decreasing tendency for $f_{ax,test}$ as the number of gaps increase (Figure (I) 4:16 (b)). So, taking REF_D324 as reference, less favorable configurations are GAP4_OL_D324 and GAP4_3L_D324, with significant decreases of 29,0% and 56,0%, respectively. Observed decreases are higher than those observed in section 3.2.1 from chapter 3.

Again, this fact must be related with the damages caused by RH cycle and the consequent enlargement of GAP4 (Figure (I) 4:14).

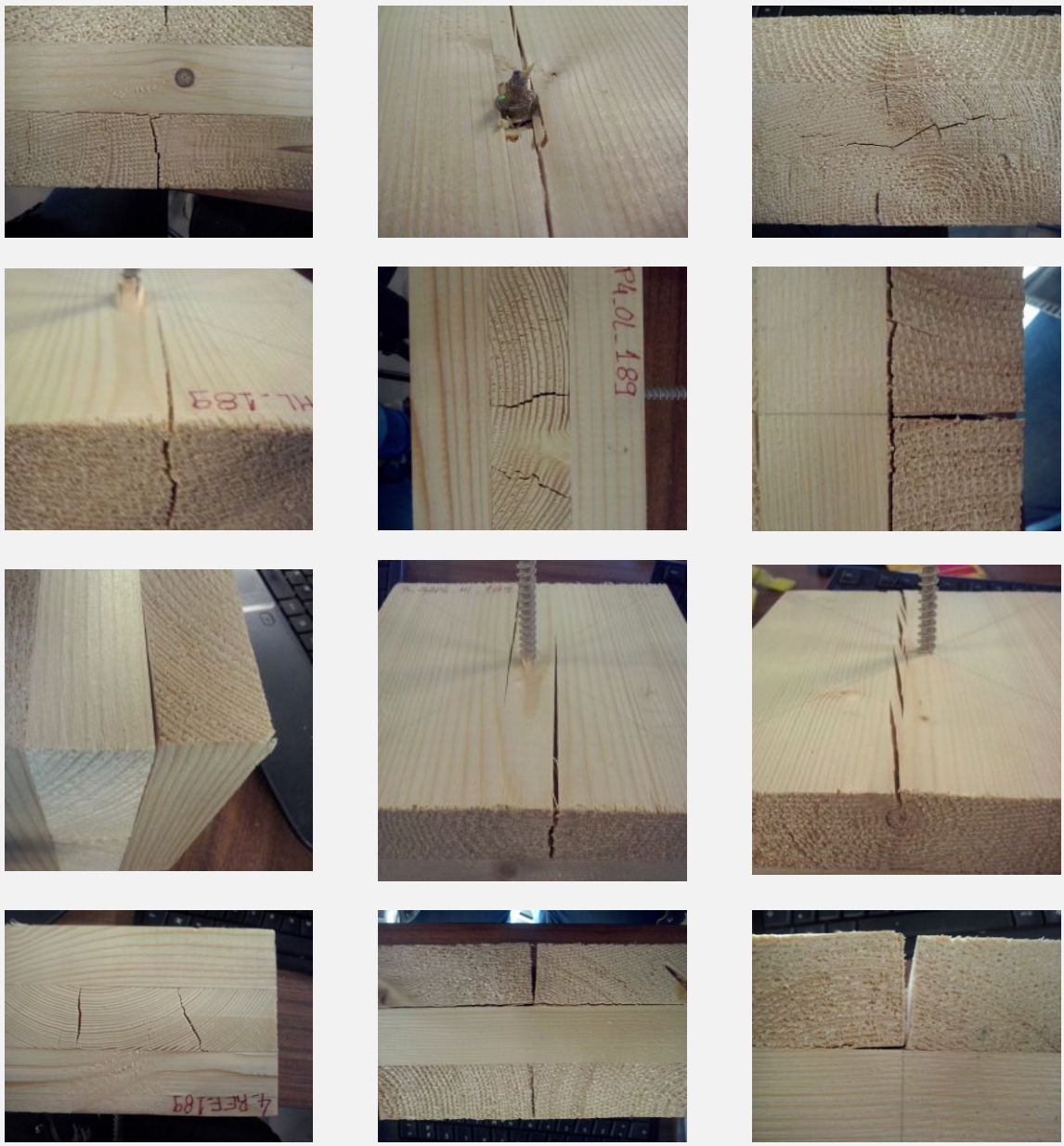

Figure (I) 4:14. Visual inspection of damages caused by RH cycle on CLT and GL specimens.

Table (I) 4:3. Mean values and descriptive statistics of $f_{ax,test}$, ρ_{12} and MC of different configurations tested on day 324.

	MEAN VALUES			DESCRIPTIVE STATISTICS						
GROUPS	MC [%]	$f_{ax,test}$ [N/MM²]	ρ_{12} [KG/M³]	N.º OF TESTS	$f_{ax,test}$ / ρ_{12} / MC	SD	COV	MIN	MAX	MEDIAN	P5
REF_D324	**13,7**	**7,97**	**452**	**10**	***0,50***	***0,06***	***7,48***	***7,69***	***8,84***	***7,48***
					7,95	**0,02**	**440**	**452**	**464**	**440**
					0,17	**0,01**	**13,4**	**13,7**	**13,9**	**13,4**
GAP0_FL_D324	13,5	7,94	461	8	*0,68*	*0,09*	*6,77*	*8,08*	*8,57*	*6,77*
					16,36	0,04	444	456	495	444
					0,08	0,01	13,4	13,6	13,6	13,4
GAP0_ML_D324	13,2	7,09	438	8	*0,44*	*0,06*	*6,58*	*7,02*	*7,83*	*6,58*
					21,78	0,05	407	445	472	407
					0,28	0,02	12,6	13,3	13,5	12,6
GAP0_OL_D324	13,4	6,98	487	9	*0,82*	*0,12*	*5,92*	*6,97*	*8,35*	*5,92*
					15,55	0,03	464	479	508	464
					0,21	0,02	13,2	13,4	13,9	13,2
GAP0_3L_D324	13,6	6,74	443	10	*0,56*	*0,08*	*5,86*	*6,64*	*7,66*	*5,86*
					16,69	0,04	424	443	482	424
					0,15	0,01	13,4	13,5	13,9	13,4
GAP4_FL_D324	13,6	6,66	451	10	*0,35*	*0,05*	*5,96*	*6,73*	*7,16*	*5,96*
					22,35	0,05	414	461	477	414
					0,20	0,01	13,4	13,5	13,9	13,4
GAP4_ML_D324	13,3	6,30	449	10	*0,47*	*0,07*	*5,58*	*6,32*	*6,96*	*5,58*
					8,70	0,02	434	448	461	434
					0,10	0,01	13,2	13,3	13,5	13,2
GAP4_OL_D324	13,5	5,66	439	10	*0,62*	*0,11*	*4,60*	*5,64*	*6,56*	*4,60*
					25,71	0,06	406	435	482	406
					0,18	0,01	13,2	13,5	13,9	13,2
GAP4_3L_D324	13,5	3,51	442	9	*0,65*	*0,19*	*2,67*	*3,51*	*4,52*	*2,67*
					15,70	0,04	416	442	472	416
					0,36	0,03	13,1	13,3	14,2	13,1
GL_D324	13,3	7,56	468	9	*0,33*	*0,04*	*7,10*	*7,61*	*8,16*	*7,10*
					28,44	0,06	432	476	504	432
					0,10	0,01	13,1	13,4	13,5	13,1

MC – moisture content, f_{ax} - maximum withdrawal resistance, ρ_{12} – density of reference, **SD** – standard of deviation, **CoV** – coefficient of variation, **P5** – 5th Percentil, **REF_D324** - configuration tested on day 324, **GAP0_FL_D324** - configuration with a gap of 0mm in first layer tested on day 324; **GAP0_ML_D324** - configuration with a gap of 0mm in middle layer tested on day 324, **GAP0_OL_D324** - configuration with a gap of 0mm in outer layers tested on day 324, **GAP0_3L_D324** - configuration with a gap of 0mm in three layers tested on day 324, **GAP4_FL_D324** - configuration with a gap of 4mm in first layer tested on day 324; **GAP4_ML_D324** - configuration with a gap of 4mm in middle layer tested on day 324, **GAP4_OL_D324** - configuration with a gap of 4mm in outer layers tested on day 324, **GAP4_3L_D324** - configuration with a gap of 4mm in three layers tested on day 324, **GL_D324** – configuration of GL tested on day 324.

Figure (I) 4:17 ((a)-(d)) compares the results obtained by similar configurations GAP0_D324/GAP4_D324 with configuration REF_D324. Differently to results observed on day 0, now it is evident the similar trend of configurations with GAP0 and GAP4 regarding REF configuration. Both present lower $f_{ax,test}$ values when comparing with REF_D324 however, the discrepancy between GAP0 and GAP4 configurations is close to that observed for tests performed on day 324: 16,1%, 11,1%, 18,9% and 47,9% for configurations GAP_FL_D324, GAP_ML_D324, GAP_OL_D324 and GAP_3L_D324, respectively.

Regarding tests performed with GL_D324, it was observed a slightly decrease of 5,1% for $f_{ax,test}$ when compared with REF_D324 configuration (Figure (I) 4:17 (e)).

Figure (I) 4:18 depicts the expected yielding failure mode observed during screw pull-out test. More detailed information about results obtained for tests performed on day 324 are shown in Annex 1:14.

6_GL_308

9_GAP0_OL_308

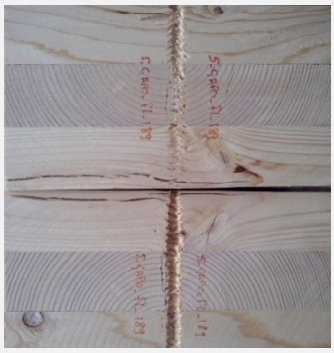

5_GAP0_FL_308

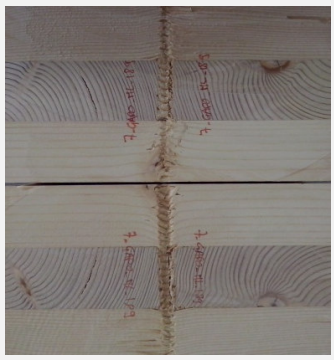

7_GAP0_ML_308

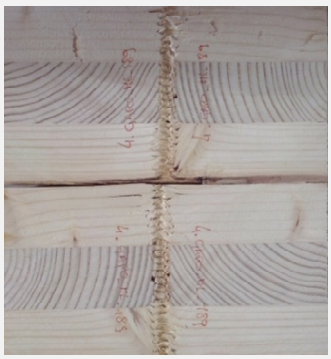

4_GAP0_ML_308

7_GAP0_FL_308

Figure (I) 4:15. Specimens defined as outliers due to the location of knots on screw path for tests performed on day 324.

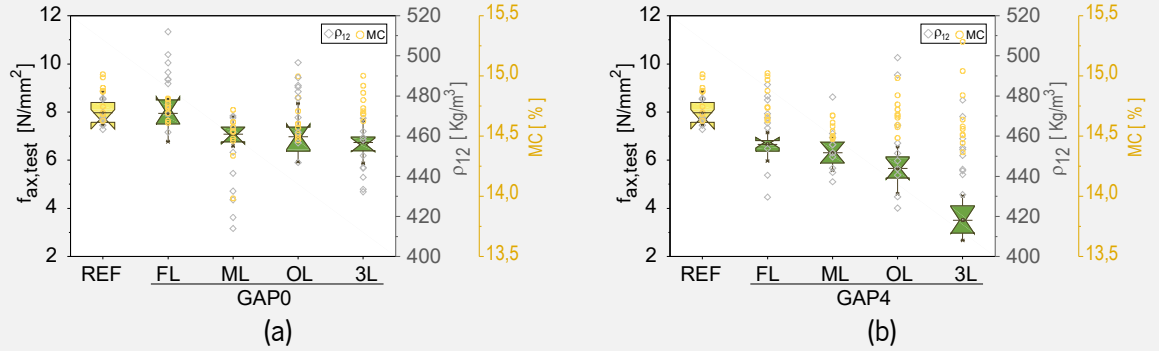

Figure (I) 4:16. Box chart with notched boxes of $f_{ax,test}$ and scatter plot of density of reference and moisture content for the following groups: (a) REF_D324 and GAP0_D324; (b) REF_D324 and GAP4_D324.

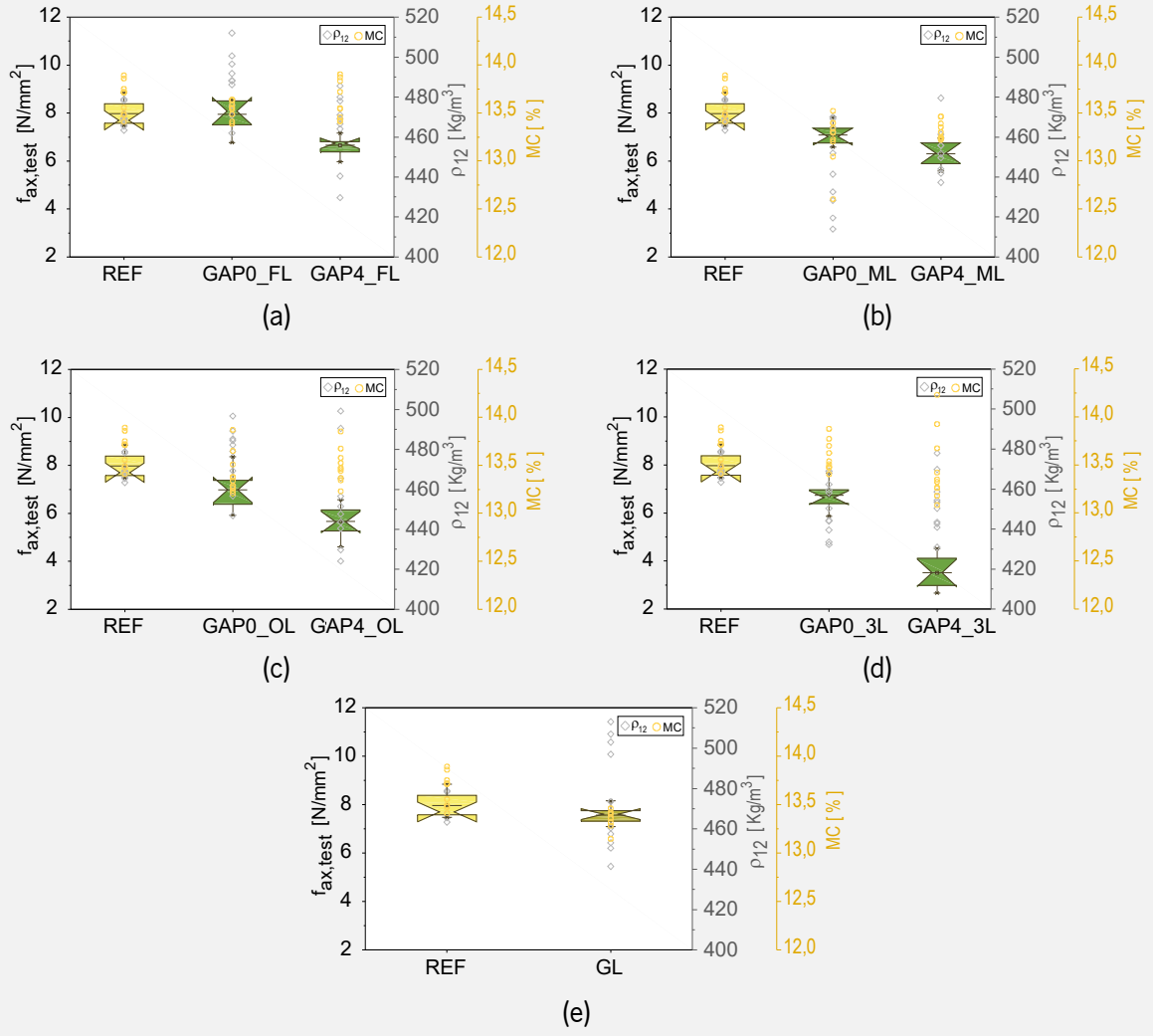

Figure (I) 4:17. Box chart with notched boxes of $f_{ax,test}$ and scatter plot of density of reference and moisture content for the following groups: (a) REF_D324 and GAP_FL_D324; (b) REF_D324 and GAP_ML_D324; (c) REF_D324 and GAP_OL_D324; (d) REF_D324 and GAP_3L_D324; and (e) REF_D324 and GL_D324.

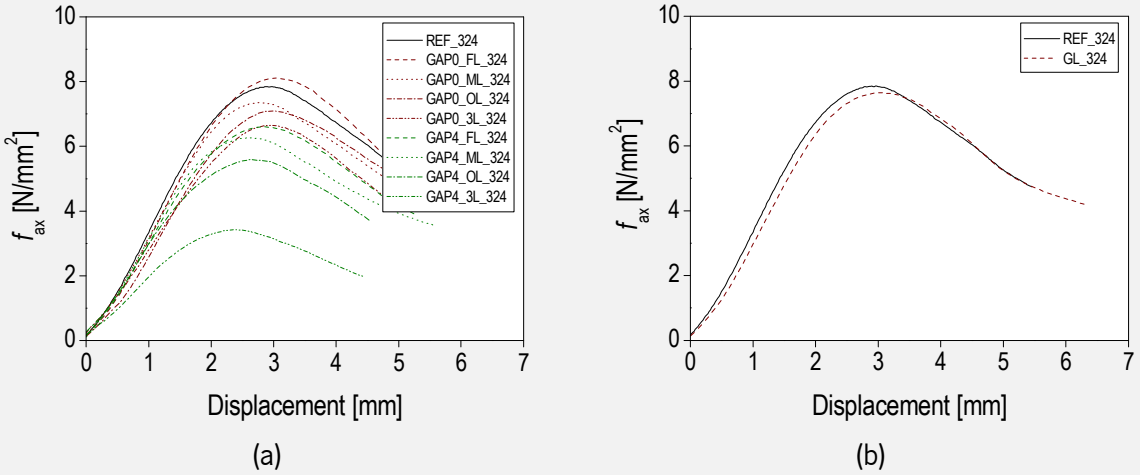

Figure (I) 4:18. Mean test curves for all configurations tested on day 324, expressing the expected yielding failure mode. (a) nine CLT configurations; (b) REF_D324 and GL_D324.

4.3 Modeling the influence of number of gaps (η_{gap}) and MC levels (η_{MC}) on withdrawal resistance of STSs inserted in main face of CLT panels

Just like the procedure presented in previous chapter, at this stage density of reference (ρ_{12}) was corrected ($\rho_{12,corr}$) considering a smaller timber volume around the STSs. Despite the reduced control during the production of specimens, regarding density distribution and location of knots, the differences observed between ρ_{12} and $\rho_{12,corr}$ are not significant (Figure (I) 3:30). Table (I) 3:6 presents density values, before and after correction, respective CoV and the ratio between ρ_{12} and $\rho_{12,corr}$ for all configurations tested before and after RH cycles. Considering values obtained for $\rho_{12,corr}$, $f_{ax.test}$ was also corrected as described in section 3.3 from chapter 3. Table (I) 4:5 shows the descriptive statistics of $f_{ax,corr}$ values that will be used to perform the analysis presented hereafter.

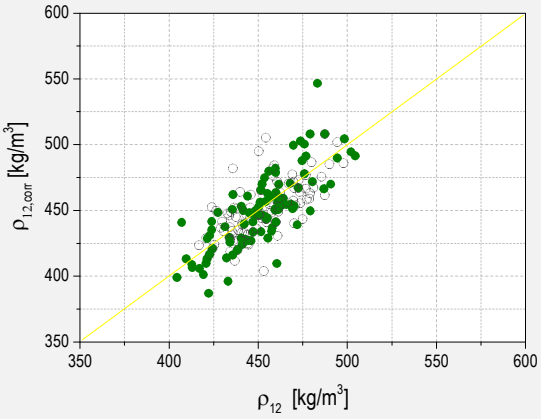

Figure (I) 4:19. Relation between density of reference concerning the entire specimen (ρ_{12}) and corrected density considering a small sample of CLT near screw location ($\rho_{12,corr}$).

Table (I) 4:4. Median values of ρ_{12} and $\rho_{12,corr}$ for different test configurations, respective CoV values and ratio between them.

GROUPS		ρ_{12} (KG/M³)	COV (ρ_{12}) [%]	$\rho_{12,corr}$ (KG/M³)	COV ($\rho_{12,corr}$) [%]	$\frac{\rho_{12}}{\rho_{12,corr}}$
REF	**D0**	460	0,01	448	0,04	1,03
	D324	462	0,01	452	0,02	1,02
GAP0_FL	**D0**	473	0,04	461	0,05	1,03
	D324	477	0,03	461	0,04	1,03
GAP0_ML	**D0**	434	0,05	431	0,08	1,01
	D324	437	0,05	438	0,05	1,00
GAP0_OL	**D0**	464	0,03	476	0,07	0,98
	D324	465	0,03	487	0,03	0,95
GAP0_3L	**D0**	438	0,03	448	0,05	0,98
	D324	441	0,03	443	0,04	0,99
GAP4_FL	**D0**	453	0,04	439	0,05	1,03
	D324	456	0,04	451	0,05	1,01
GAP4_ML	**D0**	442	0,02	444	0,04	1,00
	D324	446	0,03	449	0,02	1,00
GAP4_OL	**D0**	447	0,05	437	0,06	1,02
	D324	447	0,05	439	0,06	1,02
GAP4_3L	**D0**	442	0,03	439	0,03	1,01
	D324	445	0,03	444	0,04	1,00
GL	**D0**	460	0,06	455	0,05	1,01
	D324	471	0,06	468	0,06	1,01

ρ_{12} – density, **CoV** – coefficient of variation, **REF** - configuration without gaps, **GAP0_FL** - configuration with a gap of 0mm in first layer; **GAP0_ML** - configuration with a gap of 0mm in middle layer, **GAP0_OL**- configuration with a gap of 0mm in outer layers, **GAP0_3L**- configuration with a gap of 0mm in three layers, **GAP4_FL**- configuration with a gap of 4mm in first layer; **GAP4_ML** - configuration with a gap of 4mm in middle layer, **GAP4_OL** - configuration with a gap of 4mm in outer layers, **GAP4_3L** - configuration with a gap of 4mm in three layers; **GL** –configuration with glulam.

4.3.1 Definition of η_{gap} and η_{MC}

In order to quantify properly the influence of each GAP0/GAP4 added to the STS path (k_{gap}) as well as the influence of cyclic MC changes on CLT elements (k_{MC}), linear fittings based on the method of least squares were performed. The same bi-linear models defined in section 3.3.2. from chapter 3 (equation 3:8 and equation 3:10) were used to apply k_{gap} and k_{MC} defined in present section.

Relatively to the performed linear fittings, it is also important to note that R^2 tends to be lower than desirable and the reason for that should be related with reduced sampling.

Table (I) 4:5. Descriptive statistics of $f_{ax,corr}$ for different test configurations tested on day 0 and day 324.

$f_{ax,corr}$									
GROUPS		**SAMPLE**	**MEAN**	**SD**	**COV [%]**	**MEDIAN**	**MIN**	**MAX**	**P5**
REF	**D0**	10	7,04	0,54	0,08	7,28	5,97	7,56	5,97
	D324	10	7,99	0,52	0,07	7,76	7,45	9,05	7,45
GAP0_FL	**D0**	10	7,68	0,29	0,04	7,71	7,13	8,10	7,13
	D324	8	7,83	0,62	0,08	7,92	6,78	8,59	6,78
GAP0_ML	**D0**	9	7,50	0,36	0,05	7,45	6,93	7,99	6,93
	D324	8	7,29	0,38	0,05	7,40	6,64	7,68	6,64
GAP0_OL	**D0**	9	6,83	0,84	0,12	7,22	4,96	7,48	4,96
	D324	9	6,58	0,66	0,10	6,72	5,67	7,63	5,67
GAP0_3L	**D0**	10	7,64	0,51	0,07	7,70	6,74	8,32	6,74
	D324	10	6,86	0,50	0,07	6,78	6,10	7,74	6,10
GAP4_FL	**D0**	10	6,91	0,27	0,04	6,94	6,54	7,43	6,54
	D324	10	6,70	0,36	0,05	6,69	6,13	7,30	6,13
GAP4_ML	**D0**	10	5,83	0,34	0,06	5,79	5,36	6,34	5,36
	D324	10	6,36	0,45	0,07	6,32	5,59	7,03	5,59
GAP4_OL	**D0**	10	5,61	1,13	0,20	5,71	2,92	7,31	2,92
	D324	10	5,81	0,50	0,09	5,80	5,02	6,58	5,02
GAP4_3L	**D0**	10	3,90	0,50	0,13	4,05	3,11	4,46	3,11
	D324	9	3,51	0,66	0,19	3,34	2,58	4,57	2,58
GL	**D0**	9	7,59	0,55	0,07	7,61	6,70	8,23	6,70
	D324	9	7,39	0,49	0,07	7,33	6,68	8,25	6,68

f_{ax} - maximum withdrawal resistance, **CoV** – coefficient of variation, **SD** – standard of deviation, **P5** – 5th percentil, **REF** - configuration without gaps, **GAP0_FL** - configuration with a gap of 0mm in first layer; **GAP0_ML** - configuration with a gap of 0mm in middle layer, **GAP0_OL**- configuration with a gap of 0mm in outer layers, **GAP0_3L**- configuration with a gap of 0mm in three layers, **GAP4_FL**- configuration with a gap of 4mm in first layer; **GAP4_ML** - configuration with a gap of 4mm in middle layer, **GAP4_OL** - configuration with a gap of 4mm in outer layers, **GAP4_3L** - configuration with a gap of 4mm in three layers; **GL** – configuration with glulam.

4.3.1.1 η_{gap}

The analysis of the influence of number and width of gaps on specimens tested on DAY 0 and DAY 324 was performed as described at section 3.3.1.1 from chapter 3. So, taking REF configuration of each test day as reference (equation (4:1)), linear fittings, depicted in Figure (I) 4:20, were performed and mean k_{gap} values shown in Table (I) 2:23, were defined.

Similar to what was observed for the experimental campaign presented in previous chapter, specimens with GAP0 tested on DAY 0 present a slightly increase of f_{ax} (Figure (I) 4:20 (a)). However, the linear growing trend associated with the increasing of number of gaps is not verified here (slopes obtained for different linear fittings can be seen at tables presented in Figure (I) 4:20 (a)). Anyway, the obtained

average suggest an increase for f_{ax} of 3,3% per each GAP0 added to the STS path. On contrary, specimens with GAP0 tested on DAY 324 present a downward trend that suggest, in average, a decrease for f_{ax} of 6,7% per each GAP0 added to the STS path. As depicted in Figure (I) 4:20 (a), the downward trend is not linear once specimens with two gaps present higher decreases than specimens with three gaps.

Despite k_{gap} values obtained for configurations with GAP0, and in accordance with what is stated in previous chapter, this study consider that GAP0 has no influence on the test results. This way, the effect of RH cycles is quantified just by k_{MC} parameter.

$$\frac{f_{ax,corr,gap\ (i)(D0/D324)}}{f_{ax,corr,REF\ (mean,D0/D324)}} \quad (4:1)$$

$f_{ax,corr}$	Withdrawal resistance corrected considering density, in N/mm²;
$gap\ (i)\ (D0/D324)$	$f_{ax,corr}$ obtained in experimental campaign for remaining configurations tested on day 0 and day 324, in N/mm²;
$REF\ (mean, D0/D324)$	Mean $f_{ax,corr}$ obtained in experimental campaign for REF configuration tested on day 0 or day 324, in N/mm².

Table (I) 4:6. Obtained values for k_{gap}, depending on test day and gap width.

WIDTH OF GAPS		DAY 0	Day 324
k_{gap}	GAP0	0,03	-0,07
	GAP4	-0,11	-0,17
	GL	0,08	-0,08

Relatively to tests performed on DAY 0 for specimens with GAP4 (Figure (I) 4:20 (b)), results suggest that f_{ax} tends to decrease 10,7% per each gap added. Despite the difference of 3% of moisture content between the group tested with MC=12% ($MC_{mean,12\%}$ = 11,4%), presented in chapter 3, and the group tested on DAY 0 ($MC_{mean,DAY0}$ = 14,5%, the results obtained are close: group tested with MC=12% suggest that f_{ax} reduces 8,7% per each GAP4 added. The higher decrease presented by the group tested on Day 0 must be related with the high MC levels at lamination time, which resulted on the enlargement of the gap width after stabilization period.

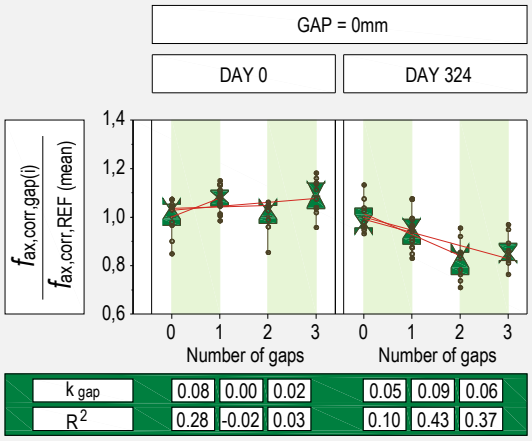

(a)

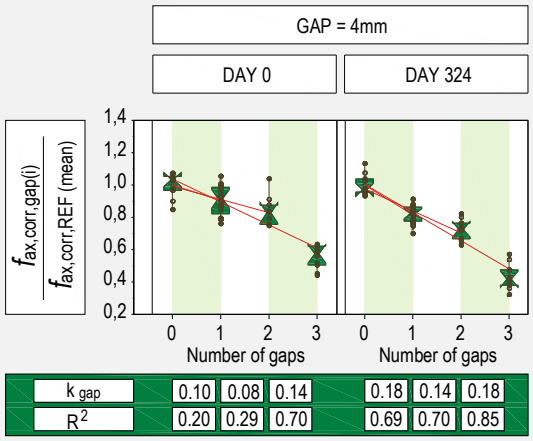

(b)

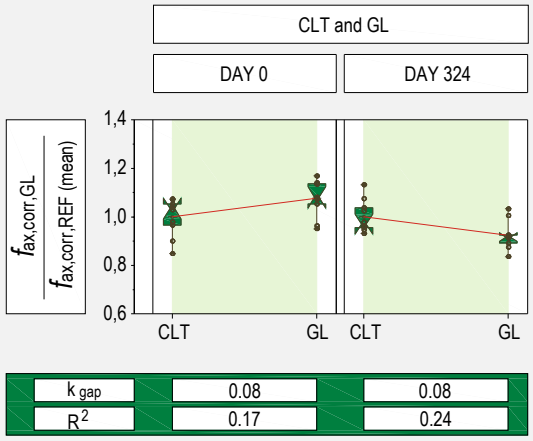

(c)

Figure (I) 4:20. Linear regressions performed between REF configuration and specimens with: (a) gaps with 0 mm; (b) gaps with 4 mm; (c) GL. k_{gap} and R^2values are presented in tables bellow respective graphs.

As expected, the group of specimens with GAP4 tested on DAY 324 registered the highest decreases of f_{ax}: 16,7% per each GAP4 added in the STS path (Figure (I) 4:20 (b)). This high decreases resulted from the damages caused by RH cycle and also with the high moisture content levels at lamination time and consequent enlargement of GAP4. This way, the group tested with MC=8% (chapter 3) presented close results, suggesting a decrease for f_{ax} of 14,4% per each GAP4 added.

Relatively to the tests performed with GL, it was observed that for the group tested on DAY 0, GL presented f_{ax} mean values 7,8 % higher than REF specimens also tested on DAY 0. However, considering the overlapping of notched boxplots (Figure (I) 4:20 (c)), the difference between GL and REF groups is not significant. Differently, Figure (I) 4:20 (c) indicate that results obtained for groups tested on DAY 324 are more significant: GL presents f_{ax} values 7,6% lower than those obtained for REF configuration with no overlapping of notched boxplots. A possible explanation for this tendency, also referred by Ringhofer et al. (2014), can be related with CLT crosswise lamination.

4.3.1.2 η_{MC}

In order to qauntify the effect of cyclic MC changes on the withdrawal resistance of STSs (η_{MC}), all tested configurations were analysed separatly. Considering test configurations tested on DAY 0 as reference (equation (3:9)), the effect of successive RH cycles was quantified (k_{MC}). k_{MC} was defined by the obtained slopes given by linear fittings performed regarding different test configurations (results can be seen at tables presented in Figure (I) 3:32).

Table (I) 3:10 shows k_{MC} values considered to apply on η_{MC} model.

$$\frac{f_{ax,corr,(D324)}}{f_{ax,corr\ (mean,D0)}} \qquad (4:2)$$

$f_{ax,corr}$	Withdrawal resistance corrected considering density, in N/mm²;
$f_{ax,corr,(D324)}$	$f_{ax,corr}$ obtained in experimental campaign for REF configuration tested on DAY 324, in N/mm²;
$f_{ax,corr,(mean,D0)}$	Mean $f_{ax,corr}$ obtained in experimental campaign for remaining configurations tested on DAY 0, in N/mm².

Table (I) 4:7. Obtained values for k_{MC}, depending on RH cycle, gap width and number of gaps.

		REF	GAP0	GAP4_FL/ML	GAP4_OL/3L	GL
K_{MC}	DAY 0 (MC≥12%)	-0,02			0,00	n.a.
	DAY 324	0,14	-0,5	-0,05		-0,03

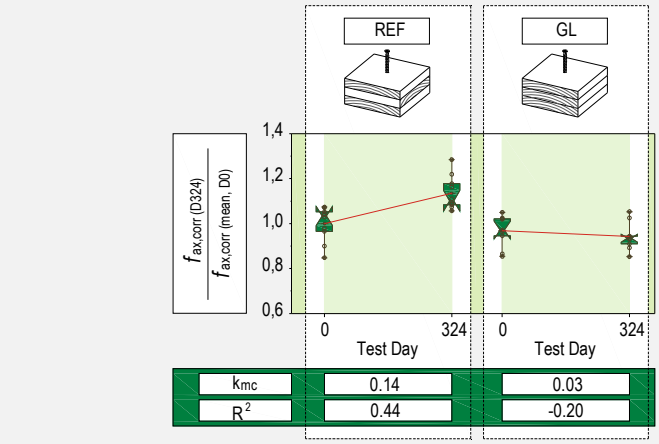

(a)

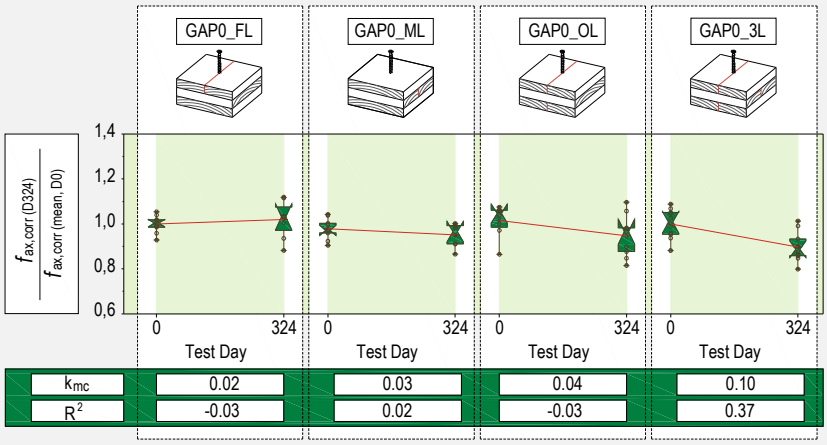

(b)

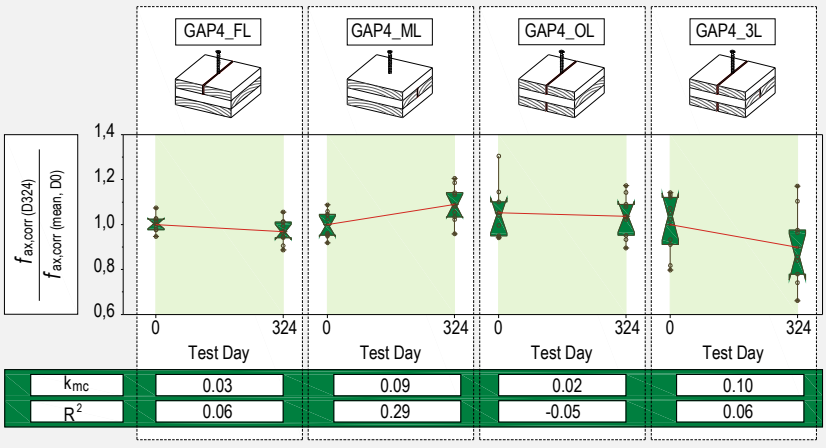

(c)

Figure (I) 4:21. Graphs of linear fittings between different moisture levels for all configurations: (a) REF configuration; (b) GAP0 configurations; and (c) GAP4 configurations. k_{MC} and R^2 values related with same linear fittings are presented bellow respective graphs.

Surprisingly, results obtained for this experimental campaign show that RH cycle resulted in an improvement of f_{ax} for REF configuration, which exhibits an increase of 13,5% (Figure (I) 3:32 (a)). This phenomenon should also be related with crosswise lamination and MIS caused by RH cycle. On contrary, GL presents a slightly decrease for f_{ax} (3,1%) at the end of RH cycles.

Despite the damages caused by RH cycles on test specimens, configurations with GAP0 also present reduced effects on withdrawal resistance. As depicted in Figure (I) 3:32 (b), decreases for f_{ax} varies between 2,0% (GAP0_FL) and 10,2% (GAP0_3L), being suggested a k_{MC} = -0,05 for all GAP0 configurations.

On the other hand, with the exception of configuration GAP4_ML_324, damages caused by RH cycles resulted in decreases for f_{ax} regarding configurations with GAP4. As depicted in Figure (I) 3:32 (c), decreases for f_{ax} varies between 3,1% (GAP4_FL) and 10,1% (GAP4_3L). Presenting the opposite trend, results obtained for configuration GAP4_ML_324 were not considered for definition of k_{MC}. Furthermore, as the increase of number of gaps does not present a linear trend, all remaining GAP4 configurations were grouped in order to suggest a k_{MC} = -0,05 for all GAP4 configurations. The reason for the increase of f_{ax} after RH cycles for configuration GAP4_ML (f_{ax} increases in average 9,0% after RH cycles) is not clear and further research is required in order to verify such tendency.

It is important to underline that GAP_3L configurations presented the highest decreases for tests performed with configurations with GAP0 and GAP4: 10,2% and 10,1%, respectively. However, considering the overlapping of boxplots, none configuration present significant decreases for f_{ax}.

4.3.2 Applying η_{gap} and η_{MC} and compare with Uibel & Blaß Model

Similar to what was presented in section 3.3.3 from chapter 3, $f_{ax,pred}$ was obtained combining the model proposed by Uibel & Blaß (2007) (equation (3:11)) and defined η_{gap} and η_{MC} models.

Table (I) 3:11 shows descriptive statistics for $f_{ax,pred}$, considering an angle of 90° between screw axis and grain direction, while Figure (I) 3:33 depicts the correlations between $f_{ax,pred}$ and $f_{ax,test}$, considering different test days and different width of gaps. Analyzing both, it is clear that predicted values are positively placed on conservative side.

Figure (I) 4:23 shows the relation between mean test results and the predicted mean values. Comparing obtained results with those presented in chapter 3, differences observed between test results and predicted withdrawal resistance are higher, suggesting that Uibel & Blaß model is too conservative.

Table (I) 4:8. Descriptive statistics of $f_{ax,pred}$ for different test configurations tested on DAY 0 and DAY 324.

GROUPS		N.TESTS	MEAN	SD	COV	MEDIAN	MIN	MAX	P5	$\frac{f_{ax,pred}}{f_{ax,test}}$
REF	**DAY 0**	10	5,94	0,19	0,03	5,97	5,50	6,22	5,50	0,85
	DAY 324	10	7,71	0,17	0,02	7,72	7,39	7,97	7,39	0,97
GAP0_FL	**DAY 0**	10	6,03	0,21	0,03	5,99	5,72	6,37	5,72	0,77
	DAY 324	8	5,96	0,15	0,03	5,92	5,78	6,26	5,78	0,75
GAP0_ML	**DAY 0**	9	5,74	0,34	0,06	5,54	5,39	6,26	5,39	0,79
	DAY 324	8	5,82	0,23	0,04	5,87	5,50	6,07	5,50	0,82
GAP0_OL	**DAY 0**	9	6,21	0,33	0,05	6,09	5,89	6,90	5,89	0,88
	DAY 324	9	6,24	0,17	0,03	6,17	6,05	6,50	6,05	0,90
GAP0_3L	**DAY 0**	10	5,89	0,25	0,04	5,86	5,61	6,37	5,61	0,77
	DAY 324	10	5,77	0,15	0,03	5,76	5,54	6,12	5,54	0,86
GAP4_FL	**DAY 0**	10	5,18	0,22	0,04	5,09	4,90	5,48	4,90	0,76
	DAY 324	9	4,73	0,21	0,05	4,84	4,41	4,98	4,41	0,71
GAP4_ML	**DAY 0**	10	5,24	0,17	0,03	5,16	5,05	5,55	5,05	0,91
	DAY 324	10	4,82	0,07	0,01	4,81	4,73	4,93	4,73	0,77
GAP4_OL	**DAY 0**	9	4,79	0,20	0,04	4,79	4,34	4,96	4,34	0,83
	DAY 324	10	3,74	0,16	0,04	3,70	3,53	4,02	3,53	0,67
GAP4_3L	**DAY 0**	10	4,10	0,10	0,02	4,07	4,00	4,27	4,00	1,09
	DAY 324	9	2,79	0,09	0,03	2,78	2,67	2,96	2,67	0,84

$f_{ax,pred}$ - predicted withdrawal resistance, obtained by Uibel & Blaß Model, η_{MC} - reduction factor of moisture influence on f_{ax}, η_{gap} - reduction factor of GAPs influence on f_{ax}, **SD** – sation, **CoV** – Coefficient of Variation, **P5** – 5th percentile, **REF** - configuration without gaps, **GAP0_FL** - configuration with a gap of 0mm in first layer; **GAP0_ML** - configuration with a gap of 0mm in middle layer; **GAP0_OL** - configuration with a gap of 0mm in outer layers; **GAP0_3L** - configuration with a gap of 0mm in three layers; **GAP4_FL** - configuration with a gap of 4mm in first layer; **GAP4_ML** - configuration with a gap of 4mm in middle layer; **GAP4_OL** - configuration with a gap of 4mm in outer layers; **GAP4_3L** - configuration with a gap of 4mm in three layers.

Regarding REF configuration, it is important to mention that $f_{ax,pred}$ is closer to $f_{ax,test}$ for tests performed on DAY 324 $\left(\frac{f_{ax,pred,D324}}{f_{ax,test,D324}} = 0{,}97\right)$ and DAY 0 $\left(\frac{f_{ax,pred,D0}}{f_{ax,test,D0}} = 0{,}85\right)$.

Again, as the effect of GAP0 was not considered for calculation of predicted values, configurations with GAP0 $\left(0{,}75 \leq \frac{f_{ax,pred,GAP0}}{f_{ax,test,GAP0}} \leq 0{,}90\right)$ present a lower range for the ratio between $f_{ax,pred}$ and $f_{ax,test}$ than configurations with GAP4 $\left(0{,}65 \leq \frac{f_{ax,pred,GAP4}}{f_{ax,test,GAP4}} \leq 1{,}09\right)$.

As expected, regarding the constraints for the definition of k_{MC} (section 4.3.1.2), configurations with GAP4 presented the configurations with the most conservative results: GAP4_FL_324 $\left(\frac{f_{ax,pred}}{f_{ax,test}} = 0{,}71\right)$ and GAP4_OL_324 $\left(\frac{f_{ax,pred}}{f_{ax,test}} = 0{,}67\right)$.

Configurations that presented the less conservative predicted values, are: GAP4_ML_D0 $\left(\frac{f_{ax,pred}}{f_{ax,test}} = 0{,}91\right)$ and GAP4_3L_D0 $\left(\frac{f_{ax,pred}}{f_{ax,test}} = 1{,}09\right)$. This happens because k_{MC} values used to obtain $f_{ax,pred}$ for configurations with GAP4 tested on DAY 0 are the same suggested for equation 3:10 (chapter 3), for a moisture range between 12% and 18%.

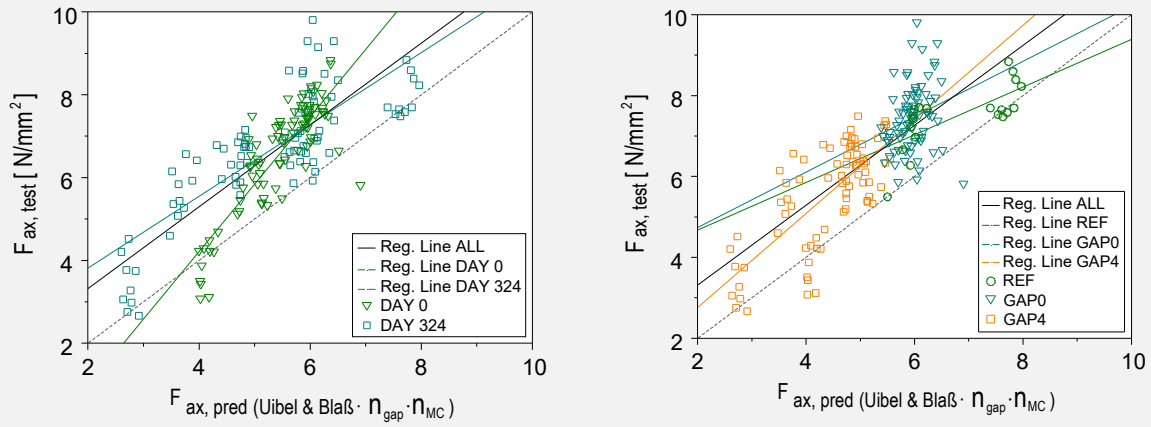

(a) (b)

Figure (I) 4:22. Correlation between $f_{ax,pred}$ and $f_{ax,test}$ for: (a) test performed on DAY 0 and DAY 324; (b) configurations REF, GAP0 and GAP4.

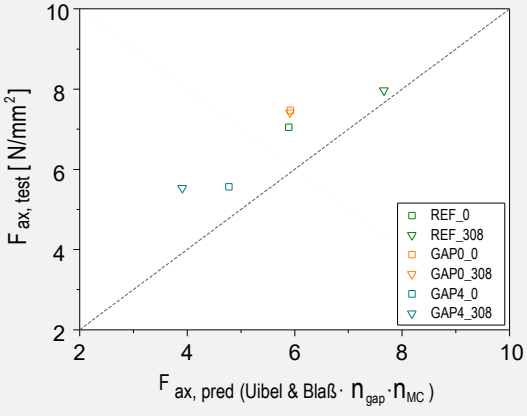

(a)

Figure (I) 4:23. Correlation between mean values obtained for $f_{ax,pred}$ and $f_{ax,test}$. a) mean values for all configurations tested on DAY 0 and DAY 324; b) mean values for GAP_FL configurations; c) mean values for GAP_ML configurations; d) mean values for GAP_OL configurations; e) mean values for GAP_3L configurations.

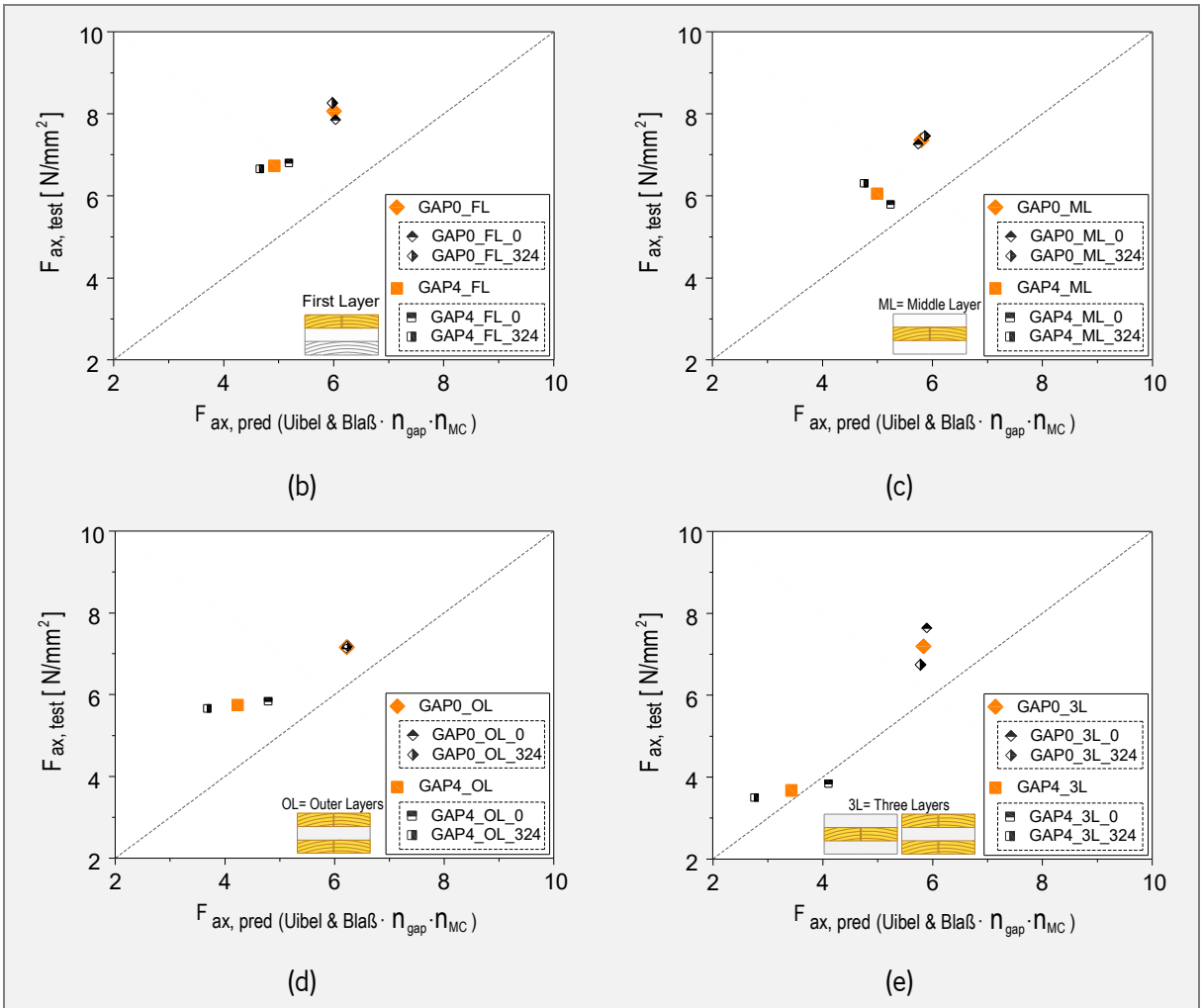

Figure (I) 4:23 (continued) Correlation between mean values obtained for $f_{ax,pred}$ and $f_{ax,test}$. a) mean values for all configurations tested on DAY 0 and DAY 324; b) mean values for GAP_FL configurations; c) mean values for GAP_ML configurations; d) mean values for GAP_OL configurations; e) mean values for GAP_3L configurations.

4.4 Main conclusion

The present research showed and discussed the results of an experimental campaign focused on the quantification of effects caused by successive RH cycles, the existence of gaps and their width on the withdrawal behavior of axially loaded STS inserted in the main face of CLT panels. RH cycles oscillated between 30 % and 90 %, number of the gaps presented in the screw path varied from 0 to 3 and gap widths were of 0mm and 4mm.

After the analysis and modeling of the test results, some important conclusions can be pointed out:

- Similar to what was observed for tests presented in chapter 3, taking REF configuration as reference, tests performed with GAP0 on DAY 0 presented a slightly improvement of f_{ax} (k_{gap}

= 0,03, however tests performed on DAY 324 presented high negative values (k_{gap} = -0,07) as result of damages caused by RH cycles;

- Taking REF_D324 as reference, less favorable configurations are GAP4_OL_D324 and GAP4_3L_D324, with significant decreases of 29,0% and 56,0%, respectively;
- The decrease of f_{ax} observed for configurations with GAP4 tested on DAY 0 must be related with the high level of moisture content at the time of CLT production;
- When comparing the effects of RH cycles on CLT (REF configuration) and GL it is observed a better performance for CLT, which exhibits an increase of f_{ax} at the end of RH cycles (k_{MC} = 0,014). Differently, GL presented a slight decrease (k_{MC} = = -0,03) of f_{ax} after being submitted to the same RH cycles. it was observed that results obtained for GL are 5,1% lower when compared with REF_D324. However, in order to properly quantify these differences more research is needed;
- The adjusted Uibel & Blaß (2007) model showed accuracy in predicting the obtained test results. However, in order to obtain less conservative results more research is required.

CHAPTER 5 (I)

5 WITHDRAWAL RESISTANCE OF SELF-TAPPING SCREWS INSERTED ON MAIN FACE OF CLT PANELS WHEN SUBMITTED TO SIMPLE CHANGES ON MOISTURE CONTEN

5.1 Experimental campaign

The present chapter presents an experimental campaign performed at Civil Department of University of Minho and at Instituto Politécnico de Bragança (IPB). This task was performed in two different laboratories, once IPB had available facilities to conditioning specimens in a high RH environment (RH=98%).

5.2 Main goals and parameters involved

The performed experiments pretend to understand the influence of three different parameters on the axial withdrawal resistance of STSs inserted on the lateral face of three layered CLT panels. The first parameter is related with increasing of MC levels on CLT elements. For that, two different MC levels were considered, namely: MC=12% (reference) and MC=25%. A group of specimens with MC levels lower than 12% were not considered once tests performed at TU Graz showed a negligible influence of MC decrease from 12% to 8% on the withdrawal resistance of self-tapping screws inserted in the main face of CLT panels. The increasing of MC level is higher (MC=25%) for this experimental campaign than that described in chapter 3. This fact is related with the fact that laboratories did not have available climatic chambers to conditioning specimens in an environment of 20°C and 90%RH. As an alternative, specimens were conditioned in a wet room with a RH that was around 98%. This way, it was not possible to test specimens considering the limits imposed by service class 2 considered by Eurocode 5. Despite being a material not suitable for such use, this experimental campaign considered service class 3 from Eurocode 5 as reference.

Second parameter is related with the possible existence of gaps on the STS path and STS location in arrangement of CLT layers. To explore this parameter, CLT was produced considering the insertion of STSs through a gap, in the center of middle layer (GAP_ML) and parallel to the grain direction, or the insertion of STSs between layers (GAP_BL) in which STS is half inserted in gaps located in outer layers and considering two grain directions (0° and 90°).

Similar to experimental campaigns presented in two previous chapters, third parameter is related with gap width, which can be 0mm (GAP0) or 4mm (GAP4).

The combination of these three parameters resulted in six different test configurations and 120 withdrawal tests. Figure (I) 5:1 presents a summary of experimental campaign and illustrates different test configurations.

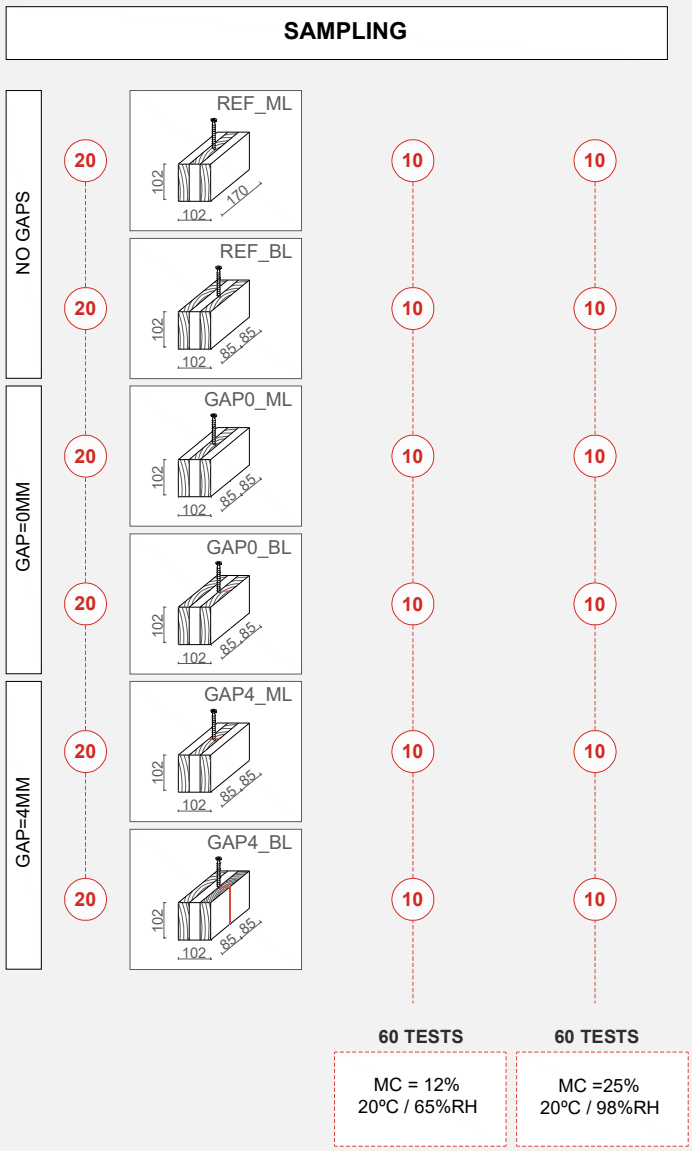

Figure (I) 5:1. Distribution of test configuration between two different test groups.

5.2.1 Production of specimens and main steps of experimental procedure

Test specimens used to present experimental campaign were produced at *Rusticasa*® and at the same time of specimens used for experimental campaign described in previous chapter (section 4.1.2. of chapter 4).

As described in previous chapter, due to high MC level at production time (CoV=0,08 and mean=18,4%), group of specimens which should present MC=12% were tested with a slightly higher MC level (around 14%).

Regarding density distribution, Table (I) 5:1 present the descriptive statistics of density distribution for all six different configurations and for both MC levels. Density values were calculated according to equation 3:1 (chapter 3) and varied between 409kg/m³ and 505kg/m³ (mean=461kg/m³). Density distribution exhibited good results with a density distribution close to a normal one, with median and mean densities close to each other, and with low CoV values between 0.02 and 0.04. Figure (I) 4:6 depicts the similarity of density distribution for groups tested with MC=14% and MC=25%.

Table (I) 5:1. Descriptive statistics of density distribution (ρ) for all six different configurations and for different MC levels.

CONF.	MC GROUP	Nº OF SPECIMENS	MEAN	SD	COV	MIN	MEDIAN	MAX	P5
REF_ML	14%	10	465	13,49	0,03	443	467	485	443
	25%	10	459	18,67	0,04	429	459	489	429
REF_BL	14%	10	471	15,42	0,03	447	468	491	447
	25%	10	482	13,87	0,03	464	477	505	464
GAP0_ML	14%	10	440	19,27	0,04	409	440	474	409
	25%	10	447	17,11	0,04	414	452	461	414
GAP0_BL	14%	10	470	10,16	0,02	450	473	485	450
	25%	10	466	14,67	0,03	444	470	486	444
GAP4_ML	14%	10	454	11,86	0,03	435	454	473	435
	25%	10	460	19,65	0,04	422	461	491	422
GAP4_BL	14%	10	448	18,00	0,04	414	449	473	414
	25%	10	460	15,80	0,03	433	461	487	433

SD – standard of deviation; **CoV** – coefficient of variation; **P5** – 5th percentile.

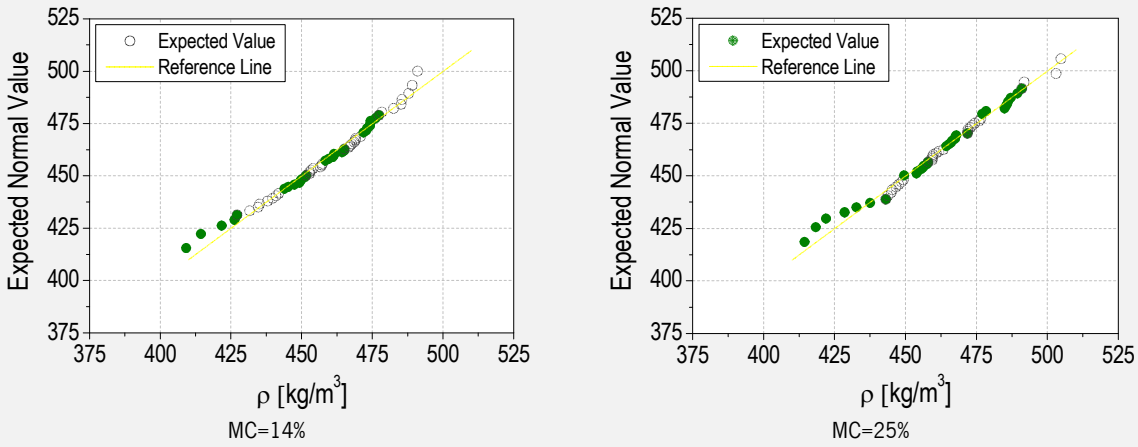

Figure (I) 5:2. Similar density distribution for different MC levels. Graphs were plotted based on Normal distribution and Rernard score method - (i – 0,3) / (n + 0,4).

5.2.2 Test procedure

Test procedure applied for the present experimental campaign follow the recommendations of EN 1382 (1999) as described in section 3.1.3 of chapter 3. Only the velocity of test had to be adjusted considering timber grain direction in order to respect the time recommended to reach F_{max} (90+/- 30 seconds). Specimens in which STS was inserted in middle layer were tested with a velocity of 1,4mm/min, while specimens in which STS was inserted between layers were tested with a velocity of 1,6mm/min.

Regarding test layout and acquisition system, it was used a similar equipment and steel frame as that described in section 4.1.3 of chapter 4.

5.3 Description of test results

Similarly to what was described in two previous chapters, first analysis of test results followed the three next steps: firstly, maximum withdrawal resistance ($f_{ax,test}$) was calculated according to equation (3:3); secondly, real moisture content at test time was defined for all tested specimens according to ISO 3130:1975; and thirdly, density of reference (ρ_{12}) was calculated as suggested at ÖNORM EN384:2010. In present section, results obtained for tests performed for groups with MC=14% and MC=25% are presented separately.

5.3.1 Test results for MC=14%

The moisture content obtained for specimens tested with MC=14% varied between 13,5% and 14,5% (13,7% ≤ Mean ≤ 14,0% and 0,01≤CoV≤0,02) and suggest a good distribution (Figure (I) 3:11). As mention in previous chapter, it is important to consider that the non-stabilization of MC level to 12% lead us to assume that some internal moisture gradients were present across the section of CLT specimens. A quantification of internal stresses was done for configuration of reference and is described in section 2.4.1.2. of chapter 2.

Table (I) 3:3 presents mean values and descriptive statistics concerning $f_{ax,test}$, ρ_{12} and MC levels regarding tests performed with MC=14%. Regarding ρ_{12} and MC levels, CoV values are positively low and median values are close to median values representing a good distribution and absence of outliers. However, CoV values registered for $f_{ax,test}$ are higher than expected (0,19≤CoV≤.0,46). This fact should be related with the existence of some outliers that will be identified ahead in the present chapter. These outliers are consequence of difficulties assuring the correct STS path between different layers, in the case

of BL configurations, and consequence of STS location on the growth rings arrangement, in the case of ML configurations.

Analyzing $f_{ax,test}$ values, highest and lowest values registered are of 10,90N/mm² and 1,12Nmm², for configurations REF_BL_14% and GAP4_BL_14%, respectively. As depicted in Figure (I) 3:12, configurations in which STS is inserted in middle layer present lower $f_{ax,test,mean}$ than configurations in which STS is inserted between layers. Obtained values suggest a reduction of $f_{ax,test,mean}$ when STS is completely inserted parallel to the grain direction of 33,9%, 33,3% and 101,0% for configurations REF, GAP0 and GAP4, respectively.

Analyzing groups with different location of STSs separately and taking REF configuration as reference (Figure (I) 3:13), it can be observed that configurations with GAP0 present non-significant decreases for $f_{ax,test}$ (13,1% for GAP0_ML and 13,9% for GAP0_BL). Differently, the non-overlapping of notched box plots suggest a significant decrease of $f_{ax,test}$for configurations with GAP4 (56,9% for GAP4_ML and 42,0% for GAP4_BL).

Figure (I) 3:14 present the typical failures of STS inserted either in middle layer (Figure (I) 3:14 (a), (b) and (f)) or between layers (Figure (I) 3:14 (c), (d), and (e)). Figure (I) 3:15 depicts the expected yielding failure mode observed during screw pull-out test. More detailed information about results obtained for tests performed with MC=14% are shown in Annex 1:1.

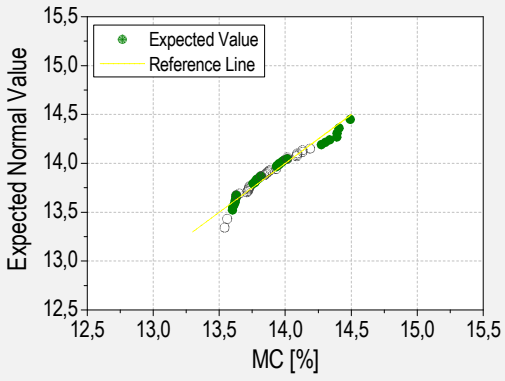

Figure (I) 5:3. Moisture distribution for group with 14% of moisture content. Graph was plotted based on Normal distribution and Renard score method - (i – 0,3) / (n + 0,4).

Table (I) 5:2. Mean values and descriptive statistics of $f_{ax,test}$, ρ_{12} and MC of different test configurations with MC=14%.

	MEAN VALUES			DESCRIPTIVE STATISTICS						
GROUPS	MC [%]	$f_{ax,test}$ [N/MM²]	ρ_{12} [KG/M³]	N.º OF TESTS	$f_{ax,test}$ / ρ_{12} / MC	SD	COV	MIN	MAX	MEDIAN	P5
REF_ML_14%	13,9	4,57	455	10		*1,68*	*0,37*	*2,84*	*8,78*	*4,21*	*2,84*
						13,71	0,03	433	480	458	433
						0,24	0,02	13,6	14,3	13,9	13,6
REF_BL_14%	14,0	6,91	466	10		*1,78*	*0,26*	*4,42*	*10,90*	*6,47*	*4,42*
						9,36	0,02	447	478	464	447
						0,24	0,02	13,8	14,4	13,9	13,8
GAP0_ML_14%	14,0	3,97	431	9		*0,76*	*0,19*	*2,62*	*5,04*	*4,03*	*2,62*
						14,64	0,03	411	460	433	411
						0,35	0,02	13,6	14,5	14,0	13,6
GAP0_BL_14%	13,8	5,95	461	9		*1,29*	*0,22*	*3,38*	*7,69*	*5,84*	*3,38*
						8,95	0,02	446	474	459	446
						0,14	0,01	13,5	14,0	13,7	13,5
GAP4_ML_14%	13,7	1,97	448	10		*0,37*	*0,19*	*1,57*	*2,83*	*1,90*	*1,57*
						11,72	0,03	432	467	444	432
						0,12	0,01	13,6	13,9	13,6	13,6
GAP4_BL_14%	14,0	4,01	444	10		*1,85*	*0,46*	*1,12*	*7,01*	*3,72*	*1,12*
						13,35	0,03	410	457	447	410
						0,12	0,01	13,8	14,1	14,0	13,8

MC – moisture content, f_{ax} - maximum withdrawal resistance, ρ_{12} – Density of reference, **SD** – standard of Deviation, **CoV** – coefficient of variation, **P5** – 5th Percentil, **REF_ML_14%** - configuration without gaps, with STSs inserted in middle layer and tested with MC=14%; **REF_BL_14%** - configuration without gaps, with STSs inserted in between layer and tested with MC=14%; **GAP0_ML_14%** - configuration with a gap of 0mm in middle layers, with STSs inserted in middle layers and tested with MC=14%; **GAP0_BL_14%** - configuration with a gap of 0mm in outer layer, with STSs inserted in between layers and tested with MC=14%; **GAP4_ML_14%** - configuration with a gap of 4mm in middle layers, with STSs inserted in middle layers and tested with MC=14%; **GAP4_BL_14%** - configuration with a gap of 4mm in outer layer, with STSs inserted in between layers and tested with MC=14%.

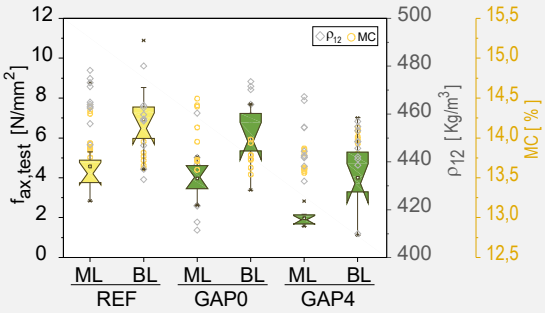

Figure (I) 5:4. Box chart with notched boxes of $f_{ax,test}$ and scatter plot of density of reference and moisture content for the following groups: REF_14%, GAP0_14% and GAP4_14%.

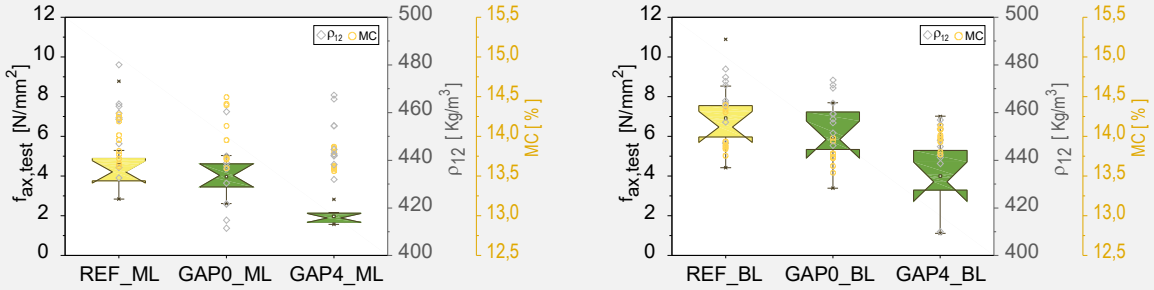

(a) (b)

Figure (I) 5:5. Box chart with notched boxes of $f_{ax,test}$ and scatter plot of density of reference and moisture content for the following groups: (a) REF_14% and GAP_ML_14%; (b) REF_14% and GAP_BL_14%.

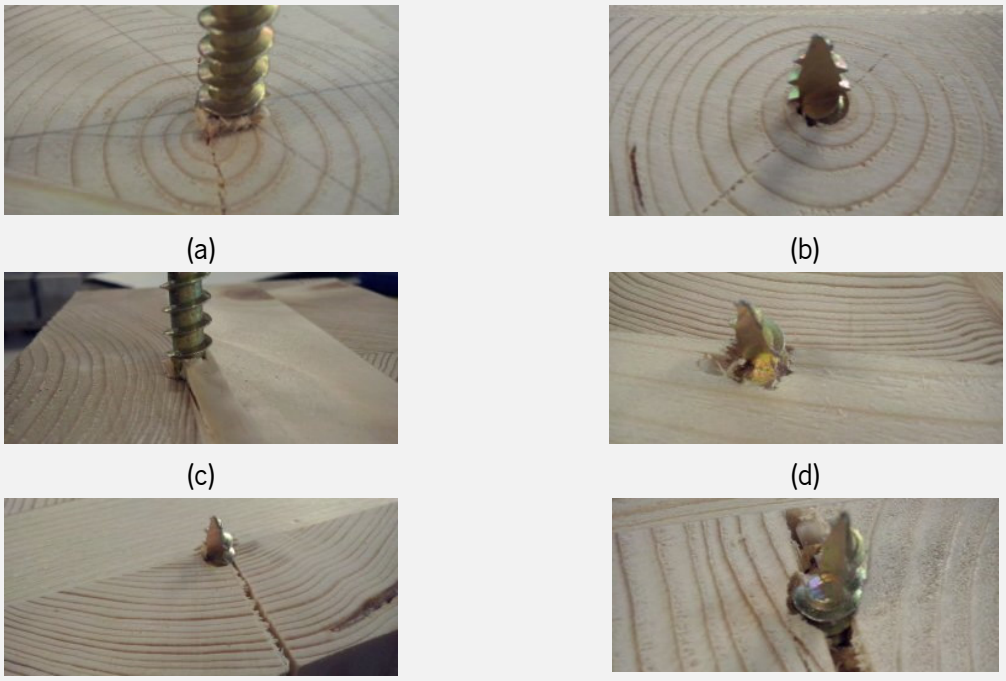

(a) (b)

(c) (d)

(e) (f)

Figure (I) 5:6. Visual inspection of failures for tests performed with 12% moisture content. (a) and (b) typical failure for configuration REF_ML_14%; (c) and (d) typical failure for configuration REF_BL_14%; (e) typical failure for configuration GAP0_BL_14%; (f) typical failure for configuration GAP4_ML_14%.

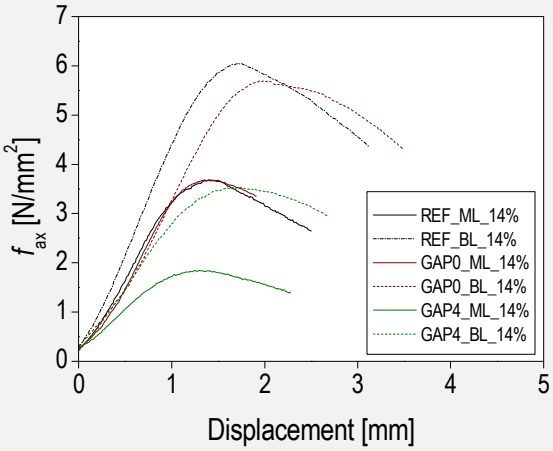

Figure (I) 5:7. Mean test curves for all configurations with 14% of moisture content, expressing the expected yielding failure mode.

5.3.2 Test results for MC=25%

The moisture content obtained for specimens tested with MC=25% varied between 23,0% and 27,1% (24,6% ≤ Mean ≤ 25,8% and 0,03≤CoV≤0,05) and suggest a good distribution (Figure (I) 5:8).

Table (I) 5:3 presents mean values and descriptive statistics concerning $f_{ax,test}$, ρ_{12} and MC levels regarding tests performed with MC=25%. Similar to what was observed for group tested with MC=14%, ρ_{12} and MC levels present low CoV values and a good distribution. However, CoV values registered for $f_{ax,test}$ are higher than expected (0,15≤CoV≤0,35).

Analyzing $f_{ax,test}$ values, highest and lowest values registered are of 5,37N/mm² and 1,13Nmm2, for configurations REF_BL_25% and GAP4_ML_25%, respectively. As depicted in Figure (I) 5:9, similar to results present in previous section, configurations in which STS is inserted in middle layer present lower $f_{ax,test,mean}$ than configurations in which STS is inserted between layers. However, obtained values suggest a smaller reduction of $f_{ax,test,mean}$ when STS is completely inserted parallel to the grain direction of 24,8%, 20,1% and 36,7% for configurations REF, GAP0 and GAP4, respectively.

Analyzing groups with different location of STSs separately and taking REF configuration as reference (Figure (I) 5:10), it can be observed that configurations with GAP0 present non-significant decreases for $f_{ax,test}$ (17,7% for GAP0_ML and 22,6% for GAP0_BL). Differently, the non-overlapping of notched box plots suggest a significant decrease of $f_{ax,test}$for configurations with GAP4 (47,0% for GAP4_ML and 37,1% for GAP4_BL). Figure (I) 5:11 depicts the expected yielding failure mode observed during screw

pull-out test. More detailed information about results obtained for tests performed with MC=25% are shown in Annex 1:16.

Table (I) 5:3. Mean values and descriptive statistics of $f_{ax,test}$, ρ_{12} and MC of different test configurations with 12% of moisture content.

	MEAN VALUES			DESCRIPTIVE STATISTICS						
GROUPS	MC [%]	$f_{ax,test}$ [N/MM²]	ρ_{12} [KG/M³]	N.º OF TESTS	$f_{ax,test}$ / ρ_{12} / MC	SD	COV	MIN	MAX	MEDIAN	P5
REF_ML_25%	25,3	3,00	455	10		*1,06*	*0,35*	*1,83*	*4,70*	*2,74*	*1,83*
						15,26	0,03	435	480	453	435
						0,98	0,04	24,1	27,1	25,0	24,1
REF_BL_25%	24,7	3,99	471	10		*0,64*	*0,16*	*3,32*	*5,37*	*3,87*	*3,32*
						9,00	0,02	459	487	470	459
						1,16	0,05	23,4	27,0	24,5	23,4
GAP0_ML_25%	25,8	2,47	437	10		*0,37*	*0,15*	*2,11*	*3,14*	*2,39*	*2,11*
						12,99	0,03	419	453	440	419
						0,93	0,04	23,9	27,1	25,9	23,9
GAP0_BL_25%	25,5	3,09	460	10		*0,49*	*0,16*	*2,03*	*3,84*	*3,13*	*2,03*
						12,40	0,03	441	472	467	441
						1,14	0,04	23,3	26,9	25,7	23,3
GAP4_ML_25%	24,6	1,59	455	10		*0,48*	*0,30*	*1,13*	*2,76*	*1,50*	*1,13*
						12,64	0,03	432	475	454	432
						0,86	0,03	23,0	25,8	24,6	23,5
GAP4_BL_25%	25,1	2,51	451	10		*0,53*	*0,21*	*1,46*	*3,20*	*2,54*	*1,46*
						10,97	0,02	432	463	455	432
						0,86	0,03	23,5	26,2	25,0	23,5

MC – moisture content, f_{ax} - maximum withdrawal resistance, ρ_{12} – Density of reference, **SD** – Standard of Derivation, **CoV** – Coefficient of Variation, **P5** – 5th Percentil. **REF_ML_25%** - configuration without gaps, with STSs inserted in middle layer and tested with MC=25%; **REF_BL_25%** - configuration without gaps, with STSs inserted in between layer and tested with MC=25%; **GAP0_ML_25%** - configuration with a gap of 0mm in middle layers, with STSs inserted in middle layers and tested with MC=25%; **GAP0_BL_25%** - configuration with a gap of 0mm in outer layer, with STSs inserted in between layers and tested with MC=25%; **GAP4_ML_25%** - configuration with a gap of 4mm in middle layers, with STSs inserted in middle layers and tested with MC=25%; **GAP4_BL_25%** - configuration with a gap of 4mm in outer layer, with STSs inserted in between layers and tested with MC=25%.

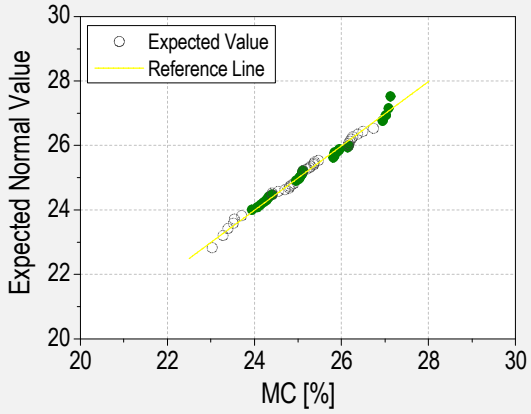

Figure (I) 5:8. Moisture distribution for group with 25% of moisture content. Graph was plotted based on Normal distribution and Rernard score method - (i – 0,3) / (n + 0,4).

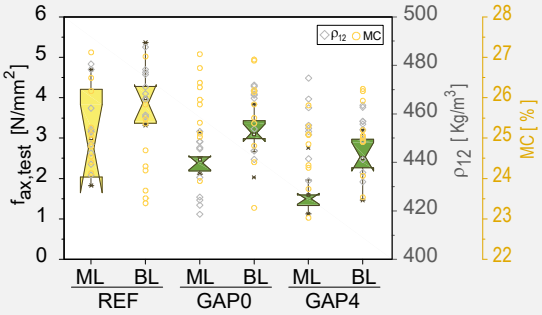

Figure (I) 5:9. Box chart with notched boxes of $f_{ax,test}$ and scatter plot of density of reference and moisture content for the following groups: REF_25%, GAP0_25% and GAP4_25%.

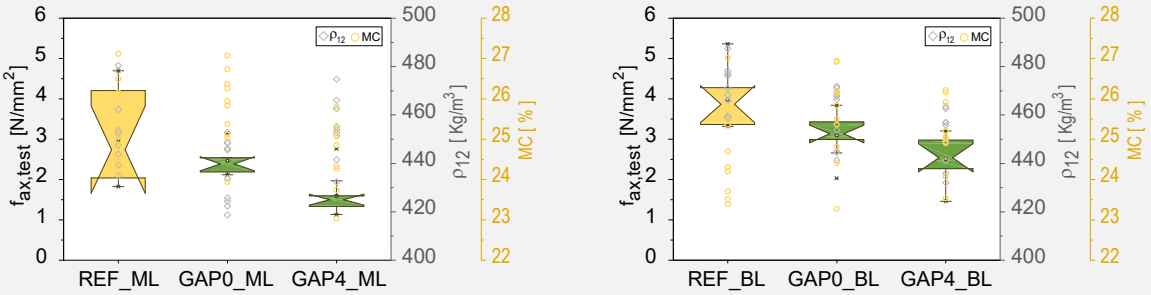

(a) (b)

Figure (I) 5:10. Box chart with notched boxes of $f_{ax,test}$ and scatter plot of density of reference and moisture content for the following groups: (a) REF_25% and GAP_ML_25%; (b) REF_25% and GAP_BL_25%.

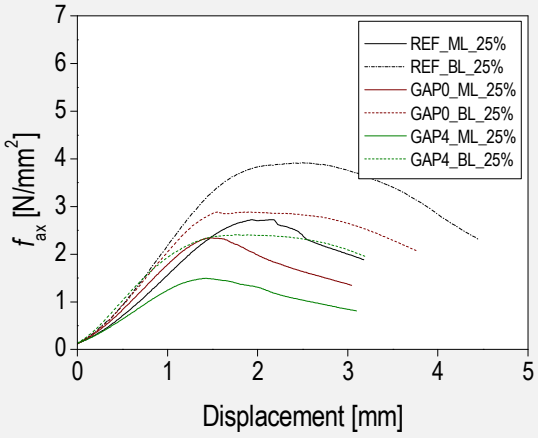

Figure (I) 5:11. Mean test curves for all configurations with 25% of moisture content, expressing the expected yielding failure mode.

5.4 Modeling the influence of gaps (η_{gap}) and MC levels (η_{MC}) on withdrawal resistance of STSs inserted in lateral face of CLT panels

Similar to the analysis performed in the two previous chapters, density of reference ρ_{12} as well as $f_{ax.test}$ were corrected considering the density values obtained when a smaller timber volume around the STSs is measured.

Before modeling the influence of gaps (η_{gap}) and MC levels (η_{MC}) on withdrawal resistance of STSs inserted in lateral face of CLT panels, some extreme outliers had to be excluded from data set, once obtained data points lie upper or lower the outer fences defined by each individual boxplot construction (Table (I) 3:8). Five samples were excluded from the test group with MC=14% and four samples were excluded from the test group with MC=25%. Table (I) 3:7 presents the descriptive statistics obtained for $f_{ax,corr}$, considering the reduction of sampling.

5.4.1 Defining η_{gap} and η_{MC}

In order to quantify properly the influence of GAP0/GAP4 located totally or partially in the STS path (k_{gap}) as well as the influence of high levels of MC on CLT elements (k_{MC}) on the withdrawal resistance of STSs inserted in lateral face of CLT elements, linear fittings based on the method of least squares were performed. The same bi-linear models defined in section 3.3.2. from chapter 3 (equation 3:8 and equation 3:10) were adjusted considering the different test configurations as well as the different moisture range studied in present section (equation (3:8) and equation (3:10)).

Table (I) 5:4. Outliers excluded from data considered for modeling of test results.

SPECIMEN NAME	NUMBER OF GAPS	GAP WIDTH [MM]	$f_{ax,corr}$ [N/MM²]	ρ_{12} [KG/M³]
8_REF_ML_14	0	n,a,	9,89	464
10_REF_ML_14	0	n,a,	7,88	457
8_REF_BL_14	0	n,a,	3,49	459
10_REF_BL_14	0	n,a,	7,87	480
7_GAP4_ML_14	1	4	2,83	454
3_GAP0_ML_25	1	0	3,21	434
6_GAP0_ML_25	1	0	3,31	426
3_GAP0_BL_25	1	0	2,06	445
8_GAP4_ML_25	1	4	1,94	463

Table (I) 5:5. Descriptive statistics of $f_{ax,corr}$ for different test configurations with MC=14% and MC=25%.

GROUPS		SAMPLE	MEAN	SD	COV [%]	MEDIAN	MIN	MAX	P5
REF_ML	**14%**	8	4,05	0,75	0,19	4,19	2,80	4,94	2,80
	25%	10	2,99	1,01	0,34	2,76	1,86	4,71	1,86
REF_BL	**14%**	8	6,26	0,72	0,11	6,46	4,75	6,94	4,75
	25%	10	3,87	0,61	0,16	3,79	3,24	5,21	3,24
GAP0_ML	**14%**	10	4,07	0,87	0,21	4,42	2,55	5,02	2,55
	25%	8	2,37	0,16	0,07	2,33	2,15	2,60	2,15
GAP0_BL	**14%**	9	6,27	0,97	0,15	6,38	4,94	7,51	4,94
	25%	9	3,17	0,33	0,10	3,17	2,59	3,76	2,59
GAP4_ML	**14%**	9	1,88	0,23	0,12	1,96	1,57	2,19	1,57
	25%	8	1,40	0,19	0,14	1,42	1,12	1,60	1,12
GAP4_BL	**14%**	10	4,09	1,70	0,42	3,98	1,11	6,52	1,11
	25%	10	2,53	0,54	0,21	2,62	1,46	3,21	1,46

f_{ax} - maximum withdrawal resistance, ρ_{12} – density of reference, **SD** – standard of deviation, **CoV** – coefficient of variation, **P5** – 5th Percentil; **REF_ML** - configuration without gaps with STSs inserted in middle layer; **REF_BL** - configuration without gaps with STSs inserted in between layer; **GAP0_ML** - configuration with a gap of 0mm in middle layers with STSs inserted in middle layers; **GAP0_BL**- configuration with a gap of 0mm in outer layer with STSs inserted in between layers; **GAP4_ML** - configuration with a gap of 4mm in middle layers with STSs inserted in middle layers; **GAP4_BL** - configuration with a gap of 4mm in outer layer with STSs inserted in between layers.

5.4.1.1 η_{gap}

In order to analise the effect of width of gaps and STSs location in withdrawal resistance of STSs (η_{gap}), both moisture groups were analysed separatly. Considering the REF_ML and REF_BL configurations of each MC group as reference (equation (3:7)), linear fittings, depicted in Figure (I) 3:31, were performed and mean k_{gap} values, shown in Table (I) 2:23, were defined. The effect of GAP0/GAP4 is represented by k_{gap} values, considering different STS locations. Values of k_{gap} were defined by the slopes given by linear fittings performed regarding different test configurations (slopes obtained for different linear fittings can be seen at tables presented in Figure (I) 3:31).

$$\frac{f_{ax,corr,gap(i)ML/BL}}{f_{ax,corr,REF\_ML/BL\ (mean)}} \quad (5:1)$$

$f_{ax,corr}$	Withdrawal resistance corrected considering density, in N/mm²;
$f_{ax,corr,gap(i)\_ML/BL}$	$f_{ax,corr}$ obtained in experimental campaign for GAP0 or GAP4 configurations considering different gap locations, in N/mm²;
$f_{ax,corr,REF\_ML/BL\ (mean\ )}$	Mean $f_{ax,corr}$ obtained in experimental campaign for REF configurations considering different gap locations, in N/mm².

As expected, and depicted in Figure (I) 3:31 (a), results obtained with linear fittings show that configurations tested with MC=14% presented none influence of GAP0 either for configuration in which STS is inserted ML or BL. Differently, group with MC=25% suggest a decrease of f_{ax} that is around 20% and 17%, for configuration in which STS is inserted ML or BL, respectively. The reason for decrease suggested by group with high MC level is not clear, once the increase of MC does not cause visible damages on GAP0. Furthermore, this tendency is opposite to what was observed for experimental campaign presented in chapter 3 (section 3.3.2.1). So, timber grain direction must have some role in suggested decrease of f_{ax}. Anyway, further research is required before state conclusions.

Figure (I) 3:31 (b) presents the results related with GAP4 configurations, suggesting that f_{ax} suffers similar decreases for both MC levels, either for ML and BL configurations. As described in Table (I) 2:23, GAP4_ML and GAP4_BL configurations present decreases for f_{ax} that are around 50,0% and 34,0%, respectively. Again, obtained results contrast with those presented in chapter 3, in which increase of MC level tend to reduce the effect of GAP4. Here, increase of MC level does not seem to influence the withdrawal capacity of STSs. The reason for that is directly related with the fact that studied locations for STSs (ML and BL) does not present so significant reductions of width for GAP4. Differently, when STSs are inserted in main face of CLT panels, GAP4 located in outer layers almost close when MC increases

to 18% (chapter 3). Another reason for different behaviors observed between STSs inserted in main or lateral faces of CLT panels can be related with timber grain direction. But, again, further research is required before fix conclusions.

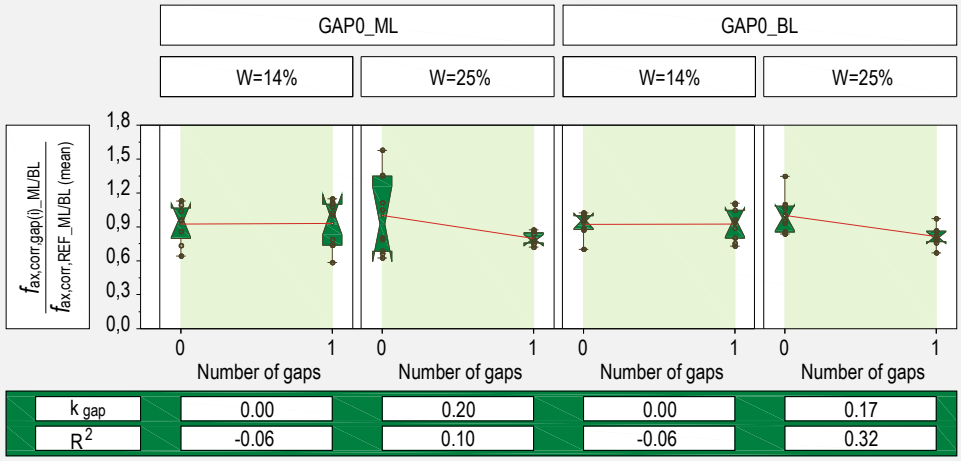

(a)

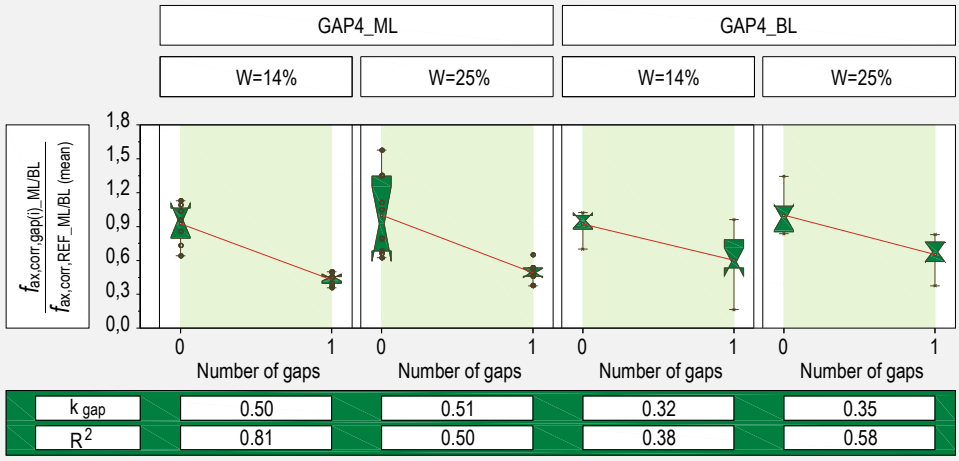

(b)

Figure (I) 5:12. Linear fittings performed between REF configuration and remaining configurations: (a) configurations with GAP0; (b) configurations with GAP4. k_{gap} and R^2values are presented in tables bellow respective graphs.

Table (I) 5:6. Obtained values for k_{gap}, depending on moisture content, gap width and STS location.

MOISTURE CONTENT		14%	25%
k_{gap}	GAP0_ML GAP0_BL	0,00	-0,19
	GAP4_ML GAP4_BL	-0,50 -0,34	

$$\eta_{gap} = \frac{f_{ax,gap(i)\_ML/BL}}{f_{ax,REF_{ML/BL},mean}} = \begin{cases} 1{,}00, when\ GAP = 0mm \\ 1{,}00 + k_{gap}, when\ GAP = 4mm \end{cases} \quad (5:2)$$

Where $f_{ax,gap(i)}$ is the mean withdrawal resistance of a given configuration, $f_{ax,REF,mean}$ is the mean withdrawal resistance of REF configuration with the same range of moisture content, k_{SL} is the effect of gap and STS location.

5.4.1.2 η_{MC}

In order to analise the effect of high levels of MC on the withdrawal resistance of STSs (η_{MC}) inserted in lateral face of CLT panels, all tested configurations were analysed separatly. Considering test configurations with MC=14% as reference (equation (3:9)), the effect of each percentage unit of MC added was quantified (k_{MC}).

$$\frac{f_{ax,corr,(MC=25\%)}}{f_{ax,corr,(mean,MC=14\%)}} \quad (5:3)$$

$f_{ax,corr}$ Withdrawal resistance corrected considering density, in N/mm².

$f_{ax,corr,(MC=25\%)}$ $f_{ax,corr}$ obtained in experimental campaign for configurations with MC=8% or MC=25%, in N/mm²;

$f_{ax,corr,(mean,MC=14\%)}$ Mean $f_{ax,corr}$ obtained in experimental campaign for configurations with MC=12, in N/mm².

Surprisingly, the results obtained with present experimental campaign suggest that the increasing of MC levels does not influence differently configurations with different STS locations. This way, k_{MC} was defined by the average obtained between slopes given by individual linear fittings performed for REF, GAP0 and GAP4 configurations (these individual results can be seen at tables presented in Figure (I) 3:32).

Table (I) 3:10 summarizes k_{MC} values obtained by linear fittings depicted in Figure (I) 3:32. Regarding REF configurations, obtained results are very similar to that obtained for REF configuration presented in chapter 3. Either for STSs inserted in the main face of CLT panels or for STSs inserted in lateral face of

CLT panels, it was suggested that f_{ax} decreases 2,0% per each percentage unit of MC added. Analyzing differences registered for different locations of STSs, REF_ML configuration presented a slightly higher influence of increasing of MC levels (f_{ax} decreases 3,0% per each percentage unit of MC added) due to the fact that STSs are totally inserted parallel to the grain direction. However, as the difference obtained between REF_ML and REF_BL configurations was so small, it was decided that k_{MC} = -0,02.

Similar to what was observed in chapter 3 (section 3.3.2.2), GAP0 configurations suggest a decrease of f_{ax} as MC level increases. For STSs inserted in main face of CLT panels, it was suggested that f_{ax} decreases 2,0% per each percentage unit of MC added (for 12%≤MC≤18%). Here, it is suggested that f_{ax} decreases 4,0% per each percentage unit of MC added (for 14%≤MC≤25%), when STSs are inserted in lateral face of CLT panels, independent of locations of STSs. This fact suggests that timber resistance presents a greater weakening in the direction parallel to the grain when MC level increases.

Concerning GAP4 configurations, present experimental campaign also suggested a higher decrease of f_{ax} as MC level increase, when comparing with results obtained for experimental campaign presented in chapter 3. As depicted in Figure (I) 3:32 (c) and summarized in

Table (I) 3:10, here it is suggested that f_{ax} decreases 2,0% and 3,0% per each percentage unit of MC added (for 14%≤MC≤25%) for GAP4_ML and GAP4_BL configurations, respectively. Differently, for configuration in which STS in inserted in main face of CLT panels f_{ax} tends not to be affected by increase of MC level as the number of GAP4 increases. As explained in previous section, GAP4 does not close significantly in the locations for STSs tested in present experimental campaign. As observed in chapter 3, GAP4 tends to close as the MC level increases, especially for GAP4 located in outer parts of outer layers. Furthermore, obtained results for REF and GAP0 configurations suggest that increasing of MC level tend to result in higher decreases for f_{ax} when STSs are inserted parallel to the grain direction.

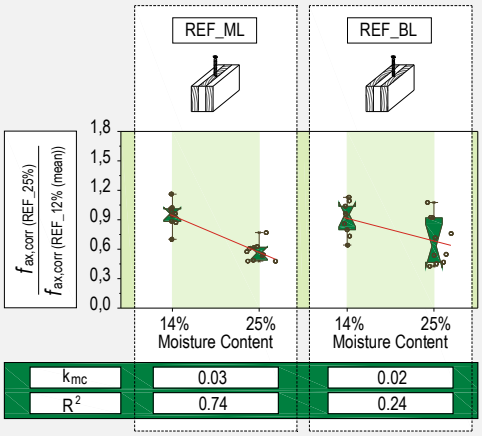

(a)

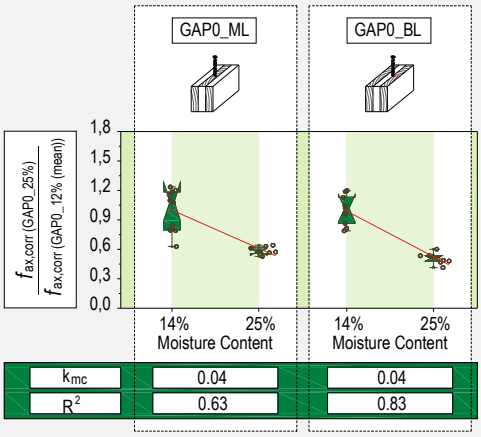

(b)

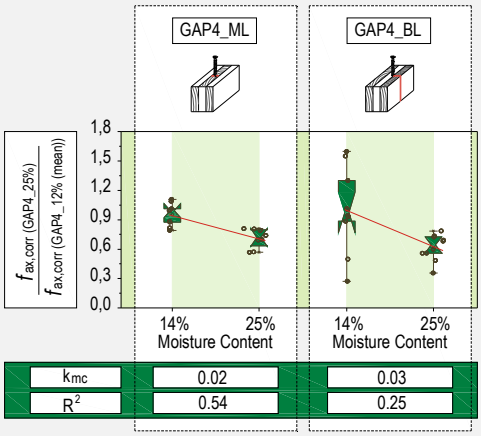

(c)

Figure (I) 5:13. Graphs of linear fittings between different MC levels for all configurations: (a) REF configurations; (b) GAP0 configurations; and (c) GAP4 configurations. k_{MC} and R^2 values related with same linear fittings are presented bellow respective graphs.

Table (I) 5:7. Obtained values for k_{MC}, depending on moisture content, gap width and number of gaps.

	MOISTURE RANGE	REF_ML AND REF_BL	GAP0_ML AND GAP0_BL	GAP4_ML AND GAP4_BL
k_{MC}	**14%-25%**	-0,02	-0,04	-0,03

$$\eta_{MC} = \frac{f_{ax,MC(i)}}{f_{ax,MC(12)}} = 1{,}00 + k_{MC} \cdot (MC - 14), when\ 14\% \leq MC \leq 25\% \quad (5:4)$$

Modeling the influence of width of gaps and location of STSs (η_{gap}) as well as the influence of increasing of MC level (η_{MC}) on withdrawal resistance of STSs inserted in lateral face of CLT panels, resulted in two models (equations (3:8) and (3:10)). The obtained values for k_{gap} and k_{MC}, presented in Table (I) 2:23and

Table (I) 3:10, respectively, are the variables that should be applied in the suggested models. The obtained models are an important step to introduce the influences of the studied variables on practical applications. However, despite being based on results obtained with rigorous experimental tests, the presented models should still be verified and some further research is needed. The width of the gaps as well as the location of STSs are variables that should be deeply studied in order to complement the proposed models.

5.4.2 Applying η_{gap} and η_{MC} to Uibel & Blaß Model

Similar to what was presented in section 3.3.3 from chapter 3, $f_{ax,pred}$ was obtained combining the model proposed by Uibel & Blaß (2007) (equation (3:11)) and defined η_{gap} and η_{MC} models.

Table (I) 3:11 shows descriptive statistics for $f_{ax,pred}$, considering an angle of 0° between screw axis and grain direction, while Figure (I) 3:33 depicts the correlations between $f_{ax,pred}$ and $f_{ax,test}$, considering different MC levels and different width of gaps. Analyzing both, a good data trend is observed and it is clear that predicted values are not so conservative as those obtained for tests in which an angle of 90° between screw axis and grain direction was considered. It is important to mention here that, as a conservative measure, for configurations in which STSs are inserted half parallel and half perpendicular to the grain direction (BL), $f_{ax,pred}$ was always calculated considering an angle of 0° between screw axis and grain direction.

Table (I) 5:8. Descriptive statistics of $f_{ax,pred}$ for different test configurations with 14% and 25% of moisture content.

GROUPS		N.TESTS	MEAN	SD	COV	MEDIAN	MIN	MAX	P5	$\frac{f_{ax,pred}}{f_{ax,test}}$
REF_ML	14%	8	4,76	0,23	0,05	4,77	4,37	5,05	4,37	1,20
	25%	10	3,55	0,16	0,04	3,55	3,27	3,76	3,27	0,76
REF_BL	14%	8	4,64	0,42	0,09	4,40	4,34	5,37	4,34	1,16
	25%	10	3,69	0,12	0,03	3,67	3,47	3,84	3,47	1,38
GAP0_ML	14%	10	4,62	0,40	0,09	4,61	3,90	5,36	3,90	1,31
	25%	8	2,38	0,19	0,08	2,40	2,13	2,73	2,13	0,95
GAP0_BL	14%	9	4,66	0,21	0,05	4,65	4,30	4,90	4,30	0,76
	25%	9	2,53	0,22	0,09	2,47	2,28	2,96	2,28	0,79
GAP4_ML	14%	9	2,34	0,18	0,08	2,29	2,15	2,70	2,15	1,26
	25%	8	1,56	0,08	0,05	1,57	1,45	1,68	1,45	1,14
GAP4_BL	14%	10	3,01	0,18	0,06	3,00	2,67	3,31	2,67	0,98
	25%	10	2,01	0,10	0,05	2,02	1,85	2,19	1,85	0,84

$f_{ax,pred}$ - predicted withdrawal resistance, obtained by Uibel & Blaß Model, η_{MC} - reduction factor of moisture influence on f_{ax}, η_{gap} - reduction factor of GAPs influence on f_{ax}, **SD** – Standard of Derivation, **CoV** – Coefficient of Variation, **P5** – 5th percentil. **REF_ML** - configuration without gaps with STSs inserted in middle layer; **REF_BL** - configuration without gaps with STSs inserted in between layer; **GAP0_ML** - configuration with a gap of 0mm in middle layers with STSs inserted in middle layers; **GAP0_BL**- configuration with a gap of 0mm in outer layer with STSs inserted in between layers; **GAP4_ML** - configuration with a gap of 4mm in middle layers with STSs inserted in middle layers; **GAP4_BL** - configuration with a gap of 4mm in outer layer with STSs inserted in between layers.

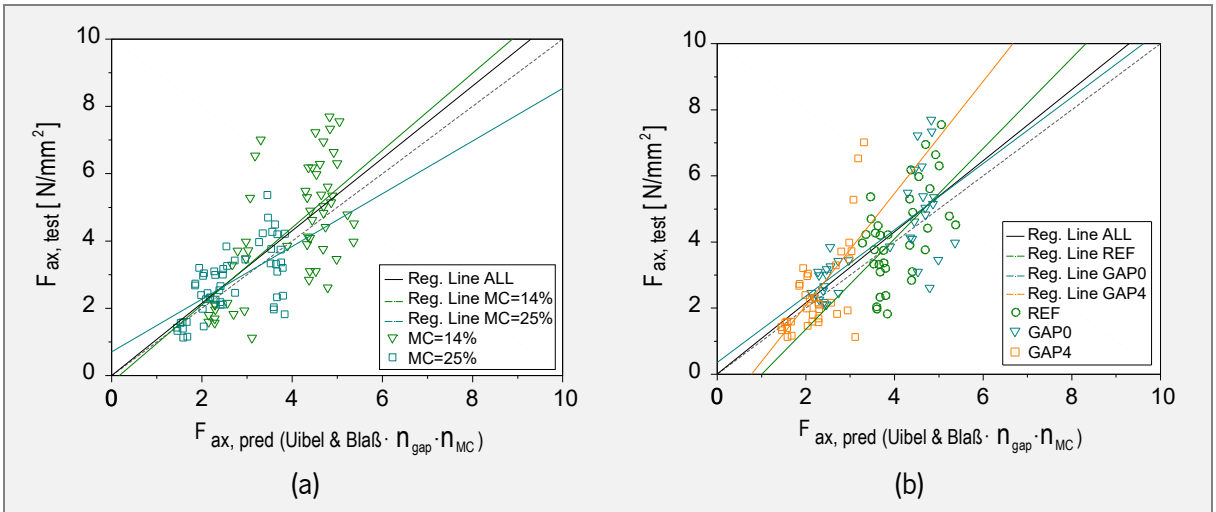

Figure (I) 5:14. Correlation between $f_{ax,pred}$ and $f_{ax,test}$ for: (a) test groups with MC=14% and MC=25%; (b) configurations REF, GAP0 and GAP4.

Figure (I) 3:34 shows the relation between mean test results and the predicted mean values. Comparing obtained results with those presented in chapter 3, it can be observed that Uibel & Blaß model is not so

conservative when an angle of 0° between screw axis and grain direction is considered. Regarding REF configuration, it is important to mention that $f_{ax,pred}$ tend to be higher than $f_{ax,test}$ for all tested configurations, with the exception of configuration REF_ML_25%, which suggests that $\frac{f_{ax,pred}}{f_{ax,test}} = 0{,}76$.

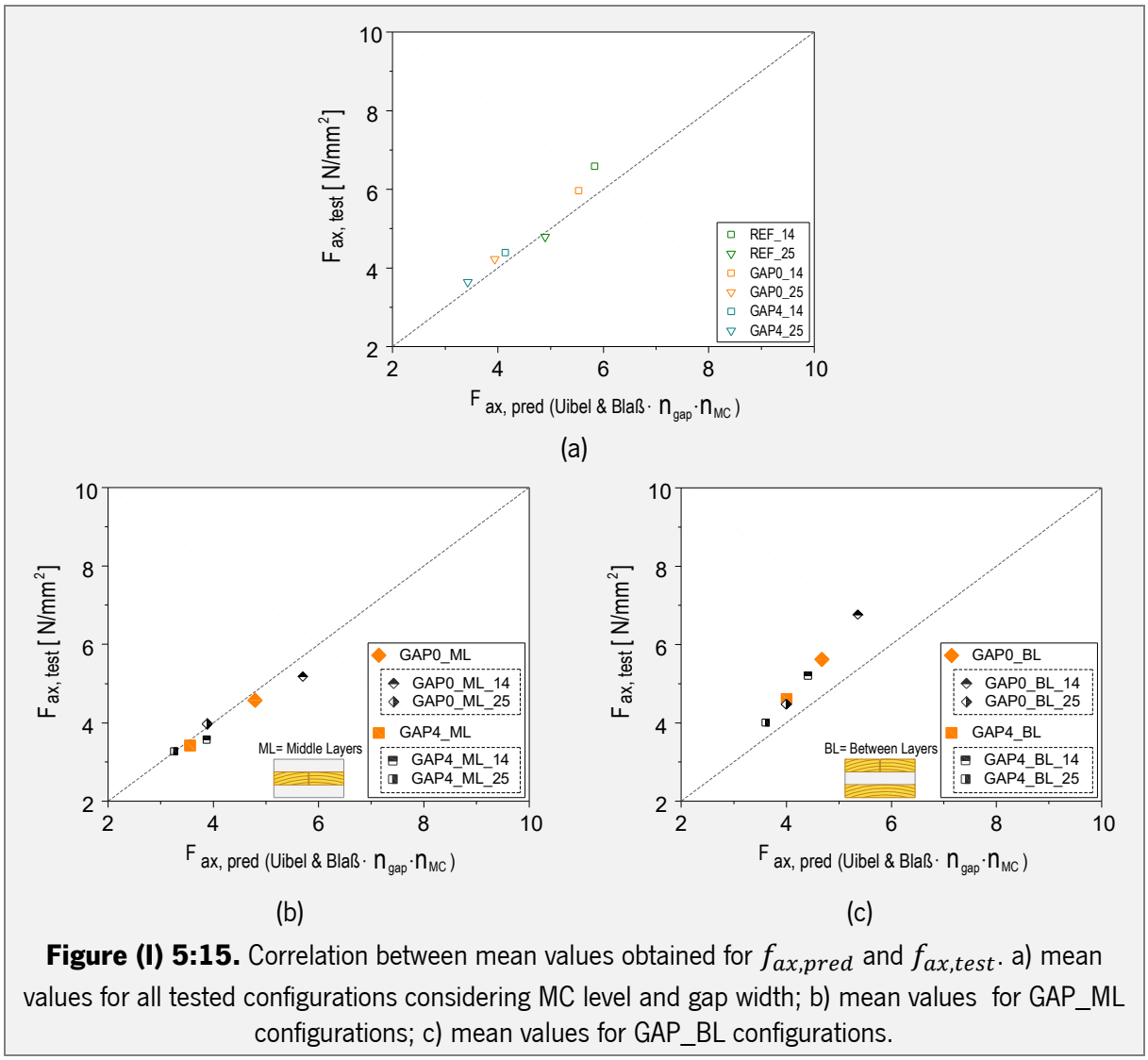

Figure (I) 5:15. Correlation between mean values obtained for $f_{ax,pred}$ and $f_{ax,test}$. a) mean values for all tested configurations considering MC level and gap width; b) mean values for GAP_ML configurations; c) mean values for GAP_BL configurations.

Similar to REF configurations, configurations with GAP0_ML and GAP4_ML present non-conservative results. Configurations with GAP0_ML ($0{,}95 \leq \frac{f_{ax,pred,GAP0\_ML}}{f_{ax,test,GAP0\_ML}} \leq 1{,}31$) present a higher range for the ratio between $f_{ax,pred}$ and $f_{ax,test}$ than configurations with GAP4 ($1{,}14 \leq \frac{f_{ax,pred,GAP4\_ML}}{f_{ax,test,GAP4\_ML}} \leq 1{,}26$) As the location of STSs was not considered for calculation of $f_{ax,pred}$, configurations with GAP0_BL ($0{,}76 \leq \frac{f_{ax,pred,GAP0\_BL}}{f_{ax,test,GAP0\_BL}} \leq 0{,}79$) and GAP4_BL ($0{,}84 \leq \frac{f_{ax,pred,GAP4\_BL}}{f_{ax,test,GAP4\_BL}} \leq 0{,}98$)presented the most conservative results.

5.5 Main conclusions

The present research showed and discussed the results of an experimental campaign focused on the quantification of effects caused by increasing of MC levels, the existence of gaps and their width and the location of STSs on the withdrawal behavior of axially loaded STSs inserted in the lateral face of CLT panels.

Moisture content covered a range between 14 % and 25 %, gap widths were of 0mm and 4mm and locations of STSs were in middle layer and between layers.

After the analysis and modeling of the test results, some important conclusions can be pointed out:

- As expected, results obtained for configurations in which STS is inserted between layers present higher f_{ax} values than ML configurations. Regarding group with MC=14%, f_{ax} is 35,3%, 35,1% and 54,0% higher for REF_BL_14%, GAP0_BL_14% and GAP4_BL_14% when comparing with similar ML configurations. Considering group with MC=25% the differences observed are a bit smaller: f_{ax} is 22,7%, 25,2% and 44,7% higher for REF_BL_25%, GAP0_BL_25% and GAP4_BL_25% when comparing with similar ML configurations;
- Differently of what was observed in chapter 3, GAP0 configurations with high MC levels present a slightly decrease of f_{ax}, independent of STS location, resulting in a $k_{gap} = -0{,}19$. This fact should be related with timber grain direction;
- Regarding k_{MC}, location of STSs do not affect the results. In other words, similar values for k_{MC} were obtained for REF, GAP0 and GAP4 configurations, independent of STS location;
- Also different of what was observed in chapter 3, high MC levels associated with GAP4 configurations do not present a $k_{MC} = 0$. The GAP4 do not tend to close with high levels of MC in the studied STS locations.
- The adjusted Uibel & Blaß (2007) model showed accuracy in predicting the obtained test results. However, predicted values obtained for configurations in which STS is inserted totally in middle layer are a bit higher than expected. On the other hand, configurations in which STS is inserted between layers present too conservative results due to the fact that s screw is half inserted perpendicular to the grain direction. In order to obtain a better correlation more research is needed to adjust model to the studied configurations.

CHAPTER 6 (I)

6. MAIN CONCLUSIONS OF PART I

The Part I of present thesis was focused on the development of two different experimental evaluations: one was dedicated to the quantification of moisture induced strains on CLT elements considering changes to the natural moisture flow through timber fibers, other was dedicated to the quantification of withdrawal capacity of STSs inserted in CLT panels, considering either changes on moisture content as well as location and width of gaps.

Regarding the quantification of moisture induced strains (Chapter 2 – Part I), specimens were submitted to a humidity cycle (RH varied between 30% and 90% for periods of 21 days), for a total period of 168 days, and then submitted to a stabilization period (RH = 65%) for a period of 142 days. At the end of stabilization period four different configurations considering different moisture flow conditions were tested (configuration 1 (C1) allows a free moisture flow through all three timber directions; configuration 2 (C2) allows moisture flow only in tangential direction; configuration 3 (C3) allows moisture flow only in longitudinal direction; and configuration 4 (C4) allows moisture flow only in radial direction). Three different technics were used to quantify moisture induced strains, namely: DIC, LVDTs and caliper ruler.

Main conclusions taken from this experimental campaign are the following:

- When evaluating restrained strains measured in main face of CLT panels (F1) it can be stated that in longitudinal direction (X) the expected wood movements are inverted (drying periods present tensile strains while wetting periods present compressive strains), while in tangential direction (Y) restrained strains tend to reduce significantly from first to last drying cycles for all test configurations;
- As expected, regarding different moisture flow conditions, configurations that restricts moisture flow on longitudinal direction (C2 and C4) present slower water desorption and because of that suggest a tendency for lower restrained strains measured through Y direction of main face of CLT panels (F1), during drying periods;
- About released strains measured in main face (F1) of CLT panels present predominant tensile strains, no effect of different moisture flow conditions was observed and released strains tend to reduce as the number of cycles increase.
- Released strains measured in specimens from group B shows that tensile strains are predominant during RH cycle, either for inner and outer layers, however at the end of stabilization period significant compressive released strains were measured for outer layers.
- Measurements taken with LVDTs acquisition in comparison with DIC technique suggest that DIC technique present wider differences between compressive and tensile strains;

- Due to reduced swelling movements registered by LVDTs during first wetting period, both techniques present different final effects for successive RH cycles: while DIC technique suggest that RH cycles decrease the moisture induced movements caused by cross wise lamination, LVDTs acquisition suggest that successive RH cycles causes cumulative compressive strains on CLT panel;
- Measurements performed with caliper ruler showed that differences between compressive and tensile strains tend to be reduced at the center of CLT panels (S3 of inner layers), maybe because inner part of CLT panels are not significantly affected by moisture changes;
- Regarding different moisture flow conditions, measurements performed with caliper ruler suggest that configurations that seal longitudinal direction (C2 and C4) present predominance of tensile strains for inner layers and the lowest compressive strains for outer layers.

Concerning the evaluation of withdrawal capacity three experimental campaigns were carried out: first tested STSs inserted on face of CLT specimens when submitted to simple changes on moisture content (MC = 8%, 12% and 18%) (chapter 3 –Part I); second tested STSs inserted on face of CLT specimens when submitted to cyclic changes on moisture content (30% ≤ RH ≤ 90%) (chapter 4 – Part I); and third tested STSs inserted on side face of CLT specimens when submitted to increase of moisture content (MC = 12% and 25%) (chapter 5 – Part I).

Results obtained with first experimental campaign fix three main conclusions:

First experimental campaign was focused on the quantification of effects caused by simple changes on moisture content levels, the existence of gaps and their width on the withdrawal behavior of axially loaded STS inserted in the main face of CLT panels. Moisture content covered a range between 8 % and 18 %, number of the gaps presented in the STS path varied from 0 to 3 and gap widths were of 0mm and 4mm. Main conclusions related with this experimental campaign are:

- The insertion of GAP0 in the STS path can result on an improvement of f_{ax}, while the insertion of gaps with 4mm result on a decrease of f_{ax}, which tends to reduce its significance as the moisture content increases. The surprising behavior of GAP4 configurations is related with timber swelling which causes the closing of gaps and consequently results on an improvement of the withdrawal resistance. The behavior of GAP0 configurations can be related with CLT crosswise lamination. Nevertheless, further research is needed to solidify the conclusions;

- Regarding the influence of gap width and location, configurations with GAP4 present significant decreases for f_{ax} when comparing with REF and a downward trend as the number of gaps increase. The test group with MC=8% registers the highest decreases (f_{ax} decreases 14,4% per each GAP4 added), while group with MC=18% registers the lowest decreases (f_{ax} decreases 5,7% per each GAP4 added);
- Considering the influence of changes on moisture content, for a MC range between 12% and 18%, REF configuration presented a decrease for f_{ax} of 1,8% per each percentage unit of moisture content added. This result proves that the reduction of withdrawal resistance caused by increase of moisture is lower for STS inserted in CLT than for solid timber and GL;
- Still regarding effects of changes on moisture content, but in a range between 8% and 12%, REF and GAP0 configurations present similar behaviour ($\eta_{MC,REF\ and\ GAP0}$ = 1,00, for 8% ≤ MC ≤ 12%), while GAP4 configurations present a high influence of MC decease due to timber shrinkage (GAP4_3L present a decreases for f_{ax} 4,7%);
- The adjusted Uibel & Blaß (2007) model showed accuracy in predicting the obtained test results, presenting higher conservative results for configurations with GAP4.

Second experimental campaign was focused on the quantification of effects caused by successive RH cycles, the existence of gaps and their width on the withdrawal behavior of axially loaded STS inserted in the main face of CLT panels. RH cycles oscillated between 30 % and 90 %, number of the gaps presented in the screw path varied from 0 to 3 and gap widths were of 0mm and 4mm. Main conclusions associated to these experiments are the following:

- Similar to what was observed for tests presented in chapter 3, taking REF configuration as reference, tests performed with GAP0 on DAY 0 presented a slightly improvement of f_{ax} (k_{gap} = 0,03), however tests performed on DAY 324 presented high negative values (k_{gap} = -0,07) as result of damages caused by RH cycles;
- Taking REF_D324 as reference, less favorable configurations are GAP4_OL_D324 and GAP4_3L_D324, with significant decreases of 29,0% and 56,0%, respectively;
- When comparing the effects of RH cycles on CLT (REF configuration) and GL it is observed a better performance for CLT, which exhibits an increase of f_{ax} at the end of RH cycles (k_{MC} = 0,014). Differently, GL presented a slight decrease (k_{MC} = -0,03) of f_{ax} after being submitted to the same RH cycles. it was observed that results obtained for GL are 5,1% lower when compared

with REF_D324. However, in order to properly quantify these differences more research is needed;

- The adjusted Uibel & Blaß (2007) model also showed accuracy in predicting the obtained test results. However, in order to obtain less conservative results more research is required.

Third experimental campaign focused on the quantification of effects caused by increasing of MC levels, the existence of gaps and their width and the location of STSs on the withdrawal behavior of axially loaded STSs inserted in the lateral face of CLT panels. Moisture content covered a range between 14 % and 25 %, gap widths were of 0mm and 4mm and locations of STSs were in middle layer and between layers. Main conclusions related with this experimental campaign are listed below:

- As expected, results obtained for configurations in which STS is inserted between layers present higher f_{ax} values than ML configurations. Regarding group with MC=14%, f_{ax} is 35,3%, 35,1% and 54,0% higher for REF_BL_14%, GAP0_BL_14% and GAP4_BL_14% when comparing with similar ML configurations. Considering group with MC=25% the differences observed are a bit smaller: f_{ax} is 22,7%, 25,2% and 44,7% higher for REF_BL_25%, GAP0_BL_25% and GAP4_BL_25% when comparing with similar ML configurations;
- Differently of what was observed in chapter 3, GAP0 configurations with high MC levels present a slightly decrease of f_{ax}, independent of STS location, resulting in a k_{gap} = -0,19. This fact should be related with timber grain direction;
- Regarding k_{MC}, location of STSs do not affect the results significantly (- 0,02 ≤ k_{MC} ≤ - 0,04). In other words, similar values for k_{MC} were obtained for REF, GAP0 and GAP4 configurations, independent of STS location;
- Also different of what was observed in chapter 3, high MC levels associated with GAP4 configurations do not present a k_{MC} = 0,00. The GAP4 do not tend to close with high levels of MC in the studied STS locations.
- The adjusted Uibel & Blaß (2007) model showed accuracy in predicting the obtained test results. However, predicted values obtained for configurations in which STS is inserted totally in middle layer, are a bit higher than expected. On the other hand, configurations in which STS is inserted between layers present too conservative results due to the fact that screw is half inserted perpendicular to the grain direction. In order to obtain a better correlation more research is needed to adjust model to the studied configurations.

Experimental campaigns performed in present thesis were of great significance to introduce the behavior of CLT when submitted to moisture changes. Further, author got access to the missing knowledge to develop a construction system based on CLT taking into account the specificities of material regarding moisture induced effects. However, research developed is just a reduced contribution to the understanding of moisture induced effects on CLT. As already listed before, some interesting results were obtained and important conclusions pointed out. However, some conclusions could not be accurately stated due to the difficulty in interpreting some results. In fact, some causes were associated to obtained results suggesting that a lot of work still needs to be done. Some suggestions for future researches were made during the discussion presented in here, such as:

- Deep research on the quantification of moisture induced strains on CLT, using larger samples and CLT specimens with a huge number of layers, just like the material is applied in real constructions;
- Develop a study just focused on the advantages/disadvantages associated with sealing moisture flow on longitudinal direction of CLT panels;
- Present research suggest that GAP0 results in an increase of withdrawal capacity of STSs. That fact was surprising and associated to effects of cross lamination, however a deep research on the field is required to understand the phenomenon properly;
- The width of gaps is another parameter that requires more research. Widths of 1, 2 and 3 mm are our suggestion, once gaps larger than 4mm are not usual and the improvement of fabrication of CLT tends to reduce the width of possible gaps on CLT panels;
- Also the aging effects on CLT connections must be deeply studied. Present research suggests an increase of withdrawal capacity of STSs inserted in face of CLT panels after submitted to RH cyclic changes, however as these results were not expected more research is recommended;
- The comparison between withdrawal capacity of STSs inserted in CLT and GL was slightly addressed in present research. A better performance of CLT was observed but also in here a focused research must be done;
- Predicting models for withdrawal capacity must be properly developed in order to be part of future building codes;
- Full scale tests of connection elements, with a significant number of metal connectors must be also done in order to understand the effects of moisture induced effects on large scale elements.

PART II: URBAN TIMBER SYSTEM: BUILDING TALL WITH CLT CONSIDERING MOISTURE INDUCED EFFECTS

CHAPTER 1 (II)

1 STATE OF THE ART

1.1 The role of timber in modern cities

The continuous increase of the urban density all around the world forced cities to grow taller, making tall buildings a common typology in developed cities. The urban population keeps growing, foreseeing that until 2050 the world population living in cities will reach 70% (Green & Eric Karsh 2012). This reality will stress the demand for large building solutions while it is important to be aware that urban density becomes an increasingly significant part of addressing climate changes. So, it is necessary to reformulate the current construction practice in order to answer the higher standard of living and higher energy efficiency required today. Unfortunately, tall buildings are generally linked to great negative impacts on environment, raising the need to look for new environment friendly solutions. Tall timber buildings are a concept that emerged connected with this need, betting on wood sustainable profile as the key factor to reduce the negative environmental impact of construction sector. In some countries where timber has a social character, such as Sweden, German and Japan, timber is positively appreciated as a building material (Stehn & Bergström 2002). However, this subject can face serious barriers in countries where wood culture does not exist. Regardless of these difficulties, tall timber buildings are an exciting and current topic, expecting that their qualitative advantages overcome remaining socio-cultural barriers.

Cross laminated timber (CLT) is an engineered timber product that has been largely associated to the concepts of tall timber buildings due to its enhanced mechanical properties, mass and technological facilities. CLT constructions are often cited as a great sustainable solution due to their capacity for store a large amount of carbon dioxide (Green & Eric Karsh 2012, Omland & Tonning 2009).

1.1.1 Why is better to live in denser city centers? And how cities should growth to be sustainable in environmental, social and economic terms?

Main limitations of urban apartments are essentially related with reduced areas, lack of outdoor space and reduced privacy due to proximity to the neighbors (especially above and below). However, the disadvantages associated with an everyday life divided between suburbs and city centers are directly linked to the increase of the urban densities all around (Kelly et al., 2011).

Proximity to public transport, mixed-use precincts, shopping and work places and more opportunities for social interaction are the main reasons why population keeps moving to city centers even when it means an exchange from a single house to an apartment. This phenomenon is positive not only for people quality of live, increasing the time devoted to family and reducing the time wasted driving home, but also to

reduce the threat of environmental degradation and global warming (Lehmann, 2012) (Build it Green, 2008).

Growth of dense urban areas results on smaller environmental footprint than expansions on suburb green areas. Developments on urbanized areas can make use of existing infrastructure and avoid destruction of green areas. Further, cities with higher densities are able to reduce car dependency, green gas emissions and land consumption (Build it Green, 2008). But, to ensure this green city profile, development of urban areas should counter the unsustainable tendency for segregated cities, raised in the early 20th century, which divided cities by zones with different uses.

New tendency for urban development is grounded on mixed-use principles, which are based on single buildings or compact urban areas where residential, retail, office, and other uses are combined. This kind of urban development can provide significant improvements for an active social life, for a dynamic economic system and for a better environment. In social terms, this mixed use cities can provide social interaction and increase the sense of neighborhood. In economic terms, it increases the employment/population ratio and consequently improves the balance between jobs and housing. At last, in environmental terms, it offers different options for encouraging cycling and walking and use public infrastructures more efficiently. Further, it is important to note that higher building density is associated to lower carbon emission by households. This association can be even better if buildings adopt green building principles, offering long term construction quality and affordability (Qin & Han, 2013).

1.1.2 The role of tall timber in cities of the future and its sustainable profile

The described advantages associated to denser cities raises the awareness that tall buildings are the better typology for this kind of environments. It is true that tall buildings are generally linked to great negative environmental impacts due to the large amount of materials required for the structure. As it is known, tall buildings require an extra wind-load resisting system and a heavier gravity-load resisting system while low-rise buildings just need an efficient gravity-load resisting system. Besides the extra material required, tall buildings also means more energy consumed during construction process (Foraboschi et al., 2014). However, the search for new environment friendly solutions already started. Tall timber buildings are one between some other possible solutions, in which sustainable profile of wood is pointed as the key factor to reduce the negative environmental impact associated to tall buildings. Similarly to mixed-use urban concept described before, tall timber buildings has been proofing their

viability in all three main sustainability targets, namely: environmental sustainability, economical sustainability and social sustainability (see Figure (II) 1:1) (C. V Silva et al., 2013).

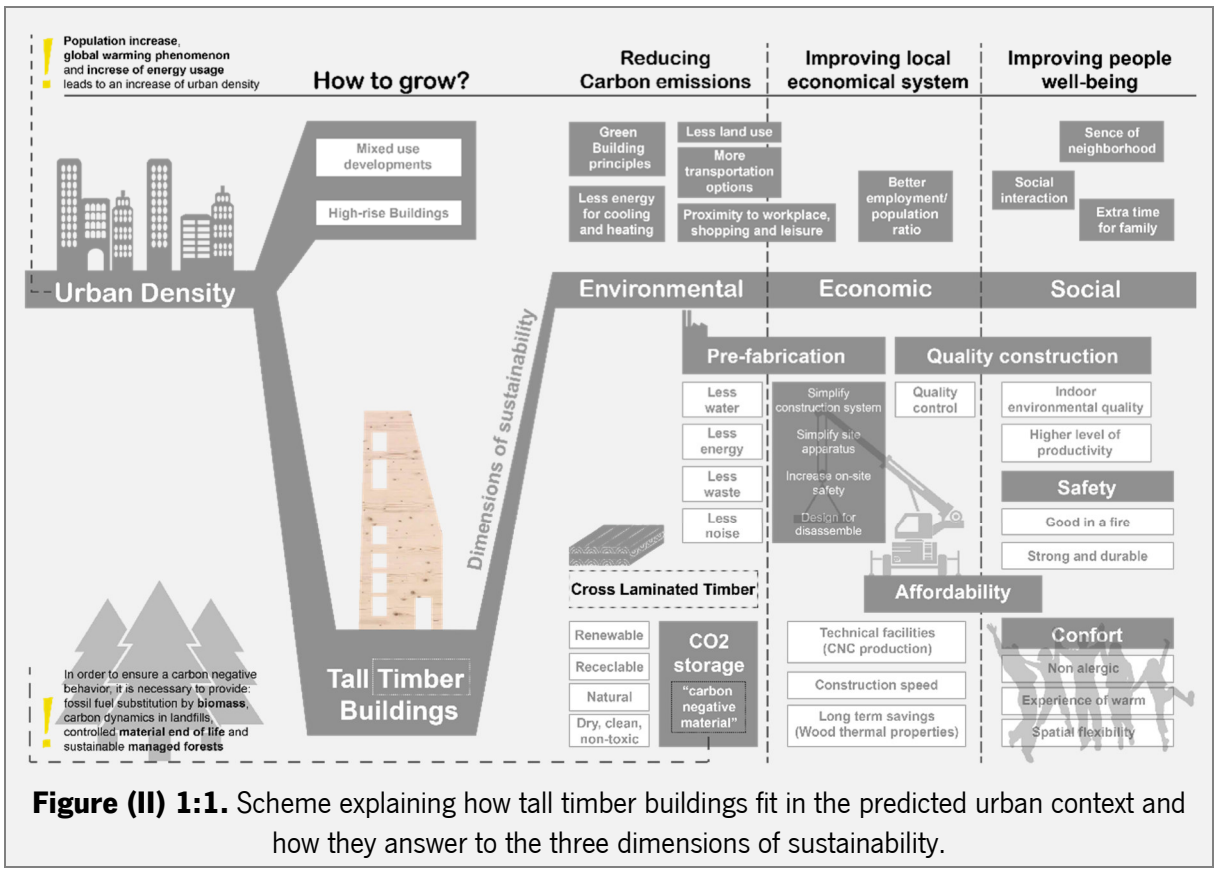

Figure (II) 1:1. Scheme explaining how tall timber buildings fit in the predicted urban context and how they answer to the three dimensions of sustainability.

1.1.2.1 Environmental sustainability

Sustainable profile linked to timber as a construction material can be a strong ally to recent European environmental policies, namely EU's 20/20/20 plan (European Commission, 2010) and 2050 Energy Roadmap (European Comission, 2012), as well as the 2030 Agenda for Sustainable Development (UN General Assembly, 2015). Indeed, timber is a natural material, renewable, recyclable and able to store carbon dioxide. This last feature is the most important once, similarly to forests, harvested timber can be used for carbon storage. However, in order to guarantee the wanted positive environmental effects, the carbon emissions during manufacturing of timber derivate materials should be reduced and these materials should have significant long lifespans assuring a useful carbon sequestration (Esbjörnsson et al., 2014). Using timber as a structural material in construction sector is one solution that fits on long-lasting carbon storage, assuring that CO_2 stored will only be emitted into the atmosphere upon combustion or decay of timber. Wood stores more carbon than the equivalent CO_2 emitted by the harvesting, processing, transport and fabrication (Cambiaso & Pietrasanta, 2014). While each ton of solid wood

panels sequester around 1,6 tons of CO_2, the production of one ton of steel and cement releases 1,5 and 1,1 tons of carbon, respectively (Stehn & Bergström, 2002).

Despite the significance of CO_2 storage, some other environmental advantages are also related with the use of timber in construction sector, such as: the substitution of high emitting building materials for timber, the use of residues resulted from timber processes in heating and power production as a substitution for fossil fuels, the decrease of energy used during buildings construction phase as well as during the whole life-cycle of buildings and the reduction of amount of waste (Christophe Sigrist et al., 1999).

If timber buildings work like carbon reservoirs, as much timber is used higher will be the amount of carbon stored. For this reason, designers responsible for the construction of multi-storey buildings using significant amounts of CLT has emphasized the environmental benefits of their choices: Stadhaus, in England, saved 310 tons of carbon during construction process and stored a 180 tons of CO_2 (Kucharek 2009); Forté, in Australia, promoted an overall saving of 1451 tons of Carbon (Heaton 2013); and a residential building erected in Wagramerstrasse, Vienna, used an amount of 2,400m^3 of CLT, which results in 1,900 tons of CO_2 storage (later this amount of wood could be converted into 19 terajoules of electricity or heat).

Just to underline the significance of ecological footprint of building environment, it is important to mention that buildings are responsible for 40% of global energy consumption, approximately 30% of the CO_2 emissions and 40% of the waste. That is why Directive 2010/31/EU on energy performance in buildings was created, forcing engineers and architects to look for almost Net Zero energy solutions with the best cost-benefit ratio. Considering that joining the gains related with CO_2 storage and pre-fabrication process with the gains associated with recycling and reuse possibilities, timber can be considered as a 'carbon negative' material and considered the perfect ally to professionals that are looking to answer environmental targets.

1.1.2.2 Economic sustainability

The economic sustainability of timber construction is closely related with savings provided by technical facilities, construction speed and long-term savings. Firstly, material production is industrialized and controlled by computerized numerical control (CNC) systems that ensure a high quality of construction elements, reduces the amount of material waste and make the execution of connections easier. Secondly, the simplicity of construction associated to timber (easy handling and prefabrication) allows a significant

reduction of construction time, simplify the site apparatus, requires reduced teams and increase the on-site safety. At last, dependent on construction system chosen, significant long-term savings related with energy consumption, operation and maintenance can be more relevant than costs resulted directly from the erection of building (Lehmann, 2012).

As consequence of advantages related with production and construction procedure, promoters of Stadhaus and Forté experienced fast construction times. With a reduced site team and less and low-tech equipment, buildings were erected in 11 and 12 months, respectively (C. Silva et al., 2012). These numbers represent approximately a saving of 30% on construction time when compared to a concrete system (Patterson 2013).

Regarding the comparison between the costs associated to timber or concrete/steel construction systems, few studies have been published. According to Green & Eric Karsh (2012), considering a comparison between an equal twenty-storey building constructed with concrete or with CLT, the final costs would be the same even considering a non-competitive price for CLT. An economic analysis performed by Winter et al. (2012), concluded that for residential buildings within a range of 4-5 stories, CLT is still 5% more expensive than a similar solution in concrete. This fact is related essentially with the large amount of timber used and with the use of gypsum boards to fulfill fire safety performance. Anyway, as mentioned before, this investment can be recovered by long term savings. Differently, Mahlum (2014) performed a comparison between an equivalent ten-storey building using CLT, steel and concrete. The conclusions pointed that CLT offers 4% of cost savings, being considered a competitive material.

1.1.2.3 Social sustainability

Finally, social sustainability is related with wellbeing of people, a dimension where quantitative and qualitative aspects should be carefully balanced. In other words, a dimension where architecture should be pragmatic, answering issues like daylight, economy and energy consumption, as well as abstract answering issues related with architectural expression and spatial organization and orientation.

As regards to functional and safety requirements, there are research initiatives that have assessed the safety of a CLT tall building in several areas, such as: fire safety (Dagenais et al., 2013) (Frangi et al., 2008), durability (McClung 2013) (Patterson, 2013), sound insulation (Hu & Adams 2013) and thermal performance (Glass et al., 2013).

Wood is a material with a restorative effect on human health. Use exposed wood in our buildings, either in interior environments or in external surfaces, offer a comfortable warm experience able to reduce stress or depression and promote people health (Lehmann et al., 2012).

1.1.3 Main Barriers and pointed solutions to overcome them

Despite the large number of advantages associated to the use of timber as structural material, described in previous sub-section, there are some important barriers to be overcome. During last century, wood was qualified as an inflammable material with low durability, fact that resulted on stagnation of timber as a construction material and allowed steel and reinforced concrete to completely domain the construction sector. In some cultural contexts, the negative connotation imposed to timber was so ingrained that the idea of building a large-scale multi-storey timber building is not well accepted, even nowadays (Langenbach, 2008). However, taking a look into the past, it is possible to find some interesting examples of tall timber buildings/structures, erected with archaic technologies that are still standing. In fact, great historic fires played a key role for the actual label imposed to structural timber, resulting in numerous regulatory barriers imposed by building codes all around the world. Figure (II) 1:2 depicts the height limits, by number of floor, imposed for timber construction in some countries. The majority of countries do not have a specific rule defining the maximum number of floors for timber buildings. However, similarly to what happens in European context, regulatory requirements do not distinguish construction materials, but their limitations related to combustible materials turn wood in an uncompetitive material and its application as structural material is limited.

Taking advantage of this reality, construction firms and industries made large investments to mechanize their concrete on-site construction. So, now, these investors are the most interested in connote timber as an old-fashioned material and keep construction sector in the same line of development. As consequence, some other barriers to structural timber were progressively being imposed, namely: construction professionals have been conditioned to a limited education focused on how construct with bricks, concrete and steel (Mahapatra & Gustavsson, 2008); large timber structures, in addition to being regarded as unsafe, are seen as a solution extremely expensive (due to the lack of a competitive market, wood price and necessity of a detailed project), with less conception freedom, with lower fire and seismic resistance and based on a material that shrinks, burn and rots (Green & Eric Karsh, 2012).

As says Fortmeyer (2011), *we climb to the myth that timber construction present risks, while concrete and steel do not.* These fears are easily justified by the lack of knowledge resulted from reduced research

dedicated to timber construction. Unfortunately, groundless or not, these fears hinder the development of timber construction sector, especially with regard to the construction in height. This way, it is mandatory to raise the awareness about positive aspects of timber, such as its strength, environmental friendliness, simple handling and appropriateness for use (Roos et al., 2010).

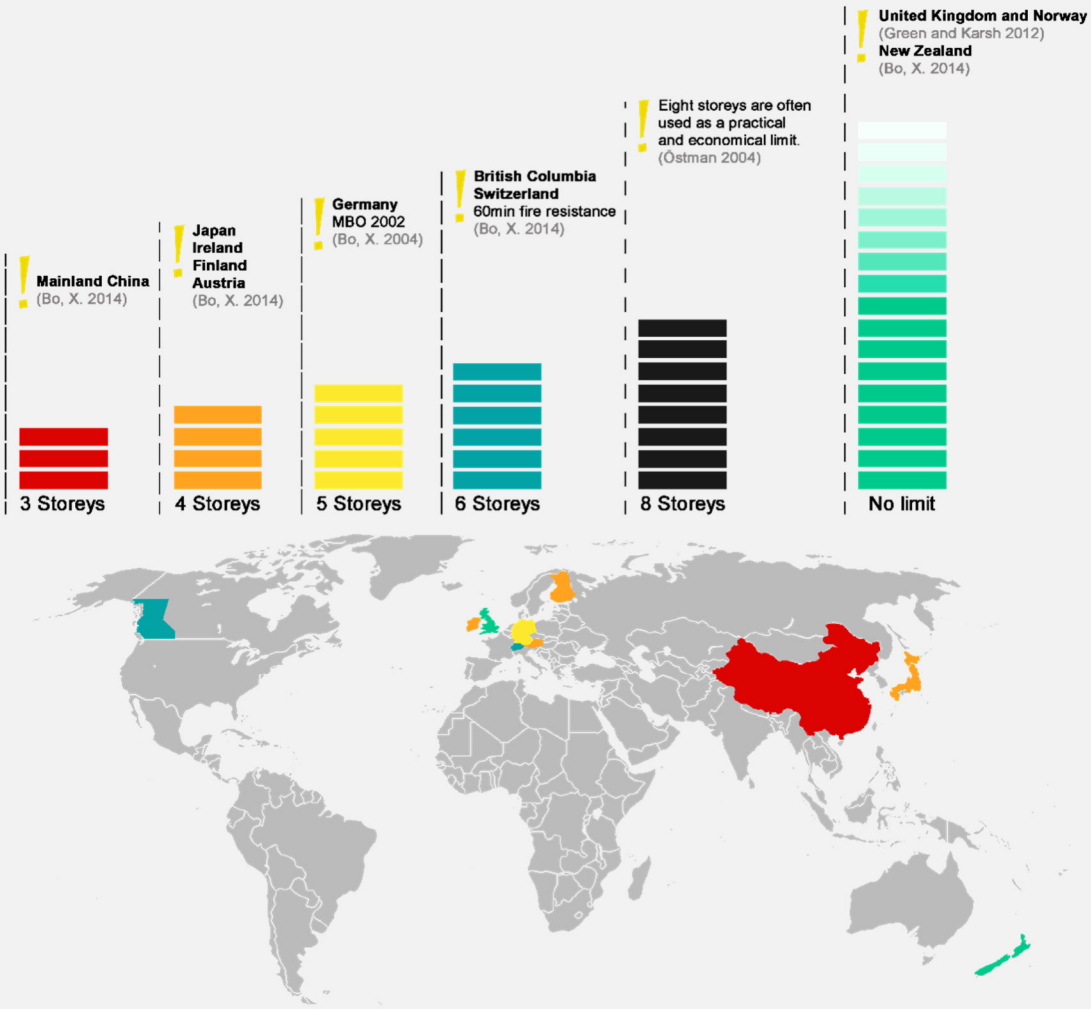

Figure (II) 1:2. Legal limitations imposed by building codes regarding number of floors for timber buildings (Xia et al., 2014) (Green & Eric Karsh, 2012) (Östman & Källsner, 2011).

On the one hand, timber construction in height seems to be a successful solution in urban contexts, where the density is increasingly and the land prices are becoming unaffordable. In other hand, *a transition from traditional (current) building practices to timber construction will require institutional changes and investments in development of knowledge, skills, logistics, and actor networks to break the path dependency of the existing construction system* (Mahapatra & Gustavsson, 2008). Multi-story timber construction is in its formative phase and the transition to a growth phase is dependent on reduction of uncertainties associated with it. Actually timber construction in height is a market for niches supported by fragile social networks that bet in innovation, climate change mitigation and positive implications for

forest health. So, the development of such niches might be based on demonstration projects that join different actors, such as: local governments, firms, universities, research institutes, users, among others. Figure (II) 1:3 locate and describe important initiatives promoting the use of timber in the construction sector.

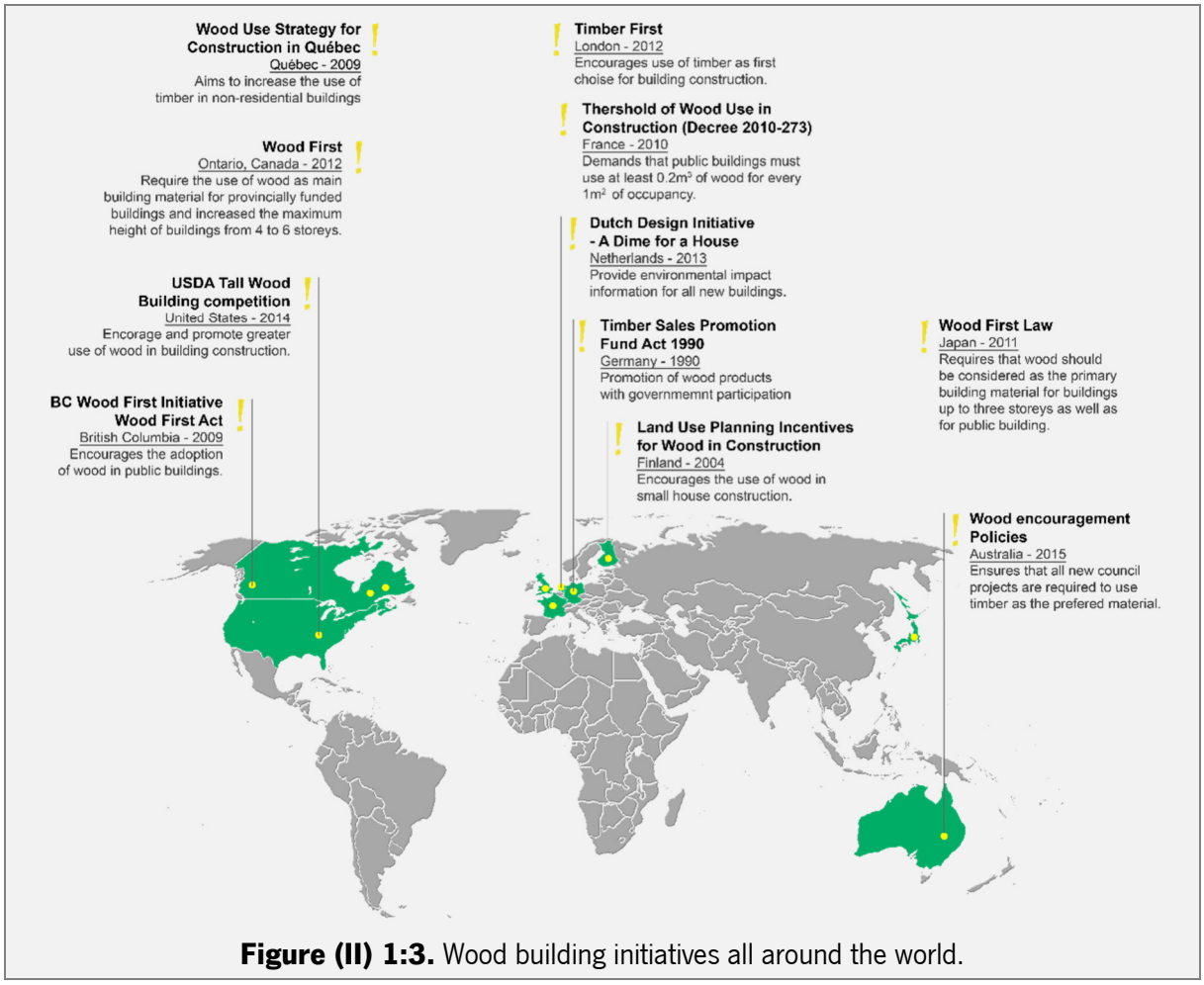

Figure (II) 1:3. Wood building initiatives all around the world.

Despite all described barriers, Green & Eric Karsh (2012) believes that *we are at a unique moment of history when wood will transition from the material we have known it to be thousands of years into the material we will know it to be for the next thousand.* In order to speed up diffusion of timber construction some actions are suggested, such as: enlarge knowledge base and promote the education of professionals; fight for institutional changes; encourage the entry of new firms in this innovative system; create a strong group of defense of timber construction; provide interchange of experience and knowledge among different actors, strengthening their network in an European level; trigger competitiveness through execution of energy and carbon taxes; and look to the development of an European standard for timber buildings based on prefabrication (Mahapatra & Gustavsson, 2008).

Despite few, the number of tall buildings that use timber as main structural material are increasing every year. So, regardless described barriers, tall timber buildings are an exciting and current topic, expecting that their qualitative advantages overcome all future obstacles. Building tall with timber can be an activity that opens the door to architects and engineers to exploit the capabilities of material by making innovative things.

1.2 The role of CLT on tall timber construction

Analyzing the progressive increase of tall timber constructions, it can be observed that CLT is a transversal material, being the leading figure in the majority of the constructed buildings as well as in the proposals for new construction systems. There are some examples of monolithic construction systems that are fully based on CLT as structural material. Some others combine CLT with concrete cores or with linear elements made from steel and other wood-based materials. In present section, CLT will be presented as a structural material and its advantages and disadvantages will be listed. Furthermore, demonstrations buildings in which CLT is applied will be described as well as their construction systems.

1.2.1 Cross laminated timber

The initial concept for cross laminated timber (CLT) panels emerged in Lausanne and Zurich (Switzerland) in the early 1990s, but it was in Australia that a synergy created between industry and academia developed the concept and presented CLT as it is known today.

CLT is a prefabricated solid engineered wood product composed of switched orthogonally bonded layers of solid-sawn timber or structural composite lumber (Figure (II) 1:4). In special configurations, consecutive layers can have the same direction, resulting in a double layer which provides specific structural capabilities (ETA-066/0138, 2011). Generally, wood species used are softwoods (spruce, pine and fir), but, although uncommon, some hardwood species (e.g. ash, beech) can also be applied. The preferential boards to use are those that are taken from the outer zones of the log (Figure (II) 1:5), which have higher mechanical properties related to stiffness and strength, and their preferential dimensions have a width to thickness ratio of 4:1 (Augustin, 2008). The timber used is stabilized with moisture content of around 12%, low enough to avoid pest or fungal attack and prevent dimensional variations and surface cracking of the panels. The density of panels at this moisture content is in the range of 470 kg/m^3 for spruce and 590kg/m^3 for larch, but the panels can be delivered with moisture content that varies in a range of 10-14% (Egmond, 2011).

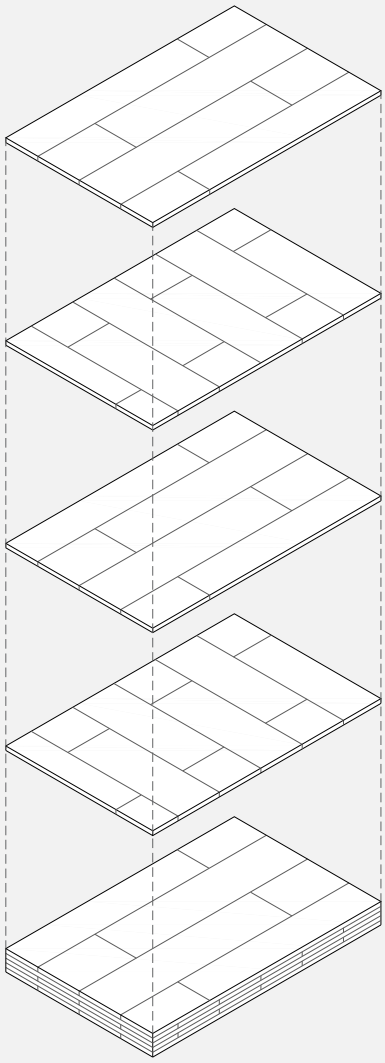

Figure (II) 1:4. Crosswise lamination of CLT panels.

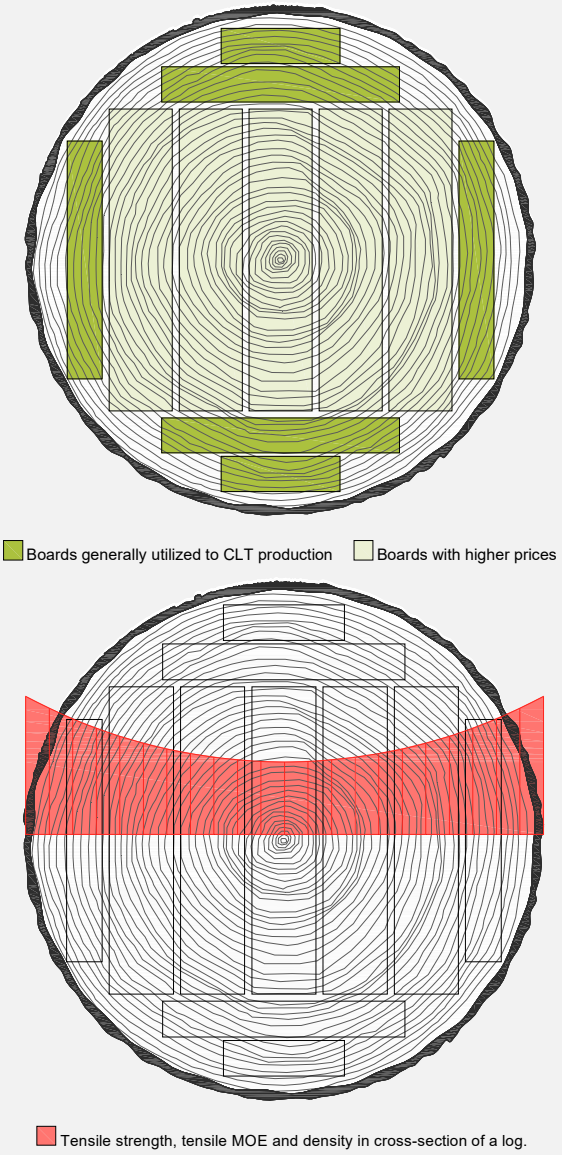

Figure (II) 1:5. Sawing pattern of the outer boards of a log. Image adapted from (Augustin, 2008).

1.2.2 Building tall with CLT

Regarding buildings with a reduced number of floors, CLT is a very attractive material possessing a significant number of qualities. The massive and isotropic *plate* allows for great freedom during designing process, allowing different building overall shapes, different spatial configurations, and freedom to define location, shape and size of openings. Further, force transferring properties of a plate structure allows floor-structures with wide spans (approximately 7.5m (Augustin, 2008)), wall-structures working as deep beams, and columns can be used as supports without main beams (Falk, 2005). However, when CLT is the only structural material of a tall building, the design freedom suggested before is limited. Structurally, CLT has been mentioned as a good material to build tall with timber once it is a massive material with

improved mechanical properties. Further, massive construction is characterized by its monolithic behavior, based on distribution of bearing walls able to provide to structure a higher level of strength and stiffness.

Vertical loads in CLT construction is not a matter of concern. Nevertheless, tall building requires the adequate stiffness to answer horizontal forces derived from wind or hazards, which means the need of increase the mass of the structure. Regarding this matter, some important aspects should be considered during building design, such as: friction locked connections with the floor, the length to height ratio of the wall and its cross section, the existence of large openings, the geometry of the building, and the type and magnitude of horizontal loads. Thus, CLT construction took refuge in a super massive system called *cellular construction* based on platform construction system[2]. It can be classified as a 'selfish system' grounded on the multi-functionality of CLT claiming that the entire building should be built up with CLT elements. In other words, it is a system in which CLT should shapes all structural elements.

Cellular construction has been recently applied in some recent tall buildings exposing some important limitations associated to this system. Beyond the stiffness requirements, this kind of system can promote progressive collapse requiring extra load paths through the increase in the number of structural walls. Consequently, this construction system is characterized by having a lot of strength capacity neglected. At the end, the building shows an enclosed external image with small openings and inner spaces excessively compartmentalized. This last is the reason why typical CLT tall buildings have been essentially limited to residential buildings.

Aware of that obstacle, enthusiasts of tall timber construction have started to encourage engineers and architects to work on new solutions able to offer greater freedom to designers and meet actual customer needs. There are already some proposals to reduce the excessive partition space, based on the location of reinforced cores or on the development of hybrid structural systems, promising to boost the emergence of new ideas. According to Wells (2011), new solutions should bet on exploration of material strength, local strengthening of bearing points and increase stiffness, in order to allow more daring and creative results.

2 CLT construction system in which floor panels rest directly on top of wall panels, forming a platform for subsequent floors.

1.2.3 Advantages and disadvantages

1.2.3.1 Mechanical properties of CLT, its fire resistance and seismic performance

Accuracy of CLT manufacture process and crosswise lamination provides improved dimensional stability and allows the fabrication of large elements (3x18m). CLT offers relatively high in-plane and out-of-plane strength and stiffness properties in both directions (Table (II) 1:1). However, it is necessary to safeguard that mechanical properties vary according to manufacturer, so consolidation with each manufacturer is required during the design process.

Relatively to fire resistance, similar to what happens with solid timber, when CLT is exposed to a fully developed fire it soon develops a charcoal layer that protects inner cross section from fire. The fire resistance of CLT panels can be designed according to the methodology suggested by Eurocode 5 (EN 1995-1-1, 2004), considering a charring rate similar to that applied to glued laminated timber made of softwood (0,7 mm/min). However, despite being proved that CLT chars at a slow and predictable rate, assuring that, in a fire situation, building will keep its structural integrity for predictable periods, majority of building standards impose special measures for fire protection, even if outer sacrifice layers are considered. Nevertheless, it is important to mention that with the advent of automatic sprinkler protection, the limitations imposed to building designers has to be revised. The efficiency of such systems has proven that firefighting and fire safety within the building are safeguarded. Sprinkler systems detect, control and suppress a fire condition prior to a significant burning of surface materials and flashover within a fire compartment.

One of the strongest points related with CLT and its construction system is related with its performance in case of earthquake. Solutions using steel brackets fixed by nails or slender screws for the connections between CLT walls and floors has demonstrated a good answer when submitted to horizontal loads (Popovski et al., 2010) (Branco et al., 2019). However, it is important to mention that shear stiffness can be compromised by large openings (NoDujic et al., 2007). Some full scale dynamic tests with multi-storey CLT buildings (3 and 7 storeys) were already performed presenting surprising absence of significant damages after being submitted to severe earthquake motions (Mohammad et al., 2011) (Ceccotti, 2008) (Campos Costa & Candeias, 2013).

Table (II) 1:1. Strength and stiffness properties of CLT according to Egmond (2011).

STRENGTH AND STIFFNESS PROPERTIES CLT (N/MM²)	
Bending Strength - Parallel to the grain direction ($f_{m,k}$)	 24
Tensile Strength - parallel to the grain direction ($f_{t,0,k}$) - normal to the grain direction ($f_{t,90,k}$)	 14 0,4
Compression Strength - parallel to the grain direction ($f_{c,0,k}$) - normal to the grain direction ($f_{c,90,k}$)	 21 2,5
Shear Strength - parallel to the grain direction (in plane of slab) ($f_{v,k}$) - rolling shear ($f_{r,k}$)	 2,5 1,0
Modulus of Elasticity - parallel to the grain direction ($E_{0,mean}$) - normal to the grain direction ($E_{90,mean}$)	 11000 340
Shear Modulus - parallel to the grain direction (G_{mean}) - normal to the grain direction ($G_{r,mean}$)	 690 60
Characteristic Density (ρ_k) Average Density (ρ_{mean})	350 420

1.2.3.2 Prefabrication

Actually, one of the main goal of construction sector is the development of practical architecture which can be built quickly, efficiently and inexpensively, inside dynamic urban environments. Considering such a goal, prefabrication of building elements or building modules out of site seems the right way to follow. This path can provide great results considering the reduction of material costs, labor, construction time and waste, however there is the risk to result on a repetitive and uninteresting architecture.

The great advantage of CLT regarding mass production method is its association with CNC methodology which allows considerable freedom to building designers without compromising advantages associated with a mass customized process.

1.2.3.3 Moisture induced effects

Hygroscopic behaviour of CLT, regarding shrinkage/swelling movements, changes on mechanical properties and moisture gradients, was explained in chapter 1 of Part I of present thesis. Putting it simple, timber hygroscopicity means that it is permanently ready to release and absorb water (absorption and

desorption phenomenon) when exposed to fluctuating atmospheric humidity. Fragiacomo et al. (2011) calls this exposure of "humidity load", which should be subdivided into various categories, such as: external conditions (sheltered or not from precipitation and sun radiation), interior conditions (heated or unheated buildings), and even the activity that the building shelters. Both indoor and outdoor structures are exposed to an environment with changing relative humidity, and the moisture content in wood structures will normally change during their use. The most severe effects often take place when the building is new. It is quite common that wood with higher moisture content (MC) is built in and then dried after the building is heated. Timber hygroscopic behaviour is a very important issue regarding the timber building physics because changes on timber moisture content affect several physical, mechanical and rheological properties of wood, such as: shrinkage/swelling, internal stresses, strength properties, durability, and decrease of connections resistance.

Regarding construction in height, the use of timber imposes a special attention to the effects of moisture content variations during design process. Tall buildings are predisposed to specific structural problems, such as: greater tendency to creep, due to higher vertical loads; crushing due to higher compressive strengths, and torsion movements due to horizontal loads. All these problems can be intensified by changes on moisture content levels and consequently interfere on the behavior of connections. Further, upper floors of tall buildings have, generally, greater exposure to the sun resulting on the development of unwanted cracks that will weaken the points of the structure where shear or tensile forces are greater, such as the connections. Other typical phenomenon on timber buildings, is the cumulative effect of shrinkage/swelling movements which, dependent on the height of the building, can result in significant changes on building height.

The experimental campaigns developed for present thesis (Part I) were crucial for the understanding of the significance of this topic on a CLT building design. Regarding compression and tensile strains caused by successive RH cycles ($30\% \leq RH \leq 90\%$), measurements performed with three layered CLT panels showed that crosswise lamination restricts moisture induced movements in tangential direction, however, as a consequence, cumulative compression/tensile internal strains can be developed in the panel (chapter 2 of Part I). Despite this restriction, tangential direction still present high moisture induced movements when compared with longitudinal direction: $1{,}8 \leq \Delta\left(\frac{T}{L}\right) \leq 12{,}8$, depending on drying or wetting periods. However, it is important to mention that when comparing with solid spruce, strains measured in tangential direction reduces significantly for CLT panels. While for solid spruce strains measured in tangential direction varies between -0,037 and 0,032, for saturated and anhydrous stages

(C. Silva, Branco, Camões, et al., 2014), for CLT strains varied between -0,012 and 0,008 for drying and wetting periods, respectively. Without any kind of restriction, radial direction is the direction that presented the highest moisture induced movements in CLT panels: $3,5 \leq \Delta\left(\frac{R}{L}\right) \leq 24,7$ and $1,5 \leq \Delta\left(\frac{R}{T}\right) \leq 3,3$, dependent on drying/wetting periods. Here it is important to mention that in solid wood tangential direction is the one that registers higher movements. According to Silva et al. (2014), $1,6 \leq \Delta\left(\frac{T}{R}\right) \leq 2,6$ for measurements taken with anhydrous and saturated specimens.

Relatively to the effect of moisture induced effects on screwed connections, chapters 3 to 5 of Part I of the present thesis also clarify that high moisture levels leads to a reduction of withdrawal resistance for STSs inserted in main face of CLT panels (1.8% per each percentage unit of MC added, when $12\% \leq MC \leq 18\%$) as well as for STSs inserted in the lateral face of CLT panels, parallel to the grain direction (3,0% per each percentage unit of MC added, when $14\% \leq MC \leq 25\%$). However, and contrary to the expectations, results obtained from tests performed after successive RH cycles, suggested an improvement of withdrawal resistance (13,5%) that must be related with crosswise lamination and consequent moisture induced stresses (MIS) caused by RH cycle

1.2.3.4 Building envelop and durability

Besides effects of wood hygroscopic behavior, moisture can also lead to timber rot, mold and mildew, which can eventually result in structural problems for the building. Wood is an organic material which needs to be protected from moisture in order to avoid the material decay. As a wood-based material, CLT demands exactly the same precautions. In fact, fungi are one of the biggest wood enemies. However, they need the right environment to live and feed on the cellulose, hemicellulose and lignin from wood cells. To perform an attack, fungi needs sufficient moisture, nutrients, oxygen, and a reasonably warm environment. Nevertheless, this kind of attack results on a reduction of the timber mechanical properties only if the same condition remains for a significant period of time (Wang et al., 2010). According to McClung (2013), wood is considered safe from decay if it is exposed to temperatures below 10°C and a maximum moisture content of 20%, which provides a safety margin for wood species with poor decay resistance.

Despite this fragility of wood, all remaining construction materials must be adequately protected from moisture sources. According to Glass et al. (2013), there are four main mechanisms of moisture movements in buildings, namely: liquid water flow; capillarity action; water vapor flow and water vapor diffusion. The liquid water flow refers to water intrusion and is the largest source of wetting, being

indispensable a proper design, detailing, and assembly of building materials. Anyway, if water intrusion happens, drying of materials must be possible by means of drainage, airflow, evaporation, and diffusion. So, durability of timber structures is dependent on wetting reduction and drying empowerment.

In the case of building enclosure, an effective drainage plane on all wall/roof surface, including a rain screen assembly, is essential to allow moisture to drain away from building elements (Build it Green, 2008). In fact, rain screen systems are known as the most effective regarding water drainage and drying of conveyed moisture. This system is characterized by the placements of an unfilled air space between cladding and water resistive barrier and structural wall assembly. This way water absorption by capillarity is avoided and an airflow which helps to dry the elements of wall assembly is created.

McClung et al. (2014) performed an experimental research focused on the evaluation of the drying potential of a variety of wall assemblies in a Southern Ontario climate. The general wall section is based on the rain screen system principles and is assembled as follows: a rainwater element, an air gap, an insulation layer, a water resistive barrier, a CLT panel, an air gap and a gypsum wall board. Materials with different permeability levels were used and results indicates that wall assemblies that used materials with higher permeability levels, such as vapor permeable membrane combined with mineral wool insulation or expanded polystyrene (EPS) insulation, presented a faster drying capacity reducing the possibility of decay initiation. In agreement with this study, Glass et al. (2013) suggest that, considering the low vapor permeability of CLT, it is desirable to improve the drying capacity of wall assembly applying vapor permeable materials for water resistive barriers and insulation layers.

Some other solutions, such as glazed curtain wall solutions, are also pointed as effective protecting timber structures from moisture accumulation. However, in such solutions, CLT has to deal with temperature issues, reduction of thermal and acoustics performances, forcing the use of high performance windows, and water vapour (condensation) (Lepage, 2012).

1.2.3.5 Acoustic performance and thermal conductibility

One of the main disadvantages of using CLT in multi-storey buildings is related with its poor acoustic performance. As consequence of its reduced mass CLT present sound transmission classes (STC) and impact insulation classes (IIC) that does not fulfil the requirements of building codes. According to Hu & Adams, Davide L. (2013), when a five layered CLT panel is considered, CLT walls elements present STC=32-34, while CLT floor elements suggest STC=39 and IIC=23. Considering that the international

building code (IBC) requires minimums of 50 either for STC or IIC, CLT must resort to additional insulation elements by means of multi-layered wall and floor assemblies.

Considering direct sound transmission, wall solutions should be constituted by two CLT panels with an air gap between or by a CLT with adjacent layers of insulation or sound absorbing materials, while floor acoustics performance can be achieved either by the application of insulation layers immediately bellow the floor finish or by applying a suspended ceiling. Wells (2011) suggests that two layers of 9mm plasterboard should be applied on each side of CLT walls with a10mm air gap, floors should be insulated by means an acoustic ceiling, while stairs and lift cores should be built with a double CLT wall with a 40mm air gap in between.

In addition, to obtain an efficient solution regarding direct sound insulation, it is necessary to detect and solve flanking sound transmissions. According to Egmond (2011), flanking sound represents 97% of total sound transmissions, when any kind of adjustments in sound transmissions is developed. This way, sound leaks, such as the connections between wall and floor elements, must be identified still during design process. One pointed solution to solve these weak points is the placement of flexible material between both CLT structural elements.

Contrary to acoustic performance, CLT has a great thermal behavior. In general, wood has a low thermal conductibility, reducing thermal bridging problems. CLT has the same thermal properties as the wood from which it is made. Besides low thermal conductibility, CLT panels have high heat capacity. According to Egmond (2011), a CLT panel with 100mm and density of 500kg/m^3 has a thermal conductivity (λ) of 0,13W/mK and a specific heat resistance (Rm) of 0,77m^2·K/W. Values for thermal resistance can be improved by simply increasing the panel thickness.

1.2.3.6 Connections

As it is well known, connections are key points for all kinds of timber structures, including CLT. Connections are essential elements that are responsible to guarantee the integrity of the structure and to provide the required strength, stiffness, stability and ductility. Further, connections should be able to transmit static and dynamic forces between structural members. In sum, the capacity of connections and its structural configuration are responsible for the ultimate behavior of a timber building. In fact, the complete collapse of a building or other less extensive accidents that may occur usually start as a local failure inside or in the vicinity of a connection (Lewandowski et al., 2015).

Construction systems full based on CLT panels are compatible with different kind of connectors (STSs, wood screws, bolts and dowels), depending on the type of elements to connect. However, as already explained in Part I of the present thesis, STSs are the solution typically recommended. These fasteners can be used to connect easily, quickly and efficiently different CLT structural elements, wall to floor, roof to walls wall to wall and floor to floor. The need to combine STSs with split rings, shear plates and tooth plates is dependent on the scale of loads. More detailed information about connections using STSs, especially regarding the consequences of moisture induced effects, can be found in section 1.2. of Chapter 1 of Part I of the present thesis.

The remaining types of metal connectors are generally used in the case of hybrid solutions, in which CLT elements are combined with other wood-based materials, concrete or steel. Another possible solution, appreciated by those who advocate the carpentry advantages, is the timber to timber connections. However, due to the complexity associated to the execution of these kind of connections, they are generally set aside. Besides the historic examples of carpentry joints, innovative solutions to timber to timber connections emerged recently. Regarding large scale connections, one interesting example is the five storey Tamedia building, in Zurique (Switzerland), designed by Shigeru Ban architects, in which linear timber laminated elements are connected together by means of hidden large hardwood elements. In the case of taller buildings, the efficiency of these kind of connections is questionable, once they should provide the proper stiffness and ductility, required to answer to horizontal loads.

1.2.3.7 Architectural considerations

CLT is a prefabricated solid engineered wood product composed of switched orthogonally bonded layers of solid-sawn timber or structural composite lumber. As final result, CLT exhibits a panel shape different of the well-known linear timber elements. Besides, cross layers provide to CLT panels higher strength and stiffness properties in their both directions, being able to take up forces in-plane as well as perpendicular to the plane. Thus, CLT panels may work as a shear wall as well as a slab (Bejder, 2012).

CLT elements introduce timber in the field of surface-based expression, known in society since 1970's when first prefabricated buildings in concrete emerged (Falk, 2005). But, better than concrete, CLT offers huge format, light weight and easier workability. The dimensions of the panels can be adjusted according to project needs, however there are dimensional limits essentially related with transport and presses. Panels can have from three up to seven layers, which means thicknesses between 42 and 500mm. Width and length of panels can go up to 4800 and 30,000mm, respectively. But, due to transportation and

assembling restrictions width and length of CLT panels are limited to 3000 and 16,500mm, respectively (Augustin, 2008).

The adaptation of CLT to engineering and architecture practices has been described by some authors. Falk (2005) defined structural behavior of structures based on timber *plates*, explaining the significance of orientation of walls and shear-walls as well as warning for stability dependency on both orientation and jointing. Regards to architectural issues, Bejder (2012) defined different possibilities to construct with CLT (Figure (II) 1:6). According to that work, there are three different ways to build with a *plate-based* system, which result in distinct final architectural expressions and spatial configurations, namely: *enclosed box, dissolved box* and *"floating" structure.*

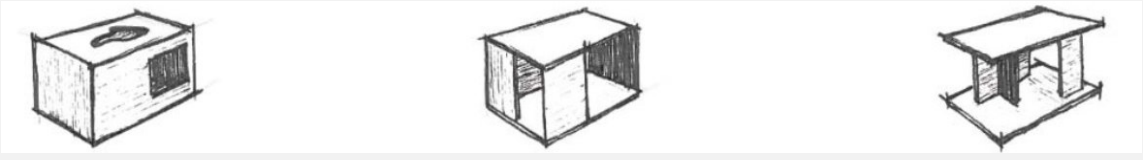

(a)	(b)	(c)

Figure (II) 1:6. Three different spatial configurations based on plate properties suggested by (Bejder, 2012). (a) Enclosed box, (b) dissolved box and (c) 'floating' structure.

1.2.4 Demonstration Buildings

Nowadays, wood is being reintroduced in construction sector and its supposed weaknesses has been demystified by science. Considered by many as the material of this century, structural timber starts a new cycle based mainly on its environmental advantages (section 1.1. of present chapter). Figure (II) 1:7 depicts a chronological evolution of large timber buildings/structures, and shows some ancient examples, the stagnation period and the recent increase of multi-storey timber buildings constructed and under construction.

Since 2006, some innovative proposals for multi-storey timber buildings are looking for a sustainable solution for our denser cities. Cross laminated timber (CLT) is a transversal material, being the leading figure in the majority of the constructed buildings and in the proposals for new construction systems. The *cellular construction* (described in sub-section 1.2.2. of present chapter) is a construction system fully based on CLT, in which CLT shapes all structural elements. Figure (II) 1:7 present the most known examples: Mühlweg project (Hermann Kaufmann Architects, Architekturbüro Reinberg and Dietrich | Untertrifaller – 2006) in Vienna, Austria; Stadhaus (Waugh Thistleton Architects - 2008) in London, England; Bridport (Karakusevic Carson Architects – 2011) in London, England; Forté (Daryl Patterson – 2013) in the Melbourn's Docklands, Australia; Via Cenni (Rossiprodi Associati - 2013), in Milan, Italy;;

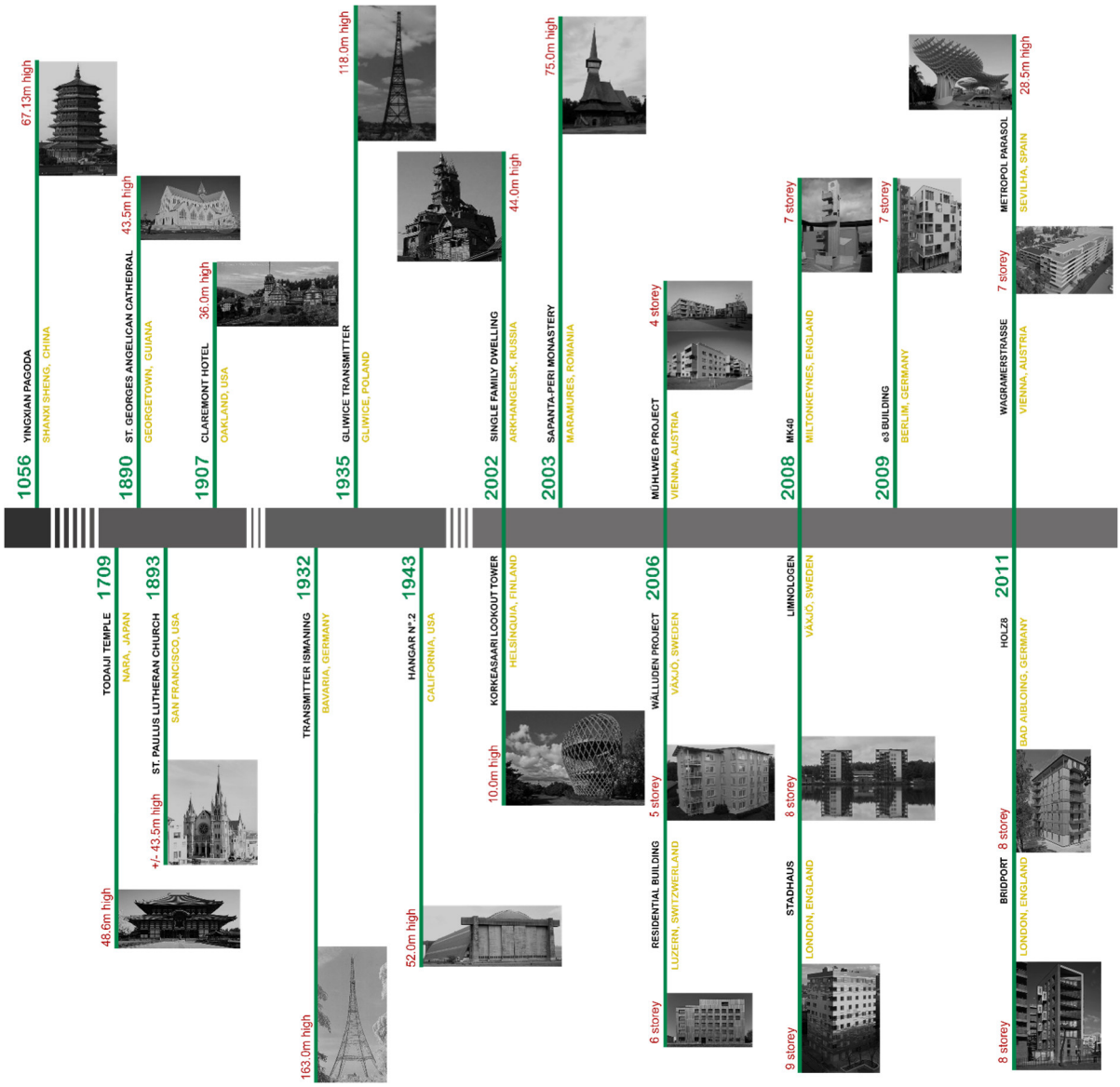

Figure (II) 1:7. Chronological evolution of large timber buildings/structures.

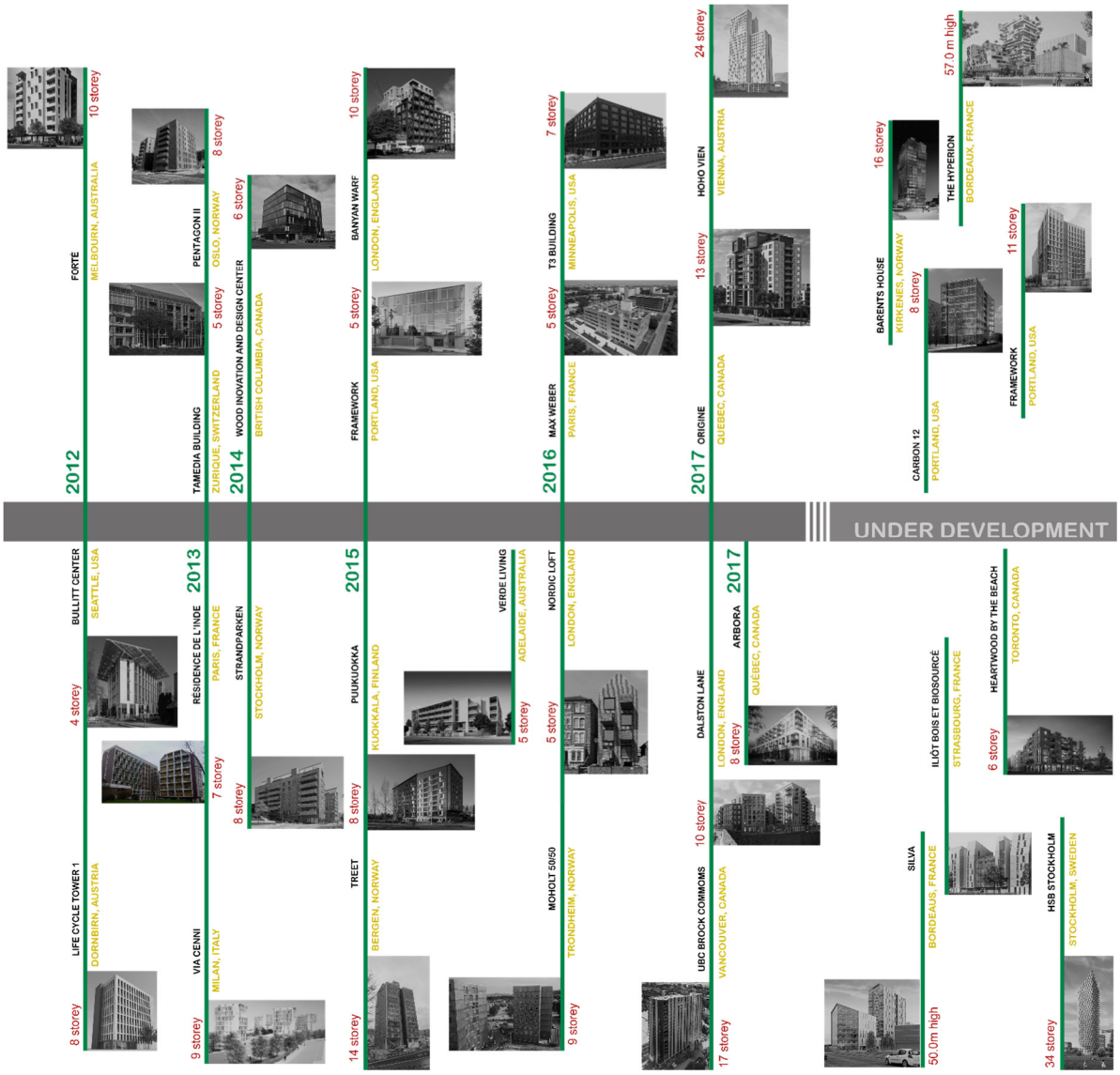

Figure (II) 1:7. Chronological evolution of large timber buildings/structures.(continued).

Pentagon II (Hoyer Finseth AS architects – 2013) in Oslo, Norway; Strandperken (Wingardhs architects - 2015) in Stockholm, Norway; Banyan Warf (Hawkins Brown architects – 2015) in London, England; Puukuokka (OOPEAA architects – 2015) in Kuokkala, Finland; Verde Living (Proske Architects – 2015) in Adelaide, Australia; Moholt 50/50 (MDH Architecture – 2016) in Trondheim, Norway; Max weber (Pascal Gontier architect – 2016) Paris, France; and Origine (Yvan Blouin Architects – 2017) in Quebec, Canada.

Some other construction systems combine CLT with strong concrete cores, such as: residential building in Wagramerstrasse (Schluder Architektur and Hagmüller Architekten - 2011) in Vienna, Austria; Holz8 in Bad Aibling (Schankula architects - 2011), in Berlin, Germany; and UBC Brock Commons (Acton Ostray architects - 2017) in Vancouver, Canada.

The structural systems and materials change as the building needs more or less spatial flexibility, small or larger openings and few or more storeys. Regarding buildings with a range of floors between 5 and 10, CLT is a very attractive material possessing a significant number of qualities. It allows floor-structures with wide spans (approximately 7.5m (Augustin, 2008)) wall-structures working as deep beams, and columns as supports without main beams (Falk (2005) and Wells (2011)). However, when CLT is the unique structural material, the design freedom becomes limited. In consequence, some innovative proposals based on hybrid and lighter concepts emerged. In order to shape more flexible buildings, other construction systems combine CLT, or other timber based panels, linear elements made either from steel or other wood-based materials and/or concrete reinforcements (cores or composite slabs). Examples of some constructed buildings are: Limnologen (Ola Malm architect – 2008) in Växjo, Sweden; E3 building (Kaden + Klingbiel architects – 2009) in Berlin, Germany; the Life Cycle Tower 1(Hermann Kaufmann ZT GmbH – 2012) at the Dornbirn, Austria; Bullitt Center (Miller Hull Partnership - 2012), in Seattle, USA; Residence De L'Inde (Intégral Lipsky+Rollet architectes – 2013) in Paris, France; the Tamedia Building (Shigeru Ban Architects - 2013), in Zurich, Switzerland; the Wood Innovation and Design Center (Michael Green Architecture - 2014), in British Columbia, Canada; the Treet (Artec - 2015), in Bergen, Norway; and the Cube (Hawkins\Brown - 2015) building, in London, England.

1.2.4.1 Describing some examples of Cellular construction

In last few years, some CLT multi-storey buildings have been built in order to prove their viability and their advantages. Many of these buildings are based on *cellular construction* system that is considered for many as a *selfish system* due to the fact that CLT shapes all structural elements and the combination with other construction materials is not considered.

Despite the excessive number of partition walls present in these type of buildings, it is possible to note some flexibility on location and orientation of bearing walls and structural cores. As result, constructed buildings present different overall shapes. The most known examples are: Stadhaus, Bridport, Forté and Via Cenni.

Developed by Waugh Thristleton Architects and Techniker engineers, Stadhaus is a nine-storey integral timber residential building, providing a total of twenty-nine apartments, which rises from a concrete podium. It presents a simple square implantation with central lift/stairwells cores, erected with double CLT walls, that work like a strengthening for lateral stability (Figure (II) 1:8). Differently, Bridport bets in a less slender but longer shape with a total of eight stories (Figure (II) 1:9). Designed by Karakusevic Carson Architects and EURBAN (timber engineering), this multi-storey residential building, containing forty-one apartments, required important measures to increase overall stability crosswise and lengthwise. The location of crosswise load bearing walls and lift/stairwell cores were the key factors to solve the different layout of the building (Figure (II) 1:9 (b)). At last, designed and constructed by Lend Lease, Forté was also erected above a concrete podium reaching a total of 10 storey and offering a total of twenty-three apartments and four townhouses (Figure (II) 1:10). It comprises an irregular plant, broking the square monotony with protrusions and angles which offer greater diversity of views to different apartments. Via Cenni is the largest CLT structure built in Europe, comprising four nine-storey buildings connected by a concrete podium (Figure (II) 1:11). Designed by architect Fabrizio Rossi Prodi, these nine-storey buildings are also based on a full timber construction composed by CLT floors and walls, including stairwell and lift core. CLT wall elements are thicker in lower levels, which are never less than 120mm (5 layers) and floor spans vary depending on CLT thickness: an element with 200mm (5 layers) allows a span up to 5.80m, while an element with 230mm (7 layers) allows a span up to 6.70m. The great challenge of this project was to build a relatively slender CLT building in an earthquake area. The building design had to fulfill the general earthquake engineering rules and was examined by a special investigation commission of the national authority.

Analyzing these four examples it is evident that *cellular construction* is not totally rigid, allowing some level of freedom to designers. However, an important limitation related with the external expression of the buildings, must be highlighted here: as a result of the excessive number of vertical load paths (inside and in the building façade) as well as the reduced size of windows, buildings will always look like extruded and enclosed boxes (C. Silva et al., 2012).

1.2.4.2 Describing some examples of hybrid construction systems

Challenging the limitations of *cellular construction* system, some innovative proposals, based on hybrid and lighter concepts, have been emerging. Combining CLT with other timber based materials, steel and/or concrete elements, it is possible to improve this construction system by exploiting what each material has the best. Here some possibilities of hybrid construction systems already used will be described.

Developed by MidrocProperty development and Ola Malm architect, Limnologen is composed by two eight-storey residential buildings which offer 134 apartments (Figure (II) 1:12). Its structural system is based on CLT load bearing elements (exterior walls, floors and apartment-separating walls), traditional framed walls (used as partition walls) and located glulam beams and columns which allowed the reduction of CLT structural walls (Serrano, 2009).

Aiming to meet the needs of towns of tomorrow, CREE (Creative Renewable Energy & Efficiency) in collaboration with architect Hermann Kaufmann, Rhomberg Bau and Arup developed a concept for a timber-concrete hybrid system. According to their developers, this system is able to reach thirty stories, however due to legal limitations, it was not possible to build such a building in Australia until today. Lyfe cycle 1, an office building with eight stories, is the first building being erected by using this hybrid construction system (Figure (II) 1:13). Its structural system is based on a glulam framed system which allows spans up to 9.45m without supports, a concrete core and a hybrid timber-concrete floor.

A residential complex with seven stories, constructed in Wagramerstrasse (Vienna, Austria), is an example of a CLT cellular construction system combined with concrete cores (Figure (II) 1:14). Developed by architects Hagmüller and Schluder, the building was designed with the shape of a long crossbar. It rises from a concrete podium and CLT structural elements are anchored in three aligned stairwells/lift cores. Concrete is also combined with CLT floor elements in order to answer fire protection requirements and increase the mass of the building.

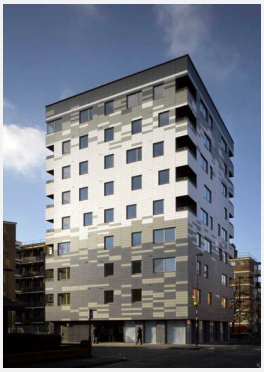

(a)

(b)

Figure (II) 1:8. Stadhaus, 24 Murray Grove, London – UK. (a) external view of building; (b) excessive compartmentalization of structural solution.

(a)

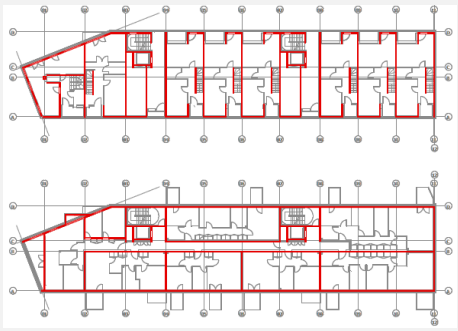

(b)

Figure (II) 1:9. Bridport building, Hackney London, UK. (a) External view; (b) CLT load bearing structure.

(a)

(b)

Figure (II) 1:10. Forté, in Melbourne's Docklands, Australia. (a) 3D external rendering; (b) Picture of works on site.

(a)

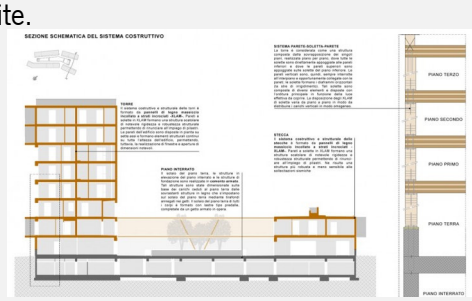

(b)

Figure (II) 1:11. Via Cenni, Milan, Italy. (a) external 3D rendering (b) vertical cross section.

Constructed in 2014, Wood Innovation and Design Center is a six-storey office building designed by MG architecture (Figure (II) 1:15). With the exception of a concrete raft slab that shapes the building foundation, it is entirely built with mass timber products: glulam columns and beams; CLT walls and stairwells/lift cores and CLT innovative staggered CLT panel design for floors. Brock Commons is a seventeen-storey building, developed by Acton Ostry architects for the University of British Columbia (Figure (II) 1:16). The building rises from a concrete podium and its structural system comprises two concrete cores, a grid of glulam columns connected between floors by means of special metal connectors and CLT floors acting as two-ways diaphragm. Vertical loads are carried by the timber structure while concrete cores provide lateral stability.

Some other hybrid systems were developed and published but not applied until today. Barents house, project by Reiulf Ramstad Architects (Reid, 2010), and FFTT system (find the forests through the trees), developed by Michael Green and Eric Karsh (Green & Eric Karsh, 2012), are two of these proposals. Both systems look for solutions able to offer greater spatial amplitude, especially suitable to non-residential uses and reach higher heights.

Barents house is a project for a timber building with 20 stories which bet in a structural system that combines CLT floors, glulam beams, columns and diagonals, and a concrete core (Figure (II) 1:17). FFTT system is able to reach 30 stories and bets on the combination of CLT walls and floors with steel beams (Figure (II) 1:18). The reduction of timber amount, and consequent reduction of space partition, is possible due to the increase in the building stiffness warranted by concrete and steel elements (C. Silva et al., 2012).

(a)

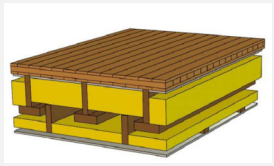

(b)

Figure (II) 1:12. Limnologen project, Växjö, Sweden. (a) External view of two of four buildings; (b) floor elements (Serrano, 2009).

(a)

(b)

Figure (II) 1:13. LifeCycle Tower ONE. (a) 3D digital external rendering of the LCT ONE in daylight; (b) Hybrid structural system.

(a)

(b)

Figure (II) 1:14. Wagramerstrasse timber building. (a) 3D external rendering; (b) Picture of works on site.

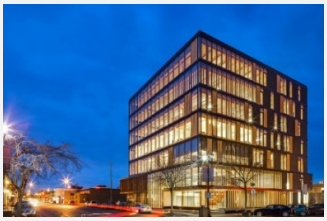

(a)

(b)

Figure (II) 1:15. Wood Innovation Design Center. (a) External view of building; (b) picture of inner space.

(a)

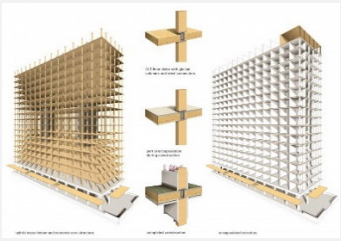

(b)

Figure (II) 1:16. Brock Commons. (a) External view of building; (b) hybrid structural system.

(a)

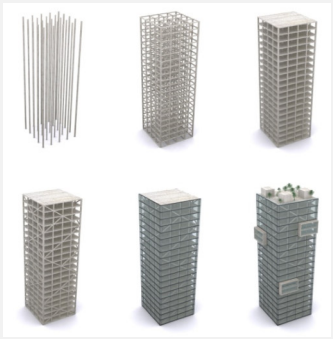

(b)

Figure (II) 1:17. Barents House Project. (a) 3D external rendering; (b) 3D structural rendering.

(a)

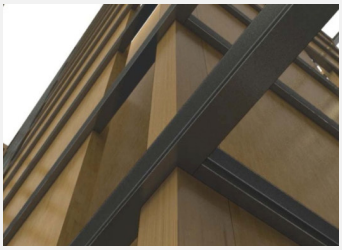

(b)

Figure (II) 1:18. FFTT system (a) 30 storey timber building model proposed by mgb Architecture + Design; (b) Hybrid timber-steel solution.

CHAPTER 2 (II)

2 URBAN TIMBER SYSTEM: A TIMBER HYBRID SOLUTION

2.1 Introduction

Based on the belief that timber is the construction material of the future, and considering all the points discussed in previous chapter, the Urban Timber system (UT system) has been developed. This system got inspiration in some constructed buildings and was designed attending to some essential principals:

- Explore the possibilities of timber as structural material promoting the rebirth of timber architecture as natural part of dense urban centers;
- Respect economic, social and environmental sustainability;
- Evaluate the advantages and disadvantages of timber based structures;
- Assuring the flexibility of the construction system, regarding the building shape, opening sizes and inner design;
- Ensure all safety building requirements;
- Explore the combination of different wood-based materials, preferring those that use low quality timber to shape advanced building products;
- Provide a fast and simple construction system;
- Offer possibilities for the building end of life;
- Consider the effects of moisture induced effects on timber based structural elements.

In order to provide a system able to shape flexible buildings, UT system was designed based on a timber hybrid construction concept that combines CLT and glulam as main structural materials. This combination of panel-shape and linear-shape elements is the key point regarding the architectural flexibility, widening the range of possibilities for architects.

UT system denies the selfish "all with CLT" concept, resulting in a lighter solution able to conceive more economical and challenging buildings. However, it is important to mention that in similarity to structures built just with CLT, UT system also chooses to work with materials that use low quality timber to shape advanced building products, enabling long-lasting carbon storage in a new assortment of wood.

Advantages associated with prefabrication were also exploited either regarding practical issues like reduction of construction time and costs, or regarding the possibilities offered by CNC technology.

As it will be described ahead in the present chapter, UT system was detailed considering safety requirements, such as structural behavior or fire safety, comfort defined by acoustic and thermal behavior, and moisture protection.

Regarding building safety, structural behavior of UT system was based on the bundled tube concept, often used on the design of multi-storey buildings. Dias (2017) developed a structural evaluation of UT system, designing a 3D model in *RFEM-5* software, a finite element software by Dlubal. The author conclude that UT system is able to shape large spans (8,8m) and consequently allows the proclaimed spatial flexibility.

Fire safety, acoustic and thermal comfort and moisture protection were evaluated based on published researches in which floor and wall sections are suggested.

The protection of timber structural elements from moisture is a crucial issue. Despite being a subject with reduced published research, the moisture effects on timber elements is of huge importance. This way, the experimental campaign presented in Part I of the present thesis was of great significance during the definition of the UT system.

In the present chapter, UT system is described and evaluated considering its structural concept and behavior, architectural considerations, production and construction processes, end of life possibilities and its detailing. Specificities related with moisture effects will be discussed in detail in next chapter.

2.2 Description of Urban Timber system (UT system) and its structural elements

Inspired in the bundled tube concept, the UT system works like a cluster of individual tubes connected together in order to make them behave as a single unit. As result, the strength and stiffness of the cross frames are improved (Ali & Moon 2007). This concept is often applied in order to achieve a greater number of floors and get a greater freedom of spatial design. One of the greatest advantages of bundled tube concept is the free location of lift and stairs cores.

The UT system is based in the combination of CLT and glulam, in which CLT shapes floors, walls and deep beams, while glulam it is used as double beams. CLT floors are directly supported by longitudinal and transversal double glulam beams. The double beams work together with CLT floors distributing the loads to the CLT walls, increasing the stiffness of the building and avoid the effect of progressive collapse. CLT walls have the function to resist all gravity loads, driving them to the foundations by means of vertical or oblique paths. At last, CLT deep beams sew up all the individual tubes in the building perimeter (Figure (II) 1:19).

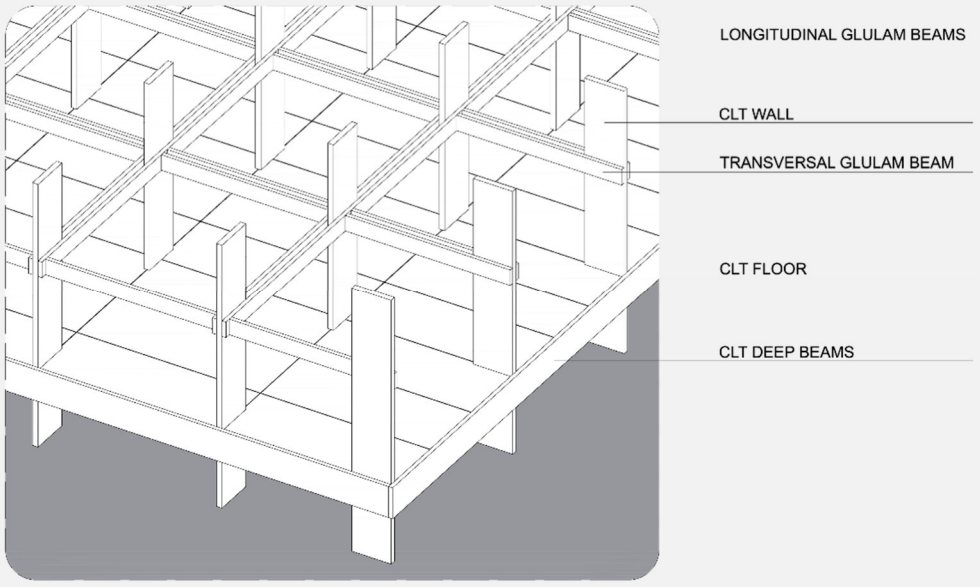

Figure (II) 1:19. Simplified Scheme of the UT system identifying main timber structural elements.

2.2.1 Structural elements

The UT system was developed based on some basic principles of structural systems. As an architect, the author of the present thesis does not have the necessary background to perform a structural design of UT system. However, collaborate in the development of a master thesis, Dias (2017), aimed to make a structural evaluation of the UT system.

To develop such work, the author considered CLT made of timber of C24 strength class and glulam of GL24h strength class. Regarding CLT, as it is not yet standardized, material characterized from Stora Enso was considered. Cross sections of CLT floors were initially pre-designed by *Calculatis*, a simple design software developed by Stora Enso. This pre-design was done in a conservative way, once CLT floor slabs were designed as unidirectional elements.

Remaining elements were designed through the elaboration of a 3D model in *RFEM-5* software*,* a finite element software by Dlubal. In the following sections, CLT walls, CLT slabs, double glulam beams and CLT deep beams will be analysed regarding its structural behavior in a 10 storey building, such as considered by Dias (2017).

2.2.1.1 CLT walls

One of the first critical reactions to the UT system, uses to be about CLT walls. Usually, the question is: Would not be better to use glulam columns instead of CLT walls? What size for CLT walls? What are the advantages of using CLT in independent small elements?

In fact, it would be possible to design the same scheme using glulam columns with smaller cross sections when comparing with CLT walls. However, in this case it was preferred to bet on CLT walls for two main reasons: one based on structural issues and the other based on aesthetic principals.

Regarding the structural issues, tall buildings have greater vulnerability to lateral forces, especially wind loads, which means that the building perimeter has more structural significance (Ali & Moon 2007). CLT walls work like shear-plates positioned in building perimeter, oriented perpendicularly to the plane facade, providing more stiffness than the corresponding elements in a frame construction (Falk 2005).

In respect to aesthetic reasons, the motivation to choose CLT walls instead of glulam columns is based in the possibility to expose CLT walls in the building. This way it is possible to expose the boards of external layers that looks like a beautiful wood cladding, instead of lamination lines that characterize glulam elements. The face of CLT walls that expose lamination lines can be hidden as depicted in Figure (II) 1:1, and final result would be perfect. Based on half miter technic, the connection between two elements, CLT wall and capping part, can be made by mechanical connections or by gluing technique.

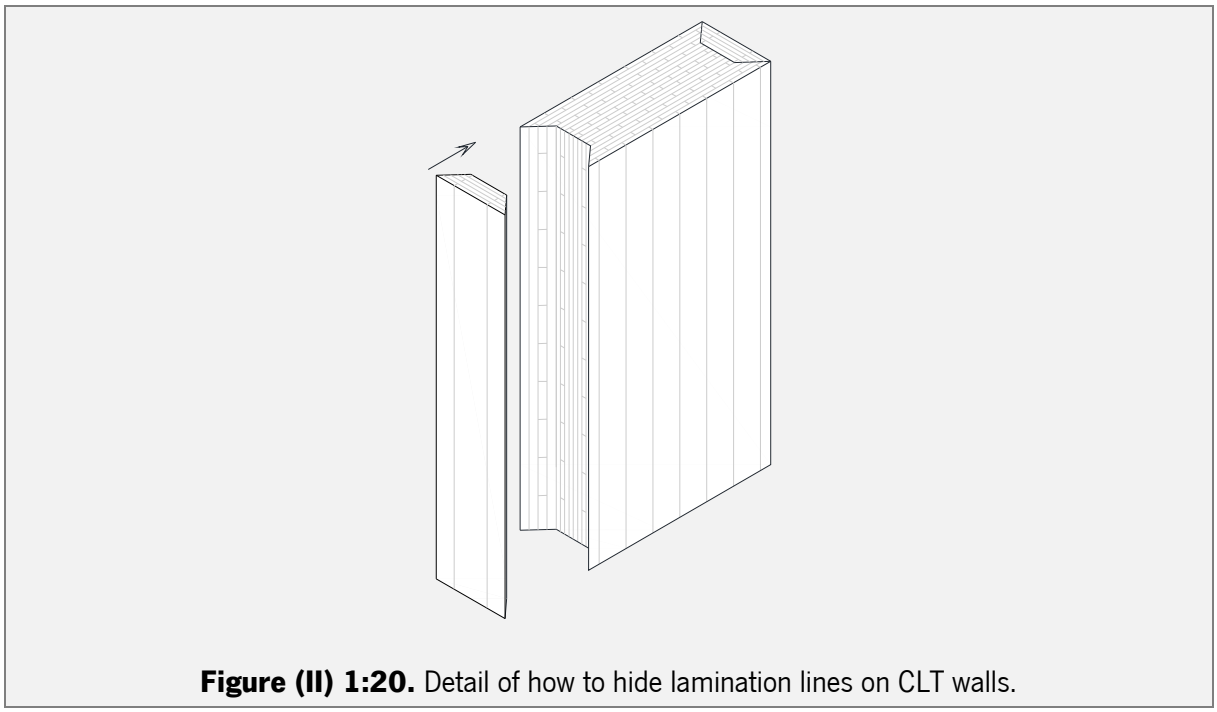

Figure (II) 1:20. Detail of how to hide lamination lines on CLT walls.

Dias (2017) performed the structural evaluation of the UT system considering the plan shown in Figure (II) 1:21. In order to answer to some structural needs, some CLT walls with different dimensions are suggested for central core and lift cores. Table (I) 3:1 exhibits the dimensions of different wall elements considered for his evaluation. The large length of CLT elements is related with construction system, theme that will be discussed in section 0, ahead in present chapter. So, in order to answer to the question

related to the dimension needs, the work developed by Dias (2017) concluded that, considering a building with 10 storeys, general CLT walls needs to have a width of 1,5m and a thickness of 600mm (Table (I) 3:1). In a first impression, a thickness of 600mm may seem too much, however, considering a building that is 10 storey high it is not that inappropriate and its impact in interior space can be hidden by separation walls or minored by means of a well-planned open space concept.

To achieve the proposed dimensions, the most important parameter to define was the buckling of the CLT walls. This parameter was successfully verified, however it imposed the need to perform experimental tests to determine the stiffness of connections between CLT walls and concrete base and between CLT walls and double glulam beams.

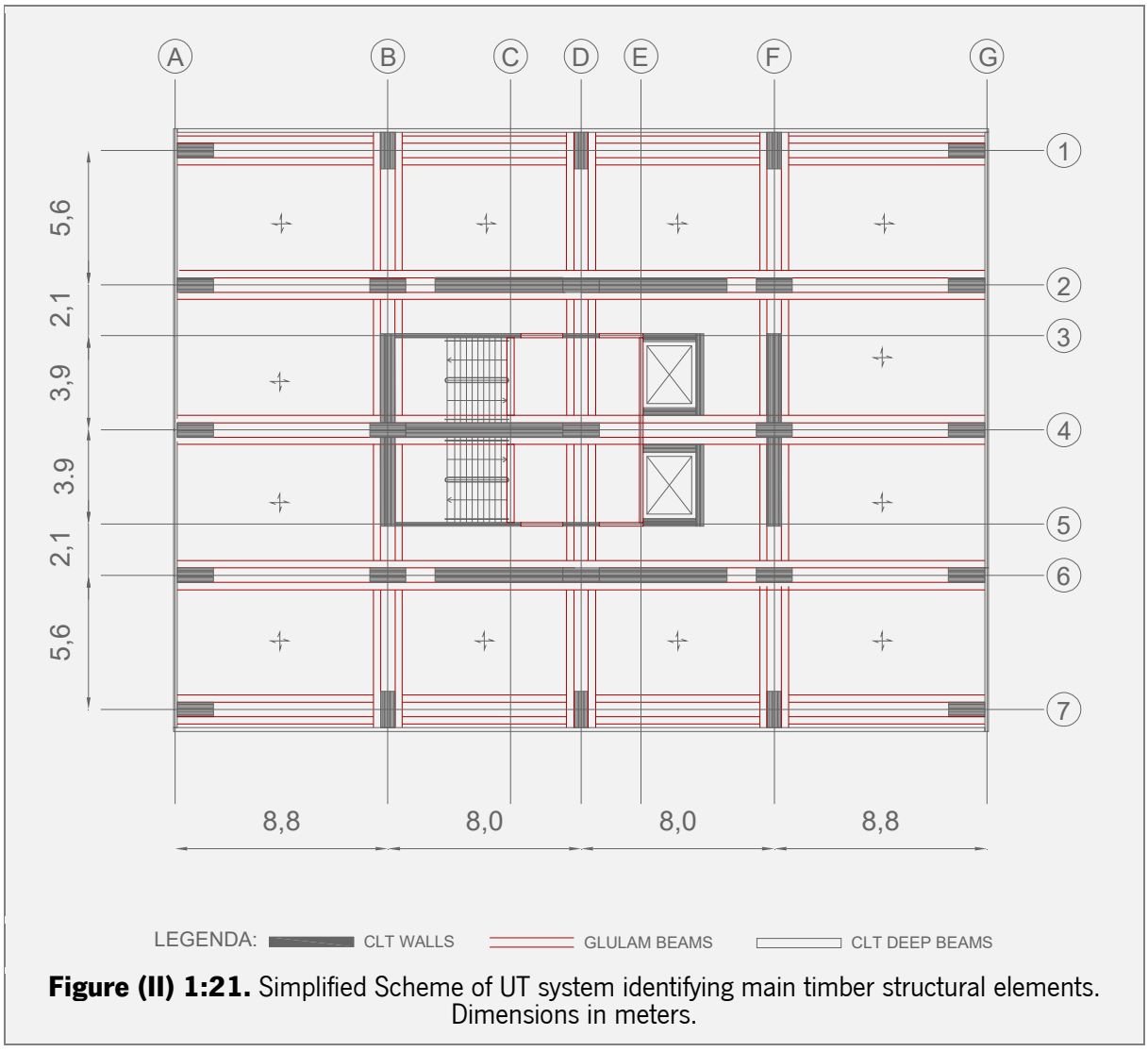

Figure (II) 1:21. Simplified Scheme of UT system identifying main timber structural elements. Dimensions in meters.

Table (II) 1:1. Dimensions of CLT walls considered by Dias (2017), depending on its location.

LOCATION OF CLT WALLS	DIMENSIONS		
	LENGTH (m)	WIDTH (m)	THICKNESS (mm)
GENERAL CLT WALLS	9,24 and 9,00 and 12,24	1,50	600
CENTRAL CORE PERIMETER	9,24 and 9,00 and 12,24	1,50 ≤ W ≤ 2,60	160
LIFT CORE	9,24 and 9,00 and 12,24	1,60 ≤ W ≤ 2,35	320

Despite the horizontal loads has been considered during the development of UT system, the connections between CLT walls and concrete foundations has to be evaluated and adapted. Generally, when it is considered a monolithic CLT construction, based on a *platform system* concept, the connection between CLT walls and concrete foundation are made by means of steel angles designed to resist tensile and shear actions. However, the UT system is based on the *ballom frame* concept and the number of CLT walls is much less. So, steel angles would not be able to resist internal stresses caused by lateral loads. Furthermore, due to reduced number of walls, this kind of connections would be susceptible to brittle failures and consequent collapse.

To overcome this issue, Dias (2017) suggested to combine UT system with Pres-lam (Prestressed Laminated timber) technology, in order to provide ductility to the structural system. This combination will be described ahead in the present chapter in section dedicated to connections.

2.2.1.2 CLT slabs

It is common to hear that one of the biggest advantages of CLT is its ability to shape slabs of solid timber which can distribute the loads in both orthogonal directions. However, in most cases, CLT slabs are calculated and applied as unidirectional structural elements. And why is that? Despite being considered a great advantage of CLT slabs, its bidirectional behavior is not easy to predict, involving a vast number of parameters, such as, support conditions, relative stiffness of panels in support zones, yielding moment of transversal and longitudinal layers, shear stress in both directions, etc.

Depending on support conditionings, designing a bidirectional CLT slab can be considered: (1) when the slab is supported by punctual elements such as columns and (2) when the slab is supported over three or four edges. Gagnon and Pirvu (2011) proposed a method of calculation for CLT slabs that is based in the following assumption:

$$if \begin{cases} \frac{l}{b} > 2, CLT\ slab\ must\ be\ calculated\ considering\ just\ the\ smaller\ span \\ \frac{l}{b} \leq 2, CLT\ slab\ must\ be\ calculated\ as\ a\ bidirectional\ element \end{cases}$$

The authors also suggest that bidirectional CLT slabs must be composed by a minimum of five layers and that for its structural design just inner layers may be considered, excluding external longitudinal layers from calculation process.

In the case of the UT system, CLT slabs are supported by glulam beams that are positioned in three or four edges of slab (Figure (II) 1:21). Dias (2017) considered for his evaluation of the UT system that major length of slabs can vary between 8,00 and 8,80 meters and the shortest length vary between 3,90 and 5,60 meters (Table (II) 1:2). Here, it is important to mention that the author concluded that the UT system allows long spans (8,8m) considering a reduced width of CLT floor elements (280mm). This way, sought after flexibility is achieved, avoiding architectural issues related with excessive partition walls.

Table (II) 1:2. Dimensions of CLT slabs considered by Dias (2017), depending on its support conditions.

SUPPORT CONDITIONS	DIMENSIONS		
	LONGEST LENGTH (m)	SHORTEST LENGTH (m)	THICKNESS (mm)
SLABS SUPPORTED ON THREE EDGES	8,00 and 8.80	5,80 and 5.45	280
SLABS SUPPORTED ON FOUR EDGES	8,00	5,45	280

2.2.1.3 Double glulam beams and CLT deep beams

The beams of the UT system are, in reality, the elements that turned this system into a hybrid one. In order to obtain a structure with less and smaller walls, those must be connected by beams and not directly by CLT floors. CLT is a super versatile material and it is also possible to shape beams with it. However, transversal layers would not be considered for its design resulting in an enormous cross section. So, as glulam is a timber derivate material that is perfect to shape linear elements, it was chosen to shape double beams of the UT system.

The concept of double timber beams is not an innovation of the UT system, buildings like Tamedia Building (Shigeru Ban Architects – 2013) or Sky believe in better building (Arup – 2014) already applied

this strategy (Figure (II) 1:22). The UT system also bet in double timber beams for some few reasons: this technique offers a simplified assembly system; the width of columns does not restring the width of beams; it is not necessary to have a super massive beam; and the space between both beams can be used to drive some infrastructures.

Considering the work developed by Dias (2017), for a building with 10 storeys, glulam beams has an unusual square cross section of 300x300mm (Table (II) 1:3). In order to do not increase too much the height of floor cross section, the width of beams was enlarged. In central core and lift core a common cross section of 160x300mm was suggested.

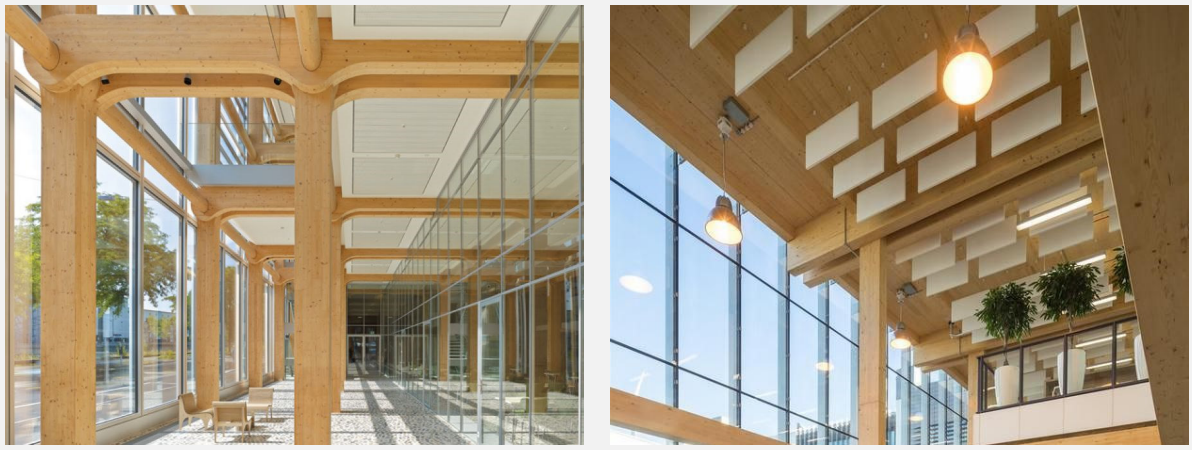

Figure (II) 1:22. Double timber beams applied in constructed buildings: at right Tamedia Building and at left Sky believes in better building.

Table (II) 1:3. Dimensions of glulam beams considered by Dias (2017), depending on its location.

LOCATION OF GLULAM BEAMS	CROSS SECTION		
	WIDTH (mm)	HEIGHT (mm)	GAP BETWEEN DOUBLE BEAMS (mm)
STAIRS	300	300	
CENTRAL CORE	160	300	
LIFT CORE	160	300	
DOUBLE BEAMS	300	300	600

2.2.2 Connections

Regardless building location, the wind and earthquake actions are the most limiting parameters when a CLT building is being designed. This way, it is mandatory to provide structural elements that add lateral stiffness to the building. In general, CLT buildings guarantee its stiffness through two main components: the ideal proportion of CLT walls, able to reduce deformations between storeys, and the connections.

The reduced number of CLT walls present in the UT system turns the connections into the most important elements in terms of ensuring the levels of stiffness required to make the structural system viable. According to Buchanan and Smith (2015), to reach the ideal stiffness level depends essentially on the design of building connections. Similarly, to other timber based construction systems, structures based on CLT structural elements demands a large quantity of connections, either they are connections between different structural elements or connections between panels belonging to the same structural element (wall-to-wall and floor-to-floor connections). Each connection origins an area where the stiffness is reduced, so it is crucial to predict the total impact of connections on global building stiffness. An efficient design and a perfect execution of connections result on various advantages for the building, namely: structural ductility in case of lateral loading; ensures proper control of building vibration; improves the quality of the final finishing touches of building and turns assemble and disassembling processes much more easy.

Regarding earthquake design, structural ductility is achieved when steel connectors, like steel dowels or self tapping screws (between others), are able to create plastic hinges. This way, brittle failures of timber structure is prevented when timber elastic phase reaches its limit. This way, definition of which are the dissipative or rigid connections is imperative and can be decisive in the structural evaluation of a timber building. Dias (2017) performed such evaluation regarding the UT system, following the recommendations of Follesa et all (2011) and defined dissipative and rigid connections as presented in Table (II) 1:4. As construction with CLT is not included in EN 1995-1-1, 2004, the design of connections must be submitted to laboratorial tests in order to correlate test results and calculation procedure.

CLT connections are usually based on simple and relatively low-tech principles, mainly based on self-tapping screws. Exploiting these advantages, the UT system suggests connections mainly based on self-tapping screws and steel dowels. The present section dedicated to the design of connections of UT system is based on bibliographic recommendations and on the research performed by Dias (2017). Anyway, it is mandatory to mention here that any proposal for connections presented in here must be object of experimental tests before that any conclusions about their structural behavior.

Table (II) 1:4. Definition of dissipative and rigid connections according the evaluation of UT system performed by Dias (2017).

DISSIPATIVE CONNECTIONS	- Connection between CLT floors and double glulam beams - connections between double timber beams and CLT walls
RIGID CONNECTIONS	- Connections between perpendicular Wall elements - connection between CLT deep beams and CLT walls - connections between CLT wall panels along the height of the building - connections between adjacent CLT floor panels

2.2.2.1 Dissipative connections

2.2.2.1.1 Connections between CLT floor panels and double glulam beams

Initially, the UT system proposes a connection between CLT floor panels and glulam beams based on the insertion of self-tapping screws (Figure (II) 1:23). As CLT floor rests on the top of glulam beam, the connection between them is based in the simple insertion of self-tapping screws perpendicular to the grain. Considering the advantages associated to this methodology (Part II – 1.2.3.6) it appears to be the most advantageous solution. It is a fast and effective solution that does not require on-site preparation of panels, like location of holes or grooves.

The evaluation of the UT system performed by Dias (2017), proposes the use of steel dowels with a diameter equal to 16mm (with a load capacity of 12,297kN - Rothoblaas) with a spacing of 15cm between each element, on the connections between floor panels and double glulam beams (Figure (II) 1:23). Contrary to what happens with self-tapping screws, this solution requires that both CLT and glulam elements reach the site with the holes, where the steel dowels will be inserted, already executed with great precision. However, it is important to mention that to fulfill this task would not be difficult considering all the advantages associated to CNC technology.

Dias (2017) justify this choice arguing that just one steel dowel does not restrict rotation between connected elements, however when steel dowels are applied as a group, rotation between elements are restricted by the high stiffness of connection. The minimum spacing between steel dowels were calculated following the recommendations of EN 1995-1-1, 2004 (

Table (II) 1:**5**).

2.2.2.1.2 Connections between double glulam beams and CLT walls

The connection between double glulam beams and CLT walls is probably the most complex connection of the entire construction system. In this connection glulam beams are in an intermediate position, transferring loads from CLT floor to CLT walls.

On his thesis, Dias (2017) choose to perform the connection between double glulam beams and CLT walls by means of steel dowels, however there is no mention how connection between perpendicular glulam beams is performed. These connections can be designed separately or together being part of a single connection. In other words, connection between CLT wall and glulam beams that are parallel to CLT walls and connection between both glulam beams, those that are parallel or perpendicular to CLT walls, can be made separately or three different elements can be connect by means of single specially designed connection.

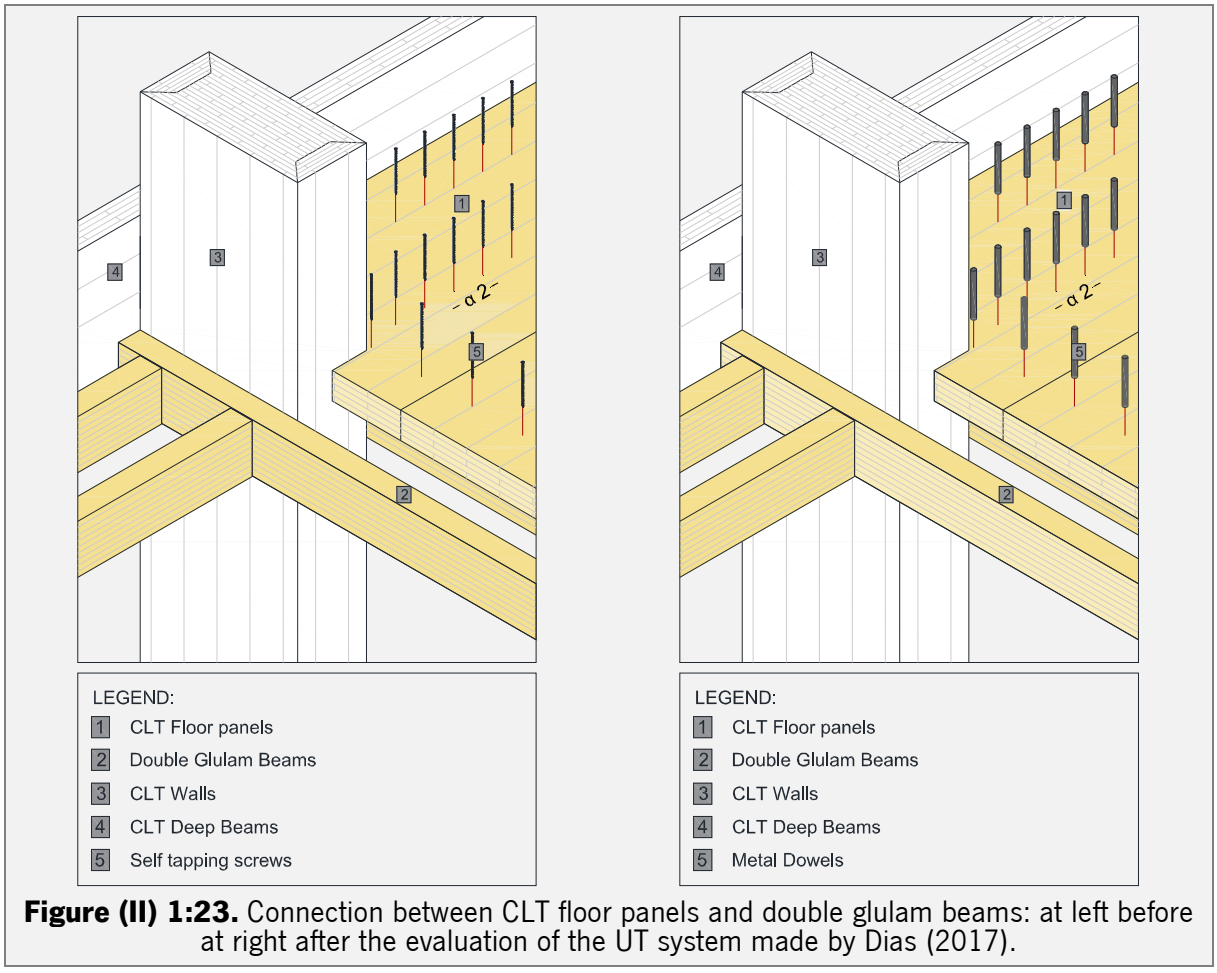

Figure (II) 1:23. Connection between CLT floor panels and double glulam beams: at left before at right after the evaluation of the UT system made by Dias (2017).

Table (II) 1:5. Definition of minimum spacing between steel dowels performed by Dias (2017), for connections between glulam beams and CLT walls, following the recommendations of (EN 1995-1-1, 2004).

	ANGLE	MINIMUM SPACING OR DISTANCE TO THE EDGE/TOP
α_1	$0° \leq \alpha \leq 360°$	48 mm
α_2	$0° \leq \alpha \leq 360°$	48mm
$\alpha_{3,t}$	$-90° \leq \alpha \leq 90°$	112mm
$\alpha_{3,C}$	$90° \leq \alpha < 150°$ $150° \leq \alpha < 210°$ $210° \leq \alpha \leq 270°$	112mm
$\alpha_{4,t}$	$0° \leq \alpha \leq 180°$	64mm
$\alpha_{4,C}$	$180° \leq \alpha \leq 360°$	48mm

α_1 – minimum spacing, parallel to grain direction, between two connectors; α_2 - minimum spacing, perpendicular to grain direction, between two connectors; $\alpha_{3,t}$ – minimum spacing to the loaded top; $\alpha_{3,C}$ – minimum spacing to the unloaded top; $\alpha_{4,t}$ - minimum spacing to the loaded edge; $\alpha_{4,C}$ - minimum spacing to the unloaded edge.

Steel dowels are preferred here once as they are produced with large lengths, being able to make double glulam beams work together with CLT wall, they improve the stiffness of connection as a cohesive set. Here the use of self tapping screws would not allow this kind of behavior, once even the long self tapping screws are produced with so large lengths.

Considering the connection between these three elements, three different solutions were developed, however, as already mentioned, all proposed solutions must be properly tested before state any final conclusion. Figure (II) 1:24, Figure (II) 1:25 and Figure (II) 1:26, depicts the three different solutions developed to connect double glulam beams with CLT walls. Figure (II) 1:24 shows a connection that is assembled by means of an external steel connector designed especially for this application. Steel connectors are positioned in both sides of CLT Walls tying at the same time parallel glulam beams to the CLT wall. Steel connectors are fixed by means of steel dowels while glulam beams that are perpendicular to CLT walls rests on U shape of steel connector. It is important to highlight that both, parallel and perpendicular glulam beams have a support on its underside. This way, delamination problems, that are frequent in this kind of connections can be reduced.

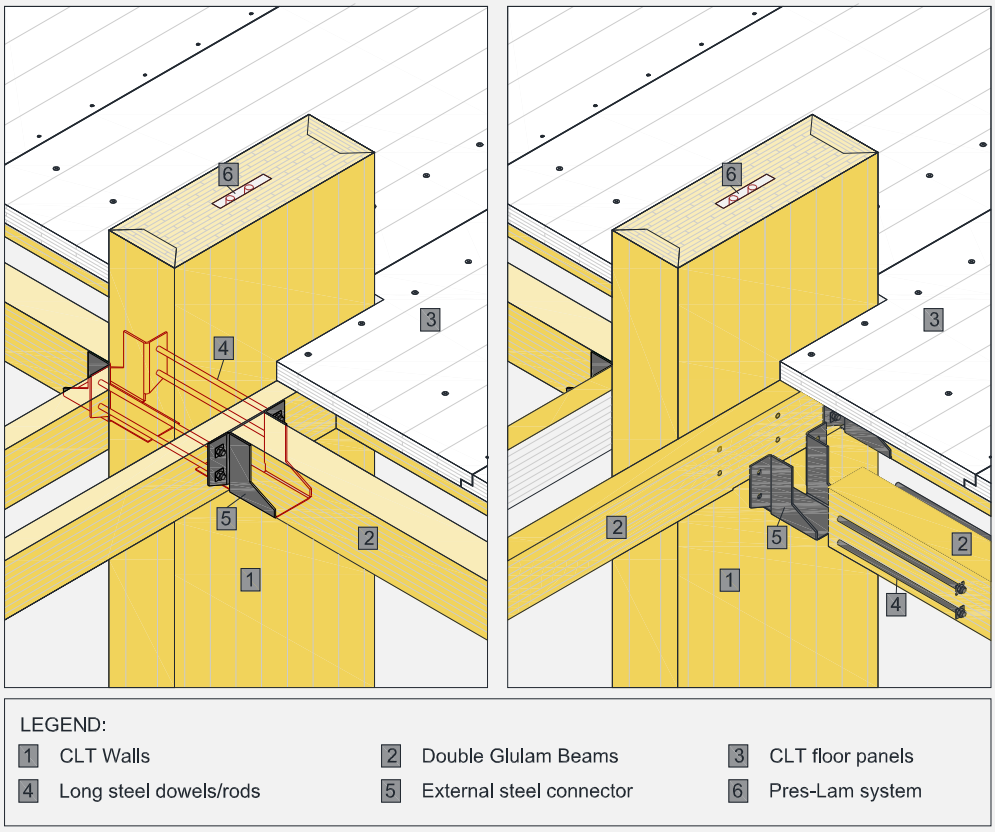

Figure (II) 1:24. Connection between double glulam beams and CLT walls by means of an external steel connector.

Figure (II) 1:25 shows a connection in which double glulam beams are connected to CLT walls by means of an internal steel connector. The need to develop a hidden solution arises essentially due to fire and aesthetic concerns. Considering a scenario in which the connection is exposed and not protected by non-flammable materials, steel connectors are considered weaknesses of structural system. Once the steel connector is hidden inside the timber element it is protected from high temperatures that can be reached in case of fire. The concept of this connection is the same of the solution presented before, parallel glulam beams are tied together with CLT walls and steel connectors by means of long steel dowels. The main difference is on the shape of steel connector that instead of a U shape it has a T shape. Perpendicular glulam beams are fixed to the steel connector by means of steel dowels/rods. In this way, perpendicular glulam beams have to be prepared on-site in order to fit perfectly in the steel connector. Here, also both parallel and perpendicular glulam beams have a support on its underside.

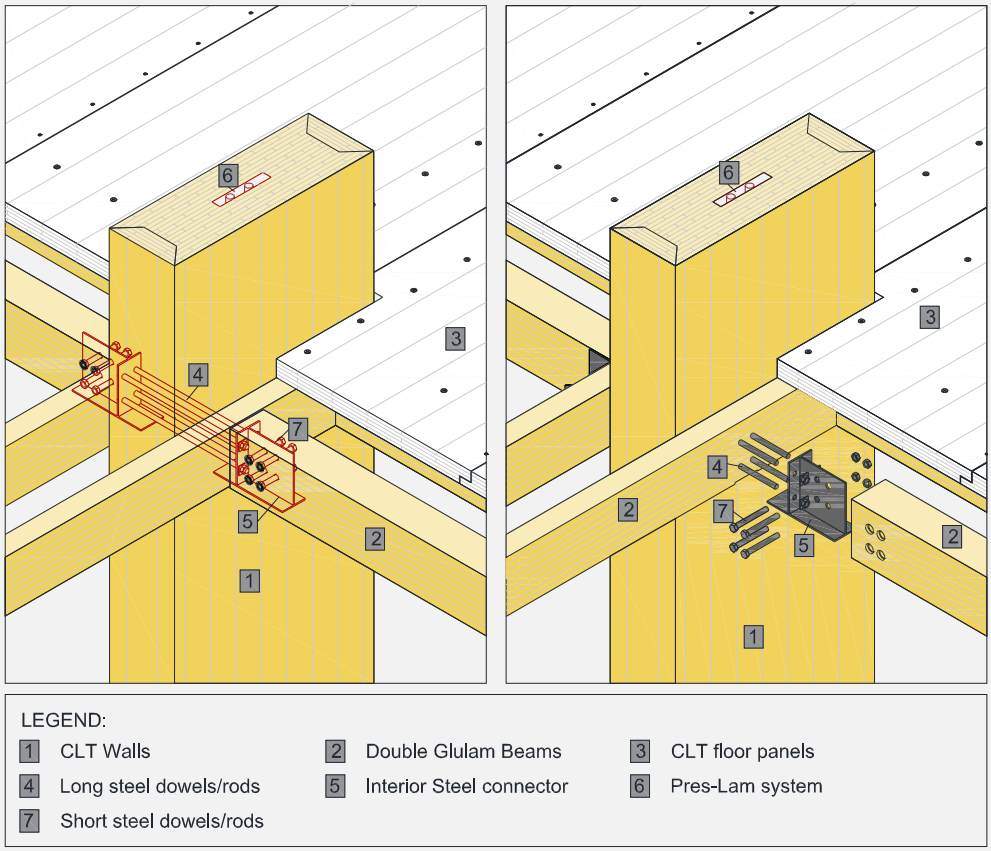

Figure (II) 1:25. Connection between double glulam beams and CLT walls by means of an internal steel connector.

At last, Figure (II) 1:26 presents a solution inspired in the timber to timber connection designed by Shigeru Ban architects to Tamedia Building. A large hardwood connector is responsible to tie together CTL walls and both, parallel and perpendicular beams. A smaller hardwood element and some self tapping screws, are used to lock CLT walls and parallel glulam beams, while perpendicular beams are fixed to large hardwood connector by means of steel dowels/rods. Here, all the elements must reach the site with all the cuts necessary to assemble the connection. The idea to apply timber to timber connections in tall timber buildings is of great interest, especially regarding environmental issues. However, to much work and research is required before state any conclusions about its efficiency.

According to Dias (2017), different possible solutions must be tested in order to quantify the stiffness of connections associated to Pres-Lam system, especially when connection are exposed to dynamic loads. According to the same author, one of the problems associated to this connection is the consequent deformation of CLT floors. This problem occurs when CLT panels are exposed to oscillation effects resulted from rotational constraint created by connection between CLT walls and glulam beams.

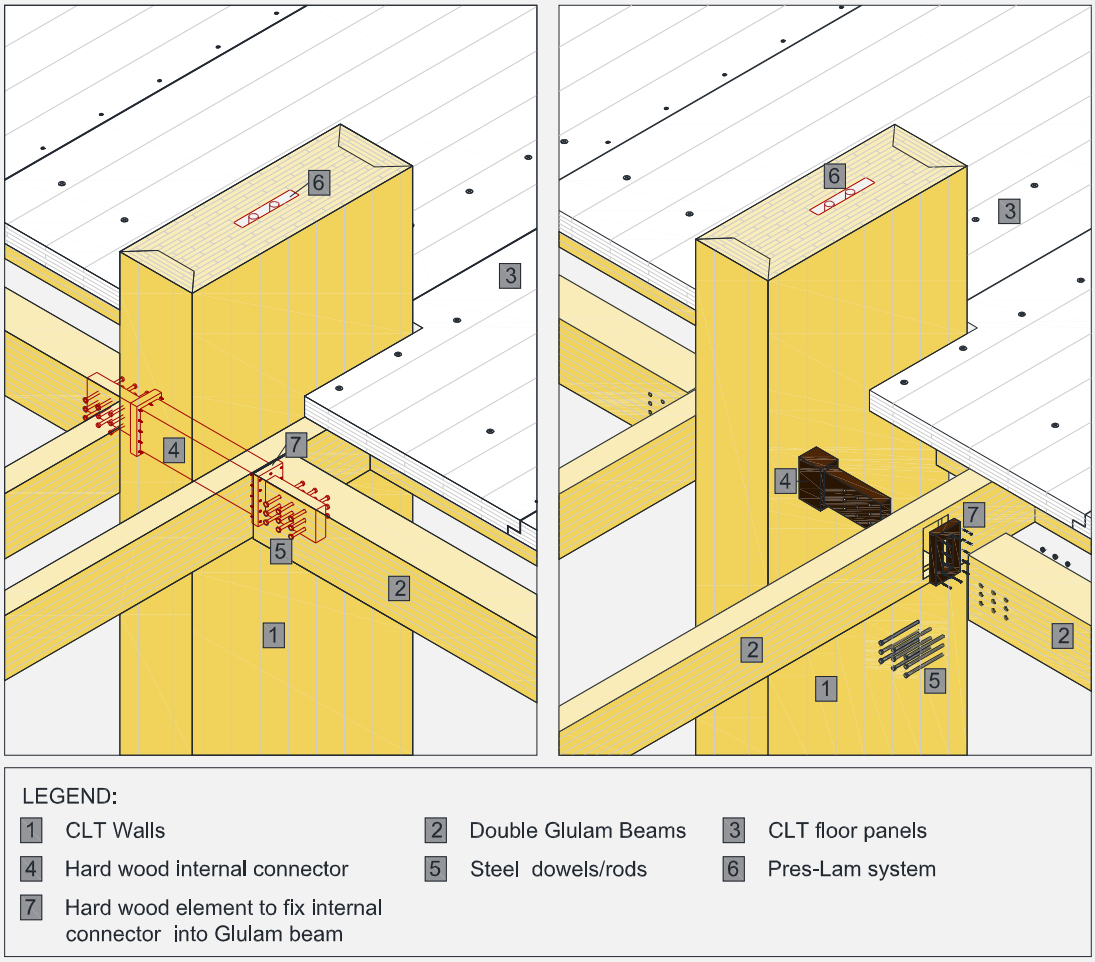

Figure (II) 1:26. Connection between double glulam beams and CLT walls by means of an internal hardwood connector.

2.2.2.2 Rigid connections

2.2.2.2.1 Connection between the reinforced concrete foundation/wall and CLT walls

As already mentioned, the need to apply Pres-Lam to the UT system, arise due to the weakness detected on the connection between the CLT wall and the reinforced concrete foundation. The contact area between both elements is too small to answer to the loads generated in a multi-storey building. Multi-storey timber buildings are characterized by a high flexibility due to the high number of connections needed and also due to the mechanical properties of timber. In structural terms, shear design for the base of the building will impose larger sections when lateral loads are considered.

Pres-Lam technology has been developed in New Zealand and it meant to be applied in large timber structures ((Palermo et al., 2006) (Smith et al., 2008) and (Iqbal et al., 2007)). During last decade, some

few commercial building has been built using this technique, namely: Nelson Marlborough Institute of Technology (Devereux et al., 2011) and Carterton Events Center (Palermo et al., 2012). Pres-Lam is constituted by high resistance pre-stress cables (Macalloy), that do not need to be continuous through all storeys, combined with located sinks (solid steel bars).

Dias (2017) estimated the located stresses on foundation when the building is subjected to extreme wind loads. He found that the maximum tension is of 539kN/m. So, due to the reduced weight of the building it can collapse when submitted to high horizontal loads. This ways, considering a building with 10 storey building, it would be necessary to apply pre-stressed bars with a diameter of 25mm of Macalloy type, located in the middle of each CLT wall.

Figure (II) 1:27 and Figure (II) 1:28 present two proposals for connection between CLT walls and the reinforced concrete foundation. Connection presented in Figure (II) 1:27 was proposed before the structural evaluation performed by Dias (2017). In that time, the connection was designed using a steel connector that rests directly in reinforced concrete foundation and is fixed by means of steel dowels/rods. The same steel connector goes inside the CLT walls by means of several steel plates. Necessary grooves on CLT wall, where the steel plates go inside, must be done previously. Steel dowels/rods would be responsible to fix steel connector to CLT walls.

The solution present in Figure (II) 1:28 resulted from the evaluation performed by Dias (2017) and is obviously based on an already tested solution proposed by Palermo *et al.*, (2012). The solution is extremely simple and the main element is the Macalloy steel bars in which pre-stress is applied. The connection is composed by lateral dowel bars casted in concrete and grouted in CLT walls and by Macalloy steel bars and Macalloy bar couplers. Lateral dowel bars work like energy dissipation devices, while pre-stressed Macalloy steel bars are responsible to answer high loads accumulated on the base of the building.

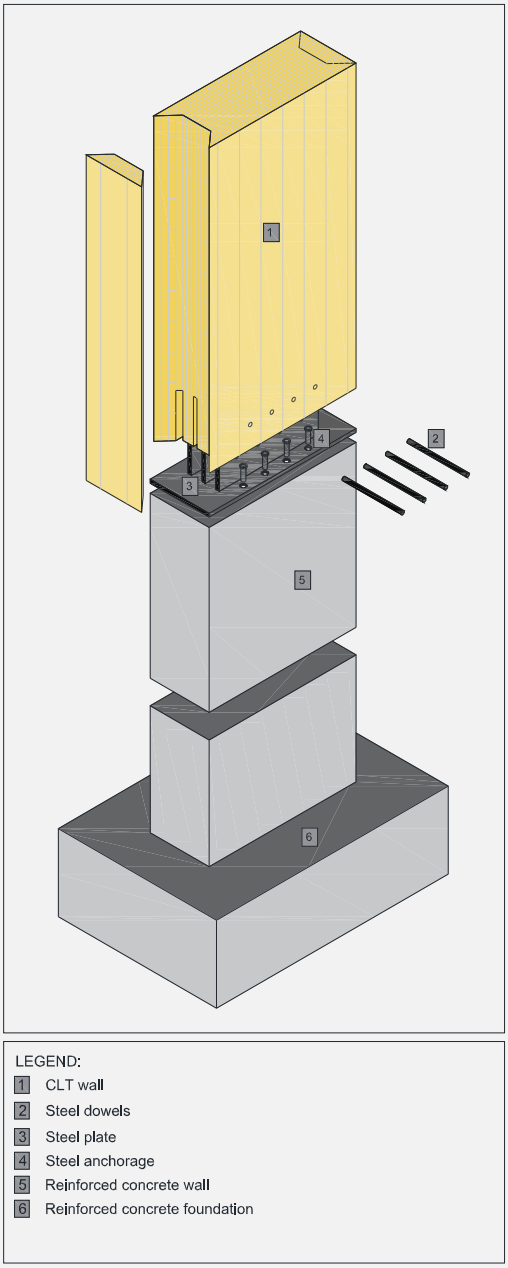

Figure (II) 1:27. Connection between reinforced concrete wall/foundation and CLT walls proposed before evaluation of the UT system.

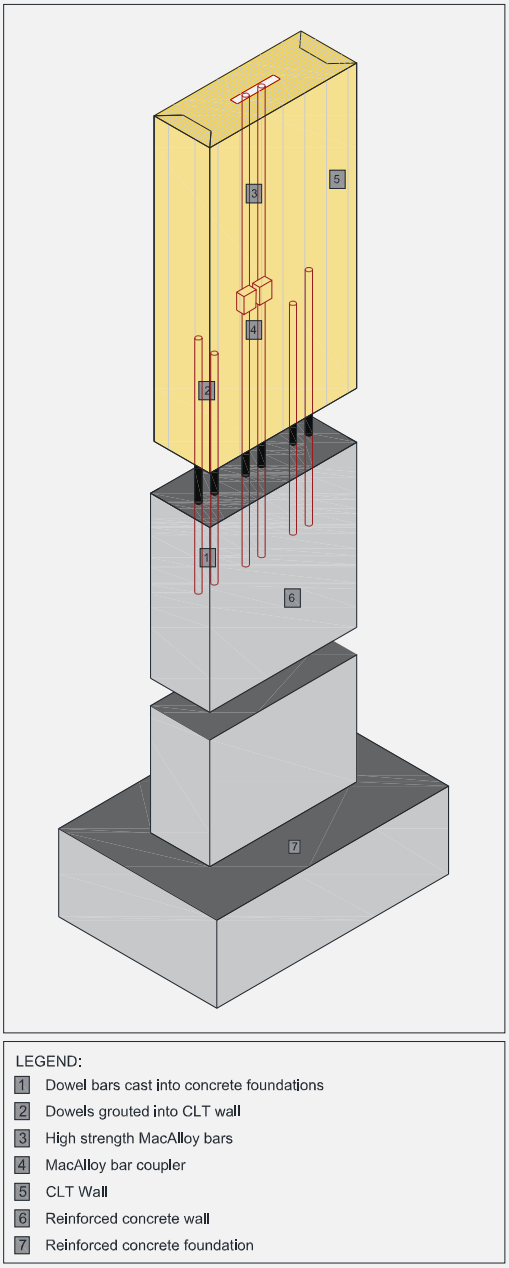

Figure (II) 1:28. Connection between reinforced concrete wall/foundation and CLT walls after Dias (2017) evaluation of the UT system.

2.2.2.2.2 Connections between CLT floors/CLT walls and CLT deep beams

CLT deep beams are strategic elements which sew up all the elements that compounds the structural system making it to work as a single unit. When a structure works like that, the stiffness of the building increases.

According to Dias (2017), the connection between CLT floors/CLT walls and CLT deep beams must be rigid and can be performed by means of self-tapping screws inserted diagonally to CLT planes. Screws are arranged under an angle of 45°, (or less if CLT deep beams are sloping) between screw axis and member axis in order to provide a higher load-carrying capacity compared to common shear connections due to the high withdrawal capacity of the self-tapping screws.

It is important to mention here that screws must always be inserted in the internal side of the building, in order to minimize the possibilities of contact with moisture sources. This subject will be discussed in more detail in the next chapter.

2.2.2.2.3 Connections between adjacent CLT floor panels

Diaphragms play a significant role on the performance of a building regarding lateral loads that can resulted from wind or earthquake actions. Together with glulam beams, diaphragms connect the elements which are responsible to resist lateral loads. Further, diaphragms are those elements which absorb lateral loads along all their perimeter, ensuring load transfer between façade elements and vertical loads resisting elements. So, the structural analysis performed by Dias (2017) shown that this kind of connections must be rigid. Regarding the dynamic behavior of a building, the research performed by Moroder (2016) shown some disadvantages associated to flexible diaphragms: increase of internal stresses in the diaphragms of lower floors and the displacements between floors are higher than displacements observed in structural walls. Generally, connections between adjacent floors are performed by self tapping screws. It is an effective and easy solution to apply.

2.2.3 Floor and wall sections

The performance of floor and wall systems, not only in the safety level but specially in terms of comfort, is a parameter of huge significance to make homes more attractive to potential buyers, in particular in cases of multi-storey timber buildings. In these cases, vertical and horizontal barriers must ensure that disturbance from one unit to the other are avoided (C. Sigrist et al., 1999).

Relatively to non-structural wall assemblies, the UT system suggests a non-load bearing light system based on gypsum boards with high levels of sound insulation. In contrast, CLT floor assemblies are a bit more complex. Figure (II) 1:29 and Figure (II) 1:30 present two possible solutions to apply in constructions which are based on the UT system. Presented proposals are based on suggestions published by Hu and Adams, Davide L. (2013). It was decided to present two possible solutions in order to keep the versatility concept always present, however both solutions suggested must be properly tested in order to guarantee its efficiency. Further, it is important to state that much more solutions are possible to apply in this structural system.

Figure (II) 1:29 shows a CLT floor assembly in which structural system is totally hidden by flooring and celling elements. According to Hu and Adams, Davide L. (2013), if a normal timber flooring system is required, it would be necessary to create an additional acoustic barrier in order to get the minimum acoustic comfort. This way, it is suggested a simple flooring solution composed by five layers, namely: timber floor, flooring underlayment, two low density wood fiberboards and flooring underlayment. Then, in order to fulfill the acoustic requirements, a ceiling structure needs to be created. So, celling must to be coated by two 15mm gypsum boards layers fixed by means of sound insulation clips. Further a 200mm fiberglass layer is located above gypsum boards. The location of rubber mat between elements is a key point reducing sound propagation.

Figure (II) 1:30 presents a solution that does not need a ceiling complement. For that, a less conventional floor system is proposed. This solution is composed by six layers, namely: pre-fabricated concrete topping with 20mm; kaft paper underlayment, subfloor of 25mm, 2 honeycomb acoustic infill of 30mm and again kaft paper underlayment. Here the huge advantage is that timber ceiling can be exposed, however it is important to alert that a concrete floor is not the suitable for residential proposes.

Both solutions respect sound transmission classes (STC) and impact insulation class (IIC) as well as reduce flanking transmissions that goes through shared structural building components (Hu & Adams, Davide L. (Adams Associates, 2013).

2.2.3.1 Fire protection

Combustibility of wood is the main reason why majority of building codes or regulatory requirements restricts the use of timber as structural material as well as the number of floors allowed (from 2 to 5 storeys for non-sprinkled buildings and from 3 to 8 storeys for sprinkled buildings (Gerard & Barber, 2013)). But, contrary to the general belief, wood can be more fire resistant than both steel and concrete:

(1) moisture content of wood delays its burning; (2) wood burns with a predicted charring rate; and (3) it creates a protective char layer which allows timber elements to be exposed for extended periods of time during a fire without sacrificing structural integrity and allowing time to evacuate the building (Mahlum et al., 2014).

Despite all these findings there is still who claims that *it is unrealistic to suppose that fire authorities will permit the unlimited use of timber for tall buildings worldwide in the near future* (Frangi et al., 2008). The main reason for this is related with specificities of fire safety for tall buildings. The worst scenario predicted in a case of a fire in a tall building is when a number of occupants located in the upper part of the building cannot leave the building nether the fire brigade can reach the fire compartment. In these cases, it is assumed that the fire cannot be extinguished and it continues until all combustible material in the fire compartment has burned.

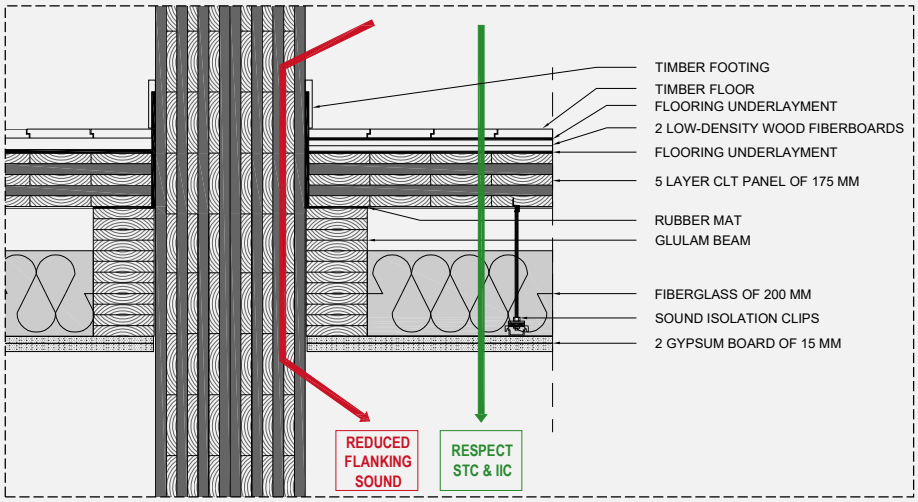

Figure (II) 1:29. Acoustic solution that hides all structural system.

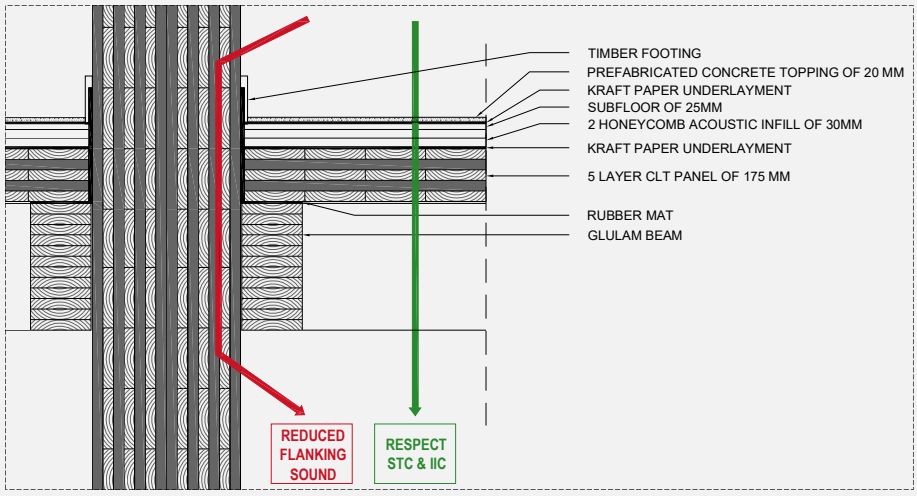

Figure (II) 1:30. Acoustic solution that exhibits part of structural system.

The UT system was obviously designed thinking on the advantages of exposed timber even if necessary to overdesign structural elements and use active fire protection devices installed for detection, alarm and suppression of fire. However, if it is not proven safe, the UT system can also use passive fire protection systems, designed to confine fire and smoke to designated zones, as well as "building encapsulation" which protects timber elements with a sufficient number of non-combustible claddings like gypsum plasterboards boards in order to prevent timber burning and consequent structural collapse.

Considering the known strength decrease of steel connections when exposed to high temperatures, the UT system looks to use embedded steel connects as much as possible. When it is not possible, encapsulation is the easiest solution.

2.3 Architectural considerations and adaptive design

2.3.1 External building appearance

The main architectural focus of the UT system is to maximize the freedom in the creative act that architecture represents. Figure (II) 1:31 shows a comparison between cellular construction and the UT system, regarding building shape possibilities. Beginning with plan shape, both structural systems allow the building to have different shapes (rectangular, triangular, hexagonal (...) or even organic shapes). The great difference between these different construction systems arises when the building is extruded. While buildings based on cellular construction system will result on a simple extrusion of plan shape, buildings based on the UT system can grow following angled paths. So, regarding general volumetric shape of building, the great innovative proposal of UT system is the possibility of creating angles between ground and façade planes.

Keeping the discussion on external view, the UT system places CLT walls perpendicular to façade allowing wider openings. This possibility combined with CLT deep beams allows to endow the building a strong sense of horizontality, what is totally impossible with a typical *cellular construction*. In a construction system that is totally based on structural walls, the continuity of opening is always broken by the location of vertical load paths on the façade plan.

Relatively to balconies and floating elements, both construction systems are compatible with them. These kind of elements are super common and in addition to its main function, it can easily be used as an architectural tool, in order to endow the building of a personalized shape.

CLT deep beams proposed by the UT system, perform an important role regarding either solar protection or aesthetic possibilities of the building. CLT deep beams can vary their height and shape and change their position relatively to floor plane, resulting in a façade system super versatile. That means that the technology behind the CLT production can be useful to architectural expression. The CNC technology enables the application of CLT panels with different shapes without impair the production process of structural elements. Despite prefabrication is often correlated with modular architecture, this does not means that it does not allow personalized solutions (Larsson et al. 2012).

In the case of buildings based on cellular construction, different shapes can also be given to the openings, offering the building a different dynamic, however vertical load paths will be always present. It is true that vertical supporting elements of the UT system are also in contact with façade elements, however the area of contact is reduced and its presence is hidden by CLT deep beams. When a rain screen walls is chosen, the presence of vertical supporting elements becomes even more unnoticed (Figure (II) 1:32).

The UT system is the result of a process that tries to dissolve the box suggested by *cellular construction*. As result, the perception of the plates as a bearing skeleton increases and the space enclosure is generated by a composition of separate elements. Considering the space configurations proposed by Bejder (2012), the *UT system* is located between the called *dissolved box* and the '*floating' structure*. Vertical elements do not define the interior space while CLT deep beams define the relation between interior and exterior.

2.3.2 Inner building flexibility

Relatively to internal spaces and its flexibility, the UT system does not offer an extreme open space concept, as proposed by Michael Green with the FFTT system, however, it allows to place interior frame lines without seriously compromising interior space planning (Figure (II) 1:31). When a construction system allows special flexibility, it is always an advantage. And why is that? Because the use of the building will not be defined by the building configuration. As more flexible is the space or as much less barriers exist in the space, more adaptive it will be. In other words, the use for the space will be defined by the owner/user and not by the architecture itself. This fact is valid for the first use, as well as for different uses that the space can shelter during its life time.

So, the goal of UT system goal was to make a space as much flexible as possible, being able to answer people shifting needs and serve a larger range of people for long periods of time. This way, *future changes can be simpler and more cost effective when planned for early in the design process and it can also*

increase a building's longevity (Build it Green, 2008). As observed in Figure (II) 1:31, cellular construction needs a lot of partition walls in order to make the building stand. So, or the building is developed for a pre-defined and definitive use or the building is doomed to failure. It is always better to bet on a structure that allows to create non fixed partition than make structural walls as definitive partitions walls.

Figure (II) 1:32depicts some possibilities allowed by the UT system in order to make inner spaces of buildings more special. As the structural walls of the UT system are perpendicular to the façade plane, they end up conditioning the interior space. Some solutions to reduce their presence in space are:

- to create inner or interior balconies with the total deep of CLT walls. This way, the structural elements will not be part of internal space and will not conditioning interior space layout;
- to create creative cuts on structural elements, making them decorative/furniture elements. CLT walls located in the facade can be used to support or to complement different kind of furniture;
- depending on its location, CLT walls can be extended in order to close a compartment that needs to be separated from others, such as the case of toilet areas.

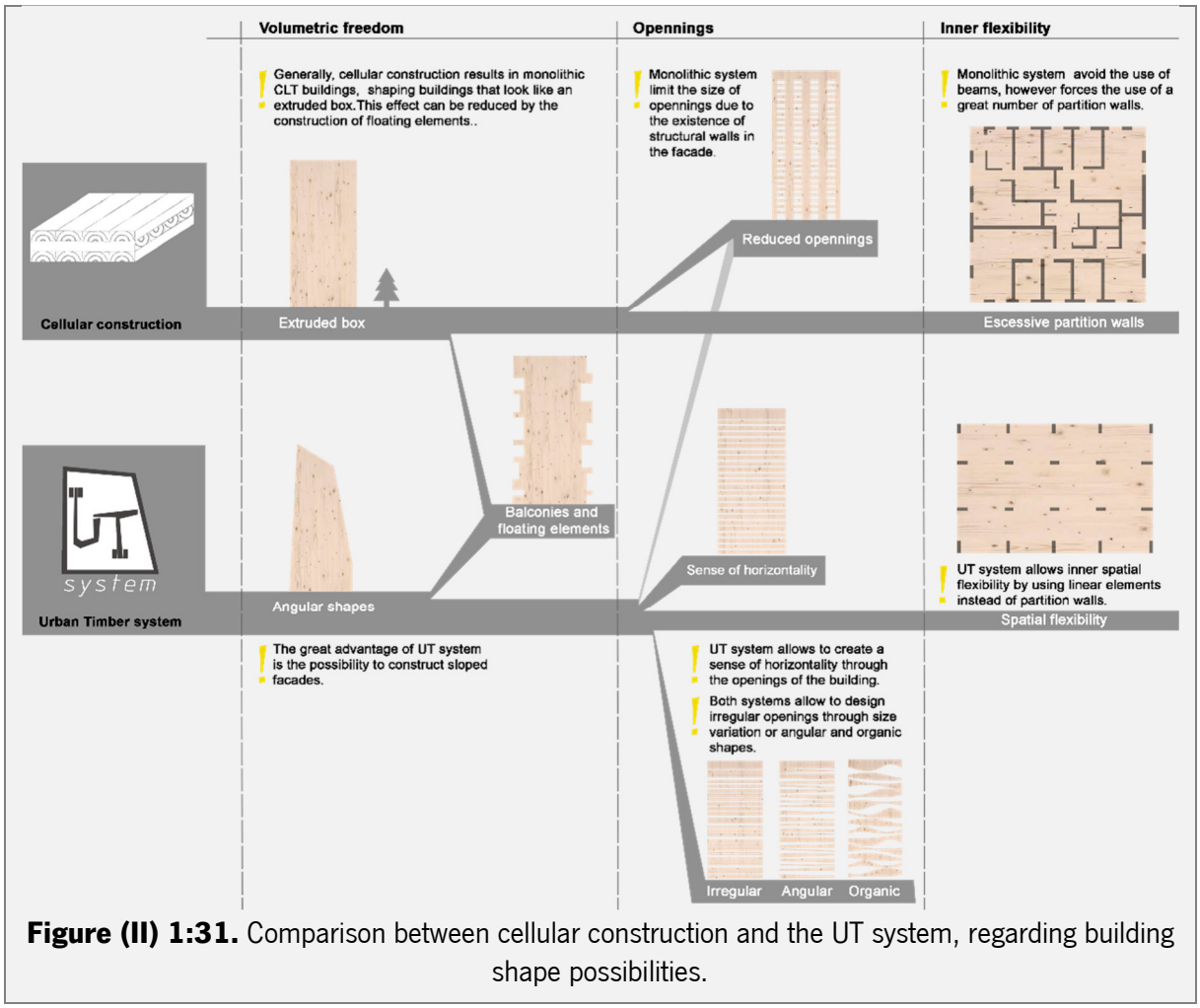

Figure (II) 1:31. Comparison between cellular construction and the UT system, regarding building shape possibilities.

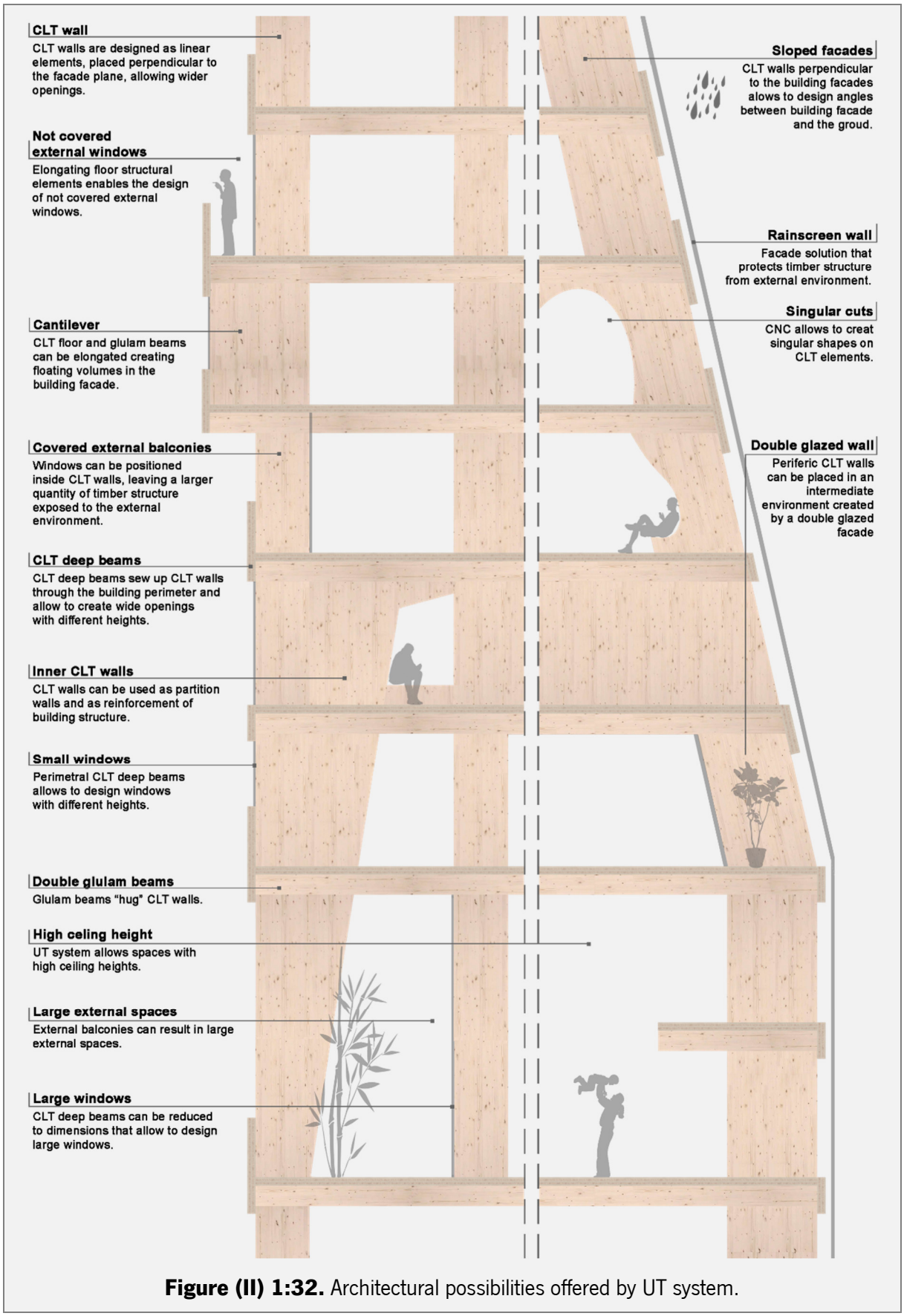

Figure (II) 1:32. Architectural possibilities offered by UT system.

Other interesting solution is the possibility to create spaces with high ceilings, once vertical structural elements can cover three storeys with just one CLT panel. This possibility is super interesting in some contexts, such as:

- creation of great building halls, when a high celling makes all the difference;
- creation of a high height balcony that allows communication between several storeys;
- double height internal spaces, not so common in multi-storey buildings.

Another goal of the UT system is to free the location of vertical cores that accommodate stairs and lift structures. According to Ali and Moon (2007), a bundled tube structure allows that freedom, however each case is different and must be studied individually. Anyway, the most favorable location is, as a general rule, the center of the building, and when the facades are always preferred to be part of using areas, that will not be a problem.

2.4 Design, production and construction

The main advantages of prefabrication were already described in chapter I of Part II of the present thesis. Considering them, the UT system tries to explore advantages of prefabrication in order to monetize the resources without compromise the quality of architecture produced and the singularity of each building.

As for any kind of construction, it is expected that a building process is initiated by a multidisciplinary team which will define in detail all production and construction process. Once project is concluded production must be initiated.

In the case of timber buildings, all structural elements must be produced using timber from sustainable managed forests that would be transformed and shaped off site following project recommendations in order to reduce as much as possible the tasks on site. It is important to guarantee that all the processes related with harvesting, transport and transformation of raw material must ensure the low level of environmental damages possible.

Digital design will be a precious ally for pre-fabricated constructions systems. This fact is of great importance once monotonous prefabricated architecture based on mass production will evolve to an original architecture based on made-to-measure components without imply a significant increase of costs (Lehmann et al., 2012). Further it is important to mention that the amount of waste on site is significantly reduced and its control is more efficient and simple.

Similarly to majority of timber systems, the UT system is a simple system based in large prefabricated elements. These elements must be produced considering the building sequence in order to guarantee the minimum number of deliveries possible. Once delivered on site, timber panels/beams are lifted by a crane and installed by a specialized team which will ensure an efficient and fast assembly. In particular case of the UT system, ballom frame system was selected as the better option, either due to construction facilities or specificities of material and structural system itself. So, in order to explore the advantages of ballom frame construction, CLT walls are produced with the height of three storeys (12,24m). Figure (II) 1:33 shows the building sequence: first the walls are erected, fixed to foundations and properly anchored, second double glulam beams are fixed to CLT walls, third CLT floors are fixed to double glulam beams and at last CLT deep beams sew-up all elements. Sequence from second to fourth steps is repeated more two times before erect CLT walls again. Erecting the building in stages of 3 stores per time is a great advantage regarding the reduction of construction time.

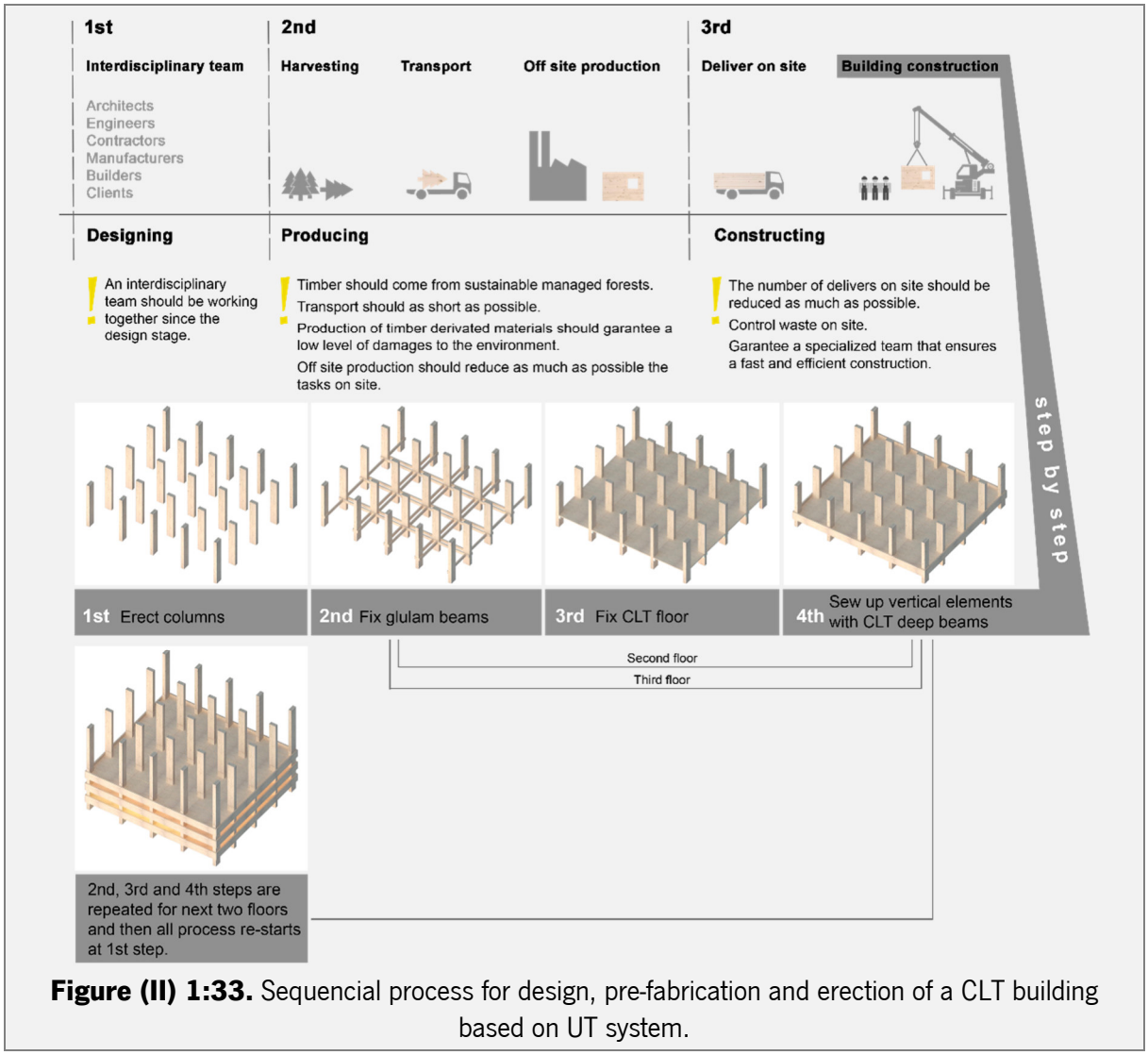

Figure (II) 1:33. Sequencial process for design, pre-fabrication and erection of a CLT building based on UT system.

2.5 Conclusions

The present chapter was dedicated to the presentation and description of the Urban Timber building as a construction system. Structural behavior, architectural considerations and construction process were the main themes discussed in here.

Regarding structural behavior, the function of each structural element was described and some possibilities of connections were presented. In order to understand in more detail the structural behavior of the UT system, Dias (2017) performed a structural evaluation of a building with 10 stories, which conclude that UT system is a feasible solution to shape future timber buildings. During his evaluation, he pointed some main problematics that must be considered:

- the connection between CLT walls and reinforced concrete foundations proved to be insufficient and the Pres-Lam system was pointed as a possible solution;
- lateral loads are a problematic that requests the development of ductility factors, especially regarding mechanical connections between timber elements. This way, it is imperative the development of experimental analysis on real scale for new solutions developed in order to quantify its behavior and verify its failure modes. This kind of researches must be developed considering each construction system individually;
- also a consequence of lateral loads is the vibration of CLT floors. The lightness of the material needs to be aided by a proper design that ensures minimum levels of vibration and the best structural behavior.

Dias (2017) also suggested some thematic for future investigations:

- to perform a complete dynamic analysis of the UT system;
- to define properly the behavior of the UT system in case of fire;
- to study deeply the effect of lateral loads on the UT system;
- to study different possibilities of connections;
- to study the influence of Pres-Lam when combined with the UT system.

Regarding connections between structural elements, Dias (2017) just define them as being dissipative or rigid connections, considering that all connections were made by metal dowels. This way, some possibilities were suggested in point 2.2.2 of the present chapter. Proposed solutions were developed taking as reference some existing solutions and considering some predicted problems such as

delamination and exhibition to fire scenarios. Obviously, all proposed solutions must be properly tested before state their efficiency.

Architectural considerations were presented always focusing on the versatility of the construction system either regarding external building appearance or inner building flexibility. In order to evaluate the advantages of the UT system, cellular construction system was used as reference of common CLT construction. Greater advantages associated to the UT system are:

- allows to shape sloped facades;
- offers the possibility to endow the building a sense of horizontality;
- the location of CLT walls are punctual resulting in a high level of spatial flexibility;
- allows the creation of high ceilings;
- CLT walls perpendicular to façades can be used as a decorative/furniture element;
- CLT walls can be placed outside the building by the creation of balconies.

As already explained, the present thesis was specially dedicated to moisture induced effects on CLT and the UT system was designed always taking into account this principle. Therefore, all research dedicated to other issues related with CLT construction were briefly studied. Obviously there is an infinity of subjects and details of the UT system that can be studied in more detail. Some suggestions are:

- to explore the architectural possibilities of the UT system, proposing different building shapes and testing its versatility by its adaptation to different uses;
- to suggest and test effective solutions able to fulfill fire safety legal requirements;
- to test connections here suggested and suggest new possibilities depending on the obtained results;
- to test the limits of the UT system regarding the number of stories;
- to test and suggest new solutions regarding floor and wall sections.

CHAPTER 3 (II)

3 INTEGRATED DESIGN OF THE UT SYSTEM CONSIDERING MOISTURE INDUCED EFFECTS

3.1 Introduction

As already observed, when timber is used as structural material it is, most of the times, hidden behind different wall coverings, either in outside façade or in inner spaces. In other words, timber is used merely as a substitute for steel or concrete, without being considered their unique aesthetic qualities and physical properties. In most examples, architecture is too often more or less reduced to an anonymous white gypsum surfaces where it is impossible to identify the structural building materials hidden underneath.

This protective measure is often taken due to the lake of knowledge about timber and its based materials. Obviously, timber construction has to proof to be safe in case of fire (Frangi et al., 2008) (Gerard & Barber, 2013), earthquakes (M. Fragiacomo et al., 2011), to be acoustically and thermally comfortable (Christophe Sigrist et al., 1999) (Hu & Chui, 2013) and moisture resistant (C. Silva, Branco, & Lourenço, 2014) (Green & Eric Karsh, 2012) (Build it Green, 2008), however, in most of times, independent of its properties, timber structural elements end up totally hidden.

In past few years, some innovative proposals for multi-storey timber buildings are looking for sustainable solutions for our denser cities. Cross laminated timber (CLT) has been a transversal material being the leading figure in majority of constructed buildings and proposals for new construction systems. For this reason, CLT was the main material selected to shape the UT system. Further, due to the lack of knowledge, the UT system was developed attending special attention to moisture effects on timber structural elements. The present chapter will use the UT system to describe and illustrate construction details which aims to prevent unwanted moisture effects.

Experimental evaluation performed focused on the effect of moisture induced effects on CLT, considering timber movements and consequent stresses created between layers, as well as the consequences on mechanical connections performed by self-tapping screws. Experimental campaign and obtained results are described in Part I of the present thesis. Obtained results were crucial to the development of the UT system, either regarding the location of structural elements or the definition of construction details. Structural elements were positioned considering swelling and shrinkage elements and the effect of such movements in the building as a unit. The connections between structural elements were also object of special attention. Different possibilities of barriers between interior and exterior spaces were considered: façade elements, eventual balconies, different positions for balconies and roof.

Despite Part I and Part II of the present thesis look to be totally independent researches, they complement each other. In fact, the contact with material and the awareness about the behavior of CLT when

submitted to moisture changes was crucial for the author to propose a construction system. It is not common to the architect to get a deep knowledge about the construction material and most of times he always applies recommendations of manufacturer without questioning or innovating. Besides the results obtained by experimental campaign developed in the scope of this thesis, bibliographic suggestions were also of great significance, once they also performed tests based on important subjects not directly studied in here.

3.2 Moisture induced effects on CLT elements

All the main concepts linked to the effects of moisture variation in CLT elements are properly explained in Chapter I of Part I of the present thesis. Anyway, a brief explanation will be made here. In very simple words, timber hygroscopicity means that the material is permanently ready to release and absorb water (absorption and desorption phenomenon) when exposed to fluctuating atmospheric humidity. Fragiacomo et al. (2011) calls this exposure of "humidity load", which should be subdivided into various categories, such as external conditions (sheltered or not from precipitation and sun radiation), interior conditions (heated or unheated buildings), and even the activity that building shelters.

Both indoor and outdoor structures are exposed to an environment with changing relative humidity and temperature, and in consequence, the moisture content in wood structures will normally change during their use. The most severe effects often take place when the building is new. It is quite common that wood with higher moisture content is built in and then dried after the building is heated. Timber hygroscopic behavior is a very important issue regard to timber building physics because changes on timber moisture content affect physical, mechanical and rheological properties of wood, such as: shrinkage/swelling, internal stresses, strength properties, durability, and decrease of connections resistance.

3.2.1 Shrinkage and swelling effects on CLT

The shrinkage/swelling capacity of CLT is not affected regarding its thickness direction, however the crosswise arrangement, shrinkage/swelling movements in-plane movements are reduced. Augustin (2008) says that moisture movements of CLT panels are too small to be measure over the panel surface: less than 1% in across the grain direction and 2% in cross-grain direction. These numbers were verified by an experimental campaign developed in the context of the presented thesis, in which high shrinkage/swelling movements were: 0,3%/-0,27% in across the grain direction (X) and 1,55%/1,28% in cross-grain direction (Y), respectively – see point 2.4.2 from chapter 2 of Part I of the present thesis.

The moisture content of mass timber elements must be controlled from the production to the end of construction, in order to ensure lowest swelling/shrinkage during the life of a building. Beyond this important caution, if the behavior of material is well known, the way it is applied can be changed/adapted in order to reduce the consequences caused by unavoidable changes caused on material properties by moisture changes. Obviously, is an advantage when solutions like cross lamination proves to be efficient on the reduction of timber movements caused by moisture changes. Anyway, if the material is properly known it is possible to work leading with its characteristics and adapt the design to them. One good example of this adaptive design is the Ballom Frame construction which reduces the shrinkage/swelling through the height of a building (Green & Eric Karsh, 2012). According to Glass et al. (2013), when Platform frame construction system is chosen to shape a timber building, quantified cumulative shrinkage over the height of the building is around 3mm per story. Three millimeters may seem insignificant, however it is reason to require special attention during the design of external envelop of the building, in order to avoid possible future damages.

Besides the simple variation of dimensions, changes on moisture content of CLT elements can cause important changes on mechanical properties of material. Gülzow et al. (2010) studied the effect of changes of moisture content on MOE and shear modulus of CLT and concluded that, similarly to solid timber, both parameters decrease at they mean level towards an increase of moisture content. However, authors emphasized that swelling of the timber grain leads to an apparent increase in the modulus of elasticity for small service loads due to internal component friction. In the other hand, cracking resulted from the reduction of moisture content leads directly to a distinct decrease in the bending stiffness perpendicular to the grain direction on the face layers.

3.2.2 Moisture induced stresses

When CLT panels are exposed to changes in the relative humidity of the ambient air, the restriction of wood movement caused by crosswise bonding of layers can result in moisture-induced stresses and deformations (warping and checking).

Moisture gradients are also an important moisture effect which may affect the stress of wood. This effect results from the slow moisture diffusion in wood when humidity load is variable or different from initial equilibrium. As previously mentioned, when wood is exposed to variable humidity conditions it absorbs and desorbs moisture from the air. However, wood needs long time periods to reach equilibrium for different levels of relative humidity, depending on timber size it can take several weeks or even months

(Time, 1998). This means that timber structures are affected by climatic variations (fast climatic changes), which do not let wood reach equilibrium. As result, moisture gradients are induced in wood sections and hence internal stresses arise. Moisture gradients combined with the restriction of wood movement caused by CLT crosswise bonding induce important differences in shrinkage and swelling of wood, which will develop so-called moisture induced-stresses (MIS), due to constrained swelling or shrinkage strains. Often MIS lead to cracks either in timber surface or in central part of timber sections. In fact, serious structural damages can occur and shape distortions may reduce the serviceability of structural elements (Kim et al., 2010) (Sjödin & Johansson, 2007).

One solution to prevent these phenomenon is based on the drastic application *of coatings on the timber surfaces exposed to weather conditions in order to reduce the moisture exchange with the environment and thus moisture induced stresses low* (Angst & Malo, 2012b). Further, to minimize the impacts of MIS in CLT panels, it is also important to use timber boards with the same moisture content. If the moisture content varies between individual boards residual stresses will develop differently as each layer shrinks or swells, what can significantly weaken the bond strength, causing joint failure and lead to excessive cracking (Harch, 2010).

3.2.3 Timber decay

Wood is an organic material which needs to be protected from moisture in order to avoid a material decay. As a timber based material, CLT demands exactly the same precautions. Fungi are one of the biggest wood enemies, however they need the right environment to live and feed on the cellulose, hemicellulose and lignin from wood cells. To perform an attack, fungi needs sufficient moisture, nutrients, oxygen, and a reasonably warm environment. Further, this kind of attack results on reduction of timber mechanical properties only if the same condition remains for a significant period of time (Wang et al., 2010). According to McClung (2013), wood is considered safe from decay if it is exposed to temperatures below 10°C and a maximum moisture content of 20%, which provides a safety margin for wood species with poor decay resistance.

3.3 The UT system answering to the conditioning of a moisture sensitive material

When a structural system based on a moisture sensitive material is developed, some special cares needs to be taken care of. As already mention before, when it is possible to adapt the design of the system to the material characteristics it is always preferable. It is important to keep always present that the material properties must be explored and not camouflaged or altered.

The UT system is an attempt to follow this principle. From definition of structural elements and the way they are linked to each other to the design of a mechanical connection, the influence of moisture induced effects were considered. Present section will describe all structural system and explain how it was thought regarding moisture induced effects on CLT.

3.3.1 Structural elements

Structural elements of the UT system are reduced to a small number of elements. There are CLT walls that work almost like columns, glulam beams that join all CLT walls, CLT floors/diaphragms that rigidify the structure and CLT deep beams that sew up all the elements.

CLT walls are the main load-carrying elements which get the loads of each floor from glulam beams and drive loads to the foundations, either through a vertical path or an oblique one. These vertical/oblique walls work also like shear walls, resisting lateral loads by being oriented perpendicular to the façades (Ali & Moon, 2007). CLT floors work together with double glulam beams, improving the building stiffness and avoiding the effect of progressive collapse. Finally, CLT deep beams sew up all individual tubes in the building perimeter.

Focusing on the adaptive design, the system is based on the Ballom Frame construction principals. Based on this decision, vertical structural elements are designed to be continuous avoiding all possibilities of accumulative shrinkage/swelling inconvenient resulted from floor structures. Similarly to FFTT system, shrinkage/swelling movements of CLT floor, especially on its thickness, will not accumulate over the building height. Further, drainage wall does not need special care to protect lateral side of CLT floor once it will not face the building facade. Being continuous, CLT walls will just accumulate the shrinkage/swelling movements developed through longitudinal direction of CLT panels (X direction indicated in experimental campaign described in chapter II of Part I). According to test results obtained within this thesis, movements on X direction will be always less than 1% even when submitted to extreme humidity changes. It must be recalled that performed tests submitted CLT specimens to RH cyclic changes that varies between 30% and 90%.

Here it is also important to mention that despite structural and architectural reasons, CLT walls are placed perpendicular to the façade reducing the area of contact with external environment. However, there is the disadvantage to put in contact with the exterior environment the face of CLT that absorbs water more quickly. In fact, the area in contact with external environment is reduced, however the protective measures against moisture must be effective.

Double glulam beams, those are placed sideward to CLT walls and fixed to them by means of steel connectors or hardwood elements. Different possibilities for this connection were presented in chapter II and will be analysed regarding moisture content issues forward in the present chapter. Here it is important to argue why double glulam beams are placed sideward of CLT walls. In terms of timber grain direction, the thickness of CLT wall will correspond to radial direction. So, considering the performed tests by the author of present thesis, in worst scenario it will swells in maximum 2% of its thickness and shrinks less than 1% of its thickness. For the building evaluated by Dias (2017), it was considered a thickness of 600mm resulting in movements of 12mm when it swells and 6mm when it shrinks. Adding to CLT wall movements, there is the movements of the glulam beams which needs also to be considered. Still considering the movements on CLT walls thickness, glulam beams will swell and shrink in tangential direction. Further glulam beams will also swell and shrink in radial direction, though its height. That is why it is suggested that CLT Floor are not directly connected to CLT walls. Similarly to glulam beams, CLT floor will swell and shrink in its radial direction without interfere with CLT Walls.

CLT deep beams will be placed in the building perimeter hugging all structural elements. In this way, it will be free to move either in radial or tangential directions without compromise the remaining structural elements that are directly in contact with them.

If the timber movements are considered high, it could be considered the possibility of reducing them by means of conditioning moisture flow through timber fibres. As observed in Chapter 2 of part I, the possibility to reduce the moisture induced strains is to condition moisture flow on longitudinal direction, however the effect of such measure must be tested on large scale panels in order to verify if such measure do not result in significant deformations.

Foundations are made of reinforced concrete in order to avoid prevention works related with subterranean termite and the use of preservative treated wood. Further, despite its low eco-friendly profile, concrete elements can be significantly smaller, when comparing to a fully concrete building due to low weight of timber. Assuming a conservative stance, the UT system resorts to reinforced concrete to shape foundations as well as underground floors and first floor. Connection between concrete and CLT walls are made 3 meters up from ground level and is performed by a built-in steel connector anchored in concrete wall and steel dowels are used to fix CLT wall or by means of Pres-lam system. If the exposed concrete is not an attractive option for designer, concrete wall can be easily covered with timber boards obtained a final look similar to CLT.

3.3.2 Façades

Despite the significance of the building envelop on its energy efficiency, indoor air quality and occupant comfort, a special attention has to be given to durability when a timber building is being designed. It is essential to control water intrusion, air flow between interior and exterior as well as water vapour diffusion. As already mentioned in the state of the art (chapter I of part II), timber buildings can last as any other. However, it is mandatory to detail the building properly in order to keep structural elements with safe levels of moisture content. So, detailing a façade of a CLT building must consider two main issues: ensure effective drainage of the façade plane and ensure a diffusion-open, but airtight solution. Unfortunately, a CLT panel cannot be used simultaneously as cladding and structural material. Similarly to solid wood, CLT is a moisture sensitive material and have to be adequately protected from any moisture sources. Obviously the main reason for that is related with durability issues and protection of timber element from rotting. However, there are other compelling reasons for such protective measures: the simple contact of panels with two distinct environments (exterior and interior) can cause significant strains in timber elements and consequently distortions on CLT panels. That is why an effective drainage of façade plane is crucial for a good performance of a timber building.

However, the accumulation of water on timber elements may not be result of a poor drainage. One of the most observed errors when a façade is detailed is the application of non-organic materials, free of hygroscopic properties, like, mineral wool, together with organic materials like timber. In a situation like this, the risk to trap water vapour between insulation material and timber element is too high. Wood is a hygroscopic material that absorb and realises water vapour naturally, so betting on a simple airtight solution will not work properly. A diffusion-open envelop, that self-regulates moisture flows, interacting with surrounding environment ensures the ideal conditions for timber elements to last. All wood-based products in the cellulose-based system offer hygroscopic properties which allow them to absorb and release moisture. Diffusion-open vapour barriers can be used to ensure airtightness, but the principle is to let the building envelope breathe by taking up, storing and releasing moisture. This gives a pleasant indoor climate and better air quality.

Aware of this real problem, countries where timber construction is much common are adapting modern building techniques to the inherent properties of timber. This means that they are looking for a solution that create an airtight but diffusion-open building envelope that self-regulates natural absorption and releasing moisture. In other words, they are looking for an organic wall that interacts with surrounding environment in order to balance humidity (Rönnelid et al., 2013). It is important to mention here that,

carefully CLT produced panels are able to airtight a building, however cracking will inevitably happen over time. So, an airtight solution may always be suggested.

Looking for an effective solution of a facade compatible with the UT system, four different possibilities for façade drainage are proposed. Figure (II) 1:34 and Figure (II) 1:35 present solutions based on the concept of rain screen system, which is known as the most efficient solution for façade drainage of multi-storey buildings (Build it Green, 2008). Figure (II) 1:37 and Figure (II) 1:38 present solutions based on the glazed curtain façade which is a much appealing solution for architects.

As already mentioned, the exposure of timber elements to two environments with different moisture levels can be a problem and cause important distortions and damages. Considering this fact, the four solutions proposed by the UT system also considering the position of CLT walls regarding the barrier between interior and exterior, trying to reduce the exposure of CLT walls to different environments: (I) when the UT system consider a rain screen system CLT wall are entirely on inside environment while CLT deep beams are the elements that make the border between interior and exterior (Figure (II) 1:34); (II) when it consider balconies in the entire perimeter of building, CLT wall are almost entirely on outside environment (Figure (II) 1:35); (III) when it consider an external continuous glazed curtain wall, entire building structure are on inside environment (Figure (II) 1:37); and (IV) when it consider a double glazed curtain wall CLT walls and deep beams are placed in an intermediate environment (Figure (II) 1:38).

3.3.2.1 Rain screen system

Rain screen system must ensure an efficient vapour permeable wall set. According to Glass *et al.* (2013), uncontrolled air leakage can cause moisture accumulation and interticial condensation and consequently CLT decay, besides other problems related with building energy performance, indoor air quality, and occupant comfort. Rönnelid, Wik and Janols (2013), suggest the substitution of mineral wool by an impregnated plywood and a weather shielding sheet. The wood fiber insulation on the other hand has very good hygroscopic capabilities, which means that water is absorbed and released in balance with the moisture level of the surroundings. Contrary to some proposals (Skogstad et al., 2011), which defend CLT air leakage, a vapour permeable and water resistant barrier is recommended. It will prevent moisture causing effects on CLT elements as will also allow drying of construction moisture and drying in service. Vapour permeable materials are desirable for all wall set in order to guarantee the desirable drying capability of entire assembly. Therefore, besides the main drainage plane, created by exterior cladding, two extra drainage planes are created: an air gap between exterior cladding and insulation layer and a

vapour permeable and water resistant barrier applied directly to CLT surface. This is a conservative solution that create two extra drainage planes that will catch the water that passes through the exterior cladding and avoid the possibility to the moisture reach timber structural elements (Glass et al., 2013). Further, a wind barrier is placed in the gap between external cladding and insulation layer, as recommended by Skogstad, Gullbrekken and Nore, (2011). This same gap should be ventilated, though openings at the top and bottom of wall assembly, in order to assure drying of materials. External cladding is fixed to a threated wood strapping, which in turn is fixed to CLT panel with compatible corrosion resistant long screws through the insulation layer. This last has to be rigid enough to avoid compression at screwing time and water resistive in order to drain the water away from the building quitly. Examples are: extruded or expanded polystyrene, mineral wool (Teibinger & Matzinger, 2013) and cork (which is an eco-friendly solution) (T. Silva, 2014).

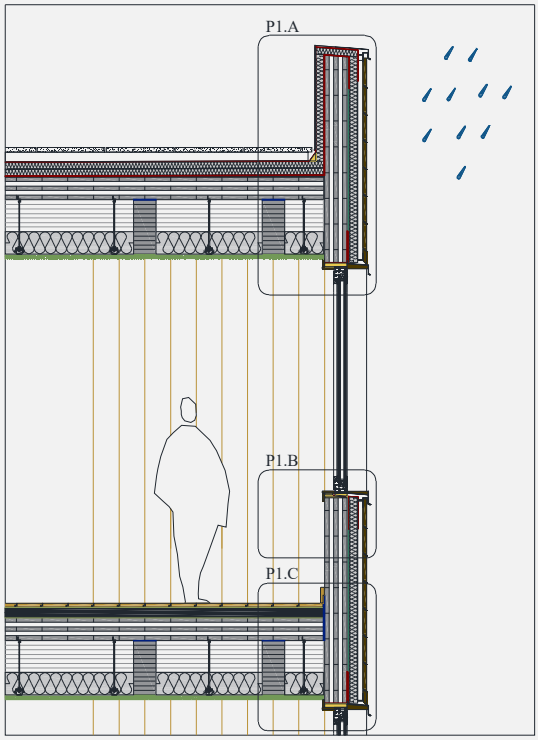

Figure (II) 1:34. Façade solution based on rain screen concept, in which water from the rain run a direct path directly to the ground.

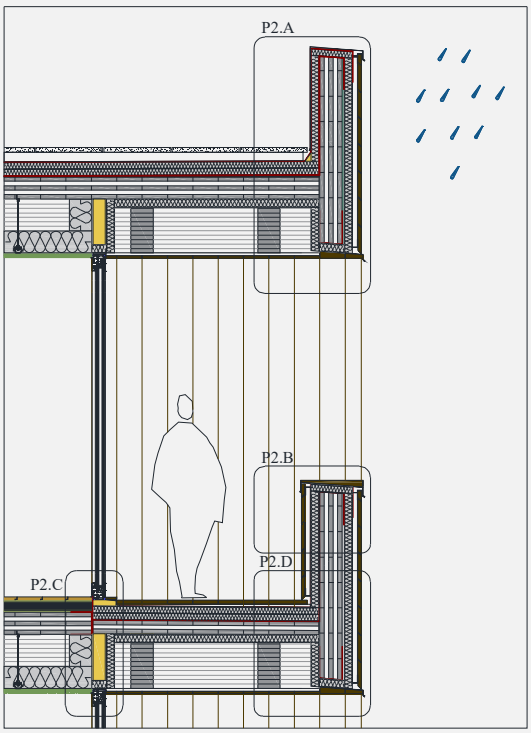

Figure (II) 1:35. Façade solution based on rain screen concept, in which water from the rain must be drained from façade plane and from external balconies.

In Figure (II) 1:36 it is shown a cross section in which it is possible to observe all layers suggested for the proposed rain screen façade. First of all, it is mandatory to mention that CLT panels tops must be sealed by means of bitumen sheet. As it was observed in part I of present thesis, CLT absorbs more water when it goes through fibre direction. In this way, the top of CLT deep beams are properly sealed once they are

elements that are exposed to external environment and must be kept with safe levels of moisture content. Then, two layers of vapour permeable water resistive membrane are placed before and after a rigid insulation element. As explained before, vapour permeable membranes will help to keep the natural hygroscopic behaviour of timber while rigid insulation layer will complement the thermal behaviour of timber as well as will help to block rain water to reach CLT panels. An air gap is placed after external cladding in order to allow the ventilation and drying of façade elements in case of heavy rain.

The main difference between the two solutions based on the rain screen system is the introduction of external balconies. The main discussion related with creation of external balconies is related with the question: Should the internal structural floor be extended to the outside environment or an independent structure must be coupled to the building? The difference between both solutions will be explained in section 3.3.3. of present chapter.

3.3.2.2 Glazed curtain wall

The other two possibilities proposed to shape façades of the UT system are based on the glazed curtain wall concept which, contrary to rain screen system, does not require the CLT elements sealing, once they are protected by a glass facade. We can tell that this might be the greatest advantage of a glazed façade. It exposes CLT structural elements in such a way that they can be contemplate either from inside or outside contributing for an eco-friendly and warm environment. The solution shown in Figure (II) 1:37 is composed by a single curtain wall while the solution shown in Figure (II) 1:38 create an inner balcony with a second layer of windows. Both solutions make the entire structure waterproof, and apparently avoid all cares related with CLT durability and building envelop design. Further, depending on the structural requirements, CLT deep beams can be reduced or avoided making the building completely transparent, alloying to explore daylight benefits and offer to the users the better views. However, not all are advantages! In a glazed curtain wall solution, instead of moisture, CLT has to deal with temperature issues and consequent demand for cooling/heating systems. High temperatures will reduce moisture content levels of timber elements, so cooling and ventilation systems will be imperative to ensure the health of structural system. Despite thermal issues, large openings will force the use of high performance windows, able to improve energy efficiency, reduce heat gain and loss, reduce noise levels, reduce condensation and improve comfort (Build it Green, 2008).

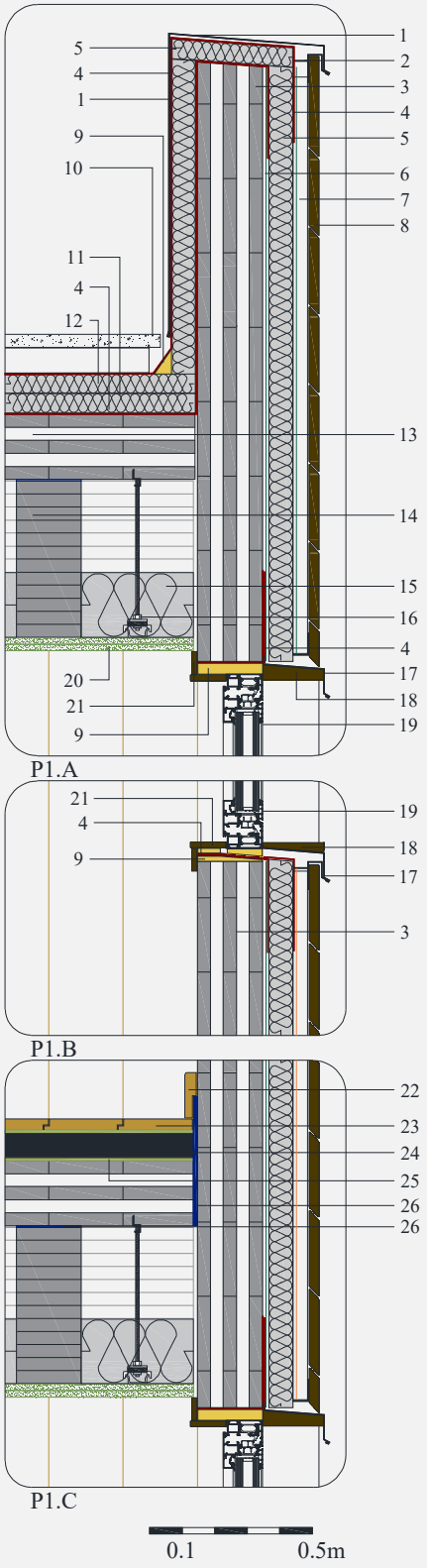

LEGEND:

1. Sloped metal roof cap-flashing with end dams
2. Bug screen
3. Five layers CLT deep beam
4. Bitumen sheet
5. Rigid insulation
6. Vapor permeable water resistive membrane/ Air/wind barrier
7. Drained and ventilated air space; wood strapping for cladding fixation
8. Non-combustible cladding
9. Shim
10. Pre-fabricated concrete plates
11. Two layers of water proof rigid insulation with staggered joints
12. Tapered rigid insulation layer
13. Five layers CLT slab
14. Glulam beam
15. Fiberglass of 200mm
16. Sound insulation clip
17. Sloped metal window flashing with end dams
18. Non combustible outer window rim
19. Window assembly
20. Two gypsum boards of 15mm
21. Timber inner window rim
22. Timber footing
23. Timber floor
24. Two low density wood fiberboards
25. Flooring underlayment
26. Rubber mat
27. Sloped metal facade flashing with end dams
28. Cover balcony
29. Non combustible balcony floor
30. Strapping for floor fixation
31. Three layers CLT floor for balconies
32. Timber section for window fixation
33. Sloped metal roof cap-flashing aligned with glass wall
34. Timber frame for glass wall fixation (UNIGLAS ®)
35. Five layers deep beam with water resistive protection
36. Fixed glass panels (UNIGLAS ®)
37. Metal connection between timber frame and CLT deep beams
38. Second inner window assembly

Figure (II) 1:36. Detailed solution in which the UT system proposes a continuous rain screen system.

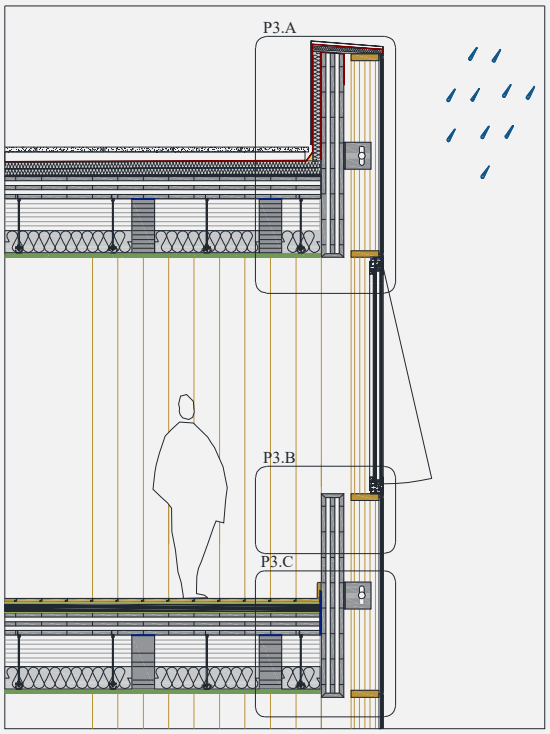

Figure (II) 1:37. Façade solution based on a simple glazed curtain wall.

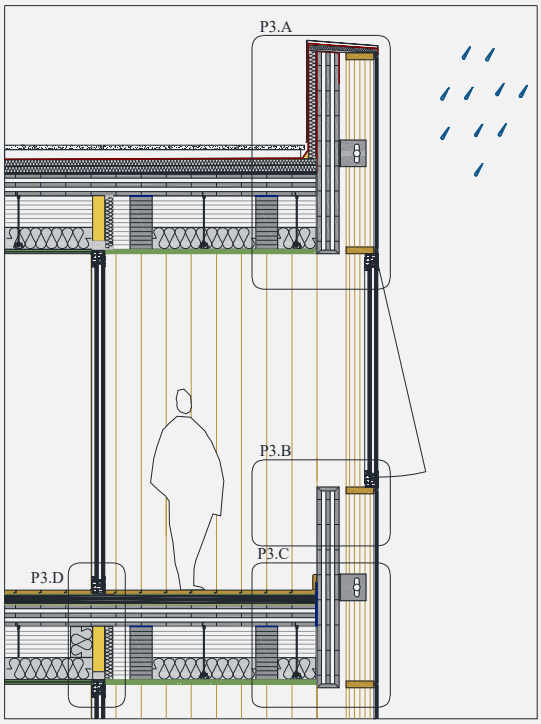

Figure (II) 1:38. Façade solution based on a double glazed curtain wall.

Considering that high temperatures can lead to a reduction of moisture content of timber elements, it is necessary to mention here that this fact may not be a serious problem to the health of timber structure. According to the study performed in present thesis (section 3.3.2 of chapter 3-Part I), at least with regarding to the behaviour of self-tapping screwed connections, while timber elements keeps its moisture content between a range of 8-12%, withdrawal capacity of connections will not be affected. Regarding moisture induced strains caused by cyclic moisture changes, present research concluded that crosswise lamination of CLT is effective on reduction of timber movements (chapter 2 – Part I). Further, performed tests also showed that strains tend to reduce as the number of cycles increase. This can mean that timber elements tend to adapt to moisture changes.

The solution shown in Figure (II) 1:38 places CLT walls in an intermediate position between indoor and external environments. It would be necessary to perform adequate studies to understand if it is a good or bad solution. However, it is evident that structural elements would be placed in a kind of greenhouse, that protect interior space from direct temperature changes from outside. So, the structural element will not suffer from sharing different environments at same time, but it will still deal with drastic changes during day and night and different seasons. Further the probability to generate condensation is higher, demanding an efficient ventilation system. Similarly, to the gap created in rain screen system, these

internal balconies must be ventilated in order to keep all the wood dry and safe from moisture accumulation. The advantage here is that the entire element is totally inside the same environment what means that it will behave equally regarding moisture/temperature induced effects.

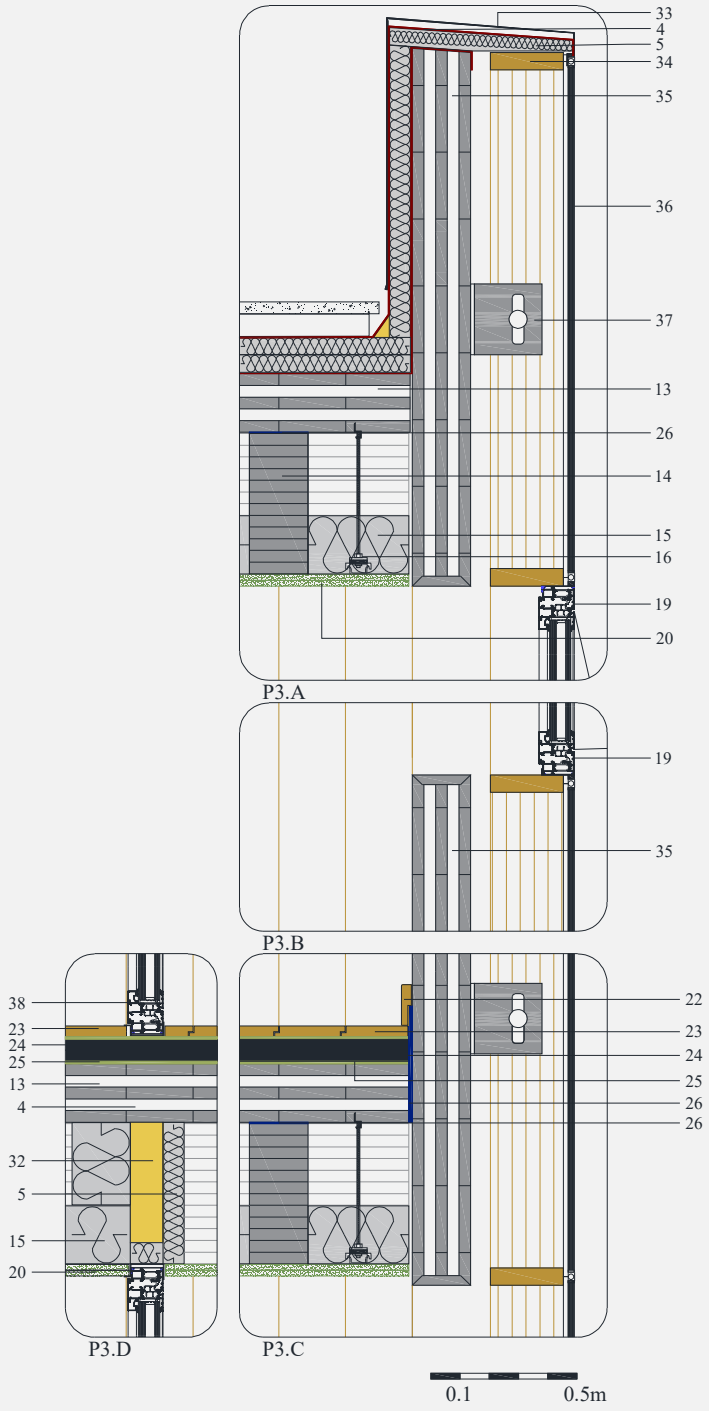

LEGEND:

1. Sloped metal roof cap-flashing with end dams
2. Bug screen
3. Five layers CLT deep beam
4. Bitumen sheet
5. Rigid insulation
6. Vapor permeable water resistive membrane/ Air/wind barrier
7. Drained and ventilated air space; wood strapping for cladding fixation
8. Non-combustible cladding
9. Shim
10. Pre-fabricated concrete plates
11. Two layers of water proof rigid insulation with staggered joints
12. Tapered rigid insulation layer
13. Five layers CLT slab
14. Glulam beam
15. Fiberglass of 200mm
16. Sound insulation clip
17. Sloped metal window flashing with end dams
18. Non combustible outer window rim
19. Window assembly
20. Two gypsum boards of 15mm
21. Timber inner window rim
22. Timber footing
23. Timber floor
24. Two low density wood fiberboards
25. Flooring underlayment
26. Rubber mat
27. Sloped metal facade flashing with end dams
28. Cover balcony
29. Non combustible balcony floor
30. Strapping for floor fixation
31. Three layers CLT floor for balconies
32. Timber section for window fixation
33. Sloped metal roof cap-flashing aligned with glass wall
34. Timber frame for glass wall fixation (UNIGLAS ®)
35. Five layers deep beam with water resistive protection
36. Fixed glass panels (UNIGLAS ®)
37. Metal connection between timber frame and CLT deep beams
38. Second inner window assembly

Figure (II) 1:39. Detailed solution in which UT system proposes a glazed curtain wall.

The glazed curtain wall is a solution composed for glass panels, opaque panels and/or operable windows, attached to a frame supported by the building load bearing structure. The efficiency of this kind of solutions, relatively to water/air infiltration, is grounded in the quality of gasket and sealant material as well as in the proper installation. However, despite its good quality, gasket and sealants can dry, shrink, crack and lose adhesion when exposed to weather for long periods, forcing to regular inspections. Further, air tightness can lead to undesirable indoor air quality problems supplying moisture able to provide slow mould grow.

Generally, this kind of assemblies also requires special attention for building thermal behaviour, that is why thermal glass is a frequent choice. But, the gain on thermal performance can lead to undesirable moisture problems derivatives from condensation effect (Sanders, 2006). There are numerous patents of glazed curtain wall systems, but for specific case of the UT system it was selected a simple solution with a timber frame (Uniglas ®), in which glass panels are glued to small timber ribs that are screwed to timber frame. This solution is depicted in Figure (II) 1:39, in which it is possible to observe that a timber frame structure is fixed to CLT deep beams by means of metal connectors. Façade panels are attached to this timber structure in such a way that water and air tightness is guaranteed, allowing timber structural elements to be exposed.

3.3.2.3 Balconies

CLT is a material that is typically produced with non-threated softwood species, which make it predisposed to decay when remain wet for long periods. Balconies are structures with a high propensity for undesirable water intrusions and accumulation. For that, secondary structures are often created in order to separate the building and balcony structures: cantilevered prefabricated steel structures (Andreas Ringhofer & Schickhofer, 2014) (Andreas Ringhofer & Schickhofer, 2013) and balconies with independent structural frame and foundations (Glass et al., 2013).

The UT system presents one single proposal that contain external balconies (Figure (II) 1:35 and Figure (II) 1:40). These balconies are covered and not cantilevered, trying to minimize durability and thermal problems. The biggest problem related with CLT balconies are related with the risk of water intrusion, which means that it is required a special care on its design and execution. A balcony has to be finished similarly to a low-slope roof (see detail P2.D in Figure (II) 1:40).

Despite the careful design, the UT system suggests the separation between inner floor and outer floor elements, instead of a single CLT plate shapes both (see detail P2.C in Figure (II) 1:40). This way, an

unexpected infiltration does not cause major damages on inner floor assembly, which is sealed with bitumen sheet when it faces balcony floor. This way, in a scenario in which CLT floor of balcony is damaged for water intrusion, the plate can be easily replaced.

The problematic point of the proposed assembly are the double glulam beams which are common for both, inner and outer floor assemblies. As double glulam beams are fixed to CLT walls in order to distribute the loads of diaphragms, there is no possibility to propose different supports for inner and outer CLT floor assemblies. So, glulam beams will be exposed to internal and external environments. In terms of water absorption, it can be controlled or reduced by means of water repellents, however distortions and damages, either on timber elements or in mechanical connections, caused by moisture variations would be a problem. The solution proposed in here suggests that the part of glulam beams that are placed in exterior must be protected by exterior cladding but assuring the ventilation of glulam elements, however further research is required in order to improve this solution and guarantee its efficiency.

The proposed solution with balconies also adopts the rain screen system for facades. Despite CLT deep beams do not affect directly thermal behaviour of building, insulation layer is continuous all around the building perimeter and balconies. This way, thermal bridges through balcony structures are not a problem.

3.3.2.4 Windows

The main concern related with a window assembly is the maximum control of water path. As mentioned before, the UT system suggests four solutions for openings which vary in windows size, location and support. However, all of them have one thing in common: the concern about control the water path keeping it out of the building.

First solution which places the windows aligned with the rain screen façade (Details P1.A and P2.A depicted in Figure (II) 1:36), proposes wider windows, not so high, which are supported on CLT deep beams. As recommended for CLT construction, the exterior side of the window assembly is placed in the same plane of vapour permeable water resistive membrane (Glass et al., 2013). The water is prevented from entering the building by means of sloped metal flashings with end dams located up and bellow the window which keep the water draining by exterior cladding. To keep unexpected water away from window sill, CLT deep beams are finished with a sloped timber shim which is covered with two self-adhered membranes which must be water resistive and vapour impermeable. First membrane overlaps the vapour permeable water resistive membrane while second overlaps the insulation layer.

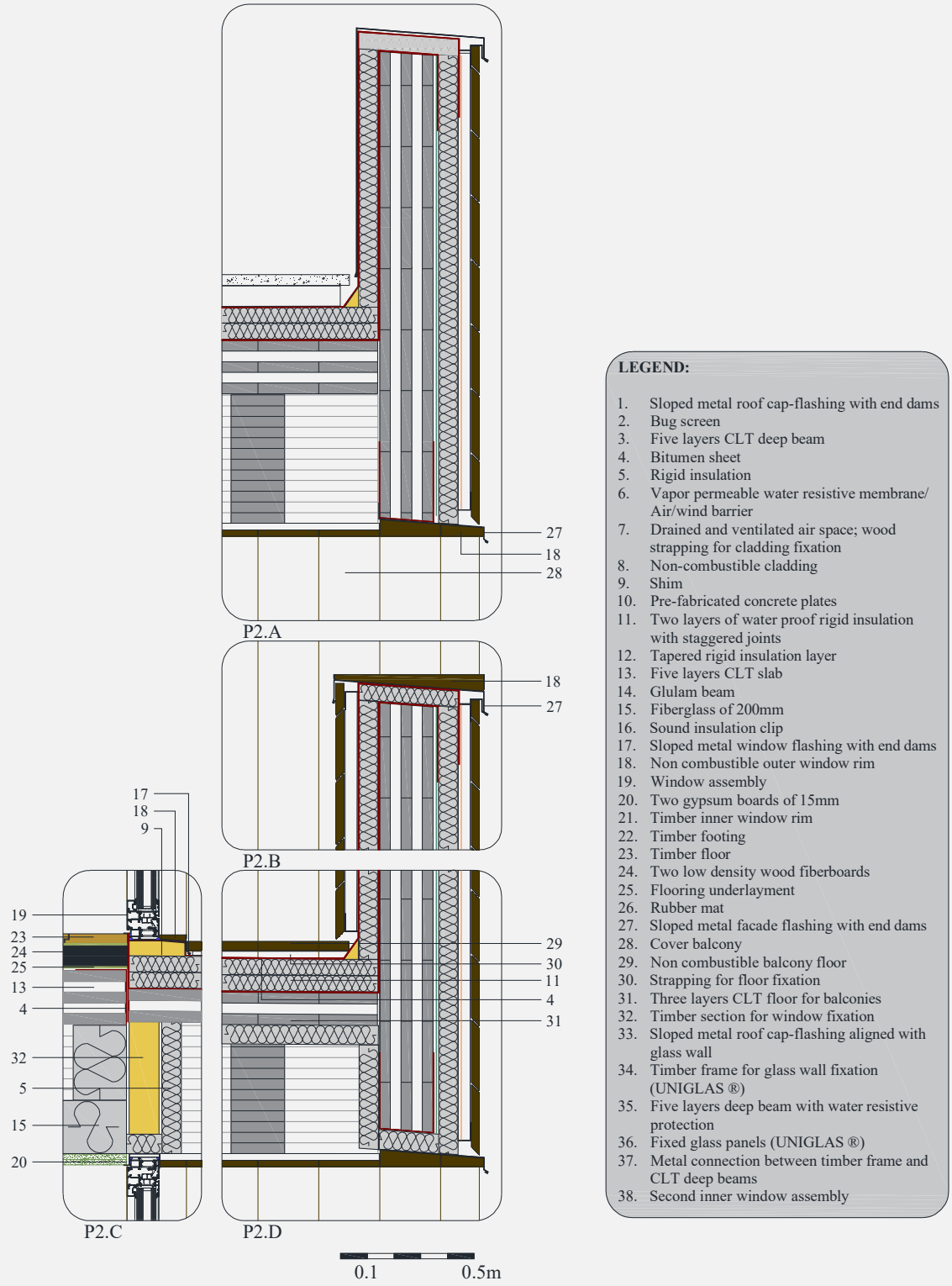

Figure (II) 1:40. Detailed solution in which UT system proposes a continuous rain screen system with external balconies.

The proposal that places balconies in the building perimeter (see detail P2.C of Figure (II) 1:40) protect window assemblies from rain by drawing back the window from façade plan, which means less possibilities of water infiltration. The difficulty of this solution is related with the drainage of balcony floor which will prevent water accumulation and consequent water infiltration inside the building. Despite the window assembly is inside, the opening in the facade remains the same. So, sloped metal flashings are also placed on top and bottom of opening, in order to keep water running through the external cladding and the tops of CLT deep beams are also protected with water proofing membranes. The balcony floor (similar to a low-slop roof assembly) meets the inner window assembly by means of two water proofing membranes, which protect inside from accumulative water, and a metal flashing, which makes the water from windows runs to balcony drainage.

Regarding Glazed curtain wall system described in section 3.3.2.2, it is important to take in consideration the significance of locating integrated windows in the system. The ventilation needs of such a system imposes the location of enough windows that ensures the adequate ventilation of the building. Further, considering low thermal behaviour and/or condensation effects, a system like this will need air conditioning and mechanical ventilation to perform well. So, it is important to consider that this kind of systems can resort to photovoltaic glass to build the glazed facade and consequently reduce the costs associated to air conditioning and mechanical ventilation.

The last proposal, based on the concept of double glass wall (see detail P3.D in Figure (II) 1:39), applies the glazed curtain wall system to building limit and add a second glass layer inside the building, creating inner balconies. The advantages of this system comparing with a single glazed curtain wall are essentially related with a better thermal behavior and with the possibility of natural ventilation. These two glass layers improve the insulation and condensation control. These inner balconies help to conserve energy by balancing interior and exterior temperatures either during cold or warm seasons (Sanders, 2006).

3.3.3 Roof

The UT system fits with aesthetics of low-slop roof assembly, which despite its higher propensity for water accumulation it does not need much more care than concrete structures. A conventional solution for a concrete low-slop roof is: application of a sloped layer; placement of water proofing membranes over the entire roof surface and bypassing parapet flashing, position of rigid insulation and sealing its joints to reduce air flow and avoid water penetration, and floor assembly for accessible roofs and for radiation protection. Extra cares related with CLT roof assemblies are: adding another layer of water proofing and

vapour resistant membrane on the top of insulation layer and ensure the removal of water accumulation near the roof-wall intersections. This last is made by the placement of a sloped shim in the roof-wall intersection (see detail P1.A in Figure (II) 1:36). Some other solutions for low-slop CLT roofs has been suggested, such as: application of closed-cell spray polyurethane foam insulation directly over a membrane on the CLT and covered with a polymeric top coat for UV protection (Glass et al., 2013); the creation of a ventilation gap, similar to rain screen wall system, that allows materials to dry easily (Andreas Ringhofer & Schickhofer, 2014) (Andreas Ringhofer & Schickhofer, 2013).

3.3.4 Connections

The main connections developed for the UT system are presented in section 2.2.2 and those that needs special care regarding moisture induced effects are the connections between CLT floors/CLT walls and CLT deep beams and the connections between double glulam beams and CLT walls.

3.3.4.1 Connections between CLT floors/CLT walls and CLT deep beams

Regarding the effects of moisture induced effects on the mechanical connections, the main concerns are obviously related with connections that are exposed to most extreme changes on relative humidity and that are more susceptible to accumulate water. Considering that, connections that are placed in façade plane are the most worrying. In façade plane the connections that can be exposed to most moisture variations are those that connects CLT floors with CLT deep beams. As explained in section 2.2.2.2.2 for these kind of connections are performed by self-tapping screws inserted diagonally from the inside side of the building. If the screws are inserted from the outside they would be ended to be an open path to water intrusion. As a result, water could accumulate in timber element and reduce the mechanical capacity of screwed connection. As evaluated in chapter 3 of part I of the present thesis, when 12%≤MC≤18% withdrawal capacity of connection reduces in a range of 1,8% per each percentage unit of moisture content added. When the timber moisture content decreases 8%≤MC≤12%, it would be expected that withdrawal capacity remains the same. However, if the screw goes through an inner gap, a reduction of withdrawal capacity can also occur. It is also important to mention that screws must be inserted diagonally in order to avoid the insertion of screws through parallel direction of timber fibers. In such case, when 14%≤MC≤25% withdrawal capacity of self-tapping screws could decrease up to 4% per each moisture content added.

3.3.4.2 Connections between double Glulam beams and CLT walls

The connection between double glulam beams and CLT walls is the most complex in the entire system, and the effects of moisture changes were also considered during its design. In section 2.2.2.1.2 were proposed three different solutions for this connection. All three solutions try to ensure that mechanical connection would allow the movements of timber elements in all three directions in case of moisture induced movements. Steel dowels were chosen in order to ensure a free movement of timber elements without damage the connection and consequently reduce its efficiency. Evaluating the possibilities of timber movements, the most worried situation is if the CLT walls swells in its thickness direction. In this situation located timber smash can occur. In the case of timber shrinkage, the consequences would not be worry because metal dowels would keep the structure safe and reduce timber cracking that could be intensified in case of screwed connections.

Another worrying situation is the possibility of delamination of glulam beams resulting in the failure the connections. That is why solutions presented in Figure (II) 1:24 and Figure (II) 1:25 suggest a metal support in the bottom of timber beam. This way, in the case of some delamination, structure collapse can be avoided and metal dowels keeps joining structural elements together.

With the exception of the solution that considers external balconies, connections between glulam beams and CLT walls are placed in internal space. Therefore, the variations on environment conditions are not expected to be extreme and predicted timber movements are low. Anyway, all suggested solutions must be properly tested also considering extreme changes on moisture content in order to predict the worst scenario. This way, the ultimate limits of suggested connections would be known.

3.4 Conclusions

In the present chapter it was described how moisture induced effects on timber elements were considered during the design of the UT system. Those effects were considered taking into account the location of structural elements, the design of different possibilities for building façade, building roof and mechanical connections between different structural elements.

It is important to state here that all proposed solutions were based on the knowledge acquired during the development of Part I of present thesis. The acquired knowledge was essential to develop the solutions here presented and discussed. However, it also must be said that all solutions must be properly tested and studied in order to guarantee their viability.

Regarding the presented study, some important conclusions must be pointed:

- The location/orientation of structural elements regarding building façade can be of significant importance when moisture induced effects are considered;
- It is important to reduce the area of contact of timber elements that create the barrier between interior and exterior spaces;
- Rain screen system is the solution most applied in multi-storey timber buildings, however glazed curtain wall is the most appealing solution for architects and it also promises to be also an effective solution regarding timber structures;
- Solution that suggest the placement of balconies in the building perimeter is the riskiest solution, once it assumes that double glulam beams share internal and external spaces of the building in such a way that the ends of glulam elements are placed in balconies. Despite protected by means of a coating and ventilated the risk of water intrusion is higher;
- Connections between CLT floors/CLT walls and CLT deep beams and connections between double glulam beams and CLT walls needs to be tested to be properly known.

In present thesis it was decided to use the knowledge obtained by experimental tests on the development of a specific structural system, however the it also could be used to create generic recommendations for designers. So, one of our recommendations for future works is the development of a guide of recommendation about how to design timber buildings considering moisture induced effects. For that, experimental work presented in present thesis would ground some recommendations, but much more experimental evaluations must be done.

CHAPTER 4 (II)

4 MAIN CONCLUSIONS OF PART II

Part II of present thesis was dedicated to the development of a structural system for multi-storey buildings, based on CLT as structural material. Based on some existing buildings and on the results obtained by experiments presented in Part I, UT system was proposed.

Chapter 1 summarizes the bibliographic research, explaining the role of timber in the cities of the future. Actually construction of this new kind of buildings has been mainly supported by qualitative reasons, such as sustainable advantages in all its three strands: environmental, social and economic. So, it is mandatory to promote a search for more feasible solutions able to support taller buildings and more versatile architectural solutions. For that, CLT is presented as a precious ally. CLT is a transversal material, being the leading figure in the majority of the constructed buildings as well as in the proposals for new construction systems. One of the advantages of this material is that it can be combined with other structural materials, such as concrete and steel. Some of the existing building and systems in development show that marriage between CLT and other structural materials in order to explore to the maximum the properties of CLT.

It is in chapter 2 that, UT system tries to render CLT as a more versatile material and more attractive to construction market. It aims to answer adequately quantitative and qualitative requests of buildings that will fill the cities of the future. Besides environmental advantages, this construction system provides spatial versatility, trying to answer more properly the demands of today's society, and its structural behavior was evaluated in order to understand its viability.

Inspired in the bundled tube concept, UT system works like a cluster of individual tubes connected together in order to make them behave as a single unit. UT system combines CLT and glulam structural elements, in which CLT shapes floors, walls and deep beams, while glulam shapes only beams. As observed in some demonstration buildings, bet in a hybrid solution can be of great advantage in order to explore the properties of the materials involved. This way, either the building structure and architectural demands have less limitations. UT system, ended to be a timber based hybrid solution, once CLT panels are combined with glulam beams.

The versatility of construction system was the central issue regarding architectural considerations. In terms of external appearance, UT system offer the possibility to shape sloped facades and it allows to endow the building a sense of horizontality by means of the shape of windows. The interior space can be drawn taking into account few limitations once, despite being placed perpendicular to the façade plane, the location of CLT walls are punctual. Furthermore, it offers the possibility to create external balconies,

CLT walls can be used as solar protection, different cuts can be made in CLT walls allowing the structure to have an active role on the definition of interior spaces.

Regarding structural behavior, UT system was evaluated by Dias (2017), who used as case study a building with 10 storeys. Structural elements were designed and its cross sections defined: CLT walls request a cross section of 600x1500mm (thickness x width); CLT slabs a thickness = 280mm; and glulam beams a cross section of 300x300mm. It was concluded that UT system is a viable solution, however much more evaluation needs to be done, especially concerning lateral loads and vibration of CLT floors.

The mechanical connections are those points that raise the most doubts. For the connection between CLT walls and reinforced concrete foundations, Dias (2017) suggested the use of Pres-Lam system, while for the remaining connections some possible solutions were pointed out. The most complex connection is the one that links CLT walls with glulam beams. For that connection three different possibilities were presented, but all of them must be properly tested before state their efficiency.

The UT system was developed considering the moisture induced effects, studied in Part I, and it is in chapter 3 that those considerations are explained. The positioning of structural elements, the design of building façade and roof and the definition of mechanical connections are the main processes in which the moisture induced effects were carefully considered. The reduction of the contact area between timber and external environment is of great significance, reason why UT system places structural walls oriented perpendicular to the façade plane. However, if a façade based on a glazed curtain wall can easily neutralize the effect of external environment in structural elements. Anyway, the problematic associated to the drastic changes in temperature and its effects on hygroscopic behavior of timber is still a problem.

Connections between structural elements also needs to predict the effect of moisture induced effects, in order to guarantee a long health to the connection. Connections based on self-tapping screws must consider that: screws cannot be inserted from exterior to the interior, preventing that moisture goes inside the timber element using screw as path; screws should preferably be inserted diagonally drilling the main face of CLT panels, avoiding the insertion through side face of panels, especially through longitudinal direction of wood fibers; during design of connections it must be considered the possibility of existence of gaps through screw path as well as the effect of moisture changes.

Connections between CLT walls and glulam beams presented in chapter 2, were developed taking into account two main issues related with wood hygroscopic behavior: the movements of timber and their

amplitude when CLT and glulam elements when submitted to changes on moisture; and the long term effects of moisture induced effects, such as the delamination of glulam beams.

The present thesis was especially dedicated to moisture induced effects on CLT and its consideration when UT system was designed. Some important conclusions were stated as a result of this topic, but as it could not be, several windows for future researches were also opened. In terms of architectural possibilities, UT system can be explored by the design of case studies in which different building shapes and different uses are proposed based on the same construction system. In terms of safety requirements, much more work can be done, since full scale tests to connections and to the structural system, fulfill fire safety requirements, and explore the limits regarding the number of stories.

BIBLIOGRAPHY

Abukari, M. H., Coté, M., Rogers, C. A., & Salenikovich, A. (2012). Withdrawal Resistance of Structural Screws in Canadian Glued Laminated Timber. *World Conference on Timber Engineering*, 134–143.

Ali, M. M., & Moon, K. S. (2007). Structural Developments in Tall Buildings: Current Trends and Future Prospects. *Architectural Science Review*, *50*(3), 205–223. https://doi.org/10.3763/asre.2007.5027

Angst, V., & Malo, K. A. (2012a). The effect of climate variations on glulam—an experimental study. *European Journal of Wood and Wood Products*, *70*(5), 603–613. https://doi.org/10.1007/s00107-012-0594-y

Angst, V., & Malo, K. A. (2012b). Effect of self-tapping screws on moisture induced stresses in glulam. *Engineering Structures*, *45*, 299–306. https://doi.org/10.1016/j.engstruct.2012.06.048

Augustin, M. (2008). Wood Based Panels. In *Handbook 1. Timber Structures* (Leonardo D, p. 243). TEMTIS.

Bejder, A. K. (2012). *Aesthetic Qualities of Cross Laminated Timber* (Issue 35) [Doctoral Thesis, Department of Civil Engineering, Aalborg University]. http://vbn.aau.dk/files/71275631/Aesthetic_Qualities_of_Cross_Laminated_Timber.pdf

Bejtka, I., & Blaß, H. J. (2002). Joints with Inclined Screws. *International Council for Research and Innovation in Building and Construction*, *September*.

Bengtsson, C. (2001). Variation of moisture induced movements in Norway spruce (Picea abies). *Annals of Forest Science*, *58*(5), 568–581. https://doi.org/10.1051/forest:2001146

Branco, J. M., Matos, F. T., & Lourenço, P. B. (2019). Lateral tests on a two-story CLT house. In I. A. for B. and S. E. (IABSE) (Ed.), *IABSE Symposium Guimarães 2019, Towards a resilient built environment, risk and asset management* (pp. 969–977). http://hdl.handle.net/1822/66255

Brandner, R. (2013). Production and Technology of Cross Laminated Timber (CLT): A state-of-the-art Report. In R. Harris, A. Ringhofer, & G. Schickhofer (Eds.), *COST Action FP1004* (pp. 2–36). https://www.researchgate.net/publication/261884030_Production_and_Technology_of_Cross_Laminated_Timber_CLT_A_state-of-the-art_Report

Buchanan, A. H., & Smith, T. (2015). The displacement paradox for seismic design of tall timber buildings. *NZSEE Conference*, 272–279.

Build it Green. (2008). *Multifamily - Green Building Guidelines* (Green Buil).

Cambiaso, F., & Pietrasanta, M. V. (2014). Innovative Timber Construction: Sustainability and Gigh Performance Building Skin. *International Journal of Engineering and Technology*, *6*(1), 47–54. https://doi.org/10.7763/IJET.2014.V6.664

Campos Costa, A., & Candeias, P. (2013). Seismic performance of multi-storey timber buildings – TUGraz building – Final report. In *TIMBER BUILDINGS Project* (WP9-TA5 LNEC). http://www.series.upatras.gr/sites/default/files/file/SERIES_TIMBER BUILDINGS_TUGraz_FinalReport (1).pdf

Ceccotti, A. (2008). New Technologies for Construction of Medium-Rise Buildings in Seismic Regions: The XLAM Case. *Structural Engineering International*, *18*(2), 156–165. https://doi.org/10.2749/101686608784218680

Crammond, G., Boyd, S. W., & Dulieu-Barton, J. M. (2013). Speckle pattern quality assessment for digital image correlation. *Optics and Lasers in Engineering*, *51*(12), 1368–1378. https://doi.org/10.1016/j.optlaseng.2013.03.014

CUAP 06.03/08. (2010). *Self-tapping screws for use in timber constructions*.

Dagenais, C. (FPInnovations), White, R. H. (Forest P. L., & Sumathipala, K. (American W. C. (2013). Fire performance of cross-laminated timber assemblies. In E. (FPInnovations) Karacabeyli & B. (AWC) Douglas (Eds.), *CLT Handbook. Cross Laminated timber* (U.S. Editi). FPInnovations.

Devereux, P., Holden, J., Buchanan, H., & Pampanin, S. (2011). NMIT Arts & Media Building - Damage Mitigation Using Post-Tensioned Timber Walls. *9th PCEE*. http://hdl.handle.net/10092/5425

Dias, F. G. (2017). *Construir em altura com CLT. O UT System aplicado a um exemplo*. Master thesis, Departamento de Engenharia Civil, Universidade do Minho.

Egmond, S. van. (2011). *Medium rise timber buildings in the Netherlands* [Master Thesis, Faculty of Civil Engineering, Delft University of Technology]. http://resolver.tudelft.nl/uuid:952bbf5e-a5b4-487f-bcae-50bb4f6d256b

Ellingsbø, P., & Malo, K. A. (2012). Withdrawal Capacity of Long Self-Tapping Screws Paralell to the Grain Direction. *World Conference on Timber Engineering*.

EN 1382. (1999). *BS EN 1382:1999 - Timber Structures - Test Methods - Withdrawal Capacity of Timber Fasteners* (pp. 2–5). BSI.

EN 1995-1-1. (2004). *EN 1995-1-1:2004. Eurocode 5 Design of timber structures. Part 1-1: General – Common rules and rules for buildings*. BSI. http://www.gradst.hr/Portals/9/PropertyAgent/1167/Files/3300/EN_1995-1-1.pdf

EN 338. (2009). *BS EN 338:2009 - Structural timber. Strength classes* (pp. 1–14). BSI.

EN 408. (2003). *EN 408:2003 Timber structures - Structural timber and glued laminated timber. Determination of some physical and mechanical properties. European Committee for Standardization.*

Esbjörnsson, A., Ford, J., & Magnusson, P. (2014). *Urban Timber - A Resilient Timber Architecture in the City and a Vision for Mass Customization* [Master Thesis, Chalmers University of Technology]. https://hdl.handle.net/20.500.12380/210252

ETA-066/0138. (2011). *KLH solid wood slabs*. EOTA.

European Comission, . (2012). *Energy roadmap 2050*. Publications Office of the European Union. https://doi.org/10.2833/10759

European Commission, . (2010). *EUROPE 2020. A strategy for smart, sustainable and inclusive growth*. http://eur-lex.europa.eu/LexUriServ/LexUriServ.do?uri=COM:2010:2020:FIN:EN:PDF

Falk, A. (2005). *Architectural Aspects of Massive Timber. Structural Form and Systems* [Doctoral Thesis, Department of Civil and Environmental Engineering, Lulea University of Technology]. https://doi.org/10.13140/2.1.3816.6409

Follesa, M., Fragiacomo, M., & Lauriola, M. (2011). A proposal for revision of the current timber part (Section 8) of Eurocode 8 Part 1. *International Council for Research and Innovation in Building and Construction. Meeting Forty Four.*

Foraboschi, P., Mercanzin, M., & Trabucco, D. (2014). Sustainable structural design of tall buildings based on embodied energy. *Energy and Buildings*, *68*(PART A), 254–269. https://doi.org/10.1016/j.enbuild.2013.09.003

Fortmeyer, R. (2011). *Why not timber high-rises?* Australian Design Review. https://www.australiandesignreview.com/architecture/why-not-timber-high-risesr/

Fragiacomo, M., Dujic, B., & Sustersic, I. (2011). Elastic and ductile design of multi-storey crosslam massive wooden buildings under seismic actions. *Engineering Structures*, *33*(11), 3043–3053. https://doi.org/10.1016/j.engstruct.2011.05.020

Fragiacomo, Massimo, Fortino, S., Tononi, D., Usardi, I., & Toratti, T. (2011). Moisture-induced stresses perpendicular to grain in cross-sections of timber members exposed to different climates. *Engineering Structures*, *33*(11), 3071–3078. https://doi.org/10.1016/j.engstruct.2011.06.018

Frangi, A., Fontana, M., & Knobloch, M. (2008). Fire Design Concepts for Tall Timber Buildings. *Structural Engineering International*, *18*(2), 148–155. https://doi.org/10.2749/101686608784218716

Frese, M., & Blaß, H. J. (2009). Models for the calculation of the withdrawal capacity of self-tapping screws. *International Council for Research and Innovation in Building and Construction*, *August*.

Gagnon, S., & Pirvu, C. (2011). CLT handbook: Cross-laminated timber. In *Special Publication SP-528E*.

Gerard, R., & Barber, D. (2013). *Fire Safety Challenges of Tall Wood Buildings - Phase 1 Final Report* (Issue December).

Gereke, T. (2009). *Moisture-induced stresses in cross-laminated wood panels* (Issue 18427). Doctoral Thesis, Department of Civil, environmental and Geomatic Engineering, Institute for Building Materials, ETH Zurich.

Glass, S. V. (Forest P. L., Wang, J. (FPInnovations), Easley, S. (Steve easley & A. I. ., & Finch, G. (RDH B. E. L. . (2013). Building enclosure design for cross-laminated timber construction. In E. (FPInnovations) Karacabeyli & B. (AWC) Douglas (Eds.), *CLT Handbook. Cross Laminated timber* (U.S. Editi). FPInnovations.

Grabner, M. (2012). The effect of moisture content variation on the withdrawal strength of self-tapping screws. *COMET Area Meeting | Holz.Bau Forschungs Gmbh*.

Grabner, M. (2013). *Ein fl ussparameter auf den Ausziehwiderstand selbstbohrender Holzschrauben in BSP-Schmal fl ächen*. Master Thesis, Institut für Holzbau und Holztechnologie, Graz University of Technology.

Green, M., & Eric Karsh, J. (2012). *Tall Wood. The Case for Tall Wood Buildings. How Mass Timber Offers a safe, economical, and Environmentally Friendly Alternative for Tall Building Structures*. http://mg-architecture.ca/tallwood/

Gülzow, A., Richter, K., & Steiger, R. (2011). Influence of wood moisture content on bending and shear stiffness of cross laminated timber panels. *European Journal of Wood and Wood Products*, *69*(2), 193–197. https://doi.org/10.1007/s00107-010-0416-z

Harch, B. (2010). *The Investigation into the Optimisation of Cross Laminated Timber Panels for use in the Australia Building Industry*. Barchelor of Engineering Dissertation, Faculty of Engineerig and Surveying, University of Southern Queensland.

Hartl, H., & Ramberger, G. (1985). *Stahlbau und konstruktiver Holzbau*.

Heaton, A. (2013). *Reflections on Building the World's Tallest Timber Building Using CLT*. DesignBUILD Source. http://designbuildsource.com.au/reflections-on-building-the-worlds-tallest-timber-building-using-clt

Hu, L. (FPInnovations), & Adams, Davide L. (Adams Associates, I. (2013). Sound insulation of cross-laminated timber assemblies. In E. (FPInnovations) Karacabeyli & B. (AWC) Douglas (Eds.), *CLT Handbook. Cross Laminated timber* (U.S. Editi). FPInnovations.

Hu, L. (FPInnovations), & Chui, Y.-H. (Uiversity of N. B. (2013). Vibration performance of cross-laminated timber floors. In E. (FPInnovations) Karacabeyli & B. (AWC) Douglas (Eds.), *CLT Handbook. Cross Laminated timber* (U.S. Editi). FPInnovations.

Iqbal, A., Pampanin, S., Buchanan, A., & Palermo, A. (2007). Improved Seismic Performance of LVL Post-tensioned Walls Coupled with UFP devices. *8th Pacific Conference on Earthquake Engineering*, 1–9. http://hdl.handle.net/11311/273363

ISO/TC 55 3131:1975. Wood - Determination of density for physical and mechanical tests. (1975).

ISO3130. (1975). *ISO/TC 55 3130:1975. Wood - Determination of moisture content for physical and mechanical tests* (Vol. 1975, pp. 0–3).

Jönsson, J. (2004). Internal stresses in the cross-grain direction in glulam induced by climate variations. *Holzforschung*, *58*(2), 154–159. https://doi.org/10.1515/HF.2004.023

Jönsson, J., & Thelandersson, S. (2003). The effect of moisture gradients on tensile strength perpendicular to grain in glulam. *Holz Als Roh- Und Werkstoff*, *61*(5), 342–348. https://doi.org/10.1007/s00107-003-0405-6

Jönsson, Johan, & Svensson, S. (2004). A contact free measurement method to determine internal stress states in glulam. *Holzforschung*, *58*(2), 148–153. https://doi.org/10.1515/HF.2004.022

Kelly, J. F., Weidmann, B., & Walsh, M. (2011). *The Housing We'd Chosse* (Grattan Institute Report ; No. 2011-5., Issue June).

Kifetew, Girma, Lindberg, H., & Wiklund, M. (1997). Tangential and radial deformation field measurements on wood during drying. *Wood Science and Technology*, *31*(1), 35–44. https://doi.org/10.1007/s002260050012

Kifetew, Grima. (1996). Application of the deformation field measurement method to wood during drying. *Wood Science and Technology*, *30*(6). https://doi.org/10.1007/BF00244440

Kim, C., Oh, J., & Lee, J. (2010). Effect of moisture content on performance of dowel-type connection. In A. Ceccoti & J.-W. van de Kuilen (Eds.), *World Conference on Timber Engineering*. https://www.researchgate.net/publication/271198762_Effect_of_moisture_content_on_performance_of_dowel-type_connection

KLH-Massivholzplatten. (2011). *ETA-06 / 0138* (Vol. 3, pp. 1–17). OIB/EOTA.

Krenn, H., & Schickhofer, G. (2009). Joints with inclined Screws and Steel Plates as outer Members. *CIB-W18/42-7-2*.

Kucharek, J.-C. (2009). Wood for the Hood. *Riba Journal*, *March*, 51–53.

Langenbach, R. (2008). Building Tall with Timber: A Paean to Wood Construction. *Structural Engineering International*, *18*(2), 130–132. https://doi.org/10.2749/101686608784218725

Larsson, M., Kaiser, A., & Girhammar, U. A. (2012). Case Study Houses 2 . 0 : Mass-Cusomised Multi-Storey Timber Buildings – Competitive high-rise timber structures from an architectural and engineering point of view. In P. Quenneville (Ed.), *World Conference on Timber Engineering* (pp. 442–447). Curran Associates, Inc.

Lecompte, D., Smits, A., Bossuyt, S., Sol, H., Vantomme, J., Van Hemelrijck, D., & Habraken, A. M. (2006). Quality assessment of speckle patterns for digital image correlation. *Optics and Lasers in Engineering*, *44*(11), 1132–1145. https://doi.org/10.1016/j.optlaseng.2005.10.004

Lehmann, S. (2012). Sustainable Construction for Urban Infill Development Using Engineered Massive Wood Panel Systems. *Sustainability*, *4*(10), 2707–2742. https://doi.org/10.3390/su4102707

Lehmann, S., Reinschmidt, A., & Mustillo, L. (2012). *Transition strategies : Accelerating social acceptance and removing the barriers to prefabricated multi-storey timber urban infill developments in Australia using CLT construction systems .* (Vol. 61, Issue December). Forest & Wood Products Australia.

Lepage, R. T. M. (2012). *Moisture Response of Wall Assemblies of Cross- Laminated Timber Construction in Cold Canadian Climates* [Master Thesis, Department of Civil Enginering, University of Waterloo]. http://hdl.handle.net/10012/6569

Lewandowski, C. M., Co-investigator, N., & Lewandowski, C. M. (2015). Summary for Policymakers. In Intergovernmental Panel on Climate Change (Ed.), *Climate Change 2013 - The Physical Science Basis* (Vol. 1, pp. 1–30). Cambridge University Press. https://doi.org/10.1017/CBO9781107415324.004

Mahapatra, K., & Gustavsson, L. (2008). Multi-storey timber buildings: breaking industry path dependency. *Building Research & Information*, *36*(6), 638–648. https://doi.org/10.1080/09613210802386123

Mahlum. (2014). *CLT feasibility study: A study of alternative construction methods in the Pacific Northwest*. https://pdf4pro.com/view/clt-feasibility-study-mahlum-198059.html

Mahlum, Co., W. C. C., & Porter Lundeen. (2014). *CLT feasibility study. A study of alternative construction methods in the pacific northwest*.

McClung, R., Ge, H., Straube, J., & Wang, J. (2014). Hygrothermal performance of cross-laminated timber wall assemblies with built-in moisture: field measurements and simulations. *Building and Environment*, *71*(January), 95–110. https://doi.org/10.1016/j.buildenv.2013.09.008

McClung, V. R. (2013). *Field Study of Hygrothermal Performance of Cross-Laminated Timber Wall Assemblies with Built-In Moisture* [Master Thesis, Department of Building Science, Ryerson University]. http://digitalcommons.ryerson.ca/dissertations/1059/

Mohammad, M., Gagnon, S., Karacabeyli, E., & Popovsky, M. (2011). Innovative Mid-Rise Timber Structures Offer New Opportunities for Designers. *Annual Convention of the Structural Engineers Association of California*.

Moroder, D. (2016). *Floor diaphragms in multistorey timber buildings* [Doctoral Thesis, Department of civil engineering, University of Canterbury]. https://doi.org/10.26021/2006

Muñoz, W., Mohammad, M., & Gagnon, S. (2010). Lateral and Withdrawal Resistance of typical CLt connections. In A. Ceccoti & J.-W. van de Kuilen (Eds.), *World Conference on Timber Engineering*. https://www.researchgate.net/publication/265521436_Lateral_and_withdrawal_resistance_of_typical_CLT_connections

NoDujic, B., Klobcar, S., & Zarnic, R. (2007). Influence of Openings on Shear Capacity of Wooden Walls. *New Zealand Timber Design Journal*, *16*(1), 5–17. https://www.researchgate.net/publication/277819809_Influence_of_openings_on_shear_capacity_of_wooden_walls

Omland, I., & Tonning, L. (2009). Can wooden architecture bond the urban past to the urban future? *International IAPS-CSBE & HOUSING Network 2009*. https://www.researchgate.net/publication/237795896_Can_wooden_architecture_bond_the_urban_past_to_the_urban_future_-_what_does_materiality_mean_for_the_genius_a_city

ÖNORM EN384:2010. (n.d.). *Structural timber — Determination of characteristic values of mechanical properties and density*. CEN.

Östman, B., & Källsner, B. (2011). *National Building Regulations In Relation To Multistorey Wooden Buildings In Europe*.

Palermo, A., Pampanin, S., Fragiacomo, M., Buchanan, A., & Deam, L. (2006). InnovativeSeismicSolutions for Multi-Storey LVL TimberBuildings. *9th World Conference OnTimberEngineering*.

Palermo, A., Sarti, F., Baird, A., & Dekker, D. (2012). From theory to practice: design, analysis and construction of dissipative timber rocking post-Tensioning wall system for Carterton Events Centre, New Zealand. *World Conference on Earthquake Engineering*.

Pan, B., & Li, K. (2011). A fast digital image correlation method for deformation measurement. *Optics and Lasers in Engineering*, *49*(7), 841–847. https://doi.org/10.1016/j.optlaseng.2011.02.023

Pan, B., Qian, K., Xie, H., & Asundi, A. (2009). Two-dimensional digital image correlation for in-plane displacement and strain measurement: a review. *Measurement Science and Technology*, *20*(6), 062001. https://doi.org/10.1088/0957-0233/20/6/062001

Pan, B., Xie, H., Wang, Z., Qian, K., & Wang, Z. (2008a). Study on subset size selection in digital image correlation for speckle patterns. *Optics Express*, *16*(10), 7037–7048. https://doi.org/10.1364/oe.16.007037

Pan, B., Xie, H., Wang, Z., Qian, K., & Wang, Z. (2008b). Study on subset size selection in digital image correlation for speckle patterns. *Optics Express*, *16*(10), 7037. https://doi.org/10.1364/OE.16.007037

Patterson, D. (2013). Forté. Creating the World's Tallest CLT Apartment Building. *US CLT Symposium*.

Pirnbacher, G., Brandner, R., & Schickhofer, G. (2009). Base Parameters of self-tapping Screws. *International Council for Research and Innovation in Building and Construction*.

Popovski, M., Schneider, J., & Schweinsteiger, M. (2010). Lateral Load Resistance of Cross-laminated Wood Panels. *World Conference on Timber Engineering*. https://www.researchgate.net/publication/265613292_Lateral_load_resistance_of_cross-laminated_wood_panels

Qin, B., & Han, S. S. (2013). Planning parameters and household carbon emission: Evidence from high- and low-carbon neighborhoods in Beijing. *Habitat International*, *37*, 52–60. https://doi.org/10.1016/j.habitatint.2011.12.017

Ranta-Maunus, A. (2001). Moisture Gradient as Loading of Curved Timber Beams. *IABSE Symposium Report*, *85*(9), 12–17. https://doi.org/10.2749/222137801796348467

Reid, R. L. (2010). Norwegian Team Designs World's Tallest Timber Building. *Civil Engineering*.

Ringhofer, A, Brandner, R., & Schickhofer, G. (2015). Withdrawal resistance of self-tapping screws in unidirectional and orthogonal layered timber products. *Materials and Structures*, *48*(5), 1435–1447. https://doi.org/10.1617/s11527-013-0244-9

Ringhofer, Andreas, Grabner, M., Silva, C. V., & Branco, J. (2014). The influence of moisture content variation on the withdrawal capacity of self-tapping screws. *Holztechnologie*, *55*(3), 33–40. http://hdl.handle.net/1822/31243

Ringhofer, Andreas, & Schickhofer, G. (2014). Multi-storey residential buildings in CLT - Interdisciplinary principles of design and construction. *WCTE 2014 - World Conference on Timber Engineering, Proceedings*. http://www.scopus.com/inward/record.url?eid=2-s2.0-84924944216&partnerID=tZOtx3y1

Ringhofer, Andreas, & Schickhofer, G. (2013). Timber-in-Town – current examples for residential buildings in CLT and tasks for the future. *Focus Solid Timber Solutions - European Conference on Cross Laminated Timber (CLT)*, 196–218.

Rönnelid, M., Wik, T., & Janols, H. (2013). *Passive cross laminated timber buildings: Final report Cerbof-project no. 76* (Solar Energy Research Center, Dalarna University, ISSN 1401-7555 ; 104). urn:nbn:se:du-13667

Roos, A., Woxblom, L., & McCluskey, D. (2010). The influence of architects and structural engineers on timber in construction – perceptions and roles. *Silva Fennica*, *44*(5), 871–884. https://doi.org/10.14214/sf.126

Sanders, R. M. (2006). Curtain Walls: Not Just Another Pretty Façade. *Journal of Architectural Technology*, *23*(1), 1–8.

Schwab, E., Steffen, A., & Korte, C. (1997). In-plane swelling and shrinkage of wood-based panels. *Holz Als Roh- Und Werkstoff*, *55*(4), 227–233.

Serrano, E. (2009). *Documentation of the Limnologen Project. Overview and Summaries of Sub Projects Results*.

Sigrist, C., Gerber, C., Weber, H., & Brunner, R. (1999). Evaluation of floor systems for multi-storey buildings. *Pacific Timber Engineering Conference*.

Sigrist, Christophe, Gerber, C., Weber, H., & Brunner, R. (1999). Evaluation of floor systems for multi-storey buildings. *Pacific Timber Engineering Conference*.

Silva, C., Branco, J. M., Camões, A., & Lourenço, P. B. (2014). Dimensional variation of three softwood due to hygroscopic behavior. *Construction and Building Materials*, *59*, 25–31. https://doi.org/10.1016/j.conbuildmat.2014.02.037

Silva, C., Branco, J. M., & Lourenço, P. B. (2012). MLCC na construção em altura. *Congresso Construção 2012 - 4º Congresso Nacional*, 1–12. http://hdl.handle.net/1822/22216

Silva, C., Branco, J. M., & Lourenço, P. B. (2014). UT System : a Structural System To Build Taller Urban Timber Houses With the Aspired Spatial Flexibility. *41st IAHS WORLD CONGRESS*, 1–12. https://doi.org/10.13140/2.1.3833.2486

Silva, T. (2014). *Explorar a Potencialidade de um Edifício Construído com Madeira Lamelada Colada Cruzada (MLCC). Da organização espacial interior à relação interior - exterior*. Master Thesis, Department of Architecture, University of Minho.

Silva, C. V, Branco, J. M., & Lourenço, P. B. (2013). A project contribution to the development of sustainable multi- storey timber buildings. In L. Bragança, M. Pinheiro, & R. Mateus (Eds.), *Portugal SB13 - Contribution of Sustainable Building to Meet EU 20-20-20 Targets* (pp. 379–386). IISBE Portugal, University of Minho, Instituto Superior Técnico. http://hdl.handle.net/1822/26947

Sjödin, J., & Johansson, C.-J. (2007). Influence of initial moisture induced stresses in multiple steel-to-timber dowel joints. *Holz Als Roh- Und Werkstoff*, *65*(1), 71–77. https://doi.org/10.1007/s00107-006-0136-6

Skogstad, H. B., Gullbrekken, L., & Nore, K. (2011). Air leakages through cross laminated timber (CLT) constructions. *NSB 2011 9th Nordic Symposium on Building Physics*, 89–96.

Smith, T., Pampanin, S., Buchanan, A. H., & Fragiacomo, M. (2008). Feasibility and Detailing of Post-tensioned Timber Buildings for Seismic Areas. *New Zealand Society of Earthquake Engineering*.

Sousa, H. S., Branco, J. M., & Lourenço, P. B. (2014). Characterization of Cross-Sections from Old Chestnut Beams Weakened by Decay. *International Journal of Architectural Heritage*, *8*(3), 436–451. https://doi.org/10.1080/15583058.2013.826303

Sousa, R. (2010). *Avaliação Experimental da Estabilidade Dimensional de Elementos em Pinho Bravo e Madeira Tratada Termicamente* [Master Thesis, Department of civil engineering, University of Minho]. http://hdl.handle.net/1822/24768

Stehn, L., & Bergström, M. (2002). Integrated design and production of multi-storey timber frame houses – production effects caused by customer-oriented design. *International Journal of Production Economics*, *77*(3), 259–269. https://doi.org/10.1016/S0925-5273(00)00153-5

Svensson, S., Turk, G., & Hozjan, T. (2011). Predicting moisture state of timber members in a continuously varying climate. *Engineering Structures*, *33*(11), 3064–3070. https://doi.org/10.1016/j.engstruct.2011.04.029

Teibinger, M., & Matzinger, I. (2013). Technical Brochure "Construction with Cross-Laminated Timber in Multi-Storey Buildings: Focus on Building Physics" available. *Bauphysik*, *35*(5), 345–345. https://doi.org/10.1002/bapi.201390039

Time, B. (1998). *Hygroscopic Moisture Transport in Wood* (Issue February). Doctoral Thesis, Department of Building and Construction Engineering, Norwegian University of Science and Technology.

Uibel, T., & Blaß, H. J. (2007). Edge Joints with Dowel Type Fasteners in Cross Laminated Timber. *International Council for Research and Innovation in Building and Construction. Working Commission W18–Timber Structures. 40th Meeting.* https://www.researchgate.net/publication/36452723_Edge_Joints_with_Dowel_Type_Fasteners_in_Cross_Laminated_Timber

UN General Assembly. (2015). Transforming our world: the 2030 agenda for sustainable development. In *A/RES/70/1*. http://www.un.org/ga/search/view_doc.asp?symbol=A/RES/70/1&Lang=E

Wallner, B. (2012). *Versuchstechnische Evaluierung feuchteinduzierter Kräfte in Brettschicholz verursacht durch das Einbringen von Schraubstangen*. Master Thesis, Institut fur Holzbau und Holztechnologie, Technische Universitat Graz.

Wang, J., Clark, J., Symons, P., & Morris, P. (2010). Time to Initiation of Decay in Plywood, OSB, and Solid Wood Under Critical Moisture Conditions. *International Conference on Building Envelope Systems and Technology.*

Wells, M. (2011). Tall Timber Buildings : Applications of Solid Timber Construction in Multistory Buildings. *Council on Tall Buildings and Urban Habitat*, *1*. https://global.ctbuh.org/resources/papers/download/319-tall-timber-buildings-applications-of-solid-timber-construction-in-multistory-buildings.pdf

Winter, W., Weber, G., Hernández, S., & Brigola, B. (2012). Strategies to increase use of timber in multi-storey buildings - case studies. In P. Quenneville (Ed.), *World Conference on Timber Engineering* (pp. 262–269). Curran Associates, Inc. https://www.researchgate.net/publication/289047278_Strategies_to_increase_use_of_timber_in_multistorey_buildings_-_Case_studies

Xia, B., O'Neill, T., Zuo, J., Skitmore, M., & Chen, Q. (2014). Perceived obstacles to multi-storey timber-frame construction: an Australian study. *Architectural Science Review*, *57*(3), 169–176. https://doi.org/10.1080/00038628.2014.912198

ANNEX

Annex 1:1

C1_BEFORE CUT_Y DIRECTION_STRAIN_F1

	A1	A2
DAY 35	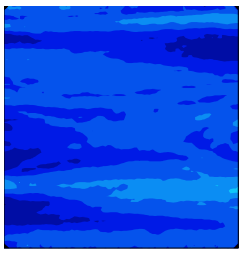 A1_C1_35_F1	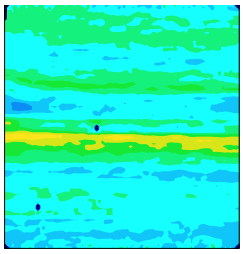 A2_C1_35_F1
DAY 56	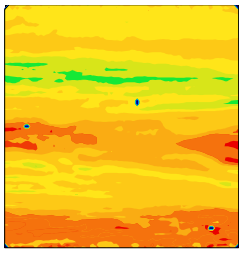 A1_C1_56_F1	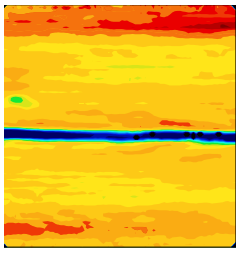 A2_C1_56_F1
DAY 161	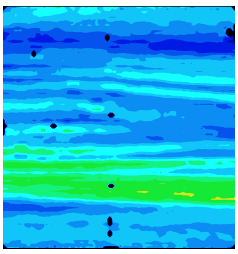 A1_C1_161_F1	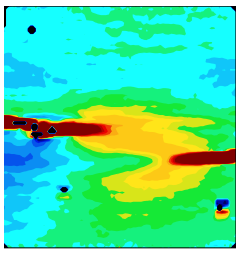 A2_C1_161_F1
DAY 182	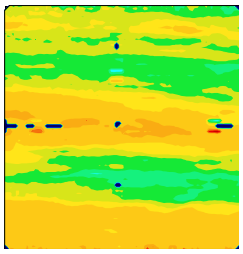 A1_C1_182_F1	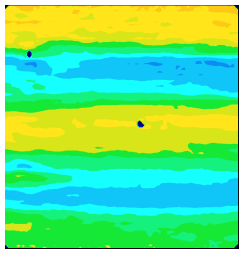 A2_C1_182_F1
DAY 324	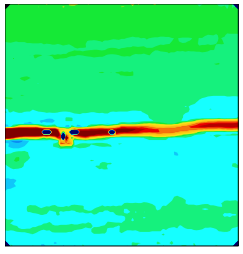 A1_C1_324_F1	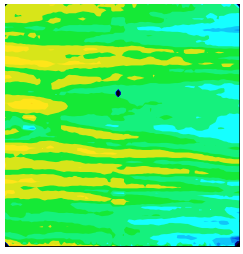 A2_C1_324_F1

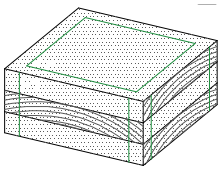

C1

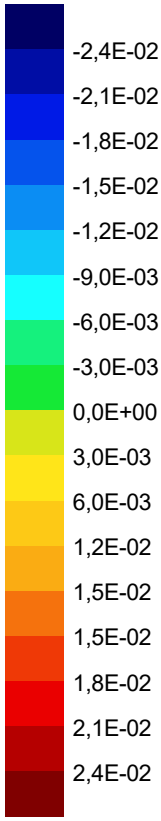

C2_BEFORE CUT_Y DIRECTION_STRAIN

	A1	A2
DAY 35	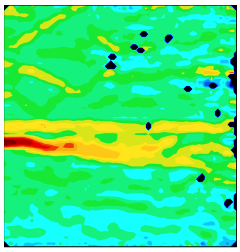 A1_C2_35_F1	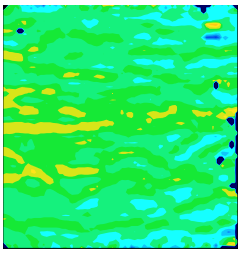 A2_C2_35_F1
DAY 56	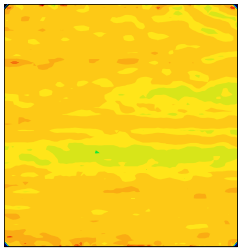 A1_C2_56_F1	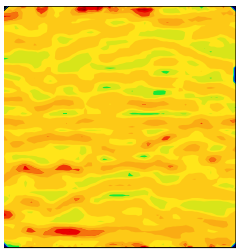 A2_C2_56_F1
DAY 161	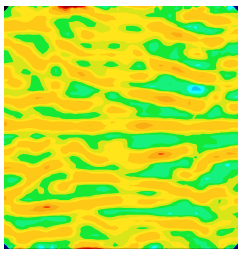 A1_C2_161_F1	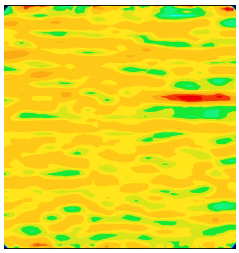 A2_C2_161_F1
DAY 182	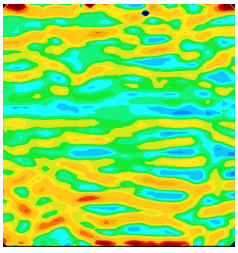 A1_C2_182_F1	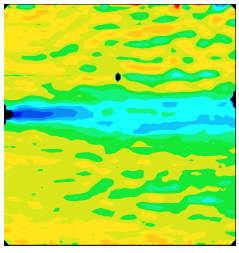 A2_C2_182_F1
DAY 324	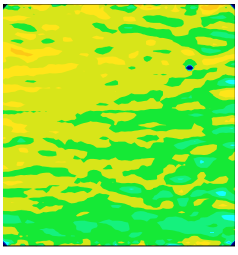 A1_C2_324_F1	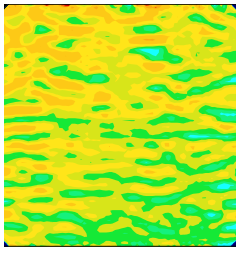 A2_C2_324_F1

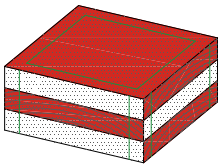

C2

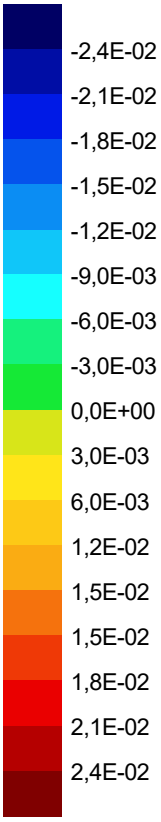

C3_BEFORE CUT_Y DIRECTION_STRAIN

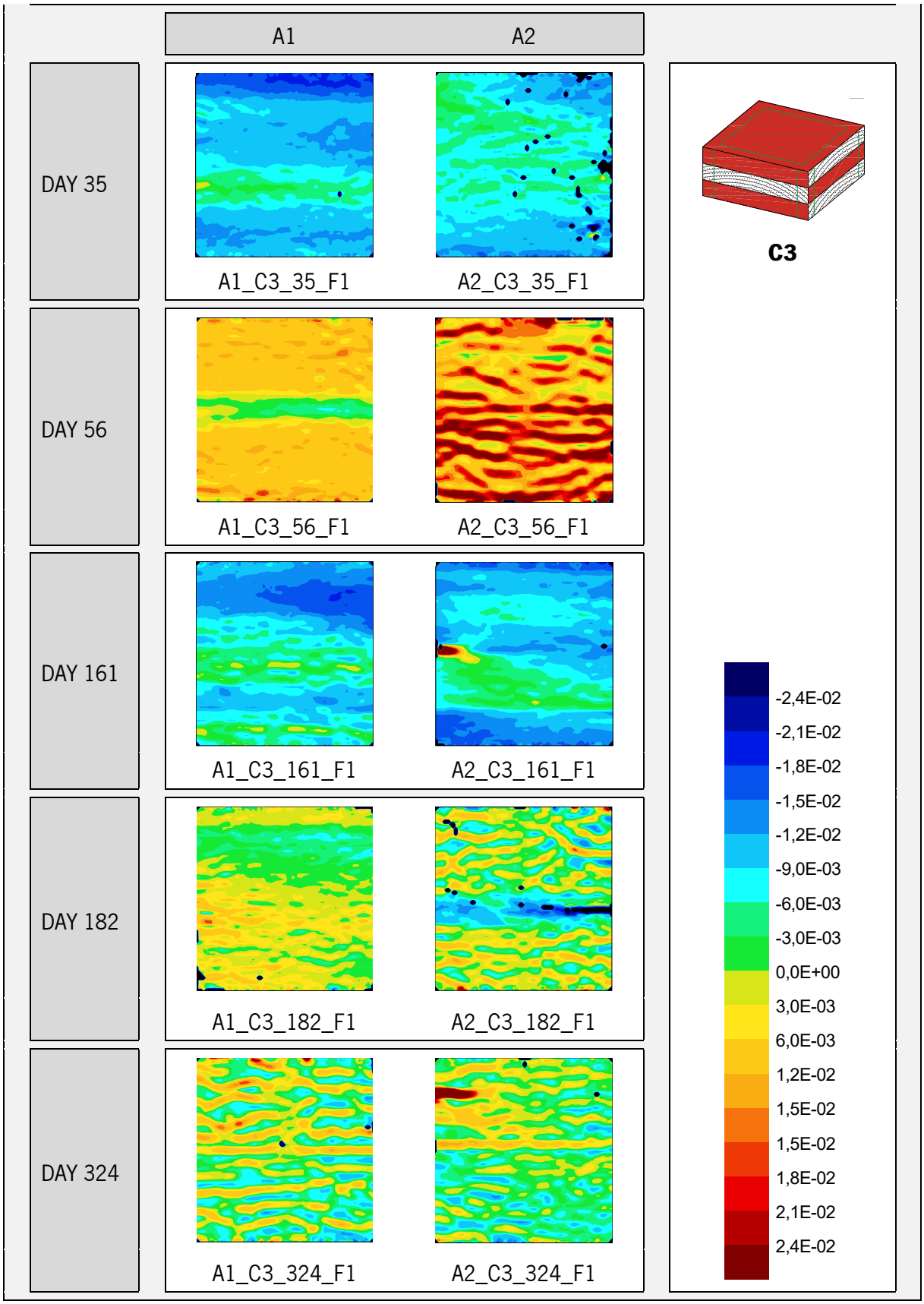
A1
A2
DAY 35
DAY 56
DAY 161
DAY 182
DAY 324
A1_C3_35_F1
A2_C3_35_F1
A1_C3_56_F1
A2_C3_56_F1
A1_C3_161_F1
A2_C3_161_F1
A1_C3_182_F1
A2_C3_182_F1
A1_C3_324_F1
A2_C3_324_F1
C3
-2,4E-02
-2,1E-02
-1,8E-02
-1,5E-02
-1,2E-02
-9,0E-03
-6,0E-03
-3,0E-03
0,0E+00
3,0E-03
6,0E-03
1,2E-02
1,5E-02
1,5E-02
1,8E-02
2,1E-02
2,4E-02

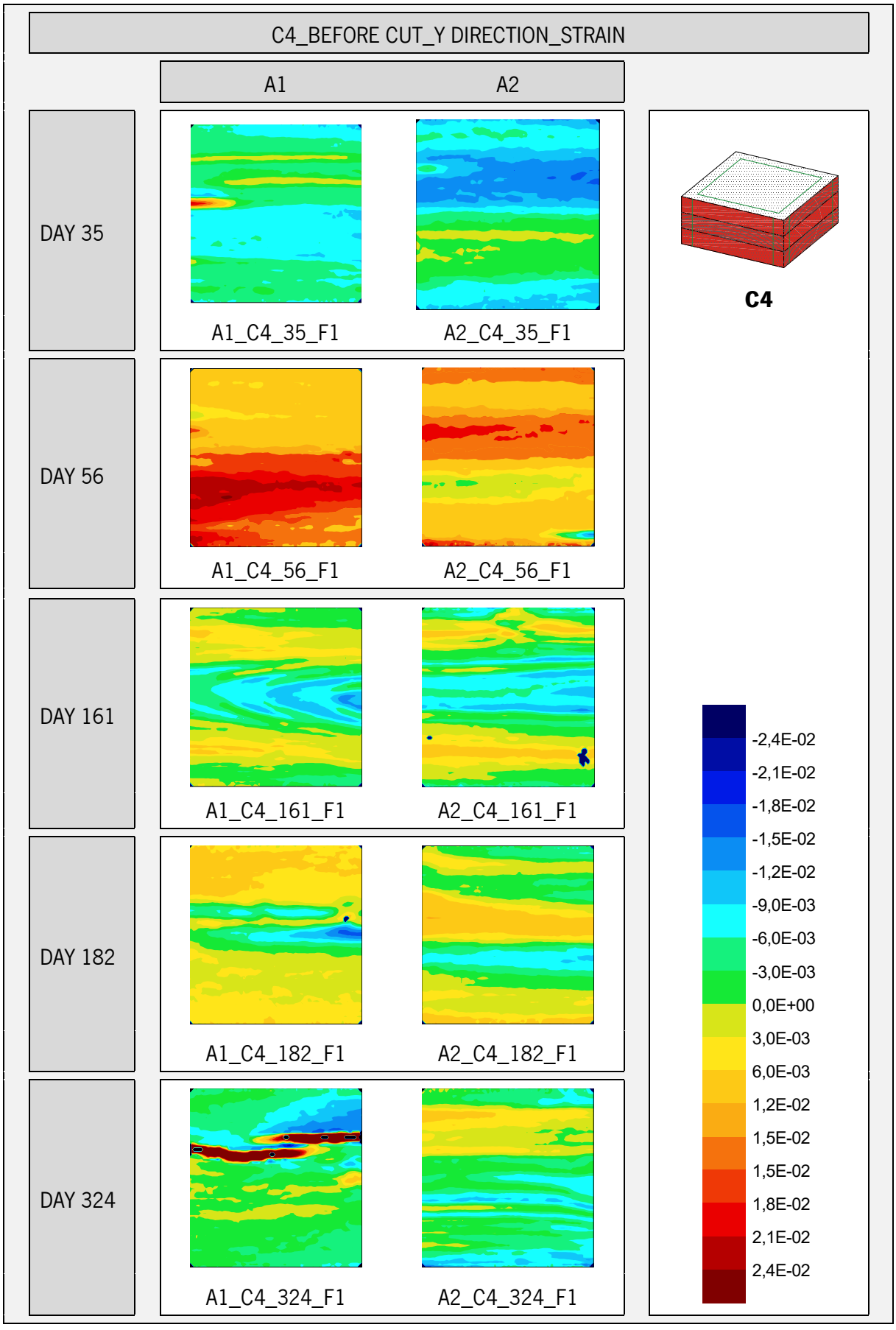
C4_BEFORE CUT_Y DIRECTION_STRAIN
A1
A2
DAY 35
DAY 56
DAY 161
DAY 182
DAY 324
A1_C4_35_F1
A2_C4_35_F1
A1_C4_56_F1
A2_C4_56_F1
A1_C4_161_F1
A2_C4_161_F1
A1_C4_182_F1
A2_C4_182_F1
A1_C4_324_F1
A2_C4_324_F1
C4
-2,4E-02
-2,1E-02
-1,8E-02
-1,5E-02
-1,2E-02
-9,0E-03
-6,0E-03
-3,0E-03
0,0E+00
3,0E-03
6,0E-03
1,2E-02
1,5E-02
1,5E-02
1,8E-02
2,1E-02
2,4E-02

Annex 1:2

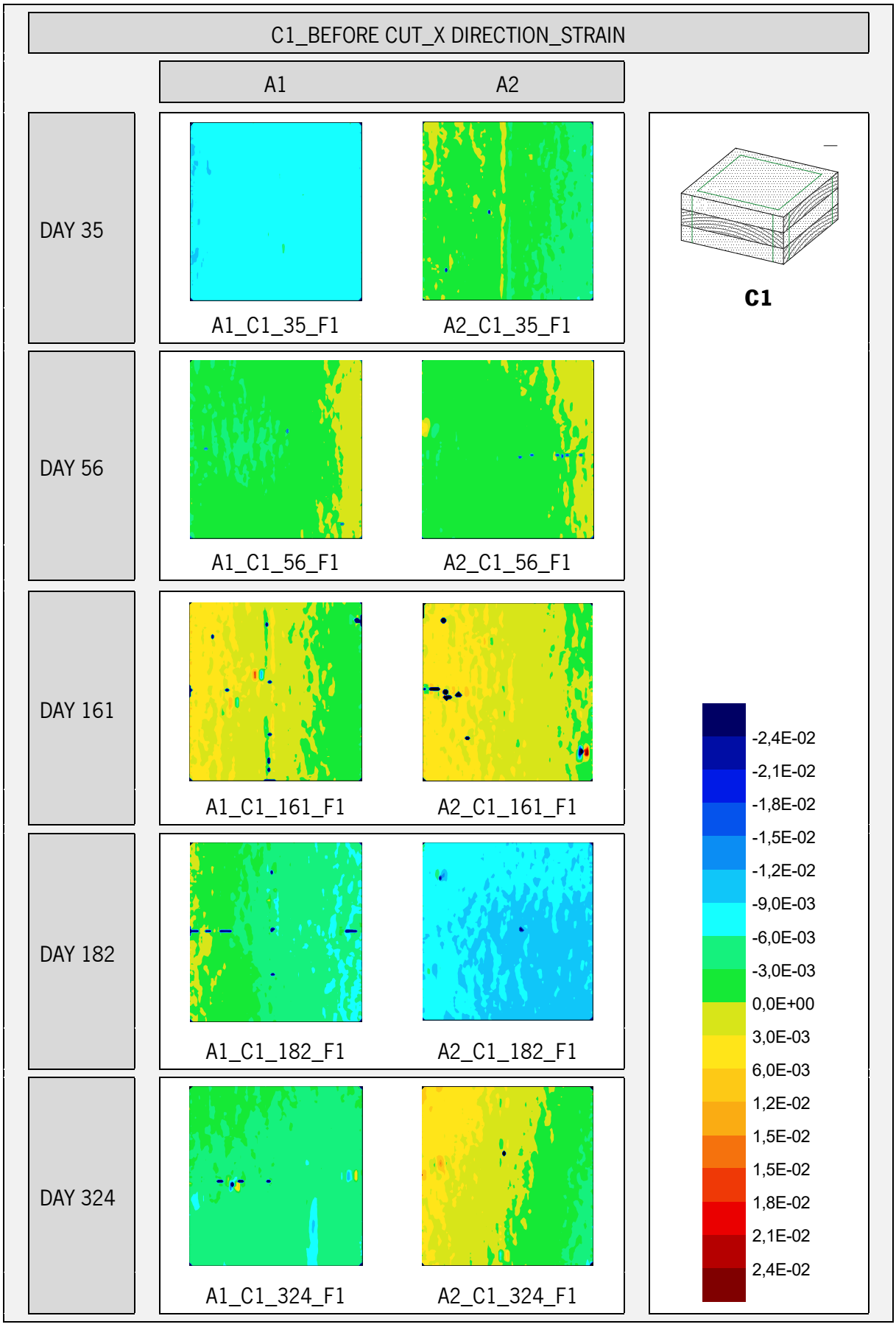
C1_BEFORE CUT_X DIRECTION_STRAIN
A1
A2
DAY 35
DAY 56
DAY 161
DAY 182
DAY 324
A1_C1_35_F1
A2_C1_35_F1
A1_C1_56_F1
A2_C1_56_F1
A1_C1_161_F1
A2_C1_161_F1
A1_C1_182_F1
A2_C1_182_F1
A1_C1_324_F1
A2_C1_324_F1
C1
-2,4E-02
-2,1E-02
-1,8E-02
-1,5E-02
-1,2E-02
-9,0E-03
-6,0E-03
-3,0E-03
0,0E+00
3,0E-03
6,0E-03
1,2E-02
1,5E-02
1,5E-02
1,8E-02
2,1E-02
2,4E-02

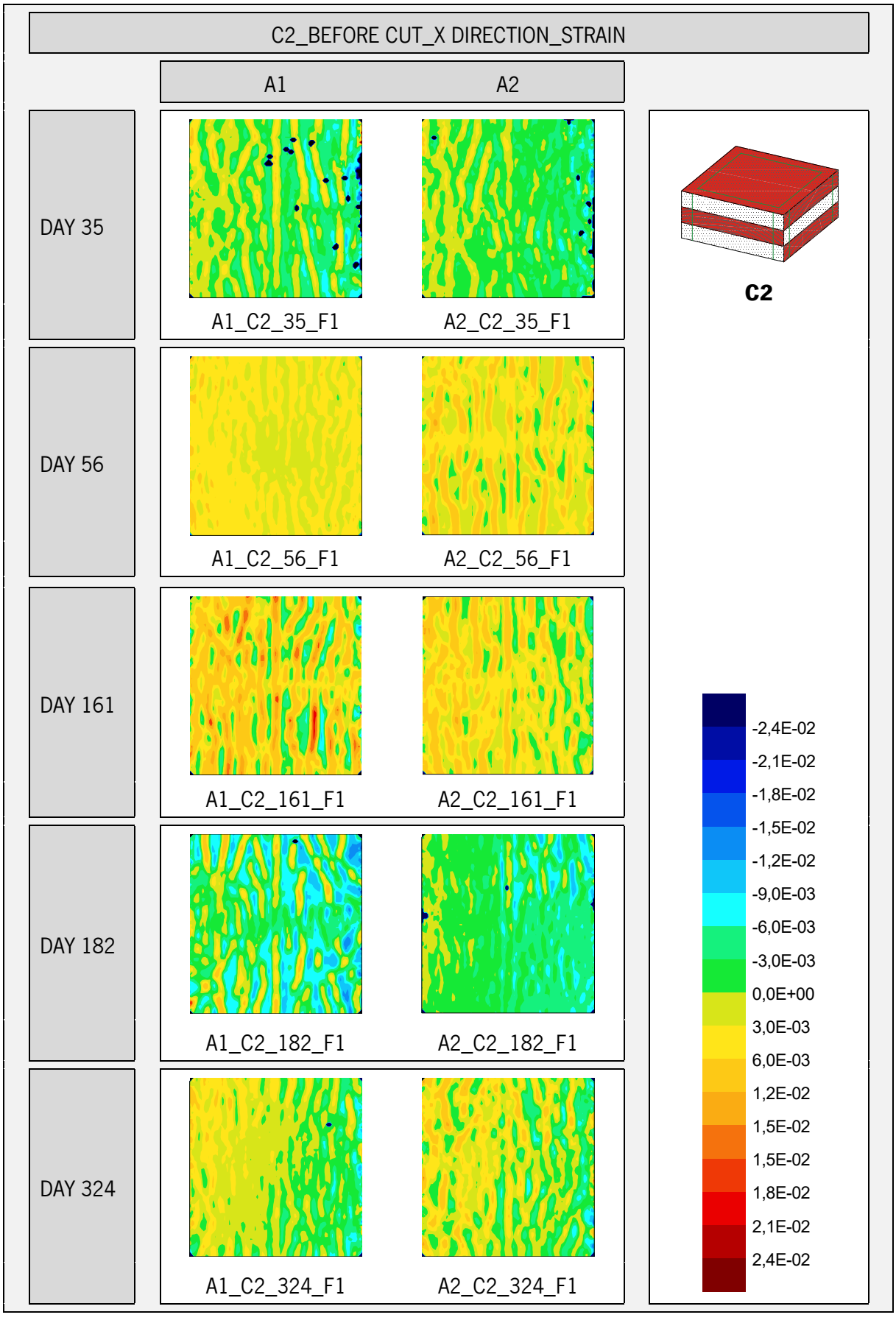
C2_BEFORE CUT_X DIRECTION_STRAIN
A1
A2
DAY 35
DAY 56
DAY 161
DAY 182
DAY 324
A1_C2_35_F1
A2_C2_35_F1
A1_C2_56_F1
A2_C2_56_F1
A1_C2_161_F1
A2_C2_161_F1
A1_C2_182_F1
A2_C2_182_F1
A1_C2_324_F1
A2_C2_324_F1
C2
-2,4E-02
-2,1E-02
-1,8E-02
-1,5E-02
-1,2E-02
-9,0E-03
-6,0E-03
-3,0E-03
0,0E+00
3,0E-03
6,0E-03
1,2E-02
1,5E-02
1,5E-02
1,8E-02
2,1E-02
2,4E-02

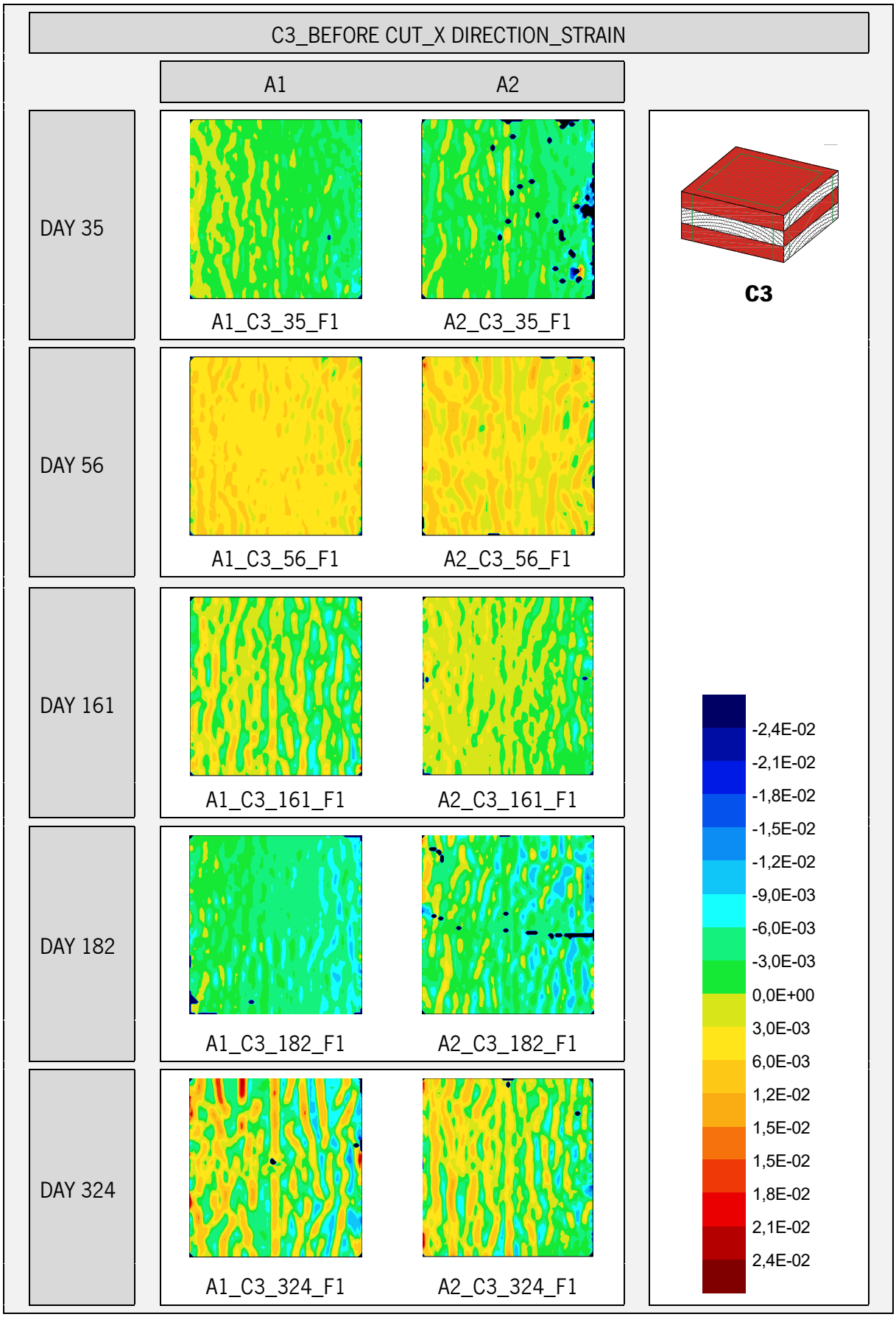
C3_BEFORE CUT_X DIRECTION_STRAIN
A1
A2
DAY 35
A1_C3_35_F1
A2_C3_35_F1
DAY 56
A1_C3_56_F1
A2_C3_56_F1
DAY 161
A1_C3_161_F1
A2_C3_161_F1
DAY 182
A1_C3_182_F1
A2_C3_182_F1
DAY 324
A1_C3_324_F1
A2_C3_324_F1
C3
-2,4E-02
-2,1E-02
-1,8E-02
-1,5E-02
-1,2E-02
-9,0E-03
-6,0E-03
-3,0E-03
0,0E+00
3,0E-03
6,0E-03
1,2E-02
1,5E-02
1,5E-02
1,8E-02
2,1E-02
2,4E-02

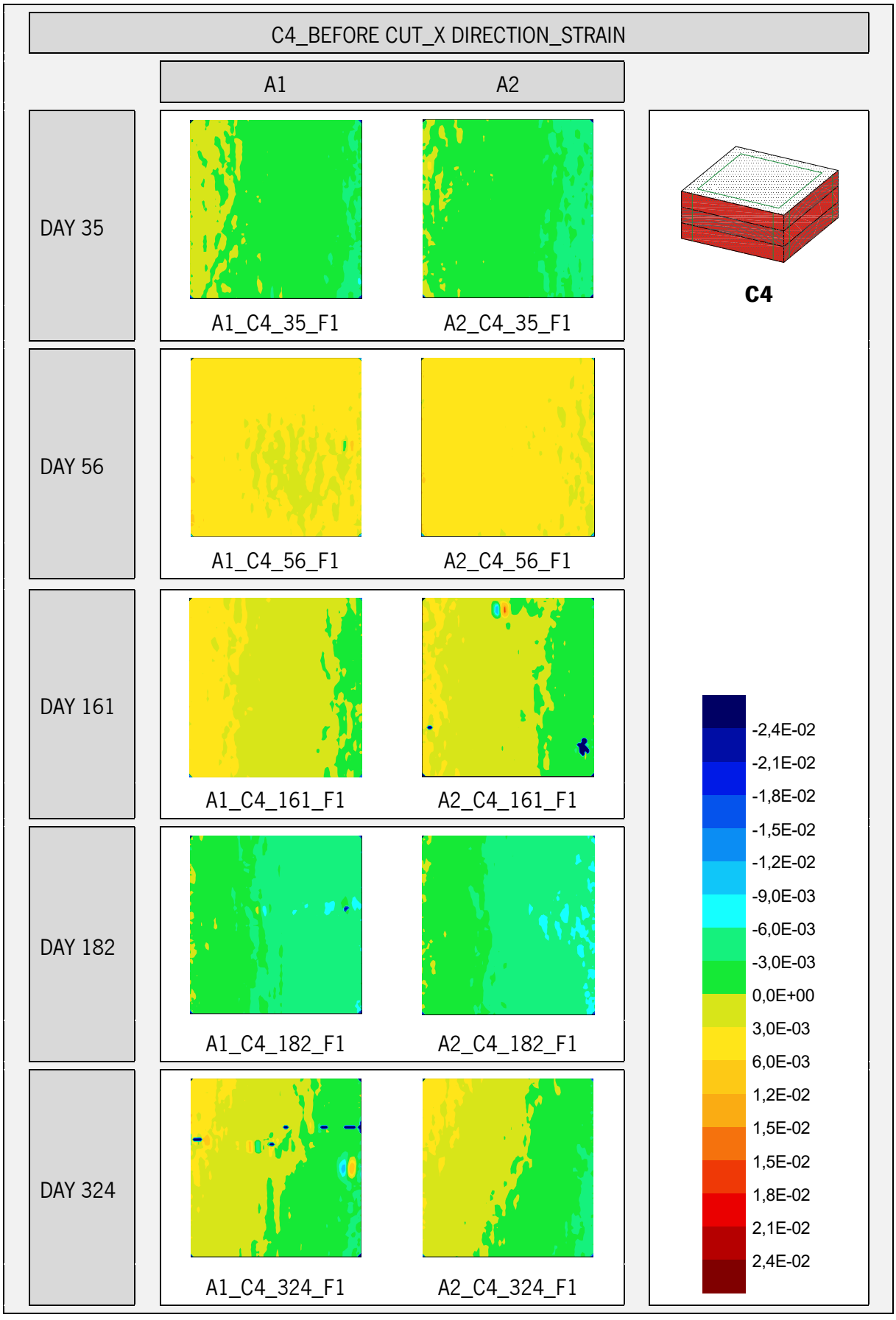
C4_BEFORE CUT_X DIRECTION_STRAIN
A1
A2
DAY 35
DAY 56
DAY 161
DAY 182
DAY 324
A1_C4_35_F1
A2_C4_35_F1
A1_C4_56_F1
A2_C4_56_F1
A1_C4_161_F1
A2_C4_161_F1
A1_C4_182_F1
A2_C4_182_F1
A1_C4_324_F1
A2_C4_324_F1
C4
-2,4E-02
-2,1E-02
-1,8E-02
-1,5E-02
-1,2E-02
-9,0E-03
-6,0E-03
-3,0E-03
0,0E+00
3,0E-03
6,0E-03
1,2E-02
1,5E-02
1,5E-02
1,8E-02
2,1E-02
2,4E-02

Annex 1:3

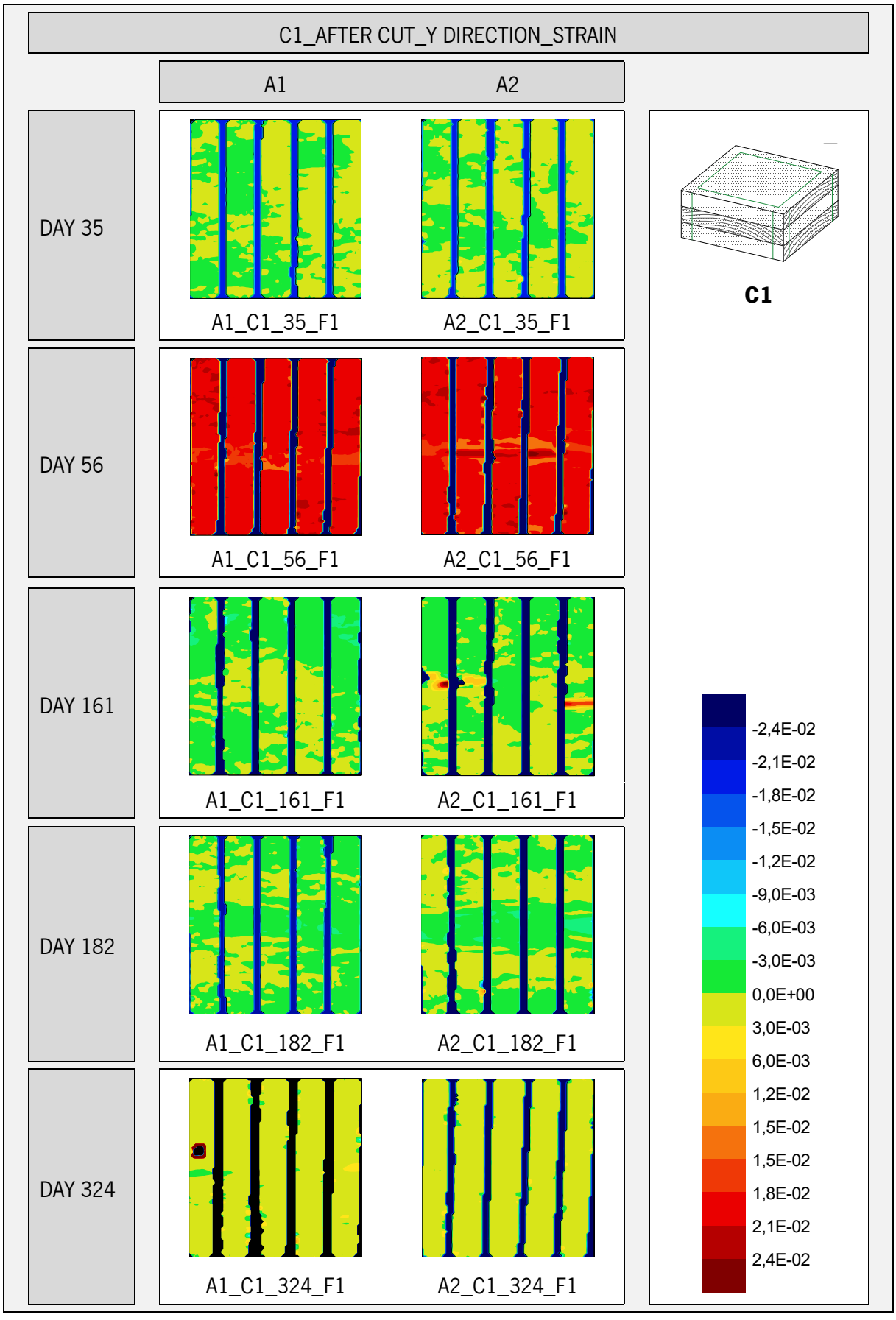
C1_AFTER CUT_Y DIRECTION_STRAIN
A1
A2
DAY 35
DAY 56
DAY 161
DAY 182
DAY 324
A1_C1_35_F1
A2_C1_35_F1
A1_C1_56_F1
A2_C1_56_F1
A1_C1_161_F1
A2_C1_161_F1
A1_C1_182_F1
A2_C1_182_F1
A1_C1_324_F1
A2_C1_324_F1
C1
-2,4E-02
-2,1E-02
-1,8E-02
-1,5E-02
-1,2E-02
-9,0E-03
-6,0E-03
-3,0E-03
0,0E+00
3,0E-03
6,0E-03
1,2E-02
1,5E-02
1,5E-02
1,8E-02
2,1E-02
2,4E-02

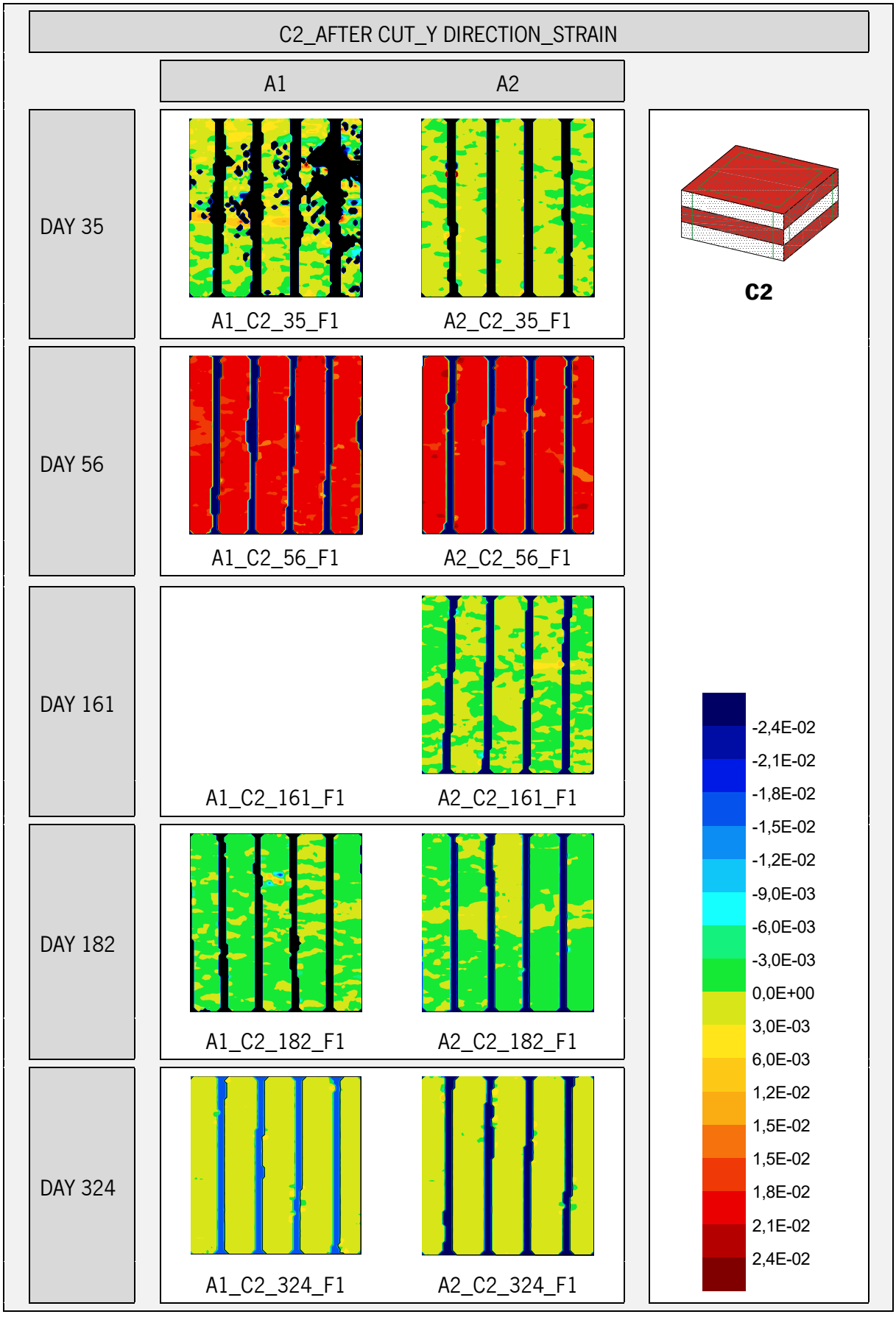
C2_AFTER CUT_Y DIRECTION_STRAIN
A1
A2
DAY 35
DAY 56
DAY 161
DAY 182
DAY 324
A1_C2_35_F1
A2_C2_35_F1
A1_C2_56_F1
A2_C2_56_F1
A1_C2_161_F1
A2_C2_161_F1
A1_C2_182_F1
A2_C2_182_F1
A1_C2_324_F1
A2_C2_324_F1
C2
-2,4E-02
-2,1E-02
-1,8E-02
-1,5E-02
-1,2E-02
-9,0E-03
-6,0E-03
-3,0E-03
0,0E+00
3,0E-03
6,0E-03
1,2E-02
1,5E-02
1,5E-02
1,8E-02
2,1E-02
2,4E-02

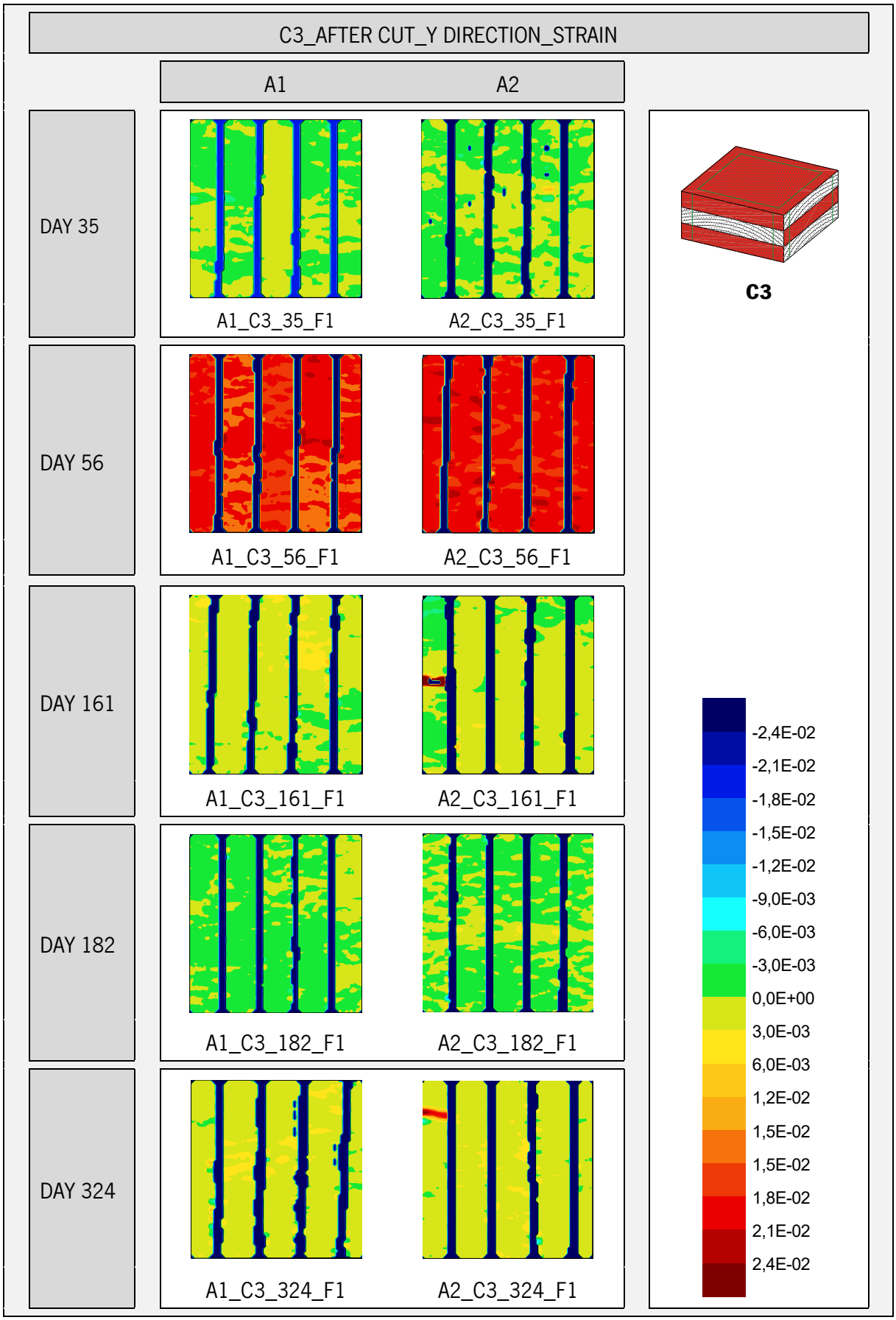
C3_AFTER CUT_Y DIRECTION_STRAIN
A1
A2
DAY 35
DAY 56
DAY 161
DAY 182
DAY 324
A1_C3_35_F1
A2_C3_35_F1
A1_C3_56_F1
A2_C3_56_F1
A1_C3_161_F1
A2_C3_161_F1
A1_C3_182_F1
A2_C3_182_F1
A1_C3_324_F1
A2_C3_324_F1
C3
-2,4E-02
-2,1E-02
-1,8E-02
-1,5E-02
-1,2E-02
-9,0E-03
-6,0E-03
-3,0E-03
0,0E+00
3,0E-03
6,0E-03
1,2E-02
1,5E-02
1,5E-02
1,8E-02
2,1E-02
2,4E-02

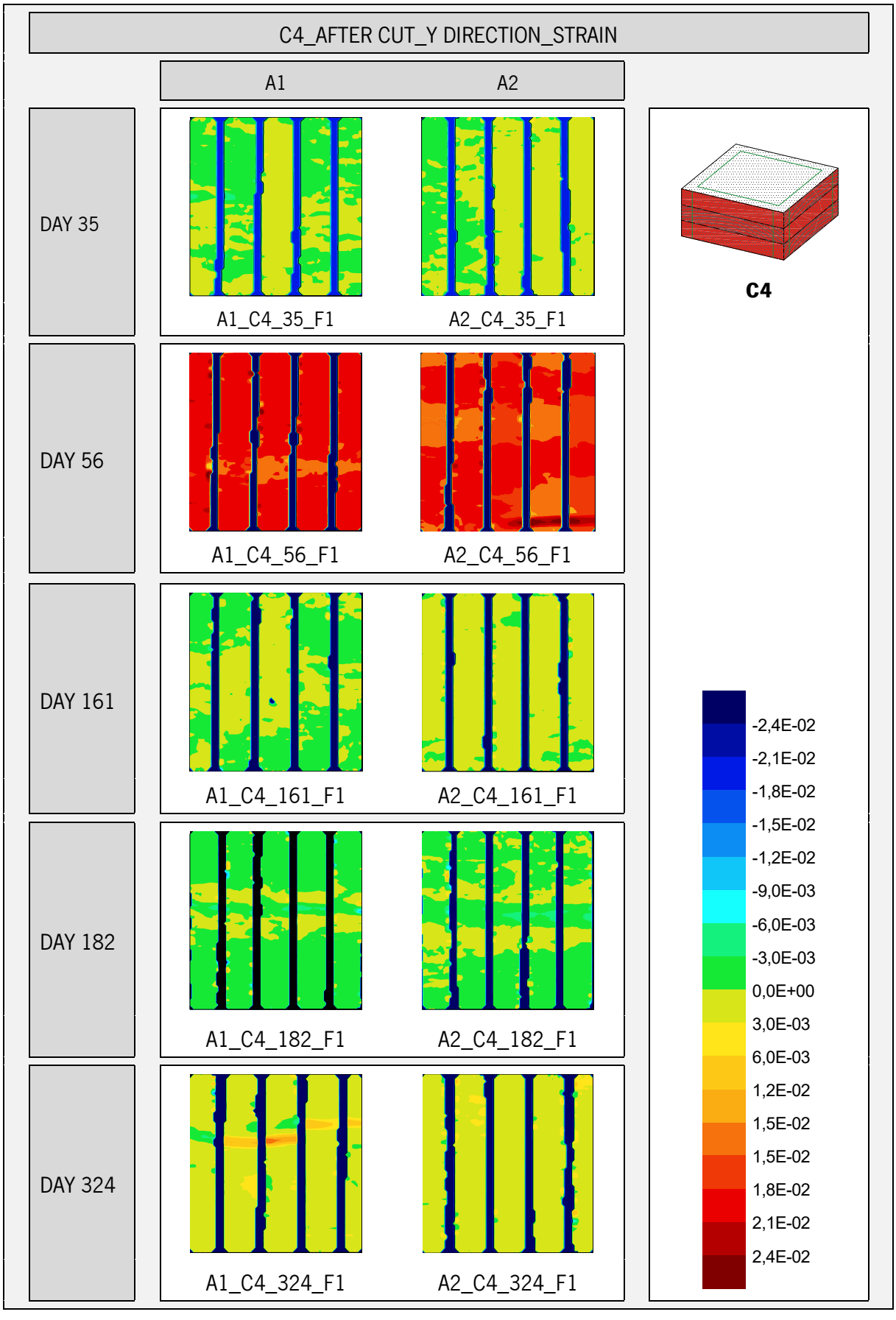
C4_AFTER CUT_Y DIRECTION_STRAIN
A1
A2
DAY 35
DAY 56
DAY 161
DAY 182
DAY 324
A1_C4_35_F1
A2_C4_35_F1
A1_C4_56_F1
A2_C4_56_F1
A1_C4_161_F1
A2_C4_161_F1
A1_C4_182_F1
A2_C4_182_F1
A1_C4_324_F1
A2_C4_324_F1
C4
-2,4E-02
-2,1E-02
-1,8E-02
-1,5E-02
-1,2E-02
-9,0E-03
-6,0E-03
-3,0E-03
0,0E+00
3,0E-03
6,0E-03
1,2E-02
1,5E-02
1,5E-02
1,8E-02
2,1E-02
2,4E-02

Annex 1:4

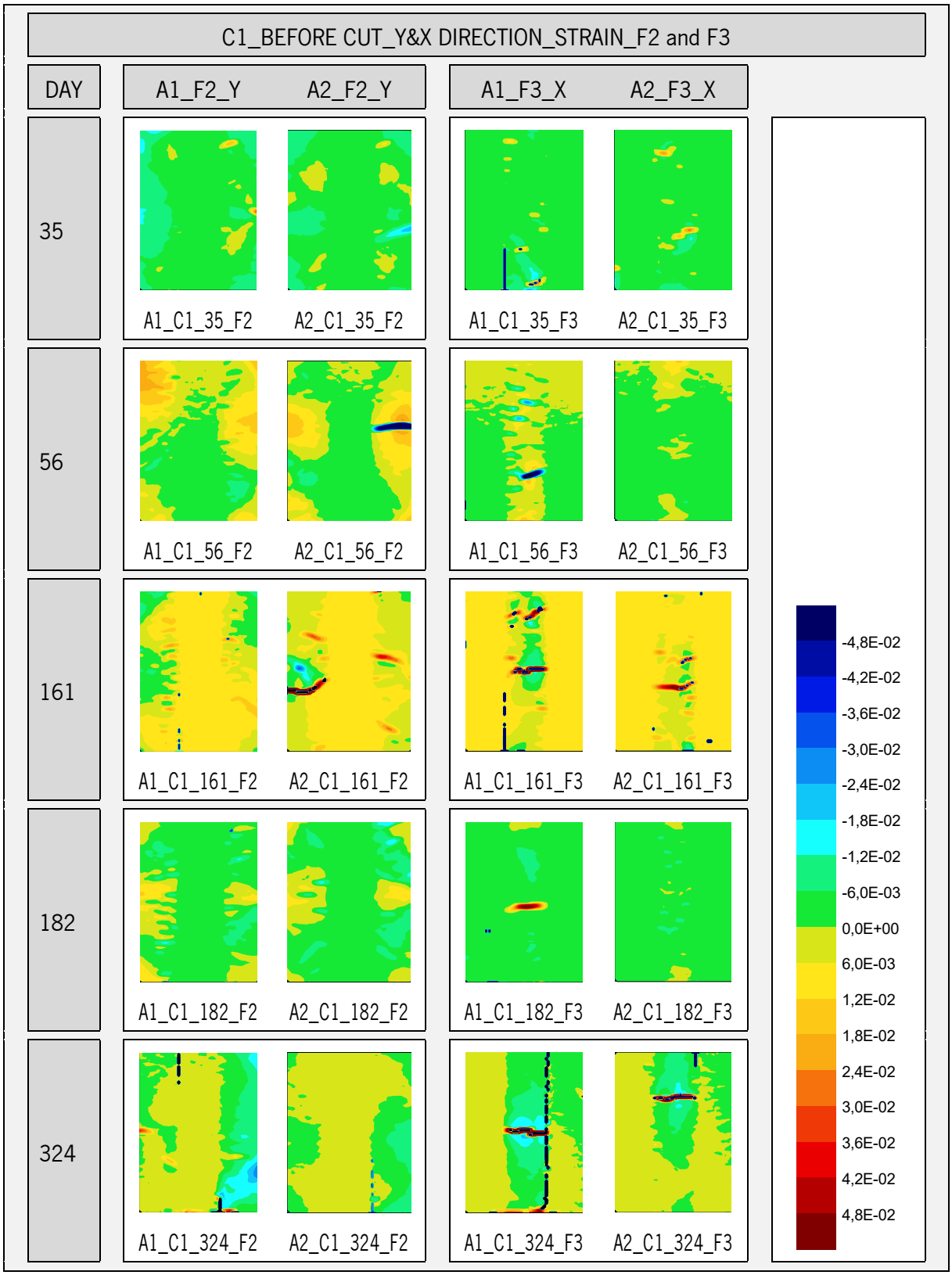
C1_BEFORE CUT_Y&X DIRECTION_STRAIN_F2 and F3
DAY
A1_F2_Y
A2_F2_Y
A1_F3_X
A2_F3_X
35
A1_C1_35_F2
A2_C1_35_F2
A1_C1_35_F3
A2_C1_35_F3
56
A1_C1_56_F2
A2_C1_56_F2
A1_C1_56_F3
A2_C1_56_F3
161
A1_C1_161_F2
A2_C1_161_F2
A1_C1_161_F3
A2_C1_161_F3
182
A1_C1_182_F2
A2_C1_182_F2
A1_C1_182_F3
A2_C1_182_F3
324
A1_C1_324_F2
A2_C1_324_F2
A1_C1_324_F3
A2_C1_324_F3
-4,8E-02
-4,2E-02
-3,6E-02
-3,0E-02
-2,4E-02
-1,8E-02
-1,2E-02
-6,0E-03
0,0E+00
6,0E-03
1,2E-02
1,8E-02
2,4E-02
3,0E-02
3,6E-02
4,2E-02
4,8E-02

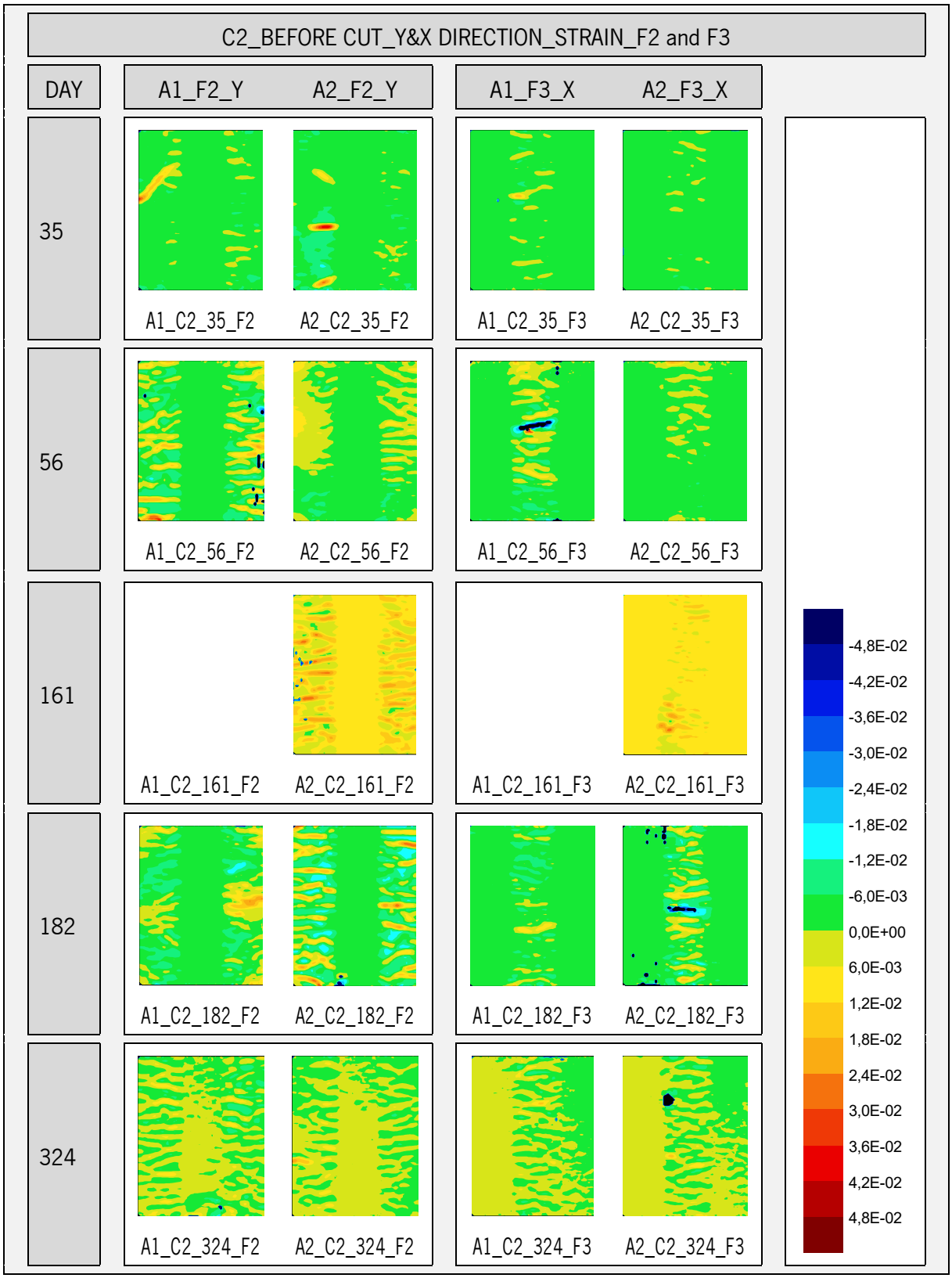
C2_BEFORE CUT_Y&X DIRECTION_STRAIN_F2 and F3
DAY
A1_F2_Y
A2_F2_Y
A1_F3_X
A2_F3_X
35
A1_C2_35_F2
A2_C2_35_F2
A1_C2_35_F3
A2_C2_35_F3
56
A1_C2_56_F2
A2_C2_56_F2
A1_C2_56_F3
A2_C2_56_F3
161
A1_C2_161_F2
A2_C2_161_F2
A1_C2_161_F3
A2_C2_161_F3
182
A1_C2_182_F2
A2_C2_182_F2
A1_C2_182_F3
A2_C2_182_F3
324
A1_C2_324_F2
A2_C2_324_F2
A1_C2_324_F3
A2_C2_324_F3
-4,8E-02
-4,2E-02
-3,6E-02
-3,0E-02
-2,4E-02
-1,8E-02
-1,2E-02
-6,0E-03
0,0E+00
6,0E-03
1,2E-02
1,8E-02
2,4E-02
3,0E-02
3,6E-02
4,2E-02
4,8E-02

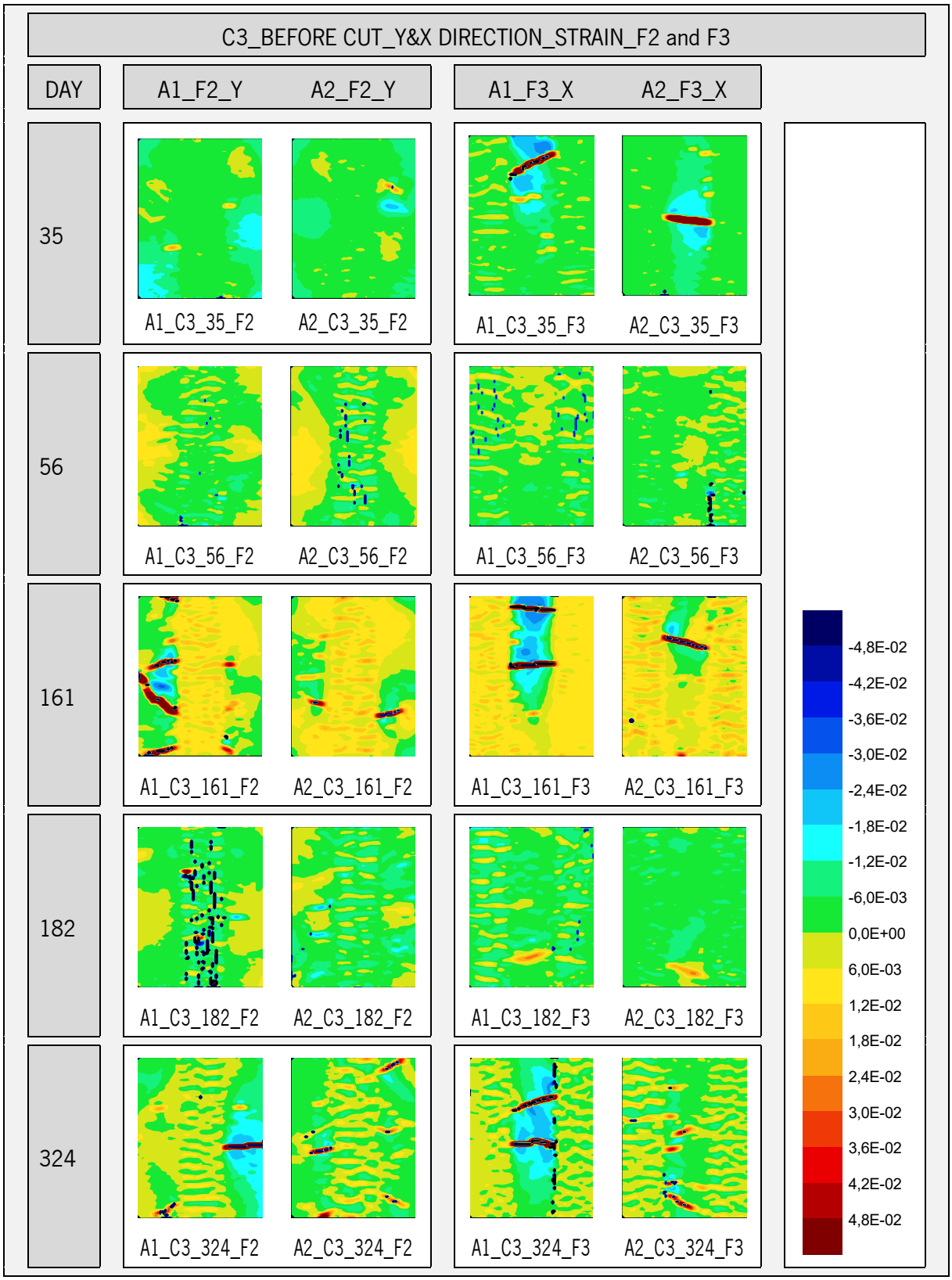
C3_BEFORE CUT_Y&X DIRECTION_STRAIN_F2 and F3
DAY
A1_F2_Y
A2_F2_Y
A1_F3_X
A2_F3_X
35
A1_C3_35_F2
A2_C3_35_F2
A1_C3_35_F3
A2_C3_35_F3
56
A1_C3_56_F2
A2_C3_56_F2
A1_C3_56_F3
A2_C3_56_F3
161
A1_C3_161_F2
A2_C3_161_F2
A1_C3_161_F3
A2_C3_161_F3
182
A1_C3_182_F2
A2_C3_182_F2
A1_C3_182_F3
A2_C3_182_F3
324
A1_C3_324_F2
A2_C3_324_F2
A1_C3_324_F3
A2_C3_324_F3
-4,8E-02
-4,2E-02
-3,6E-02
-3,0E-02
-2,4E-02
-1,8E-02
-1,2E-02
-6,0E-03
0,0E+00
6,0E-03
1,2E-02
1,8E-02
2,4E-02
3,0E-02
3,6E-02
4,2E-02
4,8E-02

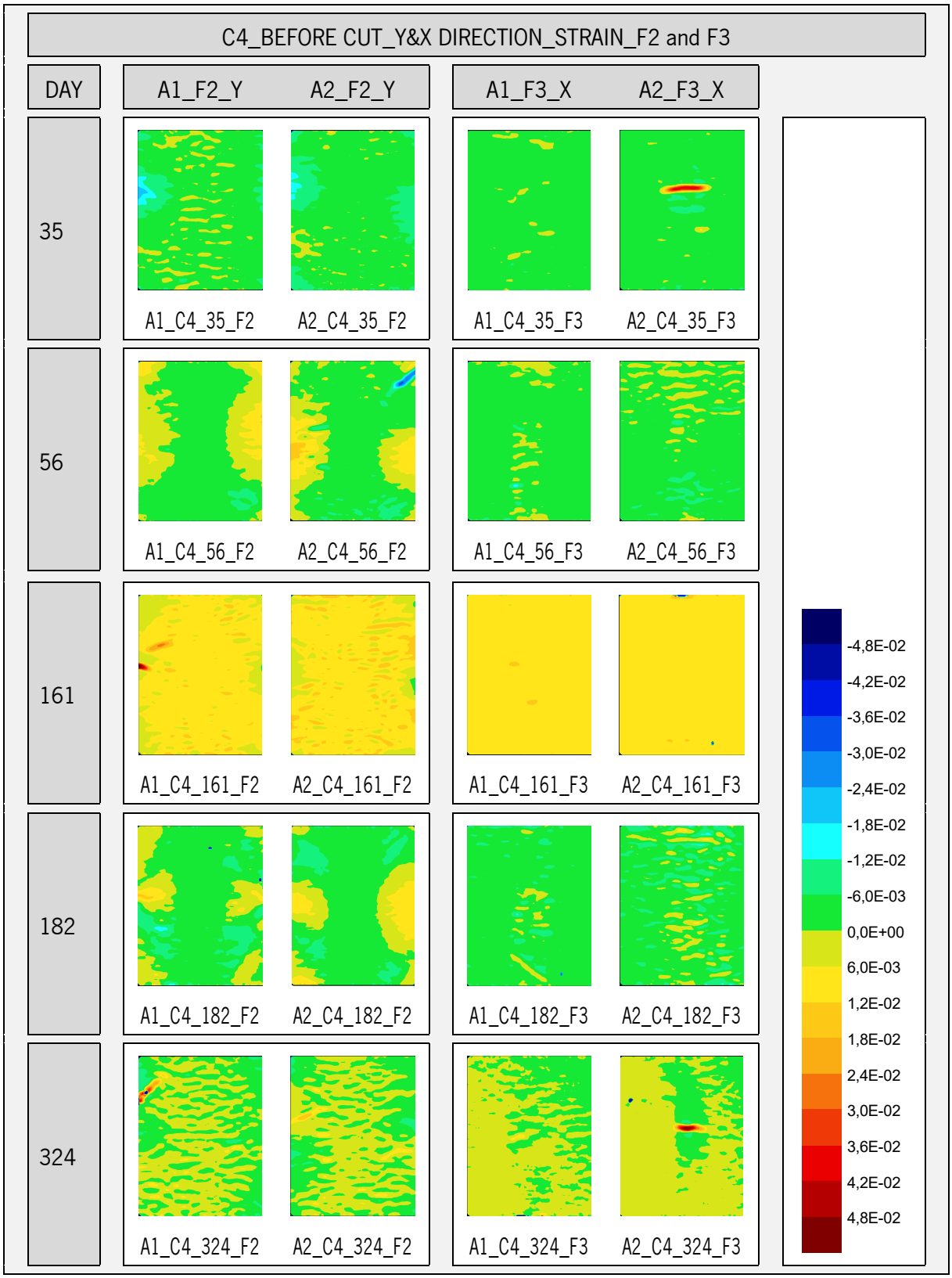
C4_BEFORE CUT_Y&X DIRECTION_STRAIN_F2 and F3
DAY
A1_F2_Y
A2_F2_Y
A1_F3_X
A2_F3_X
35
A1_C4_35_F2
A2_C4_35_F2
A1_C4_35_F3
A2_C4_35_F3
56
A1_C4_56_F2
A2_C4_56_F2
A1_C4_56_F3
A2_C4_56_F3
161
A1_C4_161_F2
A2_C4_161_F2
A1_C4_161_F3
A2_C4_161_F3
182
A1_C4_182_F2
A2_C4_182_F2
A1_C4_182_F3
A2_C4_182_F3
324
A1_C4_324_F2
A2_C4_324_F2
A1_C4_324_F3
A2_C4_324_F3
-4,8E-02
-4,2E-02
-3,6E-02
-3,0E-02
-2,4E-02
-1,8E-02
-1,2E-02
-6,0E-03
0,0E+00
6,0E-03
1,2E-02
1,8E-02
2,4E-02
3,0E-02
3,6E-02
4,2E-02
4,8E-02

Annex 1:5

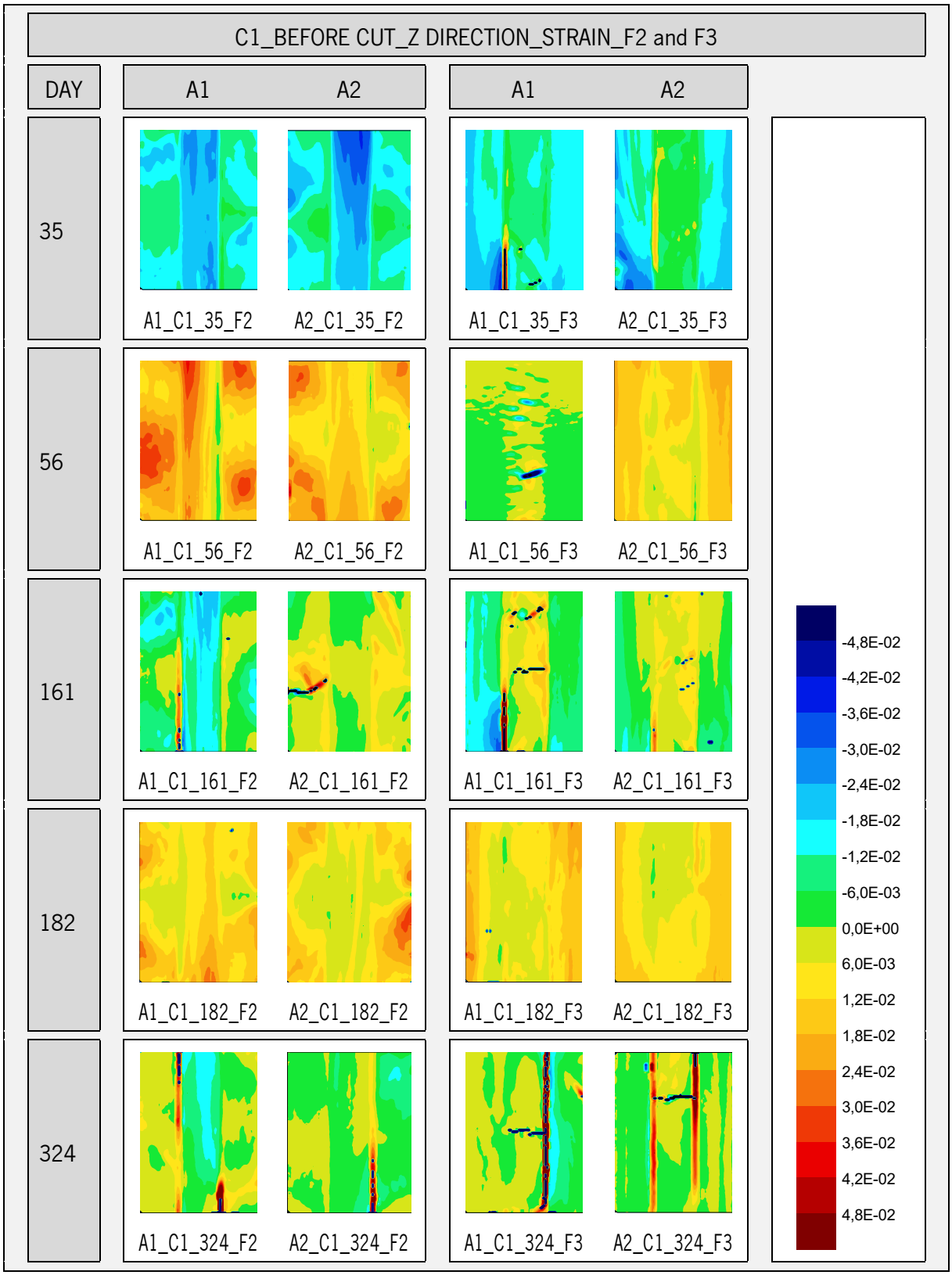
C1_BEFORE CUT_Z DIRECTION_STRAIN_F2 and F3
DAY
A1
A2
A1
A2
35
A1_C1_35_F2
A2_C1_35_F2
A1_C1_35_F3
A2_C1_35_F3
56
A1_C1_56_F2
A2_C1_56_F2
A1_C1_56_F3
A2_C1_56_F3
161
A1_C1_161_F2
A2_C1_161_F2
A1_C1_161_F3
A2_C1_161_F3
182
A1_C1_182_F2
A2_C1_182_F2
A1_C1_182_F3
A2_C1_182_F3
324
A1_C1_324_F2
A2_C1_324_F2
A1_C1_324_F3
A2_C1_324_F3
-4,8E-02
-4,2E-02
-3,6E-02
-3,0E-02
-2,4E-02
-1,8E-02
-1,2E-02
-6,0E-03
0,0E+00
6,0E-03
1,2E-02
1,8E-02
2,4E-02
3,0E-02
3,6E-02
4,2E-02
4,8E-02

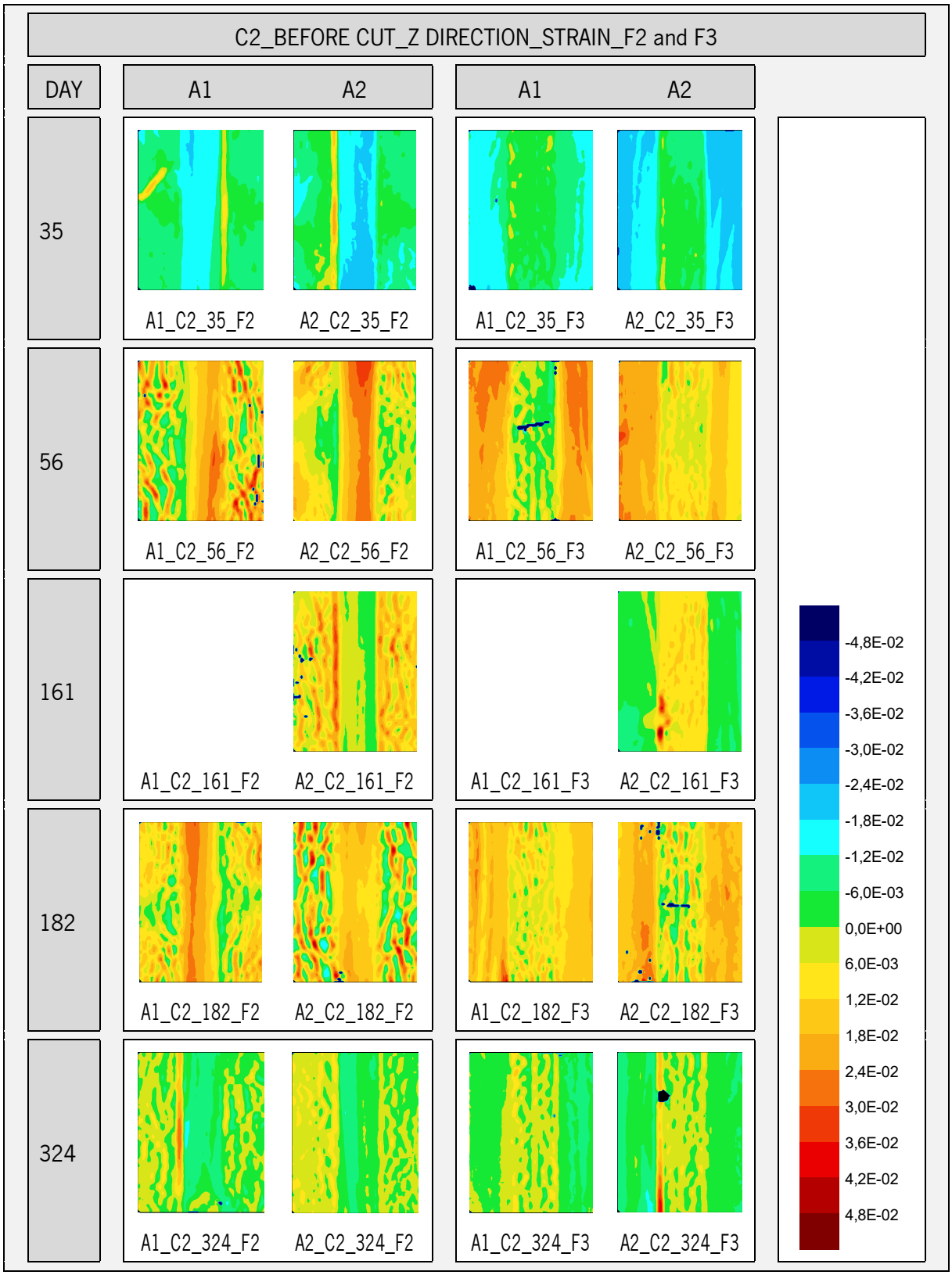
C2_BEFORE CUT_Z DIRECTION_STRAIN_F2 and F3
DAY
A1
A2
A1
A2
35
A1_C2_35_F2
A2_C2_35_F2
A1_C2_35_F3
A2_C2_35_F3
56
A1_C2_56_F2
A2_C2_56_F2
A1_C2_56_F3
A2_C2_56_F3
161
A1_C2_161_F2
A2_C2_161_F2
A1_C2_161_F3
A2_C2_161_F3
182
A1_C2_182_F2
A2_C2_182_F2
A1_C2_182_F3
A2_C2_182_F3
324
A1_C2_324_F2
A2_C2_324_F2
A1_C2_324_F3
A2_C2_324_F3
-4,8E-02
-4,2E-02
-3,6E-02
-3,0E-02
-2,4E-02
-1,8E-02
-1,2E-02
-6,0E-03
0,0E+00
6,0E-03
1,2E-02
1,8E-02
2,4E-02
3,0E-02
3,6E-02
4,2E-02
4,8E-02

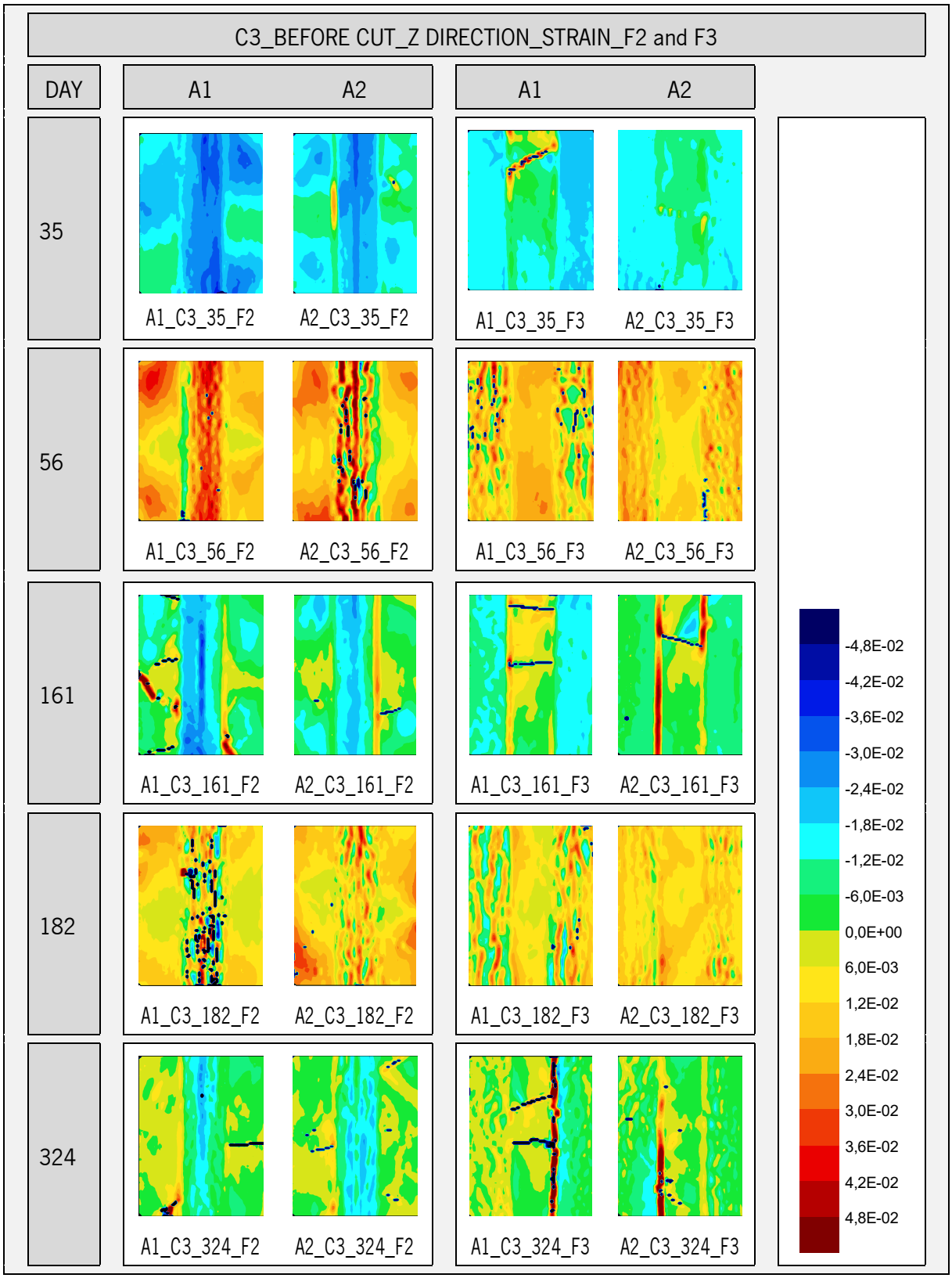
C3_BEFORE CUT_Z DIRECTION_STRAIN_F2 and F3
DAY
A1
A2
A1
A2
35
A1_C3_35_F2
A2_C3_35_F2
A1_C3_35_F3
A2_C3_35_F3
56
A1_C3_56_F2
A2_C3_56_F2
A1_C3_56_F3
A2_C3_56_F3
161
A1_C3_161_F2
A2_C3_161_F2
A1_C3_161_F3
A2_C3_161_F3
182
A1_C3_182_F2
A2_C3_182_F2
A1_C3_182_F3
A2_C3_182_F3
324
A1_C3_324_F2
A2_C3_324_F2
A1_C3_324_F3
A2_C3_324_F3
-4,8E-02
-4,2E-02
-3,6E-02
-3,0E-02
-2,4E-02
-1,8E-02
-1,2E-02
-6,0E-03
0,0E+00
6,0E-03
1,2E-02
1,8E-02
2,4E-02
3,0E-02
3,6E-02
4,2E-02
4,8E-02

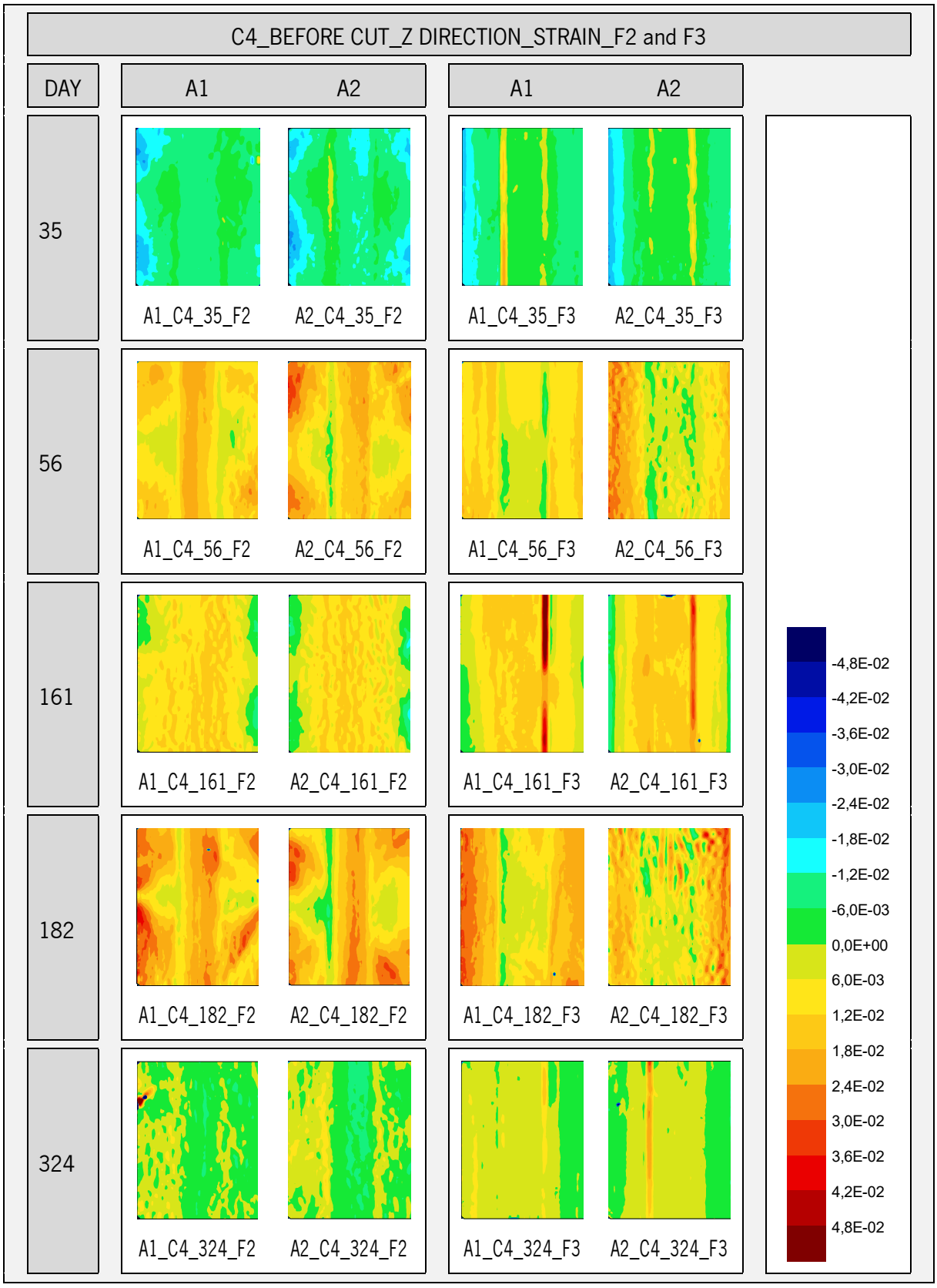
C4_BEFORE CUT_Z DIRECTION_STRAIN_F2 and F3
DAY
A1
A2
A1
A2
35
A1_C4_35_F2
A2_C4_35_F2
A1_C4_35_F3
A2_C4_35_F3
56
A1_C4_56_F2
A2_C4_56_F2
A1_C4_56_F3
A2_C4_56_F3
161
A1_C4_161_F2
A2_C4_161_F2
A1_C4_161_F3
A2_C4_161_F3
182
A1_C4_182_F2
A2_C4_182_F2
A1_C4_182_F3
A2_C4_182_F3
324
A1_C4_324_F2
A2_C4_324_F2
A1_C4_324_F3
A2_C4_324_F3
-4,8E-02
-4,2E-02
-3,6E-02
-3,0E-02
-2,4E-02
-1,8E-02
-1,2E-02
-6,0E-03
0,0E+00
6,0E-03
1,2E-02
1,8E-02
2,4E-02
3,0E-02
3,6E-02
4,2E-02
4,8E-02

Annex 1:6

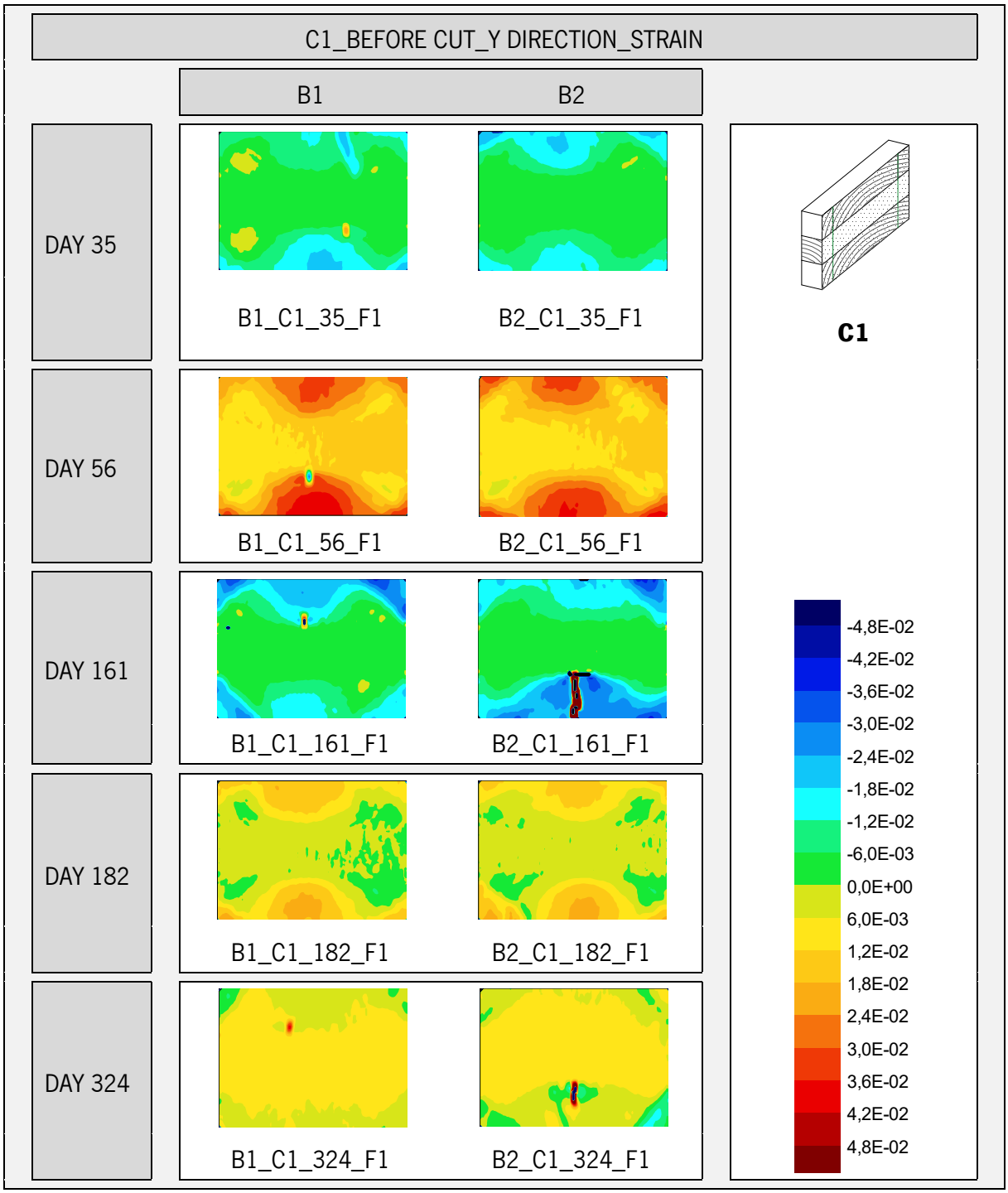
C1_BEFORE CUT_Y DIRECTION_STRAIN
B1
B2
DAY 35
DAY 56
DAY 161
DAY 182
DAY 324
B1_C1_35_F1
B2_C1_35_F1
B1_C1_56_F1
B2_C1_56_F1
B1_C1_161_F1
B2_C1_161_F1
B1_C1_182_F1
B2_C1_182_F1
B1_C1_324_F1
B2_C1_324_F1
C1
-4,8E-02
-4,2E-02
-3,6E-02
-3,0E-02
-2,4E-02
-1,8E-02
-1,2E-02
-6,0E-03
0,0E+00
6,0E-03
1,2E-02
1,8E-02
2,4E-02
3,0E-02
3,6E-02
4,2E-02
4,8E-02

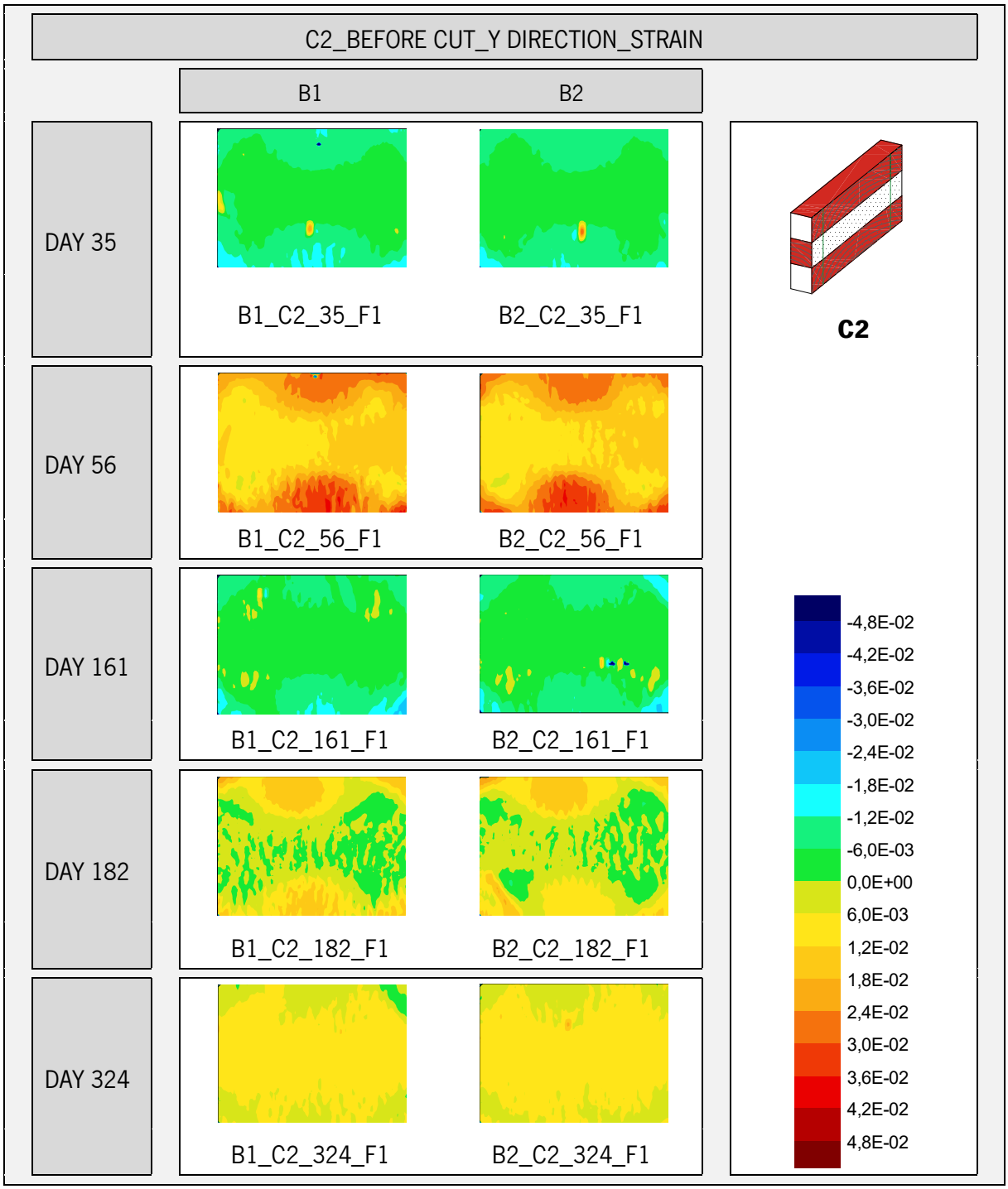
C2_BEFORE CUT_Y DIRECTION_STRAIN
B1
B2
DAY 35
DAY 56
DAY 161
DAY 182
DAY 324
B1_C2_35_F1
B2_C2_35_F1
B1_C2_56_F1
B2_C2_56_F1
B1_C2_161_F1
B2_C2_161_F1
B1_C2_182_F1
B2_C2_182_F1
B1_C2_324_F1
B2_C2_324_F1
C2
-4,8E-02
-4,2E-02
-3,6E-02
-3,0E-02
-2,4E-02
-1,8E-02
-1,2E-02
-6,0E-03
0,0E+00
6,0E-03
1,2E-02
1,8E-02
2,4E-02
3,0E-02
3,6E-02
4,2E-02
4,8E-02

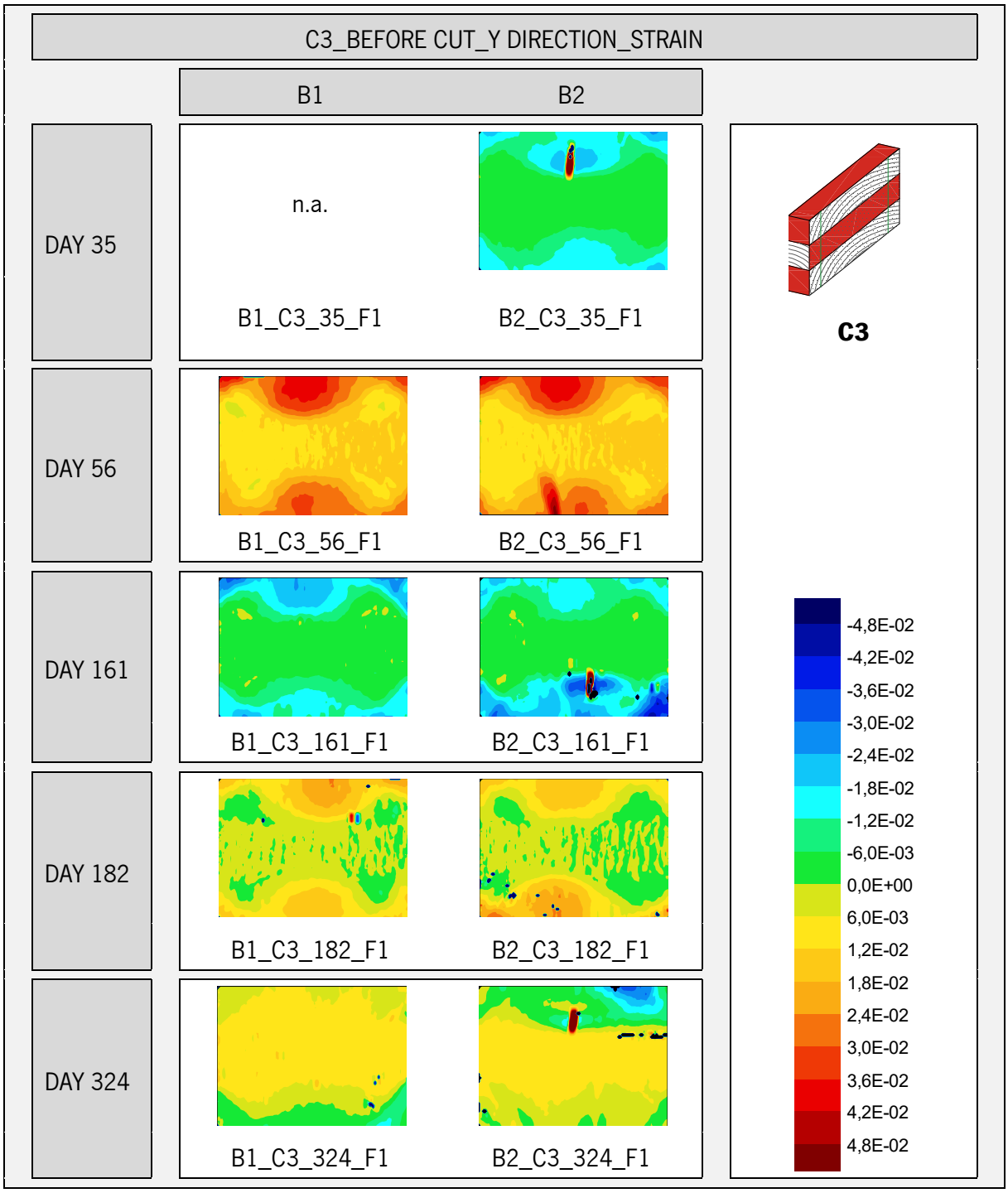
C3_BEFORE CUT_Y DIRECTION_STRAIN
B1
B2
DAY 35
n.a.
B1_C3_35_F1
B2_C3_35_F1
DAY 56
B1_C3_56_F1
B2_C3_56_F1
DAY 161
B1_C3_161_F1
B2_C3_161_F1
DAY 182
B1_C3_182_F1
B2_C3_182_F1
DAY 324
B1_C3_324_F1
B2_C3_324_F1
C3
-4,8E-02
-4,2E-02
-3,6E-02
-3,0E-02
-2,4E-02
-1,8E-02
-1,2E-02
-6,0E-03
0,0E+00
6,0E-03
1,2E-02
1,8E-02
2,4E-02
3,0E-02
3,6E-02
4,2E-02
4,8E-02

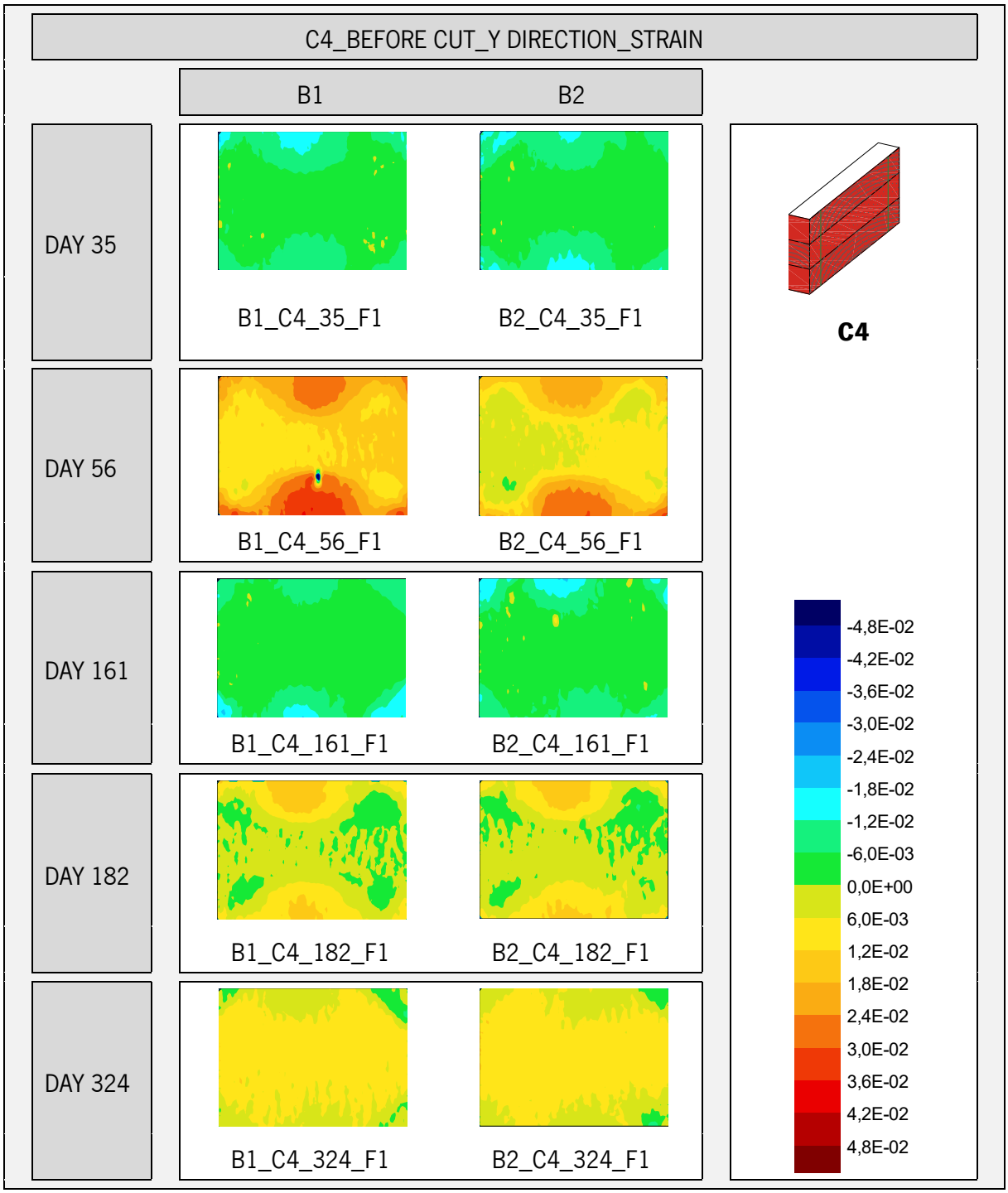
C4_BEFORE CUT_Y DIRECTION_STRAIN
B1
B2
DAY 35
DAY 56
DAY 161
DAY 182
DAY 324
B1_C4_35_F1
B2_C4_35_F1
B1_C4_56_F1
B2_C4_56_F1
B1_C4_161_F1
B2_C4_161_F1
B1_C4_182_F1
B2_C4_182_F1
B1_C4_324_F1
B2_C4_324_F1
C4
-4,8E-02
-4,2E-02
-3,6E-02
-3,0E-02
-2,4E-02
-1,8E-02
-1,2E-02
-6,0E-03
0,0E+00
6,0E-03
1,2E-02
1,8E-02
2,4E-02
3,0E-02
3,6E-02
4,2E-02
4,8E-02

Annex 1:7

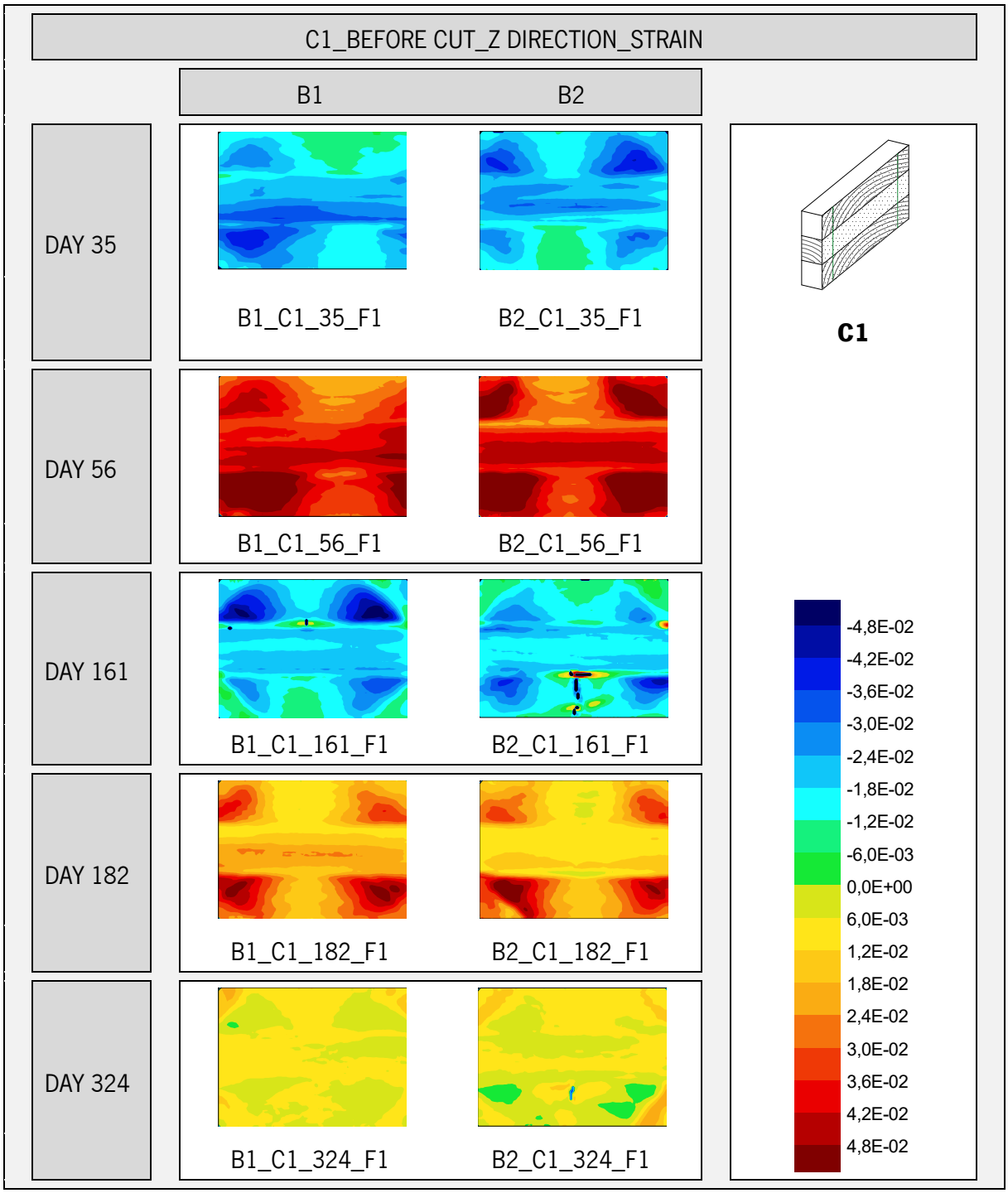
C1_BEFORE CUT_Z DIRECTION_STRAIN
B1
B2
DAY 35
DAY 56
DAY 161
DAY 182
DAY 324
B1_C1_35_F1
B2_C1_35_F1
B1_C1_56_F1
B2_C1_56_F1
B1_C1_161_F1
B2_C1_161_F1
B1_C1_182_F1
B2_C1_182_F1
B1_C1_324_F1
B2_C1_324_F1
C1
-4,8E-02
-4,2E-02
-3,6E-02
-3,0E-02
-2,4E-02
-1,8E-02
-1,2E-02
-6,0E-03
0,0E+00
6,0E-03
1,2E-02
1,8E-02
2,4E-02
3,0E-02
3,6E-02
4,2E-02
4,8E-02

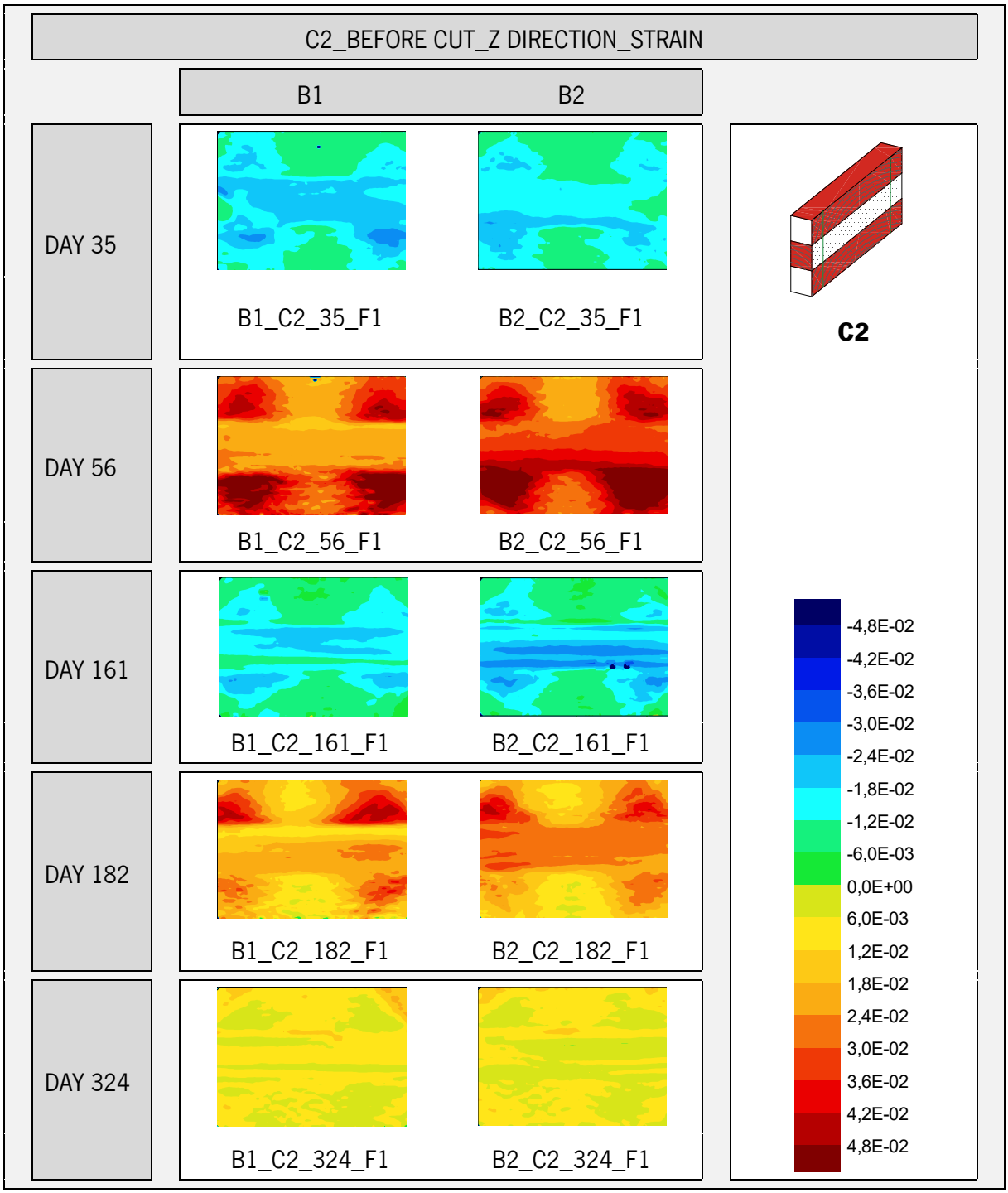
C2_BEFORE CUT_Z DIRECTION_STRAIN
B1
B2
DAY 35
DAY 56
DAY 161
DAY 182
DAY 324
B1_C2_35_F1
B2_C2_35_F1
B1_C2_56_F1
B2_C2_56_F1
B1_C2_161_F1
B2_C2_161_F1
B1_C2_182_F1
B2_C2_182_F1
B1_C2_324_F1
B2_C2_324_F1
C2
-4,8E-02
-4,2E-02
-3,6E-02
-3,0E-02
-2,4E-02
-1,8E-02
-1,2E-02
-6,0E-03
0,0E+00
6,0E-03
1,2E-02
1,8E-02
2,4E-02
3,0E-02
3,6E-02
4,2E-02
4,8E-02

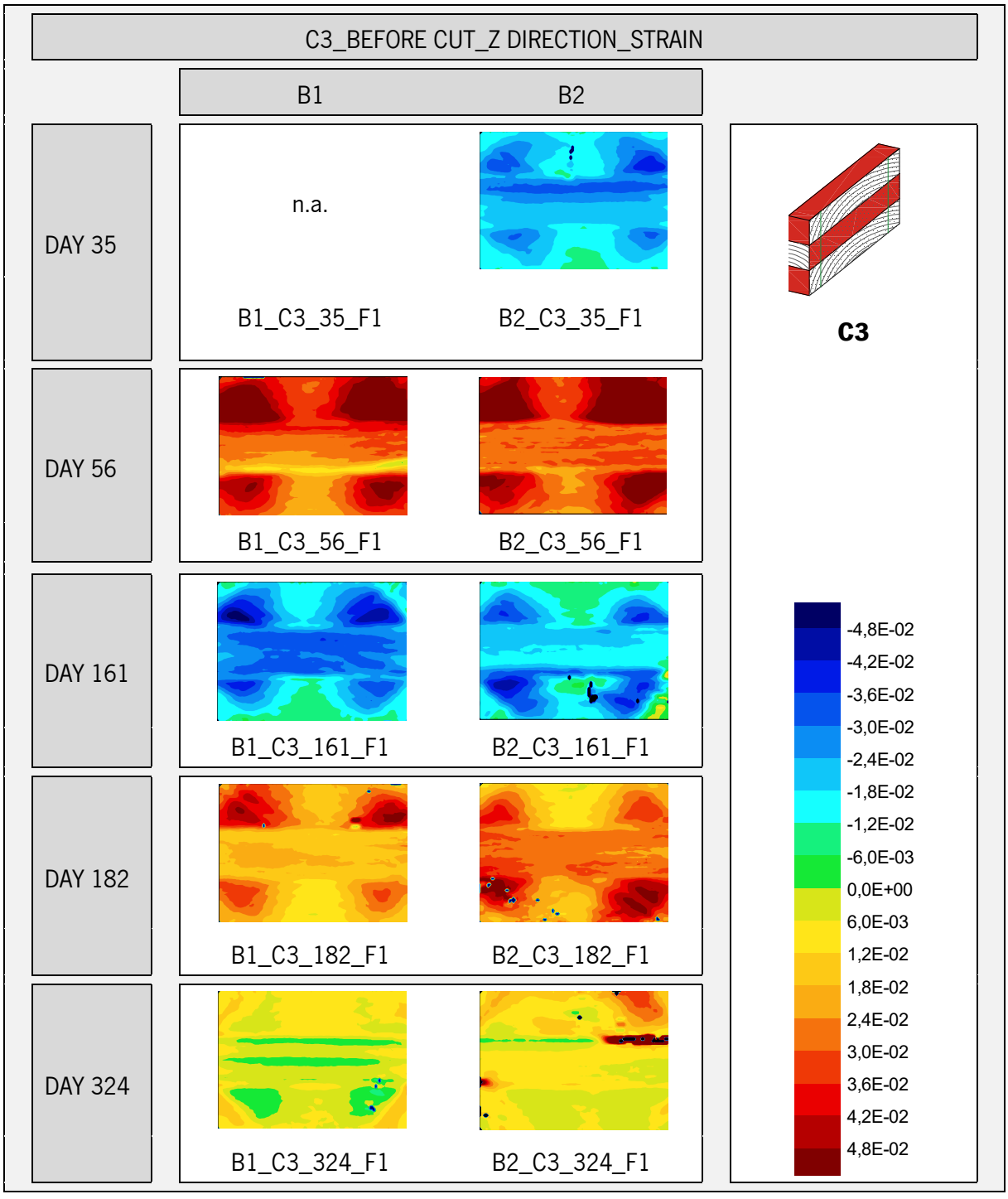
C3_BEFORE CUT_Z DIRECTION_STRAIN
B1
B2
DAY 35
n.a.
B1_C3_35_F1
B2_C3_35_F1
DAY 56
B1_C3_56_F1
B2_C3_56_F1
DAY 161
B1_C3_161_F1
B2_C3_161_F1
DAY 182
B1_C3_182_F1
B2_C3_182_F1
DAY 324
B1_C3_324_F1
B2_C3_324_F1
C3
-4,8E-02
-4,2E-02
-3,6E-02
-3,0E-02
-2,4E-02
-1,8E-02
-1,2E-02
-6,0E-03
0,0E+00
6,0E-03
1,2E-02
1,8E-02
2,4E-02
3,0E-02
3,6E-02
4,2E-02
4,8E-02

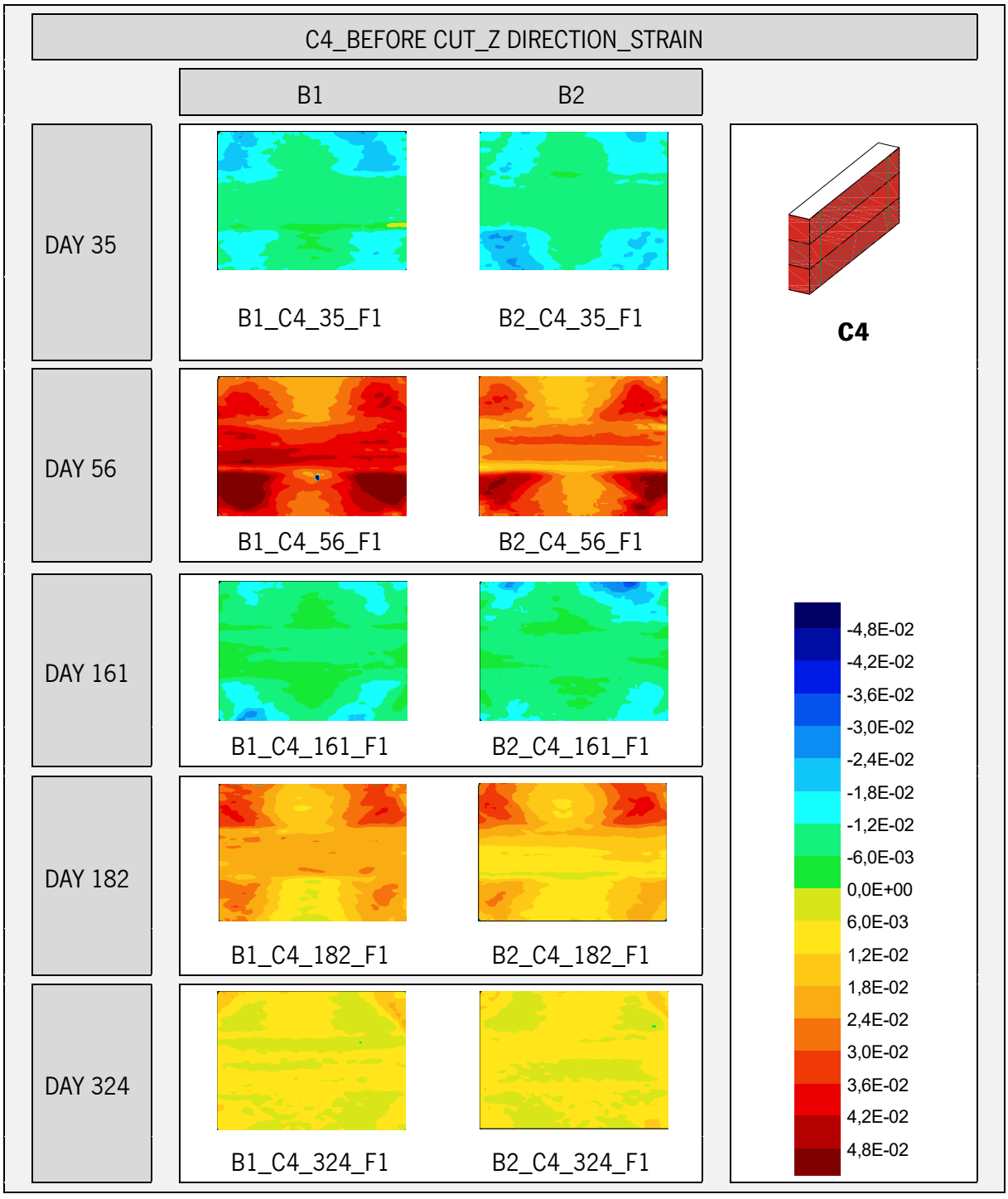
C4_BEFORE CUT_Z DIRECTION_STRAIN
B1
B2
DAY 35
B1_C4_35_F1
B2_C4_35_F1
DAY 56
B1_C4_56_F1
B2_C4_56_F1
DAY 161
B1_C4_161_F1
B2_C4_161_F1
DAY 182
B1_C4_182_F1
B2_C4_182_F1
DAY 324
B1_C4_324_F1
B2_C4_324_F1
C4
-4,8E-02
-4,2E-02
-3,6E-02
-3,0E-02
-2,4E-02
-1,8E-02
-1,2E-02
-6,0E-03
0,0E+00
6,0E-03
1,2E-02
1,8E-02
2,4E-02
3,0E-02
3,6E-02
4,2E-02
4,8E-02

Annex 1:8[i]

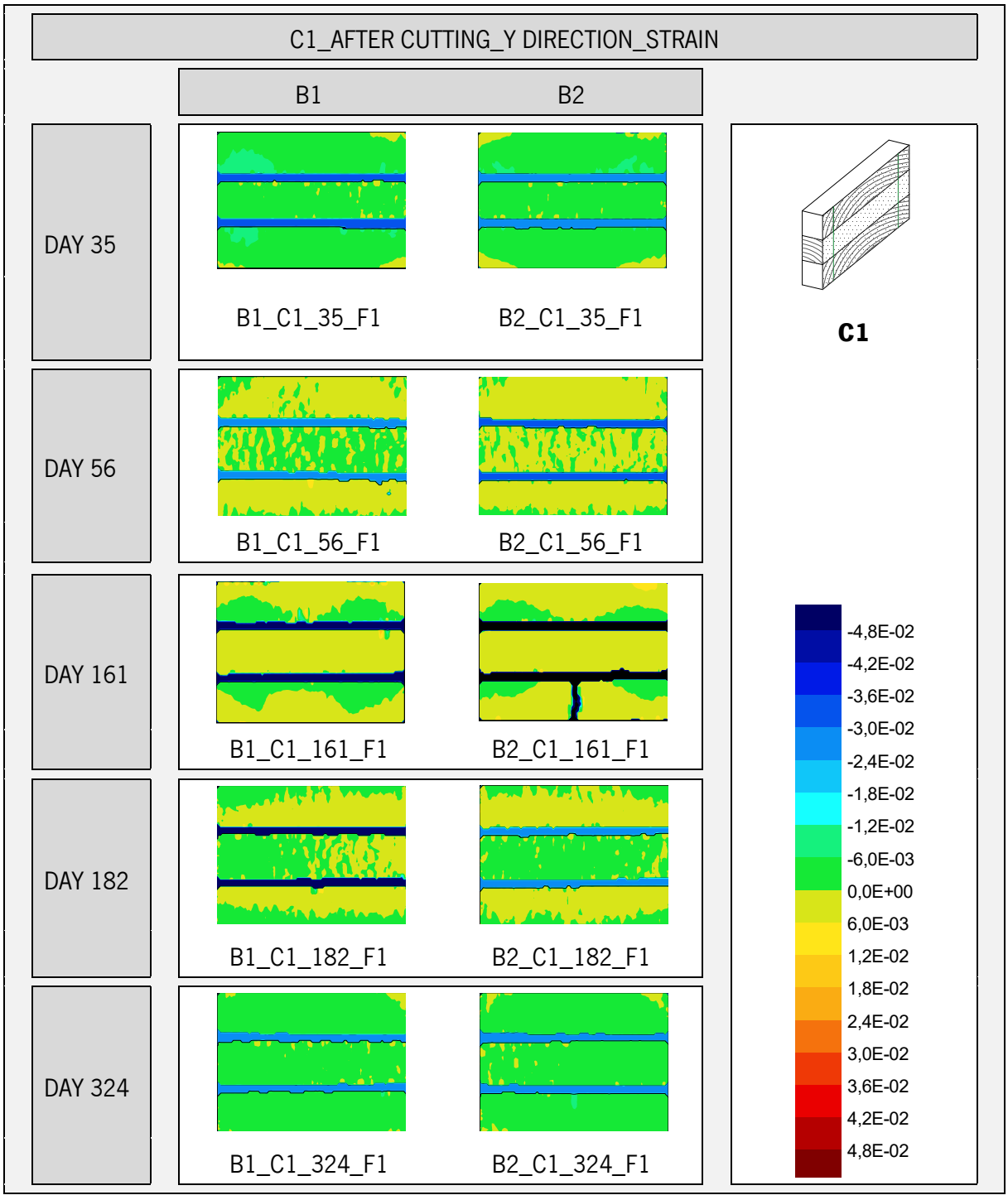
C1_AFTER CUTTING_Y DIRECTION_STRAIN
B1
B2
DAY 35
DAY 56
DAY 161
DAY 182
DAY 324
B1_C1_35_F1
B2_C1_35_F1
B1_C1_56_F1
B2_C1_56_F1
B1_C1_161_F1
B2_C1_161_F1
B1_C1_182_F1
B2_C1_182_F1
B1_C1_324_F1
B2_C1_324_F1
C1
-4,8E-02
-4,2E-02
-3,6E-02
-3,0E-02
-2,4E-02
-1,8E-02
-1,2E-02
-6,0E-03
0,0E+00
6,0E-03
1,2E-02
1,8E-02
2,4E-02
3,0E-02
3,6E-02
4,2E-02
4,8E-02

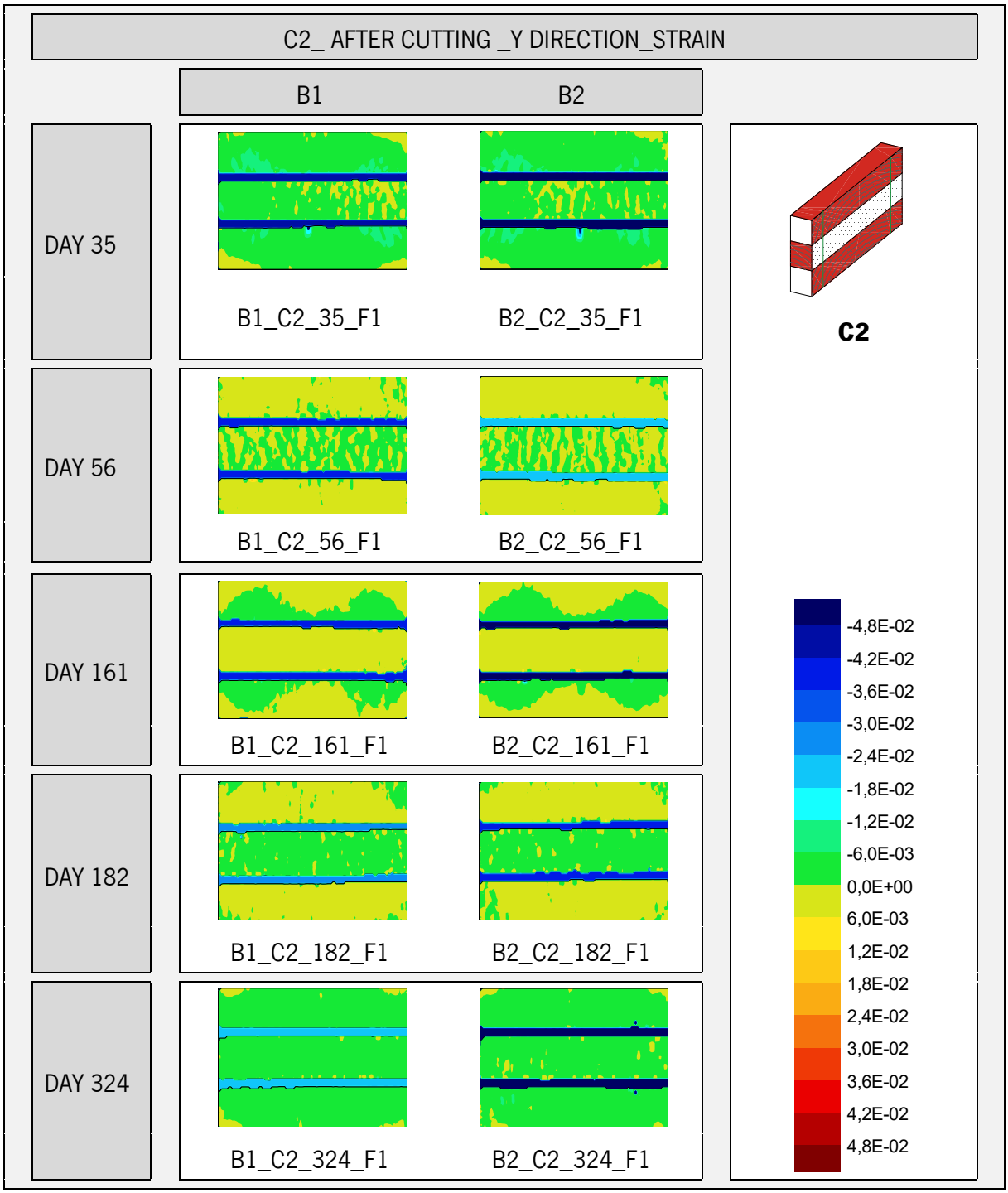
C2_ AFTER CUTTING _Y DIRECTION_STRAIN
B1
B2
DAY 35
DAY 56
DAY 161
DAY 182
DAY 324
B1_C2_35_F1
B2_C2_35_F1
B1_C2_56_F1
B2_C2_56_F1
B1_C2_161_F1
B2_C2_161_F1
B1_C2_182_F1
B2_C2_182_F1
B1_C2_324_F1
B2_C2_324_F1
C2
-4,8E-02
-4,2E-02
-3,6E-02
-3,0E-02
-2,4E-02
-1,8E-02
-1,2E-02
-6,0E-03
0,0E+00
6,0E-03
1,2E-02
1,8E-02
2,4E-02
3,0E-02
3,6E-02
4,2E-02
4,8E-02

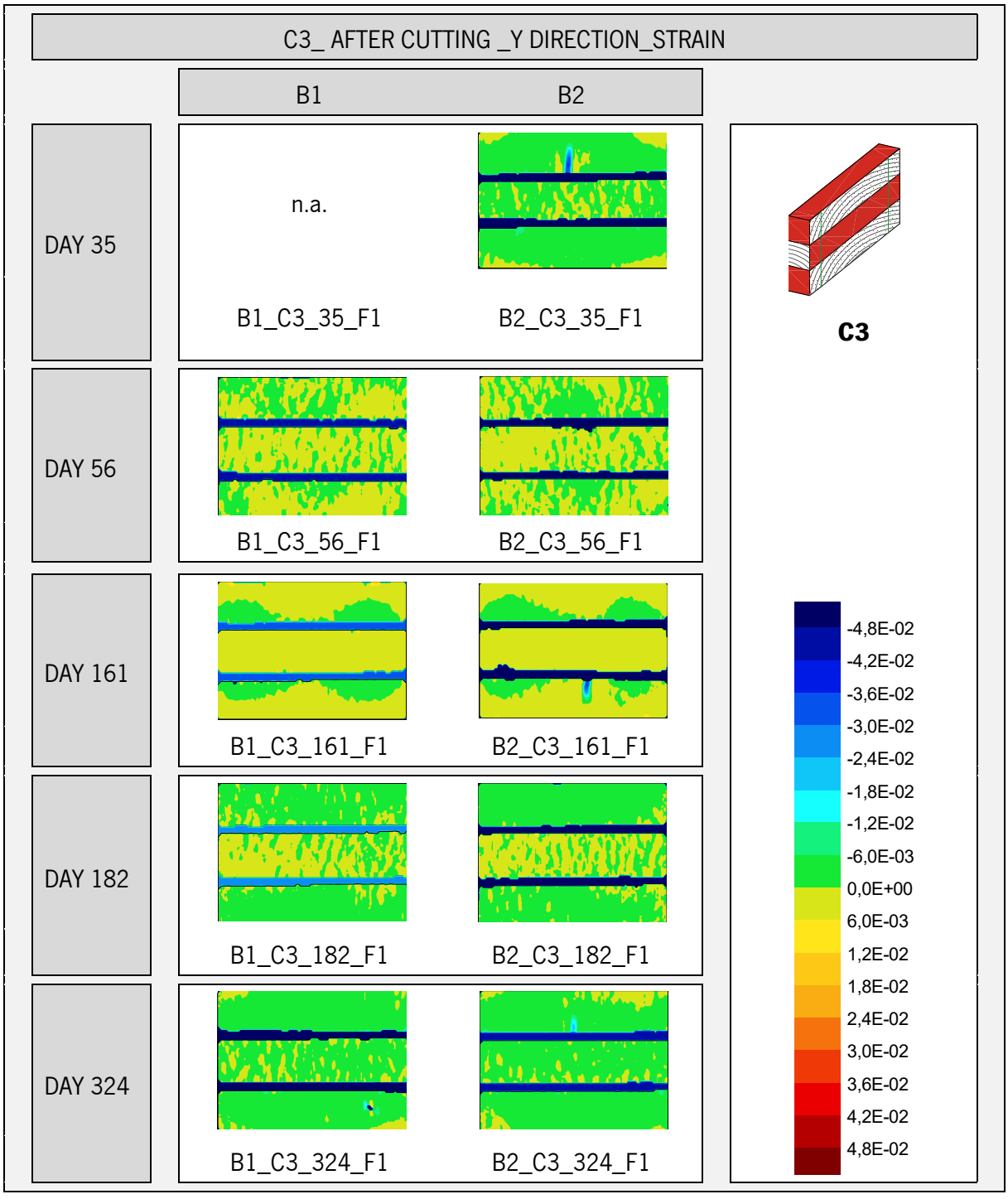
C3_ AFTER CUTTING _Y DIRECTION_STRAIN
B1
B2
DAY 35
n.a.
B1_C3_35_F1
B2_C3_35_F1
DAY 56
B1_C3_56_F1
B2_C3_56_F1
DAY 161
B1_C3_161_F1
B2_C3_161_F1
DAY 182
B1_C3_182_F1
B2_C3_182_F1
DAY 324
B1_C3_324_F1
B2_C3_324_F1
C3
-4,8E-02
-4,2E-02
-3,6E-02
-3,0E-02
-2,4E-02
-1,8E-02
-1,2E-02
-6,0E-03
0,0E+00
6,0E-03
1,2E-02
1,8E-02
2,4E-02
3,0E-02
3,6E-02
4,2E-02
4,8E-02

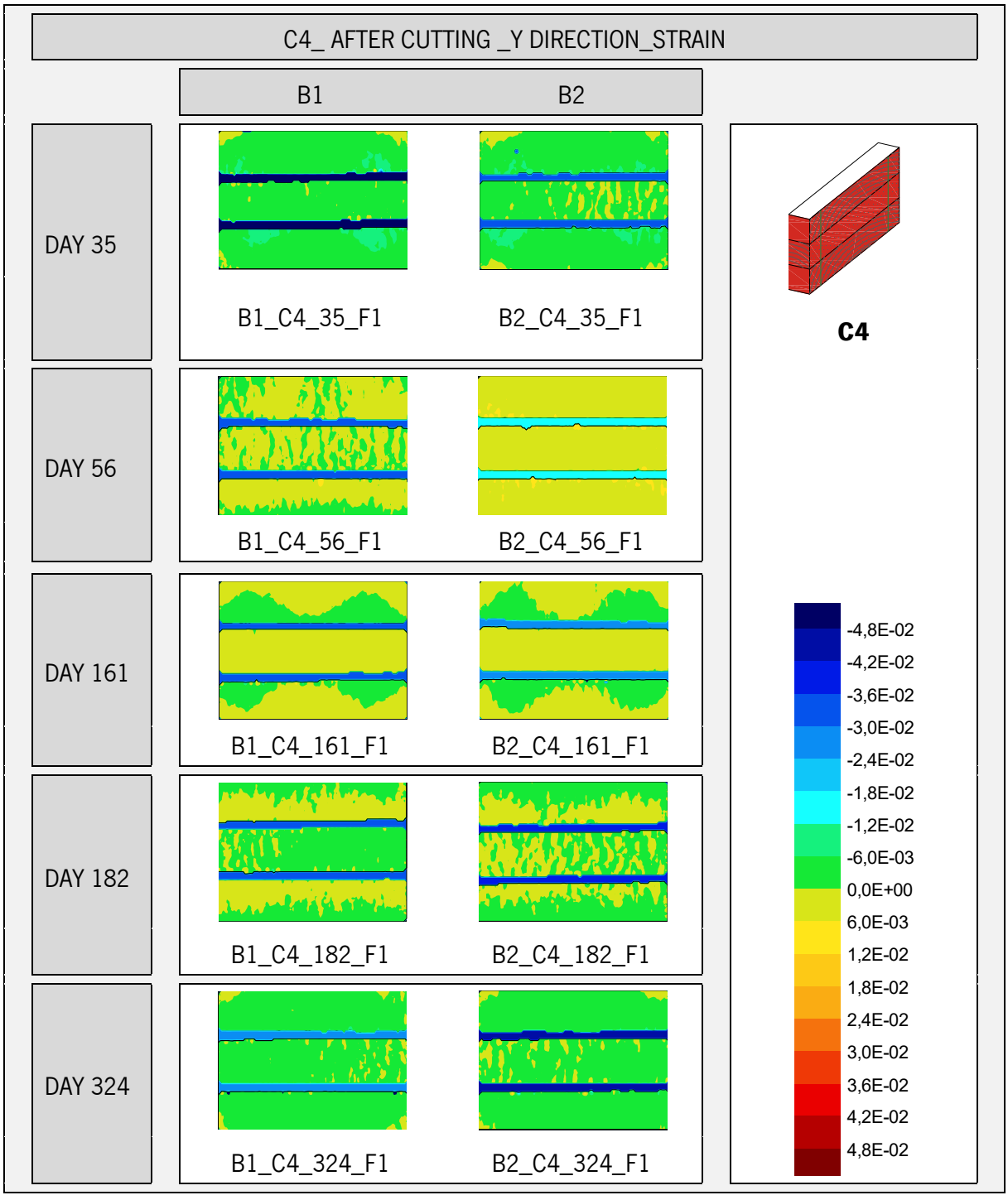
C4_ AFTER CUTTING _Y DIRECTION_STRAIN
B1
B2
DAY 35
DAY 56
DAY 161
DAY 182
DAY 324
B1_C4_35_F1
B2_C4_35_F1
B1_C4_56_F1
B2_C4_56_F1
B1_C4_161_F1
B2_C4_161_F1
B1_C4_182_F1
B2_C4_182_F1
B1_C4_324_F1
B2_C4_324_F1
C4
-4,8E-02
-4,2E-02
-3,6E-02
-3,0E-02
-2,4E-02
-1,8E-02
-1,2E-02
-6,0E-03
0,0E+00
6,0E-03
1,2E-02
1,8E-02
2,4E-02
3,0E-02
3,6E-02
4,2E-02
4,8E-02

Annex 1:9

RESULTS OBTAINED FOR THE RATIO $\frac{E_{static}}{E_{dyn}}$

SPECIMEN	ENTIRE SPECIMEN				PARALLEL TO THE GRAIN	PERPENDICULAR TO THE GRAIN	
	CROSS 1 AND 2	CROSS 3 AND 4	GLUED A+B+C	CUT A+B+C	LAYER B	LAYER A	LAYER C
SP1	5,95	1,59*	0,33	0,32*	0,31*	n.a.	0,54*
SP2	9,31*	0,69	0,36	0,16	0,15	0,11	0,16
SP3	8,70*	0,45	0,36	0,15	0,14	0,12	0,18
SP4	6,44	0,24	0,17	0,15	0,16	0,19	0,12
SP5	4,77	0,66	0,18	0,15	0,14	0,17	0,24
SP6	5,05	0,24	0,47	0,13	0,11	0,16	0,18
SP7	3,97	0,32	0,42	0,19	0,18	0,21	0,26
SP8	4,57	0,35	0,35	0,14	0,14	0,17	0,17
SP9	4,84	1,47*	0,47	0,14	0,13	0,16	0,17
SP10	4,59	1,16*	0,34	0,19	0,16	0,16	0,37*
SP11	3,58	0,33	0,37	0,21	0,19	0,17	0,20
SP12	4,20	0,50	0,44	0,22	0,15	0,31*	0,12
SP13	5,80	0,29	0,33	0,15	0,14	0,22	0,17
SP14	3,50	0,33	0,31	0,16	0,16	0,25	0,20
SP15	2,70	0,27	0,20	0,15	0,13	0,25	0,16
SP16	3,64	0,23	0,20	0,17	0,17	0,24	0,14
SP17	6,07	0,25	0,19	0,16	0,14	0,15	0,11
SP18	n.a.	n.a.	n.a.	n.a.	0,20	0,14	n.a.
SP19	2,66	0,23	0,30	0,24*	0,17	0,16	0,16
SP20	2,17	0,20	0,20	0,20	0,19	0,17	0,16
SP21	2,14	0,28	0,24	0,24*	0,21	0,18	0,16
SAMPLE	**20**	**20**	**20**	**20**	**21**	**40**	
MEAN	**4,73**	**0,50**	**0,31**	**0,18**	**0,17**	**0,19**	
COV	**0,408**	**0,828**	**0,316**	**0,254**	**0,256**	**0,402**	
MINIMUM	**2,14**	**0,20**	**0,17**	**0,13**	**0,11**	**0,11**	
MAXIMUM	**9,31**	**1,59**	**0,47**	**0,32**	**0,31**	**0,54**	

*Values considered outliers on data analysis

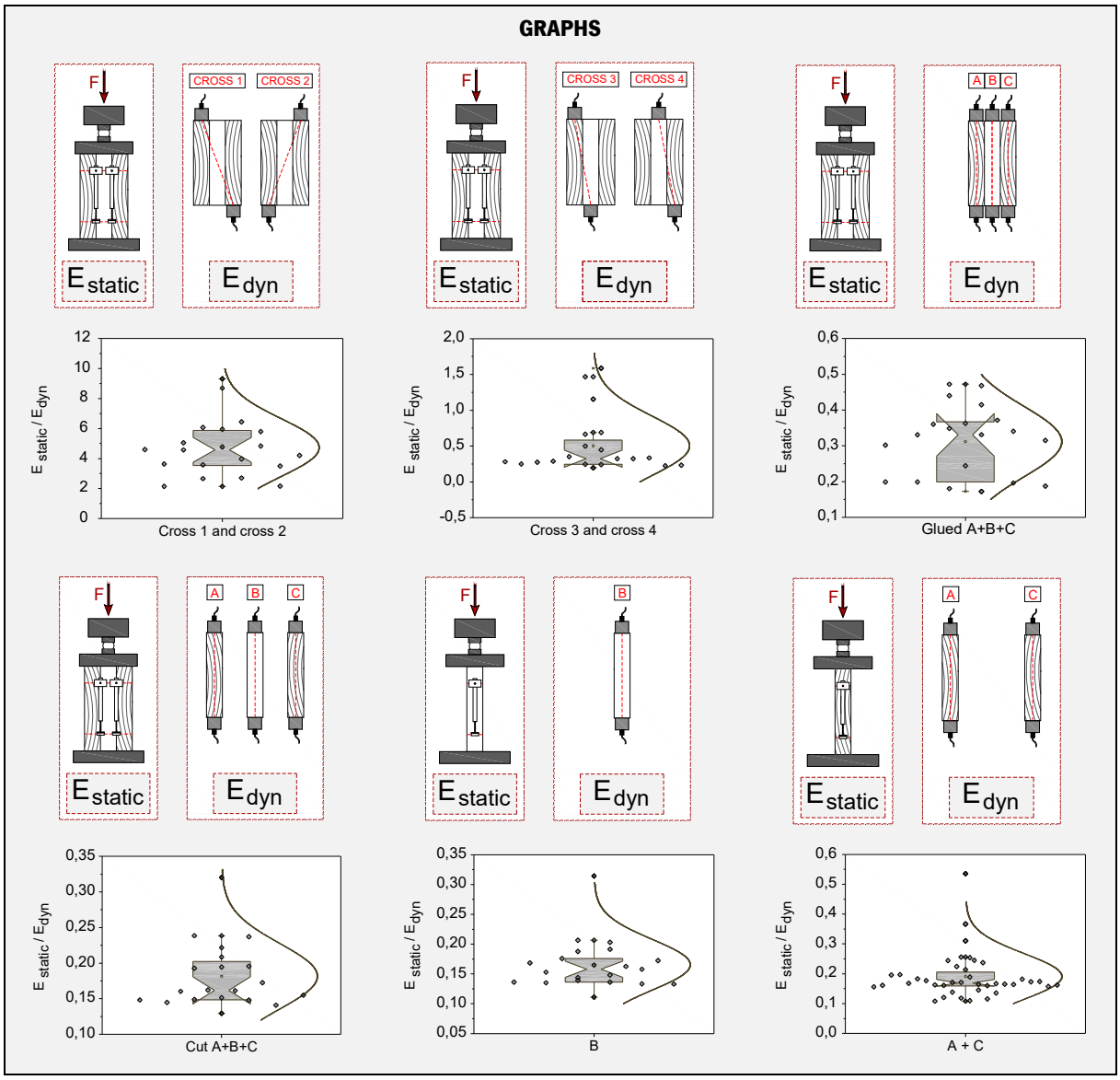
GRAPHS
F
CROSS 1
CROSS 2
E static
E dyn
CROSS 3
CROSS 4
A B C
E static / E dyn
Cross 1 and cross 2
Cross 3 and cross 4
Glued A+B+C
Cut A+B+C
B
A + C

Annex 1:10

REF_12%

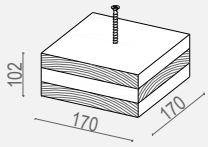

	WEIGHT AT TEST TIME [g] [mean values]	DRY WEIGHT [g] [mean values]	MC [%]	f_{ax} [N/mm²]	ρ [kg/m³]
1_REF_12%	1120,7	1012,43	10,69%	5,41	375,91
2_REF_12%	1222,75	1105,53	10,60%	5,62	409,91
3_REF_12%	1304,27	1175,08	10,99%	6,26	437,59
4_REF_12%	1360,17	1213,51	12,09%	6,74	458,21
5_REF_12%	1380,51	1233,89	11,88%	6,56	464,65
6_REF_12%	1415,72	1262,1	12,17%	6,65	477,62
7_REF_12%	1446,45	1286,07	12,47%	6,62	488,15
8_REF_12%	1495,26	1331,62	12,29%	5,83	504,42
9_REF_12%	1623,06	1447,44	12,13%	6,99	547,46
10_REF_12%	1643,32	1475,32	11,39%	7,56	553,12
MEAN VALUES	**1401,22**	**1254,30**	**11,67%**	**6,42**	**471,70**

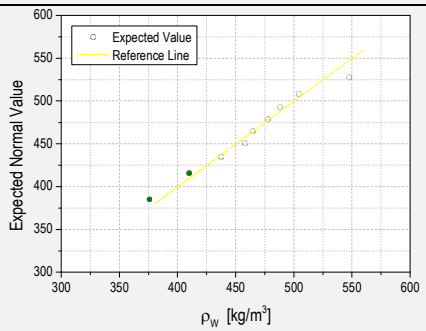

Q-Q plot of density distribution for configuration REF_12%

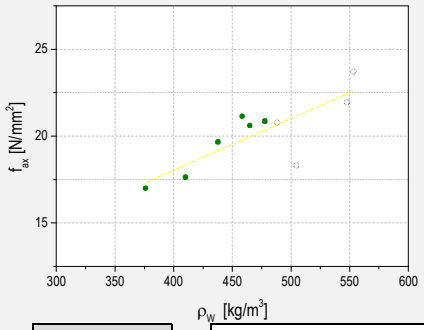

k_ρ	$6.11 + 0.03 \cdot \rho$
R-Square	**0.62**

Linear fitting of correlation between f_{ax} and density for configuration REF_12%

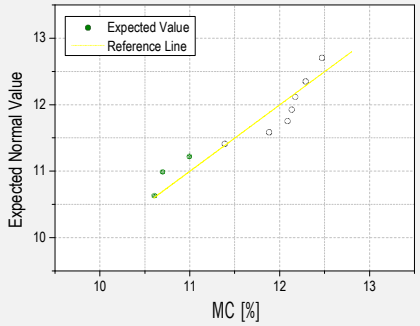

Q-Q plot of moisture content distribution for configuration REF_12%

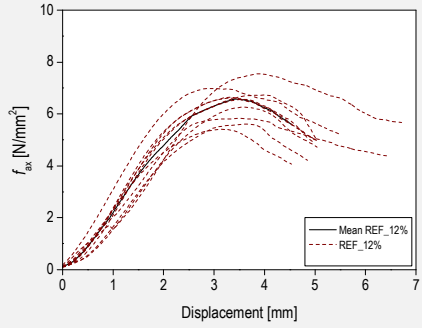

Relation between f_{ax} and displacement for REF_12% tests

	MAXIMUM	MINIMUM	SD	CoV	MEDIAN	P5
f_{ax}	7,56	5,41	0,65	0,10	6,59	5,41
ρ	553,12	375,91	55,91	0,12	471,13	375,91
MC	12,47	10,60	0,69	0,06	11,98	10,60

GAP0_FL_12%

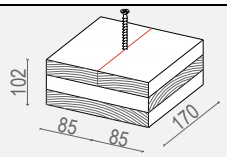

	WEIGHT AT TEST TIME [g] [mean values]	DRY WEIGHT [g] [mean values]	MC [%]	f_{ax} [N/mm²]	ρ [kg/m³]
1_GAP0_FL_12%	1168,96	1057,11	10,58%	5,45	392,72
2_GAP0_FL_12%	1186,74	1074,95	10,40%	6,00	399,23
3_GAP0_FL_12%	1294,05	1171,59	10,45%	6,57	435,02
4_GAP0_FL_12%	1305,34	1179,74	10,65%	6,74	438,23
5_GAP0_FL_12%	1356,17	1216,49	11,48%	7,12	456,70
6_GAP0_FL_12%	1377,85	1235,42	11,53%	7,16	463,81
7_GAP0_FL_12%	1420,29	1275,4	11,36%	6,58	478,66
8_GAP0_FL_12%	1432,27	1286,47	11,33%	6,41	482,39
9_GAP0_FL_12%	1472,97	1324,13	11,24%	8,32	495,12
10_GAP0_FL_12%	1517,63	1372,86	10,55%	8,41	511,13
MEAN VALUES	**1353,23**	**1219,42**	**10,96%**	**6,88**	**455,30**

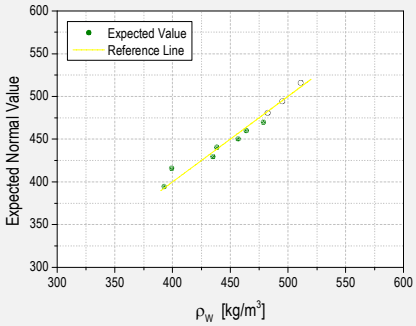

Q-Q plot of density distribution for configuration GAP0_FL_12%

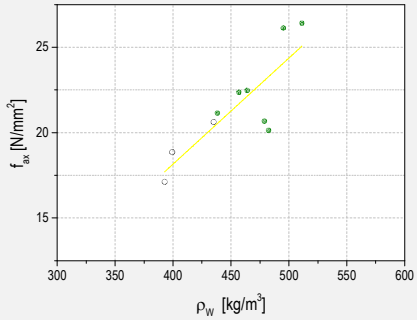

k_ρ	$-6.69 + 0.06 \cdot \rho$
R-Square	**0.66**

Linear fitting of correlation between f_{ax} and density for configuration GAP0_FL_12%

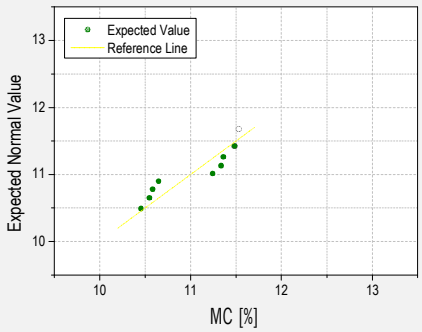

Q-Q plot of moisture content distribution for configuration GAP0_FL_12%

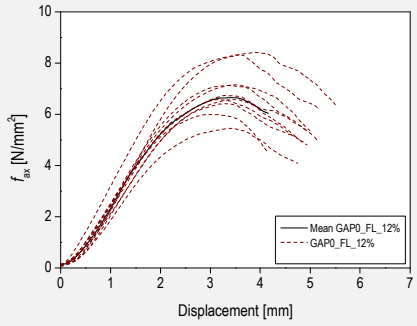

Relation between f_{ax} and displacement for GAP0_FL_12% tests

	MAXIMUM	MINIMUM	SD	CoV	MEDIAN	P5
f_{ax}	8,41	5,45	0,93	0,14	6,66	5,45
ρ	511,13	392,72	39,18	0,09	460,25	392,72
MC	11,53	10,40	0,47	0,04	10,94	10,40

GAP0_ML_12%

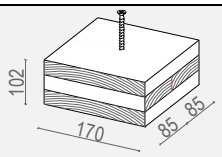

	WEIGHT AT TEST TIME [g] [mean values]	DRY WEIGHT [g] [mean values]	MC [%]	f_{ax} [N/mm²]	ρ [kg/m³]
1_GAP0_ML_12%	1174,39	1060,93	10,69%	6,06	395,83
2_GAP0_ML_12%	1212,21	1094,06	10,80%	6,13	408,22
3_GAP0_ML_12%	1299,59	1171,01	10,98%	6,62	436,76
4_GAP0_ML_12%	1326,3	1201,36	10,40%	6,16	446,39
5_GAP0_ML_12%	1350,39	1214,9	11,15%	6,42	455,26
6_GAP0_ML_12%	1373,96	1226,87	11,99%	6,71	462,99
7_GAP0_ML_12%	1412,11	1265,29	11,60%	7,32	475,55
8_GAP0_ML_12%	1434,97	1290,86	11,16%	7,50	483,64
9_GAP0_ML_12%	1470,18	1318,93	11,47%	6,47	495,74
10_GAP0_ML_12%	1483,28	1332,03	11,35%	7,18	499,92
MEAN VALUES	**1353,74**	**1217,62**	**11,16%**	**6,66**	**456,03**

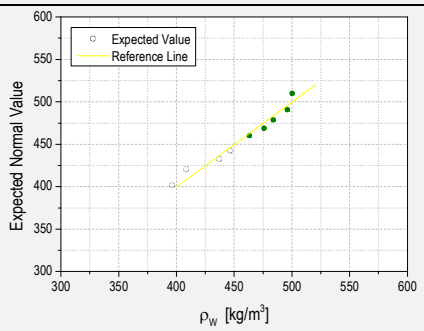

Q-Q plot of density distribution for configuration GAP0_ML_12%

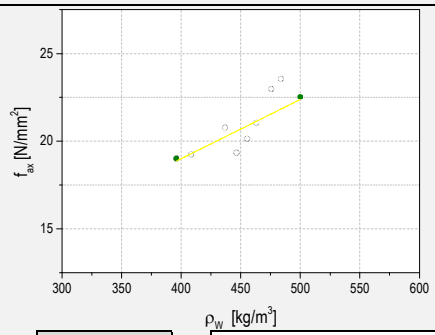

k_ρ	$6.11 + 0.03 \cdot \rho$
R-Square	**0.62**

Linear fitting of correlation between f_{ax} and density for configuration GAP0_ML_12%

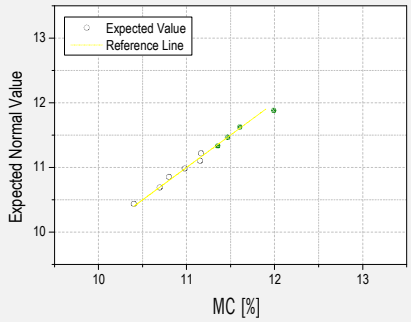

Q-Q plot of moisture content distribution for configuration GAP0_ML_12%

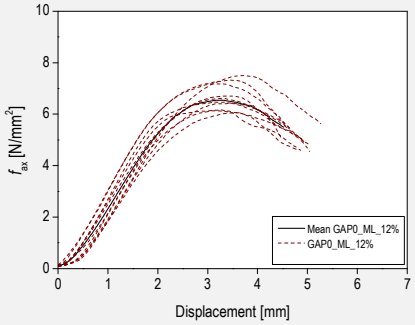

Relation between f_{ax} and displacement for GAP0_ML_12% tests

	MAXIMUM	MINIMUM	SD	CoV	MEDIAN	P5
f_{ax}	7,50	6,06	0,52	0,08	6,54	6,06
ρ	499,92	395,83	35,07	0,08	459,13	395,83
MC	11,99	10,40	0,47	0,04	11,16	10,40

GAP0_OL_12%

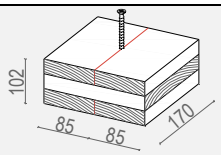

	WEIGHT AT TEST TIME [g] [mean values]	DRY WEIGHT [g] [mean values]	MC [%]	f_{ax} [N/mm^2]	ρ [kg/m^3]
1_GAP0_OL_12%	1180,85	1069,57	10,40%	5,90	395,76
2_GAP0_OL_12%	1205,34	1091,58	10,42%	6,38	404,20
3_GAP0_OL_12%	1304,64	1173,43	11,18%	6,60	439,31
4_GAP0_OL_12%	1321,51	1192,81	10,79%	6,72	444,87
5_GAP0_OL_12%	1359,45	1222,33	11,22%	7,73	457,58
6_GAP0_OL_12%	1387,95	1239,63	11,96%	7,13	468,36
7_GAP0_OL_12%	1430,07	1287,56	11,07%	7,47	481,06
8_GAP0_OL_12%	1453,2	1303,79	11,46%	7,26	489,56
9_GAP0_OL_12%	1510,29	1358,29	11,19%	7,02	509,07
10_GAP0_OL_12%	1550,09	1390,68	11,46%	7,64	523,26
MEAN VALUES	**1370,34**	**1232,97**	**11,12%**	**6,99**	**461,30**

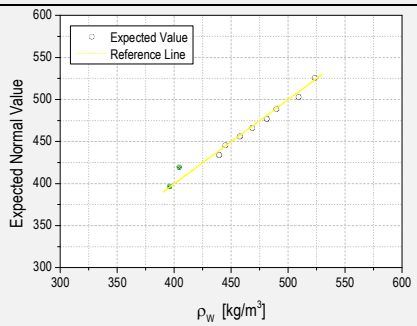

Q-Q plot of density distribution for configuration GAP0_OL_12%

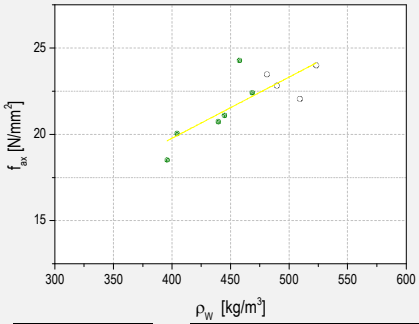

k_ρ	$5.62 + 0.01 \cdot \rho$
R-Square	**0.60**

Linear fitting of correlation between f_{ax} and density for configuration GAP0_OL_12%

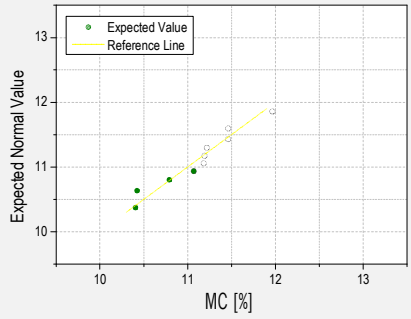

Q-Q plot of moisture content distribution for configuration GAP0_OL_12%

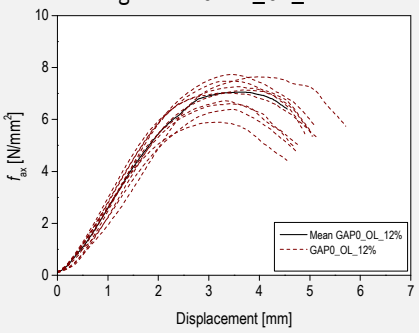

Relation between f_{ax} and displacement for GAP0_OL_12% tests

	MAXIMUM	MINIMUM	SD	CoV	MEDIAN	P5
f_{ax}	7,73	5,90	0,59	0,08	7,08	5,90
ρ	523,26	395,76	41,75	0,09	462,97	395,76
MC	11,96	10,40	0,48	0,04	11,19	10,40

GAP0_3L_12%

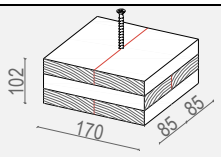

	WEIGHT AT TEST TIME [g] [mean values]	DRY WEIGHT [g] [mean values]	MC [%]	f_{ax} [N/mm²]	ρ [kg/m³]
1_GAP0_3L_12%	1168,83	1058,2	10,45%	6,71	392,24
2_GAP0_3L_12%	1183,85	1070,71	10,57%	6,34	397,81
3_GAP0_3L_12%	1287,3	1154,51	11,50%	7,32	433,46
4_GAP0_3L_12%	1305,72	1174,96	11,13%	7,41	439,68
5_GAP0_3L_12%	1357,05	1223,16	10,95%	7,21	456,26
6_GAP0_3L_12%	1383,04	1245,9	11,01%	7,92	465,15
7_GAP0_3L_12%	1422,32	1274,59	11,59%	7,87	478,99
8_GAP0_3L_12%	1429,37	1278,39	11,81%	7,56	481,97
9_GAP0_3L_12%	1481,77	1326,88	11,67%	7,40	499,94
10_GAP0_3L_12%	1498,42	1341,47	11,70%	7,35	505,15
MEAN VALUES	**1351,77**	**1214,88**	**11,24%**	**7,31**	**455,07**

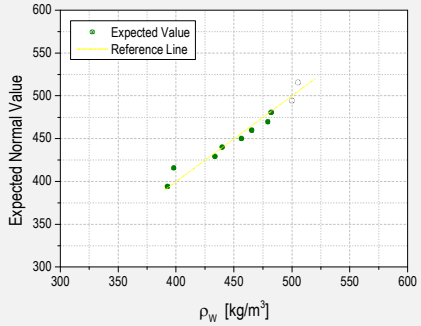

Q-Q plot of density distribution for configuration GAP0_3L_12%

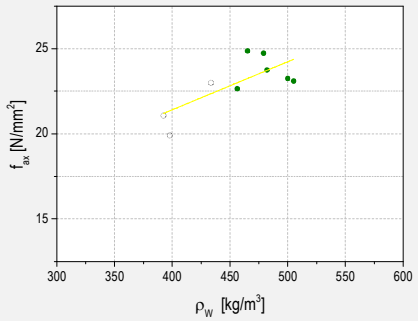

k_ρ	$10.14 + 0.03 \cdot \rho$
R-Square	**0.48**

Linear fitting of correlation between f_{ax} and density for configuration GAP0_3L_12%

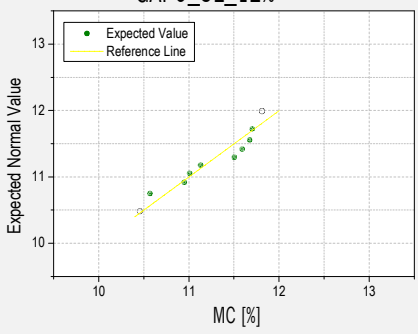

Q-Q plot of moisture content distribution for configuration GAP0_3L_12%

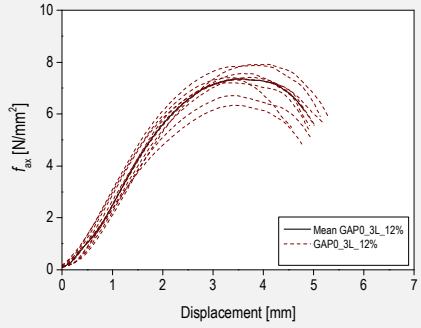

Relation between f_{ax} and displacement for GAP0_3L_12% tests

	MAXIMUM	MINIMUM	SD	CoV	MEDIAN	P5
f_{ax}	7,92	6,34	0,48	0,07	7,38	6,34
ρ	553,12	375,91	55,91	0,12	471,13	375,91
MC	11,81	10,46	0,49	0,04	11,32	10,46

GAP4_FL_12%

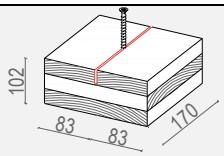

	WEIGHT AT TEST TIME [g] [mean values]	DRY WEIGHT [g] [mean values]	MC [%]	f_{ax} [N/mm²]	ρ [kg/m³]
1_GAP4_FL_12%	1185,74	1063,94	11,45%	5,12	398,39
2_GAP4_FL_12%	1216,77	1088,54	11,78%	5,25	409,63
3_GAP4_FL_12%	1290,4	1158,62	11,37%	5,23	433,38
4_GAP4_FL_12%	1314,85	1180,46	11,38%	5,51	441,01
5_GAP4_FL_12%	1357,86	1204,09	12,77%	5,89	457,50
6_GAP4_FL_12%	1377,07	1235,56	11,45%	6,07	463,72
7_GAP4_FL_12%	1403,23	1246,39	12,58%	6,15	472,85
8_GAP4_FL_12%	1432,65	1280,04	11,92%	6,07	482,93
9_GAP4_FL_12%	1476,03	1317,51	12,03%	7,09	498,05
10_GAP4_FL_12%	1513,6	1348,89	12,21%	6,92	509,88
MEAN VALUES	**1356,82**	**1212,40**	**11,90%**	**5,93**	**456,73**

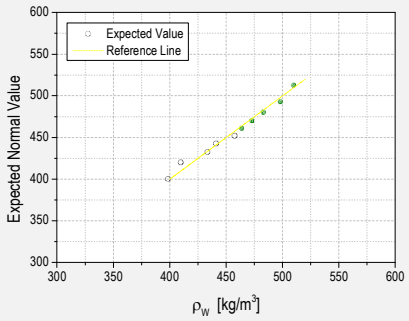

Q-Q plot of density distribution for configuration GAP4_FL_12%

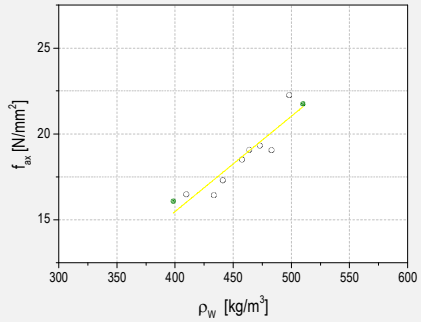

k_ρ	$-6.73 + 0.06 \cdot \rho$
R-Square	**0.87**

Linear fitting of correlation between f_{ax} and density for configuration GAP4_FL_12%

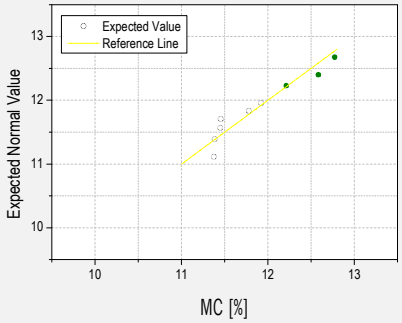

Q-Q plot of moisture content distribution for configuration GAP4_FL_12%

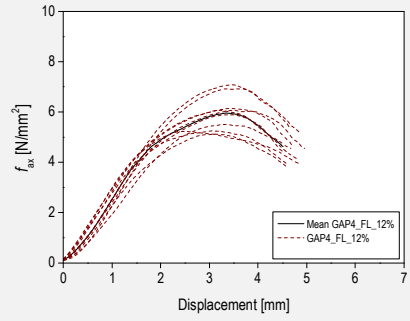

Relation between f_{ax} and displacement for GAP4_FL_12% tests

	MAXIMUM	MINIMUM	SD	CoV	MEDIAN	P5
f_{ax}	7,09	5,12	0,68	0,12	5,98	5,12
ρ	509,88	398,39	36,43	0,08	460,61	398,39
MC	12,77	11,37	0,51	0,04	11,85	11,37

GAP4_ML_12%

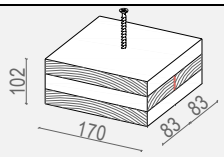

	WEIGHT AT TEST TIME [g] [mean values]	DRY WEIGHT [g] [mean values]	MC [%]	f_{ax} [N/mm²]	ρ [kg/m³]
1_GAP4_ML_12%	1197,43	1079,69	10,90%	5,29	405,43
2_GAP4_ML_12%	1225,04	1103,72	10,99%	5,42	414,34
3_GAP4_ML_12%	1291,02	1165,41	10,78%	5,50	438,08
4_GAP4_ML_12%	1330,62	1195,01	11,35%	5,84	451,42
5_GAP4_ML_12%	1360,49	1220,11	11,51%	5,96	461,28
6_GAP4_ML_12%	1387,81	1245,37	11,44%	5,85	471,13
7_GAP4_ML_12%	1407,62	1265,09	11,27%	5,95	476,94
8_GAP4_ML_12%	1412,56	1270,05	11,22%	6,11	481,94
9_GAP4_ML_12%	1475,08	1322,96	11,50%	6,30	499,82
10_GAP4_ML_12%	1511,9	1357,34	11,39%	6,74	512,16
MEAN VALUES	**1359,96**	**1222,48**	**11,23%**	**5,89**	**461,26**

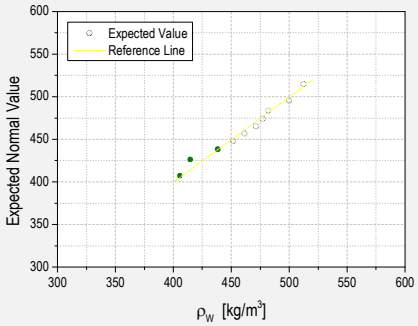

Q-Q plot of density distribution for configuration GAP4_ML_12%

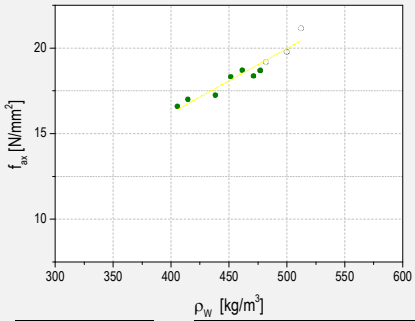

k_ρ	$1.12 + 0.00 \cdot \rho$
R-Square	**0.91**

Linear fitting of correlation between f_{ax} and density for configuration GAP4_ML_12%

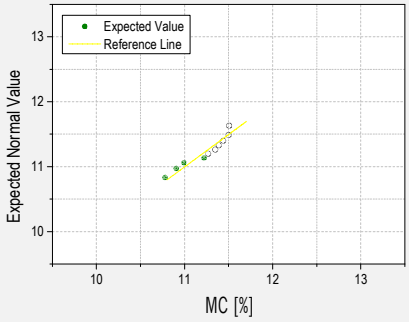

Q-Q plot of moisture content distribution for configuration GAP4_ML_12%

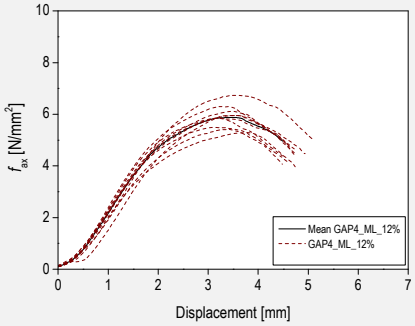

Relation between f_{ax} and displacement for GAP4_ML_12% tests

	MAXIMUM	MINIMUM	SD	CoV	MEDIAN	P5
f_{ax}	6,74	5,29	0,43	0,07	5,90	5,29
ρ	512,16	405,43	34,64	0,08	466,20	405,43
MC	11,51	10,78	0,26	0,02	11,31	10,78

GAP4_OL_12%

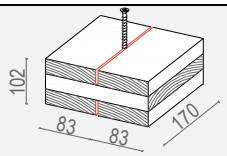

	WEIGHT AT TEST TIME [g] [mean values]	DRY WEIGHT [g] [mean values]	MC [%]	f_{ax} [N/mm²]	ρ [kg/m³]
1_GAP4_OL_12%	1195,76	1078,95	10,83%	4,49	408,73
2_GAP4_OL_12%	1215,02	1097,48	10,71%	4,51	414,80
3_GAP4_OL_12%	1291,95	1161,86	11,20%	5,26	441,10
4_GAP4_OL_12%	1302,8	1173,21	11,05%	4,61	444,31
5_GAP4_OL_12%	1363,08	1217,69	11,94%	5,14	466,86
6_GAP4_OL_12%	1370,82	1226,03	11,81%	5,89	468,83
7_GAP4_OL_12%	1405,65	1266,56	10,98%	5,83	480,91
8_GAP4_OL_12%	1417,96	1265,99	12,00%	5,58	485,56
9_GAP4_OL_12%	1495,36	1331,28	12,32%	5,83	513,59
10_GAP4_OL_12%	1551	1394,16	11,25%	6,53	529,99
MEAN VALUES	**1360,94**	**1221,32**	**11,41%**	**5,37**	**465,47**

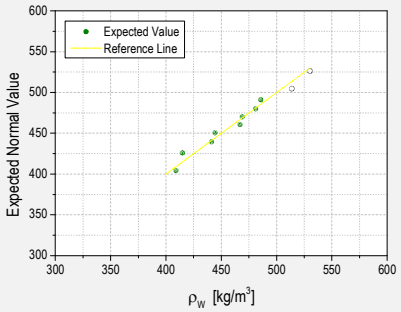

Q-Q plot of density distribution for configuration GAP4_OL_12%

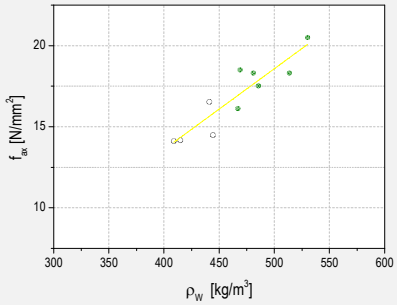

k_ρ	$-6.30 + 0.05 \cdot \rho$
R-Square	**0.81**

Linear fitting of correlation between f_{ax} and density for configuration GAP4_OL_12%

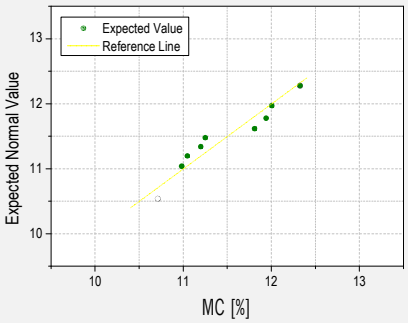

Q-Q plot of moisture content distribution for configuration GAP4_OL_12%

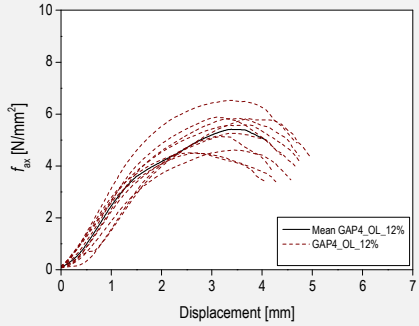

Relation between f_{ax} and displacement for GAP4_OL_12% tests

	MAXIMUM	MINIMUM	SD	CoV	MEDIAN	P5
f_{ax}	6,53	4,49	0,68	0,13	5,42	4,49
ρ	529,99	408,73	39,39	0,08	467,84	408,73
MC	12,32	10,71	0,56	0,05	11,22	10,71

GAP4_3L_12%

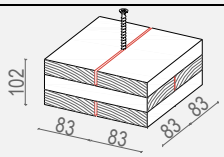

	WEIGHT AT TEST TIME [g] [mean values]	DRY WEIGHT [g] [mean values]	MC [%]	f_{ax} [N/mm^2]	ρ [kg/m^3]
1_GAP4_3L_12%	1168,74	1056,02	10,67%	3,97	401,41
2_GAP4_3L_12%	1170,46	1055,17	10,93%	3,79	403,57
3_GAP4_3L_12%	1277,31	1152,12	10,87%	4,69	439,75
4_GAP4_3L_12%	1290,67	1162,7	11,01%	4,83	444,39
5_GAP4_3L_12%	1327,13	1192,44	11,30%	5,15	456,72
6_GAP4_3L_12%	1342,9	1203,68	11,57%	4,54	462,44
7_GAP4_3L_12%	1395,9	1253,56	11,35%	4,95	481,37
8_GAP4_3L_12%	1405,47	1262,7	11,31%	5,08	484,27
9_GAP4_3L_12%	1469,13	1312,08	11,97%	5,18	507,47
10_GAP4_3L_12%	1480,75	1321,72	12,03%	5,43	512,11
MEAN VALUES	**1332,85**	**1197,22**	**11,30%**	**4,76**	**459,35**

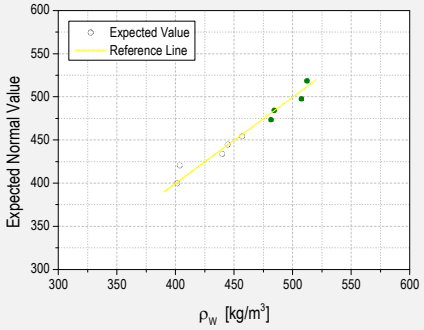

Q-Q plot of density distribution for configuration GAP4_3L_12%

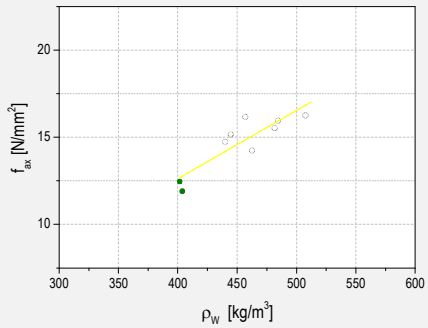

k_ρ	$-3.07 + 0.04 \cdot \rho$
R-Square	**0.80**

Linear fitting of correlation between f_{ax} and density for configuration GAP4_3L_12%

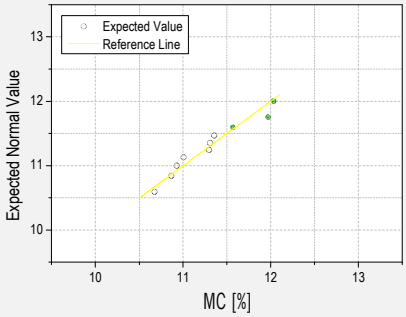

Q-Q plot of moisture content distribution for configuration GAP4_3L_12%

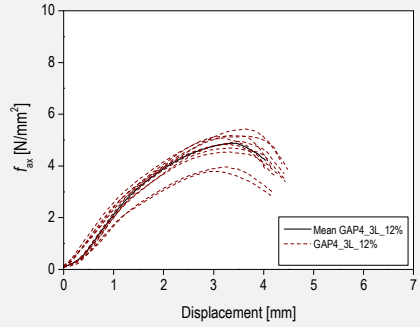

Relation between f_{ax} and displacement for GAP4_3L_12% tests

	MAXIMUM	MINIMUM	SD	CoV	MEDIAN	P5
f_{ax}	5,43	3,79	0,53	0,11	4,89	3,79
ρ	512,11	401,41	38,44	0,08	459,58	401,41
MC	12,03	10,67	0,46	0,04	11,30	10,67

Annex 1:11

REF_8%

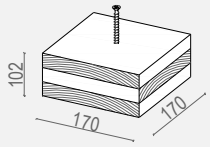

	WEIGHT AT TEST TIME [g] [mean values]	DRY WEIGHT [g] [mean values]	MC [%]	f_{ax} [N/mm²]	ρ [kg/m³]
1_REF_8%	1074,40	1000,07	7,43%	5,84	369,88
2_REF_8%	1192,38	1098,75	8,52%	5,47	409,60
3_REF_8%	1265,23	1171,57	7,99%	6,75	435,06
4_REF_8%	1282,65	1186,82	8,07%	6,25	441,38
5_REF_8%	1333,03	1223,60	8,94%	6,33	463,82
6_REF_8%	1364,65	1257,34	8,53%	6,85	477,32
7_REF_8%	1395,35	1287,23	8,40%	6,25	487,22
8_REF_8%	1444,63	1334,20	8,28%	6,94	503,67
9_REF_8%	1572,66	1448,55	8,57%	6,71	547,19
10_REF_8%	1587,98	1459,01	8,84%	7,96	548,77
MEAN VALUES	**1351,30**	**1246,71**	**8,36%**	**6,54**	**468,39**

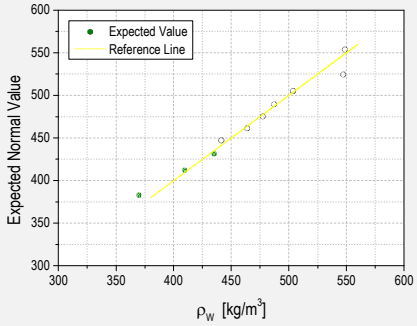

Q-Q plot of density distribution for configuration REF_8%

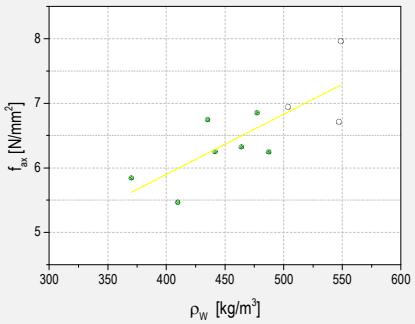

k_ρ	$2.19 + 0.01 \cdot \rho$
R-Square	**0.55**

Linear fitting of correlation between f_{ax} and density for configuration REF_8%

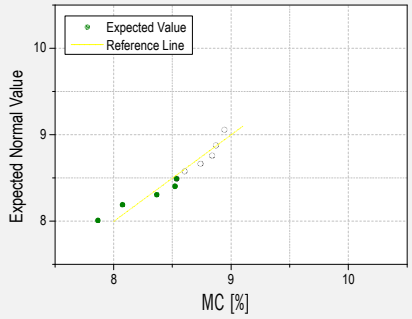

Q-Q plot of moisture content distribution for configuration REF_8%

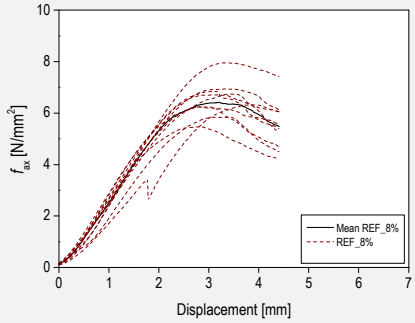

Relation between f_{ax} and displacement for REF_8% tests

	MAXIMUM	MINIMUM	SD	CoV	MEDIAN	P5
f_{ax}	7,96	5,47	0,68	0,10	6,52	5,47
ρ	548,77	369,88	57,13	0,12	470,57	369,88
MC	8,94	7,87	0,35	0,04	8,57	7,87

GAP0_FL_8%

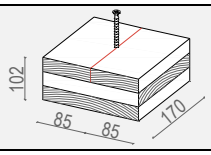

	WEIGHT AT TEST TIME [g] [mean values]	DRY WEIGHT [g] [mean values]	MC [%]	f_{ax} [N/mm²]	ρ [kg/m³]
1_GAP0_FL_8%	1129,50	1047,10	7,87%	5,80	387,53
2_GAP0_FL_8%	1148,42	1067,85	7,55%	5,75	395,45
3_GAP0_FL_8%	1262,52	1168,38	8,06%	6,85	432,65
4_GAP0_FL_8%	1270,57	1178,95	7,77%	6,74	436,85
5_GAP0_FL_8%	1316,54	1215,10	8,35%	7,00	455,14
6_GAP0_FL_8%	1332,91	1234,30	7,99%	6,69	462,11
7_GAP0_FL_8%	1374,29	1273,46	7,92%	5,95	476,91
8_GAP0_FL_8%	1386,34	1280,00	8,31%	7,29	481,26
9_GAP0_FL_8%	1426,76	1315,08	8,49%	6,73	493,80
10_GAP0_FL_8%	1475,16	1364,36	8,12%	8,12	508,47
MEAN VALUES	**1312,30**	**1214,46**	**8,04%**	**6,69**	**453,02**

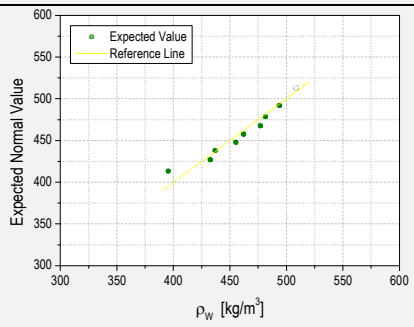

Q-Q plot of density distribution for configuration GAP0_FL_8%

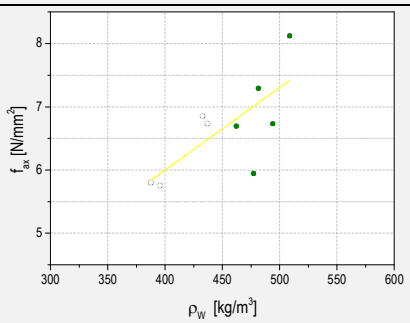

k_ρ	$0.77 + 0.01 \cdot \rho$
R-Square	**0.46**

Linear fitting of correlation between f_{ax} and density for configuration GAP0_FL_8%

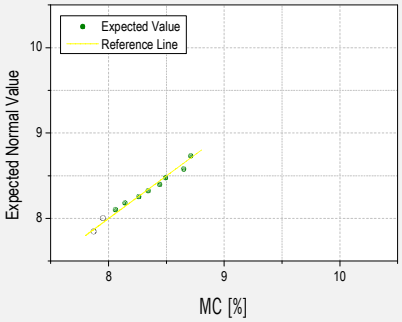

Q-Q plot of moisture content distribution for configuration GAP0_FL_8%

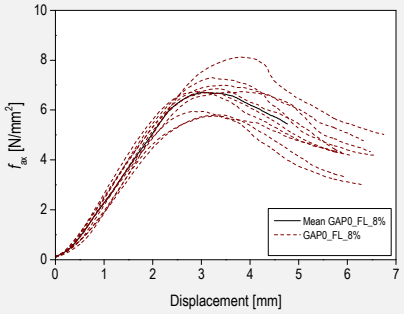

Relation between f_{ax} and displacement for GAP0_FL_8% tests

	MAXIMUM	MINIMUM	SD	CoV	MEDIAN	P5
f_{ax}	8,12	5,75	0,73	0,11	6,73	5,75
ρ	508,47	387,53	40,10	0,09	458,63	387,53
MC	8,71	7,87	0,29	0,03	8,30	7,87

GAP0_ML_8%

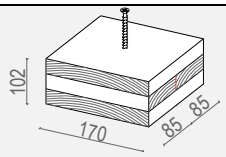

	WEIGHT AT TEST TIME [g] [mean values]	DRY WEIGHT [g] [mean values]	MC [%]	f_{ax} [N/mm²]	ρ [kg/m³]
1_GAP0_ML_8%	1138,20	1059,12	7,47%	6,14	392,83
2_GAP0_ML_8%	1180,38	1091,99	8,09%	6,01	406,60
3_GAP0_ML_8%	1244,39	1150,75	8,14%	6,34	429,53
4_GAP0_ML_8%	1272,27	1175,89	8,20%	6,06	438,60
5_GAP0_ML_8%	1301,80	1202,83	8,23%	6,30	449,40
6_GAP0_ML_8%	1334,63	1232,58	8,28%	6,80	461,46
7_GAP0_ML_8%	1369,15	1267,11	8,05%	6,82	475,03
8_GAP0_ML_8%	1387,18	1289,31	7,59%	6,40	481,52
9_GAP0_ML_8%	1417,08	1305,26	8,57%	5,91	491,38
10_GAP0_ML_8%	1444,78	1331,96	8,47%	6,15	499,44
MEAN VALUES	**1308,99**	**1210,68**	**8,11%**	**6,29**	**452,58**

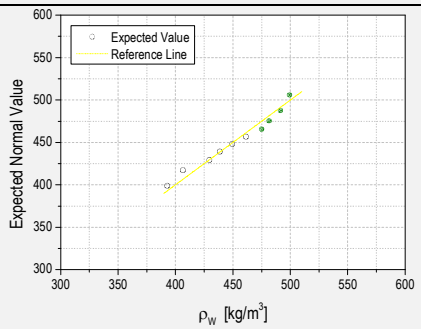

Q-Q plot of density distribution for configuration GAP0_ML_8%

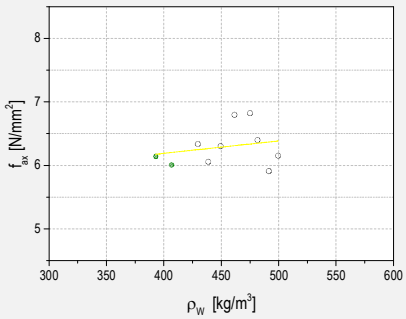

k_ρ	$5.41 + 0.00 \cdot \rho$
R-Square	**-0.07**

Linear fitting of correlation between f_{ax} and density for configuration GAP0_ML_8%

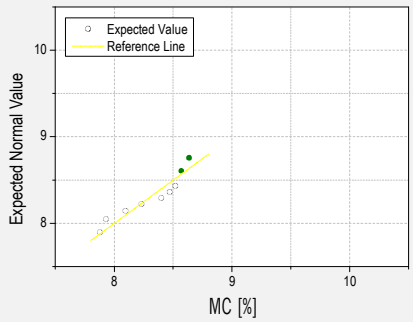

Q-Q plot of moisture content distribution for configuration GAP0_ML_8%

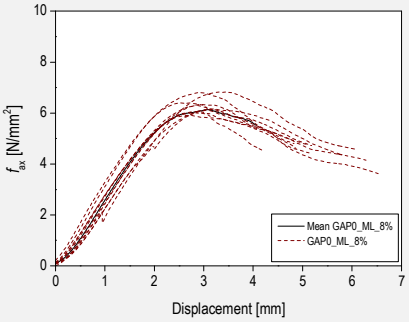

Relation between f_{ax} and displacement for GAP0_ML_8% tests

	MAXIMUM	MINIMUM	SD	CoV	MEDIAN	P5
f_{ax}	6,82	5,91	0,31	0,05	6,23	5,91
ρ	499,44	392,83	35,81	0,08	455,43	392,83
MC	8,63	7,88	0,28	0,03	8,43	7,88

GAP0_OL_8%

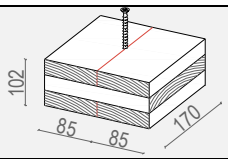

	WEIGHT AT TEST TIME [g] [mean values]	DRY WEIGHT [g] [mean values]	MC [%]	f_{ax} [N/mm²]	ρ [kg/m³]
1_GAP0_OL_8%	1124,96	1044,49	7,70%	5,92	386,40
2_GAP0_OL_8%	1166,01	1087,21	7,25%	6,29	402,79
3_GAP0_OL_8%	1257,27	1162,53	8,15%	6,46	433,38
4_GAP0_OL_8%	1282,74	1191,22	7,68%	7,14	442,56
5_GAP0_OL_8%	1313,31	1217,91	7,83%	6,96	456,41
6_GAP0_OL_8%	1338,88	1230,24	8,83%	6,60	465,50
7_GAP0_OL_8%	1384,11	1280,50	8,09%	7,10	477,87
8_GAP0_OL_8%	1403,45	1298,15	8,11%	6,92	487,46
9_GAP0_OL_8%	1446,30	1332,73	8,52%	7,26	502,40
10_GAP0_OL_8%	1476,27	1365,62	8,10%	6,59	513,52
MEAN VALUES	**1319,33**	**1221,06**	**8,03%**	**6,72**	**456,83**

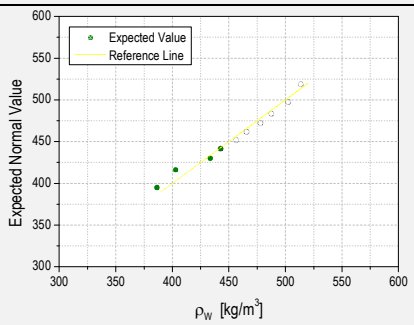

Q-Q plot of density distribution for configuration GAP0_OL_8%

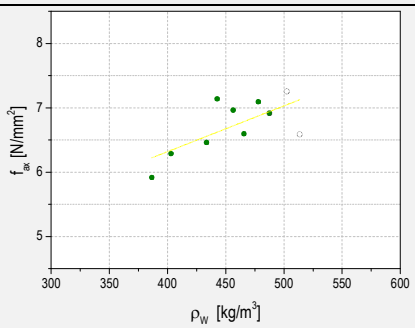

k_ρ	$3.48 + 0.01 \cdot \rho$
R-Square	**0.41**

Linear fitting of correlation between f_{ax} and density for configuration GAP0_OL_8%

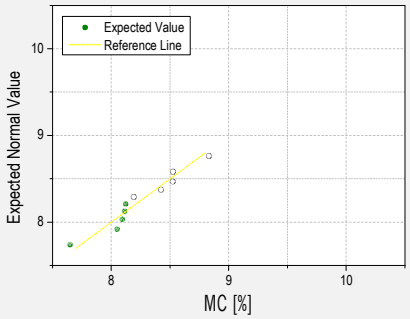

Q-Q plot of moisture content distribution for configuration GAP0_OL_8%

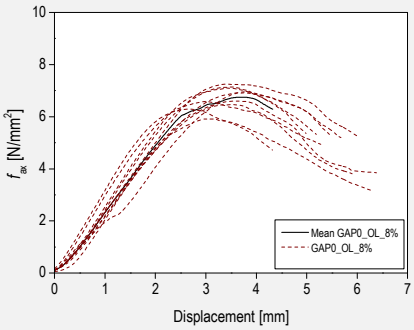

Relation between f_{ax} and displacement for GAP0_OL_8% tests

	MAXIMUM	MINIMUM	SD	CoV	MEDIAN	P5
f_{ax}	7,26	5,92	0,43	0,06	6,76	5,92
ρ	513,52	386,40	41,34	0,09	460,96	386,40
MC	8,83	7,65	0,33	0,04	8,16	7,65

GAP0_3L_8%

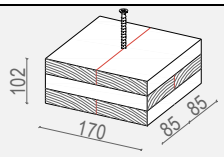

	WEIGHT AT TEST TIME [g] [mean values]	DRY WEIGHT [g] [mean values]	MC [%]	f_{ax} [N/mm²]	ρ [kg/m³]
1_GAP0_3L_8%	1118,48	1040,11	7,53%	6,42	385,60
2_GAP0_3L_8%	1145,16	1064,63	7,56%	6,62	395,19
3_GAP0_3L_8%	1252,49	1154,48	8,49%	7,31	432,55
4_GAP0_3L_8%	1268,19	1166,55	8,71%	7,58	438,26
5_GAP0_3L_8%	1321,67	1222,19	8,14%	7,32	456,01
6_GAP0_3L_8%	1345,26	1244,69	8,08%	7,52	463,73
7_GAP0_3L_8%	1371,96	1265,33	8,43%	7,56	474,42
8_GAP0_3L_8%	1388,82	1287,20	7,89%	7,59	481,84
9_GAP0_3L_8%	1440,20	1331,67	8,15%	7,77	499,45
10_GAP0_3L_8%	1442,19	1331,03	8,35%	7,75	501,47
MEAN VALUES	**1309,44**	**1210,79**	**8,13%**	**7,34**	**452,85**

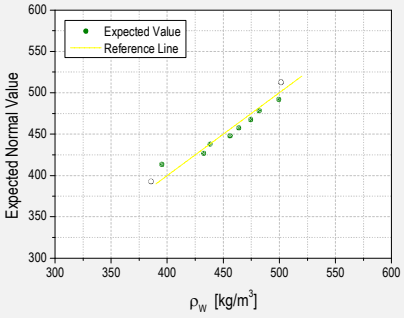

Q-Q plot of density distribution for configuration GAP0_3L_8%

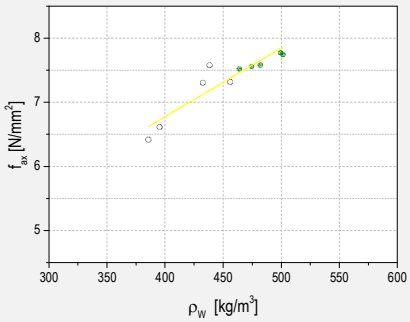

k_ρ	$2.49 + 0.01 \cdot \rho$
R-Square	**0.84**

Linear fitting of correlation between f_{ax} and density for configuration GAP0_3L_8%

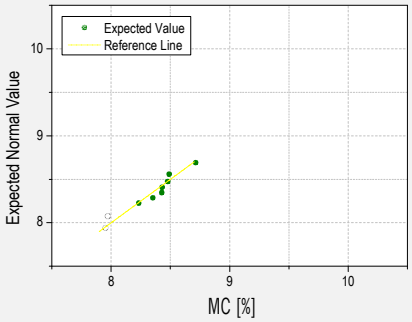

Q-Q plot of moisture content distribution for configuration GAP0_3L_8%

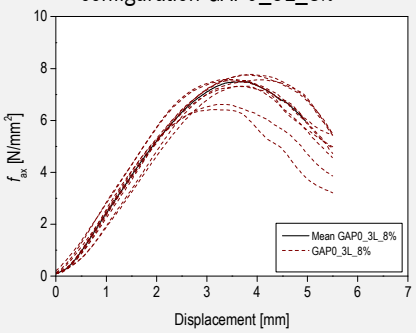

Relation between f_{ax} and displacement for GAP0_3L_8% tests

	MAXIMUM	MINIMUM	SD	CoV	MEDIAN	P5
f_{ax}	7,77	6,42	0,46	0,06	7,54	6,42
ρ	501,47	385,60	40,06	0,09	459,87	385,60
MC	8,71	7,95	0,24	0,03	8,39	7,95

GAP4_FL_8%

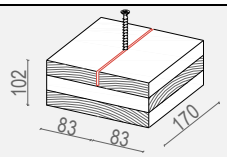

	WEIGHT AT TEST TIME [g] [mean values]	DRY WEIGHT [g] [mean values]	MC [%]	f_{ax} [N/mm²]	ρ [kg/m³]
1_GAP4_FL_8%	1148,20	1060,72	8,25%	4,84	393,73
2_GAP4_FL_8%	1182,81	1091,79	8,34%	3,93	407,84
3_GAP4_FL_8%	1245,98	1157,40	7,65%	5,63	429,67
4_GAP4_FL_8%	1266,22	1173,69	7,88%	5,21	436,22
5_GAP4_FL_8%	1304,54	1208,53	7,94%	5,16	453,54
6_GAP4_FL_8%	1329,66	1230,40	8,07%	5,25	460,50
7_GAP4_FL_8%	1352,85	1251,84	8,07%	5,31	471,30
8_GAP4_FL_8%	1375,05	1272,61	8,05%	5,83	478,79
9_GAP4_FL_8%	1414,40	1307,03	8,21%	6,62	492,16
10_GAP4_FL_8%	1444,42	1332,62	8,39%	6,21	503,60
MEAN VALUES	**1306,41**	**1208,66**	**8,09%**	**5,40**	**452,73**

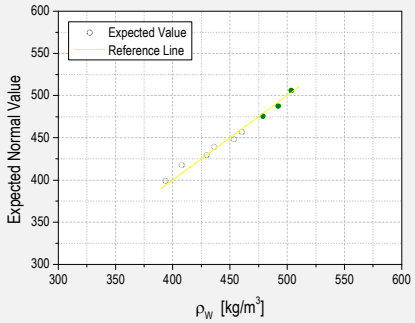

Q-Q plot of density distribution for configuration GAP4_FL_8%

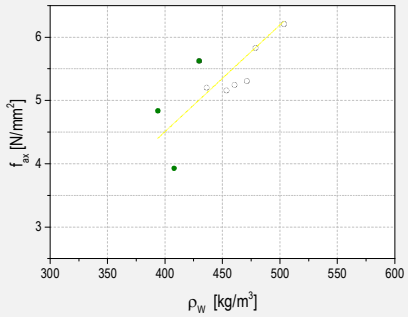

k_ρ	$-2.24 + 0.02 \cdot \rho$
R-Square	**0.62**

Linear fitting of correlation between f_{ax} and density for configuration GAP4_FL_8%

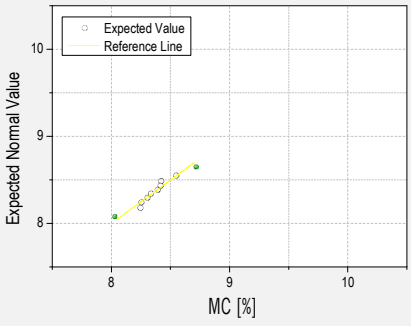

Q-Q plot of moisture content distribution for configuration GAP4_FL_8%

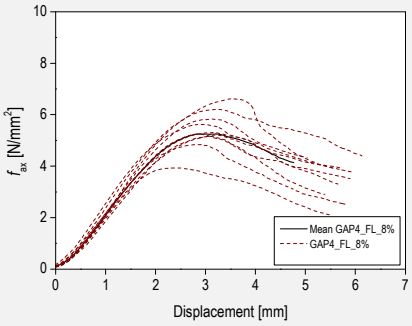

Relation between f_{ax} and displacement for GAP4_FL_8% tests

	MAXIMUM	MINIMUM	SD	CoV	MEDIAN	P5
f_{ax}	6,62	3,93	0,74	0,14	5,28	3,93
ρ	503,60	393,73	35,79	0,08	457,02	393,73
MC	8,72	8,03	0,19	0,02	8,36	8,03

GAP4_ML_8%

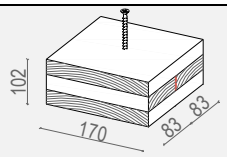

	WEIGHT AT TEST TIME [g] [mean values]	DRY WEIGHT [g] [mean values]	MC [%]	f_{ax} [N/mm²]	ρ [kg/m³]
1_GAP4_ML_8%	1145,37	1069,53	7,09%	4,72	400,45
2_GAP4_ML_8%	1177,00	1093,01	7,68%	5,00	408,77
3_GAP4_ML_8%	1252,72	1159,38	8,05%	5,27	435,78
4_GAP4_ML_8%	1268,35	1176,54	7,80%	5,32	443,19
5_GAP4_ML_8%	1311,65	1214,91	7,96%	5,50	458,69
6_GAP4_ML_8%	1332,48	1231,72	8,18%	5,50	464,98
7_GAP4_ML_8%	1362,57	1259,60	8,17%	n.a.	n.a.
8_GAP4_ML_8%	1369,95	1267,51	8,08%	5,78	480,02
9_GAP4_ML_8%	1412,59	1312,28	7,64%	n.a.	n.a.
10_GAP4_ML_8%	1467,81	1359,58	7,96%	5,84	511,23
MEAN VALUES	**1310,05**	**1214,41**	**7,86%**	**5,37**	**450,39**

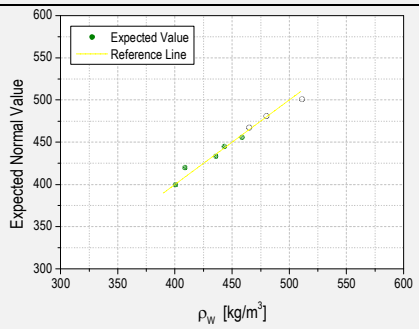

Q-Q plot of density distribution for configuration GAP4_ML_8%

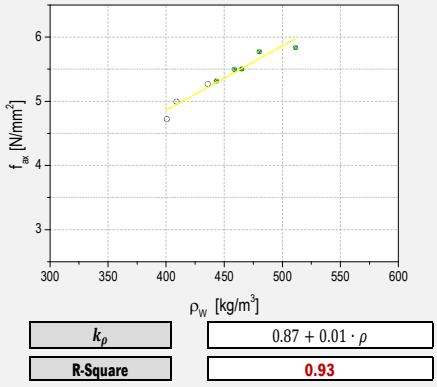

k_ρ	$0.87 + 0.01 \cdot \rho$
R-Square	0.93

Linear fitting of correlation between f_{ax} and density for configuration GAP4_ML_8%

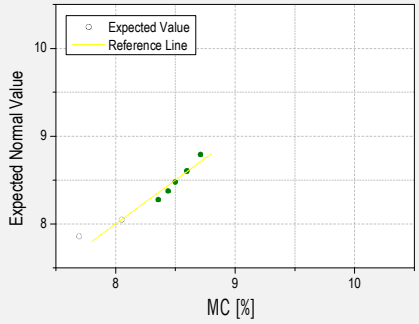

Q-Q plot of moisture content distribution for configuration GAP4_ML_8%

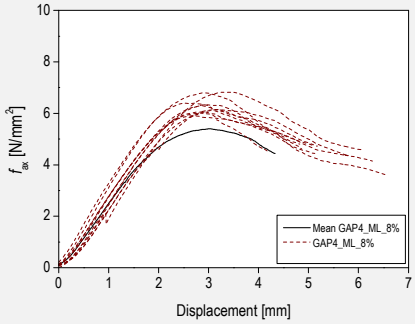

Relation between f_{ax} and displacement for GAP4_ML_8% tests

	MAXIMUM	MINIMUM	SD	CoV	MEDIAN	P5
f_{ax}	5,84	4,72	0,38	0,07	5,41	4,72
ρ	511,23	400,45	35,48	0,08	461,84	400,45
MC	8,71	7,70	0,33	0,04	8,40	7,70

GAP4_OL_8%

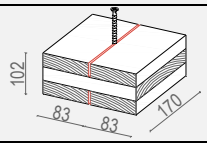

	WEIGHT AT TEST TIME [g] [mean values]	DRY WEIGHT [g] [mean values]	MC [%]	f_{ax} [N/mm²]	ρ [kg/m³]
1_GAP4_OL_8%	1159,89	1078,35	7,56%	4,64	406,93
2_GAP4_OL_8%	1185,88	1096,66	8,14%	4,52	414,74
3_GAP4_OL_8%	1239,67	1152,87	7,53%	4,36	435,25
4_GAP4_OL_8%	1262,28	1168,16	8,06%	4,25	442,45
5_GAP4_OL_8%	1309,31	1210,93	8,12%	4,67	463,45
6_GAP4_OL_8%	1325,39	1229,52	7,80%	4,63	468,35
7_GAP4_OL_8%	1358,14	1258,13	7,95%	4,44	478,36
8_GAP4_OL_8%	1377,35	1274,57	8,06%	4,79	484,23
9_GAP4_OL_8%	1438,31	1330,51	8,10%	5,20	509,34
10_GAP4_OL_8%	1465,31	1354,62	8,17%	5,32	518,63
MEAN VALUES	**1312,15**	**1215,43**	**7,95%**	**4,68**	**462,17**

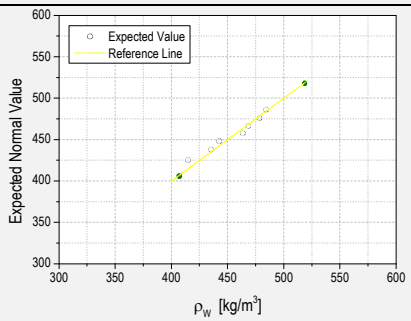

Q-Q plot of density distribution for configuration GAP4_OL_8%

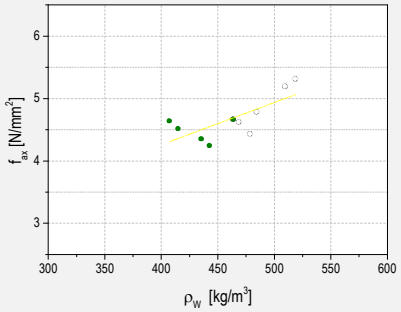

k_ρ	$1.55 + 0.01 \cdot \rho$
R-Square	**0.48**

Linear fitting of correlation between f_{ax} and density for configuration GAP4_OL_8%

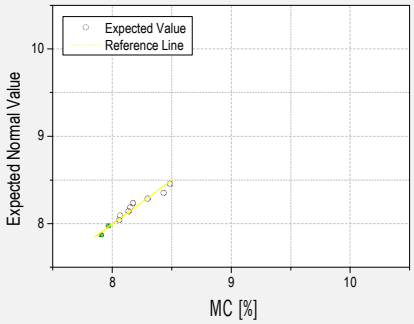

Q-Q plot of moisture content distribution for configuration GAP4_OL_8%

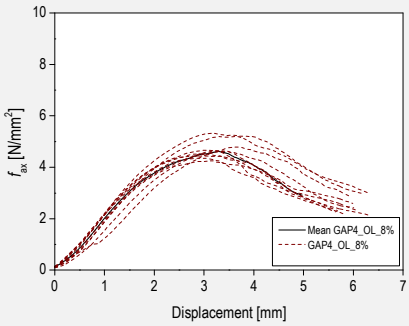

Relation between f_{ax} and displacement for GAP4_OL_8% tests

	MAXIMUM	MINIMUM	SD	CoV	MEDIAN	P5
f_{ax}	5,32	4,25	0,34	0,07	4,64	4,25
ρ	518,63	406,93	37,44	0,08	465,90	406,93
MC	8,48	7,91	0,19	0,02	8,14	7,91

GAP4_3L_8%

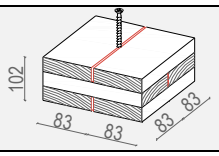

	WEIGHT AT TEST TIME [g] [mean values]	DRY WEIGHT [g] [mean values]	MC [%]	f_{ax} [N/mm²]	ρ [kg/m³]
1_GAP4_3L_8%	1137,08	1057,66	7,51%	3,25	400,30
2_GAP4_3L_8%	1144,03	1063,42	7,58%	3,49	403,15
3_GAP4_3L_8%	1239,60	1152,11	7,59%	4,27	438,83
4_GAP4_3L_8%	1250,93	1162,33	7,62%	4,04	442,77
5_GAP4_3L_8%	1286,19	1193,17	7,80%	4,46	456,17
6_GAP4_3L_8%	1295,41	1205,13	7,49%	3,85	461,20
7_GAP4_3L_8%	1338,28	1241,82	7,77%	4,47	476,28
8_GAP4_3L_8%	1361,60	1261,90	7,90%	4,13	483,52
9_GAP4_3L_8%	1412,60	1300,05	8,66%	4,66	503,70
10_GAP4_3L_8%	1429,88	1317,72	8,51%	4,34	510,76
MEAN VALUES	**1289,56**	**1195,53**	**7,84%**	**4,10**	**457,67**

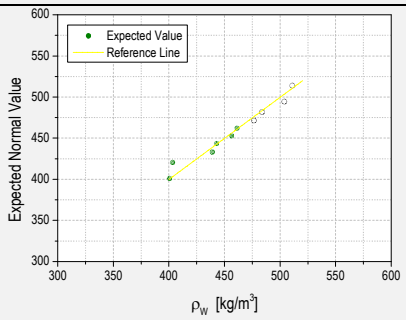

Q-Q plot of density distribution for configuration GAP4_3L_8%

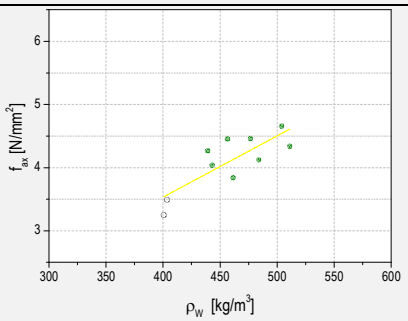

k_ρ	$-0.35 + 0.01 \cdot \rho$
R-Square	**0.62**

Linear fitting of correlation between f_{ax} and density for configuration GAP4_3L_8%

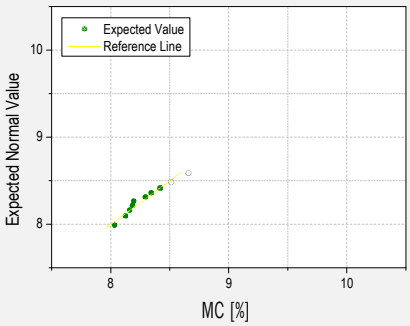

Q-Q plot of moisture content distribution for configuration GAP4_3L_8%

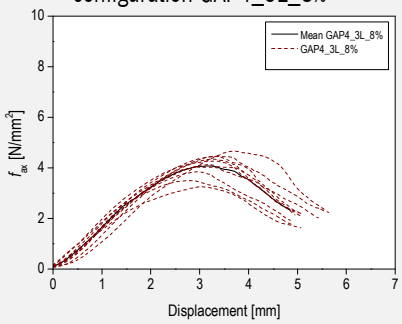

Relation between f_{ax} and displacement for GAP4_3L_8% tests

	MAXIMUM	MINIMUM	SD	CoV	MEDIAN	P5
f_{ax}	4,66	3,25	0,45	0,11	4,20	3,25
ρ	510,76	400,30	37,72	0,08	458,69	400,30
MC	8,66	8,03	0,19	0,02	8,24	8,03

Annex 1:12

REF_18%

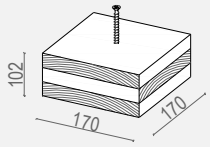

	WEIGHT AT TEST TIME [g] [mean values]	DRY WEIGHT [g] [mean values]	MC [%]	f_{ax} [N/mm²]	ρ [kg/m³]
1_REF_18%	1228,46	1046,78	17,36%	5,35	387,54
2_REF_18%	1312,31	1120,48	17,12%	5,36	415,86
3_REF_18%	1386,51	1185,36	16,97%	5,66	438,69
4_REF_18%	1443,70	1225,33	17,82%	5,66	460,74
5_REF_18%	1452,15	1234,21	17,66%	5,68	465,13
6_REF_18%	1506,92	1273,56	18,32%	5,82	482,41
7_REF_18%	1524,94	1294,65	17,79%	5,69	488,56
8_REF_18%	1598,93	1360,57	17,52%	5,92	509,86
9_REF_18%	1706,86	1458,21	17,05%	6,36	548,63
10_REF_18%	1732,48	1480,30	17,04%	7,12	554,66
MEAN VALUES	**1489,33**	**1267,95**	**17,46%**	**5,86**	**475,21**

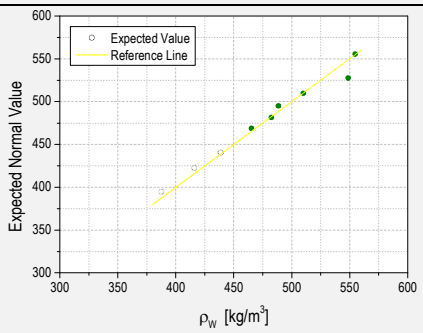

Q-Q plot of density distribution for configuration REF_18%

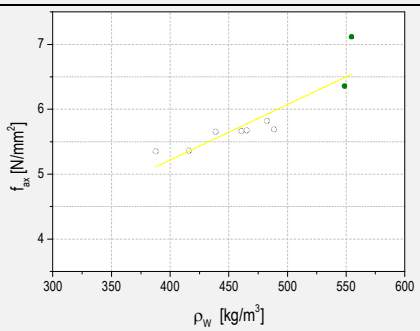

k_ρ	$1.80 + 0.01 \cdot \rho$
R-Square	**0.74**

Linear fitting of correlation between f_{ax} and density for configuration REF_18%

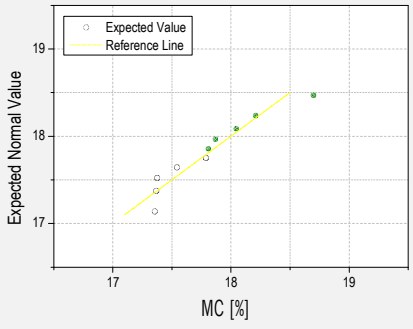

Q-Q plot of moisture content distribution for configuration REF_18%

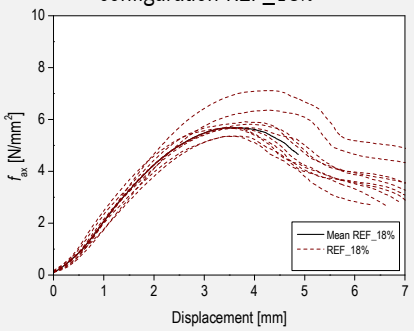

Relation between f_{ax} and displacement for REF_18% tests

	MAXIMUM	MINIMUM	SD	CoV	MEDIAN	P5
f_{ax}	7,12	5,35	0,53	0,09	5,68	5,35
ρ	554,66	387,54	53,74	0,11	473,77	387,54
MC	18,70	17,35	0,43	0,02	17,80	17,35

GAP0_FL_18%

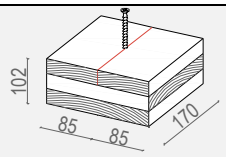

	WEIGHT AT TEST TIME [g] [mean values]	DRY WEIGHT [g] [mean values]	MC [%]	f_{ax} [N/mm²]	ρ [kg/m³]
1_GAP0_FL_18%	1240,61	1064,64	16,53%	5,81	393,56
2_GAP0_FL_18%	1280,10	1089,36	17,51%	5,13	406,00
3_GAP0_FL_18%	1368,53	1167,10	17,26%	5,80	436,35
4_GAP0_FL_18%	1419,37	1212,14	17,10%	5,89	451,95
5_GAP0_FL_18%	1429,86	1222,40	16,97%	6,12	458,46
6_GAP0_FL_18%	1457,25	1249,73	16,61%	6,28	467,75
7_GAP0_FL_18%	1497,61	1273,80	17,57%	6,38	479,16
8_GAP0_FL_18%	1510,99	1290,55	17,08%	6,83	487,32
9_GAP0_FL_18%	1578,39	1344,22	17,42%	6,44	503,05
10_GAP0_FL_18%	1619,88	1392,46	16,33%	7,76	518,57
MEAN VALUES	**1440,26**	**1230,64**	**17,04%**	**6,24**	**460,22**

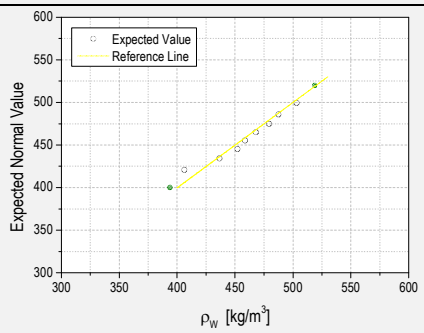

Q-Q plot of density distribution for configuration GAP0_FL_18%

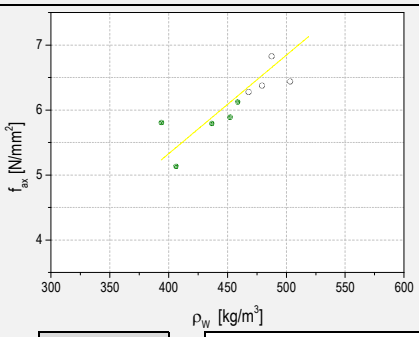

k_ρ	$-0.74 + 0.02 \cdot \rho$
R-Square	**0.71**

Linear fitting of correlation between f_{ax} and density for configuration GAP0_FL_18%

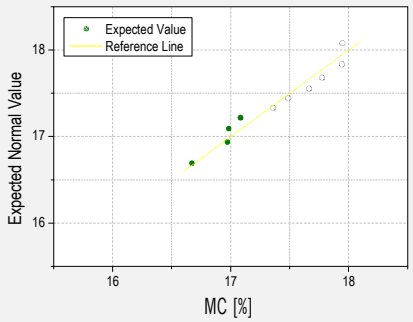

Q-Q plot of moisture content distribution for configuration GAP0_FL_18%

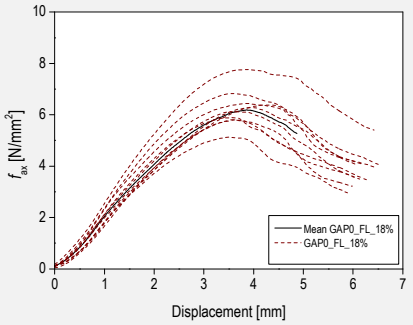

Relation between f_{ax} and displacement for GAP0_FL_18% tests

	MAXIMUM	MINIMUM	SD	CoV	MEDIAN	P5
f_{ax}	7,76	5,13	0,70	0,11	6,20	5,13
ρ	518,57	393,56	40,02	0,09	463,10	393,56
MC	17,94	16,67	0,45	0,03	17,42	16,67

GAP0_ML_18%

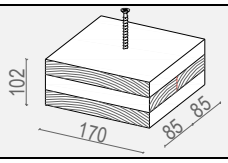

	WEIGHT AT TEST TIME [g] [mean values]	DRY WEIGHT [g] [mean values]	MC [%]	f_{ax} [N/mm²]	ρ [kg/m³]
1_GAP0_ML_18%	1280,44	1089,91	17,48%	5,58	404,22
2_GAP0_ML_18%	1281,88	1097,58	16,79%	5,40	408,55
3_GAP0_ML_18%	1375,11	1176,94	16,84%	5,57	437,28
4_GAP0_ML_18%	1397,94	1193,62	17,12%	5,61	446,76
5_GAP0_ML_18%	1425,72	1218,47	17,01%	6,14	457,49
6_GAP0_ML_18%	1465,25	1243,56	17,83%	6,21	468,38
7_GAP0_ML_18%	1492,24	1277,89	16,77%	6,61	477,81
8_GAP0_ML_18%	1519,04	1298,72	16,96%	6,48	485,15
9_GAP0_ML_18%	1540,66	1320,28	16,69%	6,15	496,67
10_GAP0_ML_18%	1557,53	1341,16	16,13%	6,54	502,31
MEAN VALUES	**1433,58**	**1225,81**	**16,96%**	**6,03**	**458,46**

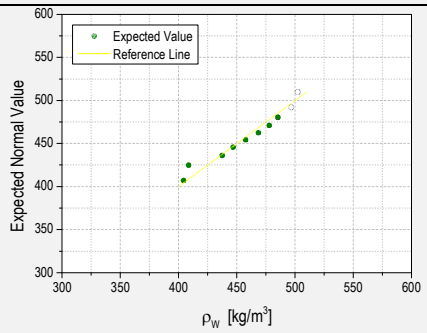

Q-Q plot of density distribution for configuration GAP0_ML_18%

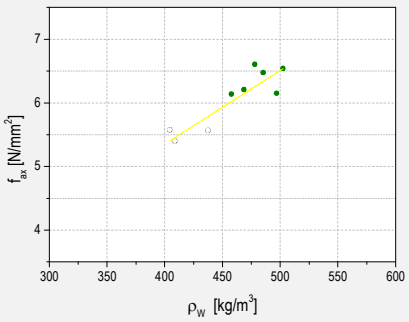

k_ρ	$0.73 + 0.01 \cdot \rho$
R-Square	**0.74**

Linear fitting of correlation between f_{ax} and density for configuration GAP0_ML_18%

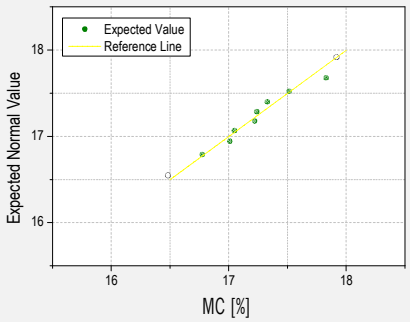

Q-Q plot of moisture content distribution for configuration GAP0_ML_18%

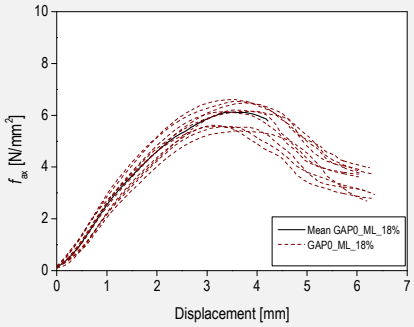

Relation between f_{ax} and displacement for GAP0_ML_18% tests

	MAXIMUM	MINIMUM	SD	CoV	MEDIAN	P5
f_{ax}	6,61	5,40	0,45	0,07	6,15	5,40
ρ	502,31	404,22	34,30	0,07	462,93	404,22
MC	17,92	16,48	0,44	0,03	17,23	16,48

GAP0_OL_18%

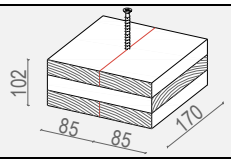

	WEIGHT AT TEST TIME [g] [mean values]	DRY WEIGHT [g] [mean values]	MC [%]	f_{ax} [N/mm²]	ρ [kg/m³]
1_GAP0_OL_18%	1267,95	1078,78	17,54%	5,26	400,65
2_GAP0_OL_18%	1301,70	1115,04	16,74%	6,11	413,32
3_GAP0_OL_18%	1382,82	1169,85	18,20%	5,81	439,55
4_GAP0_OL_18%	1406,57	1197,04	17,50%	5,81	447,88
5_GAP0_OL_18%	1432,05	1220,14	17,37%	6,15	458,55
6_GAP0_OL_18%	1473,63	1254,98	17,42%	6,50	472,60
7_GAP0_OL_18%	1514,86	1294,95	16,98%	6,57	483,56
8_GAP0_OL_18%	1525,32	1305,55	16,83%	6,93	489,63
9_GAP0_OL_18%	1593,28	1350,10	18,01%	6,77	513,21
10_GAP0_OL_18%	1660,73	1415,98	17,28%	6,57	535,40
MEAN VALUES	**1455,89**	**1240,24**	**17,39%**	**6,25**	**465,43**

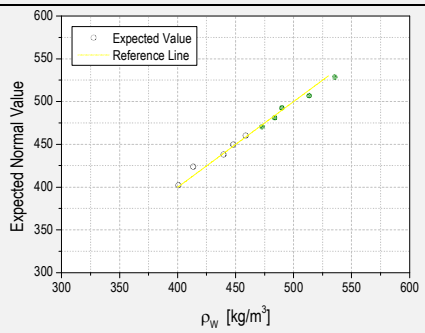

Q-Q plot of density distribution for configuration GAP0_OL_18%

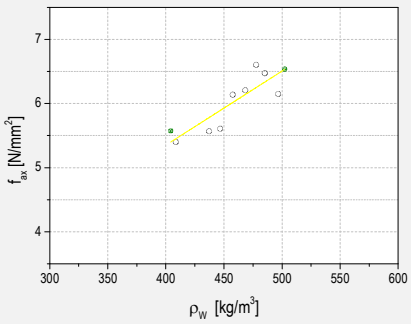

k_ρ	$1.54 + 0.01 \cdot \rho$
R-Square	**0.65**

Linear fitting of correlation between f_{ax} and density for configuration GAP0_OL_18%

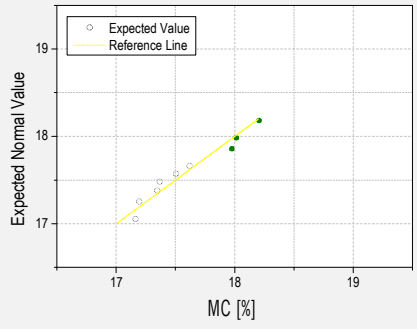

Q-Q plot of moisture content distribution for configuration GAP0_OL_18%

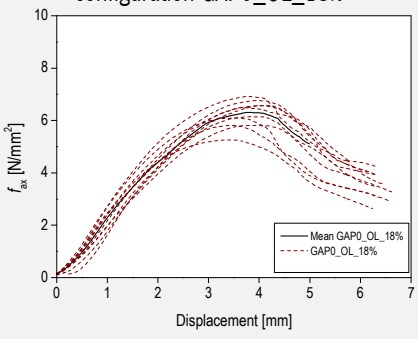

Relation between f_{ax} and displacement for GAP0_OL_18% tests

	MAXIMUM	MINIMUM	SD	CoV	MEDIAN	P5
f_{ax}	6,93	5,26	0,52	0,08	6,32	5,26
ρ	535,40	400,65	42,27	0,09	465,57	400,65
MC	18,20	17,16	0,36	0,02	17,56	17,16

GAP0_3L_18%

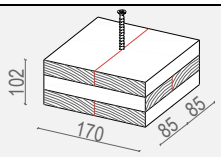

	WEIGHT AT TEST TIME [g] [mean values]	DRY WEIGHT [g] [mean values]	MC [%]	f_{ax} [N/mm²]	ρ [kg/m³]
1_GAP0_3L_18%	1251,60	1060,88	17,98%	5,65	393,27
2_GAP0_3L_18%	1268,58	1074,30	18,08%	5,85	398,33
3_GAP0_3L_18%	1368,83	1168,68	17,13%	6,33	436,69
4_GAP0_3L_18%	1396,82	1194,23	16,96%	6,17	446,73
5_GAP0_3L_18%	1438,16	1229,37	16,98%	6,43	457,92
6_GAP0_3L_18%	1468,93	1253,96	17,14%	6,41	467,97
7_GAP0_3L_18%	1498,97	1283,65	16,77%	6,66	480,53
8_GAP0_3L_18%	1530,51	1305,79	17,21%	6,42	490,71
9_GAP0_3L_18%	1558,95	1333,38	16,92%	6,65	501,43
10_GAP0_3L_18%	1587,69	1351,18	17,50%	6,10	509,38
MEAN VALUES	**1436,90**	**1225,54**	**17,27%**	**6,26**	**458,30**

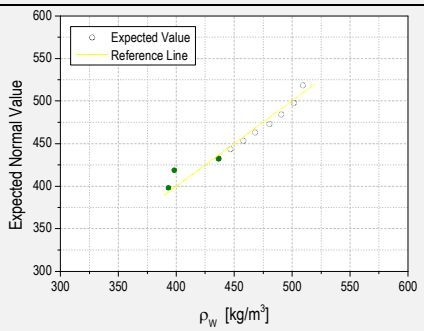

Q-Q plot of density distribution for configuration GAP0_3L_18%

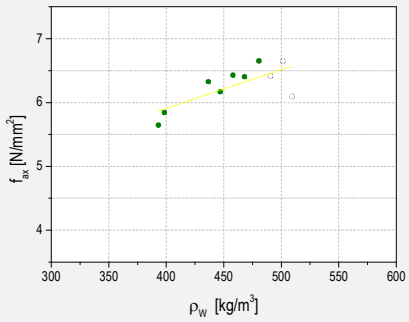

k_ρ	$3.49 + 0.01 \cdot \rho$
R-Square	**0.49**

Linear fitting of correlation between f_{ax} and density for configuration GAP0_3L_18%

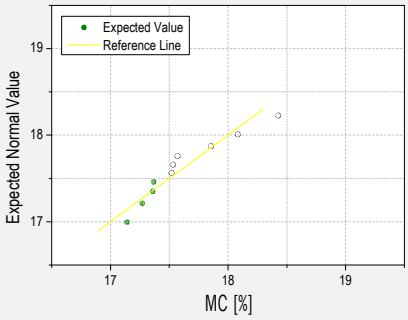

Q-Q plot of moisture content distribution for configuration GAP0_3L_18%

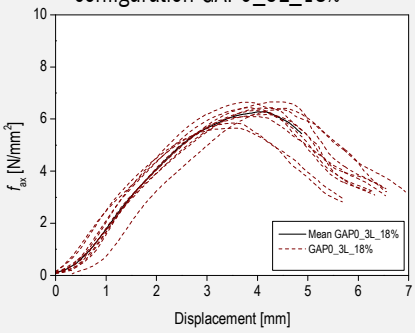

Relation between f_{ax} and displacement for GAP0_3L_18% tests

	MAXIMUM	MINIMUM	SD	CoV	MEDIAN	P5
f_{ax}	6,66	5,65	0,33	0,05	6,37	5,65
ρ	509,38	393,27	40,19	0,09	462,95	393,27
MC	18,43	17,14	0,40	0,02	17,53	17,14

GAP4_FL_18%

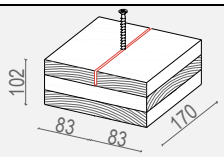

	WEIGHT AT TEST TIME [g] [mean values]	DRY WEIGHT [g] [mean values]	MC [%]	f_{ax} [N/mm²]	ρ [kg/m³]
1_GAP4_FL_18%	1278,18	1093,50	16,89%	4,50	404,88
2_GAP4_FL_18%	1310,32	1119,50	17,05%	4,90	419,70
3_GAP4_FL_18%	1364,61	1169,00	16,73%	4,78	434,00
4_GAP4_FL_18%	1397,02	1188,60	17,53%	5,00	441,54
5_GAP4_FL_18%	1438,27	1220,36	17,86%	4,90	459,01
6_GAP4_FL_18%	1472,38	1255,28	17,29%	5,80	470,80
7_GAP4_FL_18%	1488,75	1268,74	17,34%	6,05	476,03
8_GAP4_FL_18%	1521,67	1298,59	17,18%	5,90	485,83
9_GAP4_FL_18%	1570,21	1327,94	18,24%	5,57	503,38
10_GAP4_FL_18%	1600,25	1357,39	17,89%	5,65	515,43
MEAN VALUES	**1444,17**	**1229,89**	**17,40%**	**5,30**	**461,06**

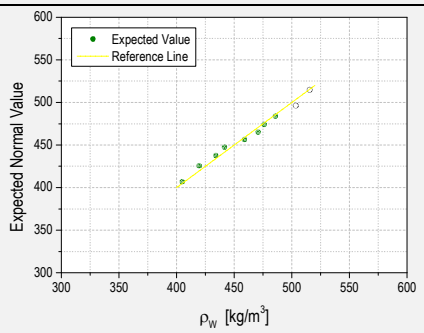

Q-Q plot of density distribution for configuration GAP4_FL_18%

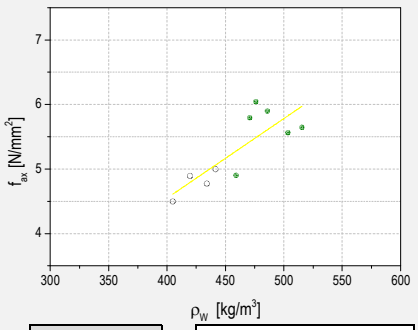

k_ρ	$-0.37 + 0.01 \cdot \rho$
R-Square	**0.62**

Linear fitting of correlation between f_{ax} and density for configuration GAP4_FL_18%

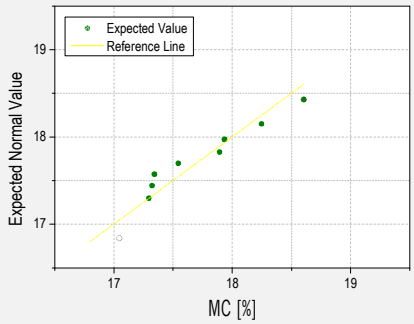

Q-Q plot of moisture content distribution for configuration GAP4_FL_18%

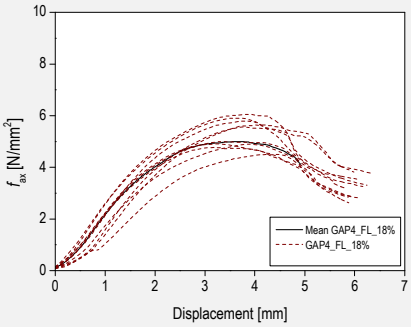

Relation between f_{ax} and displacement for GAP4_FL_18% tests

	MAXIMUM	MINIMUM	SD	CoV	MEDIAN	P5
f_{ax}	6,05	4,50	0,55	0,10	5,28	4,50
ρ	515,43	404,88	36,00	0,08	464,91	404,88
MC	18,60	17,05	0,51	0,03	17,44	17,05

GAP4_ML_18%

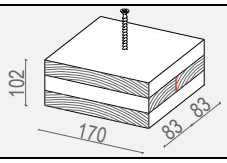

	WEIGHT AT TEST TIME [g] [mean values]	DRY WEIGHT [g] [mean values]	MC [%]	f_{ax} [N/mm²]	ρ [kg/m³]
1_GAP4_ML_18%	1283,12	1086,33	18,12%	4,67	407,97
2_GAP4_ML_18%	1307,45	1111,17	17,66%	4,85	416,14
3_GAP4_ML_18%	1372,81	1166,37	17,70%	5,02	440,35
4_GAP4_ML_18%	1410,94	1207,06	16,89%	4,88	451,81
5_GAP4_ML_18%	1438,17	1223,67	17,53%	5,38	462,31
6_GAP4_ML_18%	1468,18	1247,27	17,71%	5,18	471,16
7_GAP4_ML_18%	1489,81	1273,13	17,02%	5,78	479,24
8_GAP4_ML_18%	1494,98	1279,35	16,85%	5,72	484,33
9_GAP4_ML_18%	1559,76	1334,97	16,84%	5,90	502,06
10_GAP4_ML_18%	1622,44	1395,39	16,27%	6,21	522,87
MEAN VALUES	**1444,77**	**1232,47**	**17,26%**	**5,36**	**463,82**

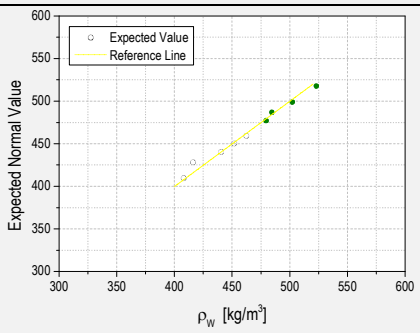

Q-Q plot of density distribution for configuration GAP4_ML_18%

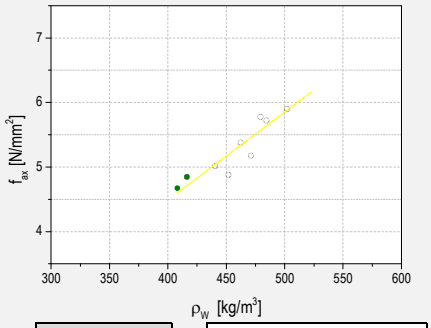

k_ρ	$-0.95 + 0.01 \cdot \rho$
R-Square	**0.88**

Linear fitting of correlation between f_{ax} and density for configuration GAP4_ML_18%

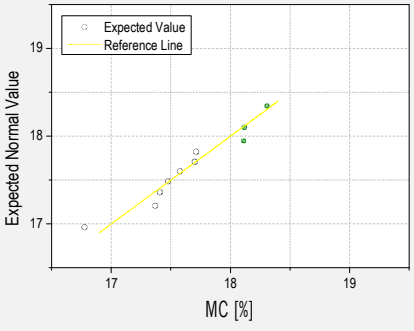

Q-Q plot of moisture content distribution for configuration GAP4_ML_18%

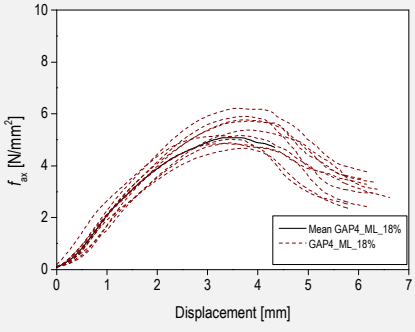

Relation between f_{ax} and displacement for GAP4_ML_18% tests

	MAXIMUM	MINIMUM	SD	CoV	MEDIAN	P5
f_{ax}	6,21	4,67	0,52	0,10	5,28	4,67
ρ	522,87	407,97	36,14	0,08	466,73	407,97
MC	18,30	16,77	0,45	0,03	17,64	16,77

GAP4_OL_18%

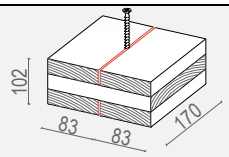

	WEIGHT AT TEST TIME [g] [mean values]	DRY WEIGHT [g] [mean values]	MC [%]	f_{ax} [N/mm²]	ρ [kg/m³]
1_GAP4_OL_18%	1281,30	1090,30	17,52%	4,34	411,92
2_GAP4_OL_18%	1311,85	1119,71	17,16%	4,67	422,36
3_GAP4_OL_18%	1372,03	1169,06	17,36%	4,67	442,05
4_GAP4_OL_18%	1386,32	1183,63	17,12%	4,68	448,11
5_GAP4_OL_18%	1441,42	1223,81	17,78%	5,75	467,43
6_GAP4_OL_18%	1448,41	1229,70	17,79%	5,24	469,23
7_GAP4_OL_18%	1494,08	1270,15	17,63%	5,85	483,61
8_GAP4_OL_18%	1516,48	1294,58	17,14%	5,57	494,31
9_GAP4_OL_18%	1588,59	1354,97	17,24%	6,06	514,71
10_GAP4_OL_18%	1634,05	1395,05	17,13%	6,24	532,59
MEAN VALUES	**1447,45**	**1233,10**	**17,39%**	**5,31**	**468,63**

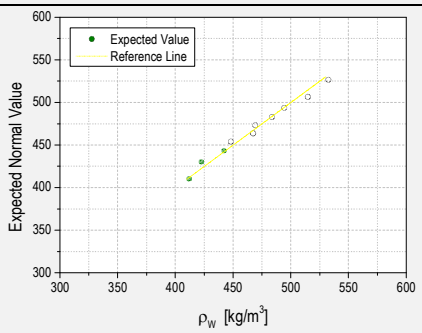

Q-Q plot of density distribution for configuration GAP4_OL_18%

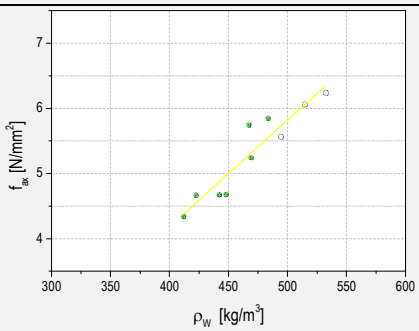

k_ρ	$-2.37 + 0.02 \cdot \rho$
R-Square	**0.87**

Linear fitting of correlation between f_{ax} and density for configuration GAP4_OL_18%

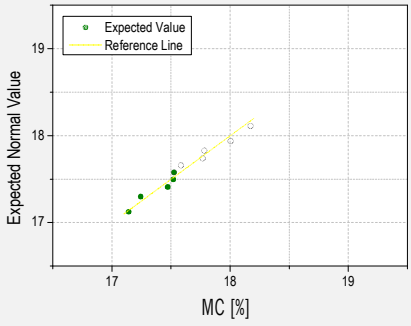

Q-Q plot of moisture content distribution for configuration GAP4_OL_18%

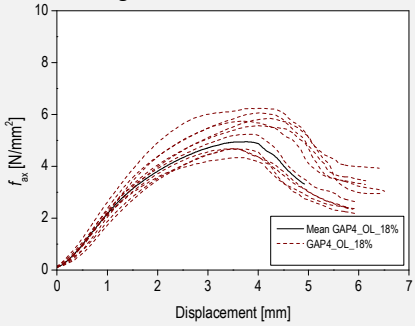

Relation between f_{ax} and displacement for GAP4_OL_18% tests

	MAXIMUM	MINIMUM	SD	CoV	MEDIAN	P5
f_{ax}	6,24	4,34	0,68	0,13	5,40	4,34
ρ	532,59	411,92	38,85	0,08	468,33	411,92
MC	18,17	17,14	0,32	0,02	17,55	17,14

GAP4_3L_18%

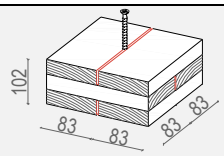

	WEIGHT AT TEST TIME [g] [mean values]	DRY WEIGHT [g] [mean values]	MC [%]	f_{ax} [N/mm²]	ρ [kg/m³]
1_GAP4_3L_18%	1244,80	1061,13	17,31%	3,77	402,44
2_GAP4_3L_18%	1254,67	1064,43	17,87%	3,95	405,40
3_GAP4_3L_18%	1361,05	1161,39	17,19%	4,43	441,81
4_GAP4_3L_18%	1367,94	1170,13	16,90%	5,11	445,74
5_GAP4_3L_18%	1408,80	1206,36	16,78%	4,94	459,29
6_GAP4_3L_18%	1433,10	1218,66	17,60%	5,29	466,42
7_GAP4_3L_18%	1473,64	1254,88	17,43%	5,09	481,39
8_GAP4_3L_18%	1492,70	1265,41	17,96%	4,96	486,56
9_GAP4_3L_18%	1553,25	1323,01	17,40%	5,37	509,53
10_GAP4_3L_18%	1560,41	1327,37	17,56%	5,03	514,97
MEAN VALUES	**1415,04**	**1205,28**	**17,40%**	**4,79**	**461,35**

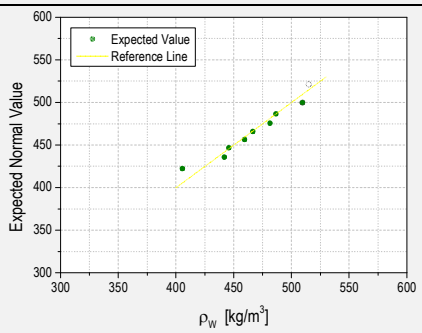

Q-Q plot of density distribution for configuration GAP4_3L_18%

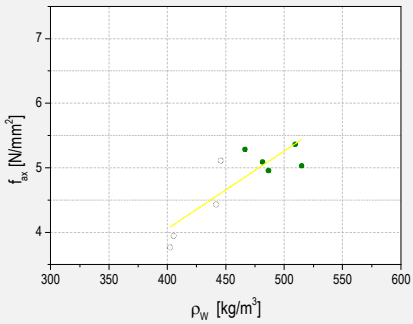

k_ρ	$-0.77 + 0.01 \cdot \rho$
R-Square	**0.67**

Linear fitting of correlation between f_{ax} and density for configuration GAP4_3L_18%

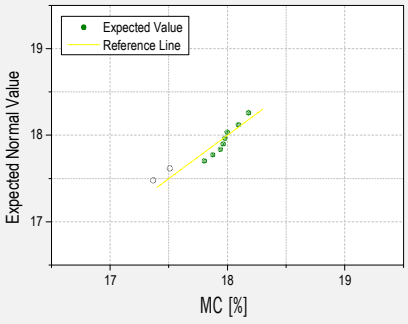

Q-Q plot of moisture content distribution for configuration GAP4_3L_18%

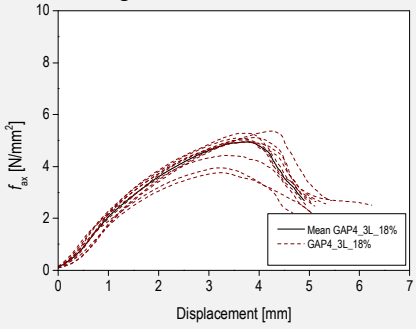

Relation between f_{ax} and displacement for GAP4_3L_18% tests

	MAXIMUM	MINIMUM	SD	CoV	MEDIAN	P5
f_{ax}	5,37	3,77	0,55	0,12	5,00	3,77
ρ	514,97	402,44	38,71	0,08	462,86	402,44
MC	18,18	17,37	0,25	0,01	17,95	17,37

Annex 1:13

REF_0

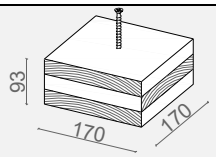

	WEIGHT AT TEST TIME [g] [mean values]	DRY WEIGHT [g] [mean values]	MC [%]	f_{ax} [N/mm²]	ρ [kg/m³]
1_REF_0	1244,52	1089,68	14,21%	5,50	458,09
2_REF_0	1233,83	1080,28	14,21%	7,22	453,98
3_REF_0	1259,04	1102,26	14,22%	7,68	463,52
4_REF_0	1266,03	1111,10	13,94%	6,27	466,00
5_REF_0	1259,70	1099,21	14,60%	6,66	464,11
6_REF_0	1262,37	1104,98	14,24%	7,44	464,72
7_REF_0	1273,57	1117,38	13,98%	7,70	468,52
8_REF_0	1267,64	1107,43	14,47%	7,65	466,85
9_REF_0	1286,20	1126,65	14,16%	6,97	473,68
10_REF_0	1281,20	1119,58	14,44%	7,42	471,46
MEAN VALUES	**1263,41**	**1105,86**	**0,14**	**7,05**	**465,09**

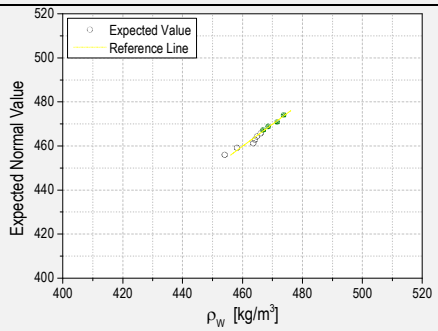

Q-Q plot of density distribution for configuration REF_0

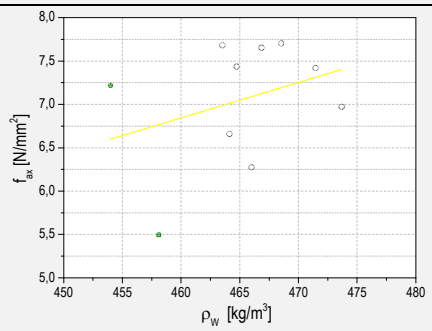

k_ρ	$-11.97 + 0.04 \cdot \rho$
R-Square	**-0.002**

Linear fitting of correlation between f_{ax} and density for configuration REF_0

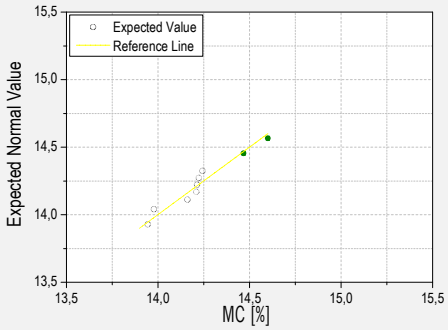

Q-Q plot of moisture content distribution for configuration REF_0

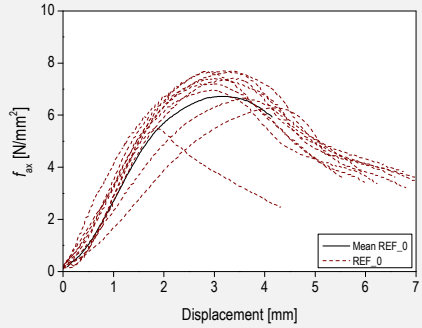

Relation between f_{ax} and displacement for REF_0 tests

	MAXIMUM	MINIMUM	SD	CoV	MEDIAN	P5
f_{ax}	7,70	5,50	0,72	0,10	7,32	5,50
ρ	473,68	453,98	5,83	0,01	465,36	453,98
MC	14,60%	13,94%	0,21	0,01	14,22%	13,94%

GAP0_FL_0

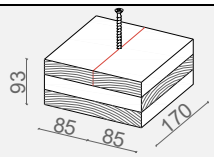

	WEIGHT AT TEST TIME [g] [mean values]	DRY WEIGHT [g] [mean values]	MC [%]	f_{ax} [N/mm²]	ρ [kg/m³]
1_GAP0_FL_0	1213,04	1059,78	14,46%	7,59	447,97
2_GAP0_FL_0	1258,36	1097,34	14,67%	7,75	460,77
3_GAP0_FL_0	1267,42	1105,65	14,63%	7,38	467,47
4_GAP0_FL_0	1300,01	1138,57	14,18%	8,20	478,88
5_GAP0_FL_0	1304,50	1141,25	14,30%	7,73	480,71
6_GAP0_FL_0	1310,32	1143,83	14,56%	7,20	477,35
7_GAP0_FL_0	1328,15	1157,72	14,72%	8,08	483,48
8_GAP0_FL_0	1334,51	1166,44	14,41%	7,86	485,90
9_GAP0_FL_0	1369,27	1191,46	14,92%	8,75	502,46
10_GAP0_FL_0	1386,76	1211,17	14,50%	8,04	505,74
MEAN VALUES	**1307,23**	**1141,32**	**14,54%**	**7,86**	**479,07**

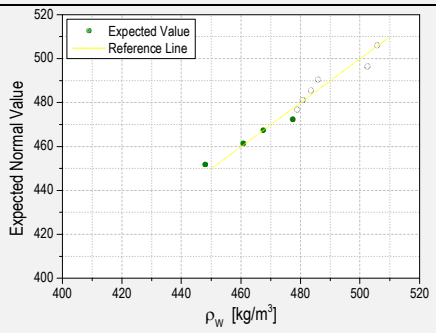

Q-Q plot of density distribution for configuration GAP0_FL_0

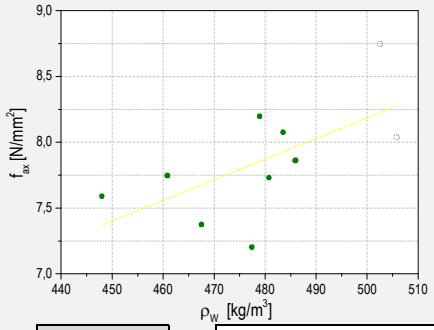

k_ρ	$0.35 + 0.02 \cdot \rho$
R-Square	**0.31**

Linear fitting of correlation between f_{ax} and density for configuration GAP0_FL_0

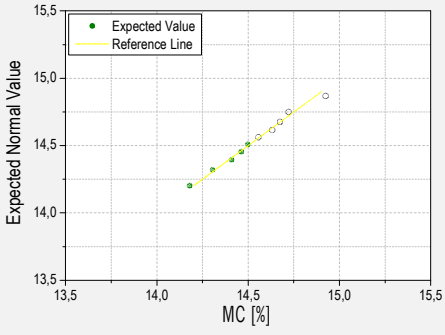

Q-Q plot of moisture content distribution for configuration GAP0_FL_0

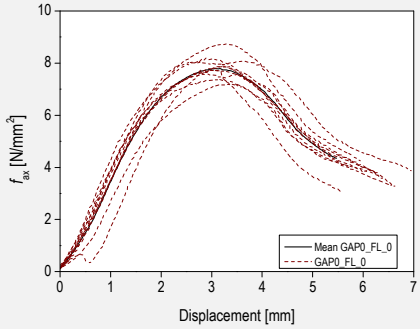

Relation between f_{ax} and displacement for GAP0_FL_0 tests

	MAXIMUM	MINIMUM	SD	CoV	MEDIAN	P5
f_{ax}	8,75	7,20	0,44	0,06	7,81	7,20
ρ	505,74	447,97	17,53	0,04	479,79	447,97
MC	14,92%	14,18%	0,22	0,01	14,53%	14,18%

GAP0_ML_0

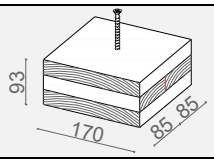

	WEIGHT AT TEST TIME [g] [mean values]	DRY WEIGHT [g] [mean values]	MC [%]	f_{ax} [N/mm²]	ρ [kg/m³]
1_GAP0_ML_0	1111,50	971,60	14,40%	7,00	409,52
2_GAP0_ML_0	1127,29	983,34	14,64%	6,98	415,30
3_GAP0_ML_0	1151,95	1007,20	14,37%	6,34	424,54
4_GAP0_ML_0	1157,27	1010,87	14,48%	6,85	426,18
5_GAP0_ML_0	1190,59	1040,01	14,48%	7,21	438,70
6_GAP0_ML_0	1209,27	1058,44	14,25%	9,21	445,96
7_GAP0_ML_0	1240,57	1083,85	14,46%	7,75	456,79
8_GAP0_ML_0	1238,68	1085,50	14,11%	8,23	456,58
9_GAP0_ML_0	1255,31	1097,23	14,41%	7,44	462,77
10_GAP0_ML_0	1261,50	1102,14	14,46%	7,53	465,25
MEAN VALUES	**1194,39**	**1044,02**	**14,41%**	**7,46**	**440,16**

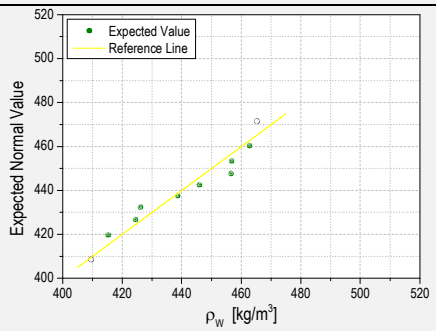

Q-Q plot of density distribution for configuration GAP0_ML_0

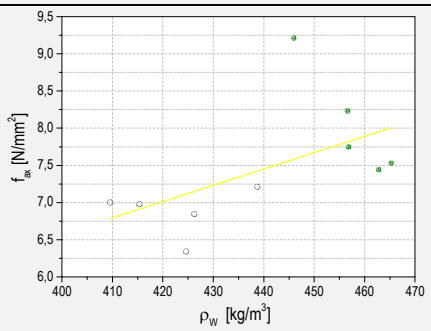

k_ρ	$-2.19 + 0.02 \cdot \rho$
R-Square	**0.22**

Linear fitting of correlation between f_{ax} and density for configuration GAP0_ML_0

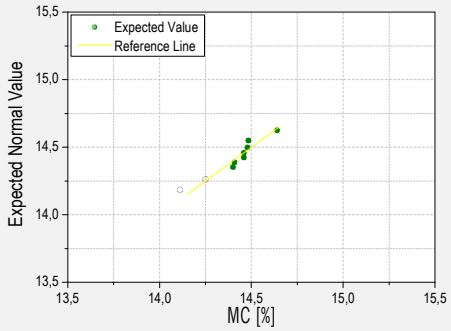

Q-Q plot of moisture content distribution for configuration GAP0_ML_0

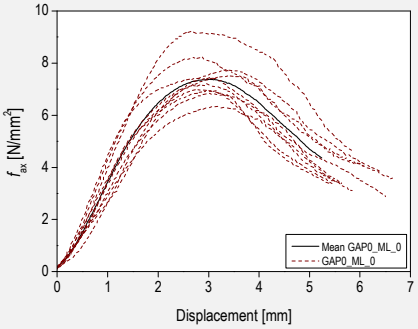

Relation between f_{ax} and displacement for GAP0_ML_0 tests

	MAXIMUM	MINIMUM	SD	CoV	MEDIAN	P5
f_{ax}	9,21	6,34	0,81	0,11	7,33	6,34
ρ	465,25	409,52	20,33	0,05	442,33	409,52
MC	14,64%	14,11%	0,14	0,01	14,43%	14,11%

GAP0_OL_0

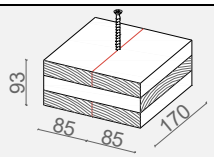

	WEIGHT AT TEST TIME [g] [mean values]	DRY WEIGHT [g] [mean values]	MC [%]	f_{ax} [N/mm²]	ρ [kg/m³]
1_GAP0_OL_0	1202,73	1053,32	14,18%	7,52	442,98
2_GAP0_OL_0	1224,69	1072,19	14,22%	7,31	451,27
3_GAP0_OL_0	1236,81	1083,21	14,18%	6,75	456,93
4_GAP0_OL_0	1253,74	1094,62	14,54%	7,48	462,60
5_GAP0_OL_0	1288,54	1127,95	14,24%	7,60	474,64
6_GAP0_OL_0	1298,15	1136,56	14,22%	7,53	478,61
7_GAP0_OL_0	1302,44	1141,47	14,10%	8,64	479,73
8_GAP0_OL_0	1309,97	1143,85	14,52%	7,49	483,58
9_GAP0_OL_0	1314,12	1149,77	14,29%	6,65	485,79
10_GAP0_OL_0	1325,75	1161,34	14,16%	5,82	489,03
MEAN VALUES	**1275,69**	**1116,43**	**0,14**	**7,28**	**470,51**

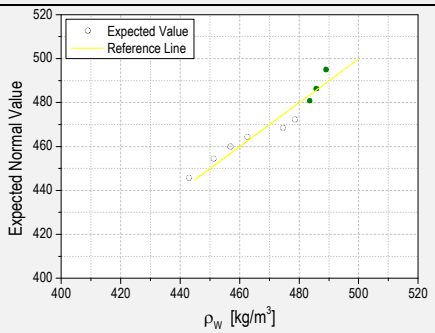

Q-Q plot of density distribution for configuration GAP0_OL_0

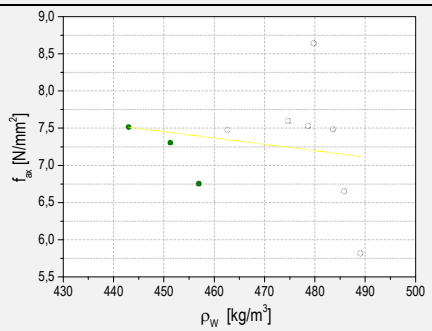

k_ρ	$11.29 - 0.009 \cdot \rho$
R-Square	**-0.09**

Linear fitting of correlation between f_{ax} and density for configuration GAP0_OL_0

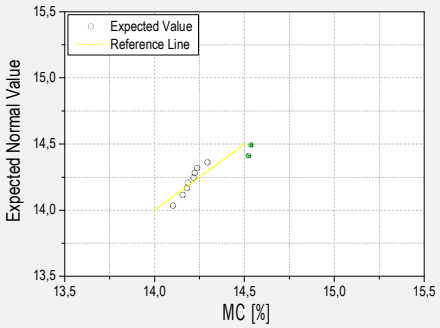

Q-Q plot of moisture content distribution for configuration GAP0_OL_0

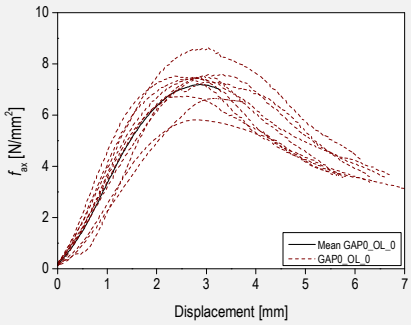

Relation between f_{ax} and displacement for GAP0_OL_0 tests

	MAXIMUM	MINIMUM	SD	CoV	MEDIAN	P5
f_{ax}	8,64	5,82	0,74	0,10	7,48	5,82
ρ	489,03	442,98	15,95	0,03	476,63	442,98
MC	14,54%	14,10%	0,15	0,01	14,22%	14,10%

GAP0_3L_0

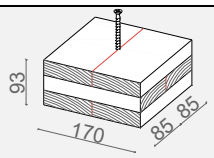

	WEIGHT AT TEST TIME [g] [mean values]	DRY WEIGHT [g] [mean values]	MC [%]	f_{ax} [N/mm²]	ρ [kg/m³]
1_GAP0_3L_0	1161,83	1013,60	14,62%	7,60	429,56
2_GAP0_3L_0	1166,01	1016,34	14,73%	7,91	430,94
3_GAP0_3L_0	1175,41	1024,75	14,70%	8,03	433,93
4_GAP0_3L_0	1192,86	1040,33	14,66%	7,08	440,51
5_GAP0_3L_0	1197,40	1045,62	14,52%	7,59	442,02
6_GAP0_3L_0	1203,16	1049,80	14,61%	7,27	444,30
7_GAP0_3L_0	1219,63	1063,23	14,71%	7,27	450,00
8_GAP0_3L_0	1223,50	1067,87	14,57%	7,94	452,18
9_GAP0_3L_0	1235,18	1078,99	14,48%	8,84	457,46
10_GAP0_3L_0	1253,75	1094,11	14,59%	6,87	462,84
MEAN VALUES	**1202,87**	**1049,46**	**0,15**	**7,64**	**444,37**

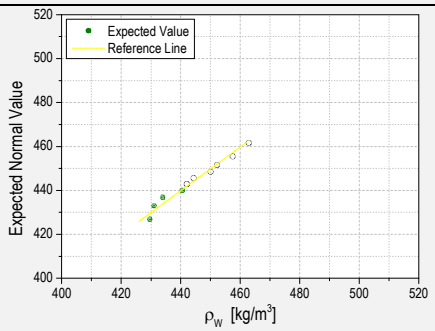

Q-Q plot of density distribution for configuration GAP0_3L_0

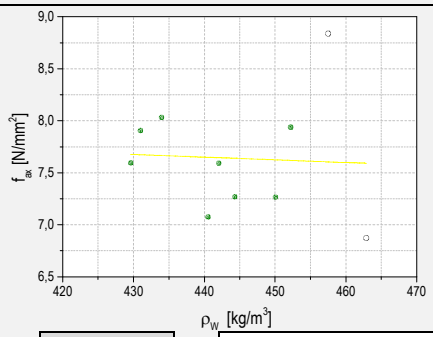

k_ρ	$8.79 - 0.003 \cdot \rho$
R-Square	**-0.12**

Linear fitting of correlation between f_{ax} and density for configuration GAP0_3L_0

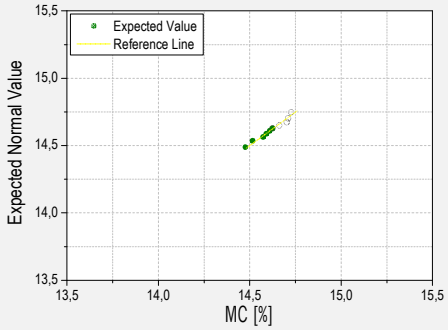

Q-Q plot of moisture content distribution for configuration GAP0_3L_0

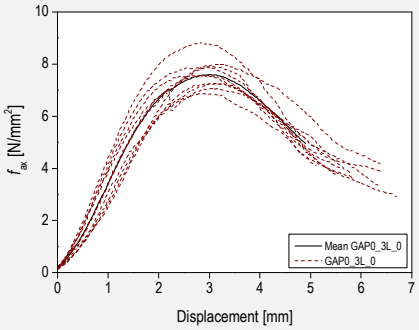

Relation between f_{ax} and displacement for GAP0_3L_0 tests

	MAXIMUM	MINIMUM	SD	CoV	MEDIAN	P5
f_{ax}	8,84	6,87	0,57	0,07	7,59	6,87
ρ	462,84	429,56	11,23	0,03	443,16	429,56
MC	14,73	14,48	0,08	0,01	14,62	14,48

GAP4_FL_0

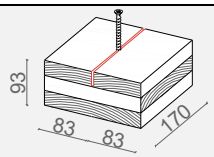

	WEIGHT AT TEST TIME [g] [mean values]	DRY WEIGHT [g] [mean values]	MC [%]	f_{ax} [N/mm²]	ρ [kg/m³]
1_GAP4_FL_0	1135,87	993,07	14,38%	6,45	422,35
2_GAP4_FL_0	1167,35	1017,32	14,75%	6,92	434,18
3_GAP4_FL_0	1207,05	1051,96	14,74%	6,80	449,11
4_GAP4_FL_0	1232,53	1074,50	14,71%	6,37	458,60
5_GAP4_FL_0	1242,61	1084,08	14,62%	6,32	462,33
6_GAP4_FL_0	1255,81	1098,18	14,35%	6,29	465,90
7_GAP4_FL_0	1259,04	1100,78	14,38%	7,37	467,19
8_GAP4_FL_0	1275,20	1116,14	14,25%	7,28	473,39
9_GAP4_FL_0	1281,77	1121,24	14,32%	6,94	476,23
10_GAP4_FL_0	1288,07	1126,31	14,36%	7,26	478,79
MEAN VALUES	**1234,53**	**1078,36**	**14,49%**	**6,80**	**458,81**

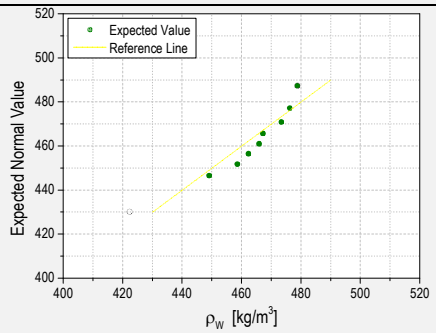

Q-Q plot of density distribution for configuration GAP4_FL_0

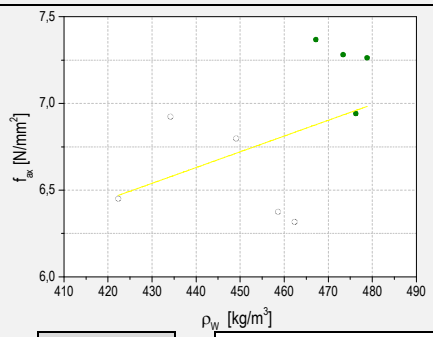

k_ρ	$2.63 + 0.01 \cdot \rho$
R-Square	**0.05**

Linear fitting of correlation between f_{ax} and density for configuration GAP4_FL_0

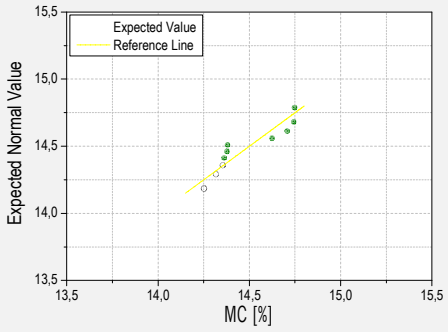

Q-Q plot of moisture content distribution for configuration GAP4_FL_0

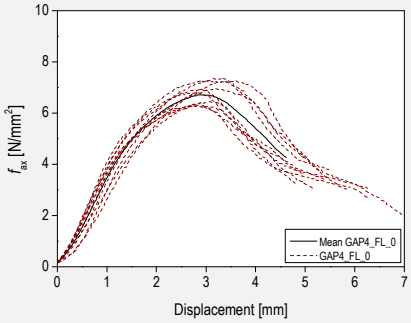

Relation between f_{ax} and displacement for GAP4_FL_0 tests

	MAXIMUM	MINIMUM	SD	CoV	MEDIAN	P5
f_{ax}	7,37	6,29	0,42	0,06	6,86	6,29
ρ	478,79	422,35	18,49	0,04	464,11	422,35
MC	14,75	14,25	0,19	0,01	14,38	14,25

GAP4_ML_0

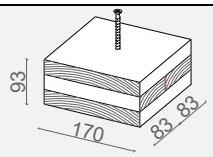

	WEIGHT AT TEST TIME [g] [mean values]	DRY WEIGHT [g] [mean values]	MC [%]	f_{ax} [N/mm²]	ρ [kg/m³]
1_GAP4_ML_0	1170,67	1022,49	14,49%	5,85	434,86
2_GAP4_ML_0	1181,65	1037,01	13,95%	5,85	438,85
3_GAP4_ML_0	1190,12	1041,32	14,29%	6,11	439,98
4_GAP4_ML_0	1193,05	1042,08	14,49%	5,33	443,35
5_GAP4_ML_0	1211,28	1057,08	14,59%	5,50	447,38
6_GAP4_ML_0	1210,53	1058,98	14,31%	5,37	449,91
7_GAP4_ML_0	1215,38	1062,00	14,44%	5,74	452,18
8_GAP4_ML_0	1223,02	1069,28	14,38%	5,40	454,83
9_GAP4_ML_0	1240,54	1084,56	14,38%	6,34	458,02
10_GAP4_ML_0	1242,23	1086,24	14,36%	6,43	462,22
MEAN VALUES	**1207,85**	**1056,10**	**14,37%**	**5,79**	**448,16**

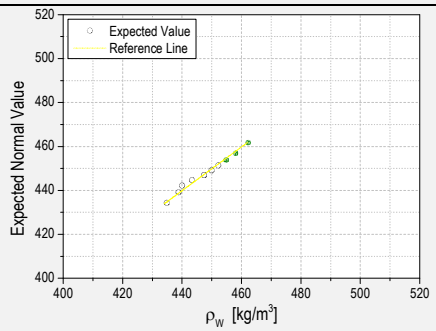

Q-Q plot of density distribution for configuration GAP4_ML_0

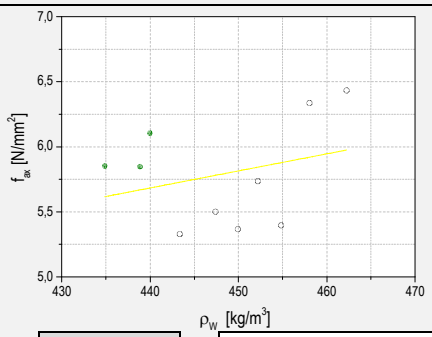

k_ρ	$-0.09 + 0.01 \cdot \rho$
R-Square	**-0.03**

Linear fitting of correlation between f_{ax} and density for configuration GAP4_ML_0

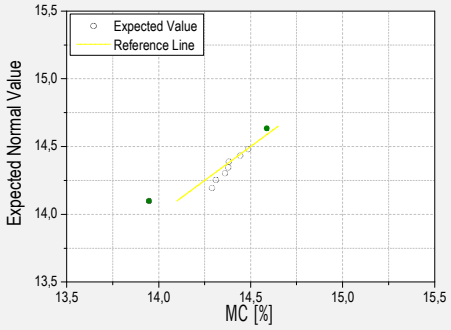

Q-Q plot of moisture content distribution for configuration GAP4_ML_0

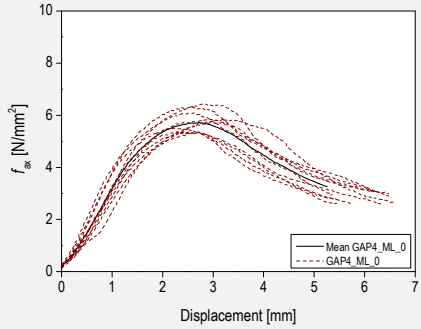

Relation between f_{ax} and displacement for GAP4_ML_0 tests

	MAXIMUM	MINIMUM	SD	CoV	MEDIAN	P5
f_{ax}	6,43	5,33	0,40	0,07	5,79	5,33
ρ	462,22	434,86	8,90	0,02	448,65	434,86
MC	14,59%	13,95%	0,17	0,01	14,38%	13,95%

GAP4_OL_0

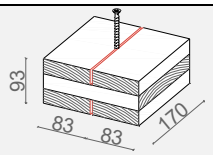

	WEIGHT AT TEST TIME [g] [mean values]	DRY WEIGHT [g] [mean values]	MC [%]	f_{ax} [N/mm²]	ρ [kg/m³]
1_GAP4_OL_0	1117,11	976,32	14,42%	2,72	418,26
2_GAP4_OL_0	1136,24	993,28	14,39%	4,69	427,44
3_GAP4_OL_0	1146,64	1003,07	14,31%	5,45	429,38
4_GAP4_OL_0	1185,09	1038,41	14,13%	6,04	441,08
5_GAP4_OL_0	1191,08	1043,64	14,13%	5,12	445,22
6_GAP4_OL_0	1210,35	1057,09	14,50%	5,19	453,37
7_GAP4_OL_0	1229,37	1076,45	14,21%	5,76	459,98
8_GAP4_OL_0	1245,42	1087,43	14,53%	6,26	469,03
9_GAP4_OL_0	1294,60	1132,18	14,35%	6,54	485,08
10_GAP4_OL_0	1319,40	1152,64	14,47%	7,49	493,79
MEAN VALUES	**1207,53**	**1056,05**	**14,34%**	**5,53**	**452,26**

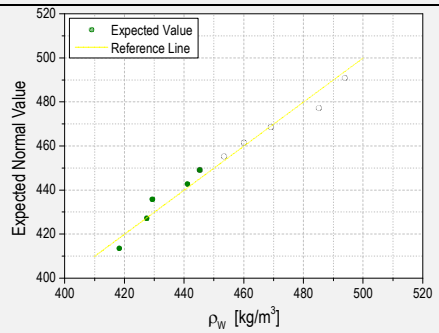

Q-Q plot of density distribution for configuration GAP4_OL_0

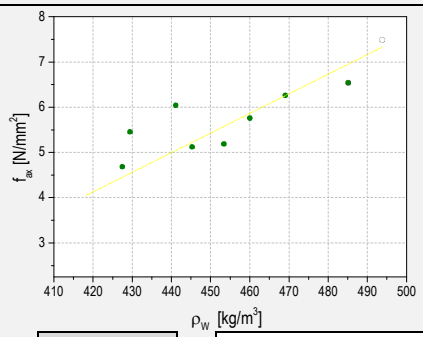

k_ρ	$-14.10 + 0.04 \cdot \rho$
R-Square	**0.69**

Linear fitting of correlation between f_{ax} and density for configuration GAP4_OL_0

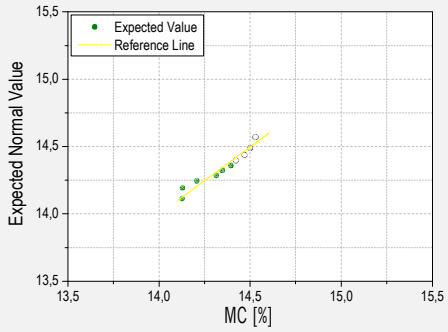

Q-Q plot of moisture content distribution for configuration GAP4_OL_0

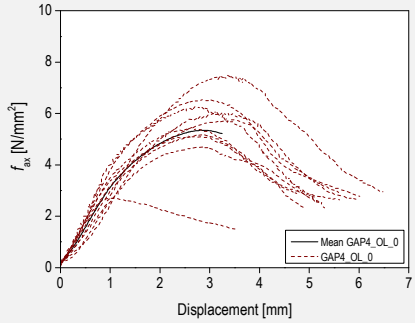

Relation between f_{ax} and displacement for GAP4_OL_0 tests

	MAXIMUM	MINIMUM	SD	CoV	MEDIAN	P5
f_{ax}	7,49	2,72	1,27	0,23	5,61	2,72
ρ	493,79	418,26	24,98	0,06	449,30	418,26
MC	14,53%	14,13%	0,15	0,01	14,37%	14,13%

GAP4_3L_0

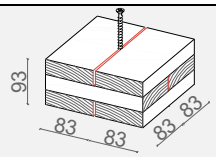

	WEIGHT AT TEST TIME [g] [mean values]	DRY WEIGHT [g] [mean values]	MC [%]	f_{ax} [N/mm²]	ρ [kg/m³]
1_GAP4_3L_0	1131,08	988,52	14,42%	3,43	425,96
2_GAP4_3L_0	1145,00	1001,20	14,36%	3,12	431,79
3_GAP4_3L_0	1164,85	1019,58	14,25%	4,29	439,29
4_GAP4_3L_0	1168,93	1023,38	14,22%	3,87	440,56
5_GAP4_3L_0	1182,89	1037,80	13,98%	4,23	445,42
6_GAP4_3L_0	1194,62	1046,12	14,20%	3,08	447,89
7_GAP4_3L_0	1193,69	1043,97	14,34%	3,50	450,22
8_GAP4_3L_0	1202,38	1051,41	14,36%	4,22	455,86
9_GAP4_3L_0	1222,80	1068,66	14,42%	4,21	460,89
10_GAP4_3L_0	1252,33	1096,80	14,18%	4,48	474,46
MEAN VALUES	**1185,86**	**1037,74**	**14,27%**	**3,84**	**447,23**

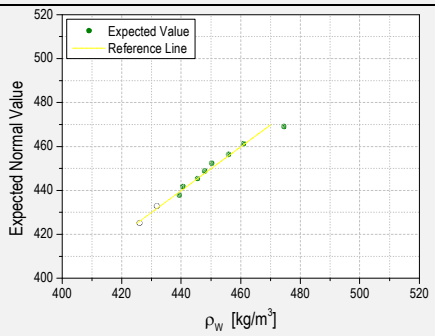

Q-Q plot of density distribution for configuration GAP4_3L_0

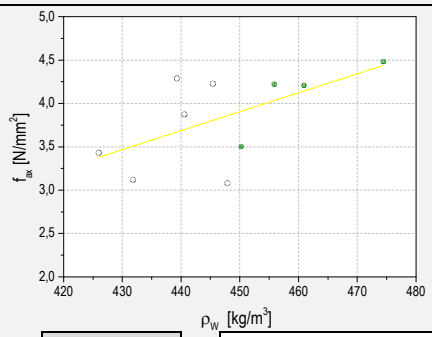

k_ρ	$-5.93 + 0.02 \cdot \rho$
R-Square	**0.28**

Linear fitting of correlation between f_{ax} and density for configuration GAP4_3L_0

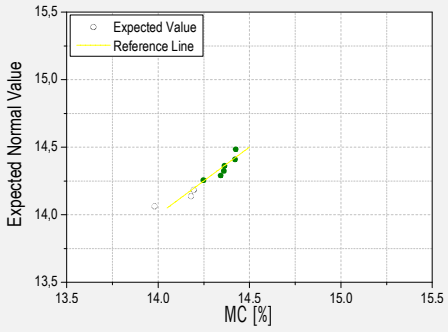

Q-Q plot of moisture content distribution for configuration GAP4_3L_0

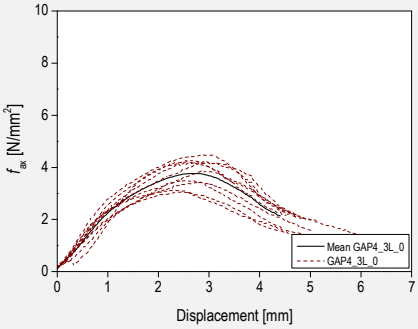

Relation between f_{ax} and displacement for GAP4_3L_0 tests

	MAXIMUM	MINIMUM	SD	CoV	MEDIAN	P5
f_{ax}	4,48	3,08	0,52	0,14	4,04	3,08
ρ	474,46	425,96	14,20	0,03	446,65	425,96
MC	14,42%	13,98%	0,14	0,01	14,29%	13,98%

GL_0

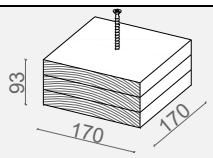

	WEIGHT AT TEST TIME [g] [mean values]	DRY WEIGHT [g] [mean values]	MC [%]	f_{ax} [N/mm²]	ρ [kg/m³]
1_GL_0	1146,85	1035,42	14,43%	7,27	437,36
2_GL_0	1166,08	1052,58	14,39%	7,62	444,35
3_GL_0	1168,47	1052,98	14,58%	7,82	445,13
4_GL_0	1186,01	1070,16	14,38%	7,61	451,32
5_GL_0	1190,27	1072,13	14,56%	7,60	452,68
6_GL_0	1214,53	1094,97	14,39%	8,29	464,70
7_GL_0	1243,51	1119,28	14,49%	10,20	472,66
8_GL_0	1307,00	1176,58	14,31%	7,22	496,30
9_GL_0	1327,92	1196,80	14,13%	7,14	503,56
10_GL_0	1330,94	1196,18	14,44%	8,41	501,81
MEAN VALUES	**1228,16**	**1106,71**	**14,41%**	**7,92**	**466,99**

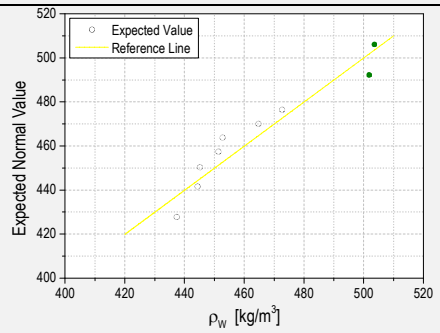

Q-Q plot of density distribution for configuration GL_0

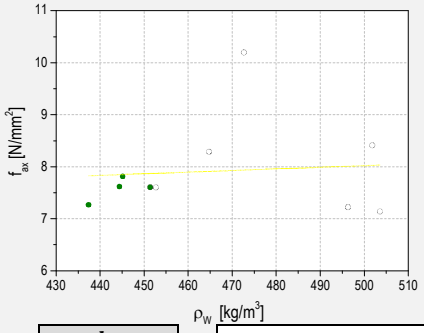

k_ρ	$6.46 + 0.003 \cdot \rho$
R-Square	**-0.12**

Linear fitting of correlation between f_{ax} and density for configuration GL_0

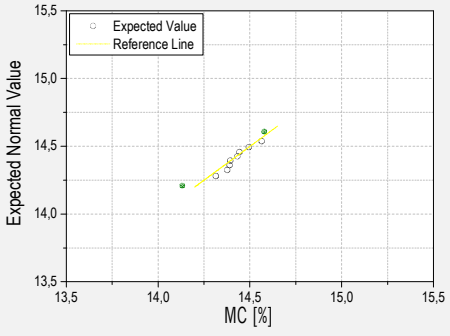

Q-Q plot of moisture content distribution for configuration GL_0

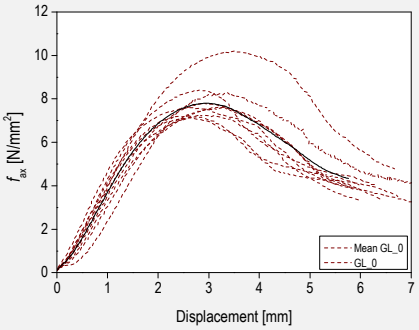

Relation between f_{ax} and displacement for GL_0 tests

	MAXIMUM	MINIMUM	SD	CoV	MEDIAN	P5
f_{ax}	10,20	7,14	0,91	0,11	7,61	7,14
ρ	503,56	437,36	25,31	0,05	458,69	437,36
MC	14,58%	14,13%	0,13	0,01	14,41%	14,13%

Annex 1:14

REF_308

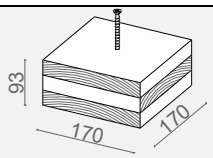

	WEIGHT AT TEST TIME [g] [mean values]	DRY WEIGHT [g] [mean values]	MC [%]	f_{ax} [N/mm²]	ρ [kg/m³]
1_REF_308	1235,46	1089,39	13,41%	7,69	463,31
2_REF_308	1242,91	1093,04	13,71%	8,39	465,43
3_REF_308	1253,87	1104,19	13,56%	7,65	469,15
4_REF_308	1247,57	1099,42	13,48%	7,53	468,20
5_REF_308	1262,64	1108,63	13,89%	8,23	471,72
6_REF_308	1249,59	1001,05	13,49%	7,58	468,05
7_REF_308	1259,56	1107,30	13,75%	8,59	471,49
8_REF_308	1249,54	1098,78	13,72%	7,48	469,33
9_REF_308	1276,41	1122,49	13,71%	7,69	478,88
10_REF_308	1281,65	1125,64	13,86%	8,84	478,26
MEAN VALUES	**1255,92**	**1094,99**	**13,66%**	**7,97**	**470,38**

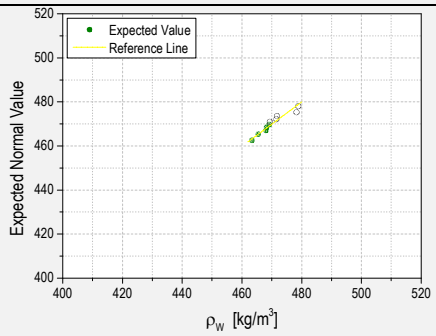

Q-Q plot of density distribution for configuration REF_308

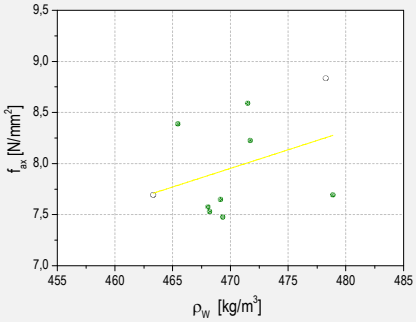

k_ρ	$-9.16 + 0.04 \cdot \rho$
R-Square	**-0.03**

Linear fitting of correlation between f_{ax} and density for configuration REF_308

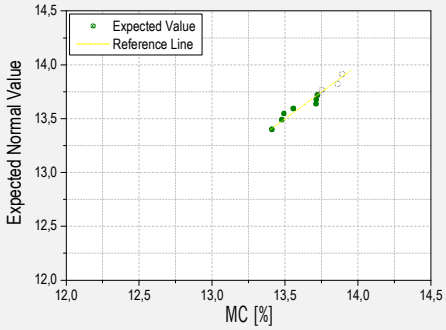

Q-Q plot of moisture content distribution for configuration REF_308

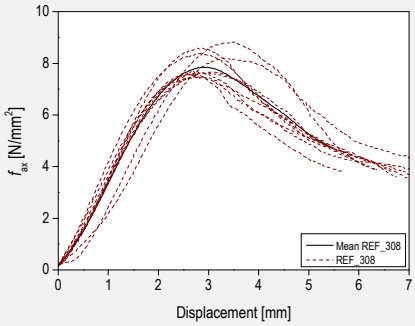

Relation between f_{ax} and displacement for REF_308 tests

	MAXIMUM	MINIMUM	SD	CoV	MEDIAN	P5
f_{ax}		7,48	0,50	0,06	7,69	7,48
ρ	478,88	463,31	5,00	0,01	469,24	463,31
MC	13,89%	13,41%	0,17	0,01	13,71%	13,41%

GAP0_FL_308

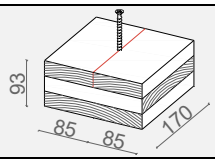

	WEIGHT AT TEST TIME [g] [mean values]	DRY WEIGHT [g] [mean values]	MC [%]	f_{ax} [N/mm²]	ρ [kg/m³]
1_GAP0_FL_308	1227,28	1080,45	13,59%	7,07	461,87
2_GAP0_FL_308	1253,74	1104,16	13,55%	6,77	470,82
3_GAP0_FL_308	1268,68	1117,17	13,56%	7,96	475,74
4_GAP0_FL_308	1294,21	1141,40	13,39%	8,02	486,12
5_GAP0_FL_308	1301,66	1145,48	13,63%	9,30	488,31
6_GAP0_FL_308	1310,11	1153,89	13,54%	8,57	491,76
7_GAP0_FL_308	1320,19	1164,09	13,41%	9,81	496,43
8_GAP0_FL_308	1332,77	1172,80	13,64%	8,14	500,57
9_GAP0_FL_308	1363,75	1200,18	13,63%	8,51	512,00
10_GAP0_FL_308	1301,06	1146,44	13,49%	8,51	488,05
MEAN VALUES	**1297,35**	**1142,61**	**13,54%**	**8,26**	**487,17**

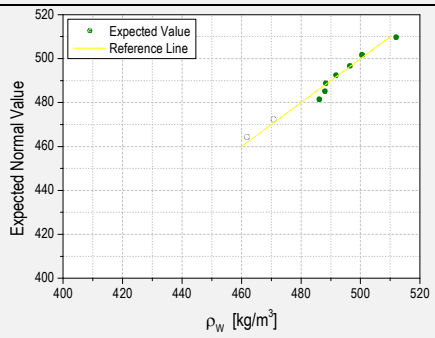

Q-Q plot of density distribution for configuration GAP0_FL_308

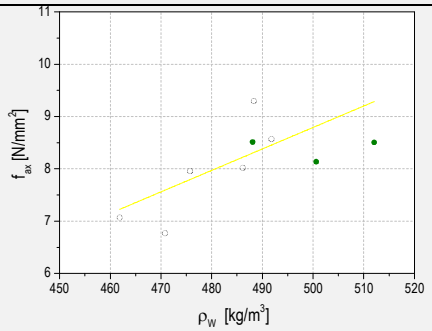

k_ρ	$-11.73 + 0.04 \cdot \rho$
R-Square	**0.37**

Linear fitting of correlation between f_{ax} and density for configuration GAP0_FL_308

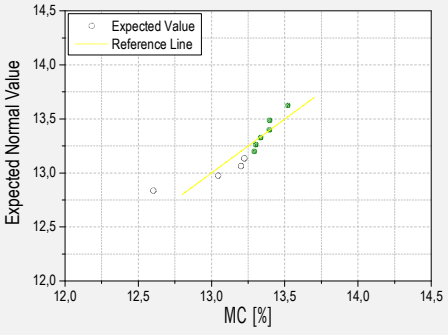

Q-Q plot of moisture content distribution for configuration GAP0_FL_308

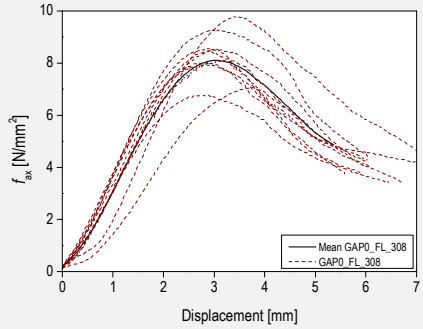

Relation between f_{ax} and displacement for GAP0_FL_308 tests

	MAXIMUM	MINIMUM	SD	CoV	MEDIAN	P5
f_{ax}	9,81	6,77	0,91	0,11	832,11%	6,77
ρ	512,00	461,87	14,70	0,03	48817,67%	461,87
MC	13,64%	13,39%	0,09	0,01	13,55%	13,39%

GAP0_ML_308

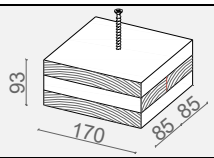

	WEIGHT AT TEST TIME [g] [mean values]	DRY WEIGHT [g] [mean values]	MC [%]	f_{ax} [N/mm²]	ρ [kg/m³]
1_GAP0_ML_308	1104,58	974,98	13,29%	7,12	413,96
2_GAP0_ML_308	1120,48	989,81	13,20%	6,90	419,48
3_GAP0_ML_308	1143,67	1009,40	13,30%	7,09	428,25
4_GAP0_ML_308	1150,63	1015,24	13,34%	8,58	432,53
5_GAP0_ML_308	1173,47	1042,13	12,60%	6,94	441,40
6_GAP0_ML_308	1207,47	1064,82	13,40%	6,61	451,96
7_GAP0_ML_308	1232,79	1087,17	13,39%	9,30	462,38
8_GAP0_ML_308	1239,80	1096,72	13,05%	7,61	464,74
9_GAP0_ML_308	1251,28	1105,14	13,22%	6,58	469,04
10_GAP0_ML_308	1249,29	1100,49	13,52%	7,83	469,93
MEAN VALUES	**1187,35**	**1048,59**	**13,23%**	**7,46**	**445,37**

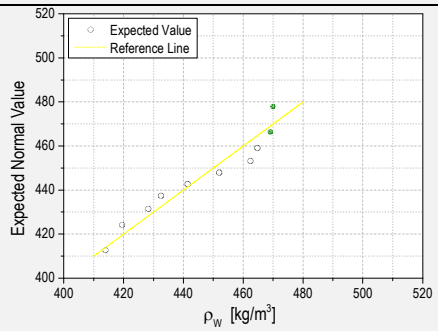

Q-Q plot of density distribution for configuration GAP0_ML_308

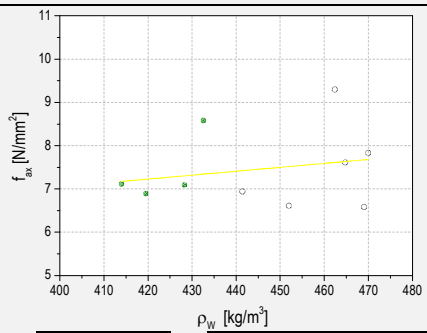

k_ρ	$3.42 + 0.009 \cdot \rho$
R-Square	**-0.07**

Linear fitting of correlation between f_{ax} and density for configuration GAP0_ML_308

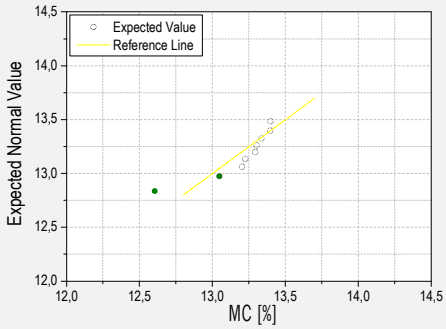

Q-Q plot of moisture content distribution for configuration GAP0_ML_308

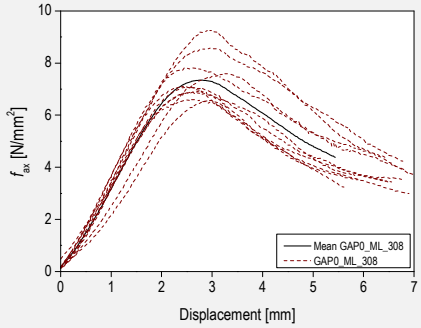

Relation between f_{ax} and displacement for GAP0_ML_308 tests

	MAXIMUM	MINIMUM	SD	CoV	MEDIAN	P5
f_{ax}	9,30	6,58	0,89	0,12	7,11	6,58
ρ	469,93	413,96	21,09	0,05	446,68	413,96
MC	13,52%	12,60%	0,26	0,02	13,30%	12,60%

GAP0_OL_308

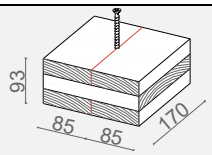

	WEIGHT AT TEST TIME [g] [mean values]	DRY WEIGHT [g] [mean values]	MC [%]	f_{ax} [N/mm²]	ρ [kg/m³]
1_GAP0_OL_308	1193,67	1053,89	13,26%	6,37	446,83
2_GAP0_OL_308	1215,69	1072,26	13,38%	7,13	456,60
3_GAP0_OL_308	1229,98	1084,85	13,38%	6,97	461,98
4_GAP0_OL_308	1250,82	1098,47	13,87%	5,92	469,22
5_GAP0_OL_308	1272,61	1122,85	13,34%	7,95	478,91
6_GAP0_OL_308	1284,59	1133,96	13,28%	7,37	482,16
7_GAP0_OL_308	1294,58	1139,10	13,65%	6,14	484,36
8_GAP0_OL_308	1291,51	1137,82	13,51%	6,60	485,17
9_GAP0_OL_308	1301,59	1149,47	13,23%	9,15	489,19
10_GAP0_OL_308	1319,60	1165,65	13,21%	8,35	496,56
MEAN VALUES	**1265,46**	**1115,83**	**13,41%**	**7,20**	**475,10**

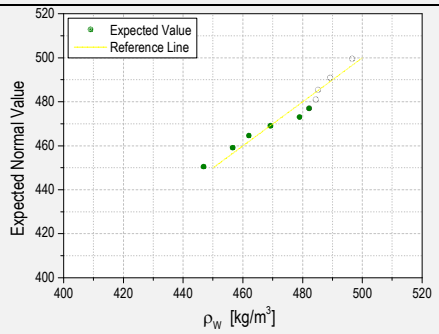

Q-Q plot of density distribution for configuration GAP0_OL_308

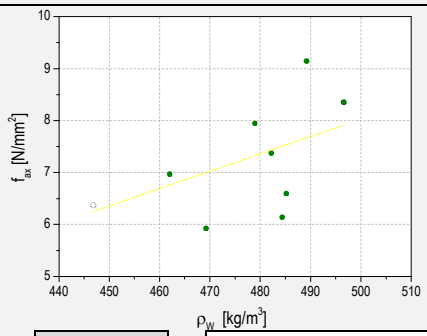

k_ρ	$-8.70 + 0.03 \cdot \rho$
R-Square	**-0.17**

Linear fitting of correlation between f_{ax} and density for configuration GAP0_OL_308

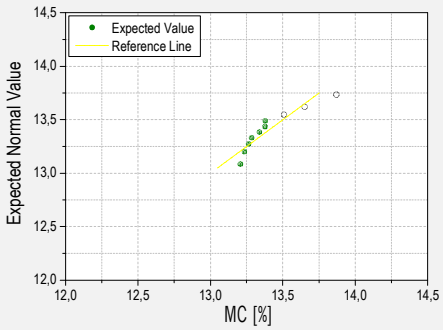

Q-Q plot of moisture content distribution for configuration GAP0_OL_308

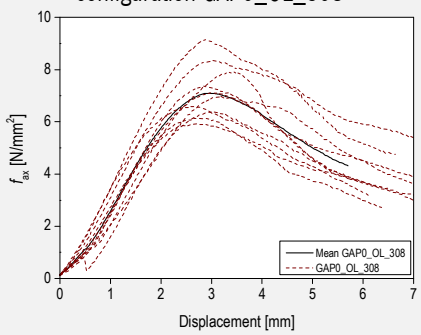

Relation between f_{ax} and displacement for GAP0_OL_308 tests

	MAXIMUM	MINIMUM	SD	CoV	MEDIAN	P5
f_{ax}	9,15	5,92	1,03	0,14	7,05	5,92
ρ	496,56	446,83	15,84	0,03	480,54	446,83
MC	13,87%	13,21%	0,21	0,02	13,36%	13,21%

GAP0_3L_380

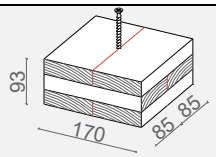

	WEIGHT AT TEST TIME [g] [mean values]	DRY WEIGHT [g] [mean values]	MC [%]	f_{ax} [N/mm²]	ρ [kg/m³]
1_GAP0_3L_308	1153,82	1013,23	13,88%	7,56	432,27
2_GAP0_3L_308	1157,59	1017,46	13,77%	6,50	433,45
3_GAP0_3L_308	1168,24	1029,22	13,51%	6,65	439,47
4_GAP0_3L_308	1183,54	1042,95	13,48%	6,29	444,32
5_GAP0_3L_308	1179,44	1040,03	13,40%	5,86	443,97
6_GAP0_3L_308	1196,71	1053,22	13,62%	6,96	450,27
7_GAP0_3L_308	1226,10	1080,52	13,47%	7,66	459,44
8_GAP0_3L_308	1217,62	1072,42	13,54%	6,63	458,06
9_GAP0_3L_308	1231,92	1085,58	13,48%	6,39	462,30
10_GAP0_3L_308	1248,95	1098,47	13,70%	6,89	468,85
MEAN VALUES	**1196,39**	**1053,31**	**13,59%**	**6,74**	**449,24**

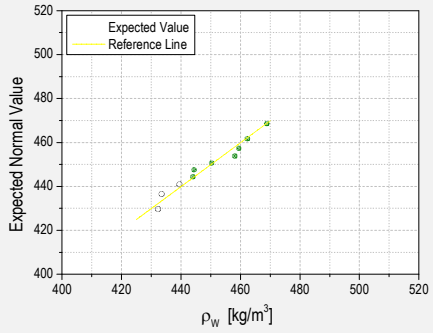

Q-Q plot of density distribution for configuration GAP0_3L_308

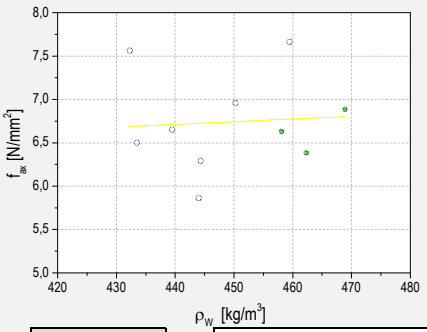

k_ρ	$5.34 - 0.003 \cdot \rho$
R-Square	**-0.12**

Linear fitting of correlation between f_{ax} and density for configuration GAP0_3L_308

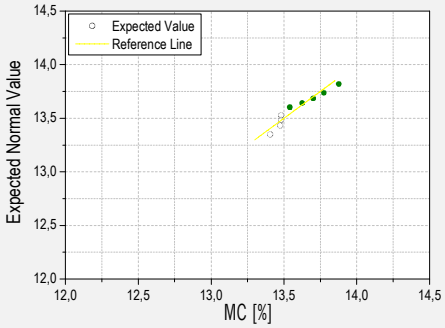

Q-Q plot of moisture content distribution for configuration GAP0_3L_308

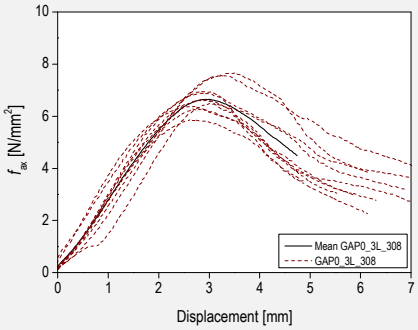

Relation between f_{ax} and displacement for GAP0_3L_308 tests

	MAXIMUM	MINIMUM	SD	CoV	MEDIAN	P5
f_{ax}	7,66	5,86	0,56	0,08	6,64	5,86
ρ	468,85	432,27	12,57	0,03	447,29	432,27
MC	13,88%	13,40%	0,15	0,01	13,52%	13,40%

GAP4_FL_308

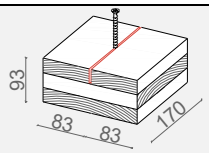

	WEIGHT AT TEST TIME [g] [mean values]	DRY WEIGHT [g] [mean values]	MC [%]	f_{ax} [N/mm²]	ρ [kg/m³]
1_GAP4_FL_308	1138,42	1000,08	13,83%	6,70	429,59
2_GAP4_FL_308	1168,32	1025,98	13,87%	6,78	440,45
3_GAP4_FL_308	1207,18	1059,83	13,90%	5,96	453,73
4_GAP4_FL_308	1228,36	1083,09	13,41%	6,81	464,02
5_GAP4_FL_308	1232,61	1085,59	13,54%	6,31	466,48
6_GAP4_FL_308	1246,86	1099,32	13,42%	6,74	469,09
7_GAP4_FL_308	1247,81	1097,26	13,72%	6,99	471,08
8_GAP4_FL_308	1269,36	1117,89	13,55%	7,16	477,95
9_GAP4_FL_308	1276,11	1124,76	13,46%	6,73	479,95
10_GAP4_FL_308	n.a.	1131,62	n.a.	6,38	485,59
MEAN VALUES	**1223,89**	**1082,54**	**13,63%**	**6,66**	**463,79**

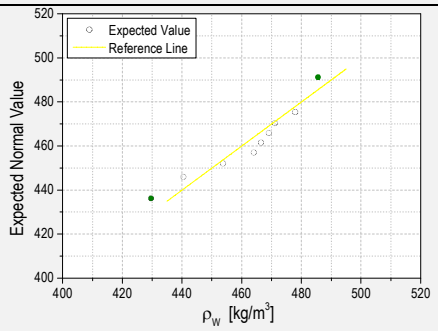

Q-Q plot of density distribution for configuration GAP4_FL_308

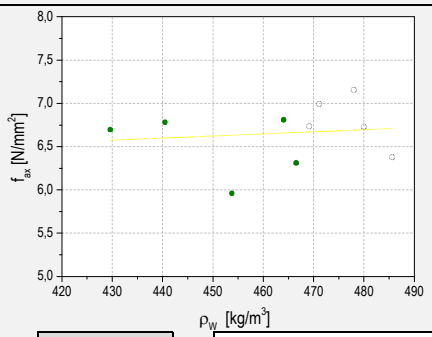

k_ρ	$5.54 + 0.002 \cdot \rho$
R-Square	**-0.12**

Linear fitting of correlation between f_{ax} and density for configuration GAP4_FL_308

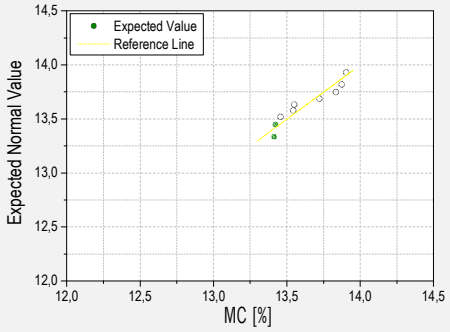

Q-Q plot of moisture content distribution for configuration GAP4_FL_308

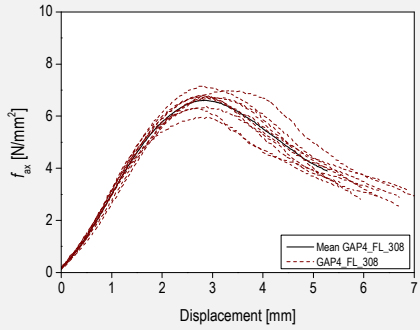

Relation between f_{ax} and displacement for GAP4_FL_308 tests

	MAXIMUM	MINIMUM	SD	CoV	MEDIAN	P5
f_{ax}	7,16	5,96	0,34834	0,05	6,73	5,96
ρ	485,59	429,59	17,76716	0,04	467,79	429,59
MC	13,90%	13,41%	0,19947	0,01	13,55%	13,41%

GAP4_ML_308

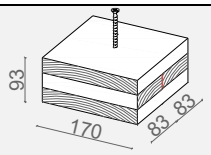

	WEIGHT AT TEST TIME [g] [mean values]	DRY WEIGHT [g] [mean values]	MC [%]	f_{ax} [N/mm²]	ρ [kg/m³]
1_GAP4_ML_308	1158,89	1021,40	13,46%	6,02	437,21
2_GAP4_ML_308	1172,28	1035,34	13,23%	5,83	441,88
3_GAP4_ML_308	1177,70	1037,95	13,46%	5,58	443,96
4_GAP4_ML_308	1192,32	1053,11	13,22%	6,36	449,60
5_GAP4_ML_308	1196,20	1055,30	13,35%	6,75	451,63
6_GAP4_ML_308	1209,95	1067,07	13,39%	6,29	455,64
7_GAP4_ML_308	1207,11	1065,90	13,25%	6,52	455,82
8_GAP4_ML_308	1219,79	1076,61	13,30%	5,89	459,24
9_GAP4_ML_308	1223,64	1080,54	13,24%	6,96	461,31
10_GAP4_ML_308	1271,04	1122,45	13,24%	6,85	479,49
MEAN VALUES	**1202,89**	**1061,57**	**13,31%**	**6,30**	**453,58**

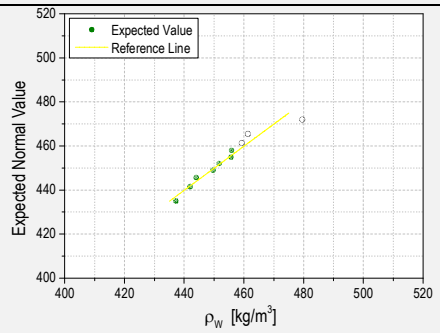

Q-Q plot of density distribution for configuration GAP4_ML_308

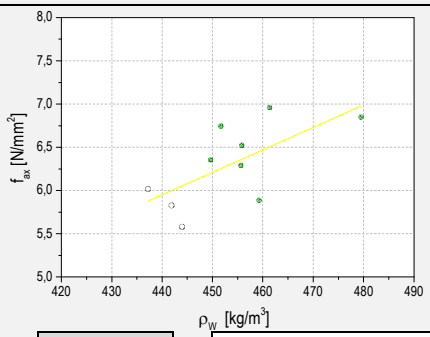

k_ρ	$-5.49 + 0.03 \cdot \rho$
R-Square	**0.37**

Linear fitting of correlation between f_{ax} and density for configuration GAP4_ML_308

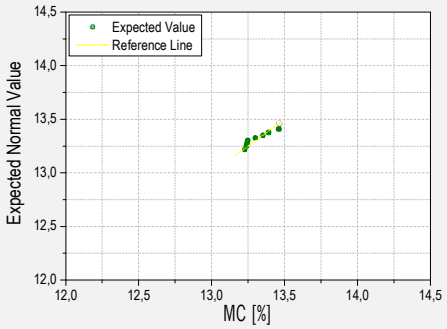

Q-Q plot of moisture content distribution for configuration GAP4_ML_308

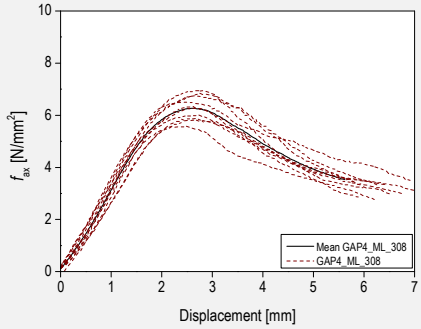

Relation between f_{ax} and displacement for GAP4_ML_308 tests

	MAXIMUM	MINIMUM	SD	CoV	MEDIAN	P5
f_{ax}	6,96	5,58	0,47	0,07	6,32	5,58
ρ	479,49	437,21	11,97	0,03	453,64	437,21
MC	13,46%	13,22%	0,10	0,01	13,27%	13,22%

GAP4_OL_308

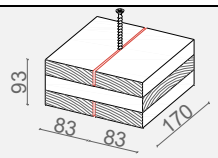

	WEIGHT AT TEST TIME [g] [mean values]	DRY WEIGHT [g] [mean values]	MC [%]	f_{ax} [N/mm²]	ρ [kg/m³]
1_GAP4_OL_308	1116,58	984,11	13,46%	4,60	424,05
2_GAP4_OL_308	1132,88	997,45	13,58%	6,14	429,73
3_GAP4_OL_308	1162,28	1024,26	13,48%	5,27	440,45
4_GAP4_OL_308	1181,93	1041,12	13,52%	5,84	447,66
5_GAP4_OL_308	1186,71	1048,06	13,23%	5,44	451,38
6_GAP4_OL_308	1203,91	1059,09	13,67%	5,07	456,46
7_GAP4_OL_308	1226,06	1080,78	13,44%	6,42	465,51
8_GAP4_OL_308	1169,63	1031,72	13,37%	5,36	443,66
9_GAP4_OL_308	1289,28	1132,42	13,85%	6,56	490,46
10_GAP4_OL_308	1311,32	1156,94	13,34%	5,93	499,10
MEAN VALUES	**1198,06**	**1055,60**	**13,49%**	**5,66**	**454,85**

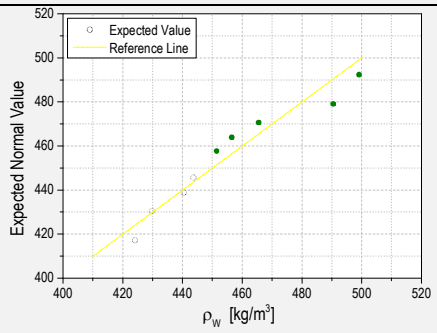

Q-Q plot of density distribution for configuration GAP4_OL_308

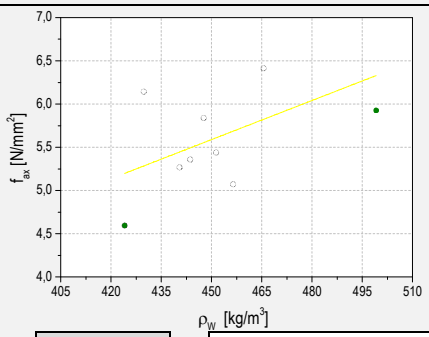

k_ρ	$-1.20 + 0.02 \cdot \rho$
R-Square	**0.26**

Linear fitting of correlation between f_{ax} and density for configuration GAP4_OL_308

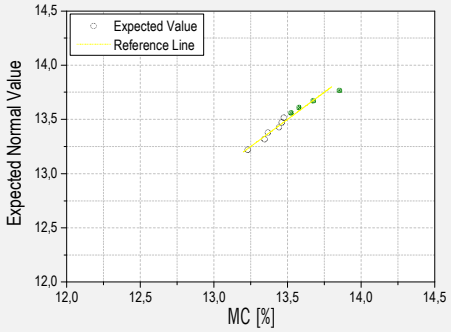

Q-Q plot of moisture content distribution for configuration GAP4_OL_308

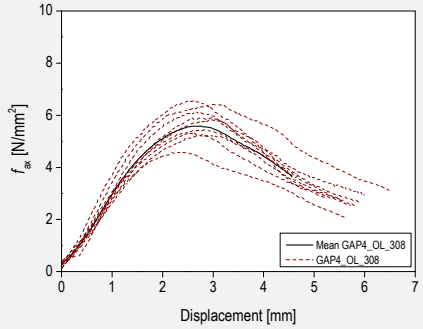

Relation between f_{ax} and displacement for GAP4_OL_308 tests

	MAXIMUM	MINIMUM	SD	CoV	MEDIAN	P5
f_{ax}	6,56	4,60	0,62	0,11	5,64	4,60
ρ	499,10	424,05	24,31	0,05	449,52	424,05
MC	13,85%	13,23%	0,18	0,01	13,47%	13,23%

GAP4_3L_308

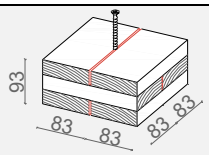

	WEIGHT AT TEST TIME [g] [mean values]	DRY WEIGHT [g] [mean values]	MC [%]	f_{ax} [N/mm²]	ρ [kg/m³]
1_GAP4_3L_308	1124,32	992,71	13,26%	2,98	430,92
2_GAP4_3L_308	1152,54	1017,56	13,27%	2,75	440,78
3_GAP4_3L_308	1153,24	1019,82	13,08%	3,75	442,73
4_GAP4_3L_308	1156,05	1019,25	13,42%	3,06	443,47
5_GAP4_3L_308	1181,40	1034,24	14,23%	4,20	450,33
6_GAP4_3L_308	1185,33	1040,44	13,93%	3,77	453,26
7_GAP4_3L_308	1186,85	1047,08	13,35%	3,27	454,30
8_GAP4_3L_308	1197,93	1053,83	13,67%	4,52	458,63
9_GAP4_3L_308	1225,98	1083,22	13,18%	4,10	469,65
10_GAP4_3L_308	1245,83	1099,35	13,32%	2,67	477,89
MEAN VALUES	**1180,95**	**1040,75**	**13,47%**	**3,51**	**452,19**

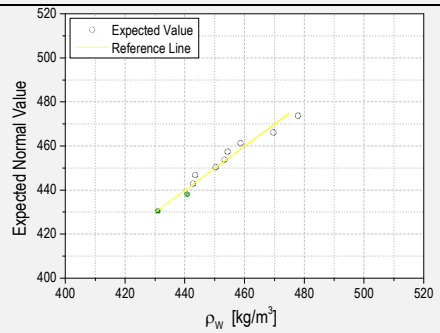

Q-Q plot of density distribution for configuration GAP4_3L_308

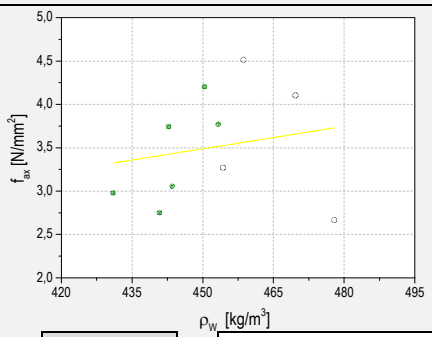

k_ρ	$-0.41 + 0.01 \cdot \rho$
R-Square	**-0.09**

Linear fitting of correlation between f_{ax} and density for configuration GAP4_3L_308

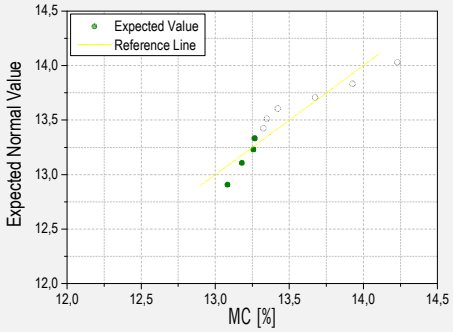

Q-Q plot of moisture content distribution for configuration GAP4_3L_308

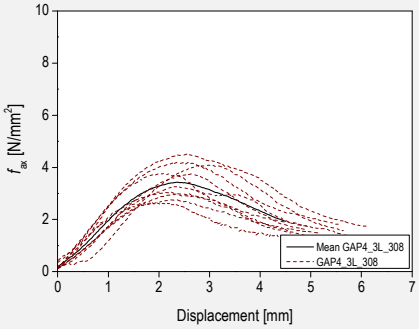

Relation between f_{ax} and displacement for GAP4_3L_308 tests

	MAXIMUM	MINIMUM	SD	CoV	MEDIAN	P5
f_{ax}	4,52	2,67	0,65	0,19	3,51	2,67
ρ	477,89	430,92	14,00	0,03	451,79	430,92
MC	14,23%	13,08%	0,36	0,03	13,34%	13,08%

GL_308

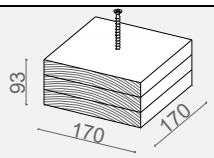

	WEIGHT AT TEST TIME [g] [mean values]	DRY WEIGHT [g] [mean values]	MC [%]	f_{ax} [N/mm²]	ρ [kg/m³]
1_GL_308		1034,01	13,42%	7,32	441,34
2_GL_308	1161,81	1058,01	13,40%	7,74	450,37
3_GL_308	1165,80	1061,89	13,36%	7,10	453,05
4_GL_308	1188,37	1079,21	13,64%	8,16	457,42
5_GL_308	1198,63	1081,11	14,39%	7,61	460,44
6_GL_308	1266,82	1147,70	13,69%	8,95	473,36
7_GL_308	1289,92	1171,86	13,32%	7,15	496,84
8_GL_308	1302,68	1183,51	13,28%	7,76	502,94
9_GL_308	1314,90	1193,50	13,36%	7,61	506,93
10_GL_308	1328,67	1207,88	13,15%	7,60	513,05
MEAN VALUES	**1235,24**	**1121,87**	**13,50%**	**7,70**	**475,58**

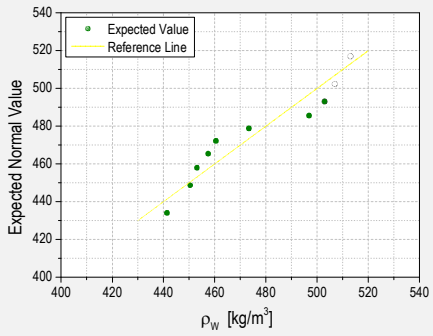

Q-Q plot of density distribution for configuration GL_308

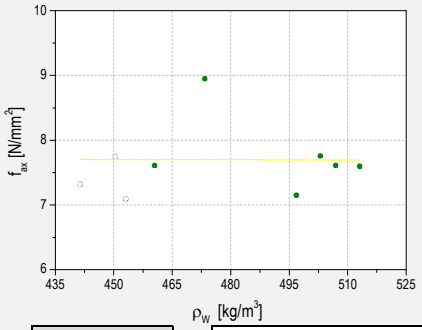

k_ρ	$7.75 - 0.00 \cdot \rho$
R-Square	**-0.12**

Linear fitting of correlation between f_{ax} and density for configuration GL_308

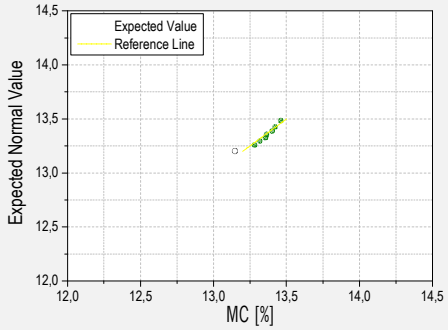

Q-Q plot of moisture content distribution for configuration GL_308

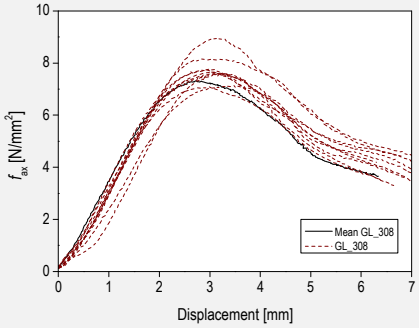

Relation between f_{ax} and displacement for GL_308 tests

	MAXIMUM	MINIMUM	SD	CoV	MEDIAN	P5
f_{ax}	8,95	7,10	0,54	0,07	7,61	7,10
ρ	513,05	441,34	26,80	0,06	466,90	441,34
MC	13,69%	13,15%	0,16	0,01	13,38%	13,15%

Annex 1:15

REF_ML_14%

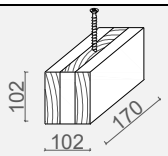

	WEIGHT AT TEST TIME [g] [mean values]	DRY WEIGHT [g] [mean values]	MC [%]	f_{ax} [N/mm²]	ρ [kg/m³]
1_REF_ML_14%	639,94	562,48	13,77%	3,90	452,78
2_REF_ML_14%	663,20	580,36	14,27%	3,10	442,54
3_REF_ML_14%	673,84	593,06	13,62%	3,76	482,48
4_REF_ML_14%	679,13	594,52	14,23%	4,89	451,55
5_REF_ML_14%	686,06	601,72	14,02%	2,84	469,02
6_REF_ML_14%	686,73	603,37	13,82%	4,52	467,61
7_REF_ML_14%	696,40	612,39	13,72%	4,79	470,81
8_REF_ML_14%	701,00	615,16	13,95%	3,79	460,95
9_REF_ML_14%	705,74	618,05	14,19%	5,30	467,21
10_REF_ML_14%	725,50	638,35	13,65%	8,78	485,48
MEAN VALUES	**685,75**	**601,95**	**13,92%**	**4,57**	**465,04**

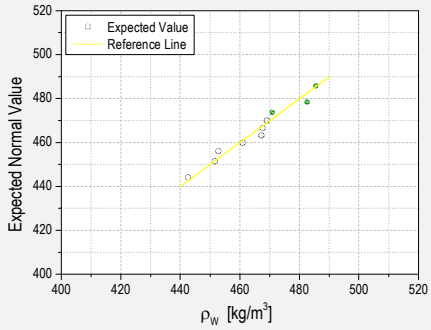

Q-Q plot of density distribution for configuration REF_ML_14%

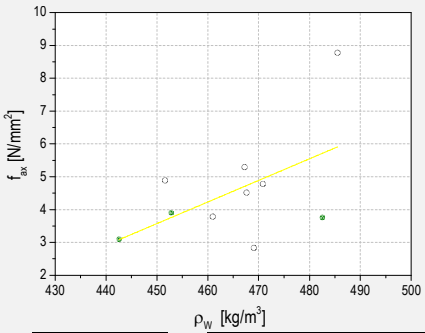

k_ρ	$-26.05 + 0.07 \cdot \rho$
R-Square	**0.19**

Linear fitting of correlation between f_{ax} and density for configuration REF_ML_14%

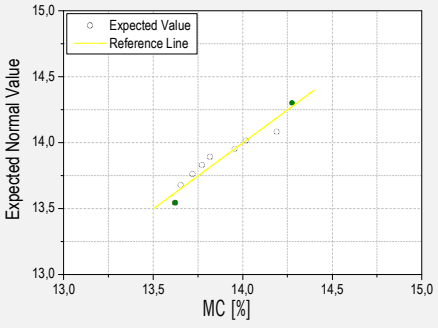

Q-Q plot of moisture content distribution for configuration REF_ML_14%

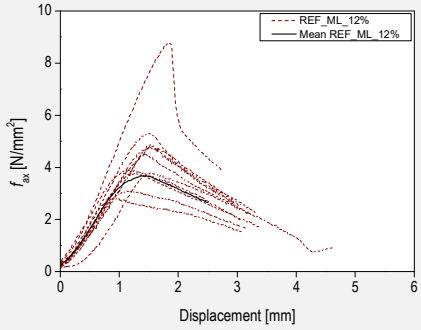

Relation between f_{ax} and displacement for REF_ML_14% tests

	MAXIMUM	MINIMUM	SD	CoV	MEDIAN	P5
f_{ax}	8,78	2,84	1,68	0,37	4,21	2,84
ρ	485,48	442,54	13,49	0,03	467,41	442,54
MC	14,27%	13,62%	0,24	0,02	13,88%	13,62%

REF_BL_14%

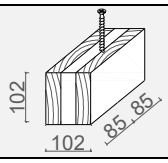

	WEIGHT AT TEST TIME [g] [mean values]	DRY WEIGHT [g] [mean values]	MC [%]	f_{ax} [N/mm²]	ρ [kg/m³]
1_REF_BL_14%	666,17	585,09	13,86%	6,18	489,11
2_REF_BL_14%	682,82	599,31	13,93%	5,98	447,39
3_REF_BL_14%	691,04	606,53	13,93%	6,95	477,28
4_REF_BL_14%	702,21	616,65	13,87%	5,62	471,87
5_REF_BL_14%	703,99	618,14	13,89%	4,42	490,98
6_REF_BL_14%	713,99	624,46	14,34%	7,55	487,85
7_REF_BL_14%	714,45	624,56	14,39%	6,64	459,68
8_REF_BL_14%	726,09	635,23	14,30%	10,90	452,76
9_REF_BL_14%	727,41	639,45	13,76%	6,31	465,04
10_REF_BL_14%	747,86	656,93	13,84%	8,53	465,02
MEAN VALUES	**707,60**	**620,64**	**14,01%**	**6,91**	**470,70**

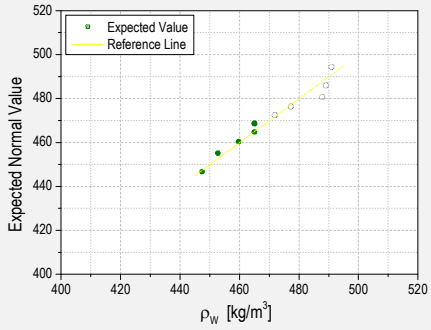

Q-Q plot of density distribution for configuration REF_BL_14%

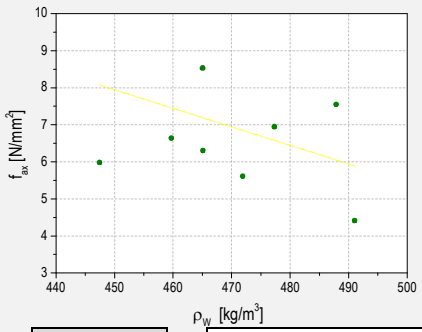

k_ρ	$30.43 - 0.05 \cdot \rho$
R-Square	**0.08**

Linear fitting of correlation between f_{ax} and density for configuration REF_BL_14%

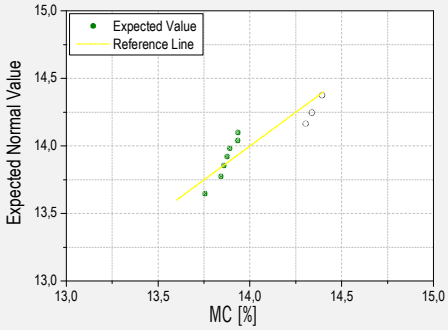

Q-Q plot of moisture content distribution for configuration REF_BL_14%

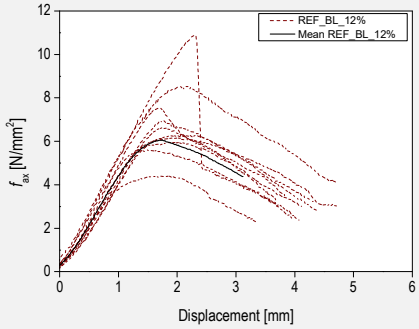

Relation between f_{ax} and displacement for REF_BL_14% tests

	MAXIMUM	MINIMUM	SD	CoV	MEDIAN	P5
f_{ax}	10,90	4,42	1,78	0,26	6,47	4,42
ρ	490,98	447,39	15,42	0,03	468,46	447,39
MC	14,39%	13,76%	0,24	0,02	13,91%	13,76%

GAP0_ML_14%

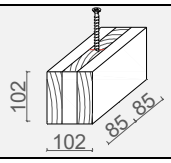

	WEIGHT AT TEST TIME [g] [mean values]	DRY WEIGHT [g] [mean values]	MC [%]	f_{ax} [N/mm²]	ρ [kg/m³]
1_GAP0_ML_14%	609,69	534,20	14,13%	4,09	441,92
2_GAP0_ML_14%	621,23	543,07	14,39%	3,10	449,20
3_GAP0_ML_14%	629,62	554,24	13,60%	3,86	409,18
4_GAP0_ML_14%	636,42	559,69	13,71%	4,13	427,15
5_GAP0_ML_14%	659,39	578,82	13,92%	3,97	456,52
6_GAP0_ML_14%	667,49	586,93	13,73%	3,46	421,69
7_GAP0_ML_14%	671,47	586,47	14,49%	2,62	437,95
8_GAP0_ML_14%	682,69	596,71	14,41%	4,62	426,23
9_GAP0_ML_14%	654,35	575,39	13,72%	5,04	453,28
10_GAP0_ML_14%	688,90	604,55	13,95%	4,83	474,06
MEAN VALUES	**652,13**	**572,01**	**14,01%**	**3,97**	**439,72**

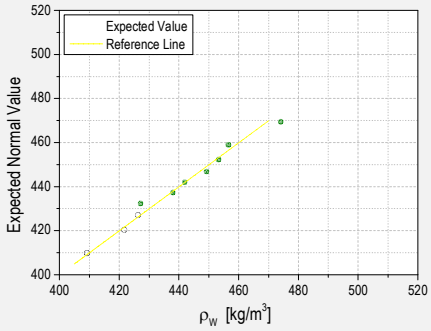

Q-Q plot of density distribution for configuration GAP0_ML_14%

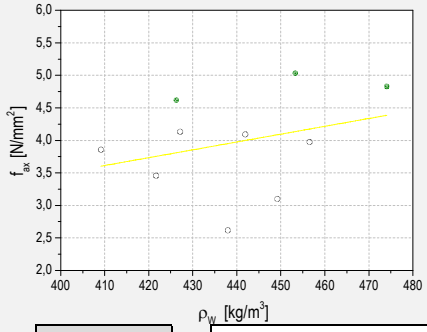

k_ρ	$-1.33 + 0.01 \cdot \rho$
R-Square	**-0.02**

Linear fitting of correlation between f_{ax} and density for configuration GAP0_ML_14%

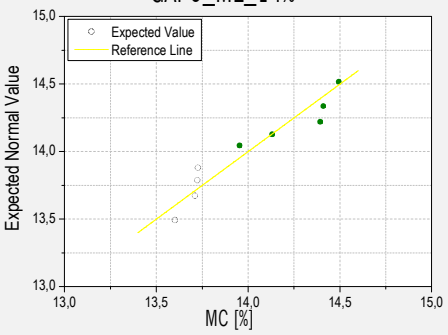

Q-Q plot of moisture content distribution for configuration GAP0_ML_14%

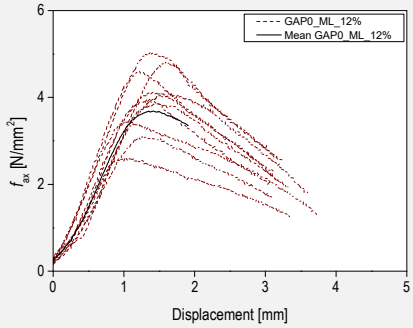

Relation between f_{ax} and displacement for GAP0_ML_14% tests

	MAXIMUM	MINIMUM	SD	CoV	MEDIAN	P5
f_{ax}	5,04	2,62	0,76	0,19	4,03	2,62
ρ	474,06	409,18	19,27	0,04	439,93	409,18
MC	14,49%5	13,60%	0,33	0,02	13,94%	13,60%

GAP0_BL_14%

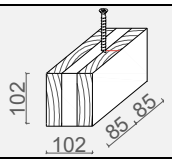

	WEIGHT AT TEST TIME [g] [mean values]	DRY WEIGHT [g] [mean values]	MC [%]	f_{ax} [N/mm²]	ρ [kg/m³]
1_GAP0_BL_14%	652,90	574,04	13,74%	6,19	476,13
2_GAP0_BL_14%	663,22	582,87	13,79%	6,28	478,34
3_GAP0_BL_14%	682,58	600,15	13,73%	5,49	471,36
4_GAP0_BL_14%	693,64	608,79	13,94%	5,35	466,59
5_GAP0_BL_14%	n.a.	n.a.	n.a.	n.a.	474,17
6_GAP0_BL_14%	702,65	617,85	13,73%	5,38	457,99
7_GAP0_BL_14%	703,84	617,51	13,98%	7,23	449,98
8_GAP0_BL_14%	709,14	624,09	13,63%	5,15	485,12
9_GAP0_BL_14%	711,29	626,46	13,54%	7,34	474,28
10_GAP0_BL_14%	722,52	634,99	13,78%	7,69	469,11
MEAN VALUES	**693,53**	**609,64**	**13,76%**	**6,23**	**470,31**

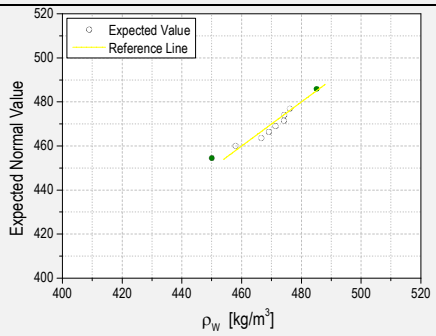

Q-Q plot of density distribution for configuration GAP0_BL_14%

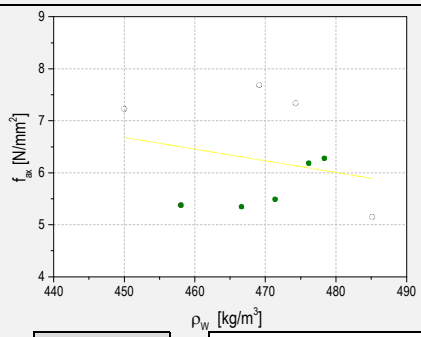

k_ρ	$16.76 - 0.02 \cdot \rho$
R-Square	**-0.07**

Linear fitting of correlation between f_{ax} and density for configuration GAP0_BL_14%

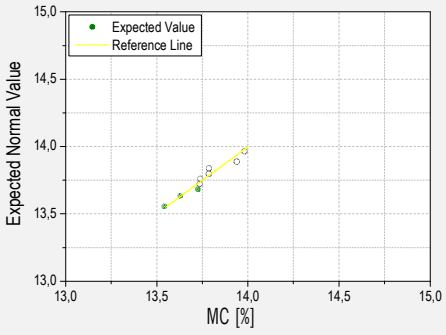

Q-Q plot of moisture content distribution for configuration GAP0_BL_14%

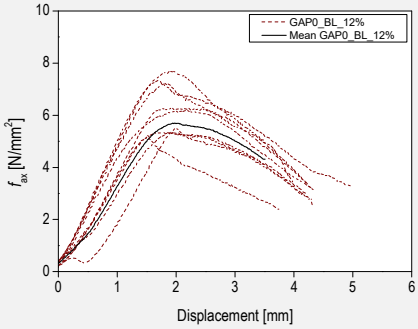

Relation between f_{ax} and displacement for GAP0_BL_14% tests

	MAXIMUM	MINIMUM	SD	CoV	MEDIAN	P5
f_{ax}	7,69	5,15	0,97	0,16	6,19	5,15
ρ	485,12	449,98	10,16	0,02	472,77	449,98
MC	13,98%	13,54%	0,14	0,01	13,74%	13,54%

GAP4_ML_14%

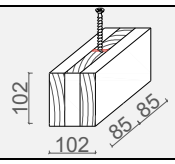

	WEIGHT AT TEST TIME [g] [mean values]	DRY WEIGHT [g] [mean values]	MC [%]	f_{ax} [N/mm²]	ρ [kg/m³]
1_GAP4_ML_14%	626,09	551,01	13,63%	1,69	461,35
2_GAP4_ML_14%	649,14	570,16	13,85%	1,97	464,25
3_GAP4_ML_14%	658,77	578,85	13,81%	2,10	451,13
4_GAP4_ML_14%	662,09	581,45	13,87%	2,13	439,71
5_GAP4_ML_14%	671,06	590,57	13,63%	1,59	445,24
6_GAP4_ML_14%	677,30	596,42	13,56%	2,16	434,55
7_GAP4_ML_14%	683,33	601,62	13,58%	2,83	457,11
8_GAP4_ML_14%	693,02	610,04	13,60%	1,80	449,55
9_GAP4_ML_14%	700,10	616,21	13,61%	1,82	472,86
10_GAP4_ML_14%	709,06	624,06	13,62%	1,57	461,39
MEAN VALUES	**673,00**	**592,04**	**13,68%**	**1,97**	**453,71**

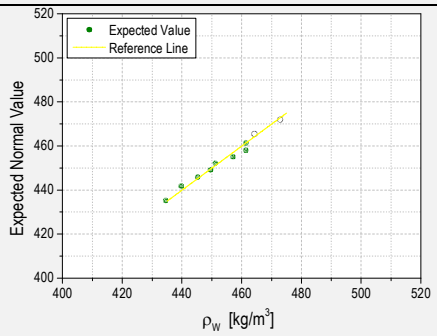

Q-Q plot of density distribution for configuration GAP4_ML_14%

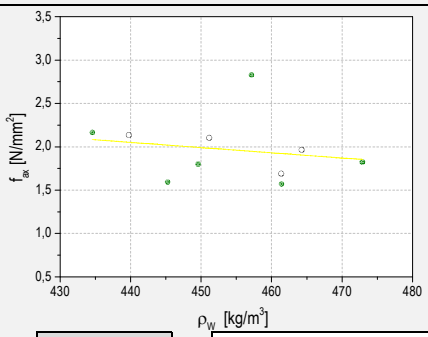

k_ρ	$4.69 - 0.06 \cdot \rho$
R-Square	**-0.08**

Linear fitting of correlation between f_{ax} and density for configuration GAP4_ML_14%

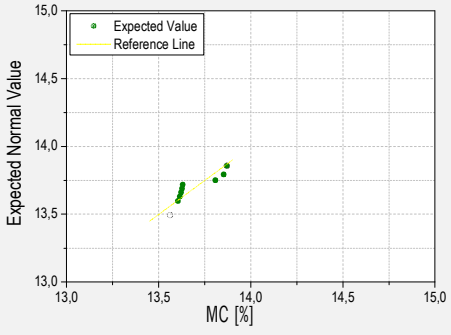

Q-Q plot of moisture content distribution for configuration GAP4_ML_14%

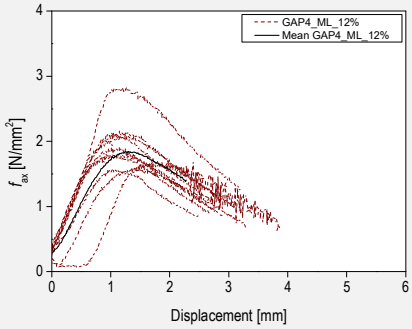

Relation between f_{ax} and displacement for GAP4_ML_14% tests

	MAXIMUM	MINIMUM	SD	CoV	MEDIAN	P5
f_{ax}	2,83	1,57	0,37	0,19	1,90	1,57
ρ	472,86	434,55	11,86	0,03	454,12	434,55
MC	13,87%	13,56%	0,12	0,01	13,62%	13,56%

GAP4_BL_14%

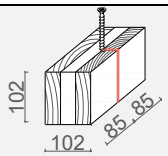

	WEIGHT AT TEST TIME [g] [mean values]	DRY WEIGHT [g] [mean values]	MC [%]	f_{ax} [N/mm²]	ρ [kg/m³]
1_GAP4_BL_14%	616,91	541,18	13,99%	3,71	414,37
2_GAP4_BL_14%	643,89	564,37	14,09%	3,29	468,56
3_GAP4_BL_14%	657,04	575,91	14,09%	5,28	473,05
4_GAP4_BL_14%	659,83	578,33	14,09%	1,93	443,83
5_GAP4_BL_14%	672,87	591,26	13,80%	3,48	454,03
6_GAP4_BL_14%	679,49	596,19	13,97%	3,98	435,07
7_GAP4_BL_14%	680,94	598,51	13,77%	6,53	457,33
8_GAP4_BL_14%	691,43	606,44	14,01%	1,12	458,36
9_GAP4_BL_14%	695,90	609,74	14,13%	3,72	431,57
10_GAP4_BL_14%	708,23	621,63	13,93%	7,01	440,91
MEAN VALUES	**670,65**	**588,36**	**13,99%**	**4,01**	**447,71**

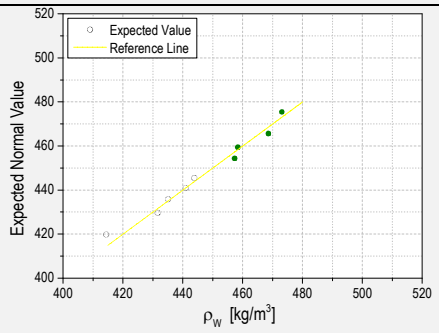

Q-Q plot of density distribution for configuration GAP4_BL_14%

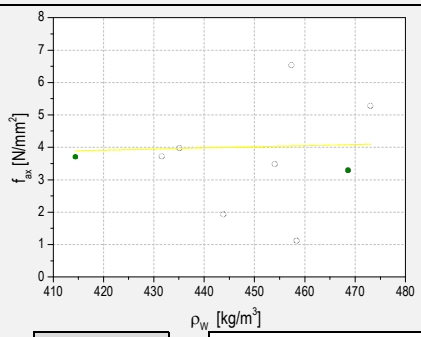

k_ρ	$2.44 + 0.004 \cdot \rho$
R-Square	**-0.12**

Linear fitting of correlation between f_{ax} and density for configuration GAP4_BL_14%

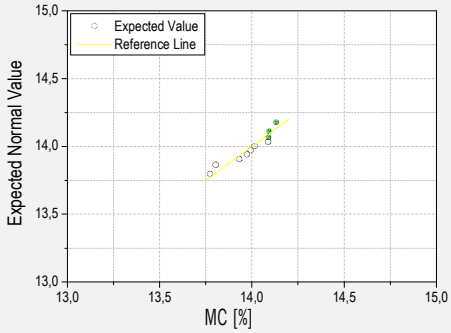

Q-Q plot of moisture content distribution for configuration GAP4_BL_14%

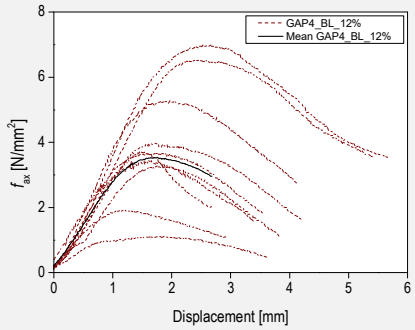

Relation between f_{ax} and displacement for GAP4_BL_14% tests

	MAXIMUM	MINIMUM	SD	CoV	MEDIAN	P5
f_{ax}	7,01	1,12	1,85	0,46	3,72	1,12
ρ	473,05	414,37	18,00	0,04	448,93	414,37
MC	14,13%	13,77%	0,12	0,01	14,00%	13,77%

Annex 1:16

REF_ML_25%

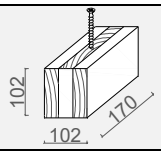

	WEIGHT AT TEST TIME [g]	DRY WEIGHT [g]	MC [%]	f_{ax} [N/mm²]	ρ [kg/m³]
1_REF_ML_25%	725,4	573,5	26,5	2,33	456
2_REF_ML_25%	736,1	588,4	25,1	3,09	460
3_REF_ML_25%	750,1	590,1	27,1	3,20	429
4_REF_ML_25%	749,1	598,0	25,3	1,97	462
5_REF_ML_25%	749,2	602,2	24,4	1,83	438
6_REF_ML_25%	749,4	603,7	24,1	4,70	458
7_REF_ML_25%	769,9	610,3	26,2	2,04	449
8_REF_ML_25%	769,9	616,2	25,0	2,38	466
9_REF_ML_25%	785,6	630,8	24,5	4,21	489
10_REF_ML_25%	798,6	639,9	24,8	4,21	485
MEAN VALUES	**758,33**	**605,31**	**25,30**	**3,00**	**459,20**

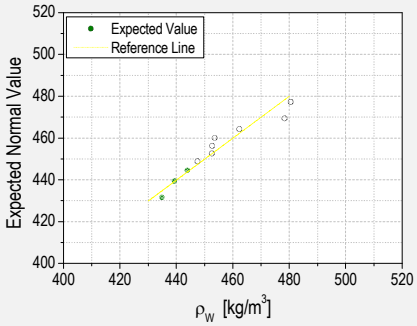

Q-Q plot of density distribution for configuration REF_ML_25%

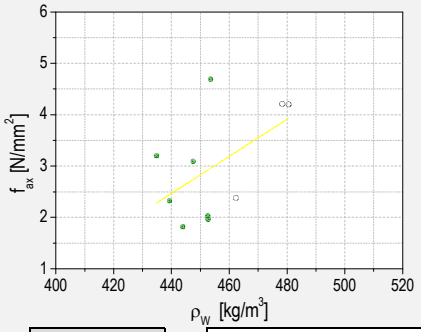

k_ρ	$-13.42 + 0.036 \cdot \rho$
R-Square	**-0.18**

Linear fitting of correlation between f_{ax} and density for configuration REF_ML_25%

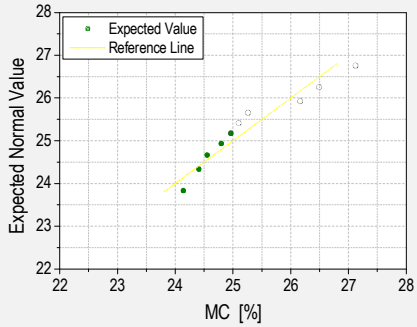

Q-Q plot of moisture content distribution for configuration REF_ML_25%

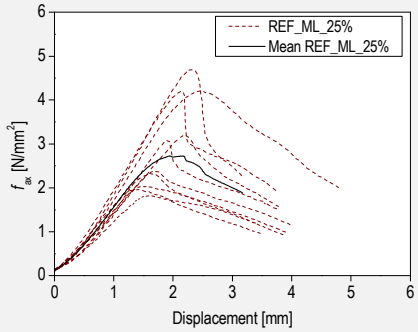

Relation between f_{ax} and displacement for REF_ML_25% tests

	MAXIMUM	MINIMUM	SD	CoV	MEDIAN	P5
f_{ax}	4,70	1,83	1,06	0,35	2,74	1,83
ρ	480	435	15,26	0,03	453	435
MC	27,1	24,1	0,98	0,04	25,0	24,1

REF_BL_25%

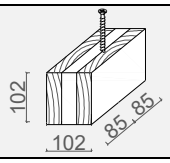

	WEIGHT AT TEST TIME [g] [mean values]	DRY WEIGHT [g] [mean values]	MC [%]	f_{ax} [N/mm²]	ρ [kg/m³]
1_REF_BL_25%	733,7	590,3	24,3	4,23	492
2_REF_BL_25%	748,9	603,0	24,2	3,33	472
3_REF_BL_25%	748,7	606,8	23,4	3,97	486
4_REF_BL_25%	771,0	614,5	25,5	3,76	477
5_REF_BL_25%	765,6	618,9	23,7	4,27	505
6_REF_BL_25%	791,0	622,7	27,0	3,32	474
7_REF_BL_25%	793,8	630,8	25,8	5,37	472
8_REF_BL_25%	797,2	639,3	24,7	4,49	503
9_REF_BL_25%	788,3	638,2	23,5	3,37	477
10_REF_BL_25%	821,5	655,3	25,4	3,75	464
MEAN VALUES	**776,0**	**622,0**	**24,7**	**3,99**	**482**

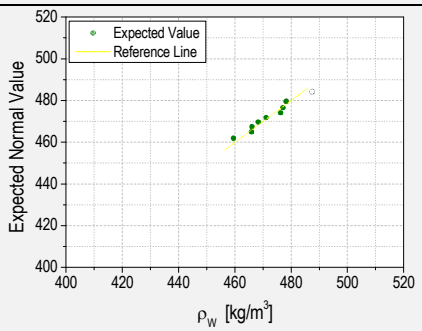

Q-Q plot of density distribution for configuration REF_BL_25%

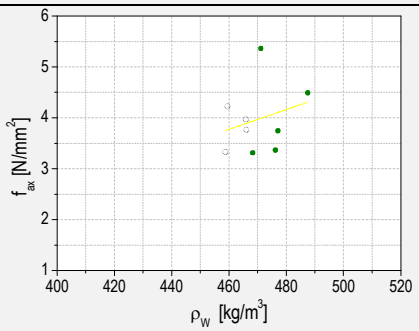

k_ρ	$-5.12 + 0.019 \cdot \rho$
R-Square	**-0.04**

Linear fitting of correlation between f_{ax} and density for configuration REF_BL_25%

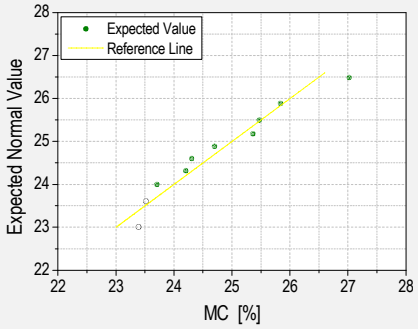

Q-Q plot of moisture content distribution for configuration REF_BL_25%

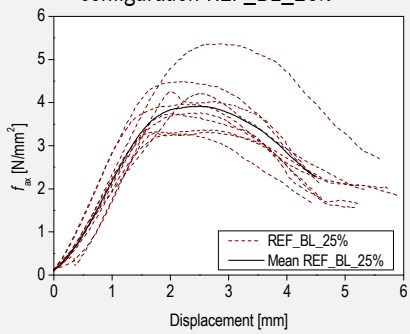

Relation between f_{ax} and displacement for REF_BL_25% tests

	MAXIMUM	MINIMUM	SD	CoV	MEDIAN	P5
f_{ax}	5,37	3,32	0,64	0,16	3,87	3,32
ρ	487	459	9,00	0,02	470	459
MC	27,0	23,4	1,16	0,05	24,5	23,4

GAP0_ML_25%

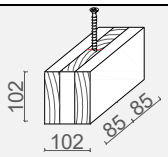

	WEIGHT AT TEST TIME [g] [mean values]	DRY WEIGHT [g] [mean values]	MC [%]	f_{ax} [N/mm²]	ρ [kg/m³]
1_GAP0_ML_25%	666,8	533,3	25,0	2,19	456
2_GAP0_ML_25%	686,5	548,7	25,1	2,11	449
3_GAP0_ML_25%	706,8	559,3	26,4	3,09	461
4_GAP0_ML_25%	723,4	570,8	26,7	2,46	418
5_GAP0_ML_25%	734,3	585,7	25,4	2,11	459
6_GAP0_ML_25%	735,8	584,2	26,0	3,14	414
7_GAP0_ML_25%	732,8	591,2	23,9	2,46	460
8_GAP0_ML_25%	753,0	596,4	26,3	2,26	447
9_GAP0_ML_25%	763,0	600,4	27,1	2,32	460
10_GAP0_ML_25%	757,7	602,2	25,8	2,54	448
MEAN VALUES	**726,0**	**577,2**	**25,8**	**2,47**	**447**

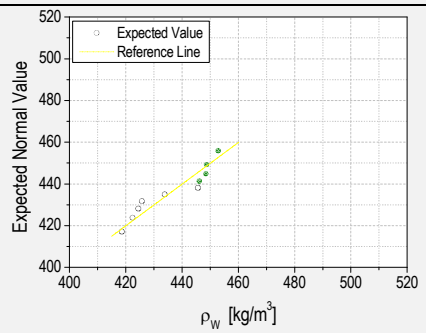

Q-Q plot of density distribution for configuration GAP0_ML_25%

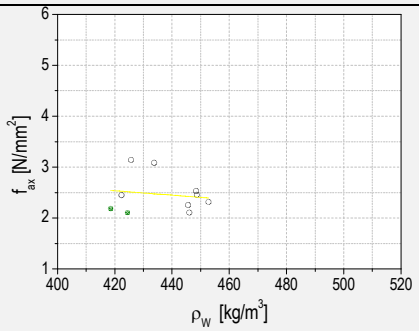

k_ρ	$4.36 - 0.004 \cdot \rho$
R-Square	**-0.10**

Linear fitting of correlation between f_{ax} and density for configuration GAP0_ML_25%

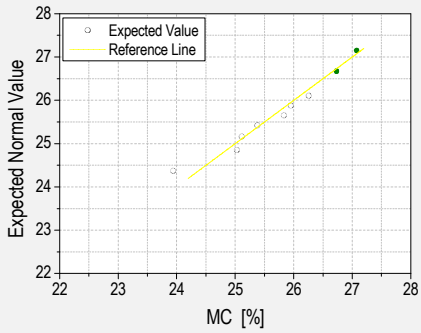

Q-Q plot of moisture content distribution for configuration GAP0_ML_25%

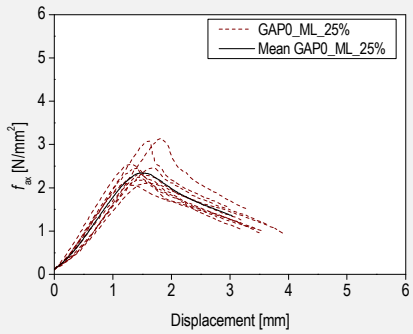

Relation between f_{ax} and displacement for GAP0_ML_25% tests

	MAXIMUM	MINIMUM	SD	CoV	MEDIAN	P5
f_{ax}	2,11	3,14	0,37	0,15	2,39	2,11
ρ	419	453	12,99	0,03	440	419
MC	23,9	27,1	0,93	0,04	25,9	23,9

GAP0_BL_25%

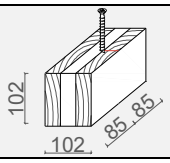

	WEIGHT AT TEST TIME [g] [mean values]	DRY WEIGHT [g] [mean values]	MC [%]	f_{ax} [N/mm²]	ρ [kg/m³]
1_GAP0_BL_25%	723,6	579,7	24,8	3,26	445
2_GAP0_BL_25%	741,5	587,6	26,2	2,99	441
3_GAP0_BL_25%	752,0	593,0	26,9	2,03	445
4_GAP0_BL_25%	765,0	604,0	25,8	3,00	468
5_GAP0_BL_25%	775,4	614,7	26,1	2,66	469
6_GAP0_BL_25%	771,9	615,7	25,4	3,84	466
7_GAP0_BL_25%	778,1	620,0	25,5	3,17	454
8_GAP0_BL_25%	774,8	622,8	24,4	3,43	468
9_GAP0_BL_25%	800,1	630,5	26,9	3,10	471
10_GAP0_BL_25%	786,2	637,8	23,3	3,45	472
MEAN VALUES	**766,9**	**610,6**	**766,9**	**3,09**	**460**

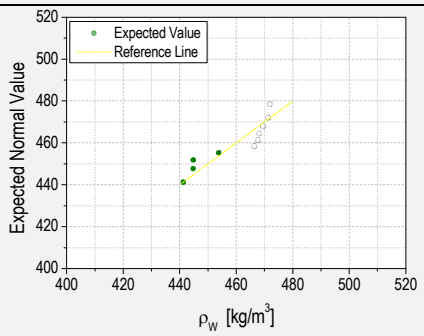

Q-Q plot of density distribution for configuration GAP0_BL_25%

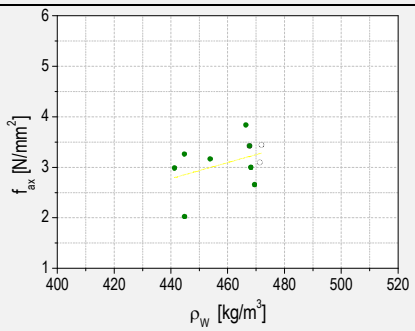

k_ρ	$-4.17 + 0.016 \cdot \rho$
R-Square	**0.05**

Linear fitting of correlation between f_{ax} and density for configuration GAP0_BL_25%

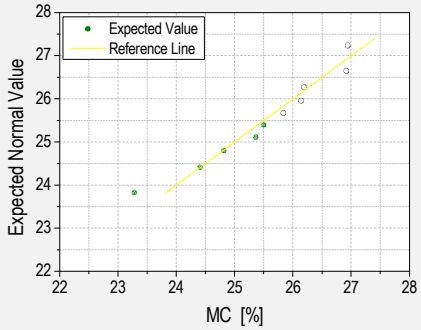

Q-Q plot of moisture content distribution for configuration GAP0_BL_25%

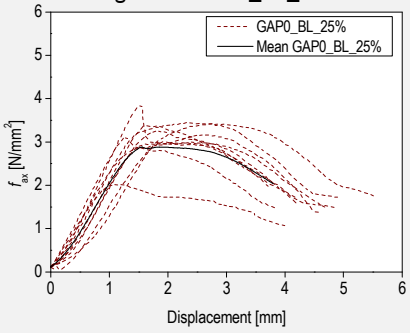

Relation between f_{ax} and displacement for GAP0_BL_25% tests

	MAXIMUM	MINIMUM	SD	CoV	MEDIAN	P5
f_{ax}	2,03	3,84	0,49	0,16	3,13	2,03
ρ	441	472	12,40	0,03	467	441
MC	23,3	26,9	1,14	0,04	25,7	23,3

GAP4_ML_25%

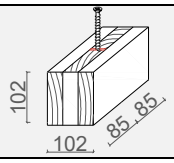

	WEIGHT AT TEST TIME [g] [mean values]	DRY WEIGHT [g] [mean values]	MC [%]	f_{ax} [N/mm²]	ρ [kg/m³]
1_GAP4_ML_25%	706,2	563,7	25,3	1,33	445
2_GAP4_ML_25%	729,3	579,7	25,8	1,43	449
3_GAP4_ML_25%	717,9	583,5	23,0	1,60	474
4_GAP4_ML_25%	732,9	585,9	25,1	1,57	478
5_GAP4_ML_25%	734,6	591,2	24,3	1,13	468
6_GAP4_ML_25%	743,9	598,3	24,3	1,59	454
7_GAP4_ML_25%	750,5	n.a.	n.a.	2,76	422
8_GAP4_ML_25%	763,5	610,4	25,1	1,97	468
9_GAP4_ML_25%	763,3	616,9	23,7	1,16	491
10_GAP4_ML_25%	791,5	633,9	24,9	1,40	454
MEAN VALUES	**743,4**	**595,9**	**24,6**	**1,59**	**460**

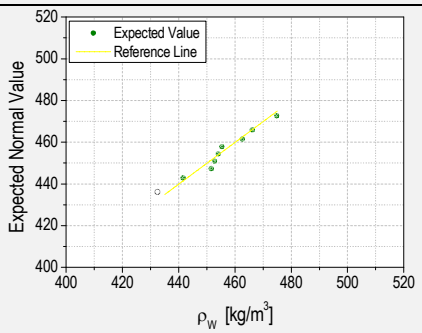

Q-Q plot of density distribution for configuration GAP4_ML_25%

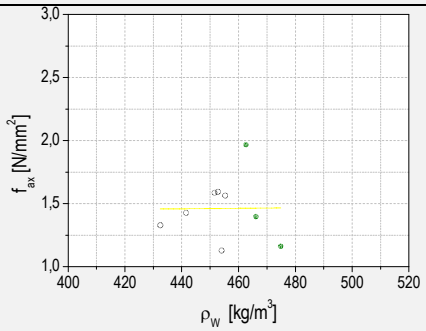

k_ρ	$1.38 + 0.000 \cdot \rho$
R-Square	**-0.14**

Linear fitting of correlation between f_{ax} and density for configuration GAP4_ML_25%

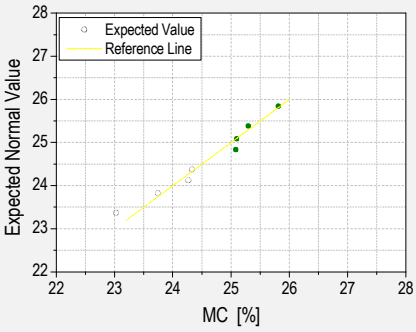

Q-Q plot of moisture content distribution for configuration GAP4_ML_25%

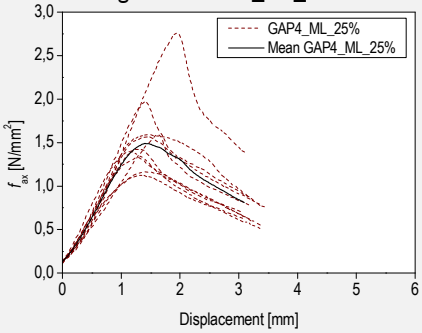

Relation between f_{ax} and displacement for GAP4_ML_25% tests

	MAXIMUM	MINIMUM	SD	CoV	MEDIAN	P5
f_{ax}	2,76	1,13	0,48	0,30	1,50	1,13
ρ	475	432	12,64	0,03	454	432
MC	25,8	23,0	0,86	0,03	24,9	23,0

GAP4_BL_25%

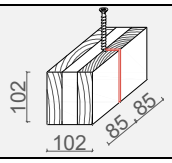

	WEIGHT AT TEST TIME [g] [mean values]	DRY WEIGHT [g] [mean values]	MC [%]	f_{ax} [N/mm²]	ρ [kg/m³]
1_GAP4_BL_25%	708,2	561,1	26,2	2,73	458
2_GAP4_BL_25%	706,8	565,8	24,9	2,40	466
3_GAP4_BL_25%	724,2	574,0	26,2	2,68	433
4_GAP4_BL_25%	730,5	583,4	25,2	1,99	487
5_GAP4_BL_25%	750,1	604,6	24,1	2,27	443
6_GAP4_BL_25%	746,4	592,8	25,9	3,20	464
7_GAP4_BL_25%	738,2	591,0	24,9	1,46	476
8_GAP4_BL_25%	758,6	606,9	25,0	2,97	455
9_GAP4_BL_25%	766,7	613,1	25,1	3,04	465
10_GAP4_BL_25%	782,7	633,6	23,5	2,32	449
MEAN VALUES	**741,2**	**592,6**	**25,1**	**2,51**	**460**

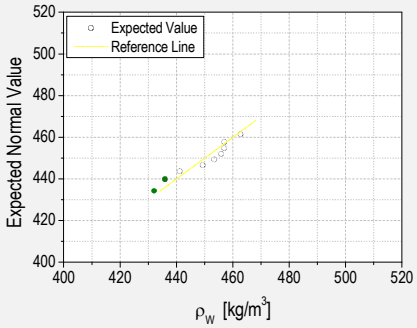

Q-Q plot of density distribution for configuration GAP4_BL_25%

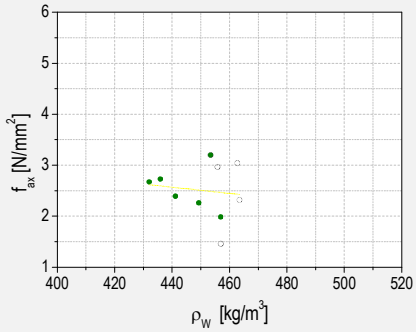

k_ρ	$5.26 - 0.006 \cdot \rho$
R-Square	**-0.11**

Linear fitting of correlation between f_{ax} and density for configuration GAP4_BL_25%

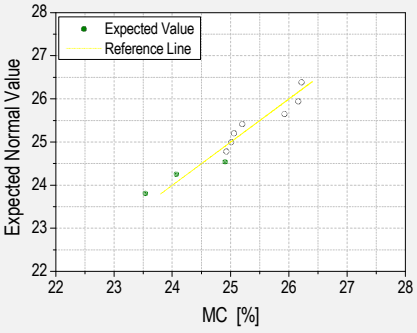

Q-Q plot of moisture content distribution for configuration GAP4_BL_25%

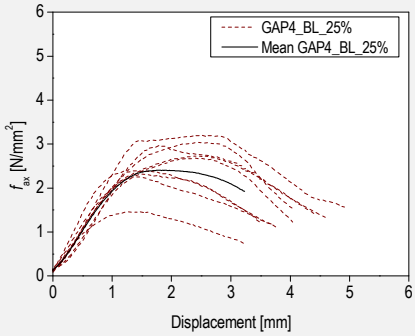

Relation between f_{ax} and displacement for GAP4_BL_25% tests

	MAXIMUM	MINIMUM	SD	CoV	MEDIAN	P5
f_{ax}	3,20	1,46	0,53	0,21	2,54	1,46
ρ	463	432	10,97	0,02	455	432
MC	26,2	23,5	0,86	0,03	25,0	23,5